NASA CR-152110

AN INVESTIGATION OF WING BUFFETING RESPONSE AT SUBSONIC AND TRANSONIC SPEEDS: PHASE I F-111A FLIGHT DATA ANALYSIS

VOLUME II - PLOTTED POWER SPECTRA

by

David B. Benepe, Atlee M. Cunningham, Jr.
and W. David Dunmyer

Prepared under Contract No. NAS 2-7091 by
GENERAL DYNAMICS CORPORATION
Fort Worth Division
Fort Worth, Texas

for

AMES RESEARCH CENTER
NATIONAL AERONAUTICS AND SPACE ADMINISTRATION

NASA CR-152110

AN INVESTIGATION OF WING BUFFETING RESPONSE AT SUBSONIC AND TRANSONIC SPEEDS: PHASE I F-111A FLIGHT DATA ANALYSIS

VOLUME II - PLOTTED POWER SPECTRA

by

David B. Benepe, Atlee M. Cunningham, Jr.
and W. David Dunmyer

Prepared under Contract No. NAS 2-7091 by
GENERAL DYNAMICS CORPORATION
Fort Worth Division
Fort Worth, Texas

for

AMES RESEARCH CENTER
NATIONAL AERONAUTICS AND SPACE ADMINISTRATION

TABLE OF CONTENTS

LIST OF TABLES

LIST OF FIGURES

LIST OF FIGURES, (Continued)

LIST OF FIGURES, (Continued)

LIST OF FIGURES, (Continued)

LIST OF FIGURES, (Continued)

LIST OF FIGURES, (Continued)

AN INVESTIGATION OF WING BUFFETING RESPONSE AT SUBSONIC AND TRANSONIC SPEEDS: PHASE I F-111A FLIGHT TEST DATA ANALYSIS

VOLUME II: PLOTTED POWER SPECTRA

by

David B. Benepe, Atlee M. Cunningham, Jr.,
and W. David Dunmyer

SUMMARY

The structural response to aerodynamic buffet during moderate to high-g maneuvers at subsonic and transonic speeds was investigated. The measurements which consisted of shear, bending moment and torque at four wing span stations, vertical accelerations at the wing tips, center of gravity and pilot's seat and lateral accelerations at the center of gravity and pilot's seat had been previously obtained during the Loads Demonstration flight program on a variable sweep fighter bomber aircraft.

Existing flight data for one wing sweep were extraced from magnetic tape records and subjected to statistical analyses to determine the power spectra and root-mean-square values of response for each of the measurements at several angles of attack for each of of seven maneuvers. The frequency content of the various responses was correlated with results of ground vibration tests to identify the response modes. The rms values of response were plotted against angle of attack to show the variations of intensity of

response during the maneuvers. The Phase I F-111A Flight Data Analysis effort is reported in three volumes. NASA CR-152109 presents a summary of the technical approach, the results and conclusions drawn from the results. NASA CR-152110 presents plotted variations of Power Spectral Density (PSD) data with frequency for each structural response item for each data sample analyzed during the course of the investigation. NASA CR-152111 presents Power Spectral Density (PSD) data in tabular form for the convenience of those who might with to perfom additional analysis.

The investigation showed that the structural response to buffet is very complex. Almost all of the natural vibration modes of the aircraft,both symmetric and antisymmetric, are excited during buffet encountered in a moderate to high-g maneuver. Some of the sensors show pronounced changes in the relative modal contributions to the total response as penetration beyond buffet onset increases. The fluctuating shear and bending moment loads on the wing are small in terms of design loads except near the wing tip. The wing structural response in torsion is larger than anticipated on the basis of previously published buffet studies and amounts to between 1/3 and 1/2 of the rms values of wing bending response at high angles of attack. For the particular aircraft geometry and structure examined, there is some evidence of bending-torsion coupling starting at angles of attack between 9 and 12 degrees at Mach number of 0.80 and 0.87.

SYMBOLS

Note:	Quantities are presented in the International System of Units (U.S. customary units in parenthesis). The work was performed using U.S. customary units.
b	wing span - m, (ft)
c.g.,C.G.	center of gravity
f	frequency, hertz
f_o	spectral base frequency or analysis bandwidth, hertz
F_Z	wing vertical shear as measured by strain gages - N, (lb)
g,G	gravitational acceleration
M	Mach number
M_X	Wing Bending Moment as measured by strain gages-N-m, (in-lb)
M_Y	Wing torsional moment - N-m, (in-lb)
S	theoretical wing area (leading and trailing edges of swept panel extended to airplane centerline)-m^2, (ft^2)
T	length of input frame in spectral analysis - seconds
T_1	start time of interval for spectral analysis - seconds
T_2	stop time of interval for spectral analysis - seconds
ΔT	time interval used for spectral analysis=T_1-T_2,sec
$\ddot{y}$	lateral acceleration-g's
$\ddot{z}$	vertical acceleration-g's
α	indicated angle of attack referenced to wing manufacturing chord plane
α_{max}	maximum indicated angle of attack - deg.

SYMBOLS, (Continued)

$\alpha_{nom,NOM}$	nominal angle of attack representing time interval ΔT-deg.
α_1	indicated angle of attack at time T_1, deg
$\Delta\alpha$	increment in indicated angle of attack during time interval ΔT, deg
β	indicated sideslip angle, deg
Ψ_T	average rms value determined from power spectral analysis

ABBREVIATIONS

Alt	altitude
Asym	antisymmetric
B.M.	bending moment
Cross-PSD, XPSD	cross power spectral density
dB	decibel
Dyn Press	dynamic pressure
FM	frequency modulation
H_Z	hertz
hor,hori	horizontal
in-lb,IN-LB	inch-pound
inbd	inboard
L	left
lb,LB	pound
L/H	left hand
LWT	left wing tip
m	meter
N	newton
N-m,N-M	newton-meter
outbd	outboard
P.S.	pilot seat
PSD	power spectral density
R	right

ABBREVIATIONS, (Continued)

R/H	right hand
rms	root-mean-square
RWT	right wing tip
Sym	symmetric
TOR	torsion
W.S.	Wing Station for strain gage measurements

SECTION I

INTRODUCTION

The phenomenon of aerodynamic buffet has been a challenge to aircraft design teams for many years. With the advent of truly high performance fighter aircraft which are capable of operating at high angles of attack, the intensity of buffet and the magnitudes of the aircraft structural responses to buffet have become important design considerations.

The state-of-the-art of buffet research is such that development of a valid method of predicting aircraft structural response to buffet appears feasible in the near future. A significant problem that exists is the dearth of published flight data to provide an adequate test of the validity of a prediction method.

This investigation, described in NASA CR-152109, NASA CR-152110, and NASA CR-152111, is an attempt to supply the data of sufficient scope in terms of the number and types of flight measurements and in terms of the depth of analysis of the measurements to use for correlation with predicted response characteristics. A secondary, though no less important, objective of the investigation is to add to the aeronautical community's understanding of buffet phenomena which has advanced rapidly in recent years.

Considerable effort has been expended in research programs conducted by the National Aeronautical and Space Administration's Ames, Langley, and Flight Research Centers (Refs. 1-7), by the

armed services (Refs. 8-14) and by airframe manufacturers (Refs. 15-17). Each of these previous efforts has contributed something of significance to our understanding of buffet and of aircraft responses to buffet.

Results of various flight test programs have shown that a most reliable indicator of maneuvering buffet onset is the abrupt change in rms response of a wing-tip accelerometer. It can also be inferred that wing-tip accelerometer response is a good indicator of the variation of buffet intensity with angle of attack. However, measurements need to be obtained of accelerations at several points on an aircraft and of the spanwise distributions of dynamic structural loads on the wing to obtain a true test of a prediction method. Additionally, power spectra data are needed for each measurement over a range of frequencies which covers the important natural vibration modes of the aircraft structure.

Recent developments in flight test instrumentation and dat recording and data processing systems permit the use of powerful techniques of random data analysis to study the buffet problem. Power spectral density (PSD) plots can be readily constructed to obtain the needed variations of response with frequency and calculate root-mean-square values (rms) of the accelerations and loads to obtain statistical measures of the variations of responses with angle of attack.

The duration of the flight maneuvers is short, therefore, the data samples are usually not long enough to strictly satisfy the mathematical criteria for obtaining a high level of confidence in the spectral or rms estimates. Nevertheless, spectral estimates and rms values are much more meaningful quantities than the peak-to-peak or half-amplitude measurements prevalent early studies of the buffet problem.

A summary of the investigation with a complete description of the technical approach, description of the aircraft, its instrumentation, the data reduction procedures, results and conclusions is presented in NASA CR-152109. This volume presents plotted variations of Power Spectral Density data with frequency for each structural response item for each data sample and analyzed during the course of the investigation. Some of this information contained in NASA CR-152109 is repeated to allow the reader to identify the specific conditions appropriate to each plot presented and to interpret the data.

The flight program from which data have been extracted for use in this study was primarily for F-111A flight loads demonstration. The test aircraft was therefore instrumented with numerous strain-gage sensors and accelerometers. Flight maneuvers included wind-up turns, pull-ups and roller coasters at various altitudes, Mach numbers, and target load factors. While it was

not a particular goal of the flight program to investigate buffeting, many of the flight test conditions were such that significant levels of buffeting occurred. An opportunity thus exists to subject the extensive flight data to analyses specifically aimed at providing detailed buffeting response characteristics.

The basic approach used in the study is described in the following paragraphs.

The various records pertinent to the Flight Loads Demonstration program were surfeyed to identify candidate flight points for the investigation. About 90 combinations of wing sweep, Mach number, altitude and target load factor were selected for initial investigation. Analog strip-charts of thirty items for instrumentation were then made for each candidate flight point. The strip charts were used primarily to identify the particular flight maneuvers in which the wing responses were of sufficient magnitude to be meaningful in the study and to eliminate points in which excessive wing spoiler activity might "contaminate" the response data.

Since the investigation was aimed at providing flight data, for comparison with predictions an additional criterion in the selection of flight points for detailed analysis was the existence of corresponding wind tunnel data in terms of wing sweep and Mach number. The investigation finally was concentrated on seven flight maneuvers all of which were performed at one

nominal wing sweep. Existing digital data for the selected flight points were then reviewed and plots were made of the variations of Mach number, angle of attack and load factor as functions of time during the particular maneuvers. Specific time intervals corresponding to nominal average angles of attack were selected for each maneuver and stochastic (statistical) analyses were performed on the outputs from seven accelerometers and twelve strain-gage sensors for each selected time interval.

The major effort in the stochastic analysis was devoted to obtaining power spectral density (PSD) plots as a function of frequency and root-mean-square (rms) values of the magnitudes of wing shear, bending moment, and torque at four wing span stations and accelerations at the wing tips, center of gravity and pilot's seat. These PSD and rms data are essential for correlation with prediction methods. In addition, the PSD plots were used to identify the frequencies and magnitudes of the major responses for each time interval. The particular vibration modes associated with the major responses were then identified insofar as possible from the results of extensive ground vibration tests performed at an earlier time on F-111A aircraft (References 18 and 19).

The variations of rms values of the various putputs (for specific ranges of frequencies) of instrumentation were plotted against angle of attack and comparisons made to observe trends with changes of altitude or Mach number.

SECTION 2

AIRCRAFT DESCRIPTION

The test aircraft was F-111A Number 13. A drawing showing the general features of the aircraft is presented as Figure 1. Detailed geometry associated with the aircraft and its components appears in Table 1. The aircraft has a variable sweep wing and a convention was adopted early in the development program that all aerodynamic coefficients would be referenced to geometric characteristics at a specific wing sweep, namely, Λ_{LE} 16 degrees. The variations of some key geometric characteristics of the wing with leading-edge sweep angle are presented in Figure 2.

Although the aircraft is fitted with a high lift system consisting of multisegment leading-edge slats and multisegment double-slotted trailing-edge flaps, these devices were in their retracted positions for all maneuvers analyzed in this study.

Two-segment upper surface spoilers on each wing are used at low wing sweeps in addition to differentially controlled all-movable horizontal tails to achieve roll control.

The aircraft has a three-axis stability augmentation system which was operational on all maneuvers analyzed in this investigation.

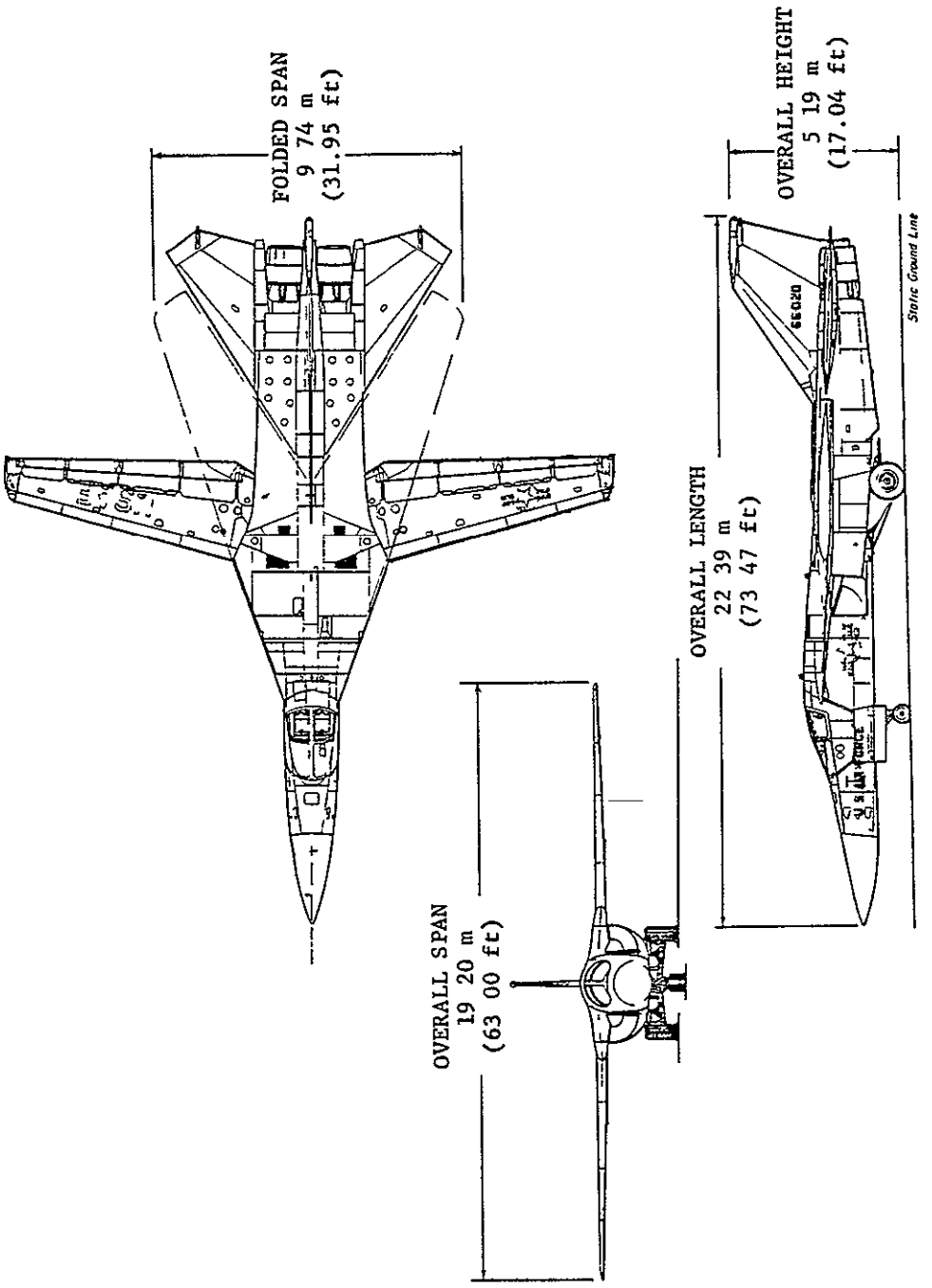

Figure 1 F-111A THREE-VIEW

Table 1

PHYSICAL CHARACTERISTICS OF THE F-111A AIRPLANE (NUMBER 13)

Wing –	
Airfoil section, at pivot	NACA 64A210 7 (modified)*
Airfoil section, tip	NACA 64A209 8 (modified)*
Sweep, deg (leading edge)	16 to 71 5
Incidence, deg	1
Dihedral, deg	1
Span area, mean aerodynamic chord	(See fig 2)
Leading-edge slats	
Area (planform projected), $ft^2(m^2)$	60 7(5 64)
Span percent of exposed wing-panel span	96 5
Deflection, maximum, deg	45
Trailing-edge flaps	
Type	Double Slotted Fowler
Area (aft of hinge line), $ft^2(m^2)$	117 8(10 94)
Span, percent of exposed wing-panel span	
Deflection, maximum, deg	37 5
Spoilers	
Area (planform projected), $ft^2(m^2)$	28 6(2 66)
Span, ft(m)	11 8(3 6)
Deflection, maximum, deg	45
Wing pivot	
Distance from airplane nose, ft(m)	40 18(12 25)
Distance from airplane centerline, ft(m)	5 86(1 79)
Horizontal tail (all movable) –	
Airfoil section	BICONVEX
Incidence, deg	1
Dihedral, deg	-1
Sweep at leading edge, deg	57 5
Span, ft(m)	29 3(8 93)
Area (exposed), $ft^2(m^2)$	174 3(15 74)
Area (movable), $ft^2(m^2)$	154 2(13 92)
Aspect ratio	1 42
Mean aerodynamic chord (exposed), in (cm)	137 5(349 3)
Deflection, maximum, deg	
As elevators	
Trailing-edge up	(approx) 25
Trailing-edge down	(approx) 10
As ailerons (total)	(approx) ±15
Surface stops	
Trailing-edge up	(approx) 31
Trailing-edge down	(approx) 16
Vertical tail –	
Airfoil section	BICONVEX
Sweep at leading edge, deg	55
Span, ft(m)	8 9(2 71)
Area, $ft^2(m^2)$	111 7(10 09)
Aspect ratio	1 42
Mean aerodynamic chord, in (cm)	159 3(404 6)
Rudder	
Span, ft(m)	7 8(2 38)
Area, $ft^2(m^2)$	29 3(2 65)
Deflection, maximum, deg	±30
Speed brake –	
Area, $ft^2(m^2)$	26 5(2 39)
Deflection, maximum, deg	77
Ventrals –	
Area (total), $ft^2(m^2)$	25(2 26)
Power plants –	
P & W TF30-P-3 engines	2

* $\Lambda_{LE} = 16^{\circ}$

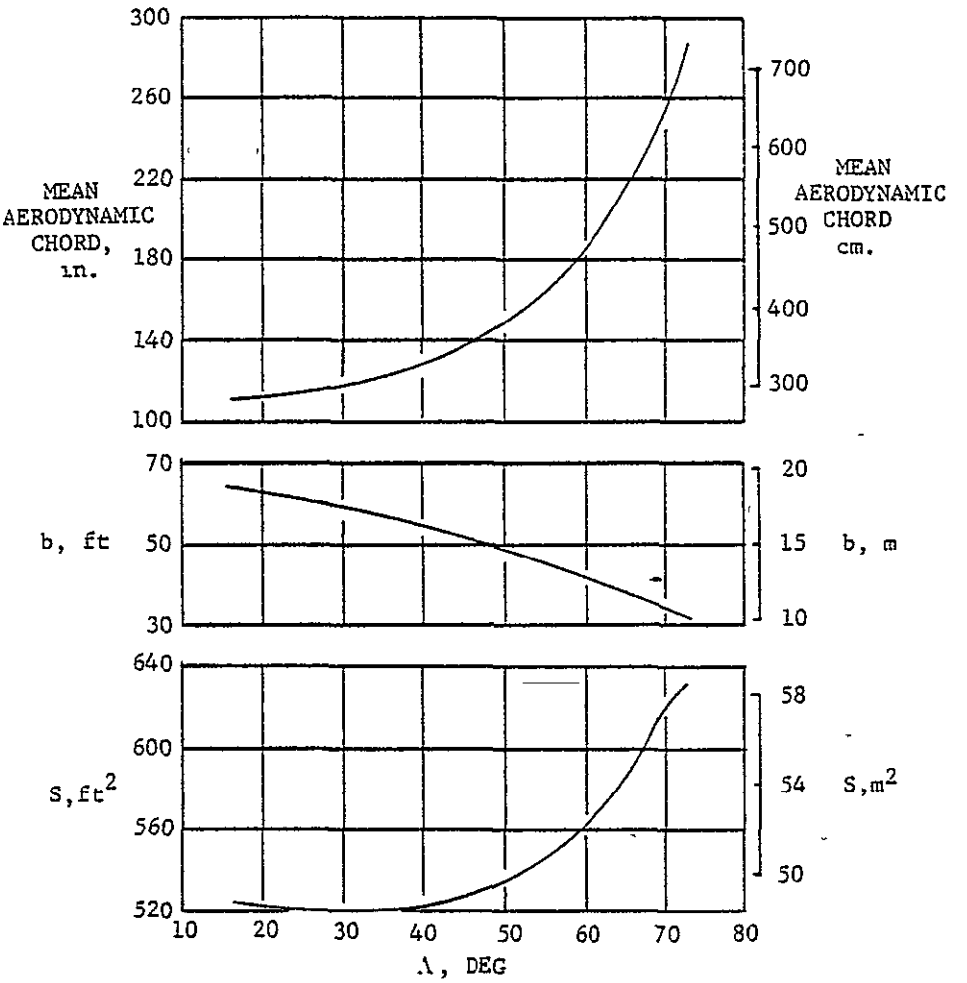

Figure 2 F-111A WING GEOMETRY AS A FUNCTION OF WING-SWEEP ANGLE

SECTION 3
AIRCRAFT INSTRUMENTATION

The instrumentation system installed in the aircraft consisted of two 30 track and one 14 track FM analog magnetic tape recorders and various transducers throughout the airplane. IRIG B time reference signals were recorded on each tape recorder to provide time correlation. The general locations of the accelerometers pertinent to the buffet study are shown in Figure 3. The actual locations in terms of aircraft geometry references are listed in Table 2.

The characteristics of the accelerometers, most of which were commercially available units, are indicated in Table 3. The accuracies quoted refer to the nominal flat frequency response up to the limit frequency quoted. No calibration data exist above the quoted limit of flat frequency response, however, the natural resonant frequencies are well beyond 100 hertz for all of the accelerometers. There is no reason to suspect a significant deviation from the basic calibration factors quoted for frequencies up to 100 hertz.

The locations of the strain gage sensors pertinent to the buffet study are shown in Figure 4. Shear, bending moment and torque were measured at each of the four indicated wing stations on the right wing. The sensitivities of these measurements were governed by the fact that the wing loads were to be measured

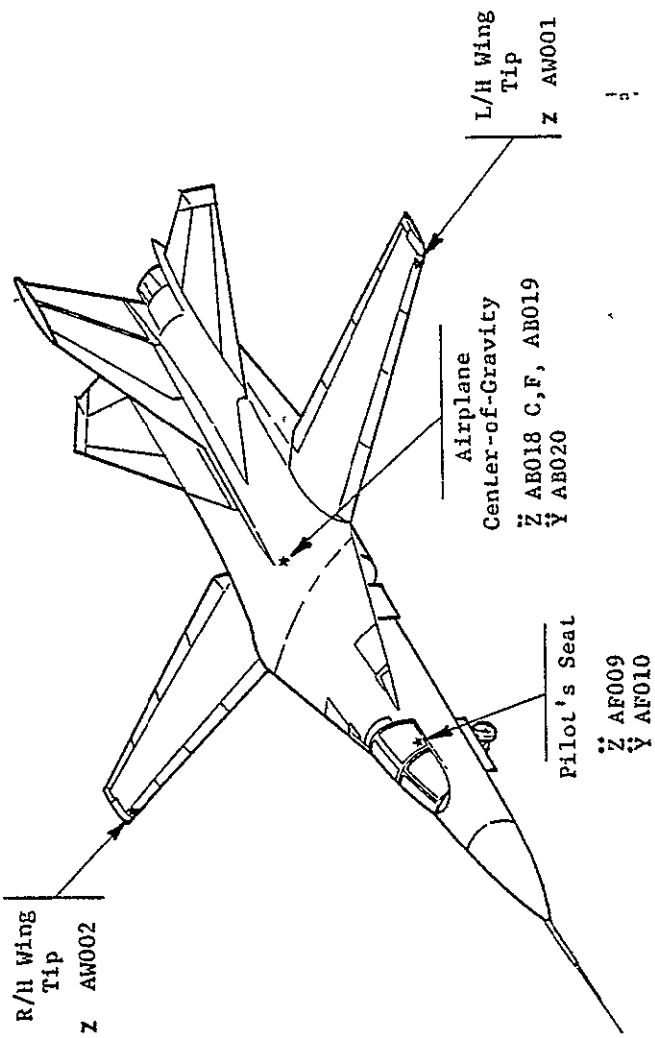

Figure 3. ACCELERATION MEASUREMENTS

Table 2

ACCELEROMETER LOCATIONS

ITEM CODE	MEASUREMENT	LOCATION					
		FUSELAGE STATION		WATERLINE		BUTT LINE	
		METERS	INCHES	METERS	INCHES	METERS	INCHES
AB018	c g vertical	12 996	(511 64)	4 740	(186 62)	0	0
AB019	c.g vertical	12 996	(511 64)	4.740	(186 62)	0	0
AB020	c g. lateral	12 996	(511 64)	4 740	(186 62)	- 023	(- 89)
AF009	Pilot seat vertica	6 462± 127	(254 40±5 0)	4 245± 127	(167 12±5 0)	- 133	(-5 25)
AF010	Pilot seat lateral	6 462± 127	(254 40±5 0)	4 245± 127	(167 12±5 0)	- 133	(-5 25)
AW001	Left wing tip - vertical	Front spar station 9 500 meters (374 inches)					
AW002	Right wing tip - vertical	Wing span station 9 157 meters (360 5 inches) @ Λ_{LE} = 16°					

Table 3

ACCELEROMETER CHARACTERISTICS

ITEM CODE	MEASUREMENT	NOMINAL FULL SCALE RANGE*	SPECIFIED ACCURACY % FULL SCALE**	SPECIFIED FLAT FREQUENCY RESPONSE TO HZ.	RESONANT# NAT. FREQ HZ	FLIGHTS
AB018	C.G. Vertical	-3 5 to +6 5	±5	25	Not Available	48, 60
AB018	C G. Vertical	±15	±3	42	530	70, 77, 78, 79
AB019	C G Vertical	±10	±5	325	--	ALL
AB020	C G. Lateral	±7 5	±5	275	--	ALL
AF009	Pilot Seat Vertical	±10	±3	32	400	ALL
AF010	Pilot Seat Lateral	±7.5	±5	275	--	ALL
AW001	Left Wing Tip Vertical	±25	±5	500	--	ALL
AW002	Right Wing Tip Vertical	±25	±5	500	--	ALL

*The actual range calibrated varied from these nominal values
**Over range of flat frequency response and at all temperatures between -70° and +250°F

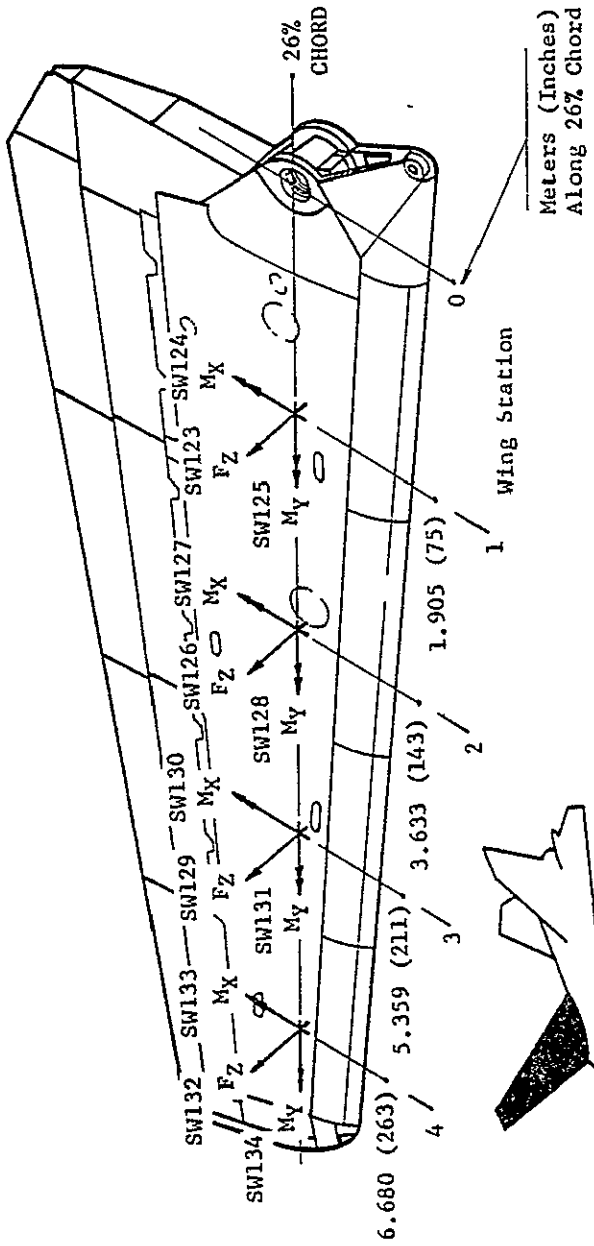

Figure 4. R/H WING-BOX LOADS MEASUREMENTS

during maneuvers at load factors up to the maximum capability of the aircraft. As a consequence the signal-to-noise ratios for the present buffet studies were lower than is desirable. The calibration slopes for each channel of information are shown in Table 4.

In several cases the frequency response upper limit for the measurements was set by the subchannel characteristics of the flight recording system. Table 5 lists the appropriate nominal limit of frequency response for each item of instrumentation based on the recorder subchannel arrangements for each flight selected for detailed analysis.

Correlating items such as angle of attack, airspeed, Mach number, altitude, gross weight, and control surface position indication of the spoilers an d horizontal tail surface deflections were also recorded on the FM tapes.

A special test nose boom was fitted to the aircraft to obtain angle of attack, sideslip angle, altitude and Mach number data.

TABLE 4

CALIBRATION SLOPES — UNITS/PERCENT OF BANDWIDTH

ITEM	MEASUREMENT	S I UNITS	U S CUST UNITS	FLT 48		FLT 60		FLT 70		FLTS 77, 78		FLT 79	
				S I	CUST	S I.	CUST	S I	CUST	S I	CUST	S I	CUST
AW001	LWT-Vert	g's	g's		50304		50304		.33578		33578		33578
AW002	RWT-Vert	g's	g's		50232		50232		33322		33322		33322
AB018C	CG-Vert	g's	g's		130		130		10690		10313		18339
AB018F	CG-Vert	g's	g's		010		010		---		---		---
AB019	CG-Vert	g's	g's		20142		20142		20172		20172		20172
AB020	CG-Vert	g's	g's		05129		05129		05052		05052		05052
AF009	P S -Vert	g's	g's		15306		15306		29280		29280		29280
AF010	P S -Lat	g's	g's		10232		10232		10128		10128		10128
AB015	Ang Roll	rad/sec^2	rad/sec^2		53569		53569		3012		3012		3012
AB016	Ang Pitch	rad/sec^2	rad/sec^2		32175		32175		0998		0998		0998
SW123	Shear-W S 1	N	lbs	8011	1801	8011	1801	11770	2464	11770	2464	11926	2681
SW124	B M -W S 1	m-N	in-lbs	22517	202896	22517	202896	37110	334383	37110	334383	37393	336937
SW125	TOR -W S 1	m-N	in-lbs	4136	37264	4136	37264	3913	35263	3913	35263	3969	35767
SW126	Shear-W S 2	N	lbs	5124	1152	5124	1152	9475	2130	9475	2130	9608	2160
SW127	B M -W S 2	m-N	in-lbs	9981	89935	9981	89935	9828	88557	9828	88557	9897	89181
SW128	TOR -W S 2	m-N	in-lbs	1251	11268	2501	22535	2798	25215	2798	25215	2834	25539
SW129	Shear-W S 3	N	lbs	2358	530	2358	530	3479	782	3479	782	3523	792
SW130	B M -W S 3	m-N	in-lbs	2800	25228	2800	25228	4160	37481	4160	37481	4197	37821
SW131	TOR -W S 3	m-N	in-lbs	1008	9084	1008	9804	964	8690	964	8690	982	8847
SW132	Shear-W S 4	N	lbs	801	180	801	180	1561	351	1561	351	1588	357
SW133	B M -W S 4	m-N	in-lbs	393	3541	393	3541	758	6835	758	6835	765	6896
SW134	TOR -W.S 4	m-N	in-lbs	188	1694	188	1694	344	3100	344	3100	349	3142
DH001C	α	deg	deg		875		875		875		875		875
DH001F	α	deg	deg		080		080		080		080		080
DH002F	β	deg	deg		080		080		080		080		080
DW001	L Inbd Spoil	deg	deg		60		60		60		60		60
DW002	R Inbd Spoil	deg	deg		60		60		60		60		60
DW003	L Outb Spoil	deg	deg		60		60		60		60		60
DW001	R Outb Spoil	deg	deg		60		60		60		60		60
DT003C	L Hor T	deg	deg		88		88		88		88		88
DT004C	R Hor T	deg	deg		88		88		88		88		88
PD016F	Mach	---	---		0034		0034		.0034		0034		0034
PD004F	Alt	m	Ft	15 24	50	15 24	50	---	---		---		---
PH022F	Alt	m	Ft	---	---	---	---	12 192	40	12 192	40	12 192	40

Table 5

FLIGHT RECORDER FREQUENCY RESPONSE CHARACTERISTICS

ITEM CODE	FLIGHTS 48, 60		FLIGHTS 70, 77, 78, 79	
	IRIG CHANNEL	FILTER FREQ. - HZ	IRIG CHANNEL	FILTER FREQ - HZ
AW001	8	45	11	110
AW002	12	160	12	160
AB018	14	330	11	110
AB019	9	60	8	45
AB020	14	330	9	60
AF009	11	110	12	160
AF010	12	160	10	80
SW123	10	80	7	35
SW124	11	110	8	45
SW125	12	160	9	60
SW126	13	220	10	80
SW127	8	45	11	110
SW128	9	60	12	160
SW129	10	80	13	220
SW130	11	110	6	25
SW131	12	160	7	35
SW132	13	220	8	45
SW133	8	45	9	60
SW134	9	60	10	80

SECTION 4

BASIC DATA PROCESSING METHODS

During the Loads Demonstration Flight Program, the FM analog magnetic tapes containing raw flight test data were processed by automated techniques. The real time data were first displayed on strip chart recorders for instrumentation verification. Next, the data were digitized at sample rates of 1 to 20 samples per second under computer control. The specific sample rates depended on user group requirements. The digitized data were then scaled, calibrated and output in computer listings and computer tapes for additional processing on an IBM System/360. Second generation computer runs were made to obtain corrected flight condition data such as gross weight, Mach number, altitude, dynamic pressure and fuel distribution at 1-second intervals.

Microfilm records of the computer listings from the original flight program data reduction were used in the present program to make plots of angle of attack, normal load factor, Mach number and dynamic pressure as functions of flight time and to identify the gross weights and altitudes for the selected flight maneuvers. The Mach number, altitude and dynamic pressure data include corrections for position error. The angles of attack are indicated angles and do not include the effect of upwash at the nose boom.

The following formula can be used to obtain an estimate of the true geometric angle of attack values if desired:

$$\alpha_T = 0.318 + 0.931\,\alpha \text{(degrees)}$$

This correction was not applied to the data presented in this report because the magnitude is not large in the range of angles of attack covered by the flight data and is within the uncertainty of the flight measurements taken under buffeting conditions with an aeroelastic aircraft.

SECTION 5

FLIGHT CONDITIONS SELECTED FOR DETAILED ANALYSIS

The seven maneuvers selected for detailed analysis are listed in Table 6. They consist of two wind-up turns, four pull ups and one roller coaster, all performed at a nominal wing sweep of 26 degrees. The Mach numbers are approximately 0.70, 0.80, and 0.87 for the three high altitude maneuvers (above 6000 meters). At the two higher Mach numbers the selected maneuvers for the three altitudes, nominally 1500, 3700 and above 6000 meters. The gross weights range from 266,000 N to 335,500 N.

Variations of angle of attack, load factor, Mach number and dynamic pressure with flight time are presented in Figure 5 for each of the selected maneuvers. Inspection of Figures 5(a) through 5(g) shows that the wind-up turns are gradual maneuvers whereas the pullups and roller coaster are rather abrupt maneuvers. As a consequence, it was feasible to select morepoints within each of the wind-up turns for stochastic analysis than for the other maneuvers.

Table 7 lists the segments of each maneuver selected for detailed analysis. In most cases the time duration of the records is one second, but some longer records were used particularly for the wind-up turn of Flight 77, S&C-R. The table also lists the indicated angle of attack at the start of each record

Table 6

SELECTED FLIGHT MANEUVERS

FLT	RUN	MANEUVER	WING SWEEP DEG	NOMINAL FLIGHT CONDITIONS		
				MACH	ALTITUDE	GROSS WEIGHT
48	6	Windup Turn	26 6	70	7,559 m (24,800 ft)	294,472 N (66,200 lb)
77	S&C-R	Windup Turn	25 6	80	6,035 m (19,800 ft)	266,004 N (59,800 lb)
78	5	Pullup	26 2	80	3,780 m (12,400 ft)	327,389 N (73,600 lb)
79	9R	Pullup	26 7	80	1,494 m (4,900 ft)	323,386 N (72,700 lb)
60	10	Roller Coaster	26 6	87	8,382 m (27,500 ft)	307,817 N (69,200 lb)
78	4	Pullup	26 3	87	3,688 m (12,100 ft)	330,503 N (74,300 lb)
70	2	Pullup	26 8	86	1,494 m (4,900 ft)	328,800 N (73,800 lb)

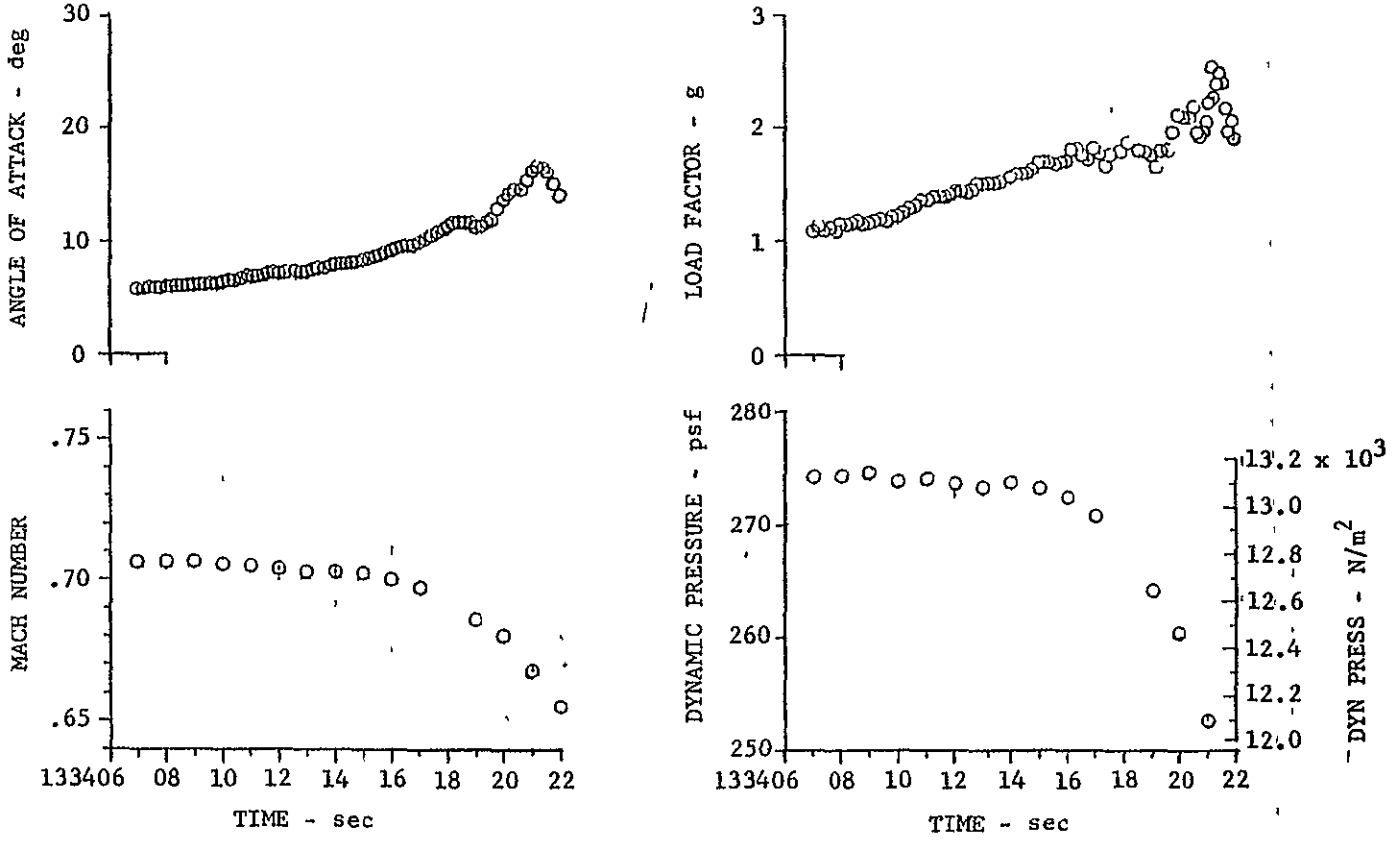

(a) FLIGHT 48, RUN 6, WINDUP TURN

Figure 6. FLIGHT CONDITIONS FOR SELECTED MANEUVERS

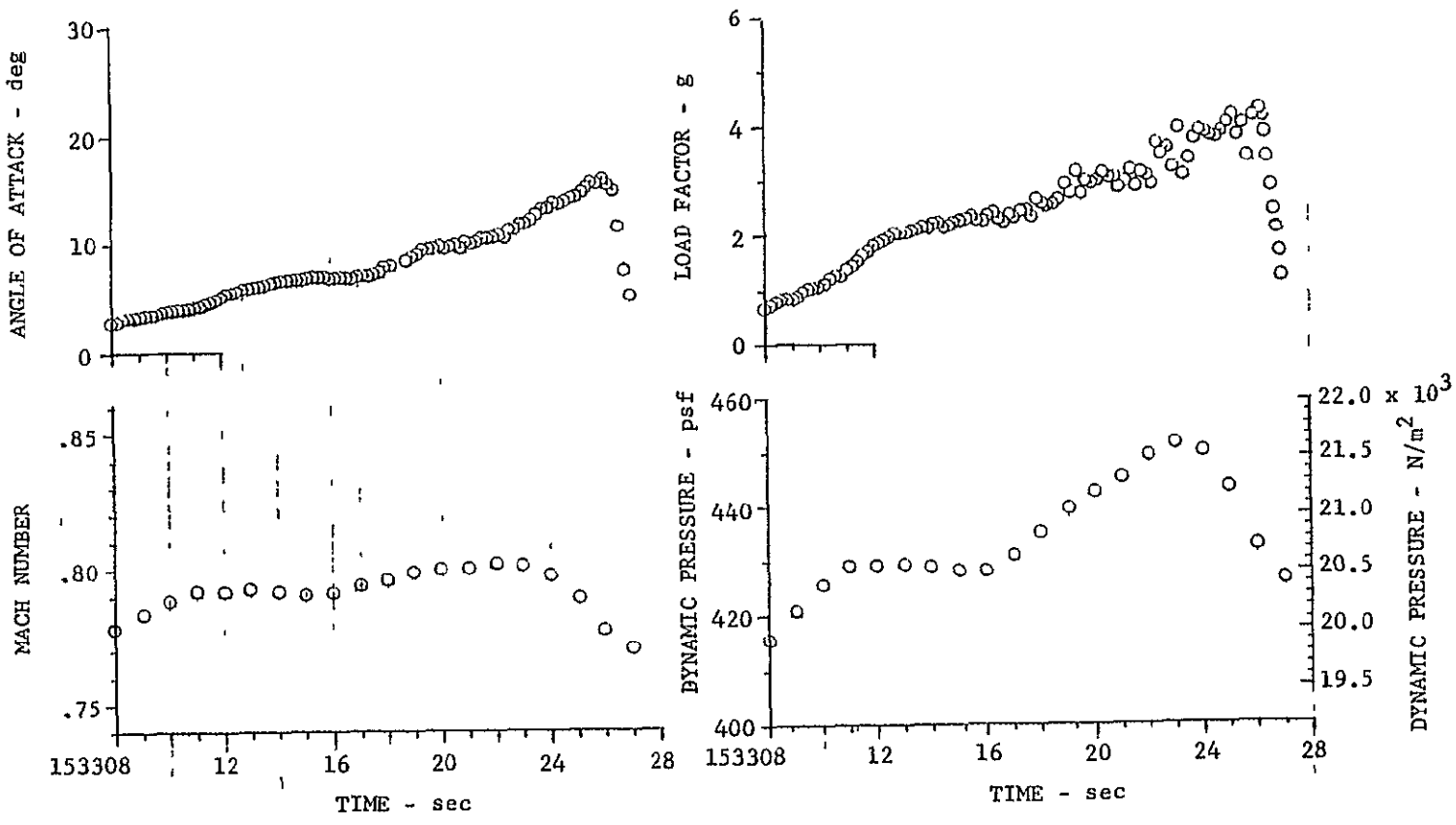

(b) FLIGHT 77, RUN S&C-R, WINDUP TURN

Figure 6. Continued

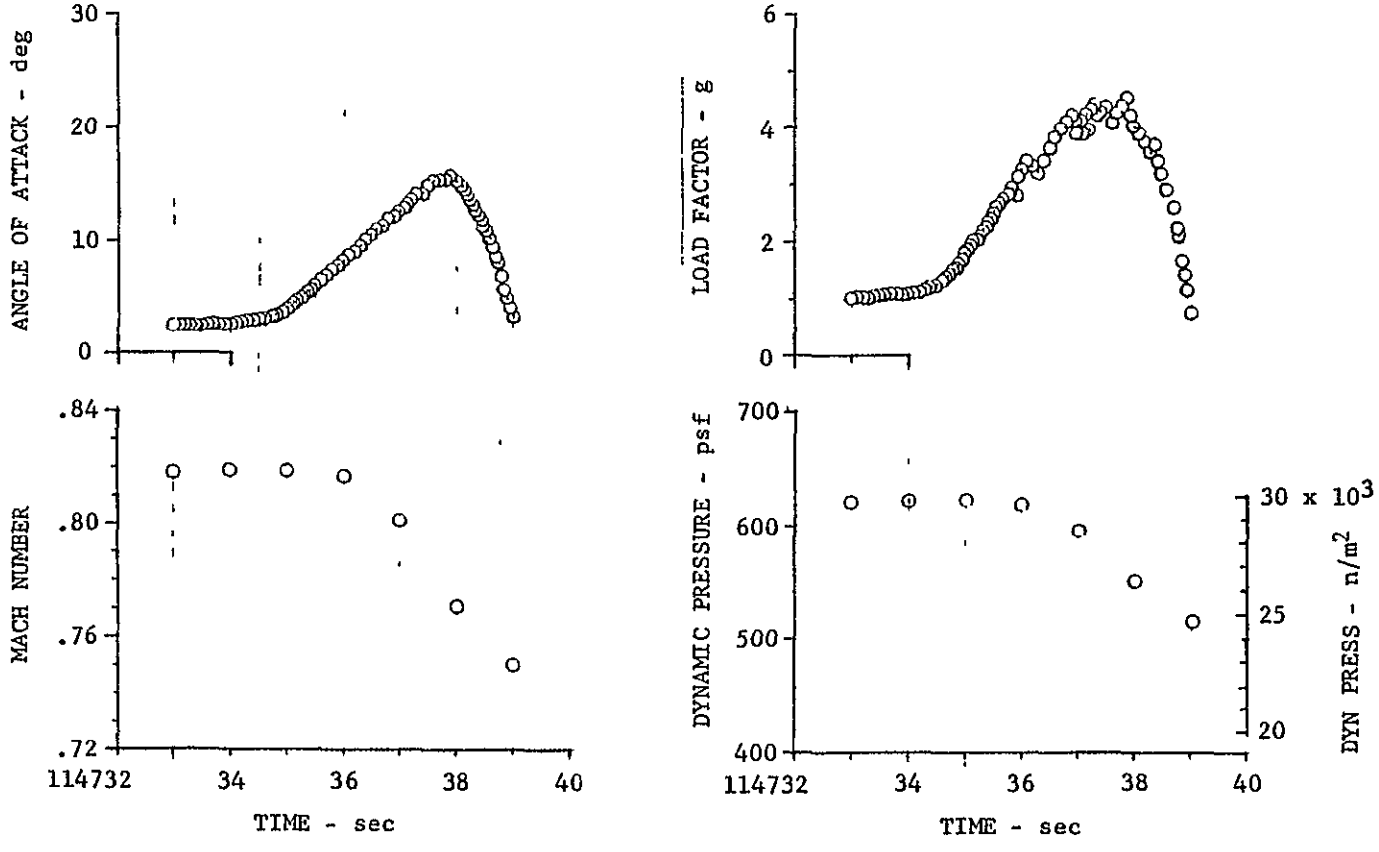

(c) FLIGHT 78, RUN 5, PULLUP

Figure 6. Continued

(d) FLIGHT 79, RUN 9R, PULLUP

Figure 6. Continued

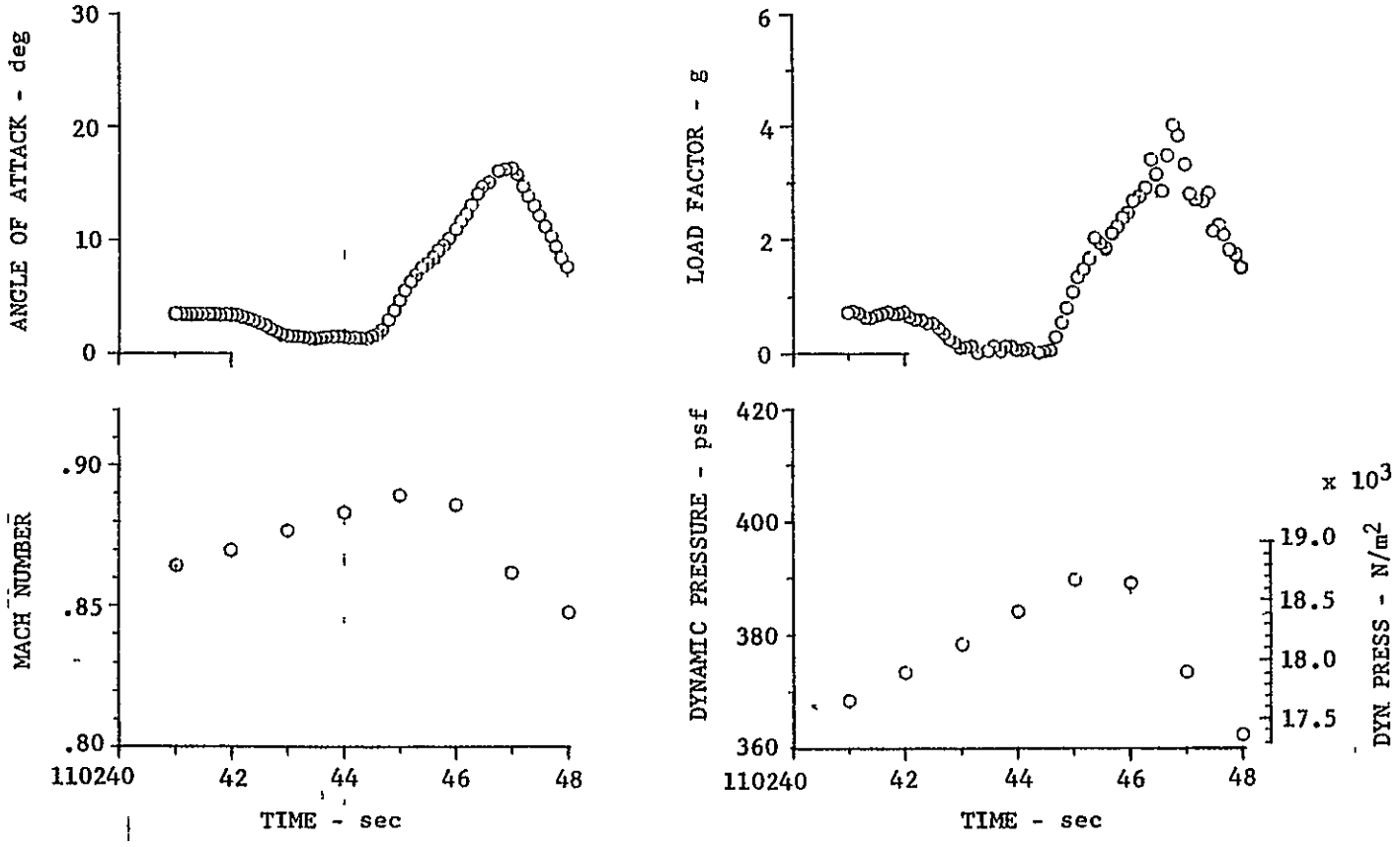

(e) FLIGHT 60, RUN 10, ROLLER COASTER

Figure 6. Continued

(f) FLIGHT 78, RUN 4, PULLUP

Figure 6. Continued

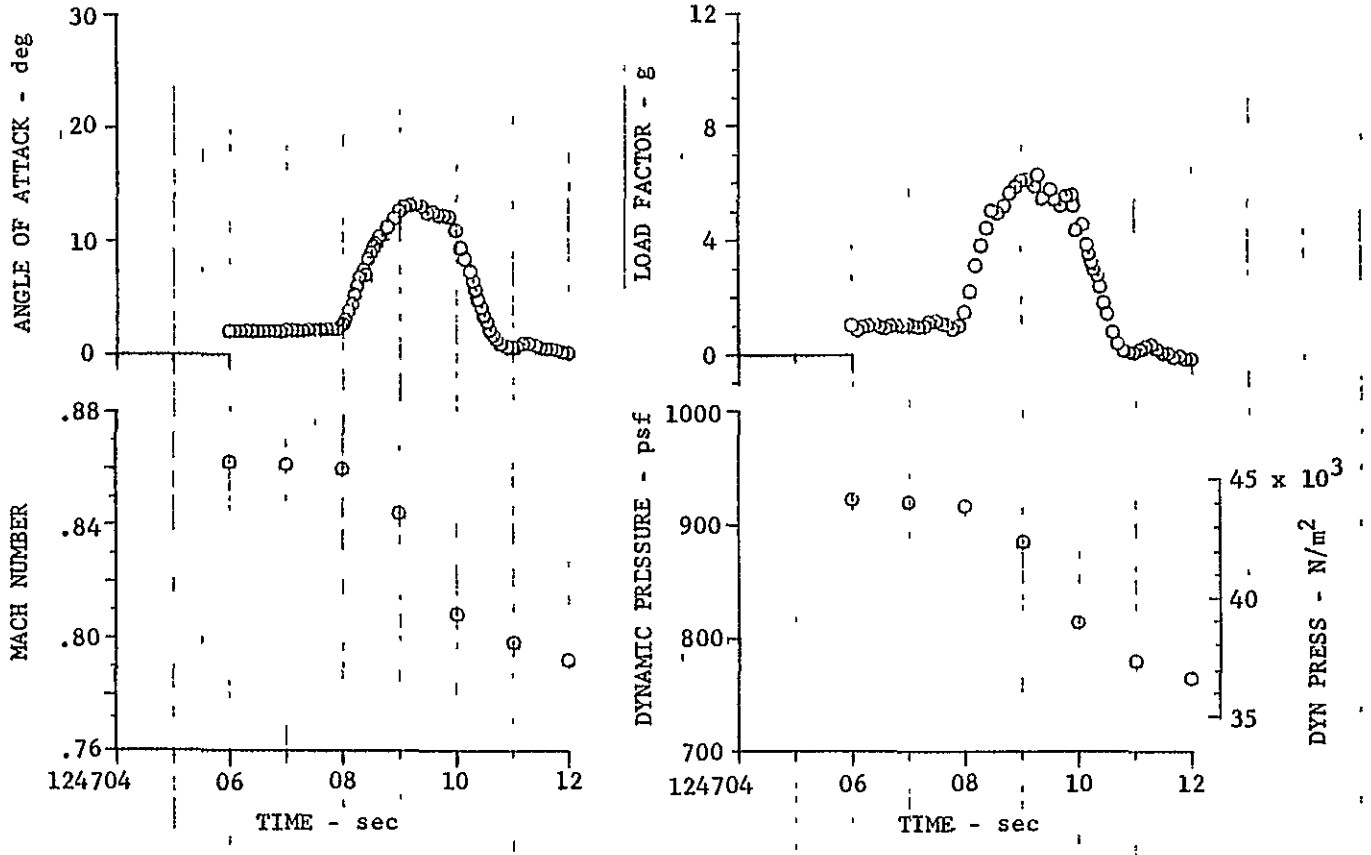

(g) FLIGHT 70, RUN 2, PULLUP

Figure 6. Concluded

TABLE 7

FLIGHT POINTS SELECTED FOR STOCHASTIC ANALYSIS

FLT	RUN	POINT	START TIME T_1	STOP TIME T_2	ΔT (SEC)	α_1 (DEG)	α_2 (DEG)	α_{MAX} (DEG)	α_{NOM} (DEG)	$\Delta\alpha$ (DEG)	PSD PLOT Fig. No.
48	6	1	133412.5	133413.5	1	7.25	7.62		7.4	0.37	9
		2	133414.0	133415 0	1	7.82	8.40		8.1	0.58	10
		3	133415.0	133416.0	1	8.72	9.55		9.1	0.83	11
		4	133416.7	133417.7	1	9.70	10.75		10.2	1.05	12
		5	133417.3	133418.3	1	10.30	11.75		11.1	1.45	13
		6	133419.0	133420.0	1	11.15	13.55		12.3	2.40	14
		7	133420.3	133421.3	1	14.25	16.60		15.3	2.35	15
		8	133420.0	133422.0	2	13.55	13.70	16.60	15.1	3.05	16

TABLE 7 CONTINUED

FLT	RUN	POINT	START TIME T_1	STOP TIME T_2	ΔT (SEC)	α_1 (DEG)	α_2 (DEG)	α_{MAX} (DEG)	α_{NOM} (DEG)	$\Delta\alpha$ (DEG)	PSD PLOT Fig. No.
77	S&C-R	1	153310.0	153311 0	1	3.72	4.22		4 0	0.50	17
		2	153311.5	153312.5	1	4.70	5.62		5.1	0.92	18
		3	153316.0	153317 0	1	6 90	7.08		7.0	0.18	19
		4	153319 0	153320.0	1	8.75	9.65		9 2	0.90	20
		5	153322.85	153323.85	1	11.45	13.00		12.2	1.55	21
		6	153325.3	153323.3	1	14 60	15.35	15.55	15.2	0.95	22
		7	153311.0	153313 0	2	4.22	5.98		5 1	1.76	23
		8	153315.5	153317.5	2	7 60	7.22		7.1	0 32	24
		9	153318 5	153320 5	2	8.45	9.65		9.2	1 24	25
		10	1533 22.50	153324 50	2	10.85	13 40		12.2	2.55	26
		11	153324.35	153326 35	2	13 40	15 35	15.55	14.8	2 15	27
		12	153323.0	153326.0	3	11 65	15.55		13.6	3.88	28

TABLE 7 CONTINUED

FLT	RUN	POINT	START TIME T_1	STOP TIME T_2	ΔT (SEC)	α_1 (DEG)	α_2 (DEG)	α_{MAX} (DEG)	α_{NOM} (DEG)	Δ (DEG)	PSD PLOT Fig. No.
78	5	1	114732.0	114733.0	1	2.60	2 60		3.60	$\pm$ 05	29
		2	114734.8	114735.8	1	3.60	7.40		5.1	3.80	30
		3	114735.7	114736.7	1	7.00	11.20		9.2	4.20	31
		4	114736.4	114737.4	1	10.10	14.40		12.2	4.30	32
		5	114737.2	114738.2	1	13.35	14.00	15.40	14.6	2.05	33
79	9R	1	100109.4	100110.4	1	2.95	5.50		4.1	2.55	34
		2	100110.3	100111.3	1	5.12	10.50		7.1	5.38	35
		3	100110.6	100111.6	1	6.30	12.10		9.2	5.80	36
		4	100111.15	100112.15	1	9.30	9.95	12.60	10.8	5.30	37

TABLE 7 CONCLUDED

FLT	RUN	POINT	START TIME T_1	STOP TIME T_2	ΔT (SEC)	α_1 (DEG)	α_2 (DEG)	α_{MAX} (DEG)	α_{NOM} (DEG)	$\Delta\alpha$ (DEG)	PSD PLOT Fig. No.
60	10	1	110241.0	110242.0	1	3.50	3.45		3.5	±.05	38
		2	110244.65	110245.65	1	2.10	8 70		5.15	6.60	39
		3	110245.2	110246.2	1	6.35	12.30		9.3	5.95	40
		4	110245.7	110246.7	1	9.07	15.60		12 3	6.53	41
		5	110246.15	110247.15	1	12.00	15.20	16.30	14.8	4.30	42
78	4	1	114454.0	114455.0	1	3.35	3.30		3.3	± 05	43
		2	114455.85	114456.85	1	4.35	8 35		6.35	4.00	44
		3	114456.55	114457.55	1	6.95	11 90		9.40	4.95	45
		4	114457.05	114458.05	1	9.10	14.55		12.0	5.45	46
		5	114457.65	114458 65	1	12.45	16.65		14.6	4.20	47
		6	114457.4	114459.4	2	11.05	11.20	16.65	13.6	3.55	48
70	2	1	124705 7	124707.7	2	2.10	2.10		2.10	±.05	49
		2	124708 5	124709 5	1	9 05	12.60	13.25	12.3	4 20	50
		3	124708.9	124709.9	1	11.95	12.05	13.25	12.5	1.30	51

(α_1), at the end of each record (α_2)and in a few cases the maximum indicated angle of attack (α_{max}) occurring during the record. The figure number for the corresponding PSD data is also listed for each point. Also presented is the increment in angle of attack during the record ($\Delta\alpha$) which is relatively large for the pullup and roller coaster maneuvers. A nominal angle of attack (α_{nom}) has been assigned to each segment which is used later to plot trends in the variations of instrument responses with angle of attack.

An adjunct to the point selection process was the determination of the buffet onset characteristics for each of the maneuvers from the time histories. The criterion used for buffet onset was the first detectable change in level of response from any of the wing instrumentation which was followed by an ever increasing level of response. The results of the buffet onset determinations are presented in Figure 6. It was possible to obtain buffet onset points for six of the seven maneuvers. The aircraft was slightly into buffet even at 1-g trim conditions for Flight 78, Run 4. Figure 6(a) shows that the variation of angle of attack for buffet onset with Mach number is smooth despite the significant differences in dynamic pressure and pitch rates for the various maneuvers. Figure 6(b) shows that the normal force coefficients for buffet onset show a slight trend of increasing with a decrease in altitude (increase in dynamic pressure). This

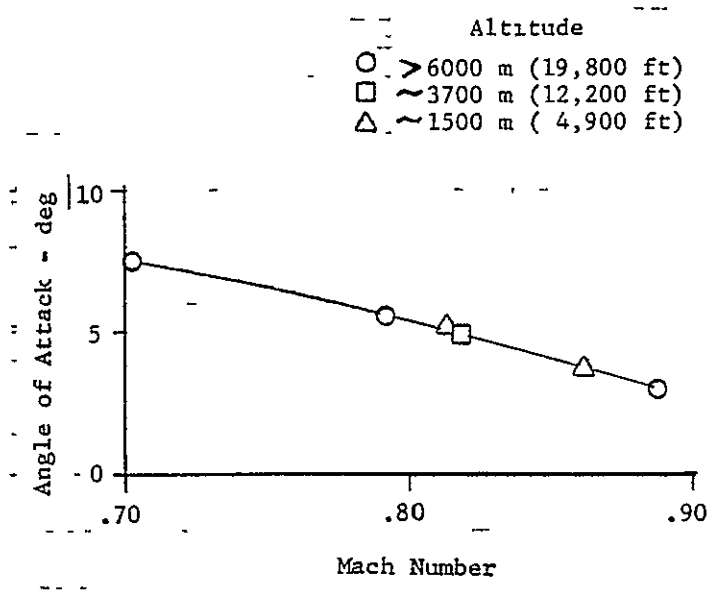

(a) ANGLE OF ATTACK

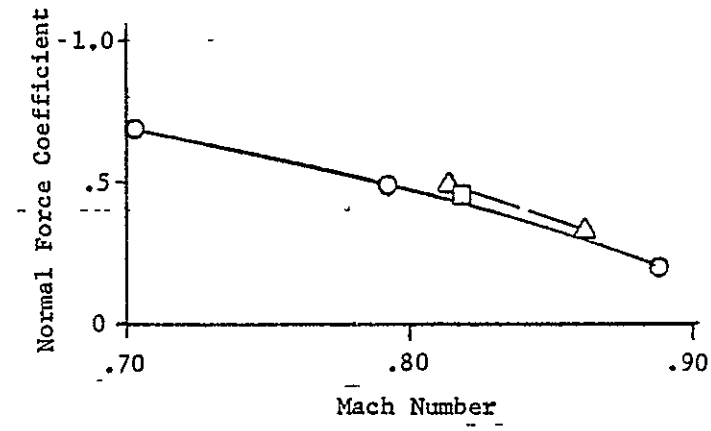

(b) NORMAL FORCE COEFFICIENT

Figure 6. ANGLE OF ATTACK AND NORMAL FORCE COEFFICIENT FOR BUFFET ONSET

result is likely due to the fact that less horizontal tail deflection is required to produce the maneuvers and the loss in lift due to tail deflection is then smaller at the lower altitudes.

SECTION 6

STOCHASTIC ANALYSIS TECHNIQUES

The analysis techniques used in this study are compatible with American National Standard (ANS S2.10-1971) recommended methods for analysis and presentation of shock and vibration data. A quick-look examination was performed on each time-history measurement to determine the data classification, degree of stationarity, record length, and recoverability.

Measurements

Data reduction was performed on the following data:

1. Shear, bending moment, and torsion at four wing stations (12 measurements).
2. Two wing-tip accelerometers (vertical).
3. Two C.G. vertical and one C.G. lateral accelerometers.
4. Pilot seat vertical and lateral accelerometers.

The analysis performed on these items consisted of PSD (including an average rms value), cross-PSD, and Probability Density and was distributed as follows:

PSD (all items)	779 plots
Cross-PSD (AW001 and AW002)	7 photographs
Probability Density	126 photographs

In addition to the plots and photographs, a digital magnetic tape recording was made of spectral coefficients of all PSD's

and Cross-PSD's. The magnetic tape format (shown in Figure 7) for a single PSD consists of two adjacent records; the first record for identification and the second for raw data.

Special-Purpose Processing

A block diagram of the special purpose stochastic equipment is shown in Figure 8. The FM signal is discriminated to recover the analog signal. Band-pass filters at 3 Hz and 100 Hz (48 dB per octave) were used to reject unwanted frequencies and to minimize aliasing effects on the sampled data. The data is calibrated at this point and converted to non-dimensional quantities. The T/D 100 Analyzer was used to compute the PSD's, Cross-PSD's, and Probability Densities. The stochastic algorithms utilized by the T/D 100 to perform these functions are discussed below.

After each PSD or Cross-PSD was plotted, the spectral coefficients were punched, in ASCII format, on perforated paper tape. This paper tape was then fed into an SEL-810A mini-computer for transcription to magnetic tape. This was done to increase storage density, for ease of handling, and for speed of subsequent playback.

Auto-Spectral Density (PSD)

The T/D 100 computes the PSD coefficients by first approximating the complex Fourier transform of the input signal. The

- RECORD 1, 3, 5, , N

WORD NUMBER	FORMAT	CONTENTS
0-2	A2	KEY, AAAAAA
3-7	A1	ITEM ID
8	A1	TEST TYPE, P FOR PSD AND X FOR CROSS PSD
9-10	A1	RUN ID
11-19	A1	FRAME NUMBER AS 011225 55
20	A1	LENGTH
21-27	A1	CONSTANT AS 2 05+01
28-143	?	JUNK

- RECORD 2, 4, 6, . ,(N+1)

WORD NUMBER	FORMAT	CONTENTS
0-2	A2	KEY, BBBBBB
3-103	I6	DATA VALUE
104-143	?	JUNK

- RECORD LAST

END OF FILE (N+2)

Figure 7. STOCHASTIC DATA TAPE FORMAT

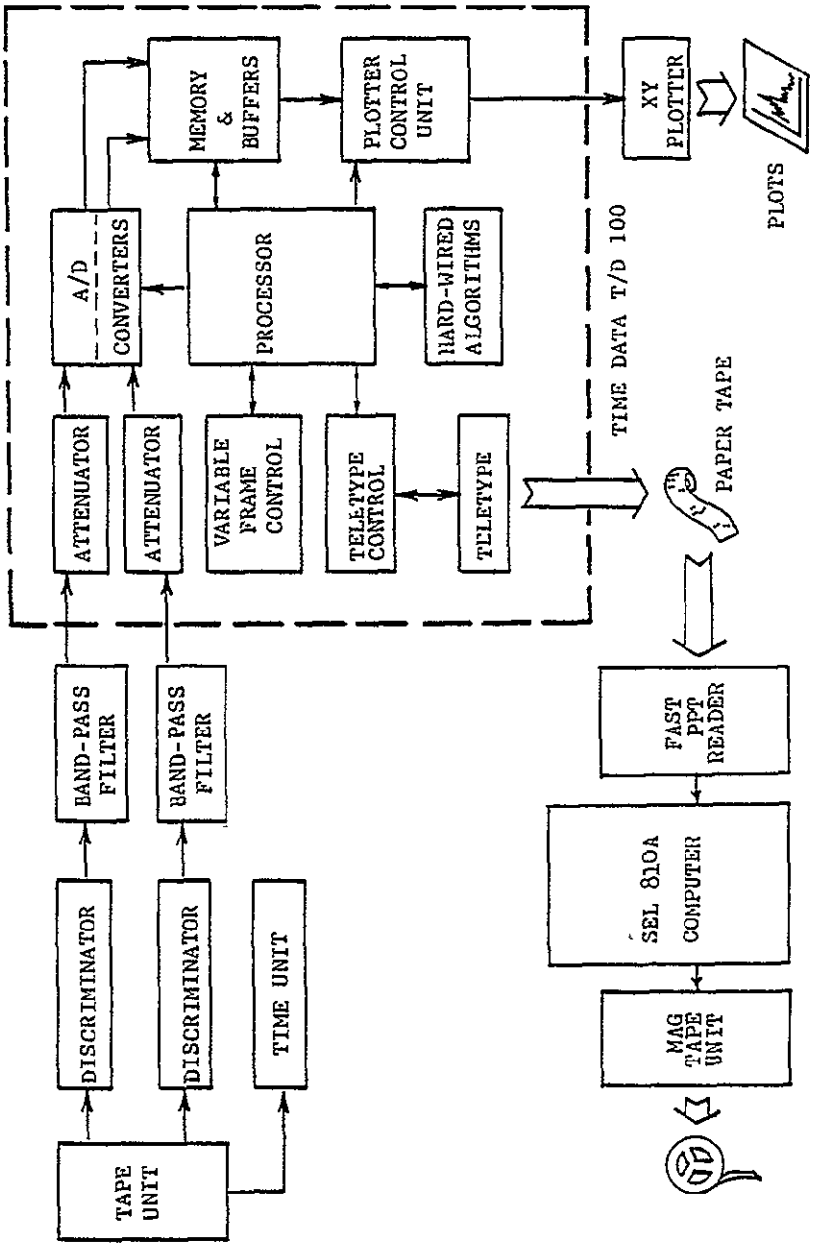

Figure 8. STOCHASTIC SPECIAL-PURPOSE EQUIPMENT

Fourier transform of the time-domain input function x(t) is given by:

$$G(jf) = \int_{-}^{+} x(t)\ (\cos\ 2\pi ft - j\ \sin\ 2\pi ft)\ dt \qquad (1)$$

where $j=\sqrt{-1}$. Since the time-domain input is sampled and quantitized in the analyzer, and only a finite number of samples are available, the finite transform is used, and, separated into its real P(f) and imaginary Q(f) components, can be written as follow follows:

$$P_T(f) = \int_{-T/2}^{T/2} x(t)\ \cos\ 2\pi ft\ \ dt \qquad (2)$$

$$Q_T(f) = \int_{-T/2}^{T/2} x(t)\ \sin\ 2\pi ft\ \ dt \qquad (3)$$

where T is the length of the input frame, which is assumed to be centered about time t=0.

Replacing the continuous input, x(t), with a set of 2N+1 discrete samples at intervals of $t_o = \frac{1}{2N}$, and replacing the sinusoidal functions by corresponding values, the continuous integrals may be expressed as the sum of products:

$$P(kf_o) = \sum_{n=-N}^{+N} x(nt_o)\ \cos\left[2\ kf_o(nt_o)\right] \qquad (4)$$

$$Q(kf_o) = -\sum_{n=-N}^{+N} x(nt_o)\ \ \sin\left[2\ kf_o(nt_o)\right] \qquad (5)$$

where k is a series of 2N integers and f_o is the base frequency which is equal to $\frac{1}{2T}$.

The PSD coefficients $\left[S(kf_o)\right]$ are then computed from (4) and (5) by the equation:

$$S(kf_o) = \left|P(kf_o)\right|^2 + \left|Q(kf_o)\right|^2 \qquad (6)$$

Cross-Spectral Density (XPSD)

The T/D 100 computes the XPSD (S_{AB}) by simultaneously computing the complex Fourier transform of channel A ($P_A + jQ_A$) and channel B ($P_B + jQ_B$) and multiplying the channel A transform by the complex conjugate of the channel B transform as follows:

$$\begin{aligned} S_{AB} &= (P_A + jQ_A)\ (P_B - jQ_B) \\ &= P_AP_B + Q_AQ_B + j\ (P_BQ_A - P_AQ_B) \end{aligned} \qquad (7)$$

The spectrum is then separated into its real ($S_{P\cdot AB}$) and imaginary ($S_{Q\cdot AB}$) components as follows:

$$\begin{aligned} S_{P\cdot AB} &= P_AP_B + Q_AQ_B \\ S_{Q\cdot AB} &= P_BQ_A + P_AQ_B \end{aligned} \qquad (8)$$

The T/D 100 then puts the real component into the channel A output buffer and the imaginary component into the channel B output buffer.

Probability Density

On the T/D 100 the Probability Density of a time-domain input is ascertained by performing an Amplitude Histogram on the input function. This algorithm counts the number of times that

each of 255 discrete amplitudes occurs at the input. Zero-amplitude occurrences appear mid-scale of the output display with negative-amplitude occurrences increasing to the left of mid-scale and positive-amplitude occurrences increasing to the right.

Average rms (Ψ_T)

The average rms of the input signal is calculated from the PSD coefficients $S(kf_o)$ by the following equation:

$$\Psi_T = \sqrt{f_o \sum_{k=0}^{2N} S(kf_o)} \tag{9}$$

where $f_o = \frac{1}{2NT}$ is the base frequency or analysis bandwidth.

SECTION 7
PRESENTATION OF DATA

During the course of the study, approximately 800 power spectral density plots were obtained. These data have two primary uses. First they permit identification of the significant modal contributions through comparison with the ground vibration test data obtained in the F-111 development program. Second they provide the data base for future assessment of prediction methods.

Natural Vibration Modes

A summary of measured natural vibration modes of the F-111A at 26 degrees leading-edge sweep is presented in Table 8. Most of the values were taken from tests previously conducted on Airplane No. 12 which is structurally the same as Airplane No. 13 (Reference 18). A few of the measurements were taken on Airplane No. 1 and were not repeated on Airplane No. 12 because the parts and associated structure had not changed (Reference 19). Data are presented for two fuel loading conditions: fuselage empty, wing empty and fuselage full, wing empty. Note that the difference in fuselage fuel load affects some of the natural frequencies.

Table 9 presents calculated values of symmetric vibration mode frequencies obtained using a math model of the aircraft structure for two gross weight conditions which represent specific loadings occuring on maneuvers investigated in this study.

TABLE 8 - MEASURED F-111A NATURAL VIBRATION MODES

Predominant Mode (Airplane No. 12 Tests)	Frequency - Hz			
	Fuse Empty, Wing Empty		Fuse. Full, Wing Empty	
	Symmetric	Antisymmetric	Symmetric	Antisymmetric
Wing First Bending	5 2	7 6	5 1	7.1
Fuselage First Vertical Bending	8 6	---	8 0	---
Fuselage First Lateral Bending	---	---	---	8.7
Wing Fore and Aft Bending	7 9	9 3	8.8	8 7
Wing Second Bending	16 9	29 2	17 8	29.0
Wing-Horizontal Tail	---	16 2, 17 5	---	17.5
First Wing Torsion	25 2	25 4	25 7	26 1
Horizontal Tail First Bending	13 6	13 3	13 8	13 1
Horizontal Tail Fore and Aft	15.2	15 3	16 3	16.2
Horizontal Tail Pitch	34 4	37 3, 31 0	30 9	29.5, 36.1
Vertical Tail Bending	---	9.9	---	9 6
Vertical Tail Torsion	---	28 0	---	11 7
Rudder Rotation	---	32 7	---	28.3
Rudder Torsion	---	45 0	---	44 8
Rotating Glove				
Leading Edge Bending	27 4			
Yaw	44.3			
Pitch	50 9			
Aft End Bending	63 8			
Spoiler Modes (From Airplane No 1 Tests)				
Spoiler No 1			46,56,62	53,60
Spoiler No 2			55,65,72	68

TABLE 9 - CALCULATED SYMMETRIC VIBRATION MODES

Mode No	Mode Description	Frequency - Hz	
		Gross Weight - Lbs	
		59,800	72,600
1	First Wing Bending	4 794	4 772
2	First Fuselage Vertical Bending	7.013	6.708
3	Horizontal Tail Bending + Sec Wing Bend + Sec Fus Bend	13 930	13 249
4	Horizontal Tail Bending + Second Wing Bending	14 828	14 723
5	Second Wing Bending	17 010	16.401
6	Third Fuselage Bending + Wing Torsion	22 853	21 618
7	First Wing Torsion	24.064	23 970
8	Horizontal Tail Second Bending	27 521	26 073
9	Third Wing Bending	30.666	30 273
10	Horizontal Tail Torsion	33 893	33 865
11	Fuselage Fourth Bending + Second Wing Torsion	37 573	36 591
12	Second Wing Torsion	39 229	37 986

These calculated mode frequencies serve the purpose of clarifying some measured responses which were not clearly identified in the ground vibration tests because of the close proximity of other modes.

Power Spectral Density Plots

All power spectral density data obtained during the Phase I investigation are presented in this Section in plotted form. Because of the large amount of data, the plots have been reduced in size from that presented in NASA CR-152109 and are assembled in a format which permits four plots per page. For ease of use the data are arranged in the following way.

Each figure number represents a data set which corresponds to a given Flight Number, Run Number and Point Number as listed in Table 7. Each data set consists of two pages of accelerometer data and one page each of the wing shear, wing bending moment and wing torsion data. The lower case letter designation for each plot corresponds to a particular item of instrumentation and is the same for all data sets. In some cases data were not obtained for a particular item of instrumentation and the corresponding plot location is so marked.

The format for each PSD plot is the same. The ordinates are normalized by the sum of the measured PSD values taken over the range from 1 to 100 Hz. The numerical value of this sum appears

as the scaling factor listed above each plot. The format for the scaling factor is:

$$SF = .XXX \pm Y\ (Z)**^2$$

where

.XXX is a decimal value.

Y is the power of 10 by which the decimal value must be multiplied.

Z is the basic unit of the scaling factor.

$**^2$ represents the fact that the units are squared.

Where appropriate, scaling factors are presented in both S.I. and U.S. Customary units.

The values plotted at frequencies of 0 and 1 Hz are used to set the scales for the automatic plotting routine and do not represent actual data. When a symbol appears on the lower bound of a plot for frequencies greater than 1 Hz, it actually represents the fact that measurement was below the dynamic threshold of the analysis equipment. Finally, although data are plotted at all frequencies from 2to 100 Hz on all the plots, the upper frequency limit of valid data varies. Table 5 should be consulted for the frequency limit appropriate for each item and flight.

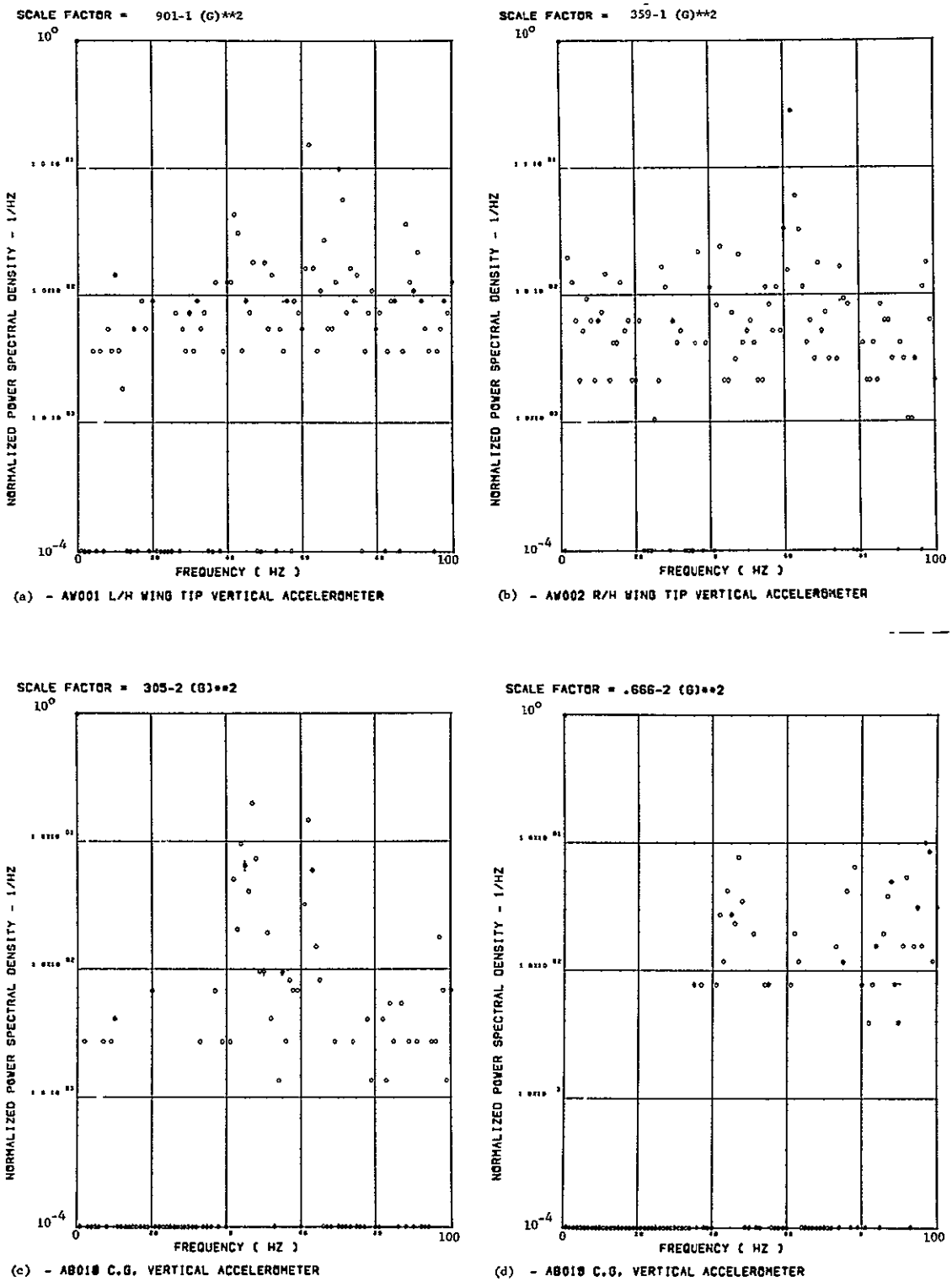

Figure 9. Power Spectra-Flight 48, Run 6, Point 1 T_1=133412.5, ΔT=1 Sec, α_{Nom}=7.4 Deg, $\Delta\alpha$=0.37 deg.

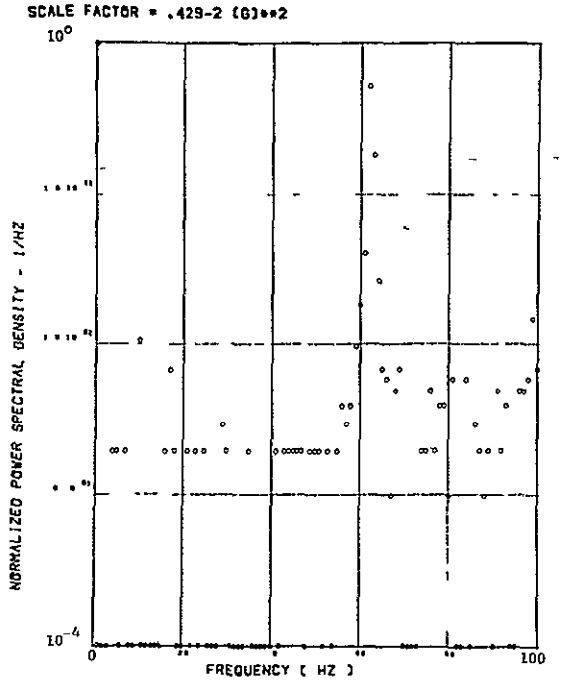

(e) - AF009 PILOT S SEAT VERTICAL ACCELEROMETER

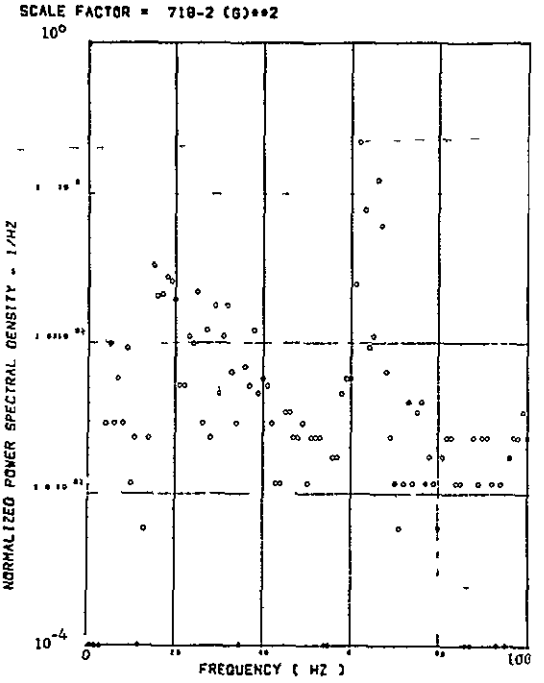

(f) - AF010 PILOT S SEAT LATERAL ACCELEROMETER

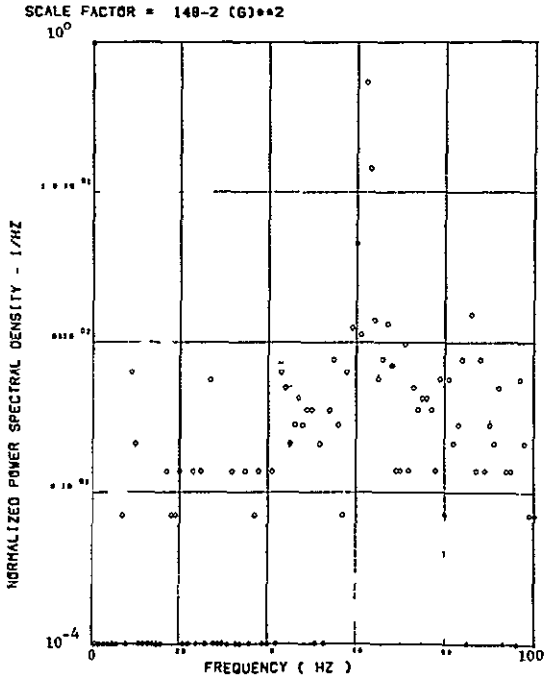

(g) - AB020 C.G. LATERAL ACCELEROMETER

Figure 9. Continued

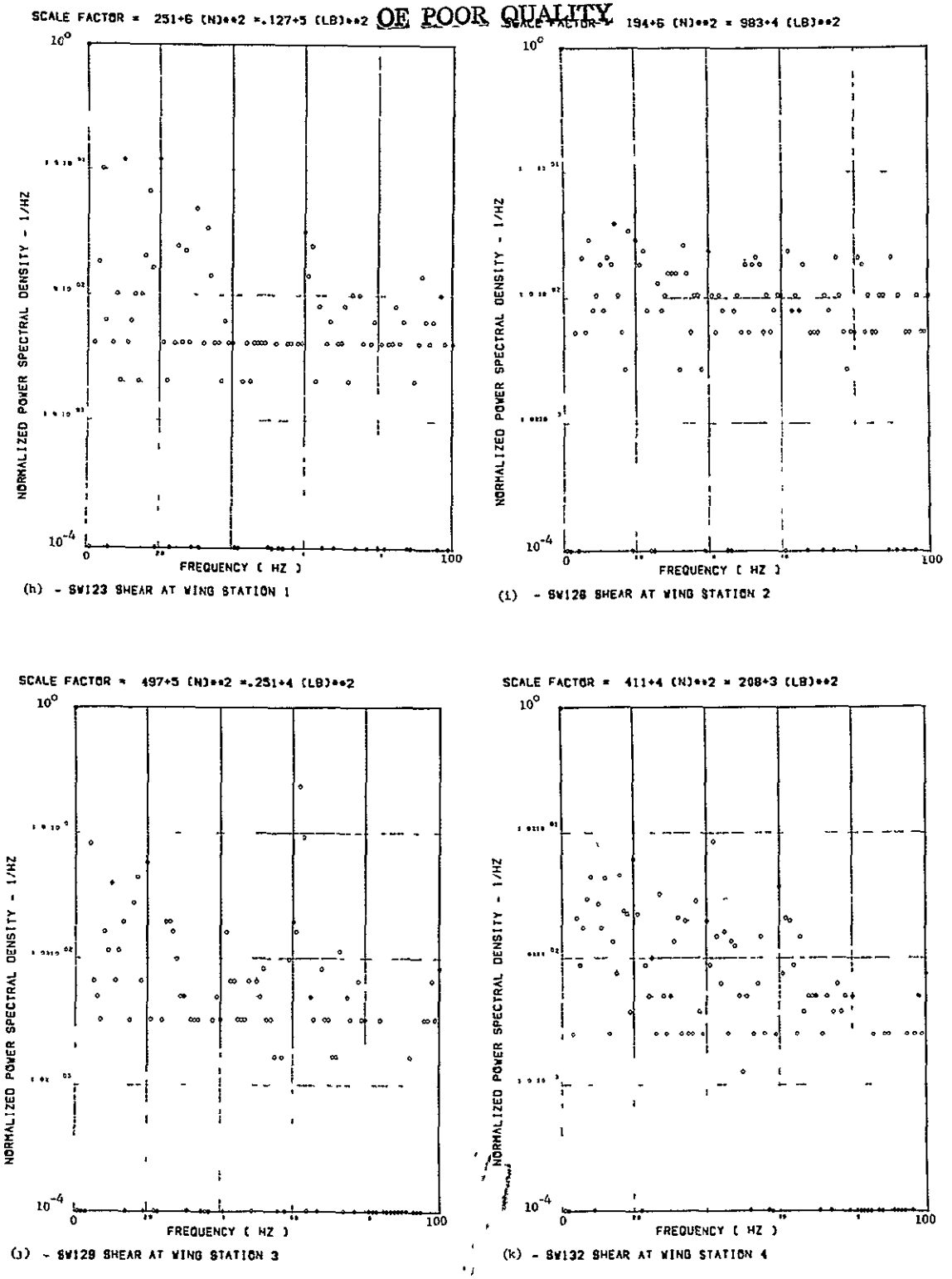

Figure 9. Continued

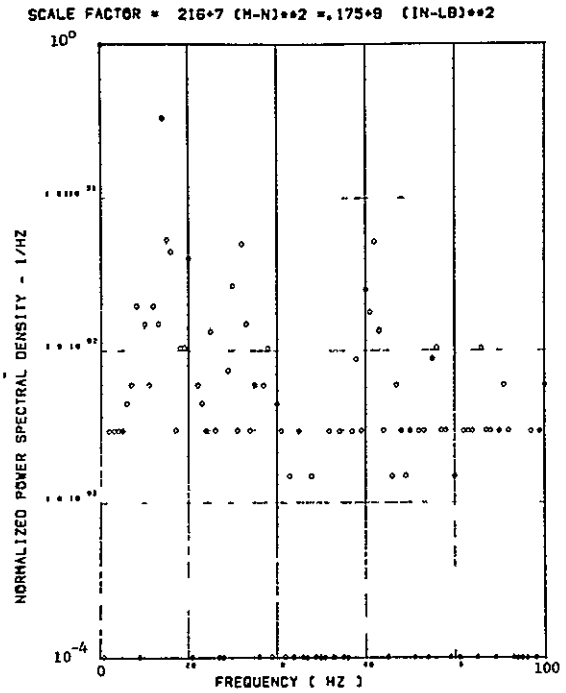

(l) - SW124 BENDING MOMENT AT WING STATION 1

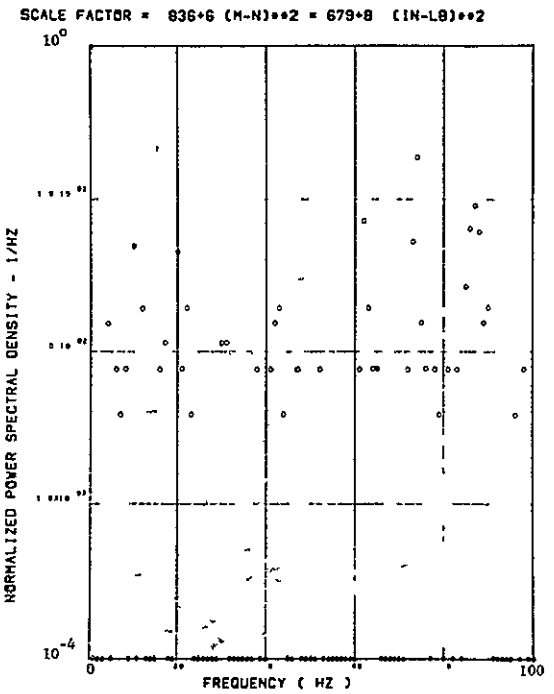

(m) - SW127 BENDING MOMENT AT WING STATION 2

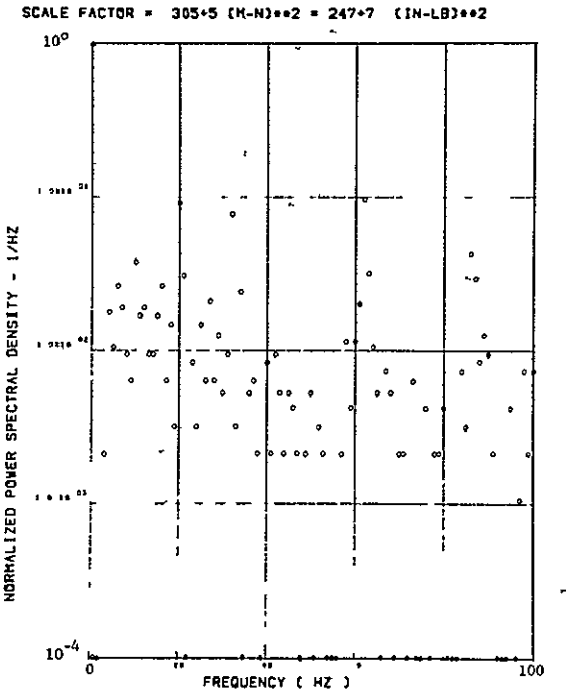

(n) - SW130 BENDING MOMENT AT WING STATION 3

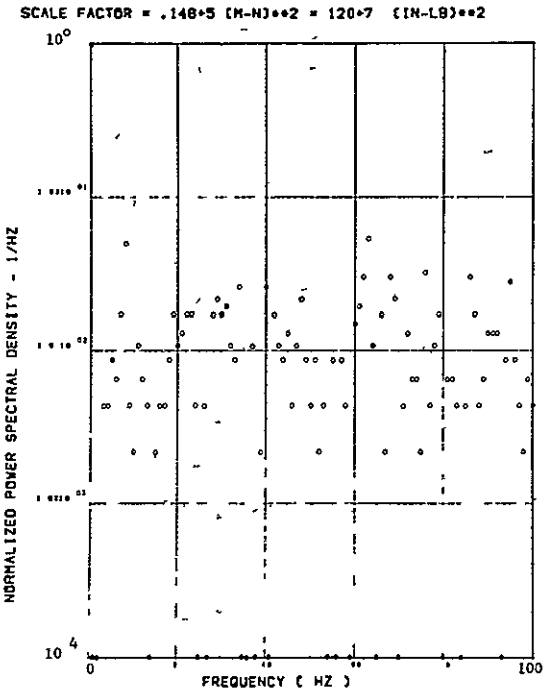

(o) - SW133 BENDING MOMENT AT WING STATION 4

Figure 9. Continued

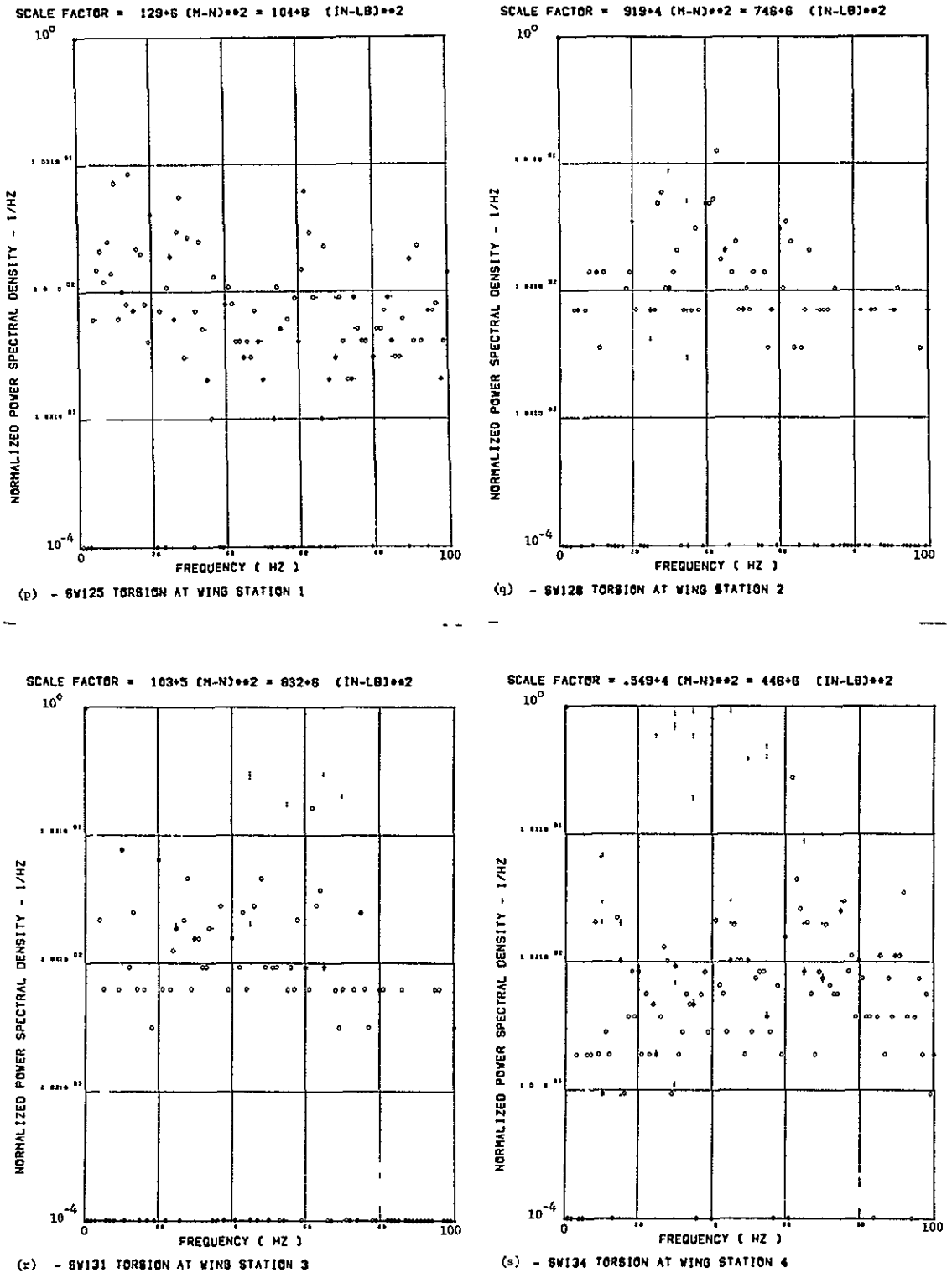

Figure 9. Concluded

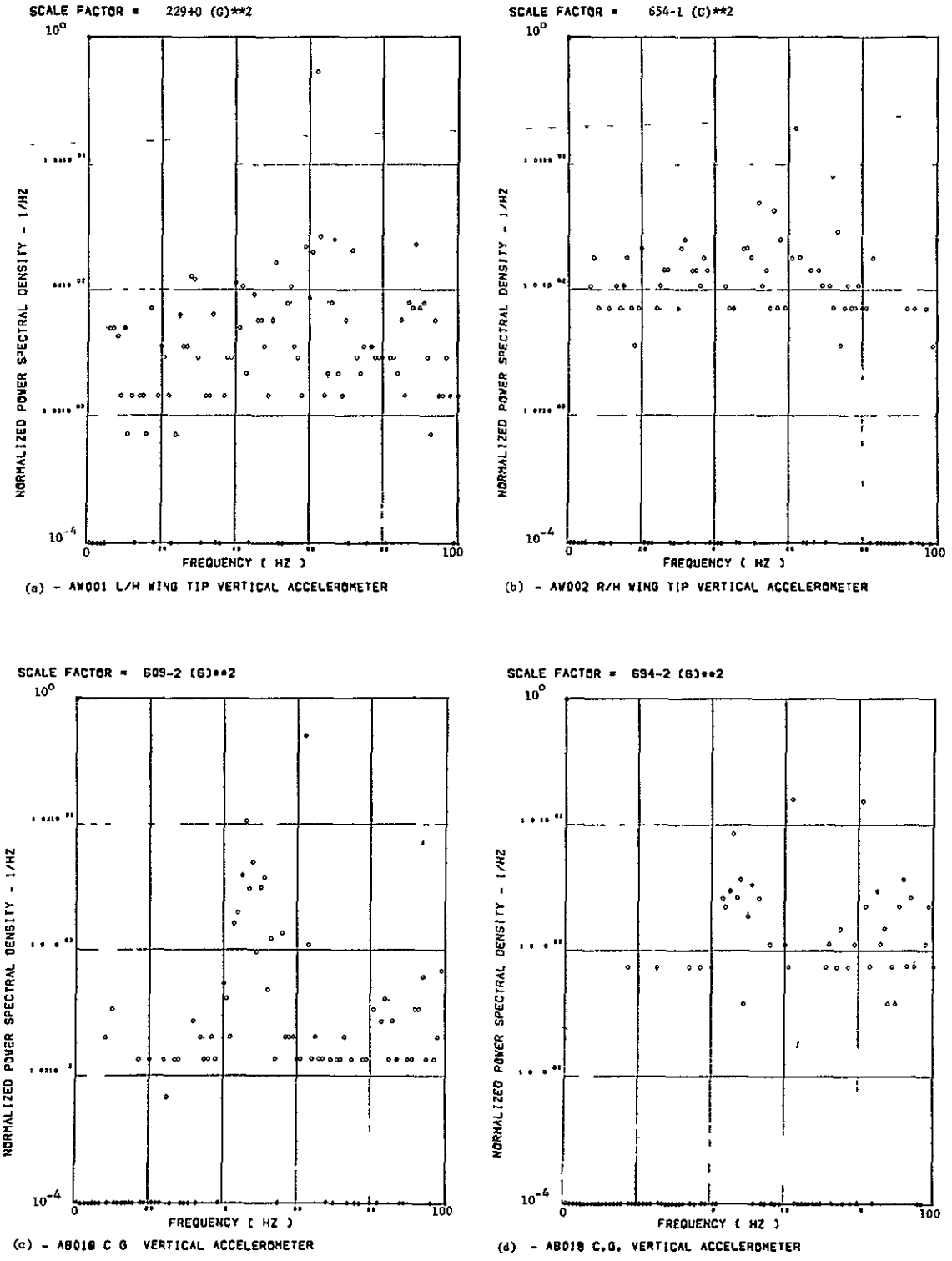

Figure 10. Power Spectra-Flight 48 Run 6, Point 2 T_1=133414.0, ΔT=1 Sec, α_{Nom}=8.1 deg, $\Delta\alpha$ = 0.58 deg.

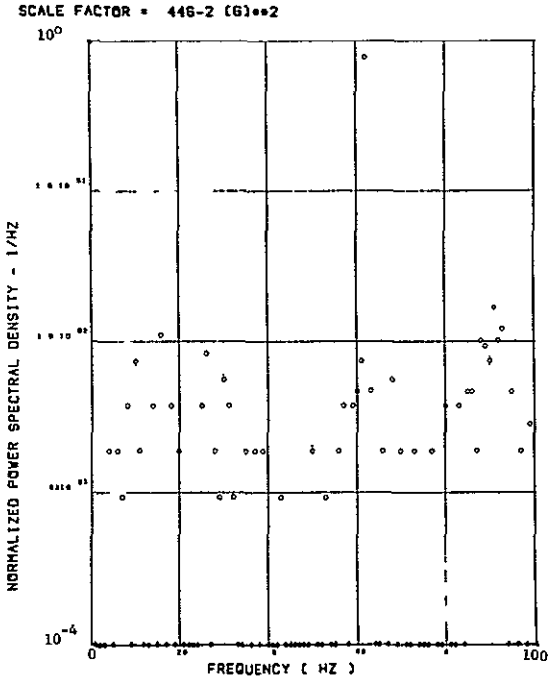

(e) - AF008 PILOT S SEAT VERTICAL ACCELEROMETER

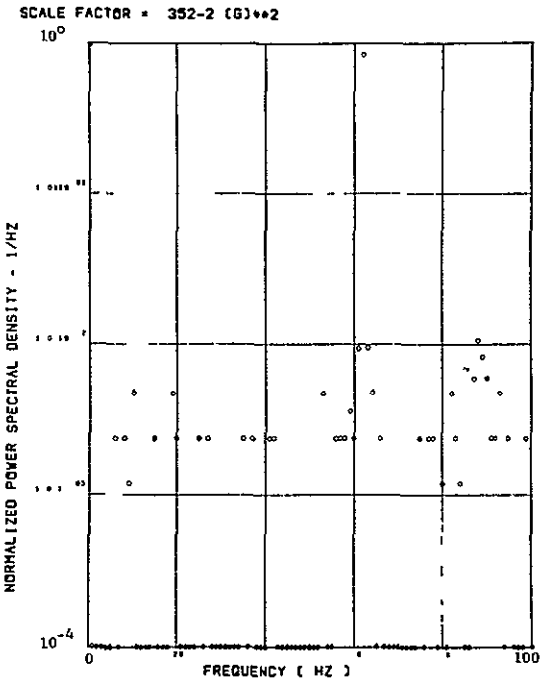

(f) - AF010 PILOT S SEAT LATERAL ACCELEROMETER

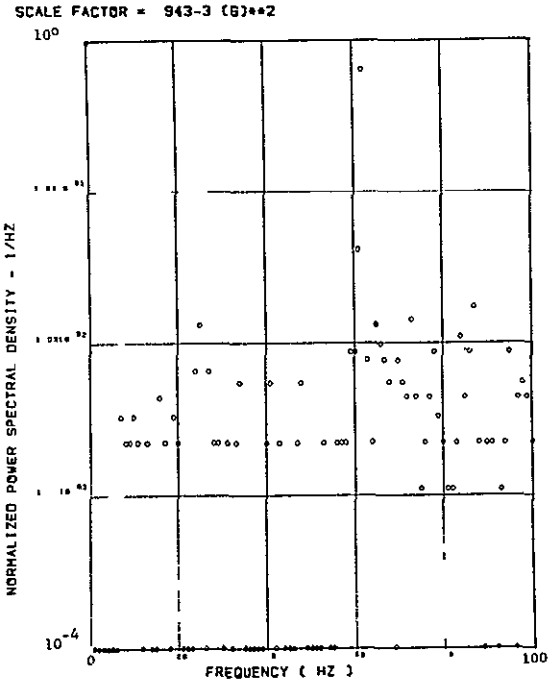

(g) - AB020 C G LATERAL ACCELEROMETER

Figure 10. Continued

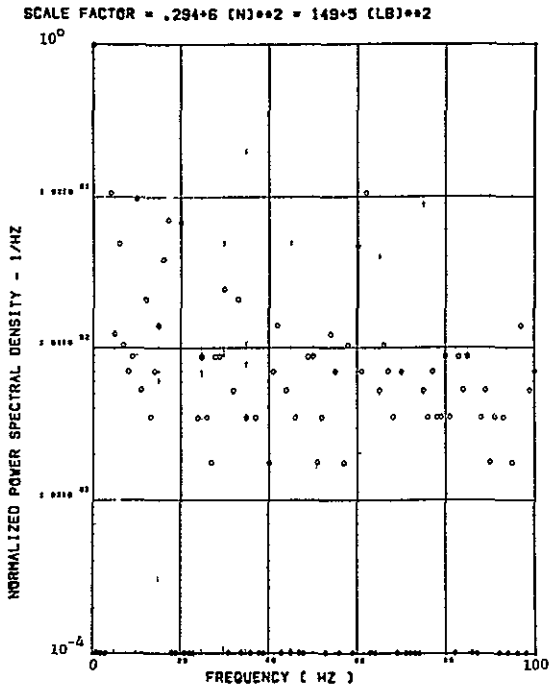

(h) - SW123 SHEAR AT WING STATION 1

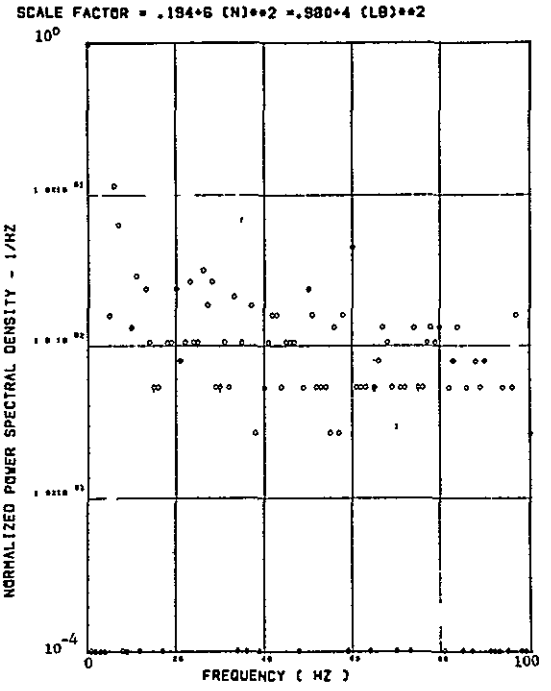

(i) - SW126 SHEAR AT WING STATION 2

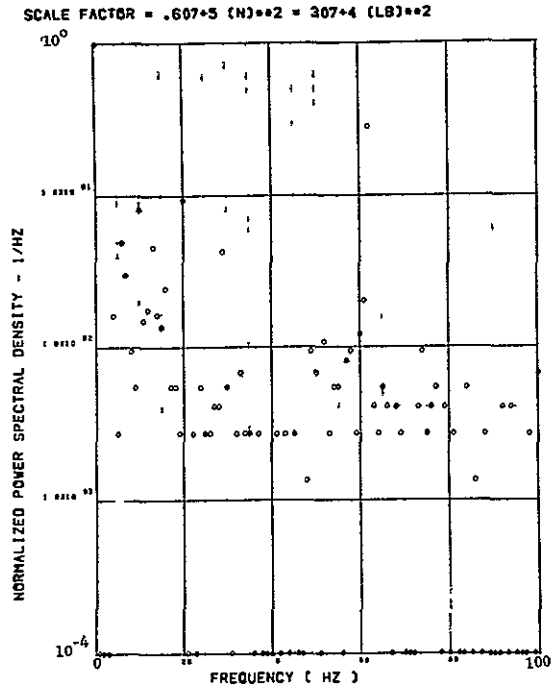

(j) - SW129 SHEAR AT WING STATION 3

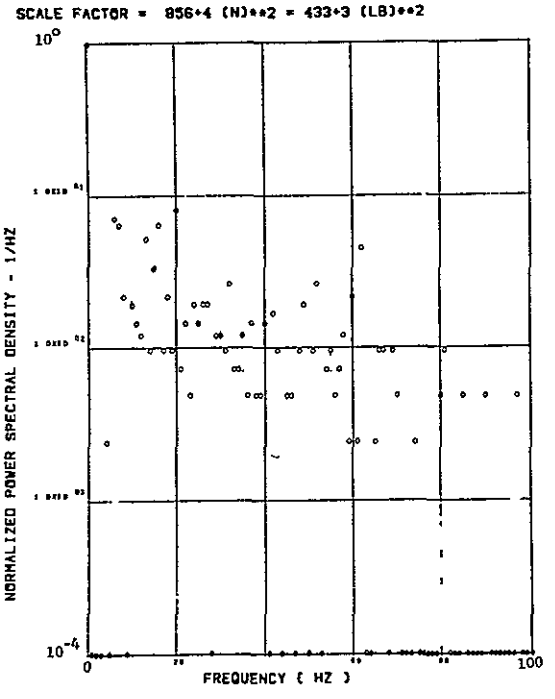

(k) - SW132 SHEAR AT WING STATION 4

Figure 10. Continued

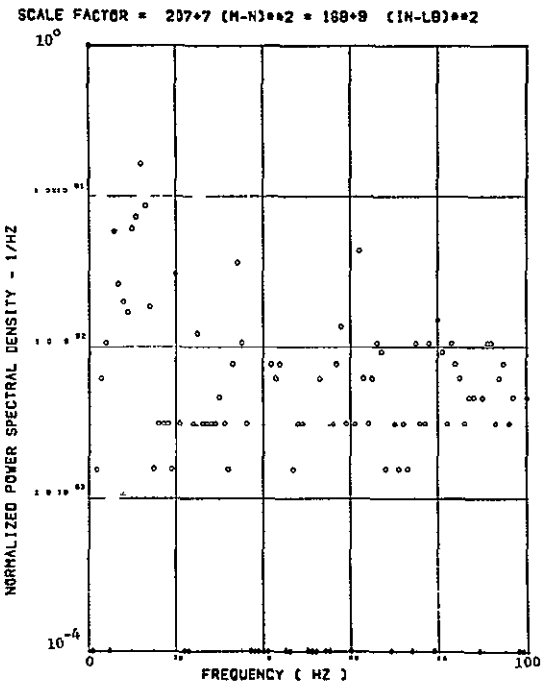

(l) - SW124 BENDING MOMENT AT WING STATION 1

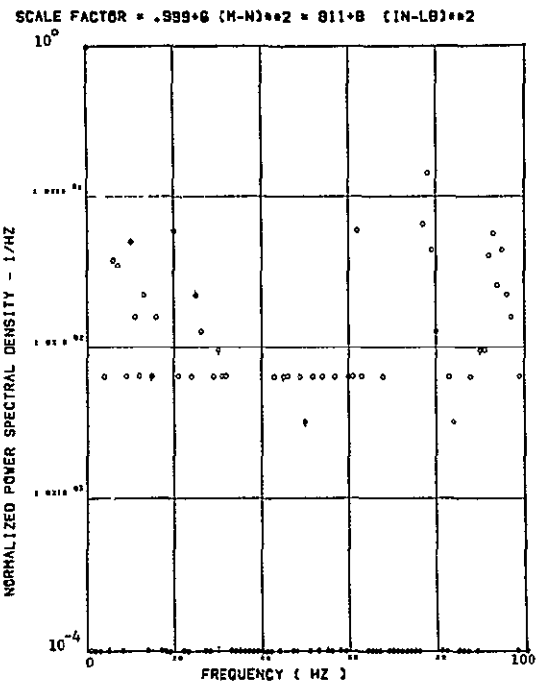

(m) - SW127 BENDING MOMENT AT WING STATION 2

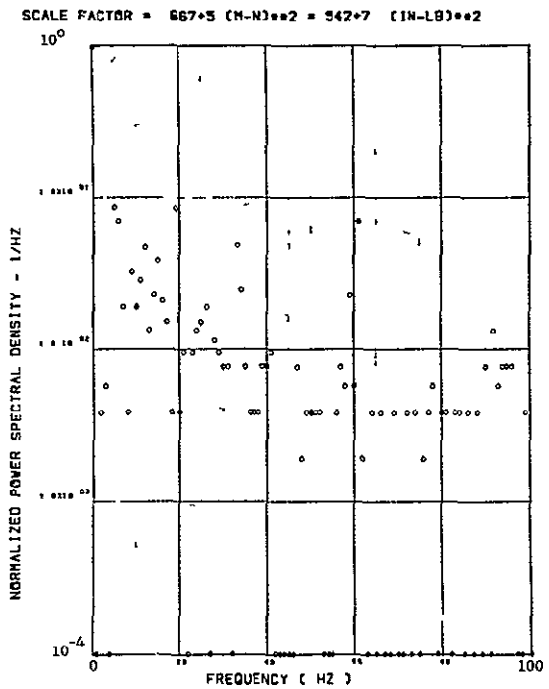

(n) - SW130 BENDING MOMENT AT WING STATION 3

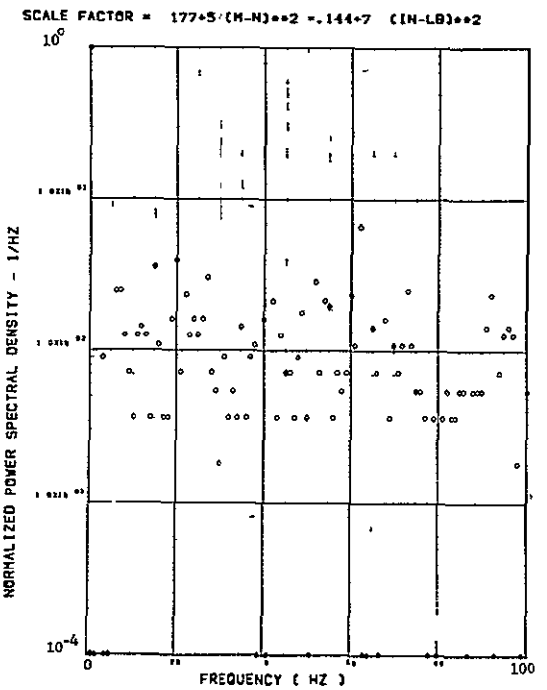

(o) - SW133 BENDING MOMENT AT WING STATION 4

Figure 10. Continued

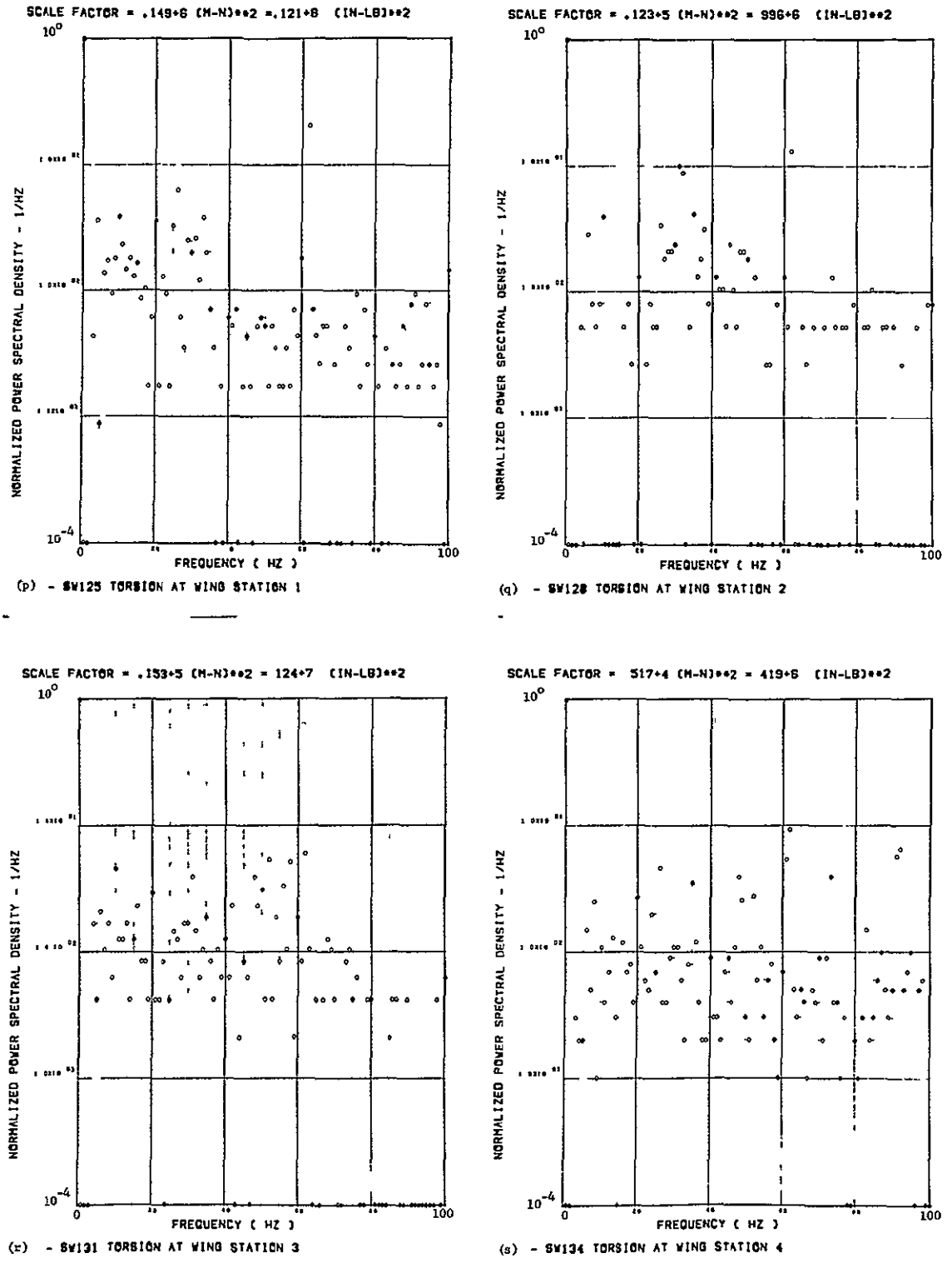

Figure 10. Concluded

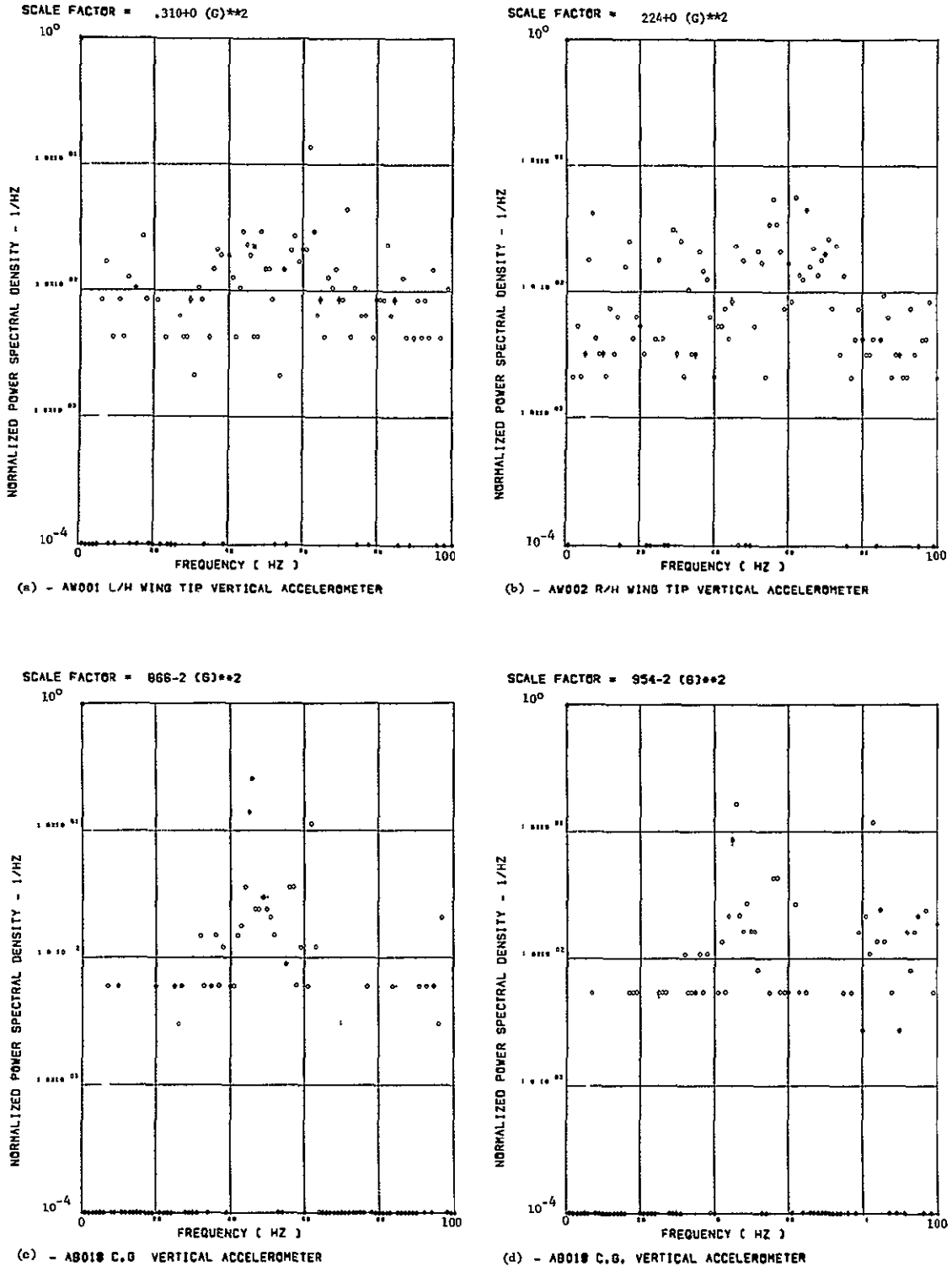

Figure 11. Power Spectra-Flight 48, Run 6, Point 3 T_1=133415.0, ΔT=1 Sec, α_{Nom}=9.1 deg, $\Delta\alpha$=0.83 deg.

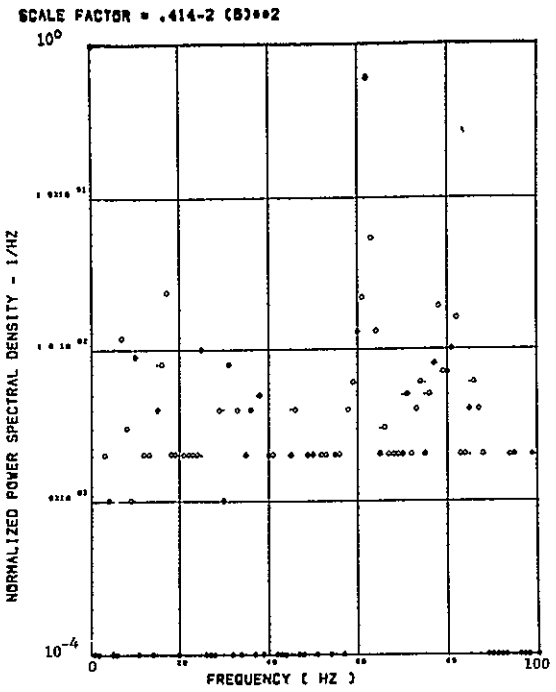

(e) - AF009 PILOT S SEAT VERTICAL ACCELEROMETER

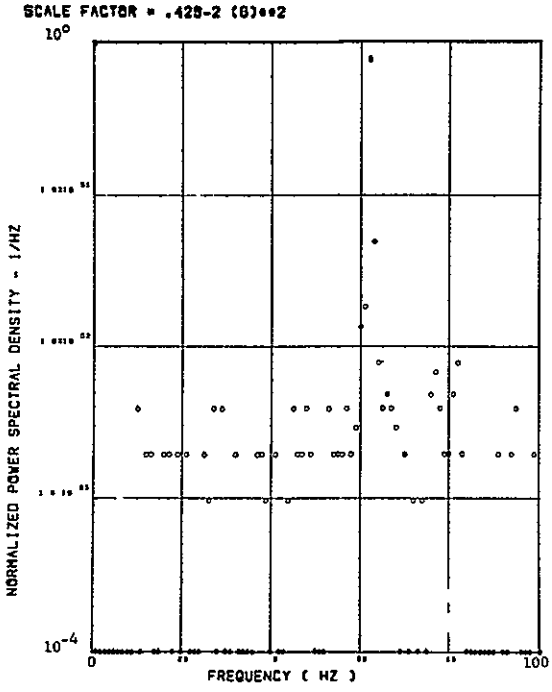

(f) - AF010 PILOT S SEAT LATERAL ACCELEROMETER

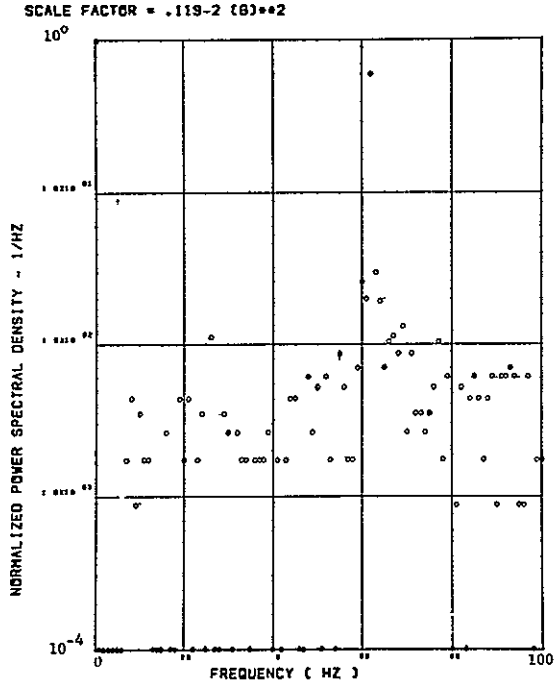

(g) - AB020 C.G. LATERAL ACCELEROMETER

Figure 11. Continued

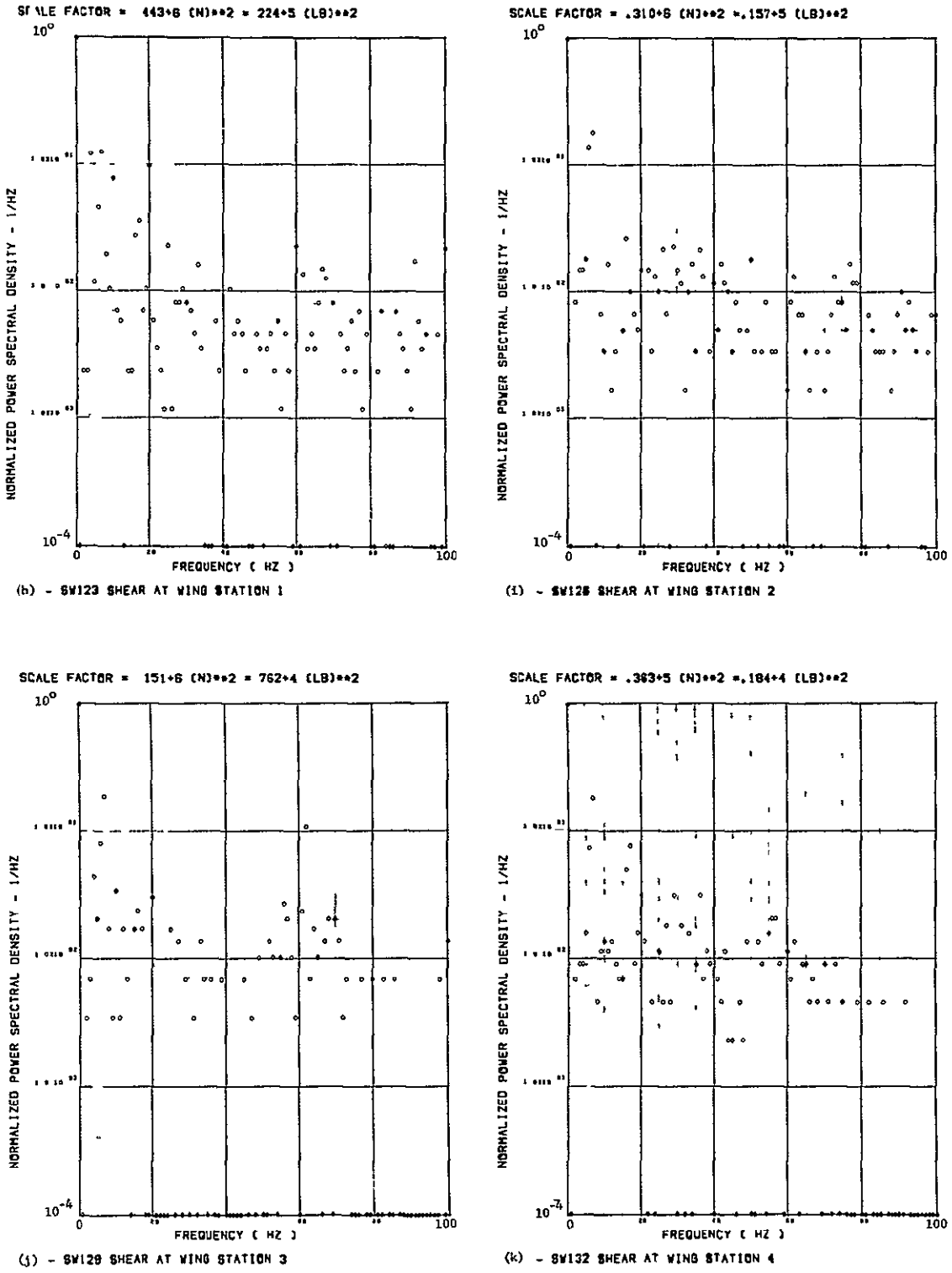

Figure 11. Continued

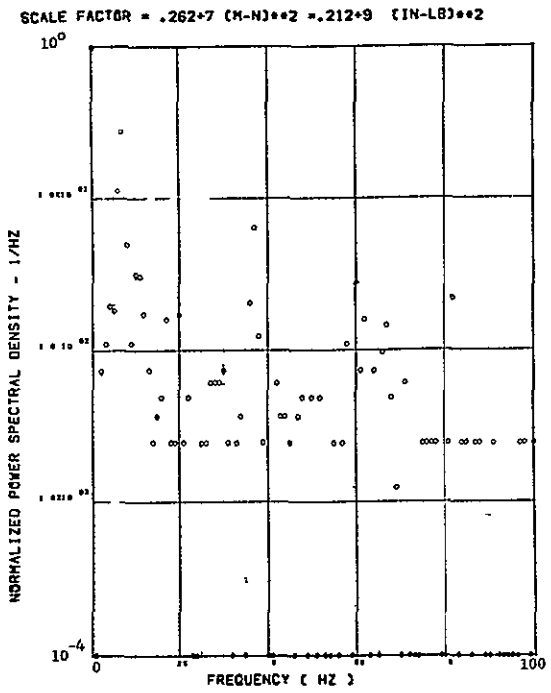

(l) - SW124 BENDING MOMENT AT WING STATION 1

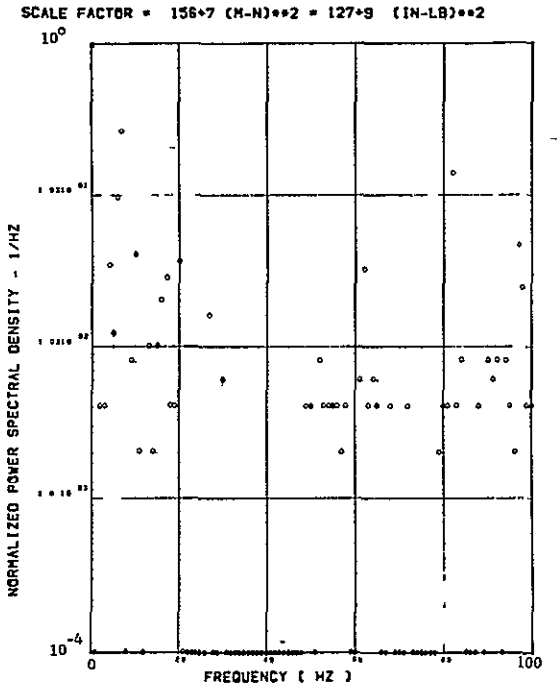

(m) - SW127 BENDING MOMENT AT WING STATION 2

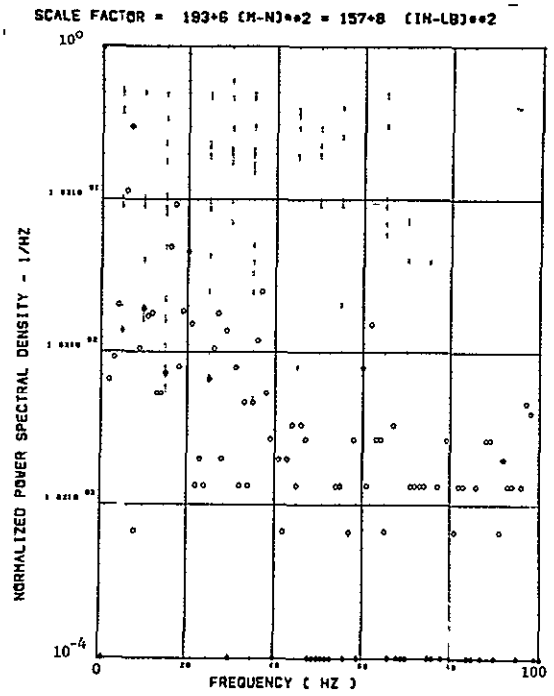

(n) - SW130 BENDING MOMENT AT WING STATION 3

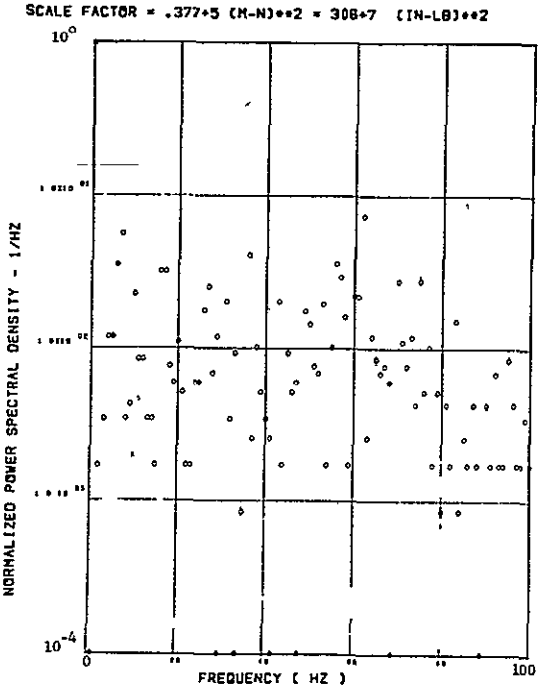

(o) - SW133 BENDING MOMENT AT WING STATION 4

Figure 11. Continued

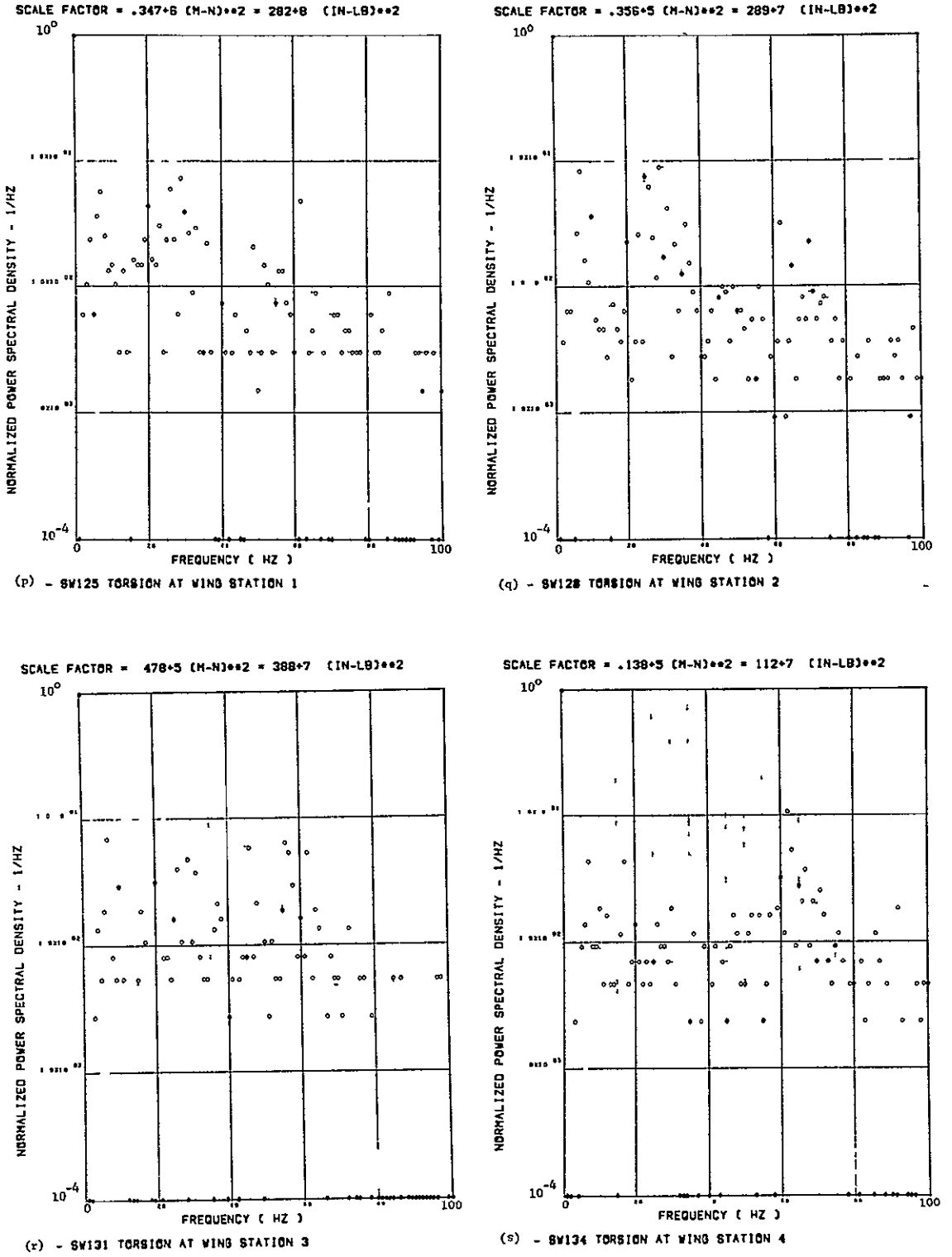

Figure 11. Concluded

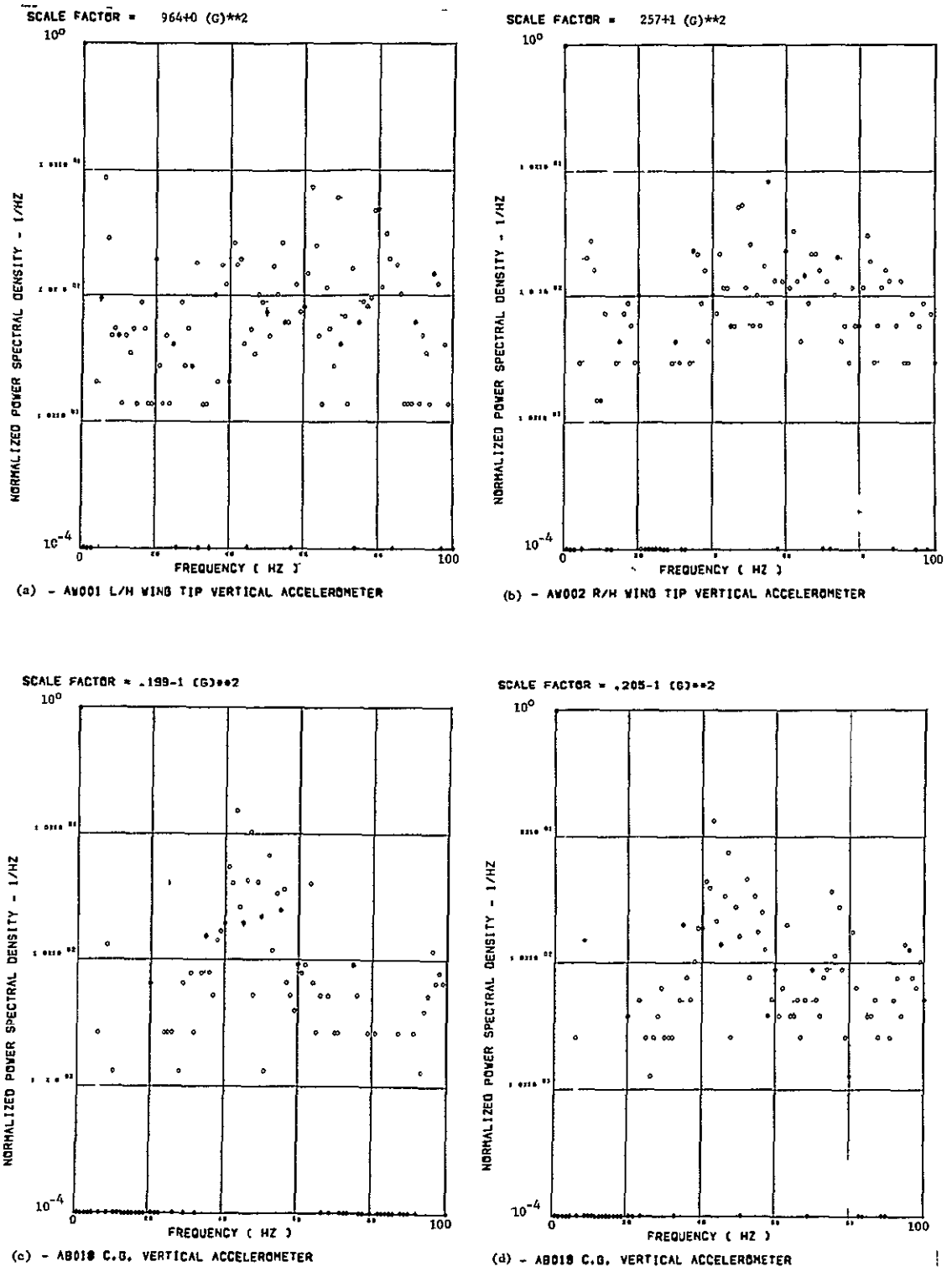

Figure 12. Power Spectra-Flight 48, Run 6, Point 4 T_1=133416.7, ΔT=1 Sec, α_{Nom}=10.2 Deg, $\Delta\alpha$=1.05 deg.

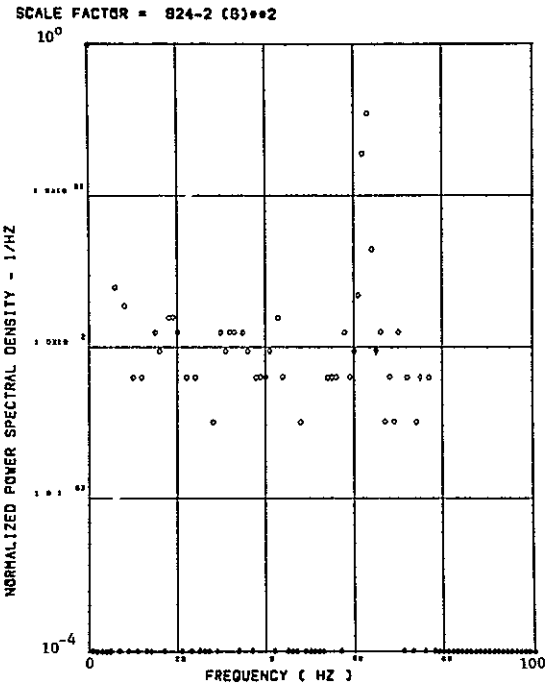

(e) - AF009 PILOT S SEAT VERTICAL ACCELEROMETER

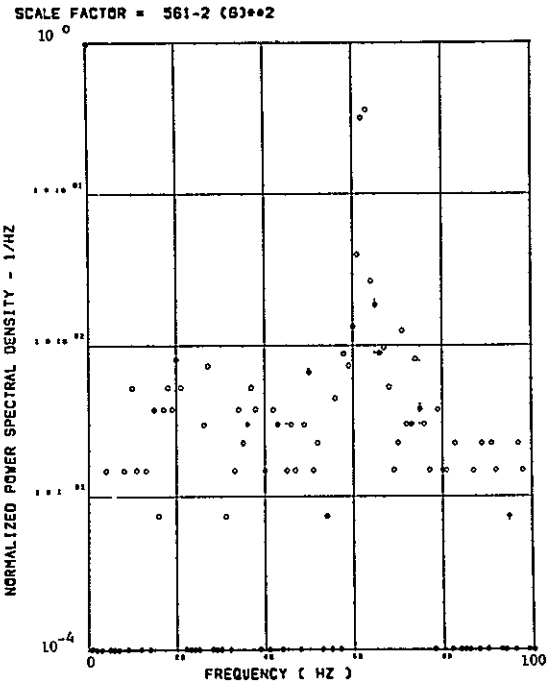

(f) - AF010 PILOT S SEAT LATERAL ACCELEROMETER

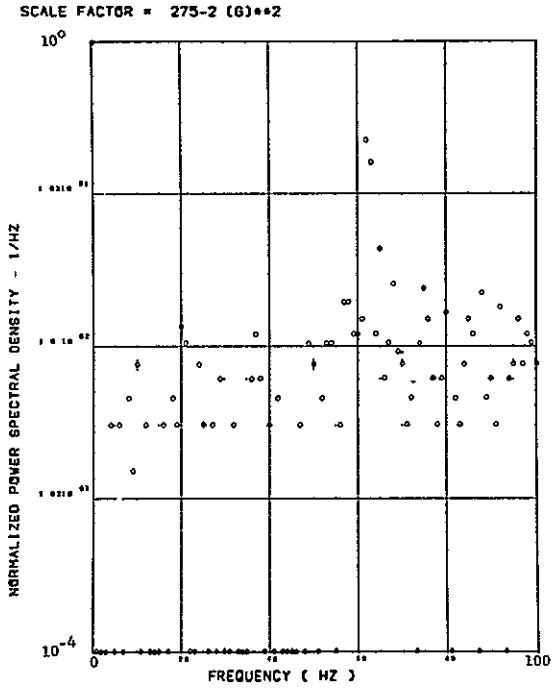

(g) - AB020 C G LATERAL ACCELEROMETER

Figure 12. Continued

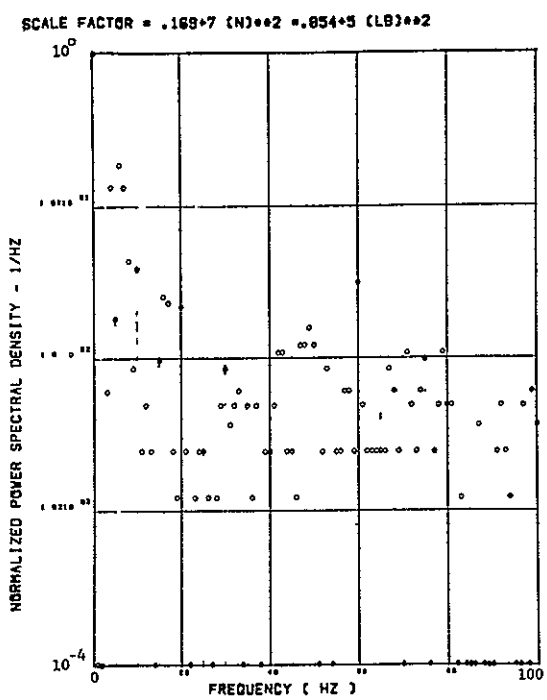

(h) - SW123 SHEAR AT WING STATION 1

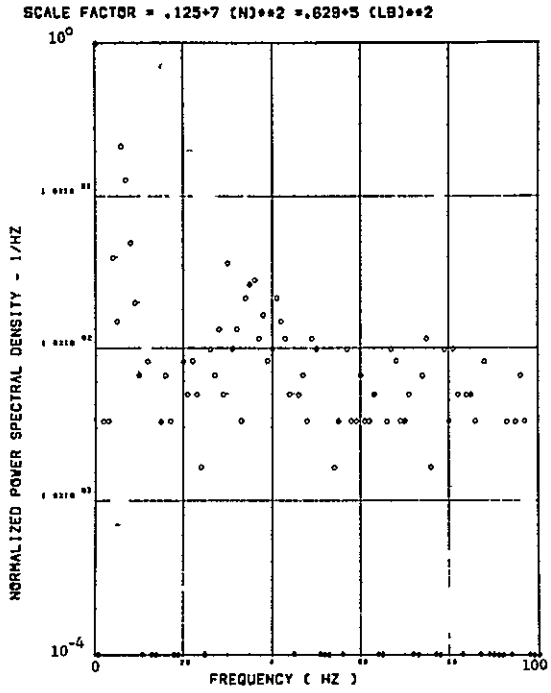

(i) - SW126 SHEAR AT WING STATION 2

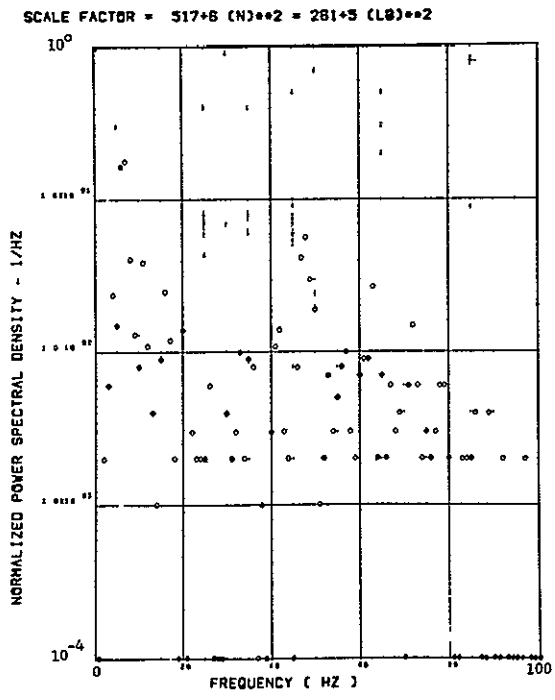

(j) - SW129 SHEAR AT WING STATION 3

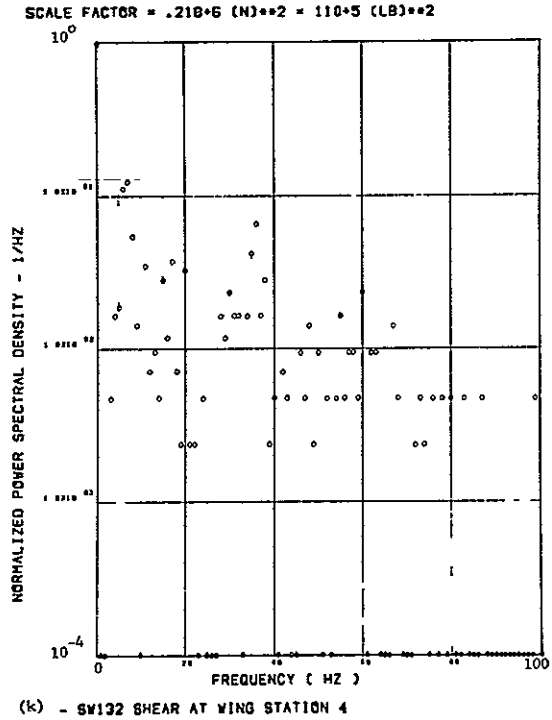

(k) - SW132 SHEAR AT WING STATION 4

Figure 12. Continued

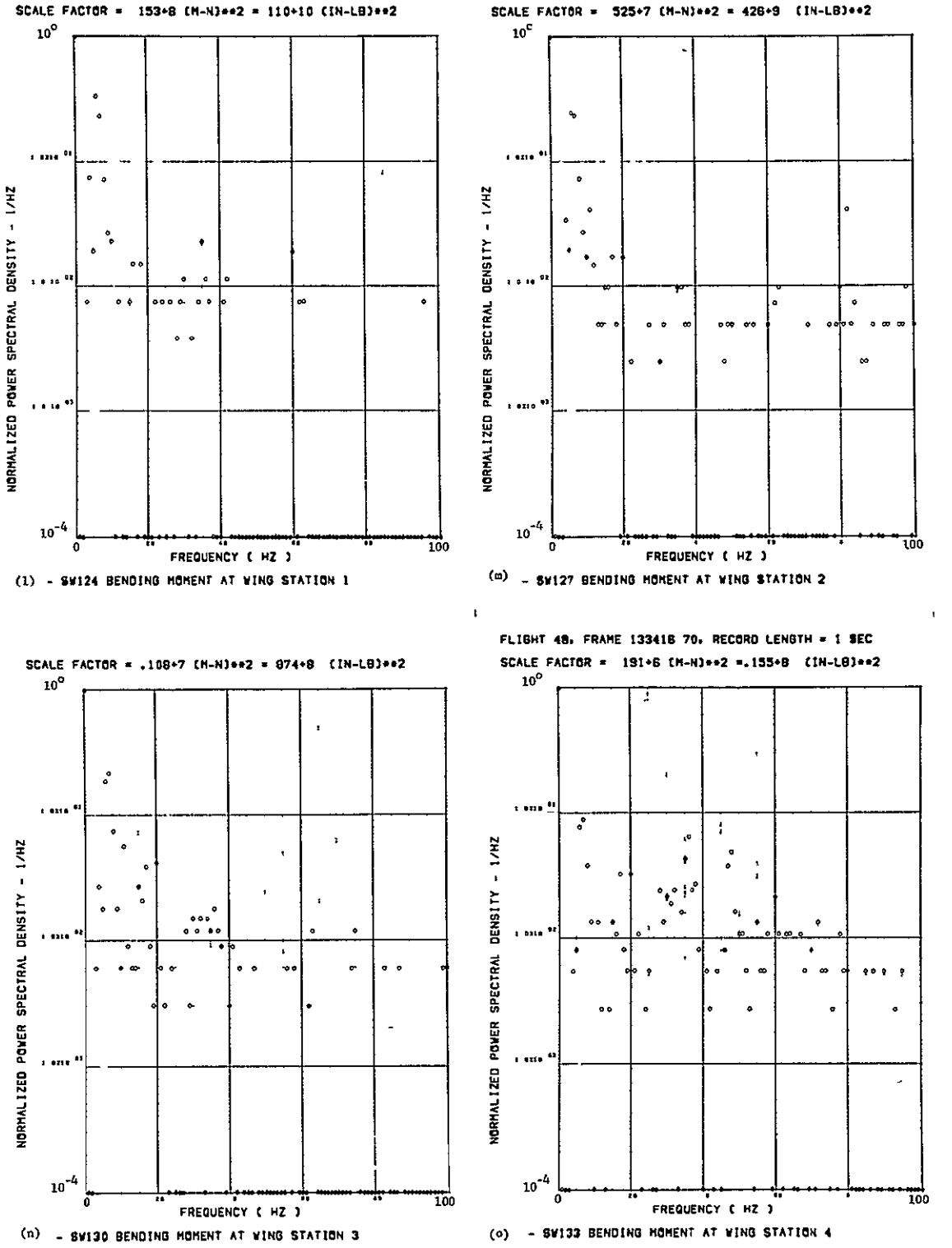

Figure 12. Continued

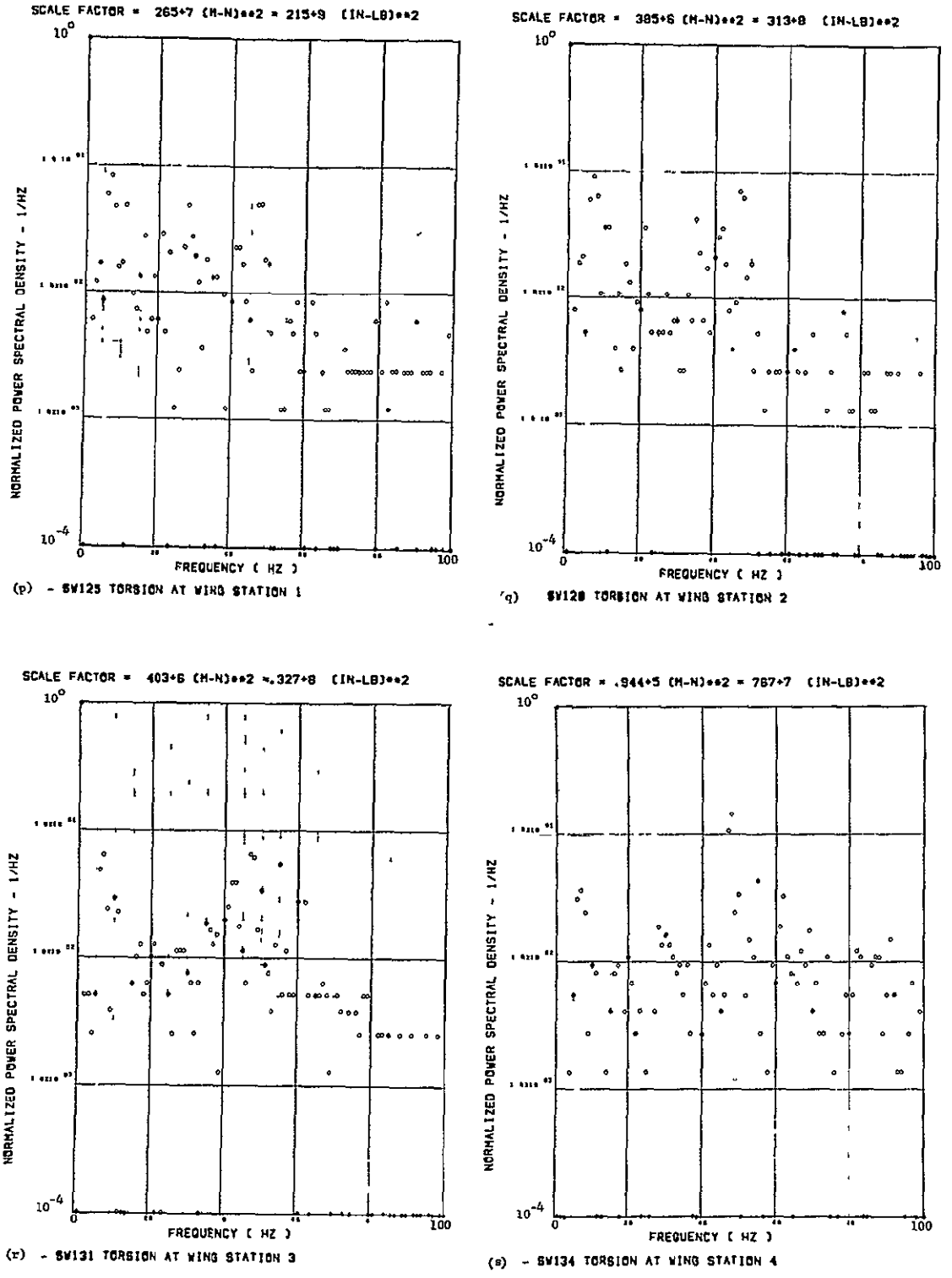

Figure 12. Concluded

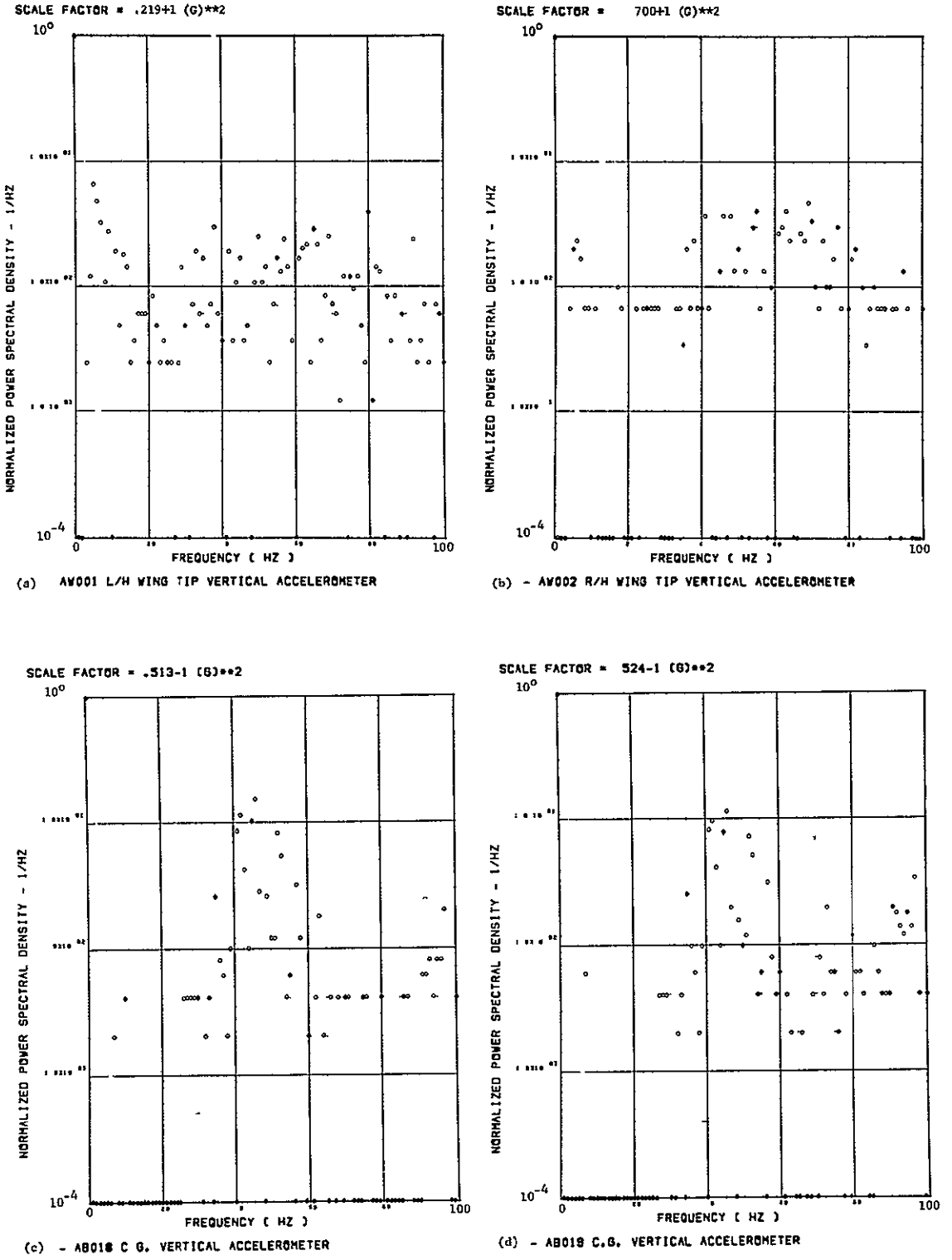

Figure 13. Power Spectra-Flight 48, Run 6, Point 5 T_1=133417.3, ΔT=1 Sec, α_{Nom}=11.1 deg, $\Delta\alpha$=1.45 deg.

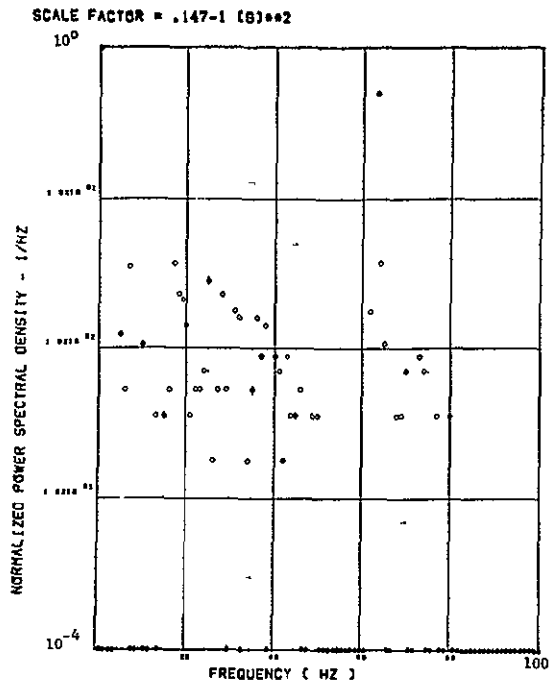

(e) - AF009 PILOT S SEAT VERTICAL ACCELEROMETER

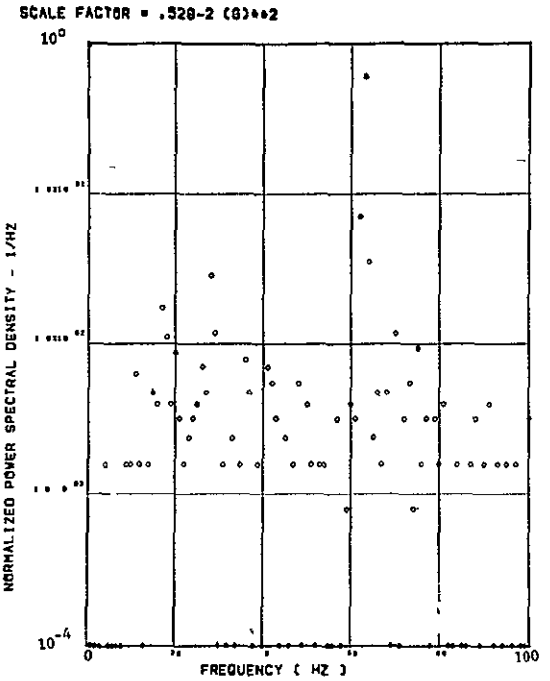

(f) - AF010 PILOT S SEAT LATERAL ACCELEROMETER

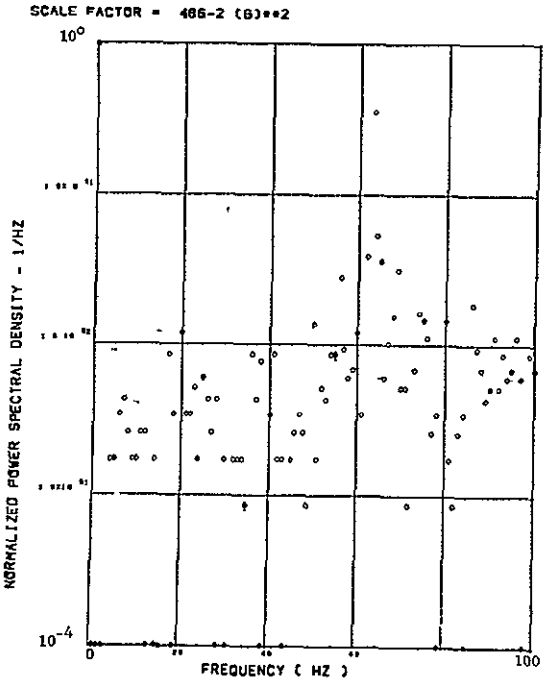

(g) - AB020 C G LATERAL ACCELEROMETER

Figure 13. Continued

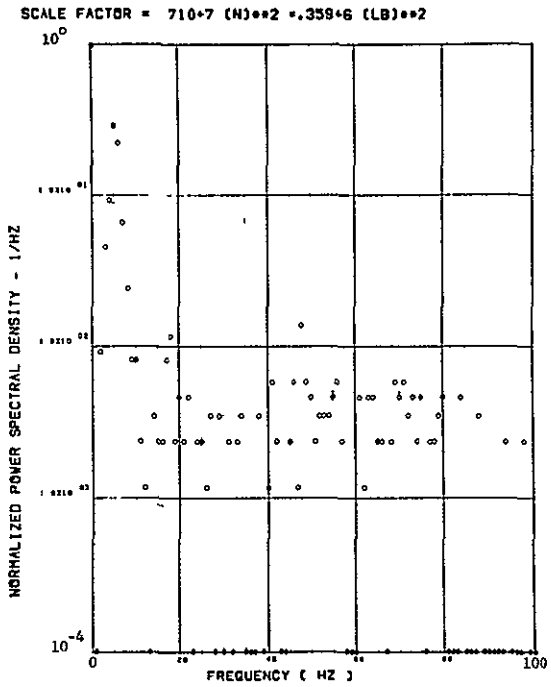

(h) - SW123 SHEAR AT WING STATION 1

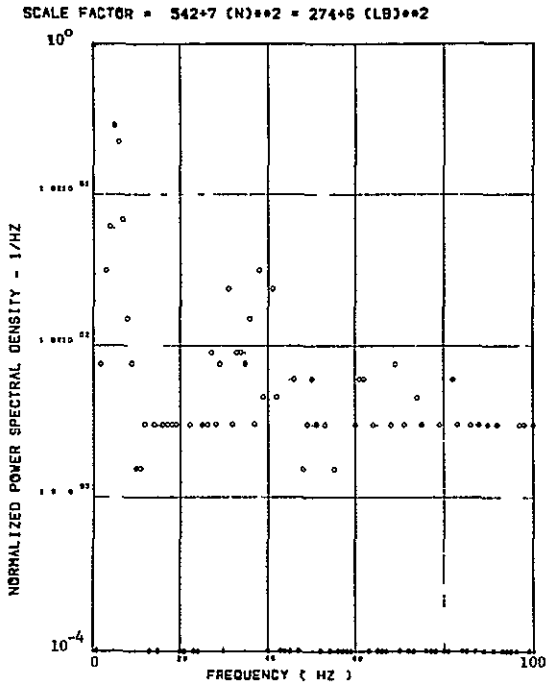

(i) - SW126 SHEAR AT WING STATION 2

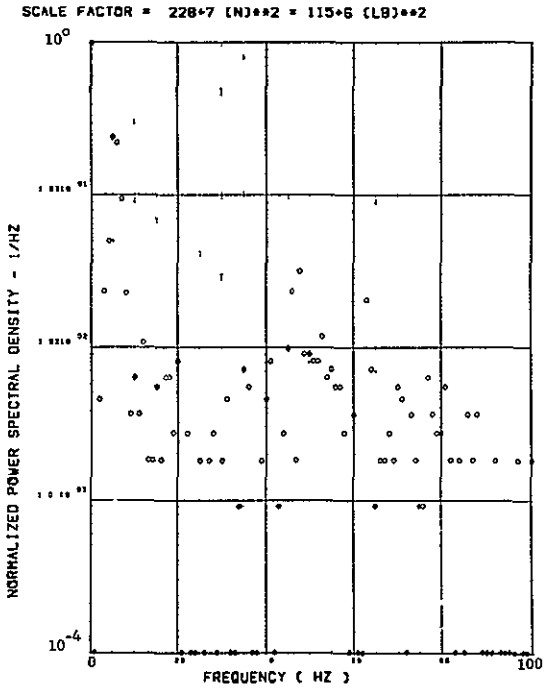

(j) - SW129 SHEAR AT WING STATION 3

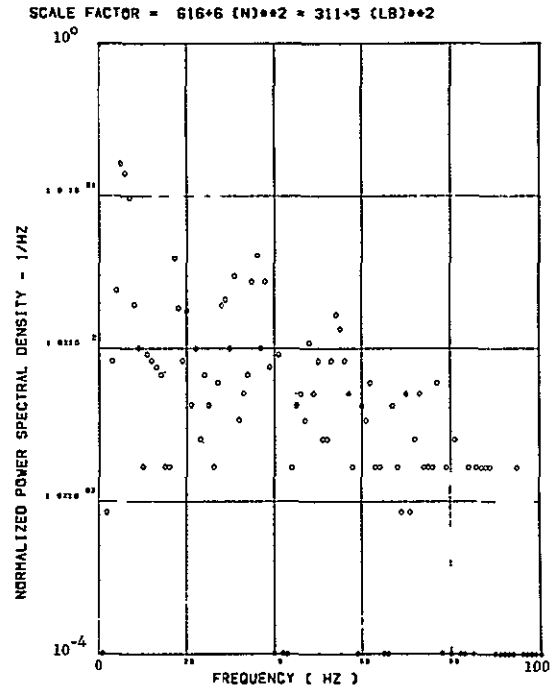

(k) - SW132 SHEAR AT WING STATION 4

Figure 13. Continued

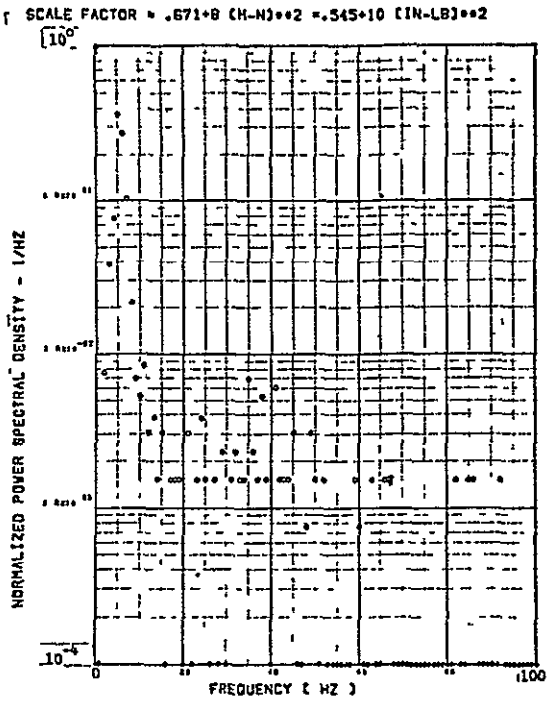

(l) - SW124 BENDING MOMENT AT WING STATION 1

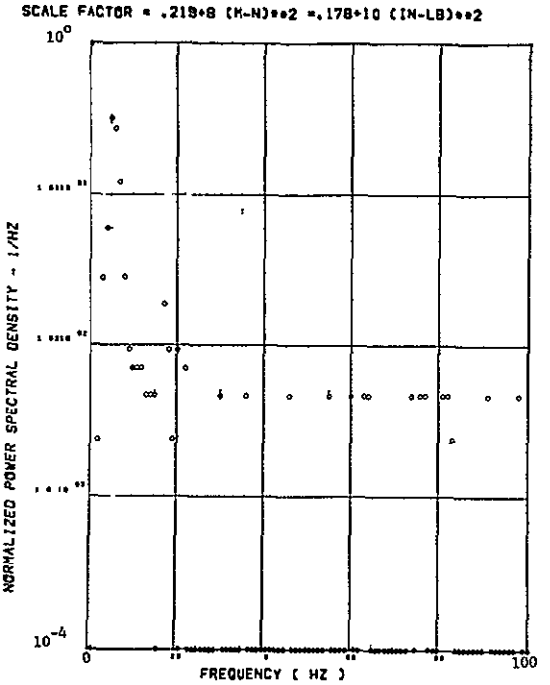

(m) - SW127 BENDING MOMENT AT WING STATION 2

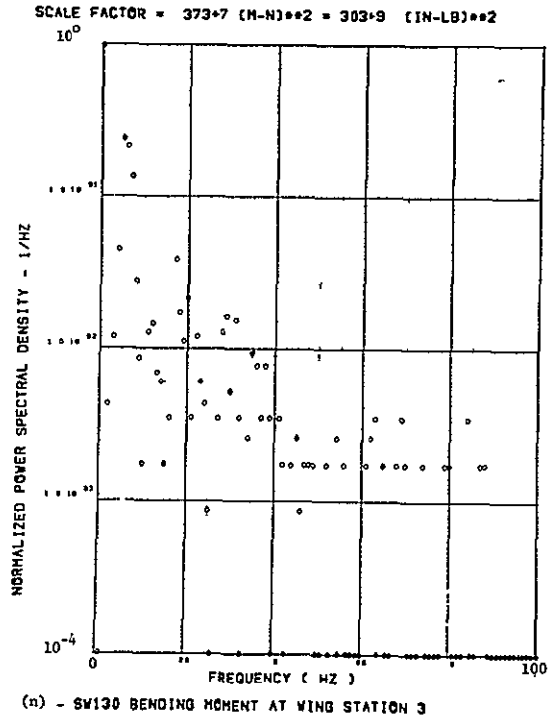

(n) - SW130 BENDING MOMENT AT WING STATION 3

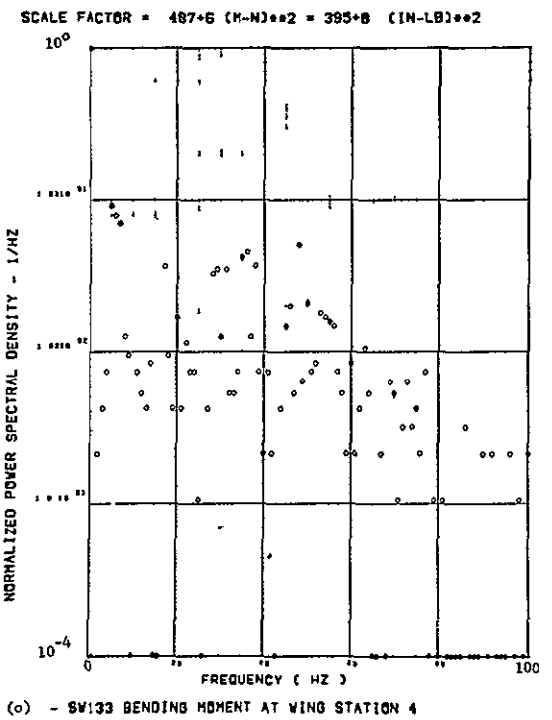

(o) - SW133 BENDING MOMENT AT WING STATION 4

Figure 13. Continued

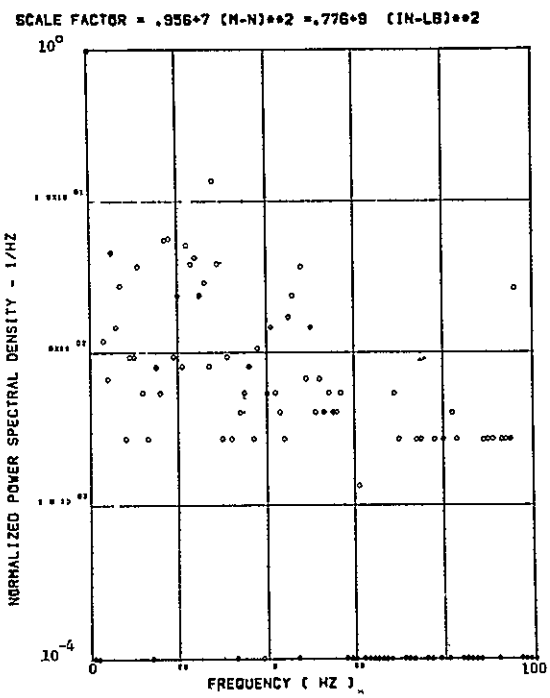

(p) - SW125 TORSION AT WING STATION 1

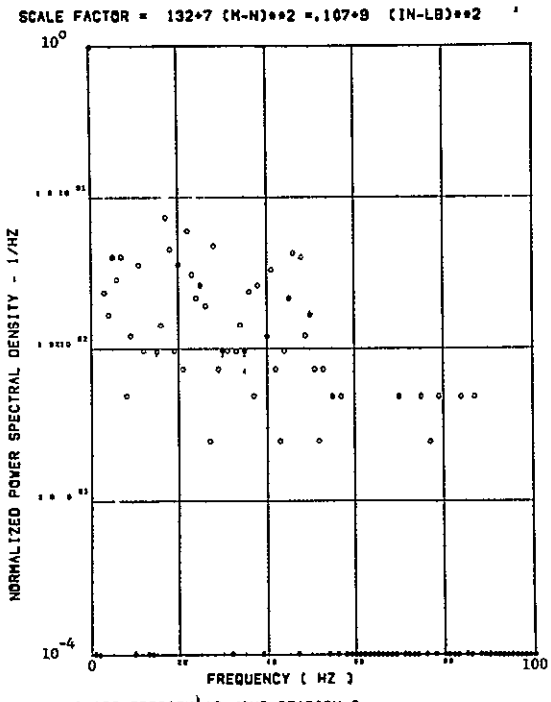

(q) - SW128 TORSION AT WING STATION 2

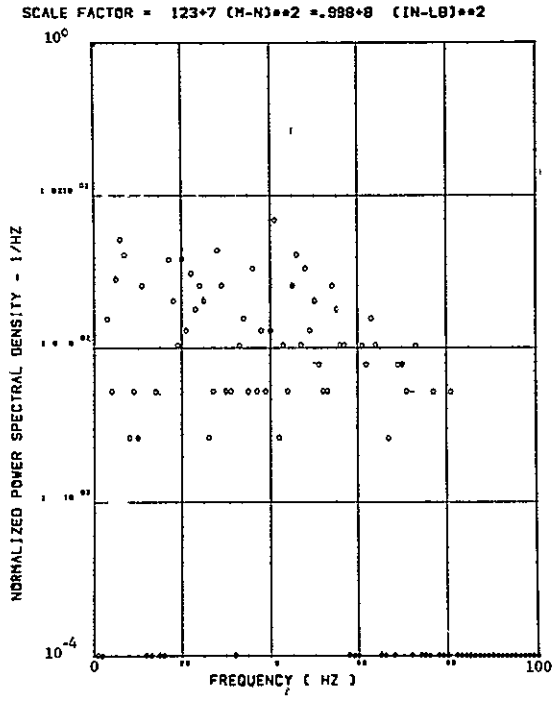

(r) - SW131 TORSION AT WING STATION 3

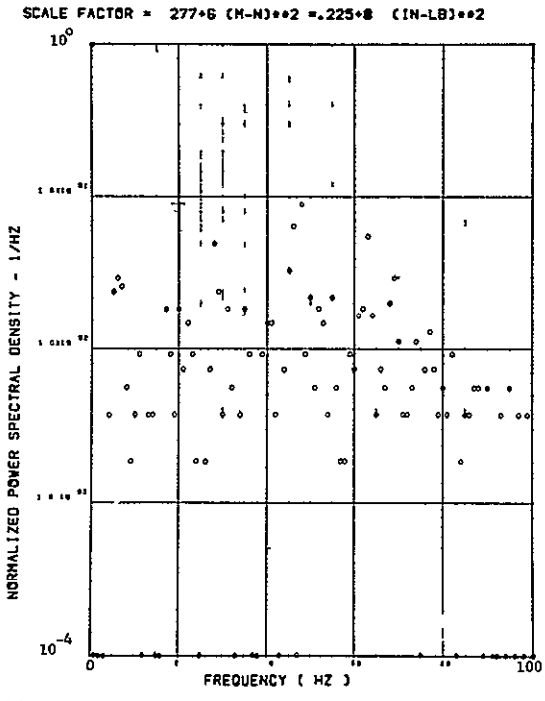

(s) - SW134 TORSION AT WING STATION 4

Figure 13. Concluded

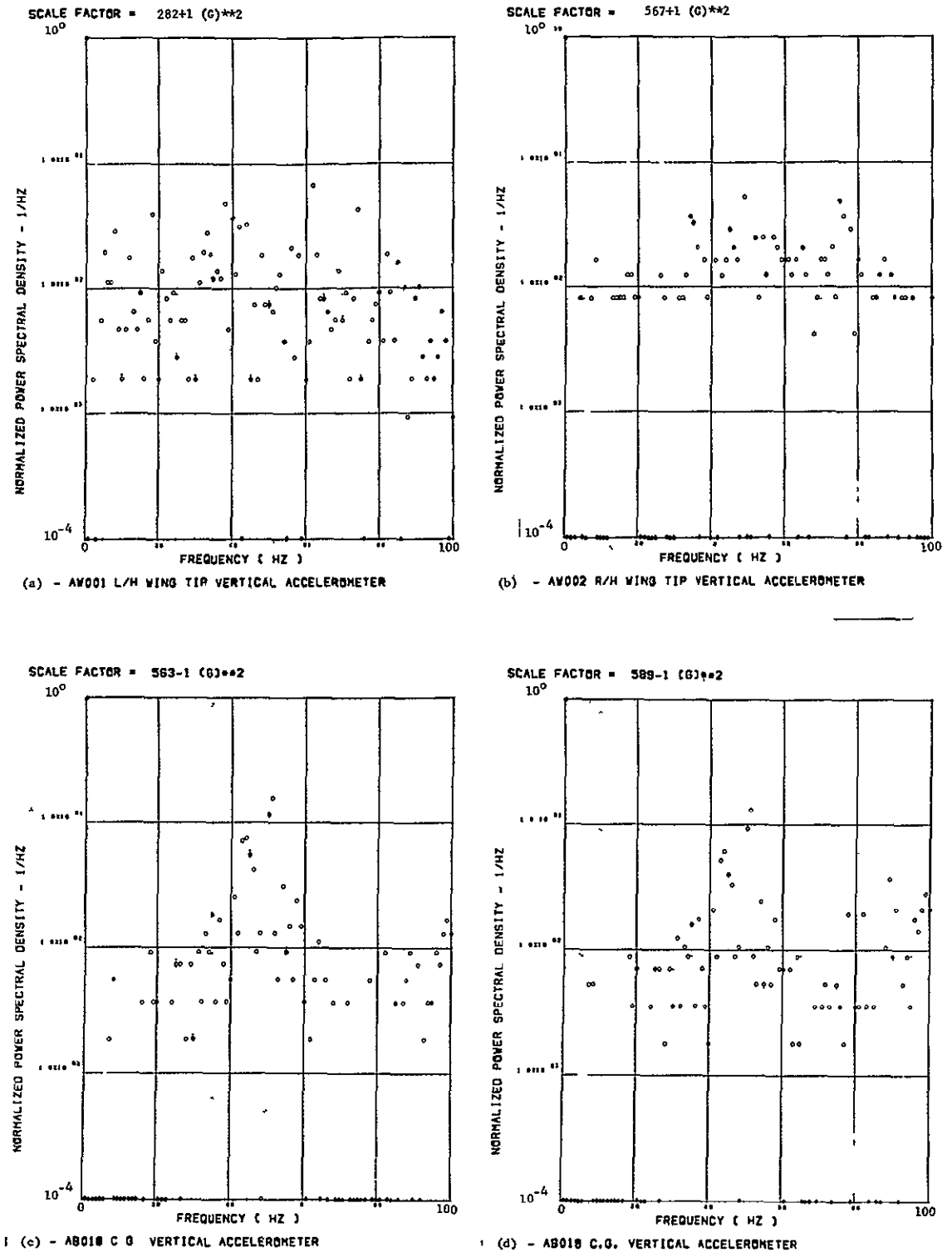

Figure 14. Power Spectra-Flight 48, Run 6, Point 6 T_1=133419.0, ΔT=1 Sec, α_{Nom}=12.3 deg, $\Delta\alpha$=2.40 deg.

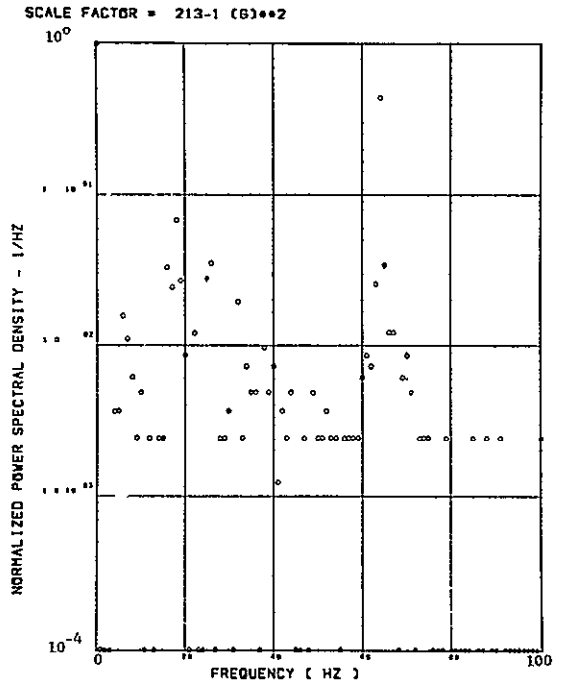

(e) - AF008 PILOT S SEAT VERTICAL ACCELEROMETER

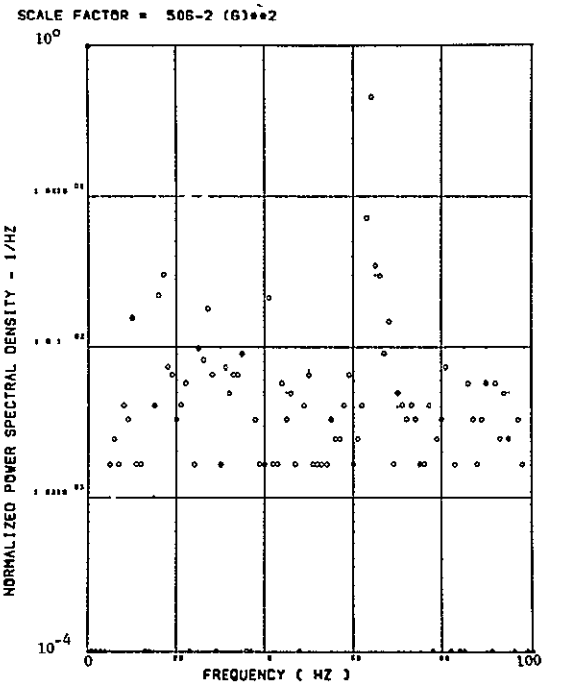

(E) - AF010 PILOT S SEAT LATERAL ACCELEROMETER

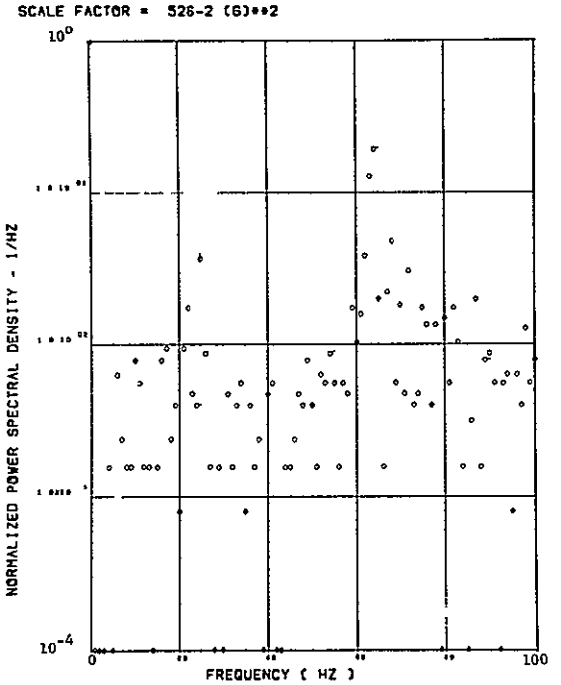

(g) - AB020 C G. LATERAL ACCELEROMETER

Figure 14. Continued

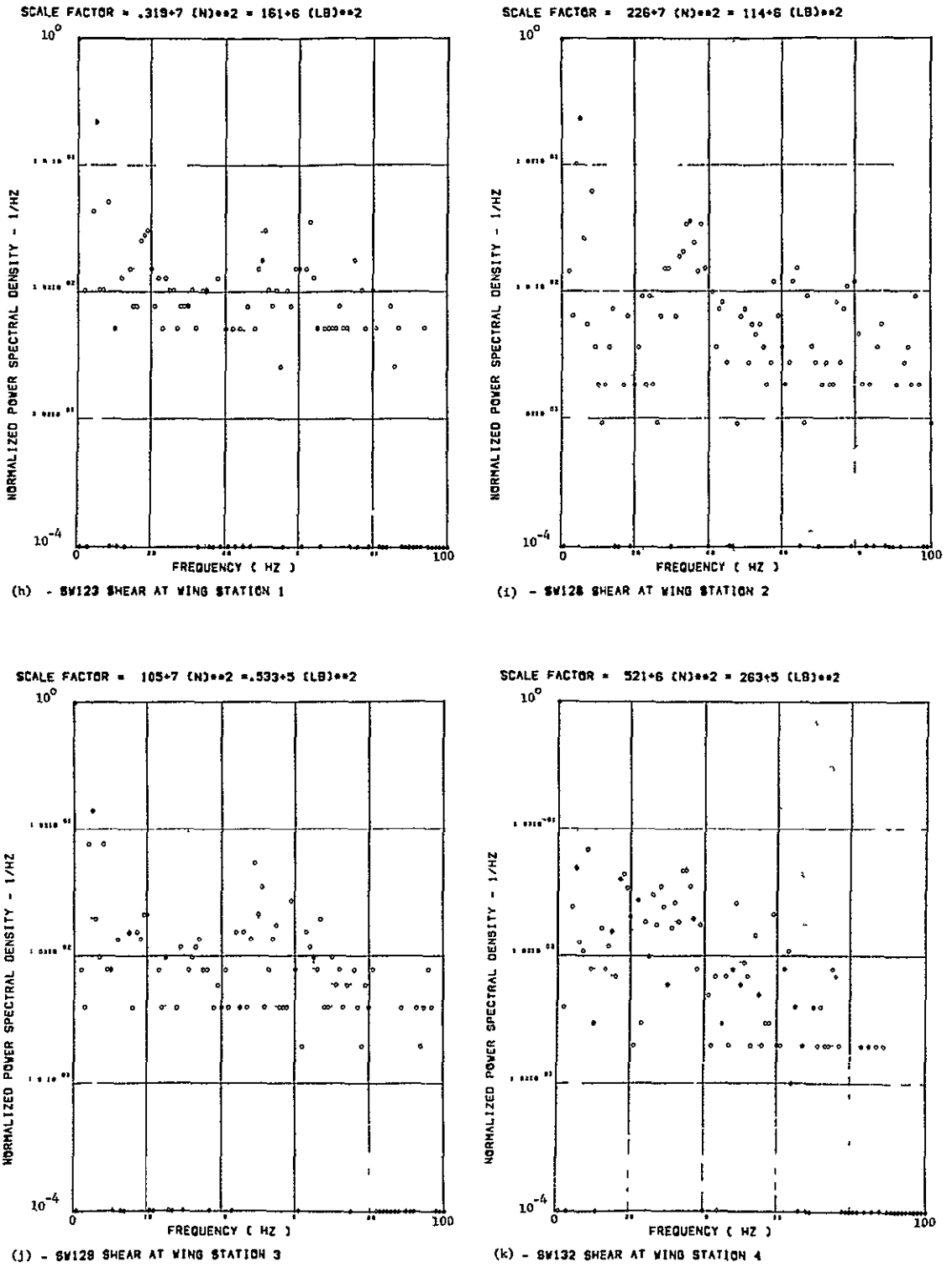

Figure 14. Continued

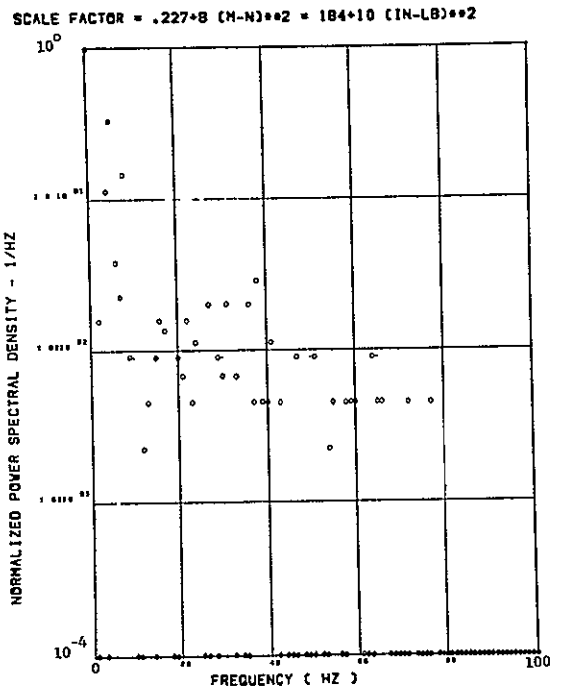

(l) - SW124 BENDING MOMENT AT WING STATION 1

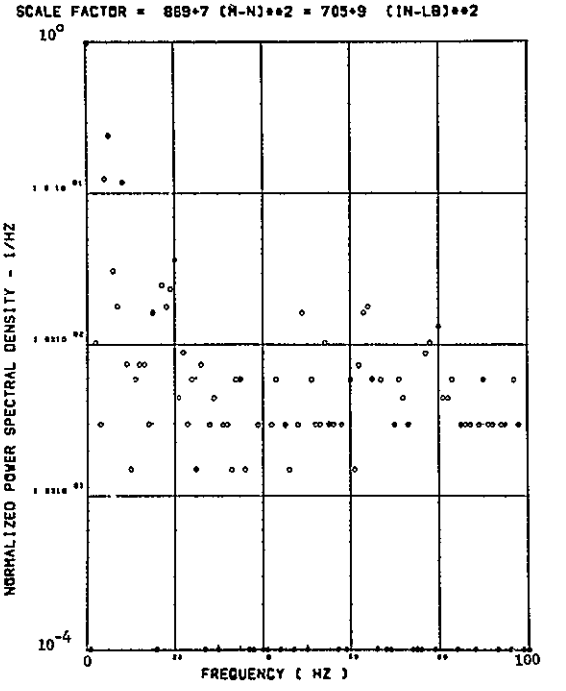

(m) - SW127 BENDING MOMENT AT WING STATION 2

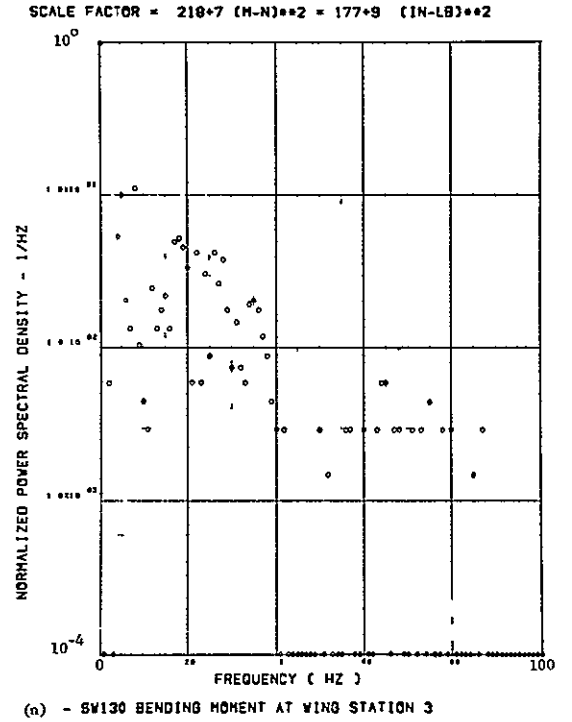

(n) - SW130 BENDING MOMENT AT WING STATION 3

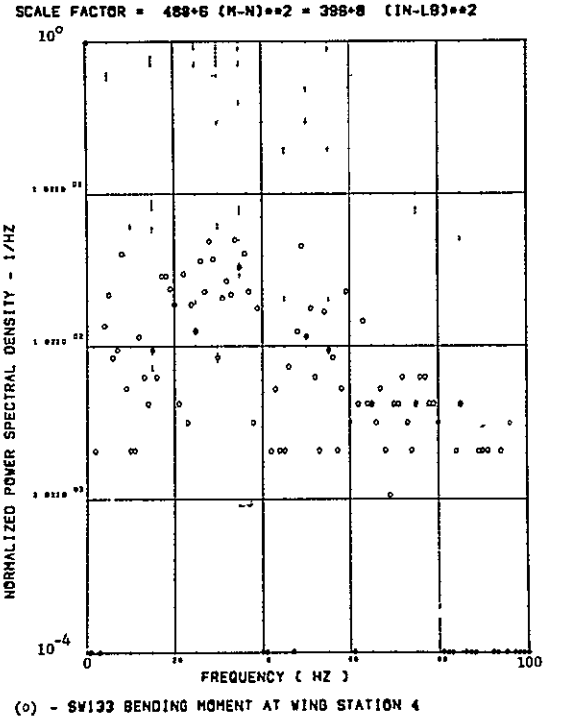

(o) - SW133 BENDING MOMENT AT WING STATION 4

Figure 14. Continued

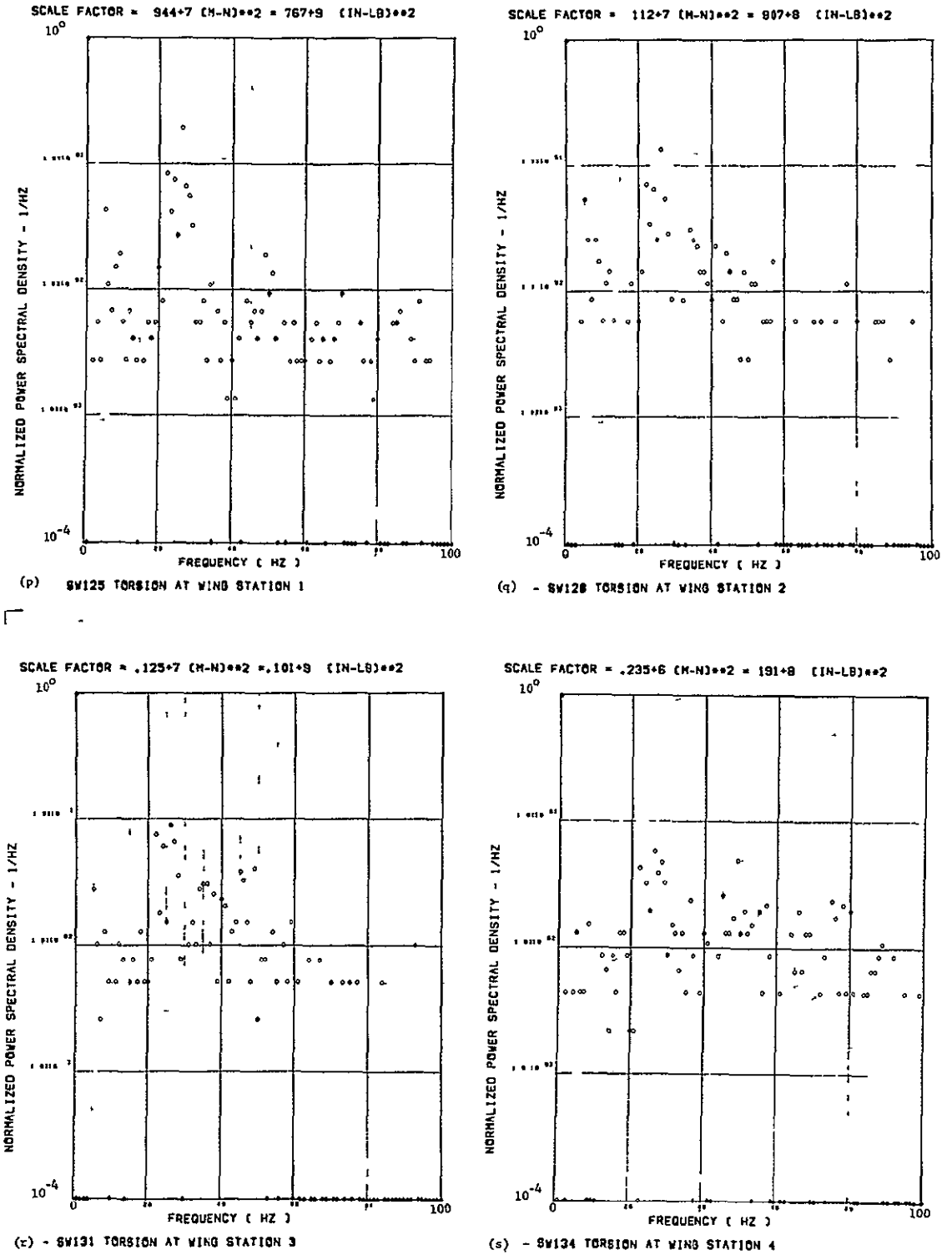

Figure 14. Concluded

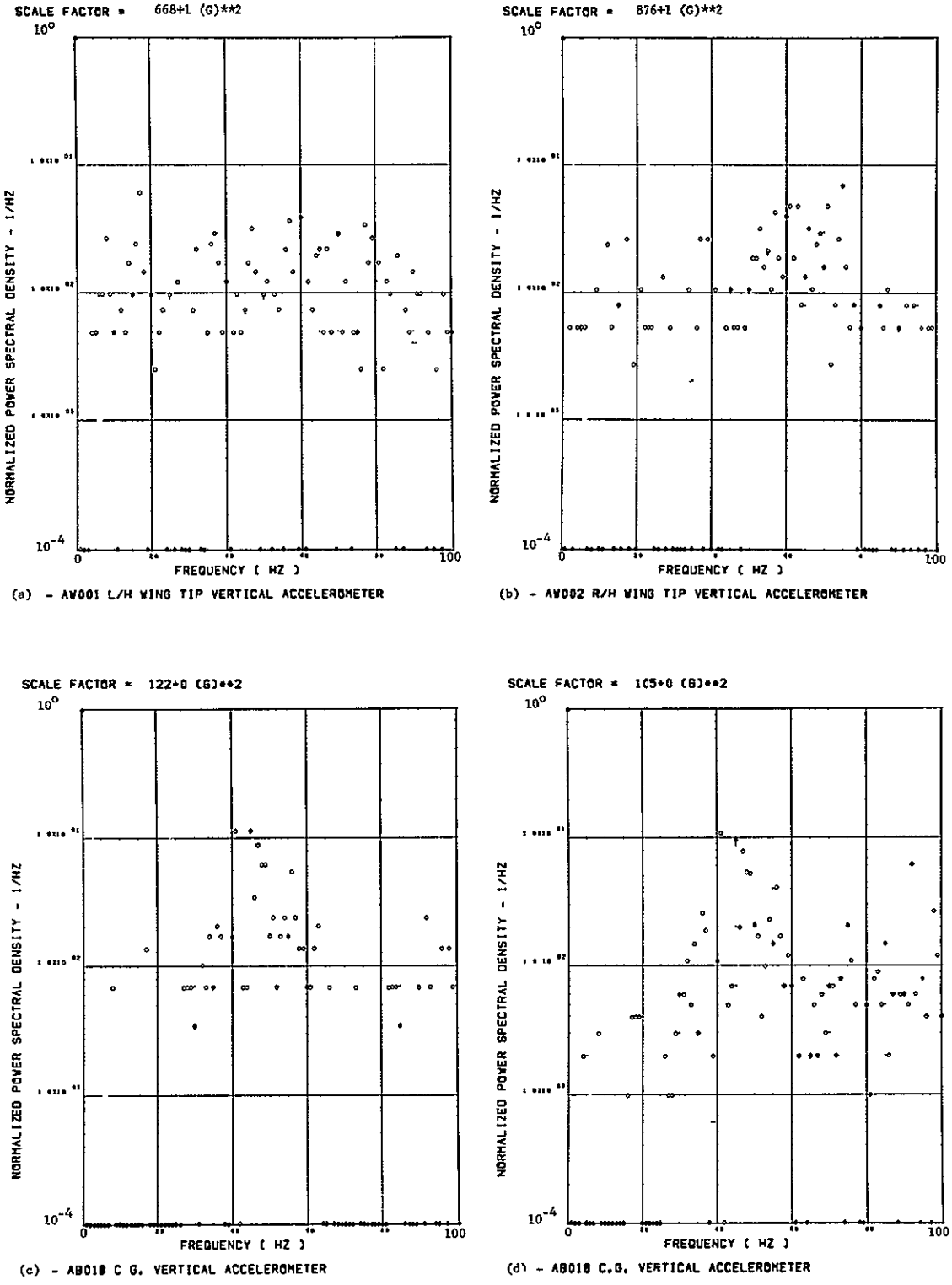

Figure 15. Power Spectra- Flight 48, Run 6, Point 7 T_1=133420.3, ΔT=1 Sec, α_{Nom}=15.3 deg, $\Delta\alpha$=2.35 deg.

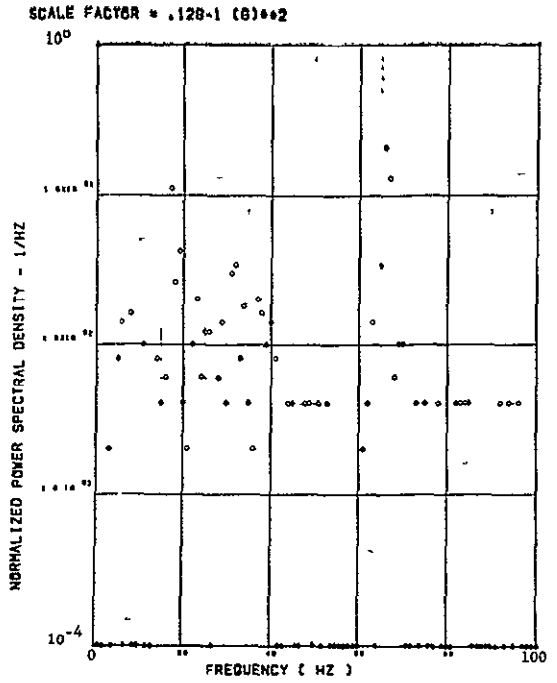

(e) - AF008 PILOT S SEAT VERTICAL ACCELEROMETER

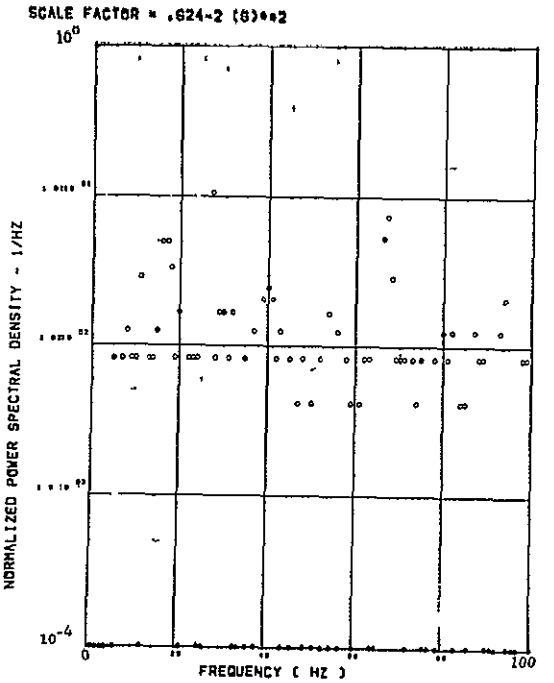

(f) - AF010 PILOT S SEAT LATERAL ACCELEROMETER

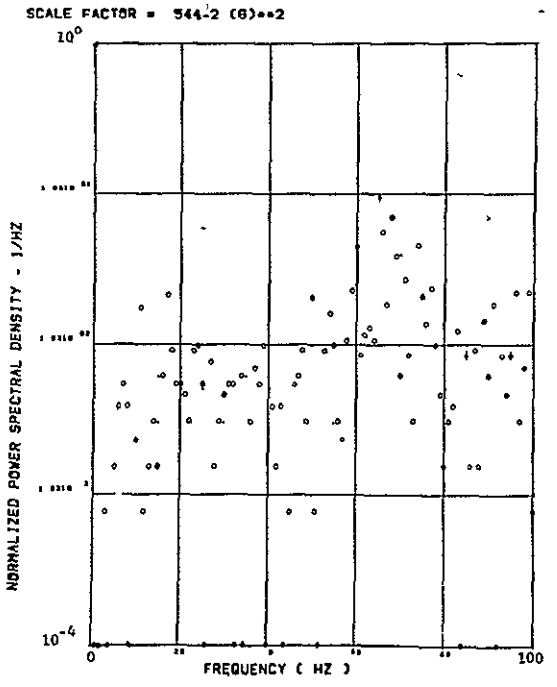

(g) - AB020 C G. LATERAL ACCELEROMETER

Figure 15. Continued

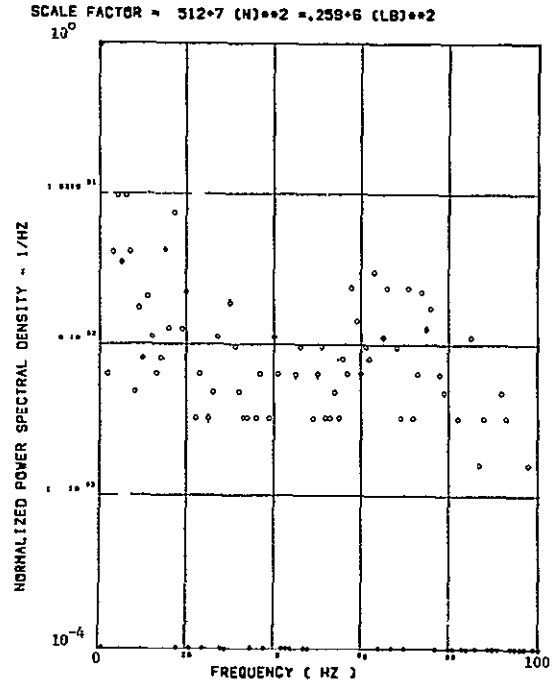

(h) - SW123 SHEAR AT WING STATION 1

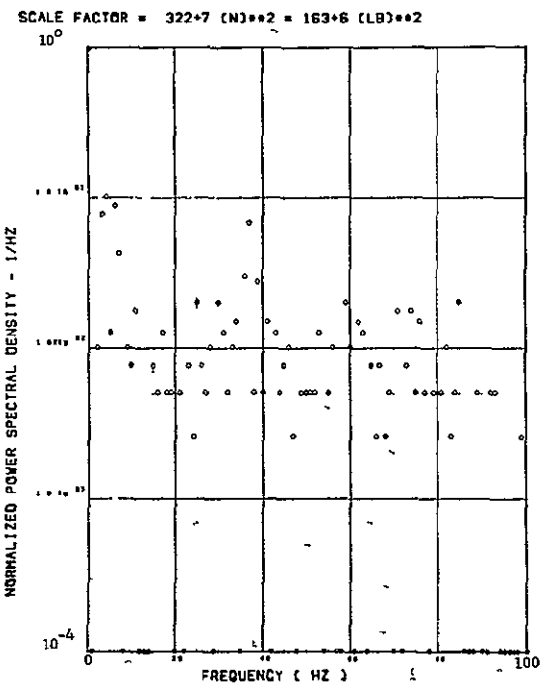

(i) - SW128 SHEAR AT WING STATION 2

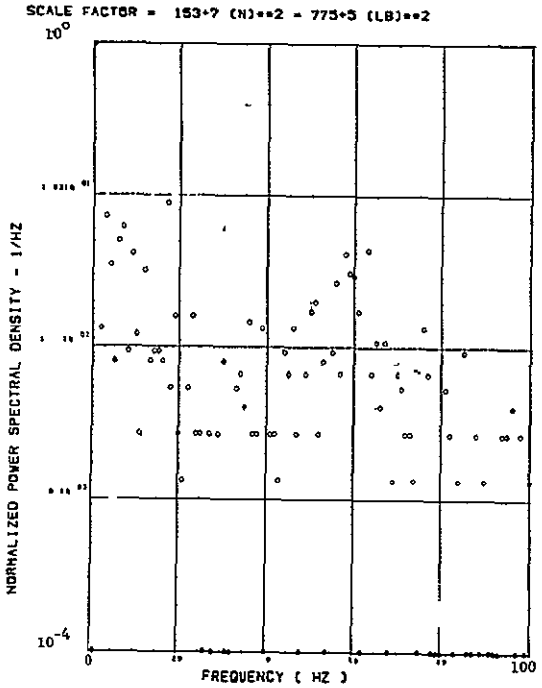

(j) - SW129 SHEAR AT WING STATION 3

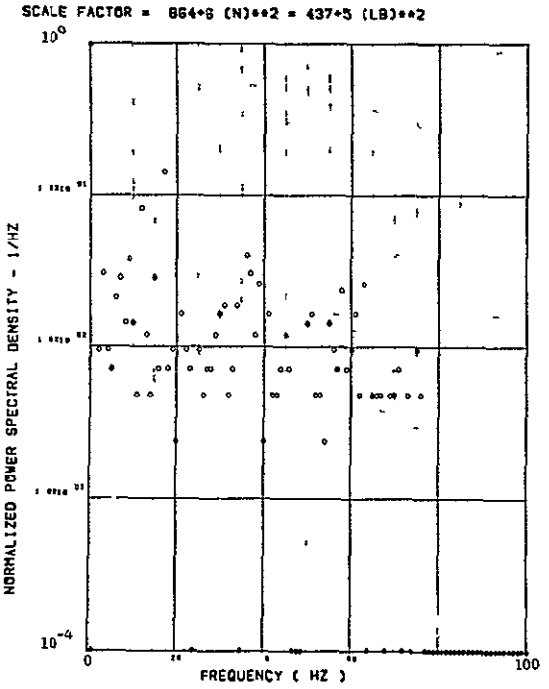

(k) - SW132 SHEAR AT WING STATION 4

Figure 15. Continued

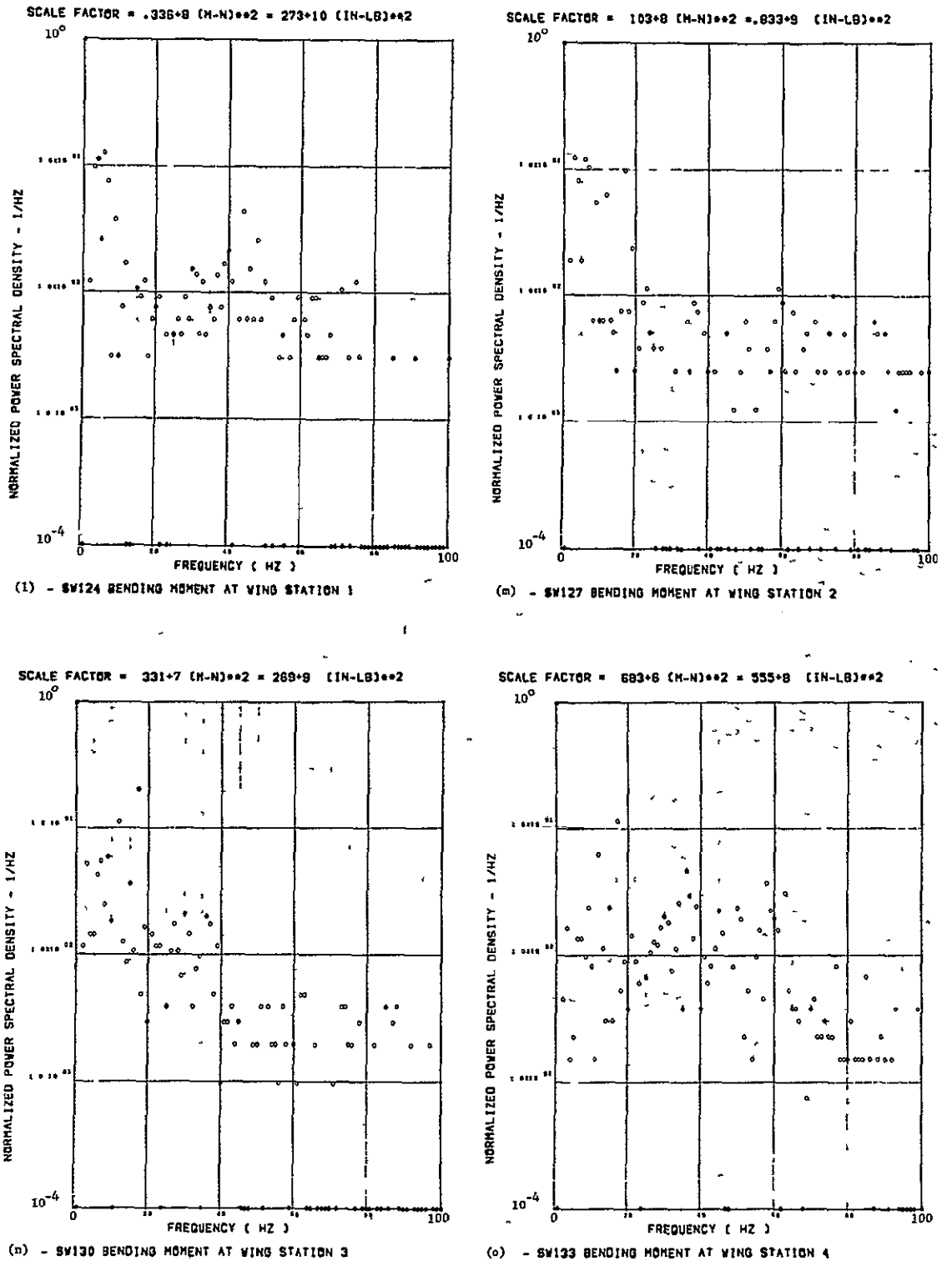

Figure 15. Continued

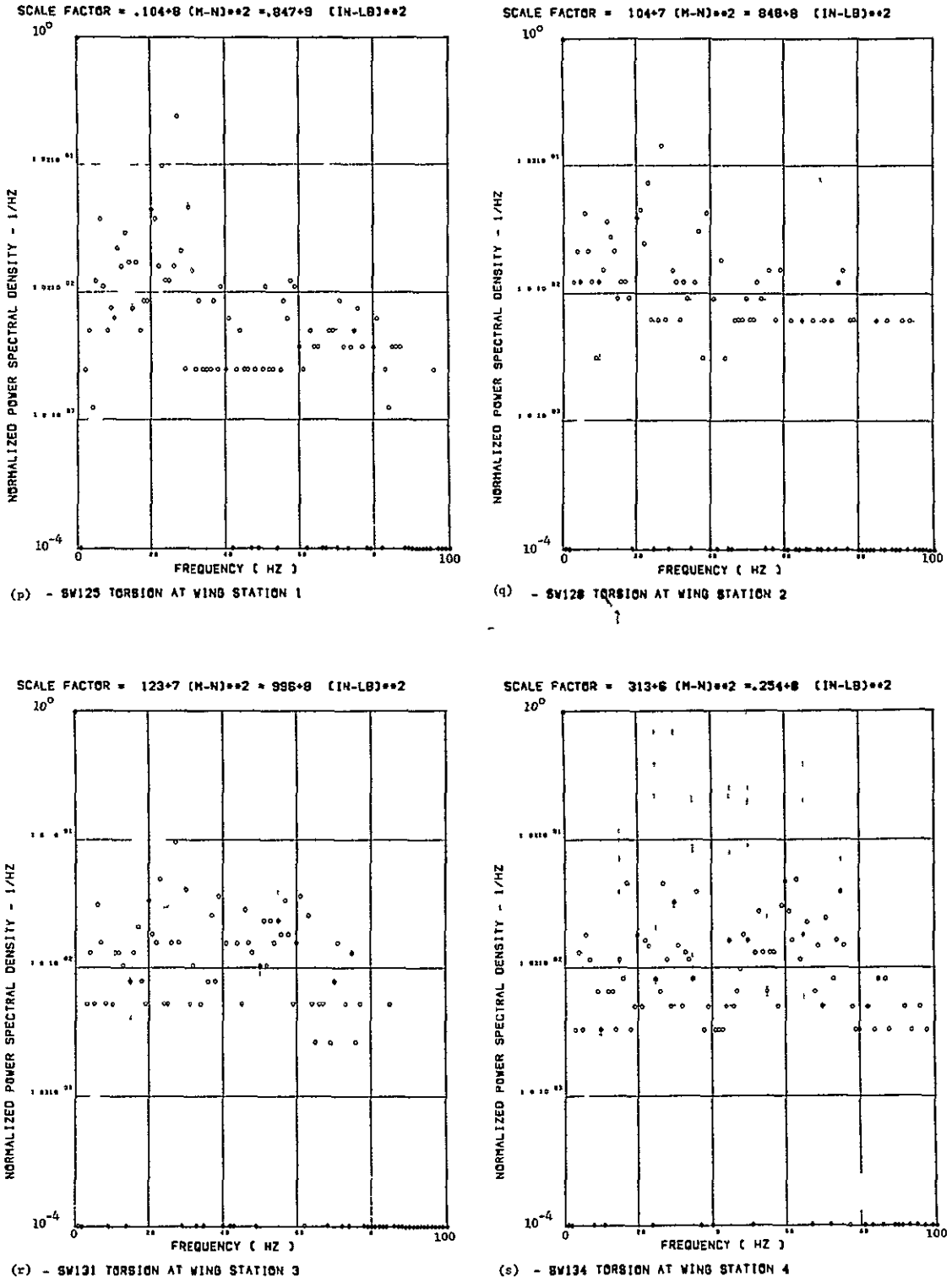

Figure 15. Concluded

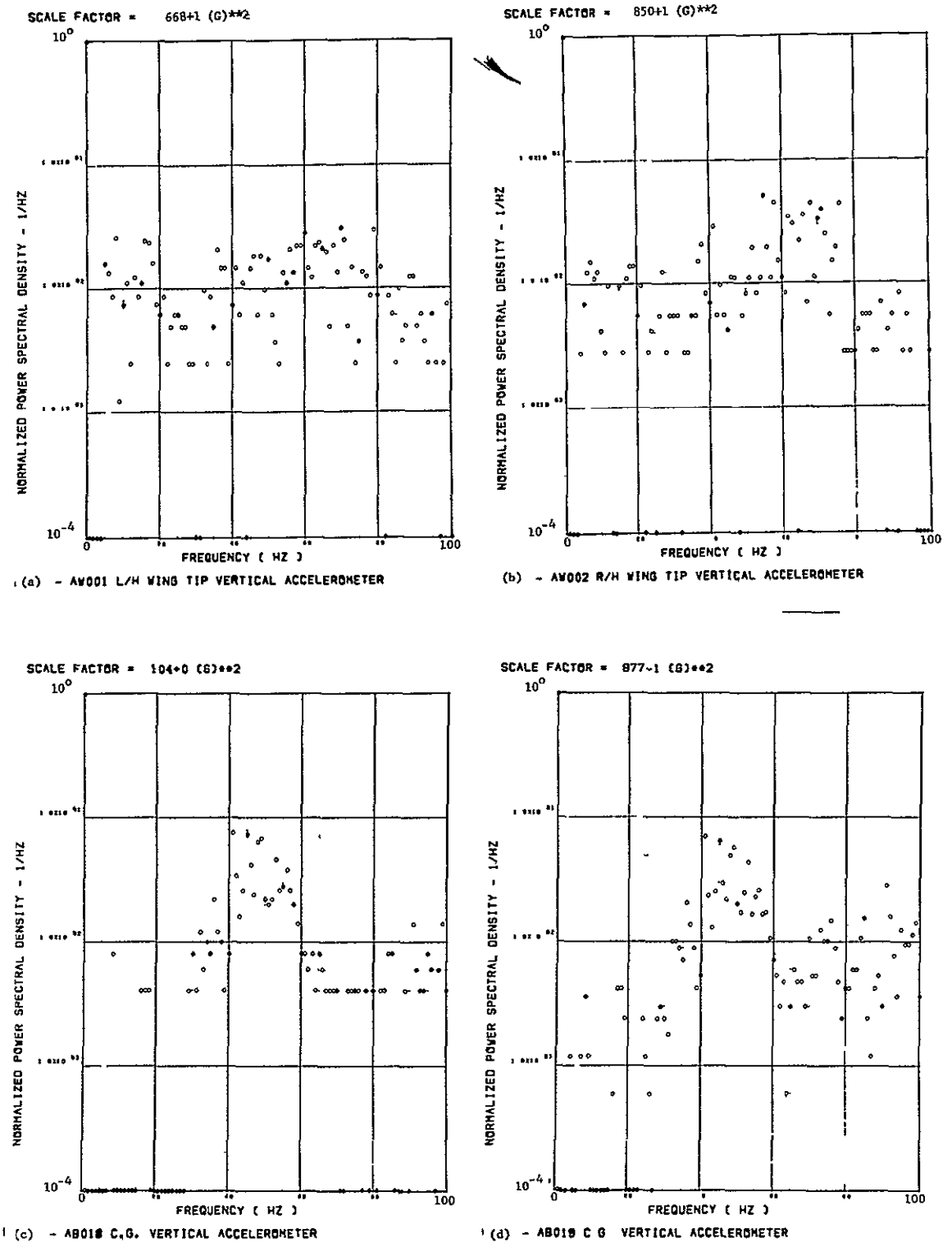

Figure 16. Power Spectra-Flight 48, Run 6, Point 8 T_1=133420.3, ΔT=2 Sec, α_{Nom}=15.1 deg, $\Delta\alpha$=3.05 deg.

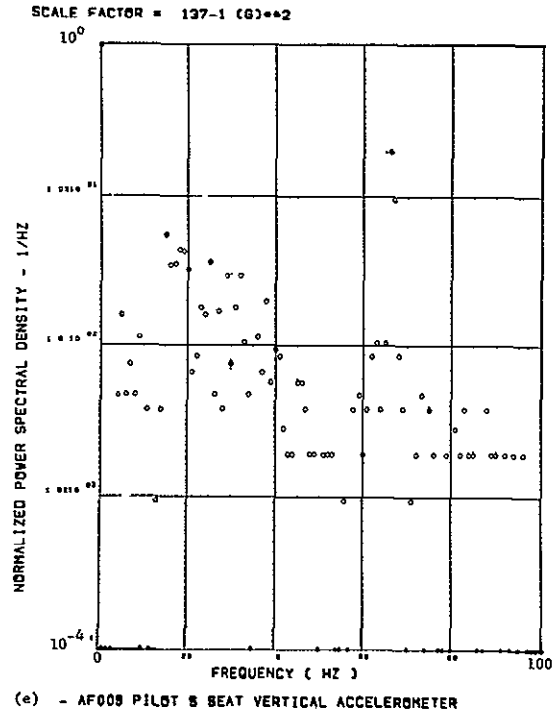

(e) - AF008 PILOT S SEAT VERTICAL ACCELEROMETER

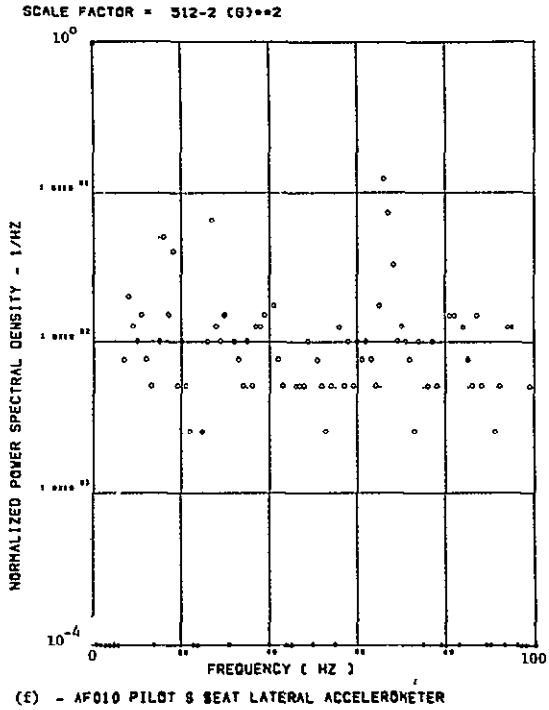

(f) - AF010 PILOT S SEAT LATERAL ACCELEROMETER

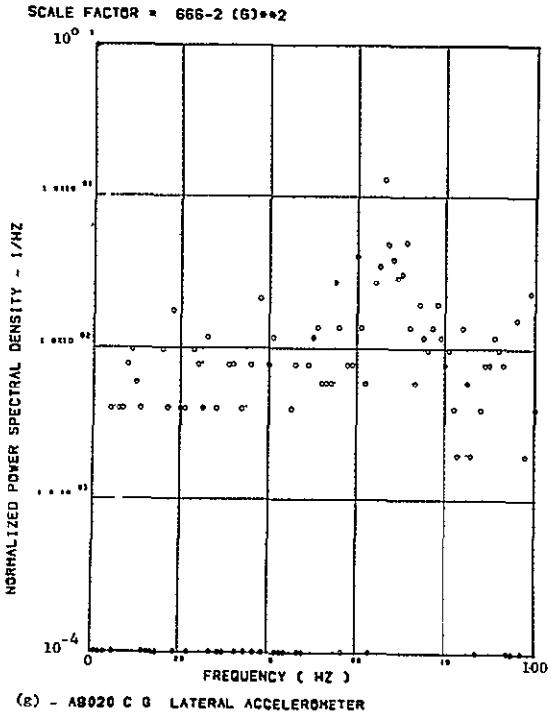

(g) - AB020 C G LATERAL ACCELEROMETER

Figure 16. Continued

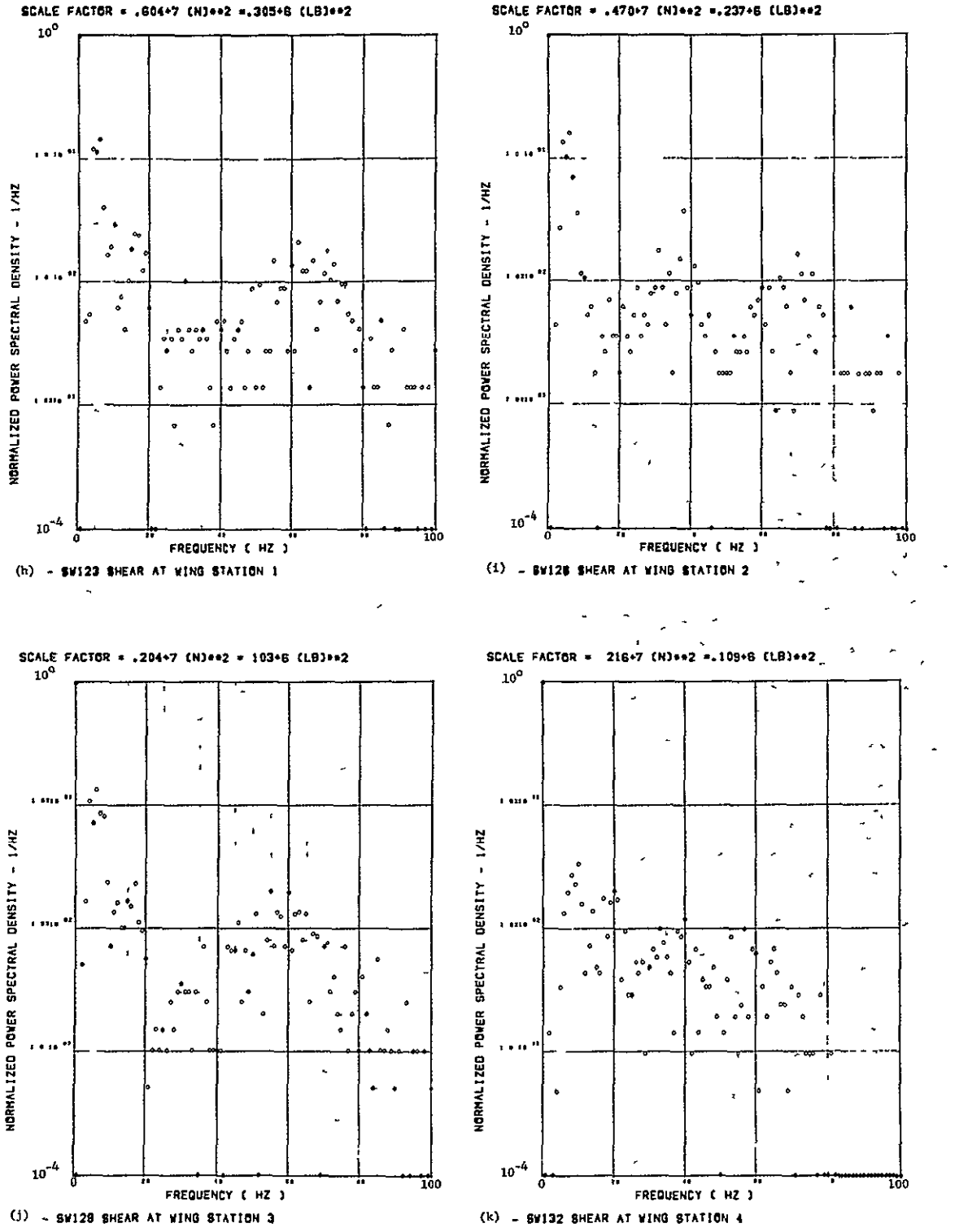

Figure 16. Continued

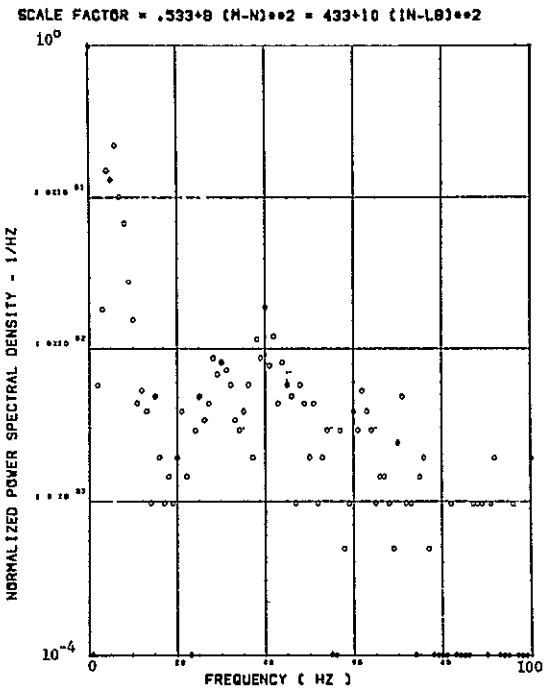

(l) - SW124 BENDING MOMENT AT WING STATION 1

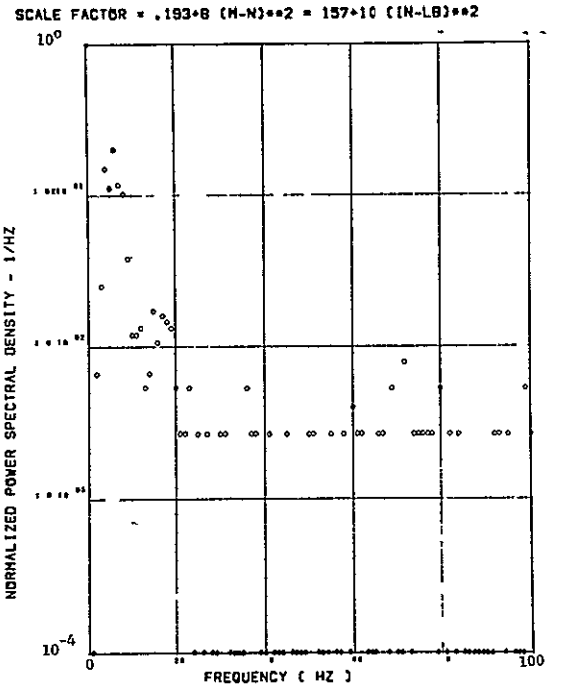

(m) - SW127 BENDING MOMENT AT WING STATION 2

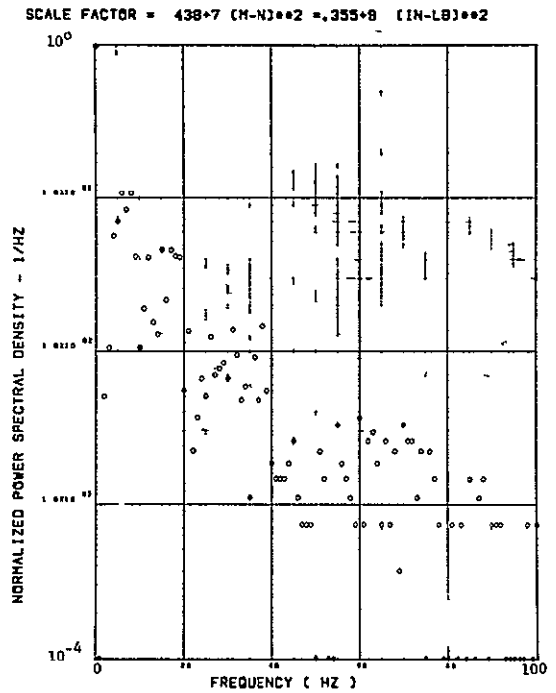

(n) - SW130 BENDING MOMENT AT WING STATION 3

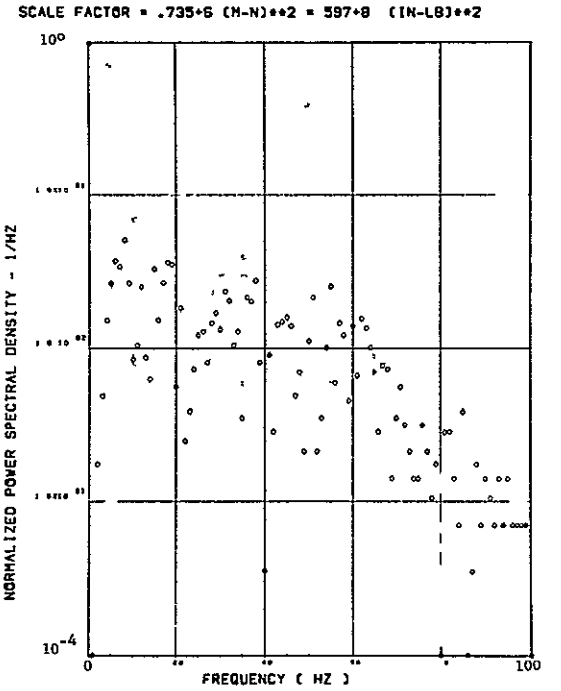

(o) - SW133 BENDING MOMENT AT WING STATION 4

Figure 16. Continued

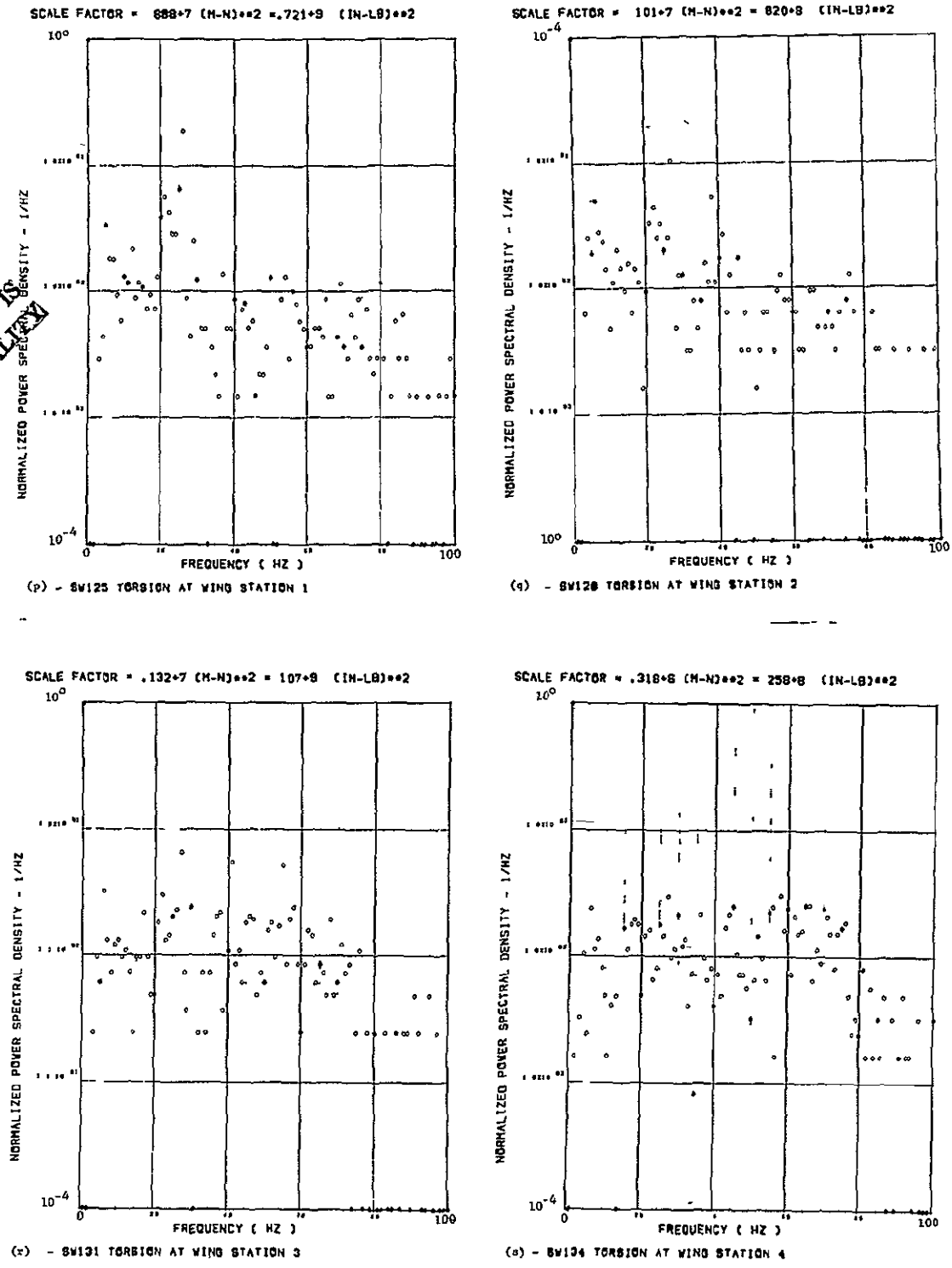

Figure 16. Concluded

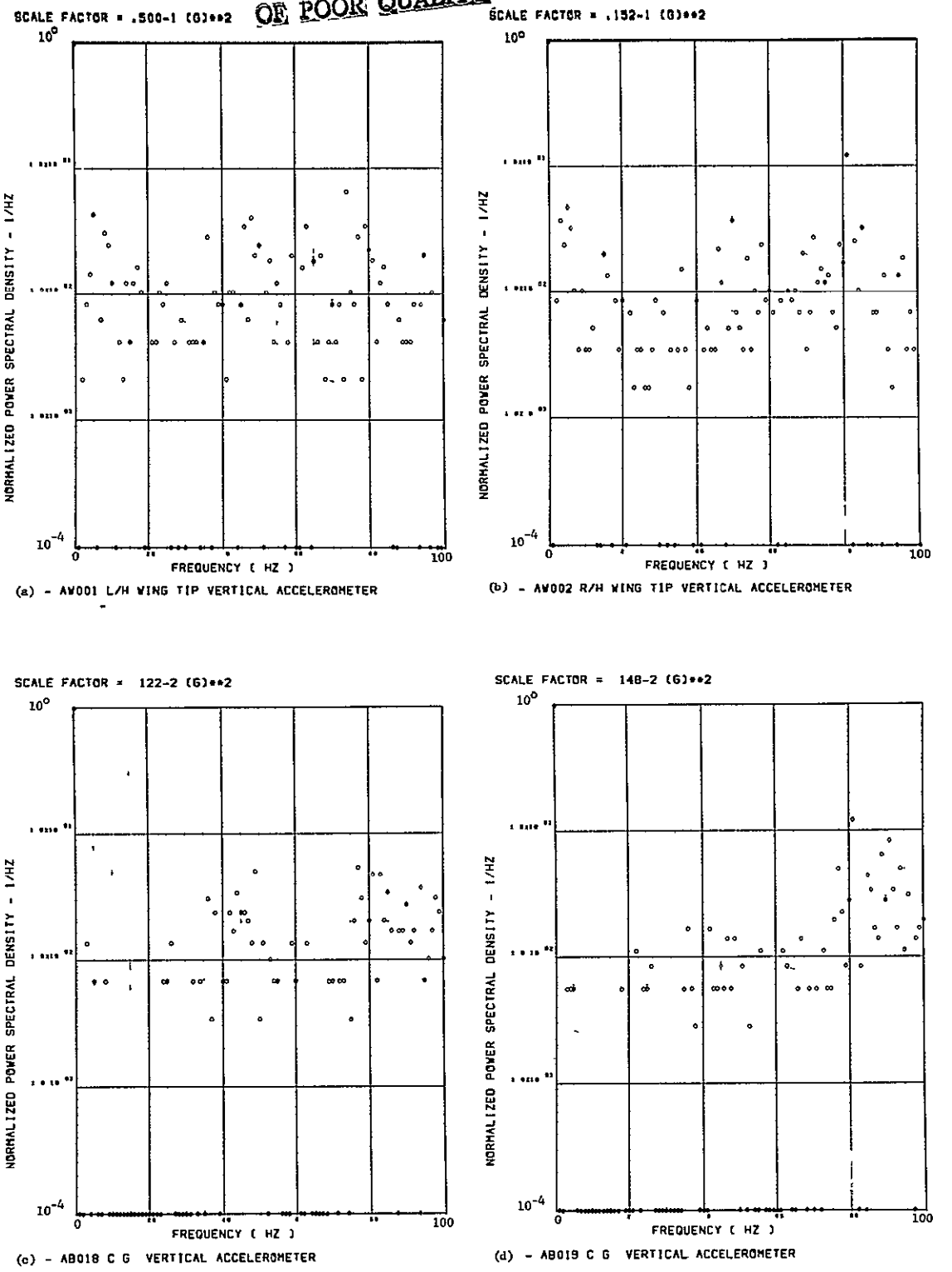

Figure 17. Power Spectra-Flight 77, Run S&C-R, Point 1 T_1=153310.0, ΔT=1 Sec , α_{Nom}=4.0 deg, $\Delta\alpha$=0.50 deg.

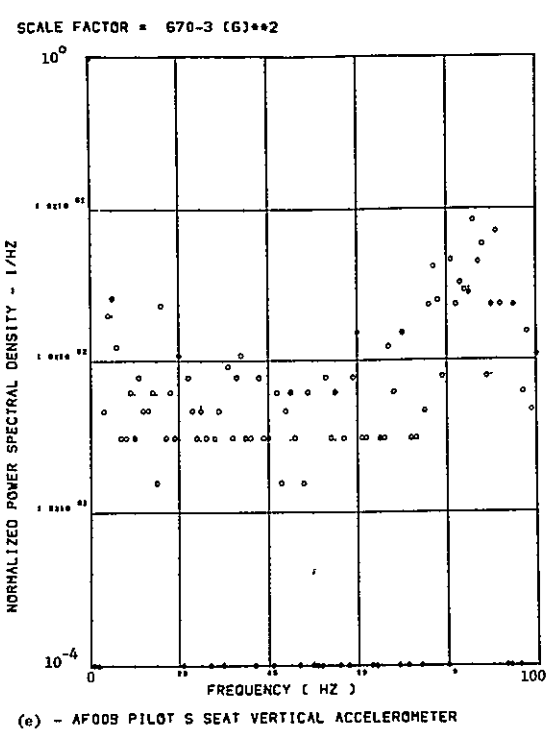

(e) - AF009 PILOT S SEAT VERTICAL ACCELEROMETER

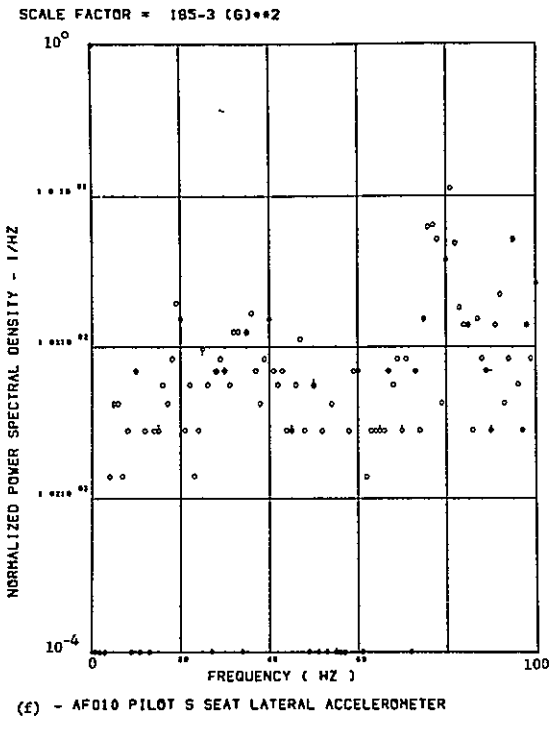

(f) - AF010 PILOT S SEAT LATERAL ACCELEROMETER

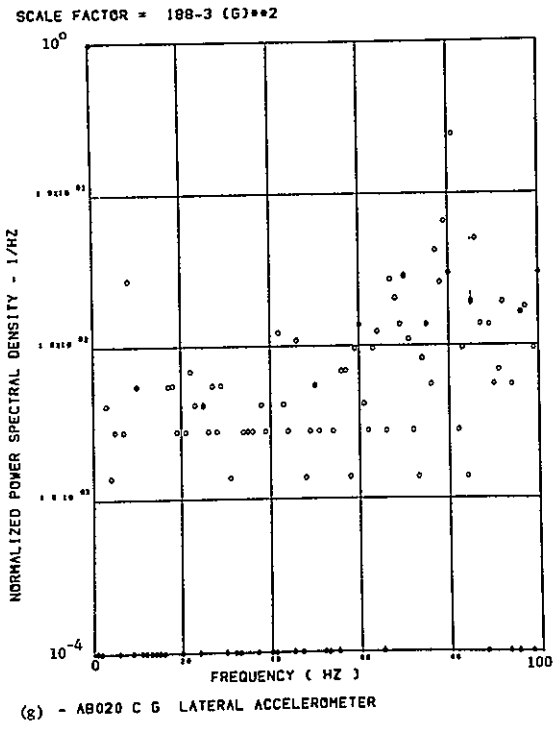

(g) - AB020 C G LATERAL ACCELEROMETER

Figure 17. Continued

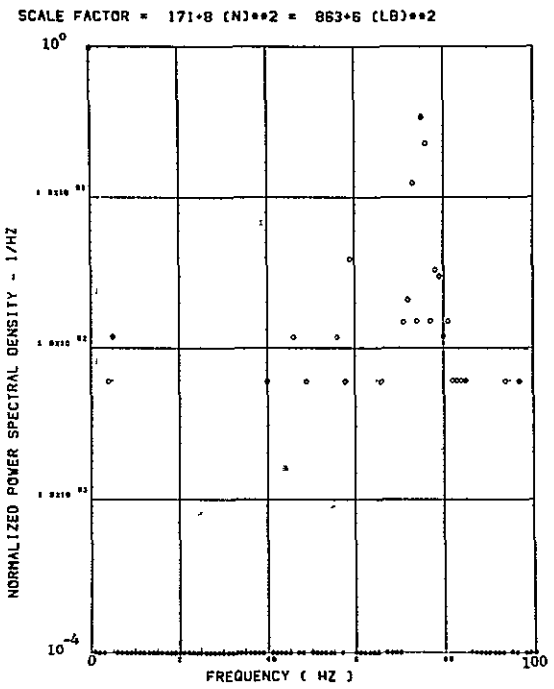

(h) - SW123 SHEAR AT WING STATION 1

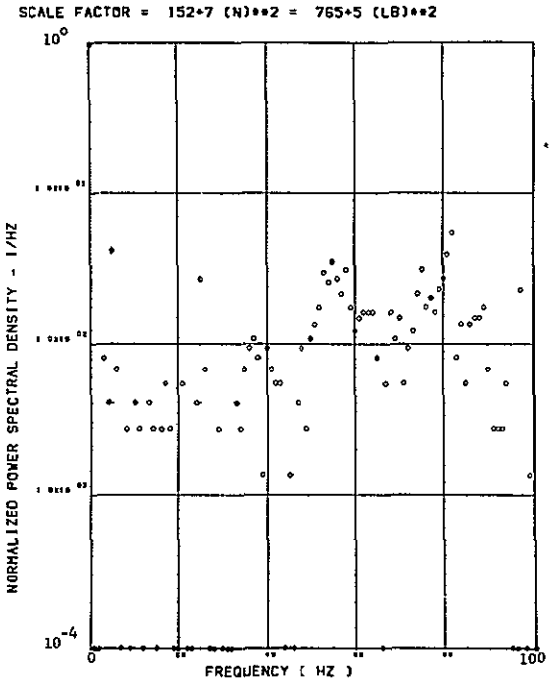

(i) - SW126 SHEAR AT WING STATION 2

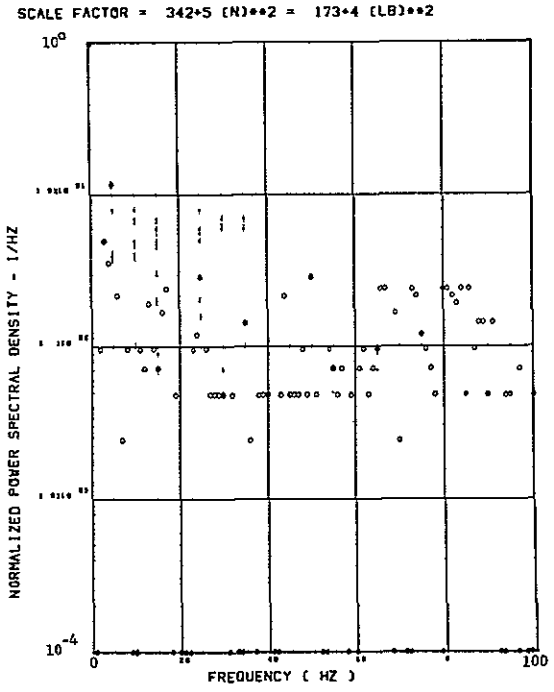

(j) - SW129 SHEAR AT WING STATION 3

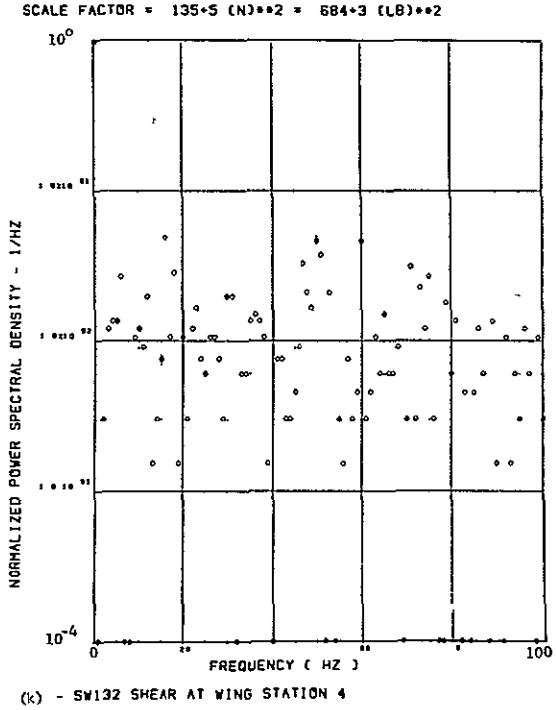

(k) - SW132 SHEAR AT WING STATION 4

Figure 17. Continued

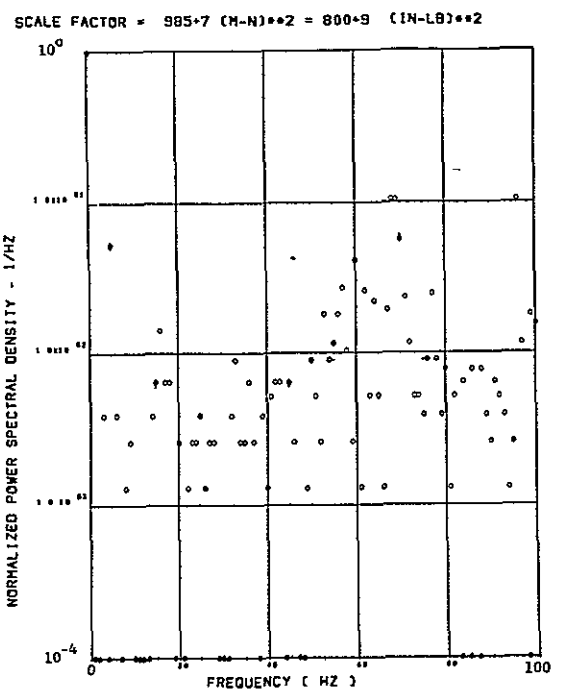

(l) - SW124 BENDING MOMENT AT WING STATION 1

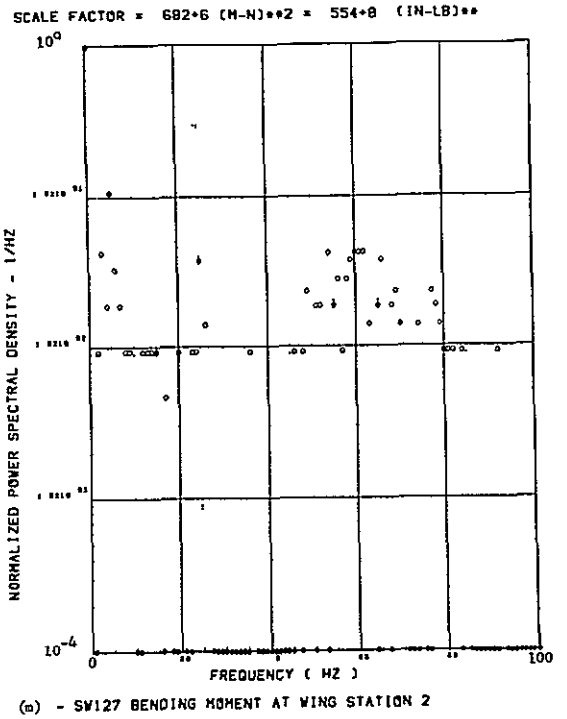

(m) - SW127 BENDING MOMENT AT WING STATION 2

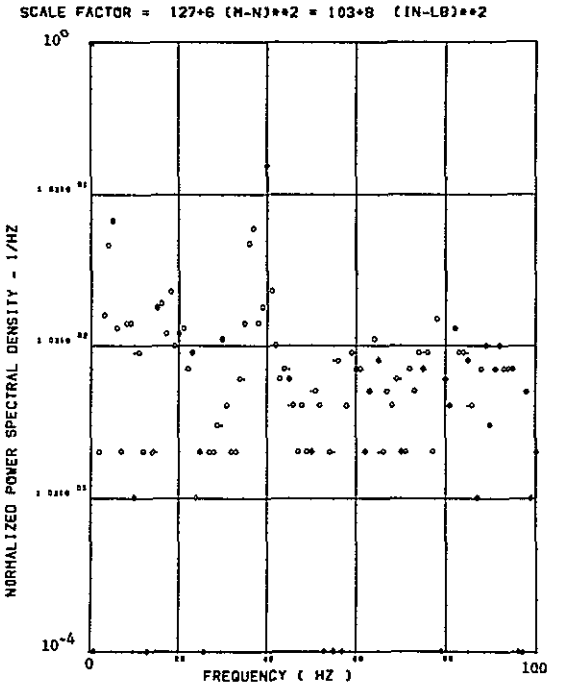

(n) - SW130 BENDING MOMENT AT WING STATION 3

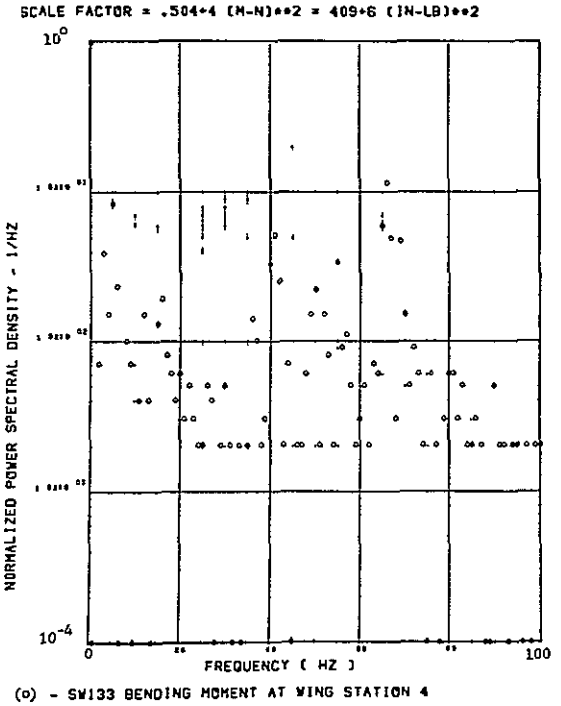

(o) - SW133 BENDING MOMENT AT WING STATION 4

Figure 17. Continued

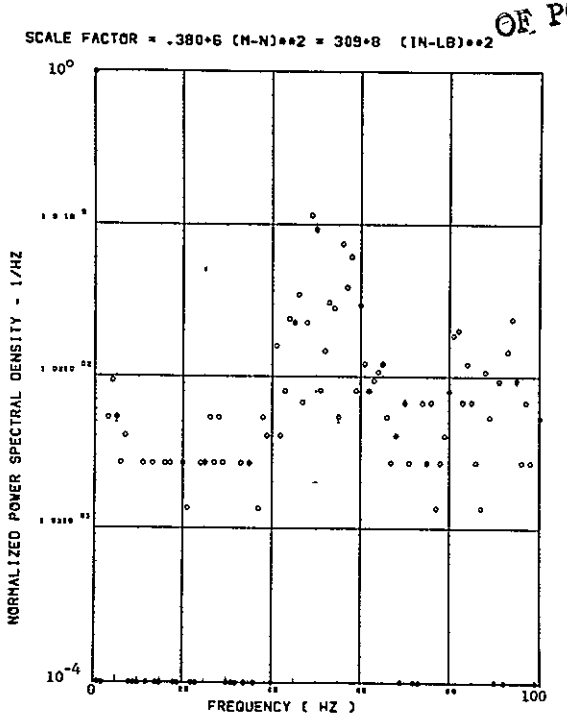

(p) - SW125 TORSION AT WING STATION 1

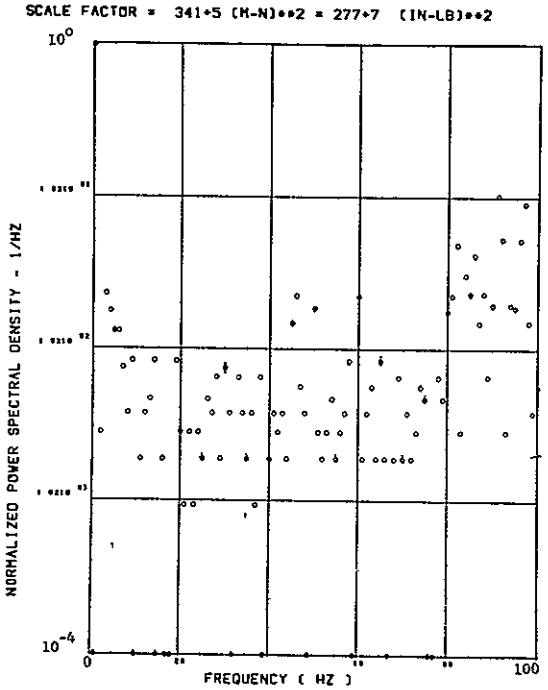

(q) - SW128 TORSION AT WING STATION 2

Data Not Available

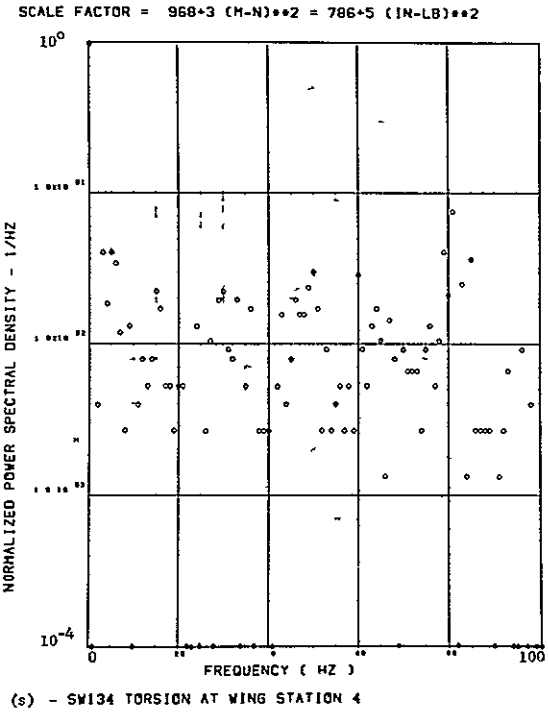

(s) - SW134 TORSION AT WING STATION 4

Figure 17. Concluded

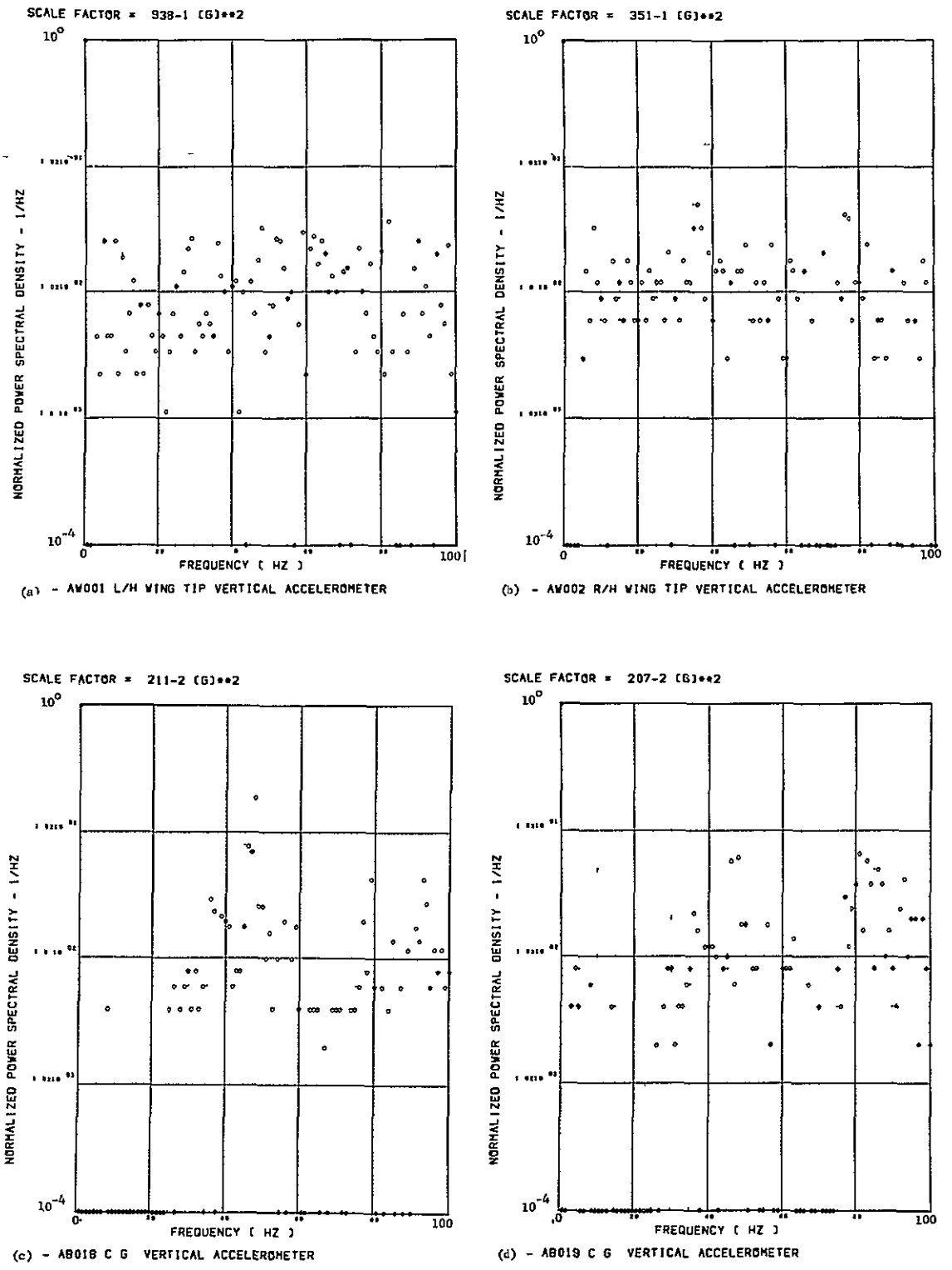

Figure 18. Power Spectra-Flight 77, Run S&C-R, Point 2 T_1=153311.5, ΔT=1 Sec, α_{Nom}=5.1 deg, $\Delta\alpha$=0.92 deg.

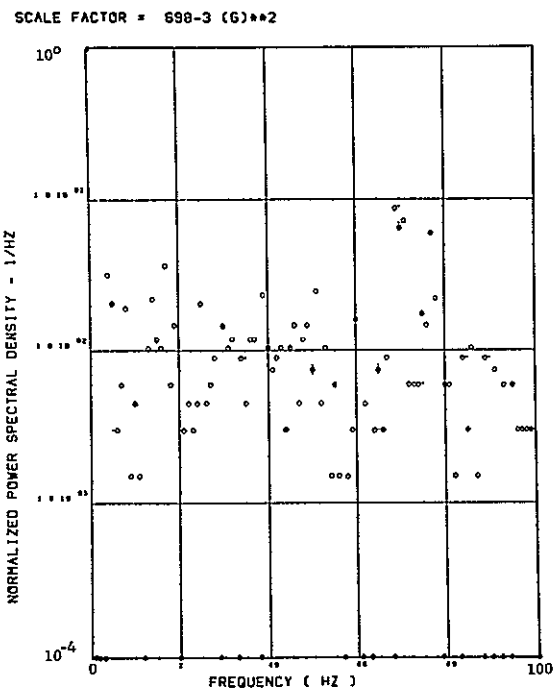

(e) - AF009 PILOT S SEAT VERTICAL ACCELEROMETER

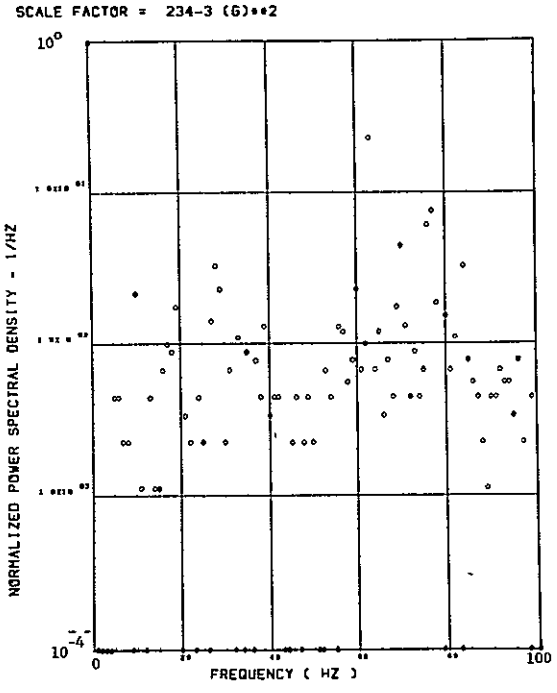

(f) - AF010 PILOT S SEAT LATERAL ACCELEROMETER

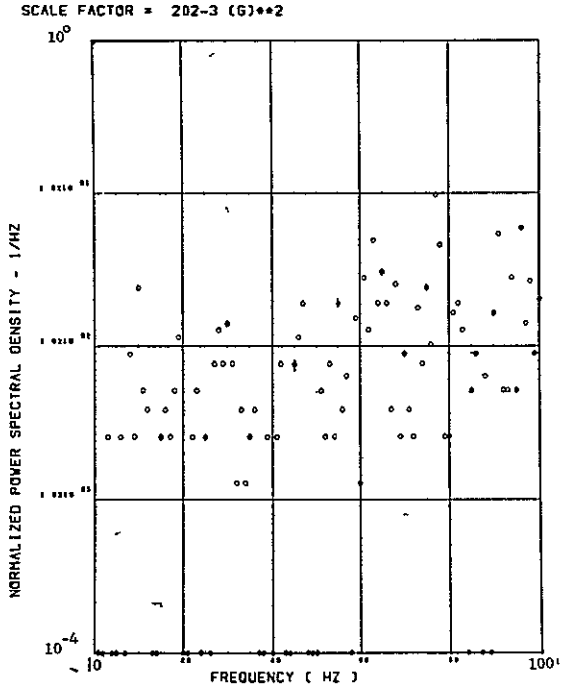

(g) - AB020 C G LATERAL ACCELEROMETER

Figure 18. Continued

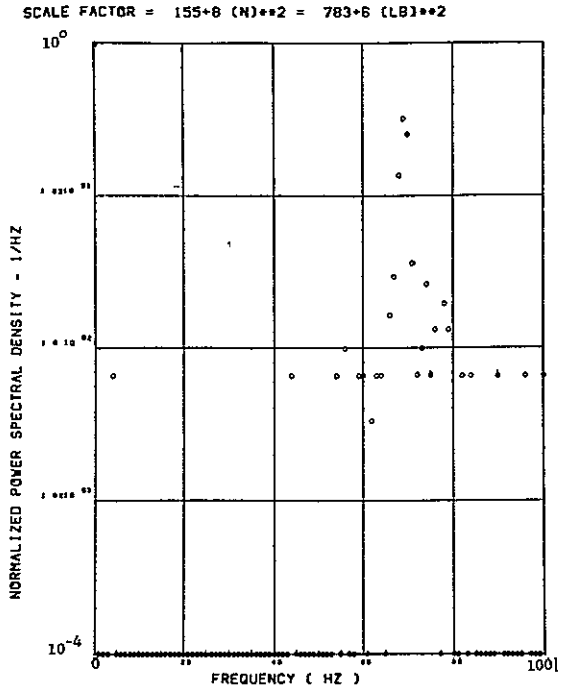

(h) - SW123 SHEAR AT WING STATION 1

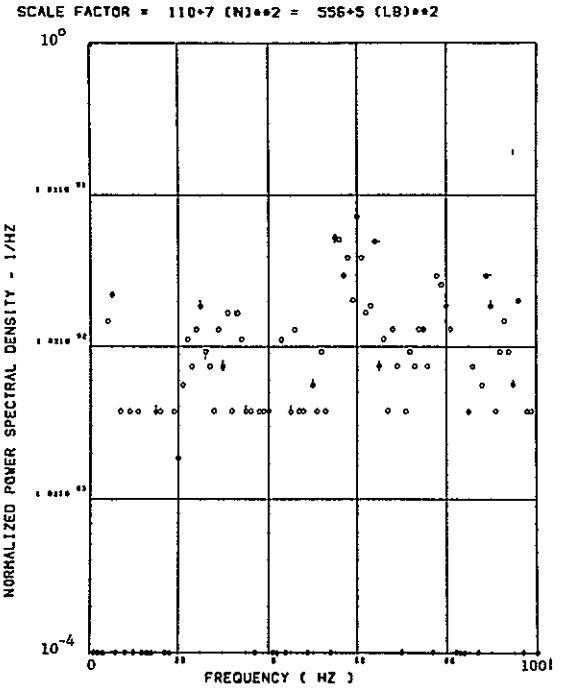

(i) - SW126 SHEAR AT WING STATION 2

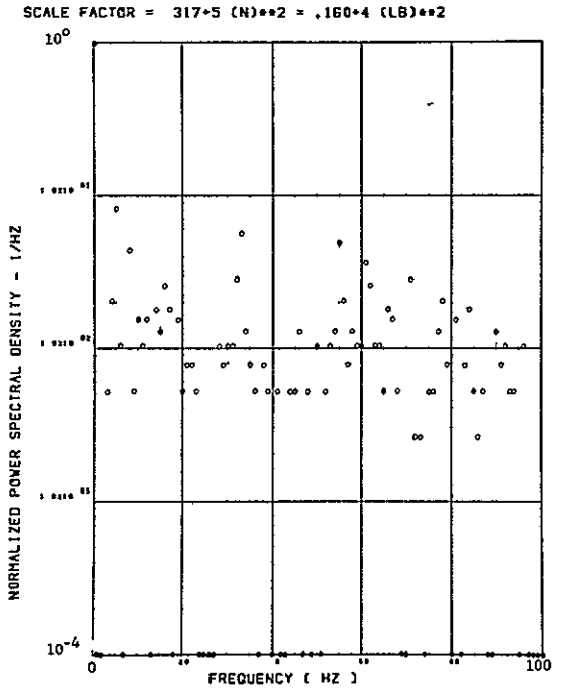

(j) - SW129 SHEAR AT WING STATION 3

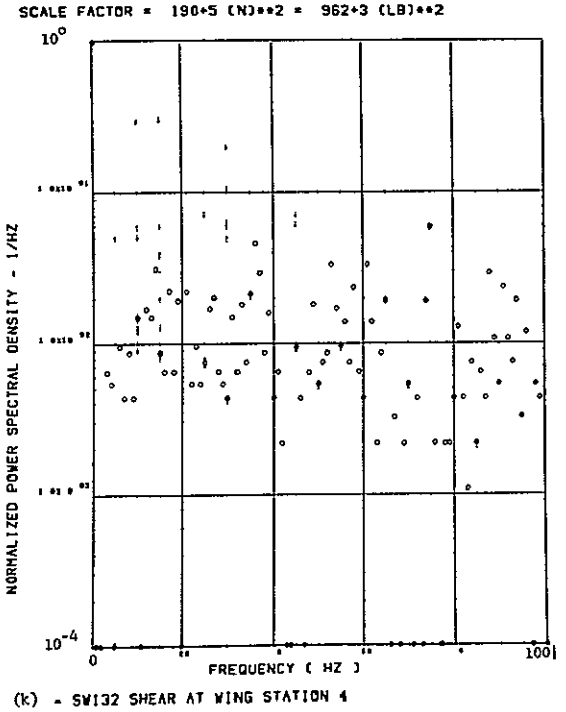

(k) - SW132 SHEAR AT WING STATION 4

Figure 18. Continued

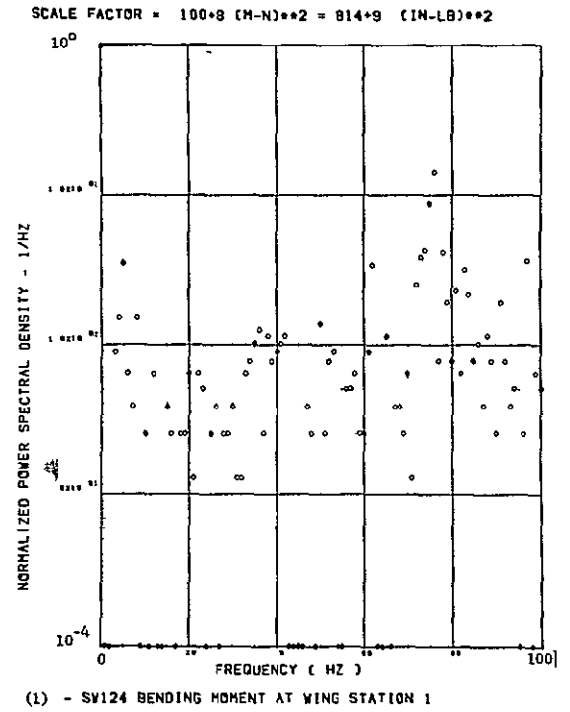

(l) - SW124 BENDING MOMENT AT WING STATION 1

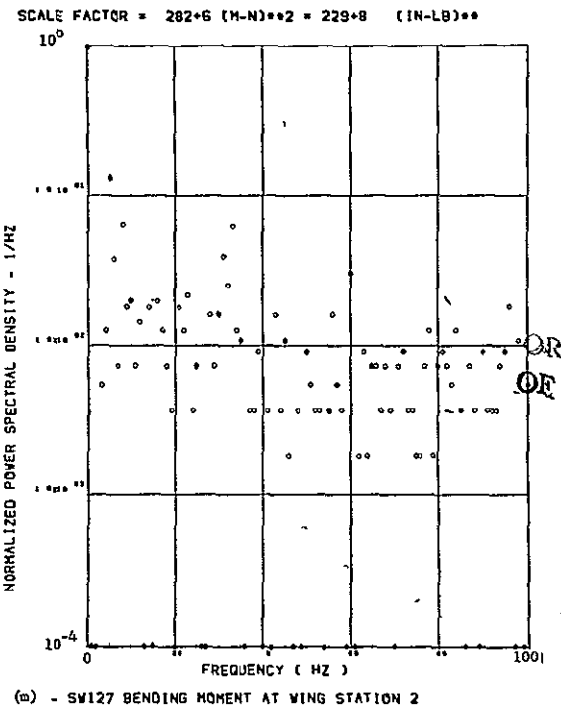

(m) - SW127 BENDING MOMENT AT WING STATION 2

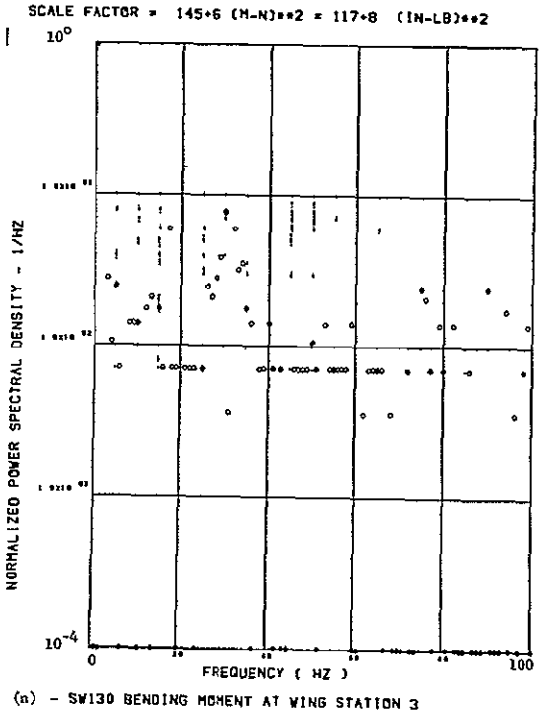

(n) - SW130 BENDING MOMENT AT WING STATION 3

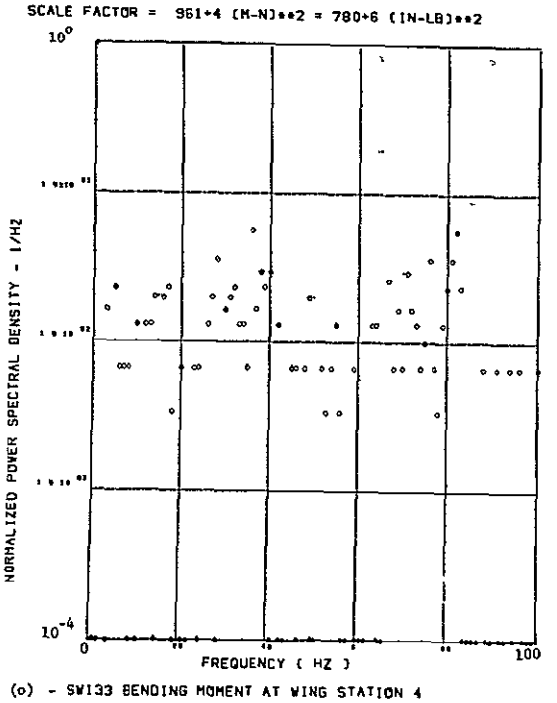

(o) - SW133 BENDING MOMENT AT WING STATION 4

Figure 18. Continued

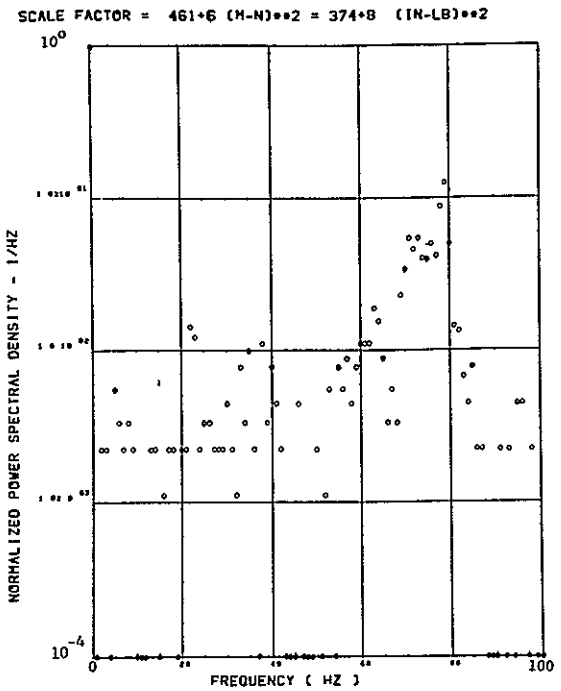

(p) - SW125 TORSION AT WING STATION 1

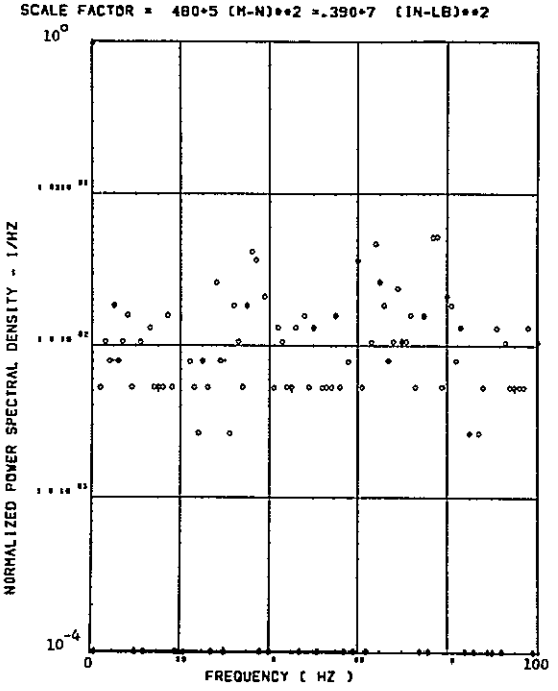

(b) - SW128 TORSION AT WING STATION 2

Data Not Available

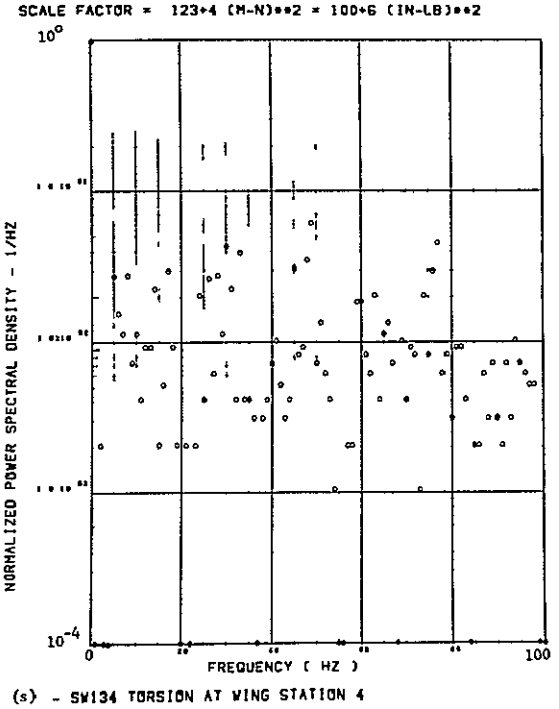

(s) - SW134 TORSION AT WING STATION 4

Figure 18. Concluded

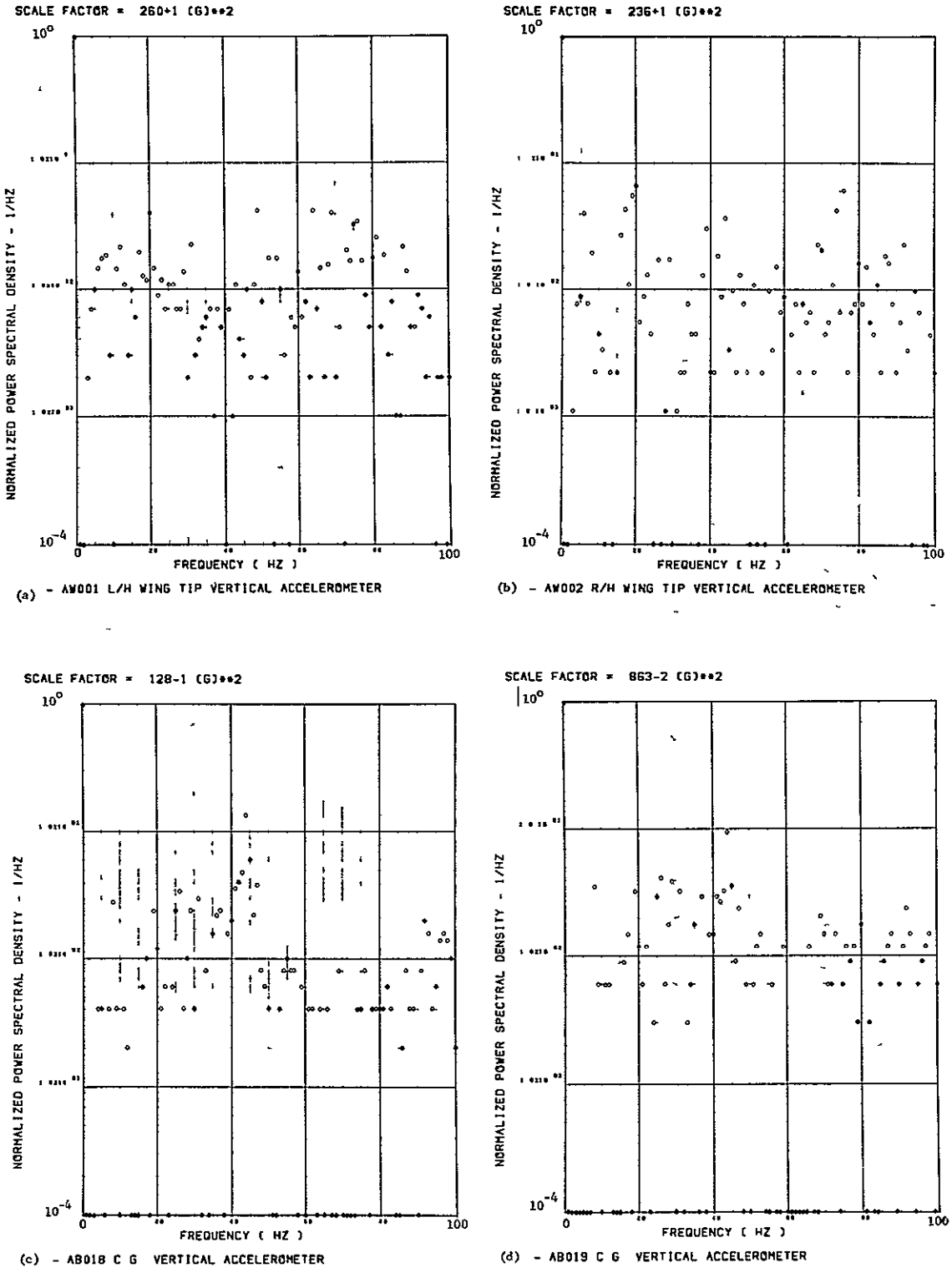

Figure 19. Power Spectra-Flight 77, Run S&C-R, Point 3, T_1=153316.0, ΔT=1 Sec, α_{Nom}=7.0 deg, $\Delta\alpha$=0.18 deg.

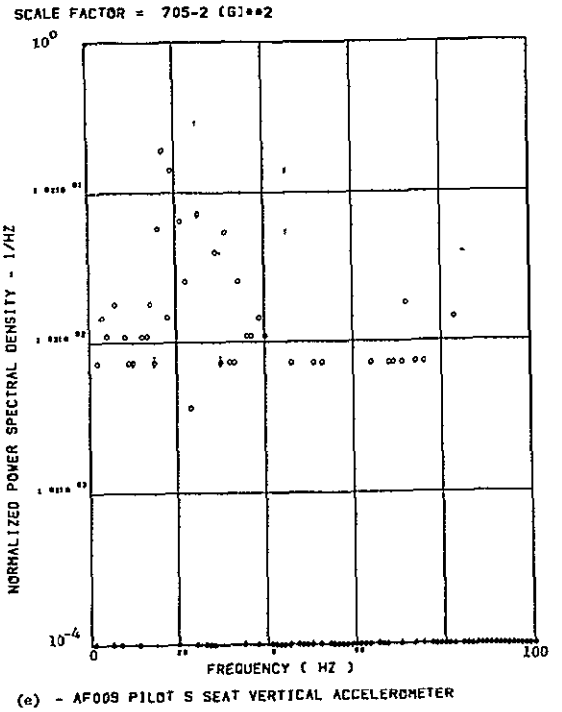

(e) - AF009 PILOT S SEAT VERTICAL ACCELEROMETER

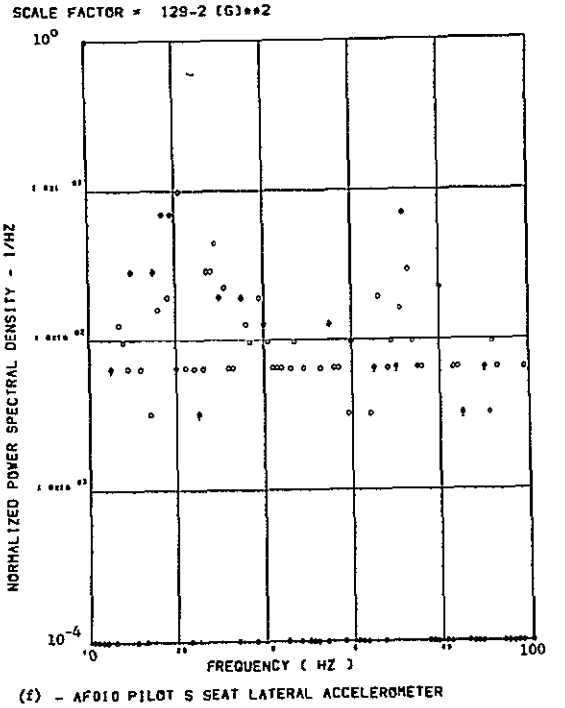

(f) - AF010 PILOT S SEAT LATERAL ACCELEROMETER

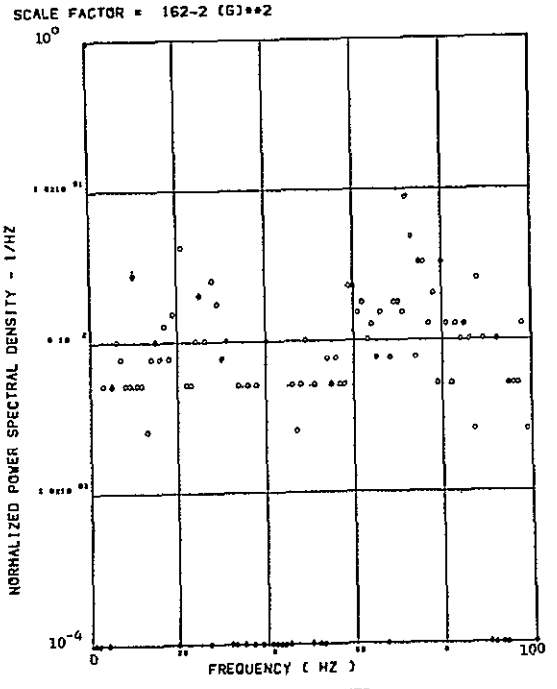

(g) - AB020 C G LATERAL ACCELEROMETER

Figure 19. Continued

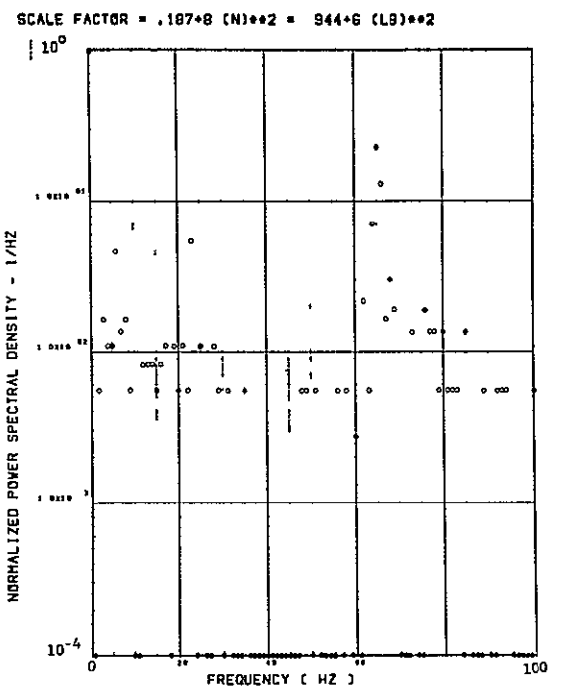

(h) - SW123 SHEAR AT WING STATION 1

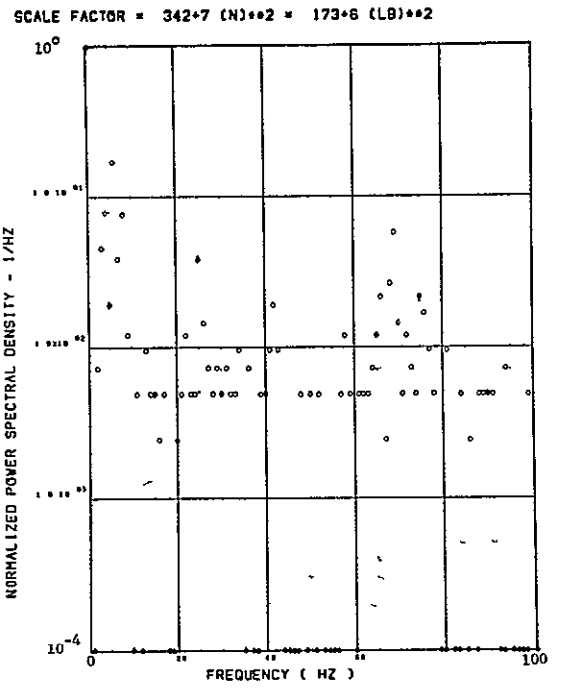

(i) - SW126 SHEAR AT WING STATION 2

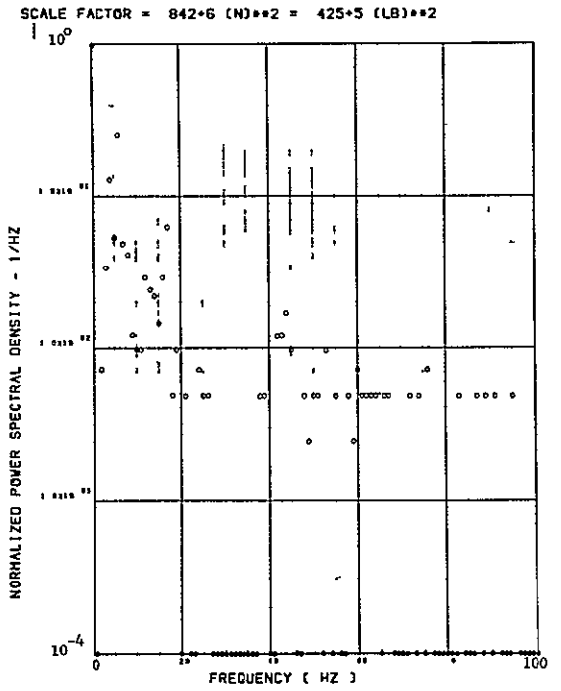

(j) - SW129 SHEAR AT WING STATION 3

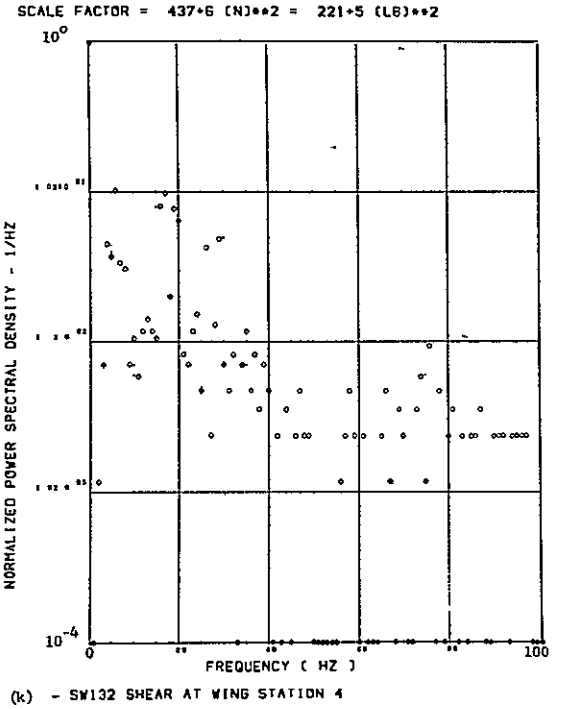

(k) - SW132 SHEAR AT WING STATION 4

Figure 19. Continued

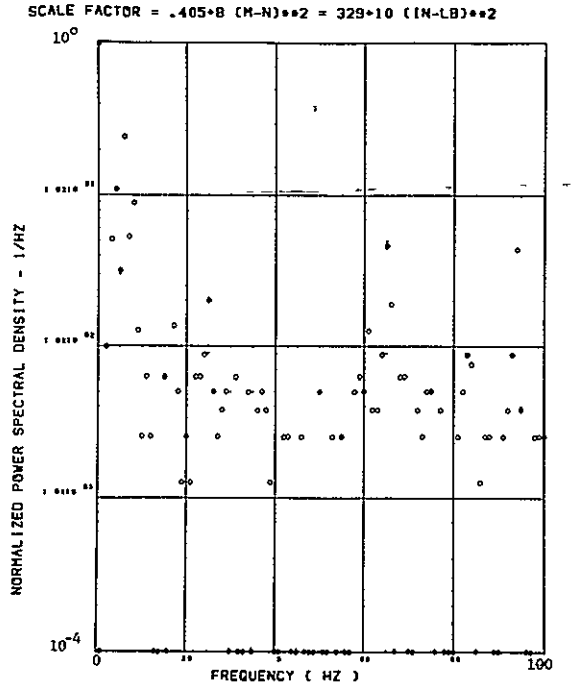

(l) - SW124 BENDING MOMENT AT WING STATION 1

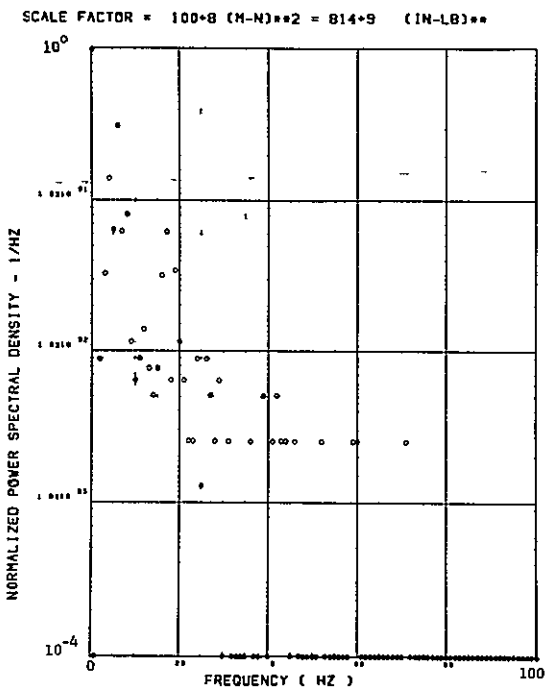

(m) - SW127 BENDING MOMENT AT WING STATION 2

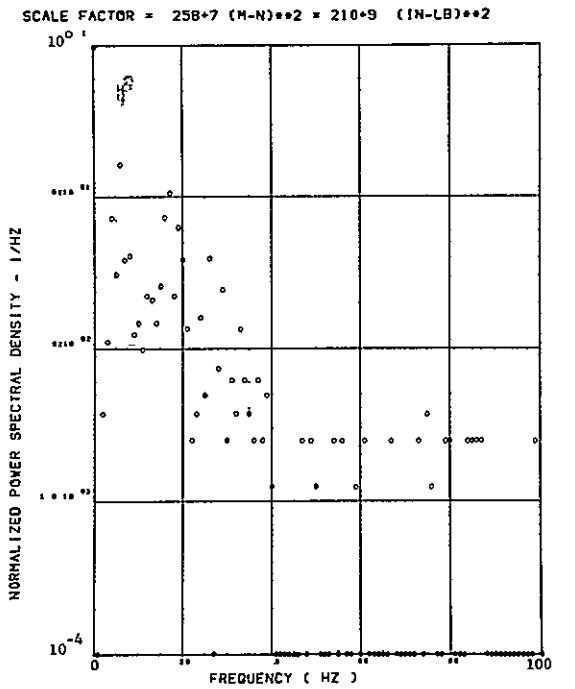

(n) - SW130 BENDING MOMENT AT WING STATION 3

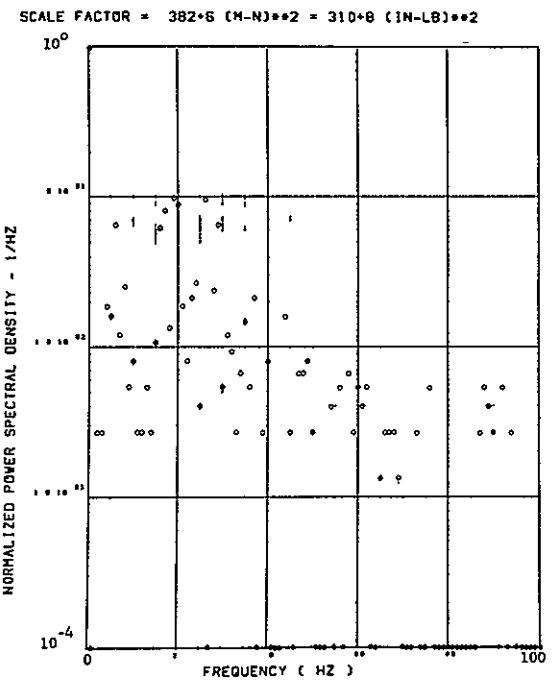

(o) - SW133 BENDING MOMENT AT WING STATION 4

Figure 19. Continued

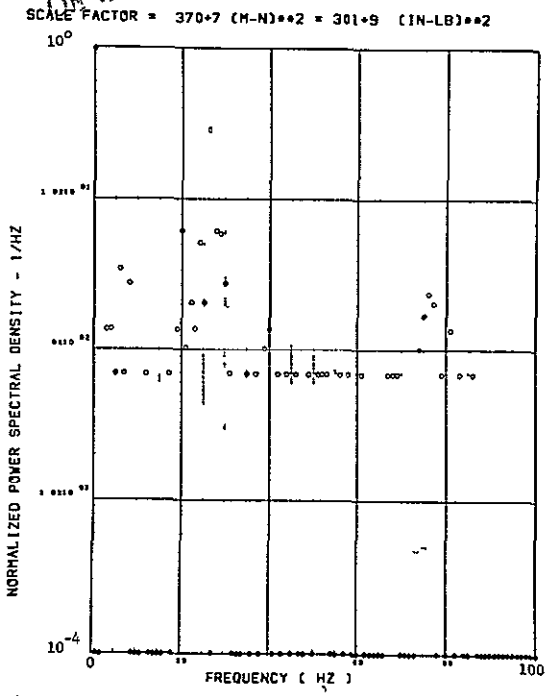

(p) - SW125 TORSION AT WING STATION 1

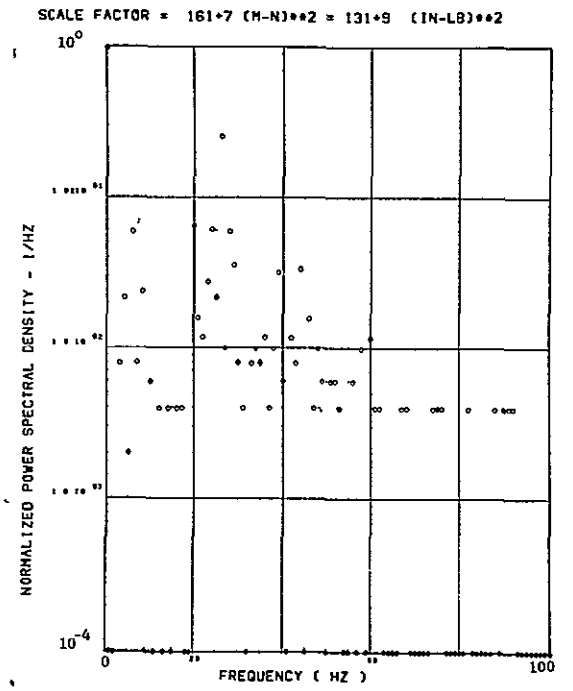

(q) - SW128 TORSION AT WING STATION 2

Data Not Available

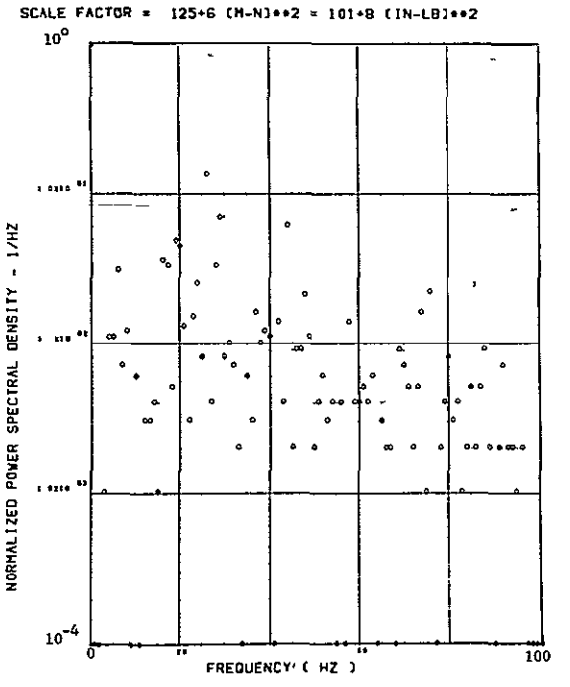

(s) - SW134 TORSION AT WING STATION 4

Figure 19. Concluded

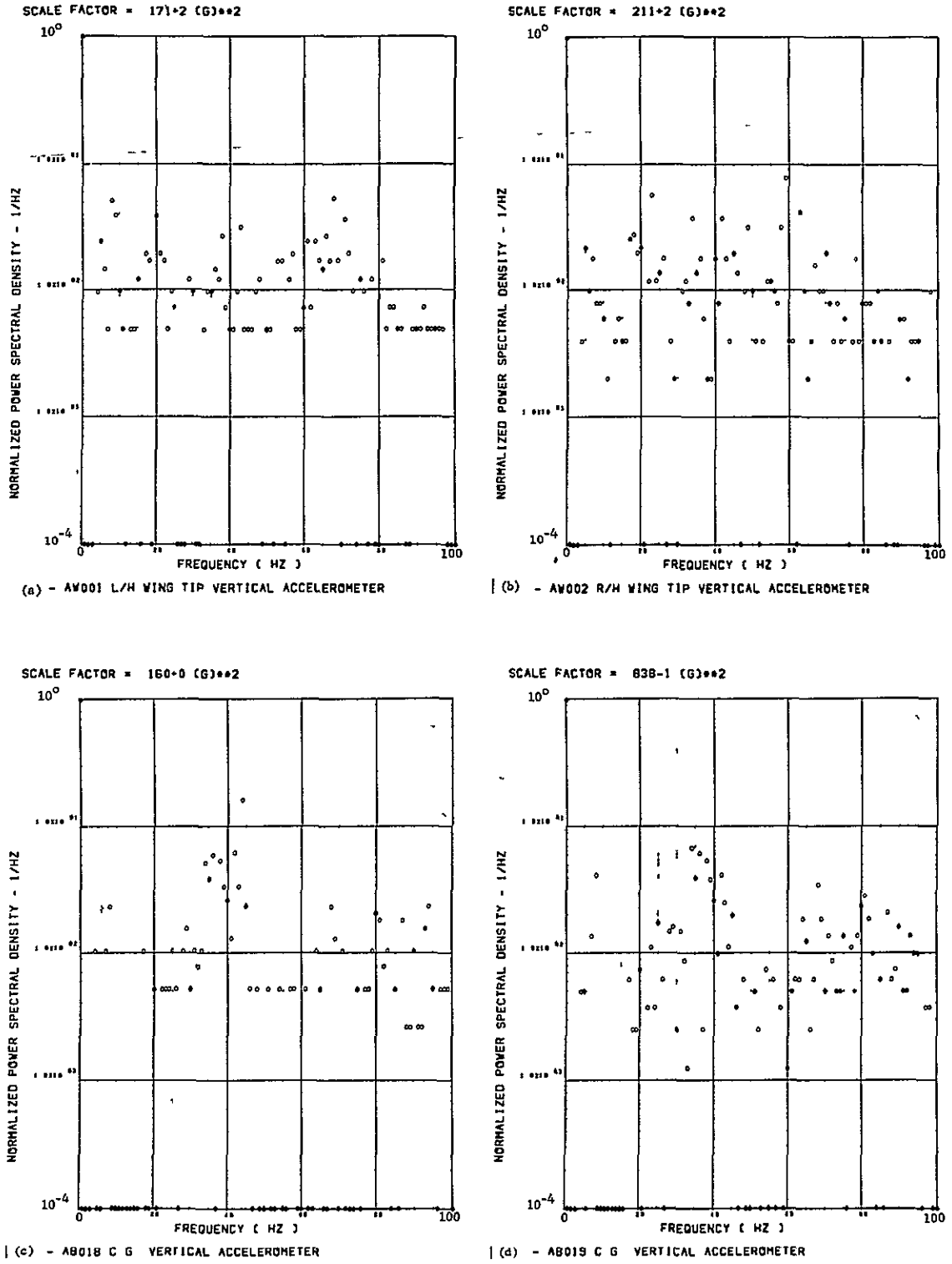

Figure 20. Power Spectra-Flight 77, Run S&C-R, Point 4 T_1=153319.0, ΔT=1 Sec, α_{Nom}=9.2 deg, $\Delta\alpha$=0.90 deg.

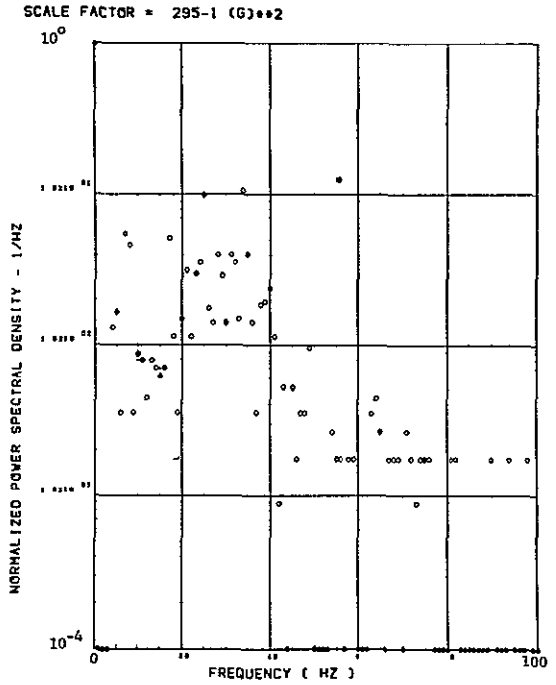

(e) - AF009 PILOT S SEAT VERTICAL ACCELEROMETER

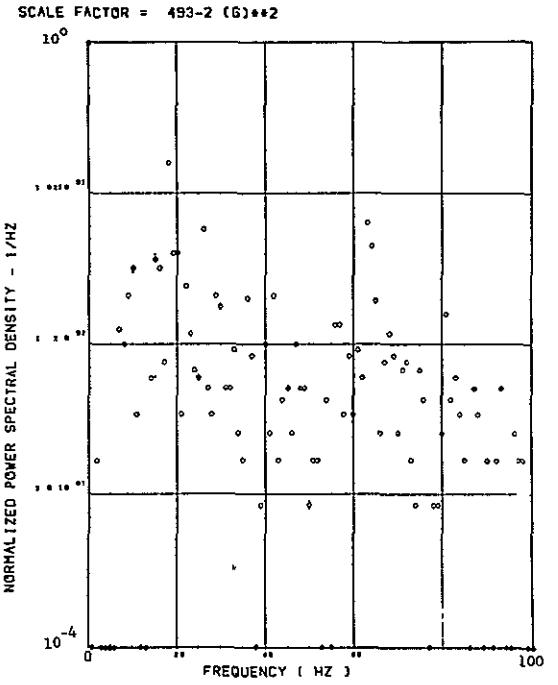

(f) - AF010 PILOT S SEAT LATERAL ACCELEROMETER

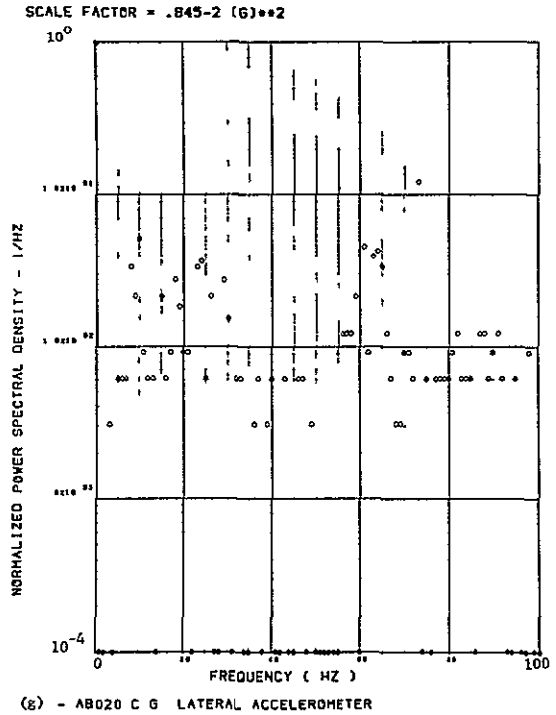

(g) - AB020 C G LATERAL ACCELEROMETER

Figure 20. Continued

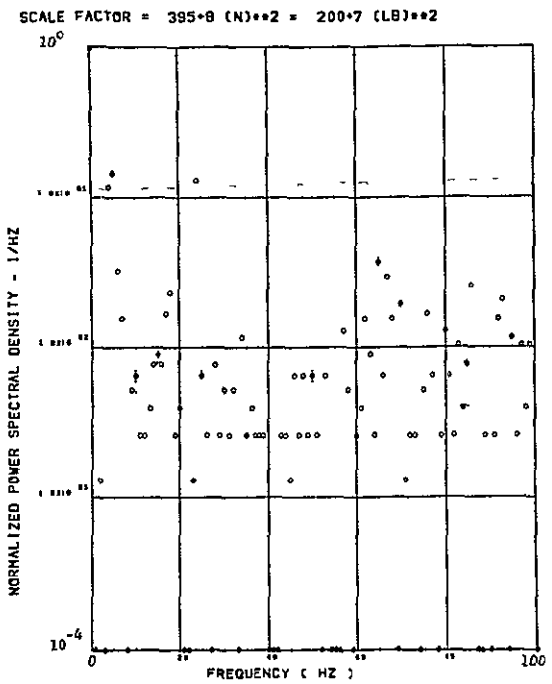

(h) - SW123 SHEAR AT WING STATION 1

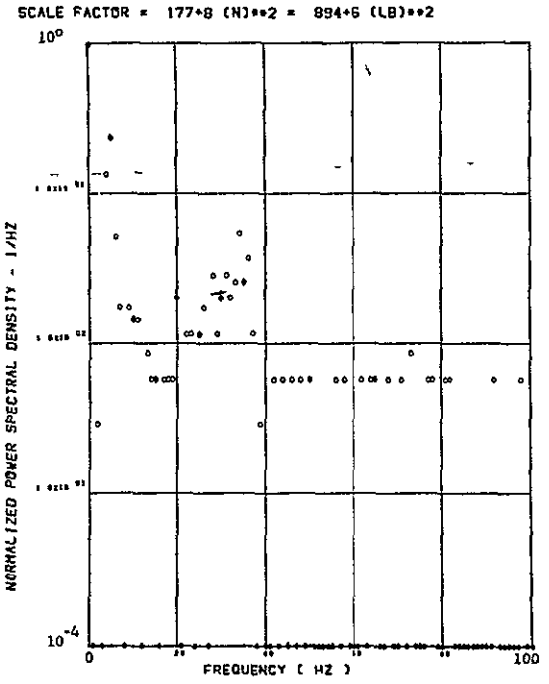

(i) - SW126 SHEAR AT WING STATION 2

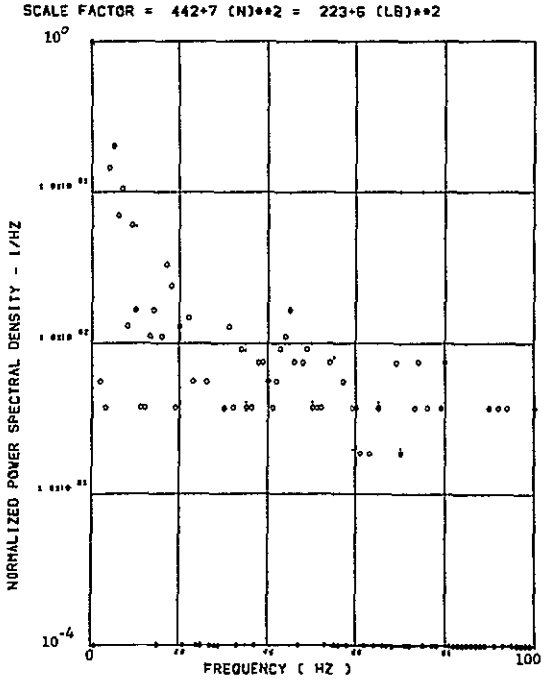

(j) - SW129 SHEAR AT WING STATION 3

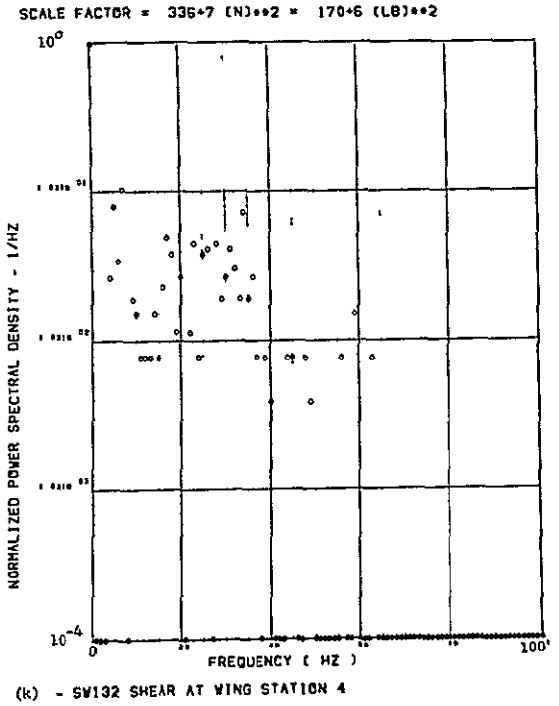

(k) - SW132 SHEAR AT WING STATION 4

Figure 20. Continued

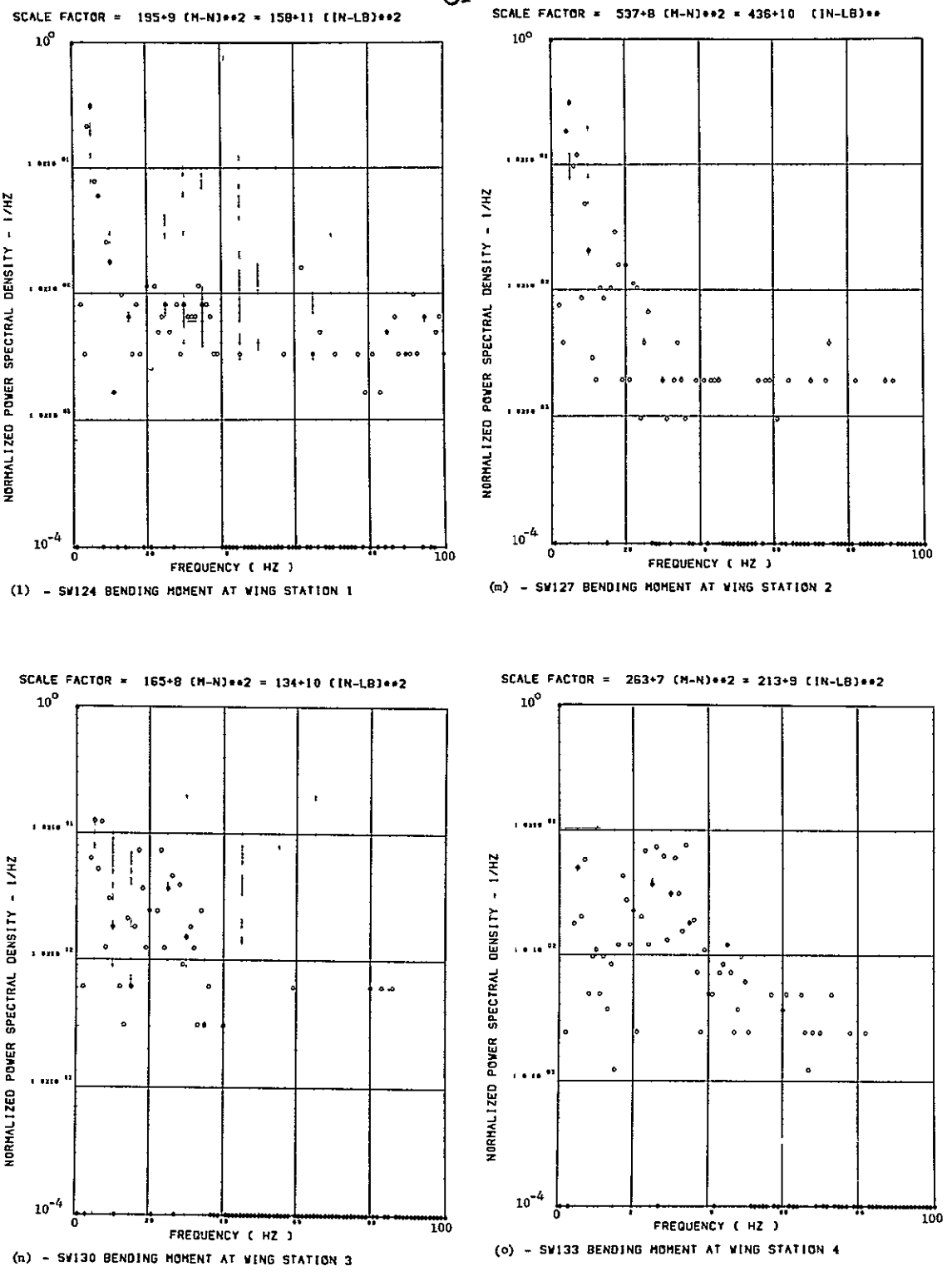

Figure 20. Continued

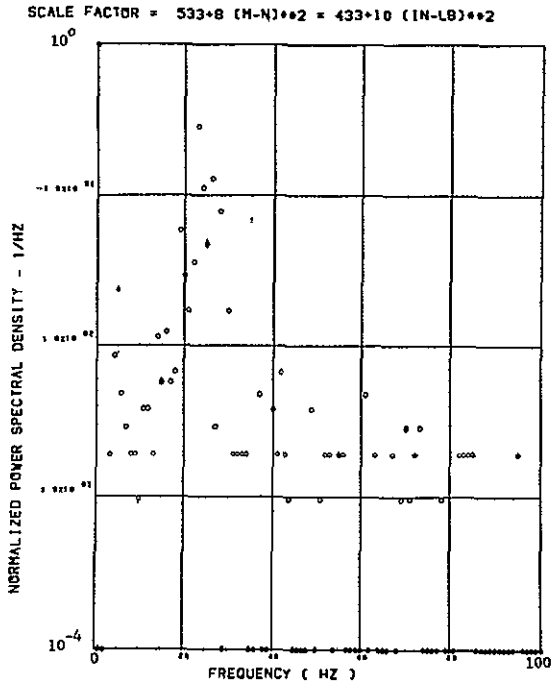

(p) - SW125 TORSION AT WING STATION 1

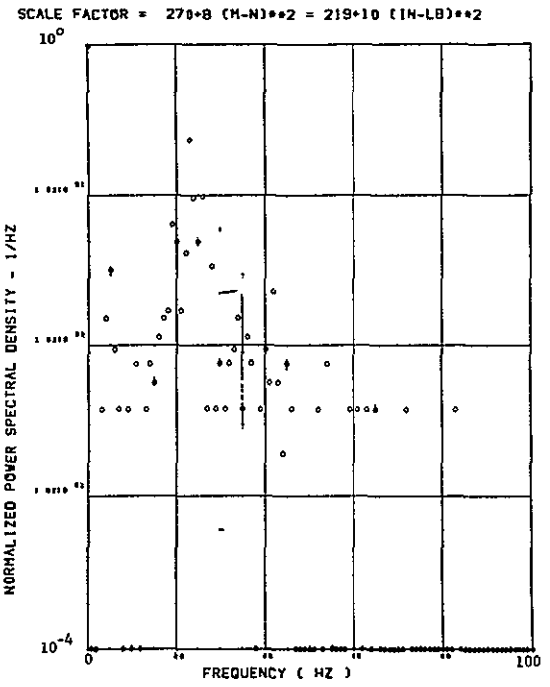

(q) - SW128 TORSION AT WING STATION 2

Data Not Available

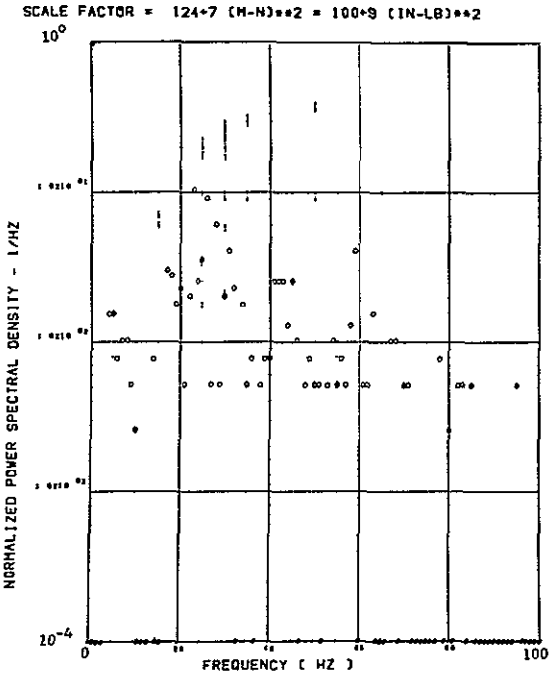

(s) - SW134 TORSION AT WING STATION 4

Figure 20. Concluded

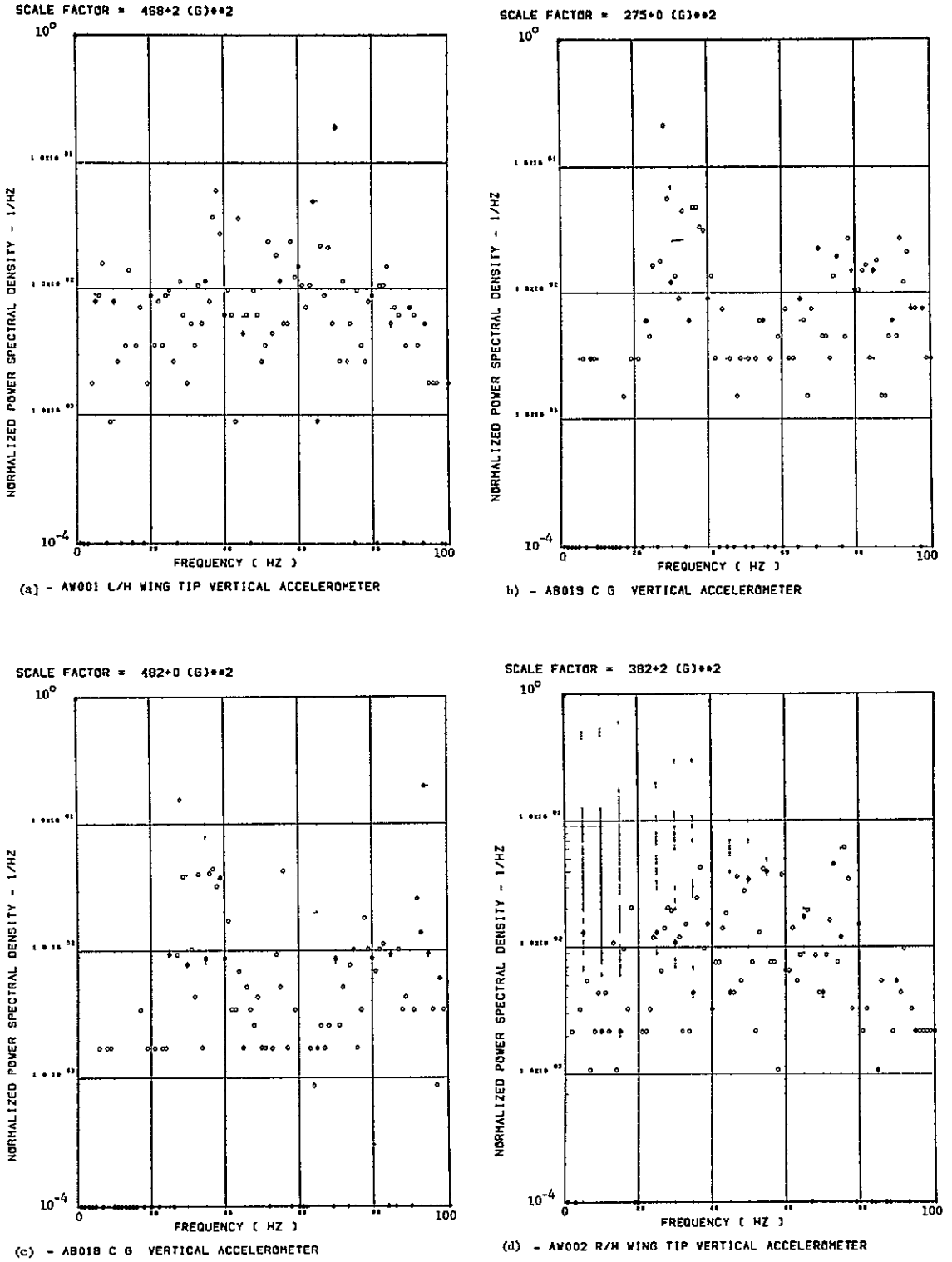

Figure 21. Power Spectra-Flight 77, Run S&C-R, Point 5, T_1=153322.85, ΔT=1 Sec, α_{Nom}=12.2 deg, $\Delta\alpha$=1.55 deg.

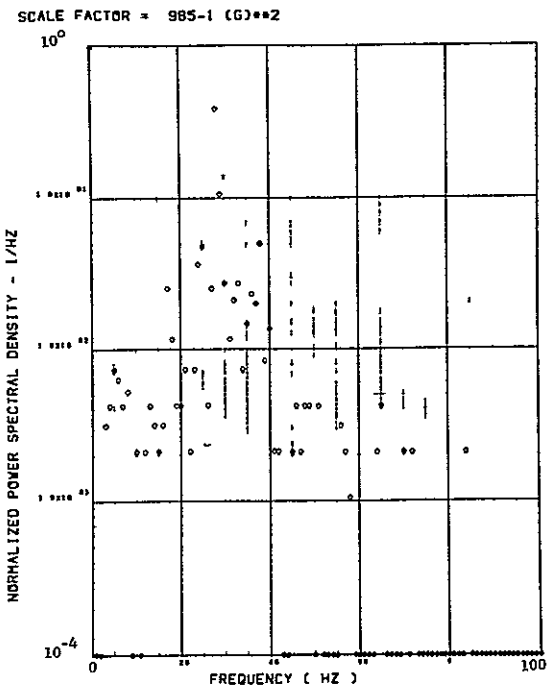

(e) - AF009 PILOT S SEAT VERTICAL ACCELEROMETER

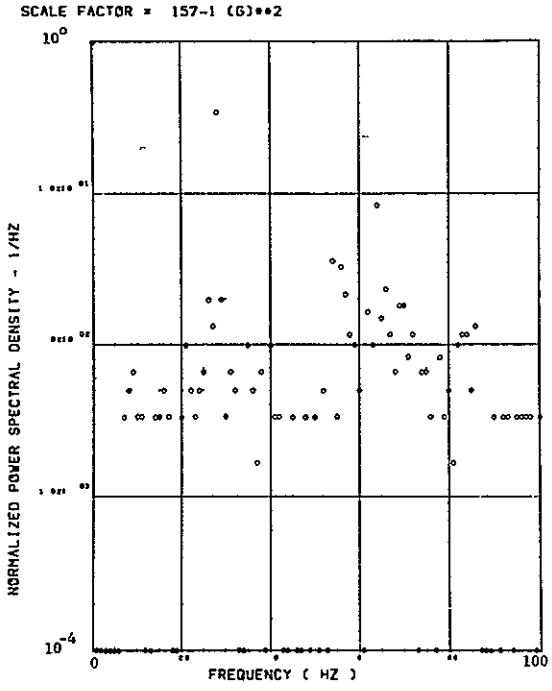

(f) - AF010 PILOT S SEAT LATERAL ACCELEROMETER

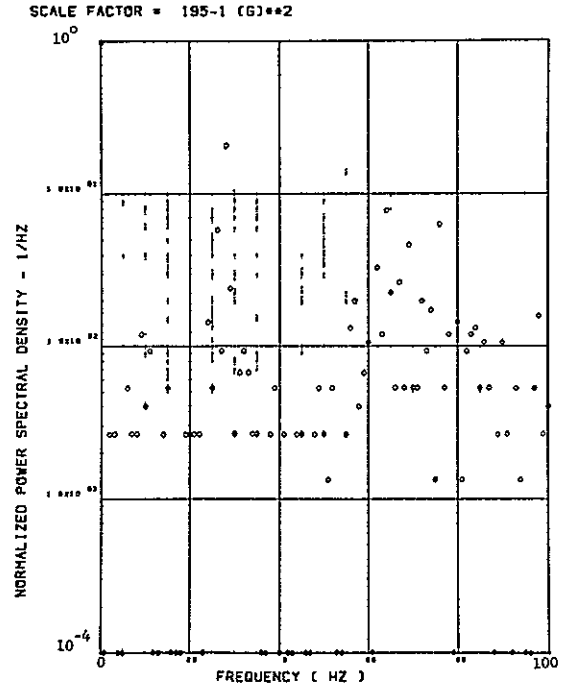

(g) - AB020 C G LATERAL ACCELEROMETER

Figure 21. Continued

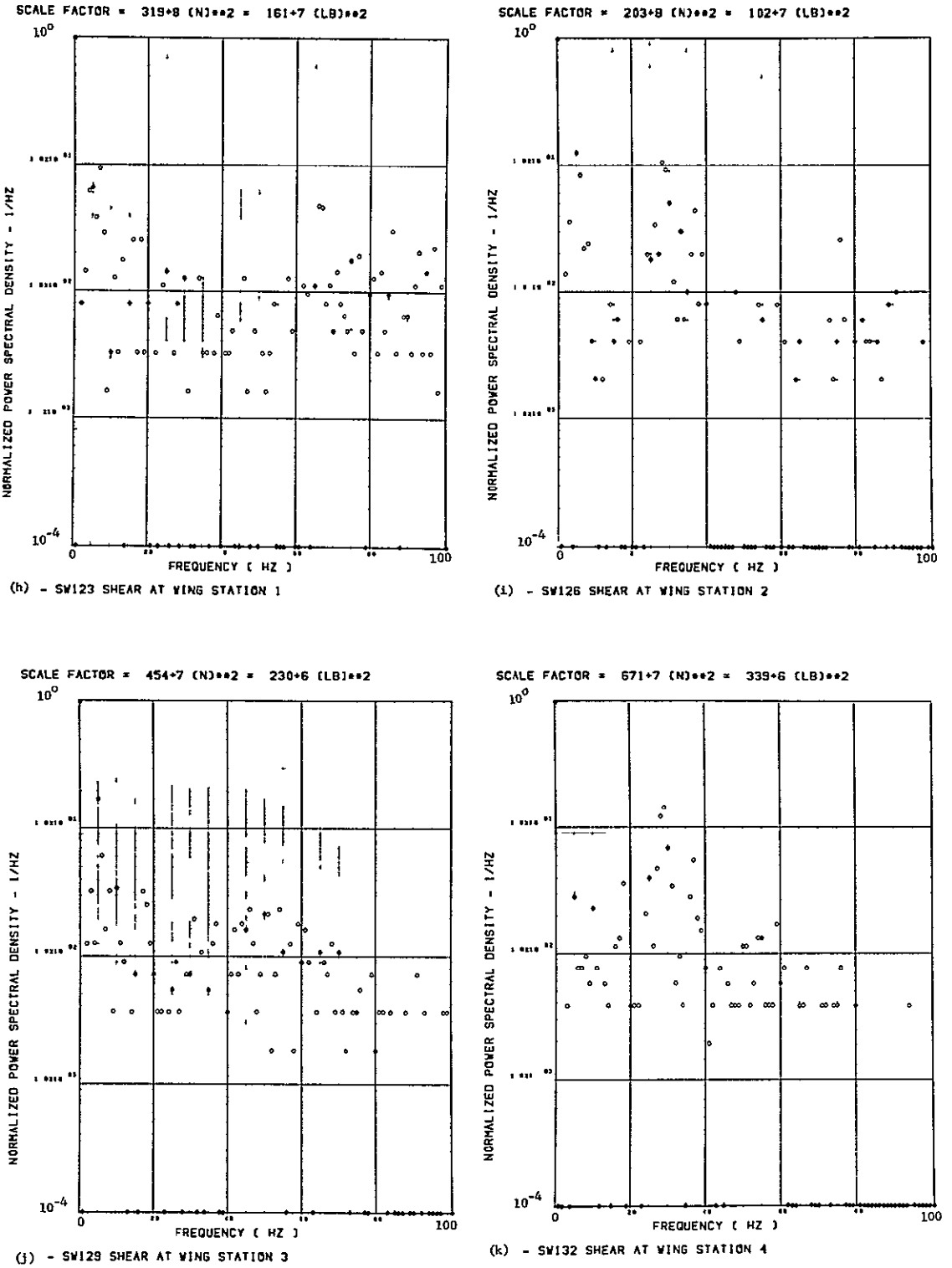

Figure 21. Continued

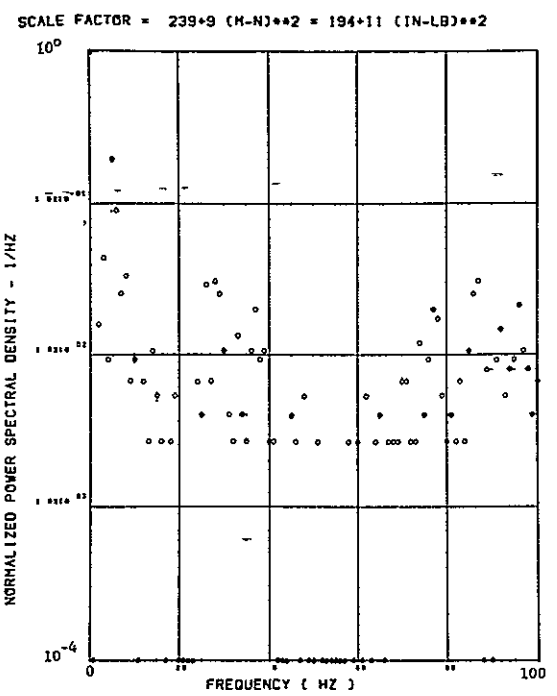

(l) - SW124 BENDING MOMENT AT WING STATION 1

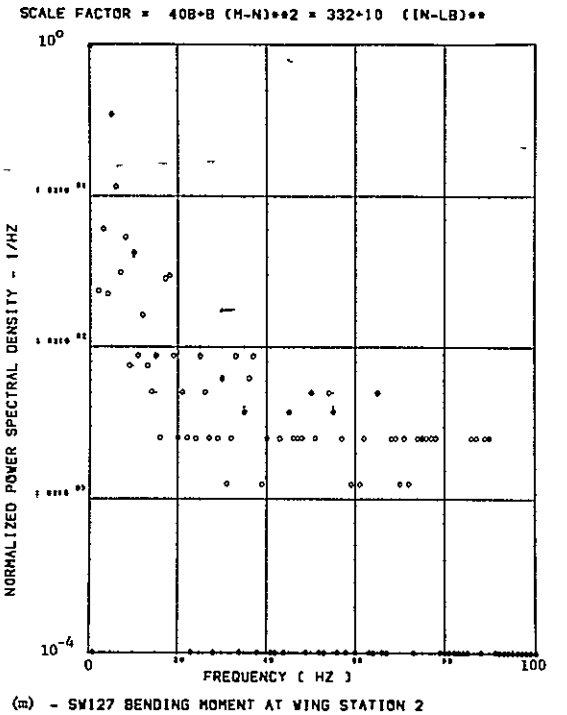

(m) - SW127 BENDING MOMENT AT WING STATION 2

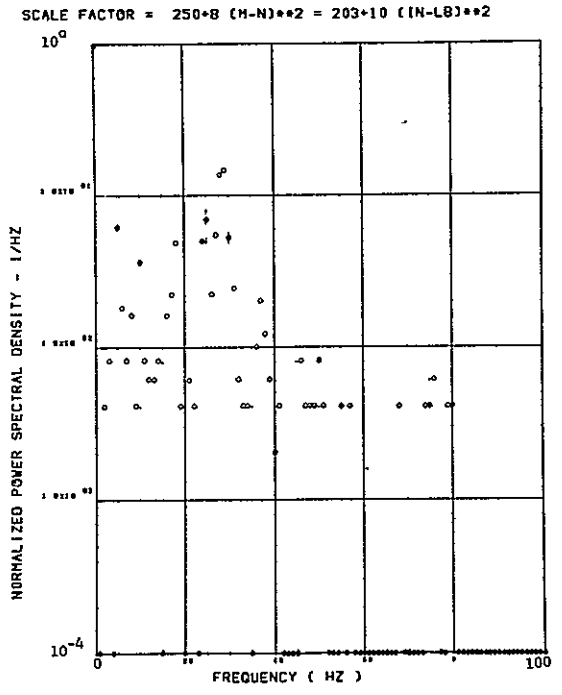

(n) - SW130 BENDING MOMENT AT WING STATION 3

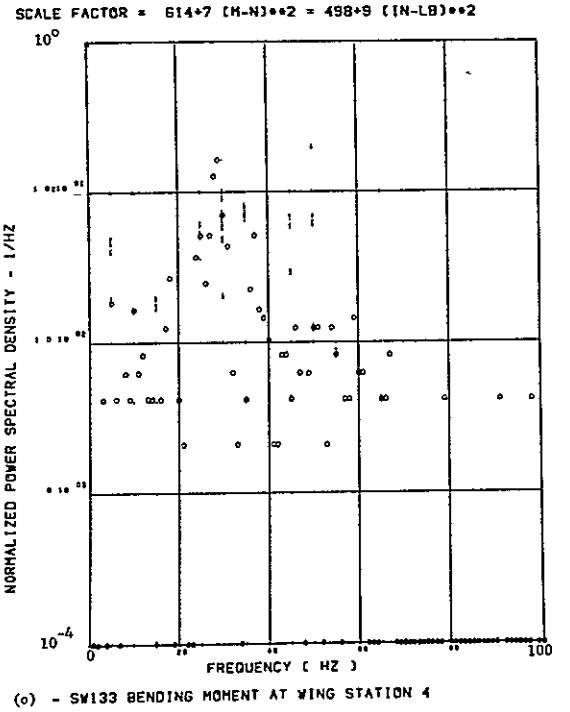

(o) - SW133 BENDING MOMENT AT WING STATION 4

Figure 21. Continued

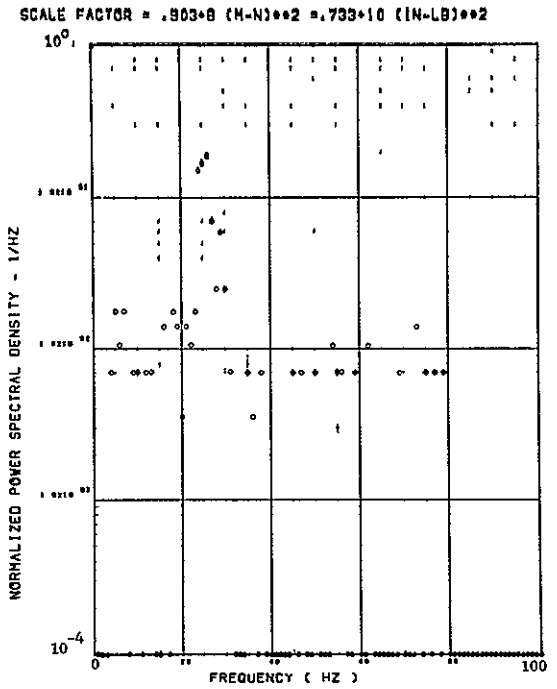

(p) - SW125 TORSION AT WING STATION 1

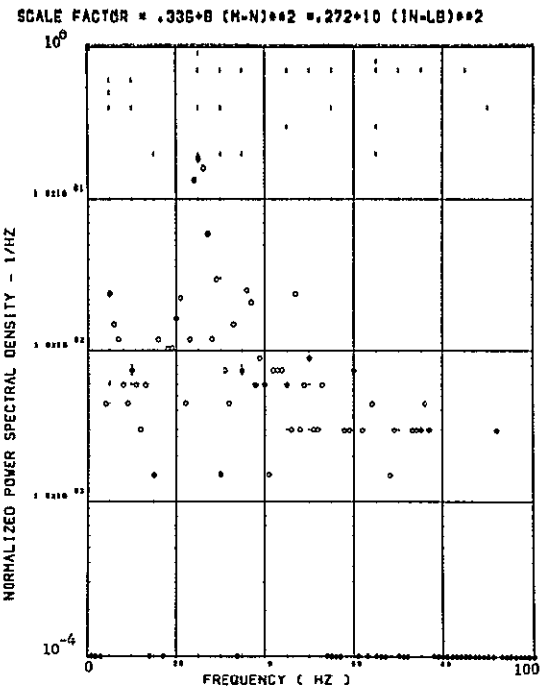

(q) - SW128 TORSION AT WING STATION 2

Data Not Available

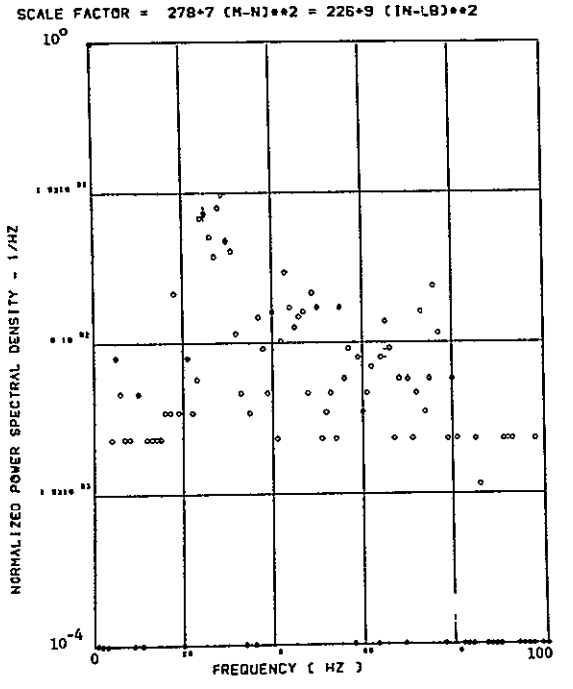

(s) - SW134 TORSION AT WING STATION 4

Figure 21. Concluded

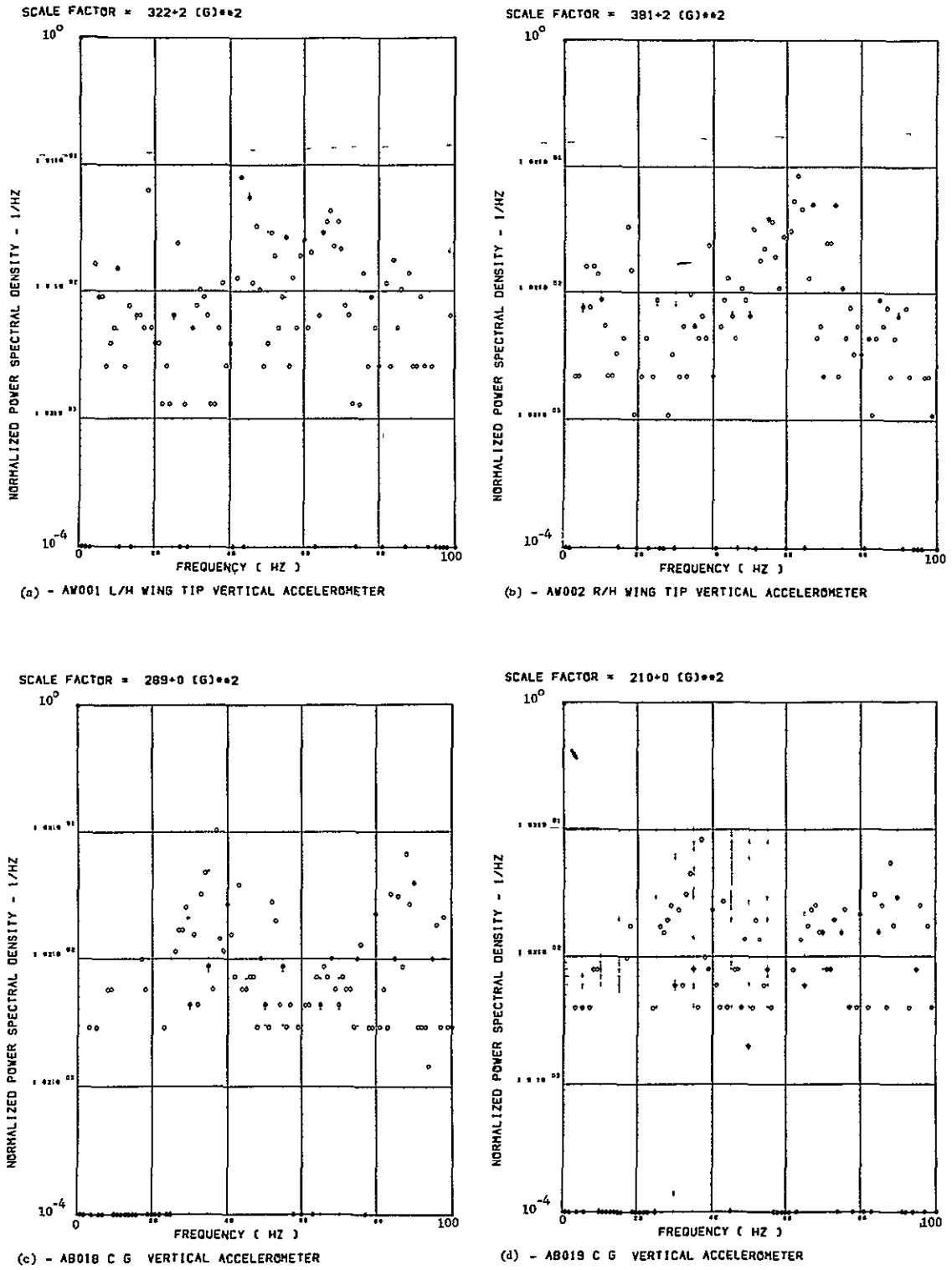

Figure 22. Power Spectra-Flight 77, Run S&C-R, Point 6, T_1=153325.3, ΔT=1 Sec, α_{Nom}=15.2 deg.

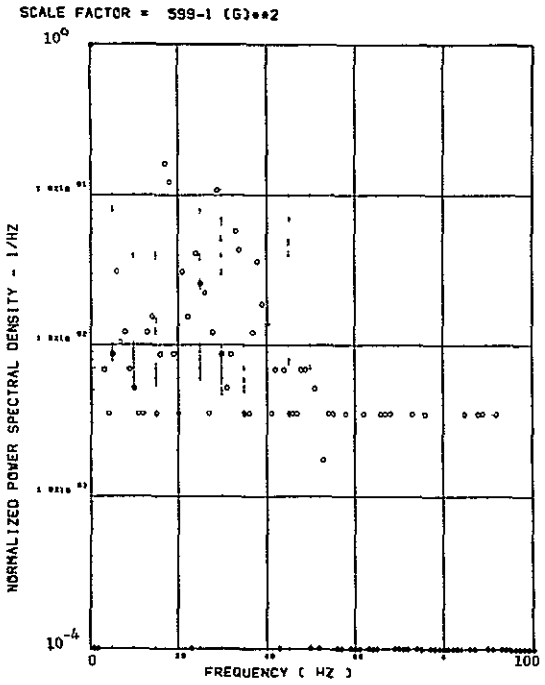

(e) - AF009 PILOT S SEAT VERTICAL ACCELEROMETER

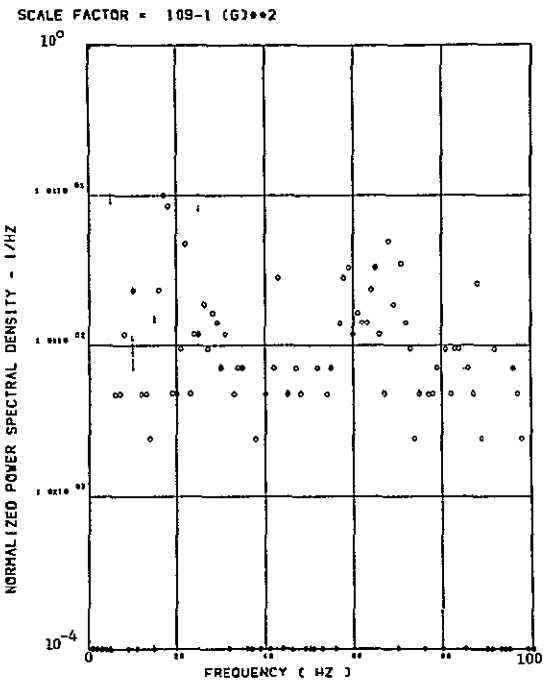

(f) - AF010 PILOT S SEAT LATERAL ACCELEROMETER

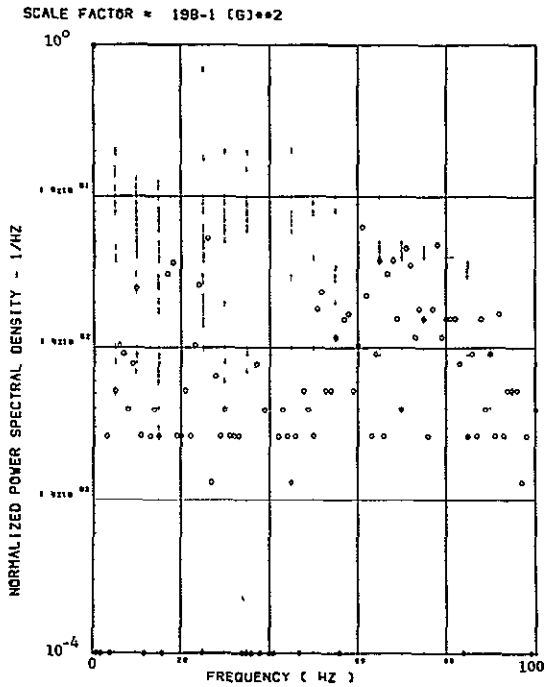

(g) - AB020 C G LATERAL ACCELEROMETER

Figure 22. Continued

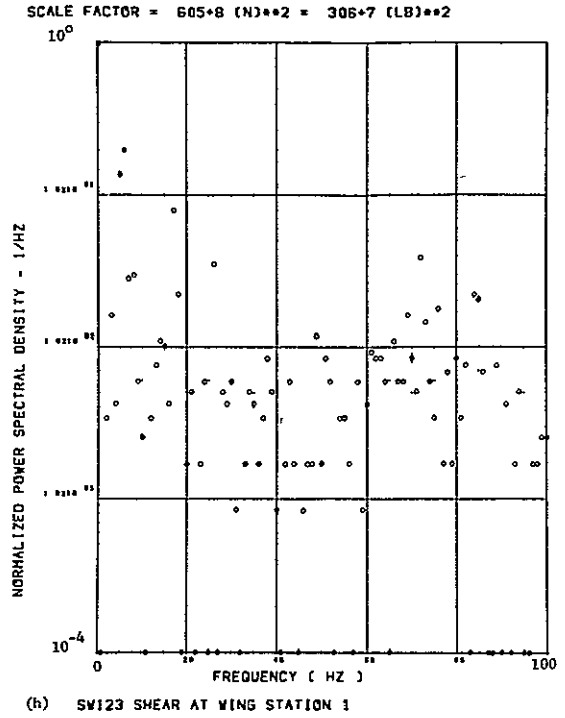

(h) SW123 SHEAR AT WING STATION 1

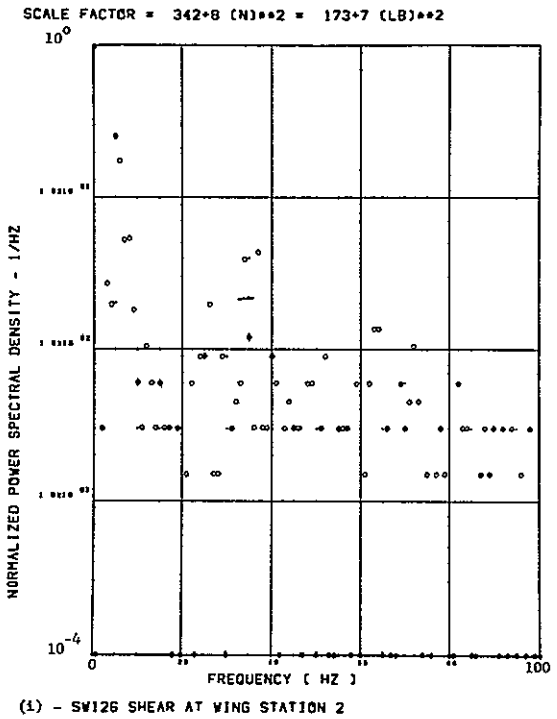

(i) - SW126 SHEAR AT WING STATION 2

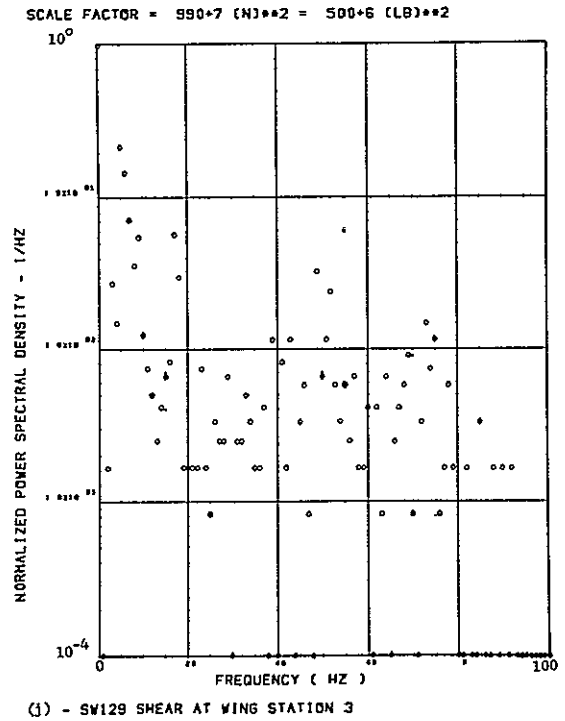

(j) - SW129 SHEAR AT WING STATION 3

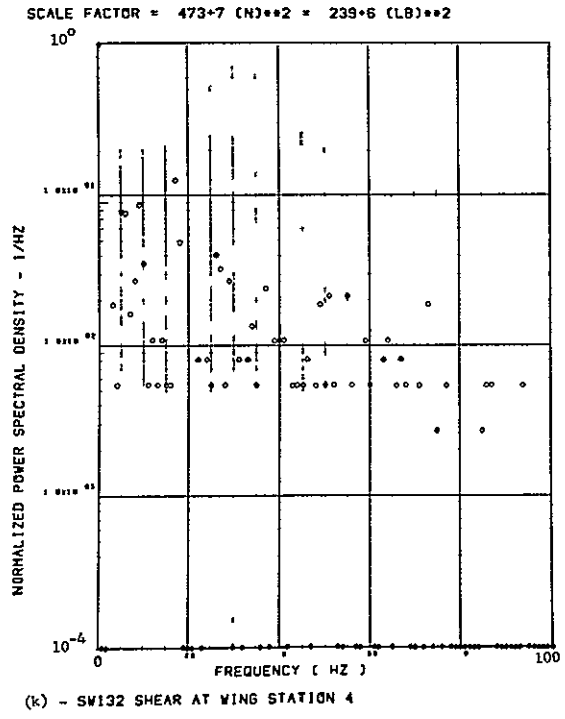

(k) - SW132 SHEAR AT WING STATION 4

Figure 22. Continued

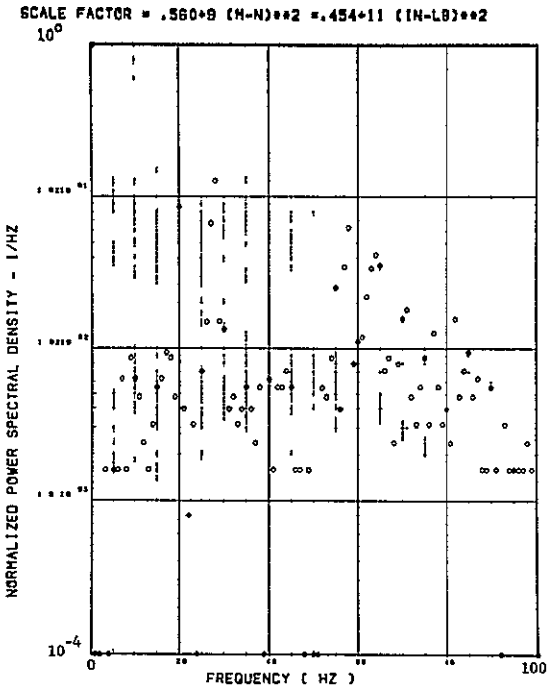

(l) - SW124 BENDING MOMENT AT WING STATION 1

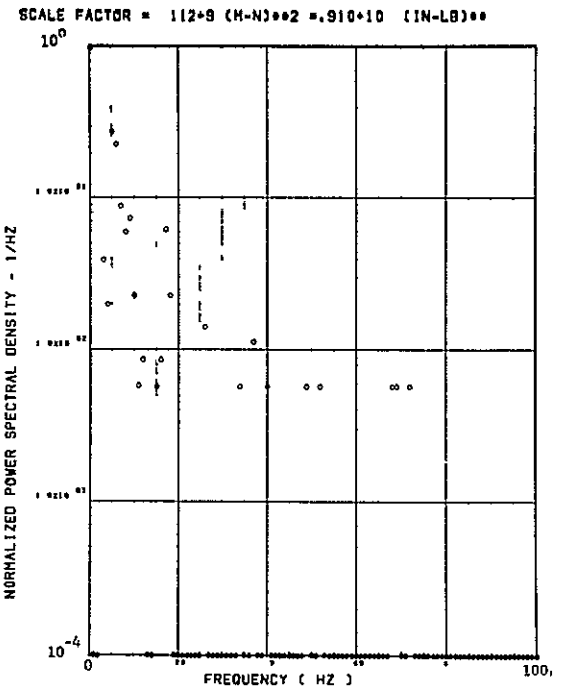

(m) - SW127 BENDING MOMENT AT WING STATION 2

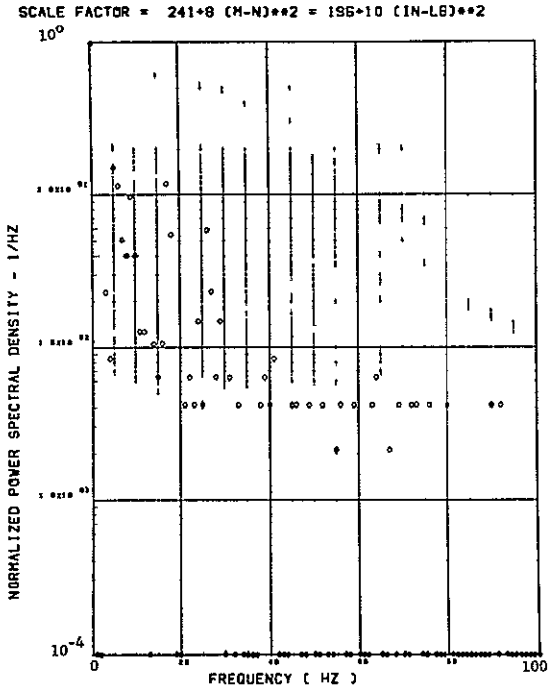

(o) - SW130 BENDING MOMENT AT WING STATION 3

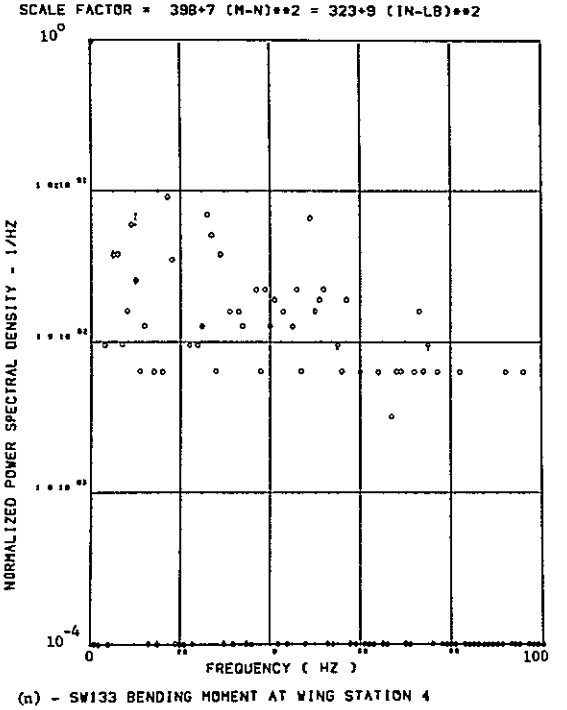

(n) - SW133 BENDING MOMENT AT WING STATION 4

Figure 22. Continued

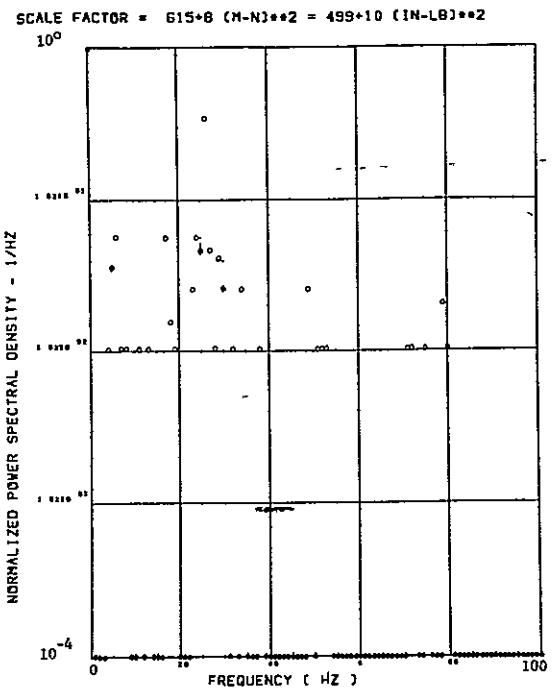

(a) - SW125 TORSION AT WING STATION 1

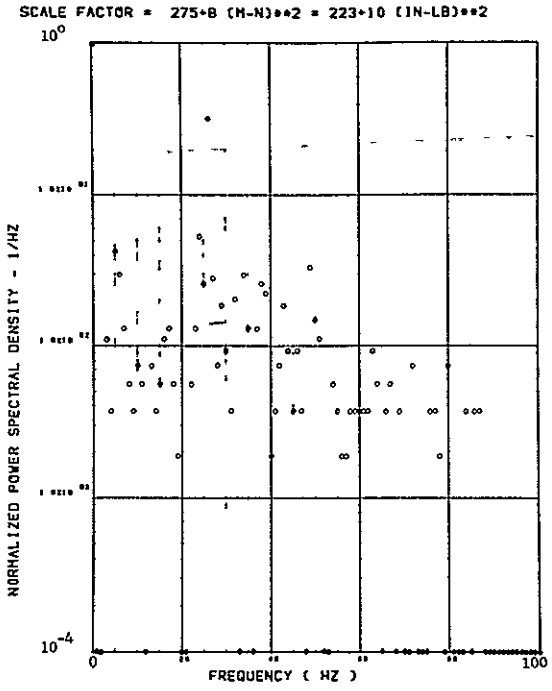

(b) - SW128 TORSION AT WING STATION 2

Data Not Available

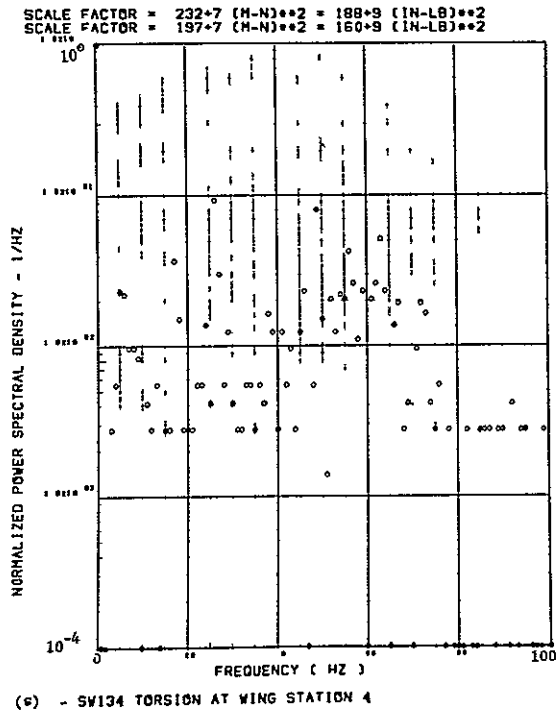

(c) - SW134 TORSION AT WING STATION 4

Figure 22. Concluded .

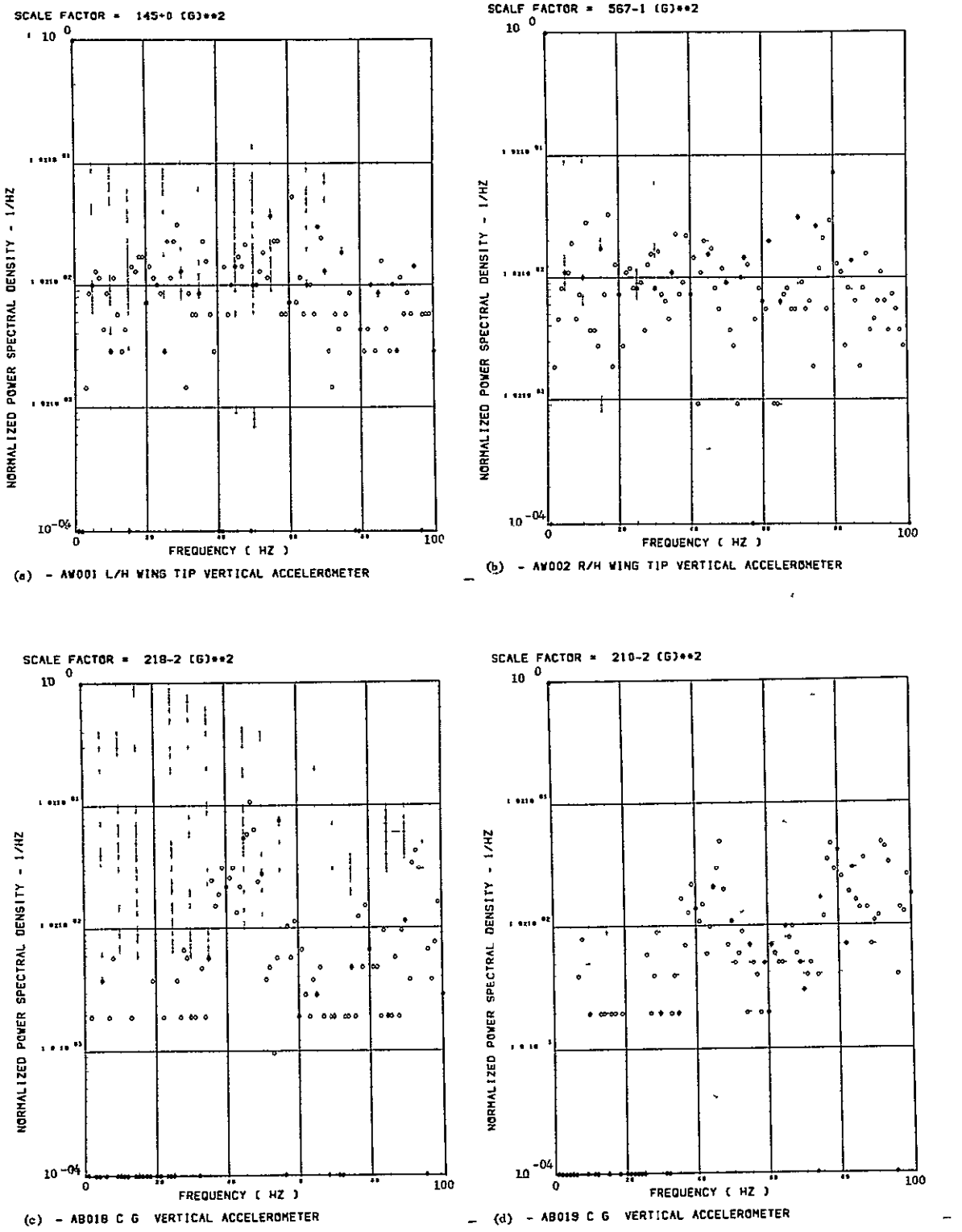

Figure 23. Power Spectra-Flight 77, Run S&C-R, Point 7, T_1=153311.0, ΔT=2 Sec, α_{Nom}=5.1 deg, $\Delta\alpha$=1.76 deg.

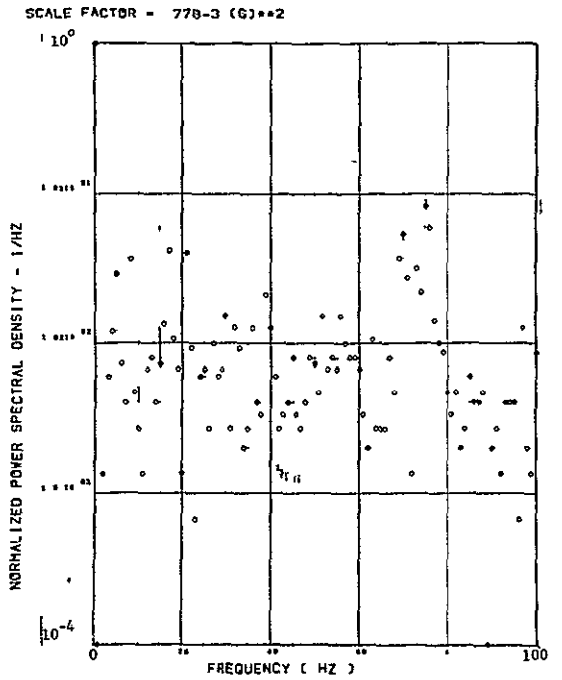

(e) - AF009 PILOT S SEAT VERTICAL ACCELEROMETER

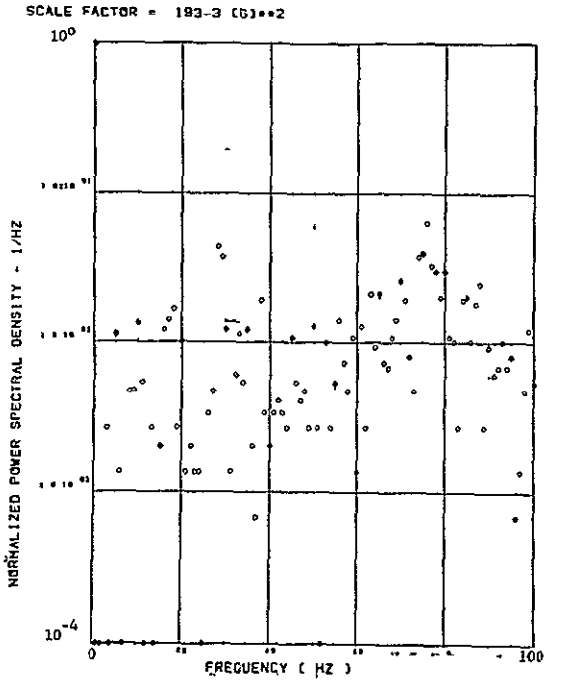

(f) - AF010 PILOT S SEAT LATERAL ACCELEROMETER

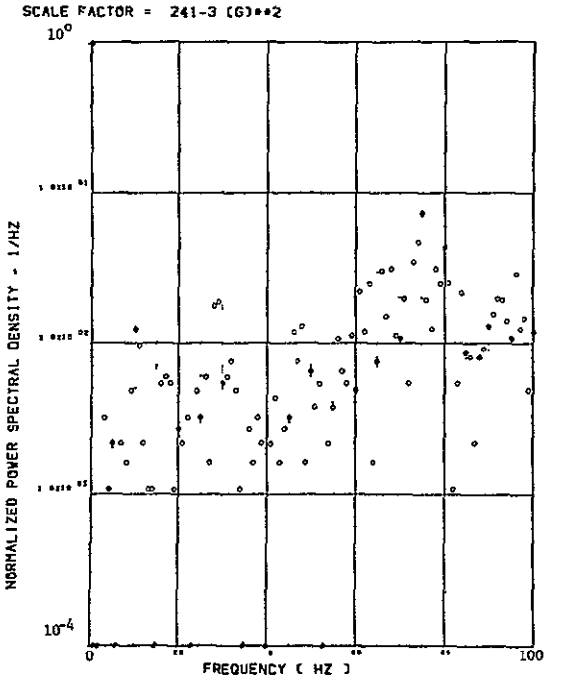

(g) - AB020 C G LATERAL ACCELEROMETER

Figure 23. Continued

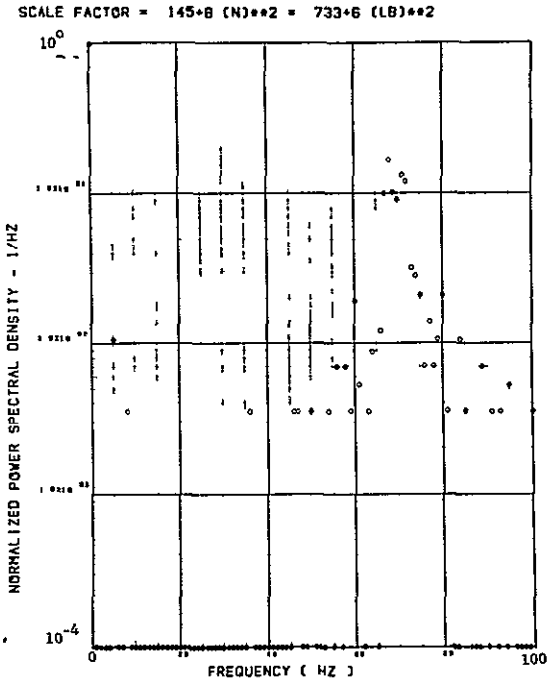

(h) - SW123 SHEAR AT WING STATION 1

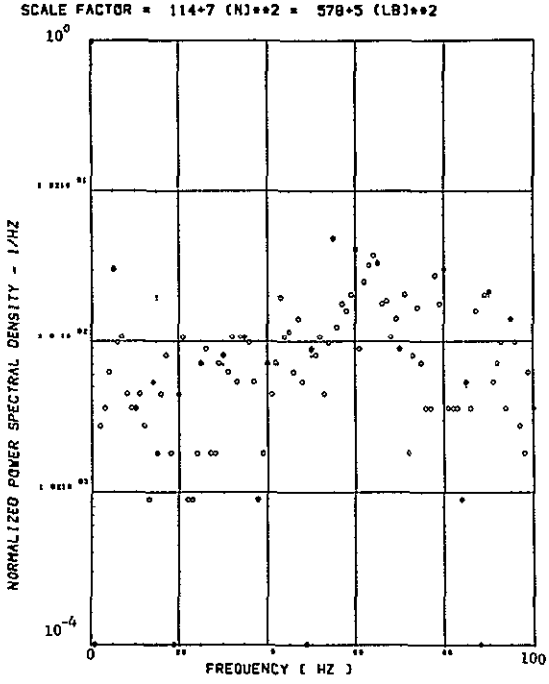

(i) - SW126 SHEAR AT WING STATION 2

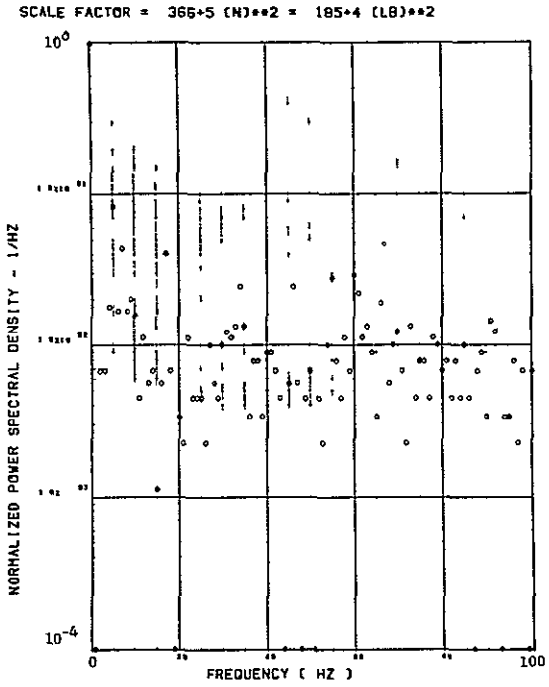

(j) - SW129 SHEAR AT WING STATION 3

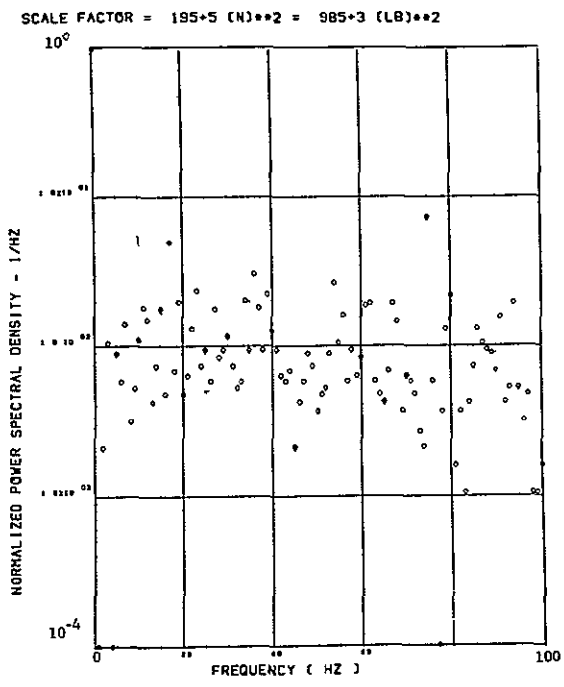

(k) - SW132 SHEAR AT WING STATION 4

Figure 23. Continued

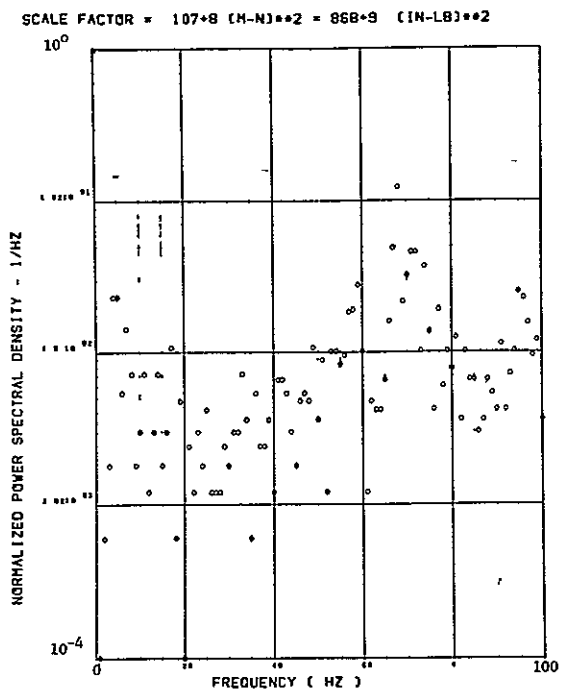

(l) - SW124 BENDING MOMENT AT WING STATION 1

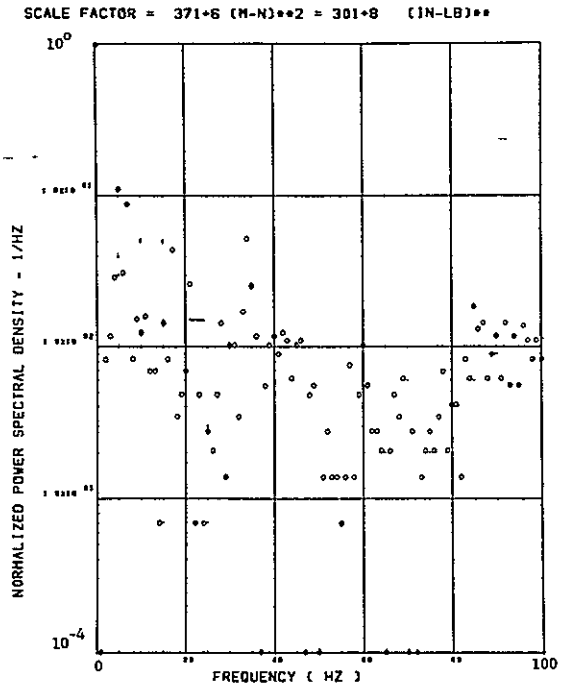

(m) - SW127 BENDING MOMENT AT WING STATION 2

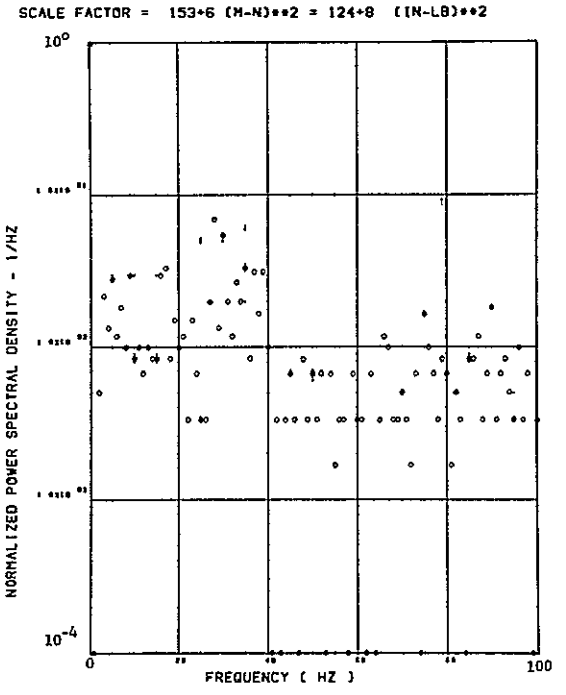

(n) - SW130 BENDING MOMENT AT WING STATION 3

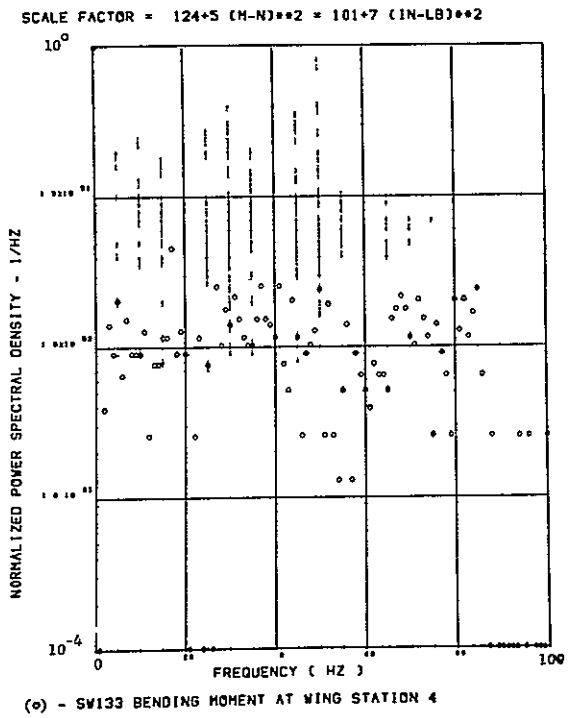

(o) - SW133 BENDING MOMENT AT WING STATION 4

Figure 23. Continued

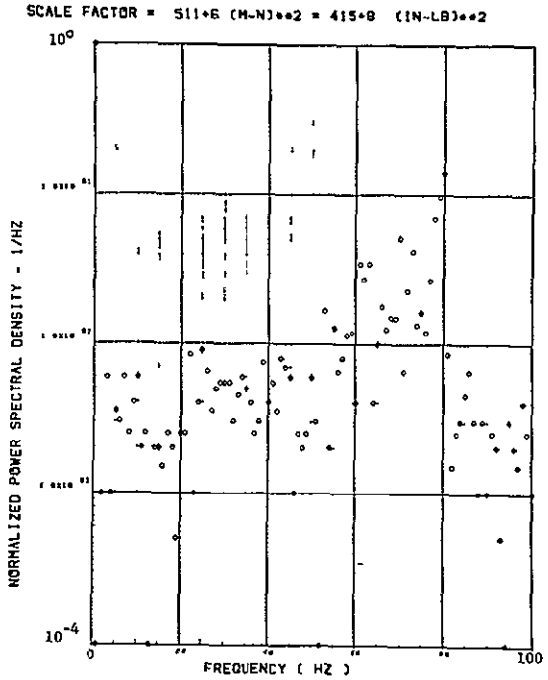

(p) - SW125 TORSION AT WING STATION 1

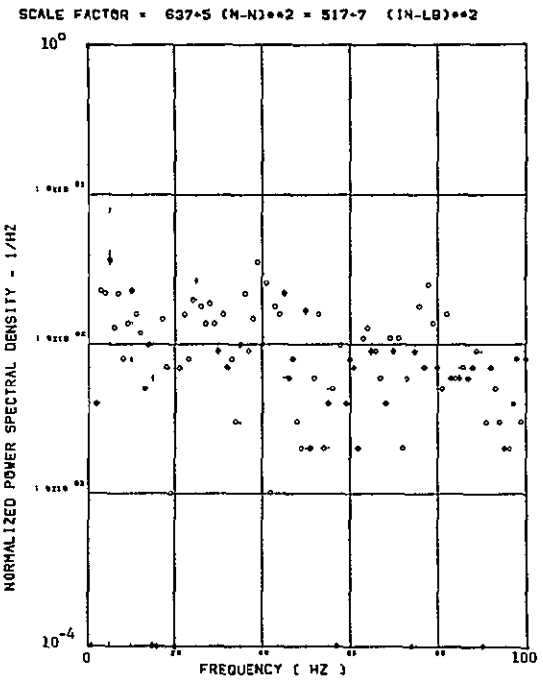

(q) - SW128 TORSION AT WING STATION 2

Data Not Available

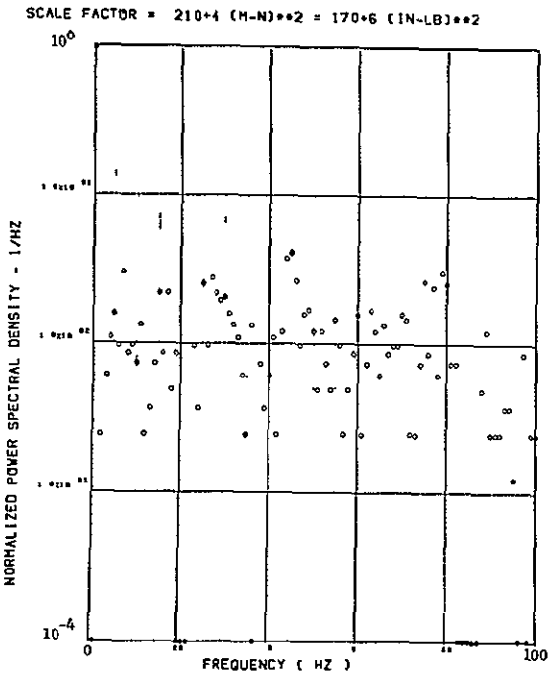

(s) - SW134 TORSION AT WING STATION 4

Figure 23. Concluded

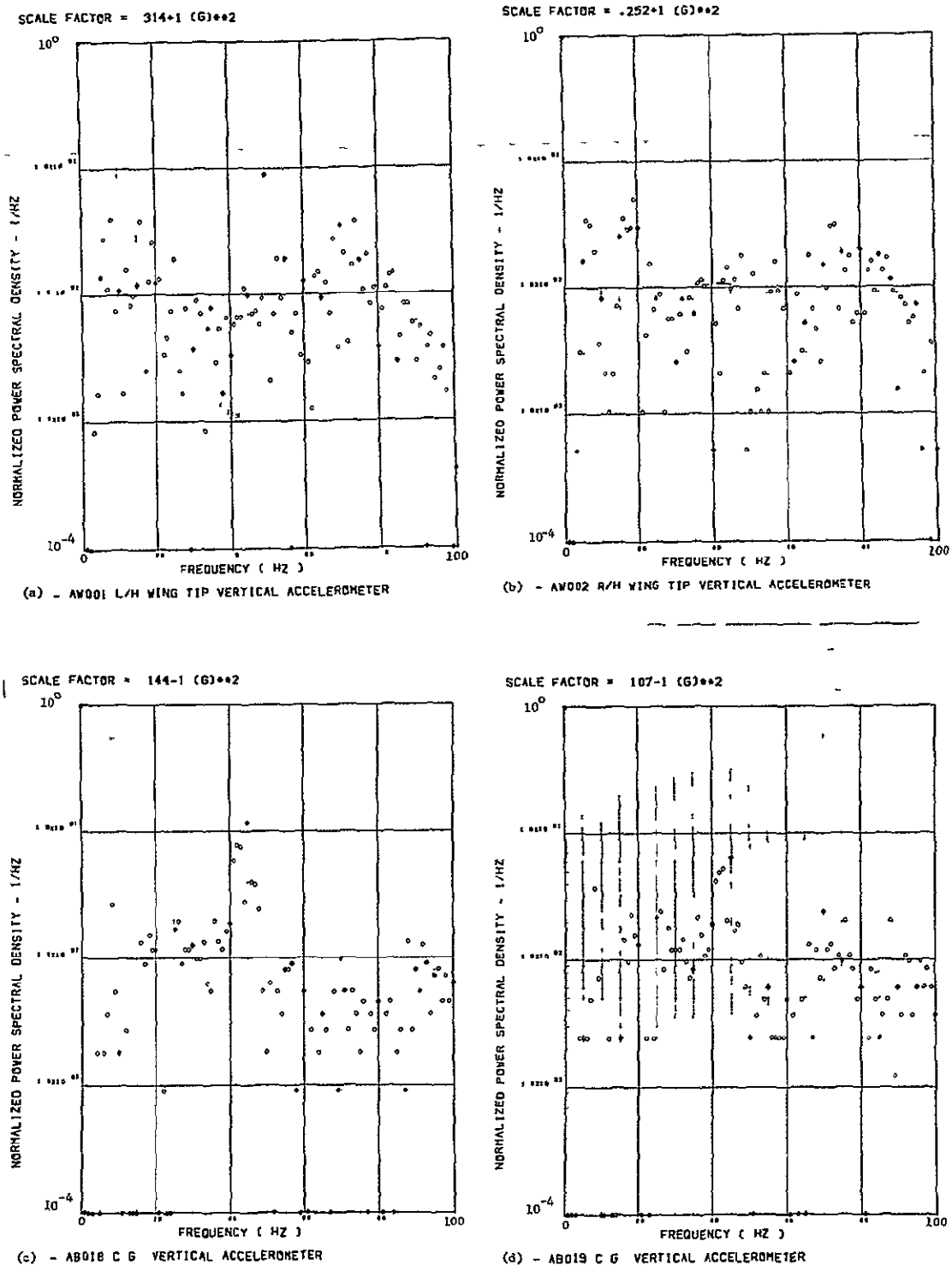

Figure 24. Power Spectra-Flight 77, Run S&C-R, Point 8, T_1=153315.5, ΔT=2 Sec, α_{Nom}=7.1 deg, $\Delta\alpha$=0.32 deg.

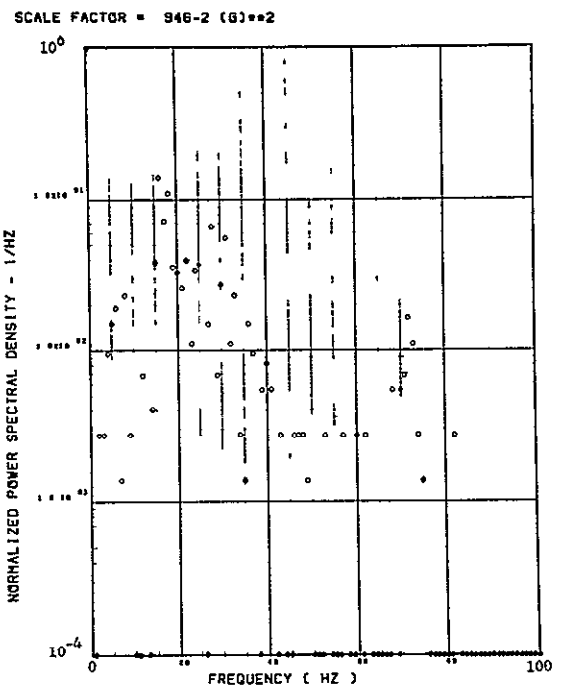

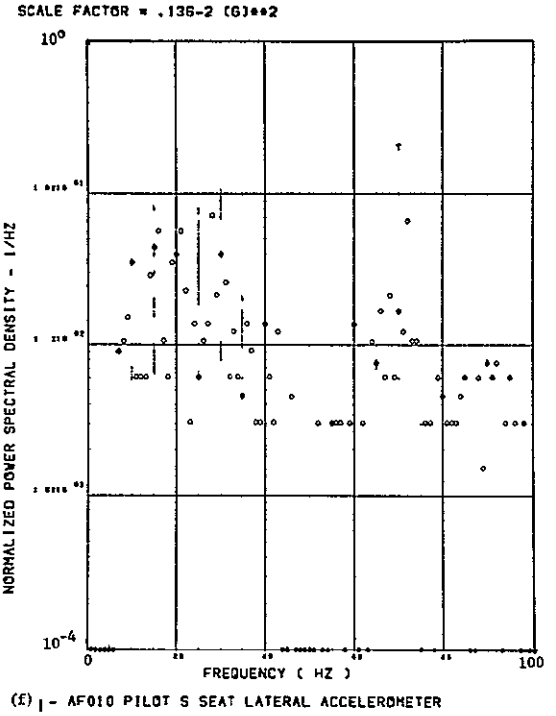

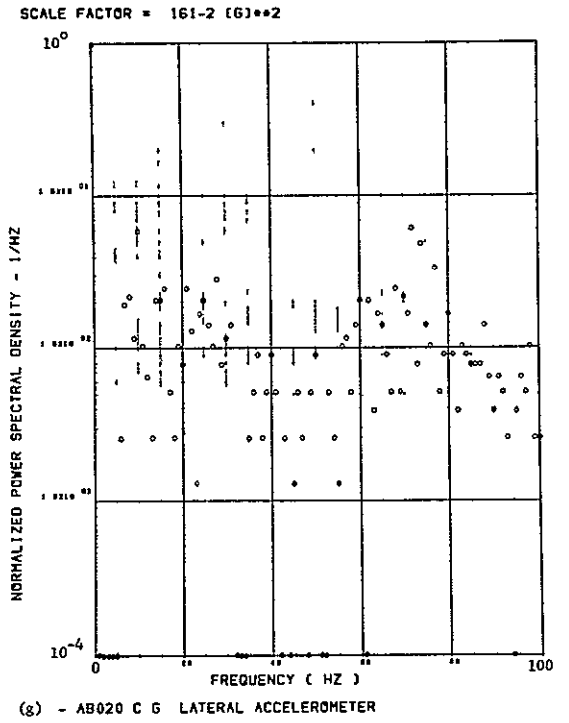

Figure 24. Continued

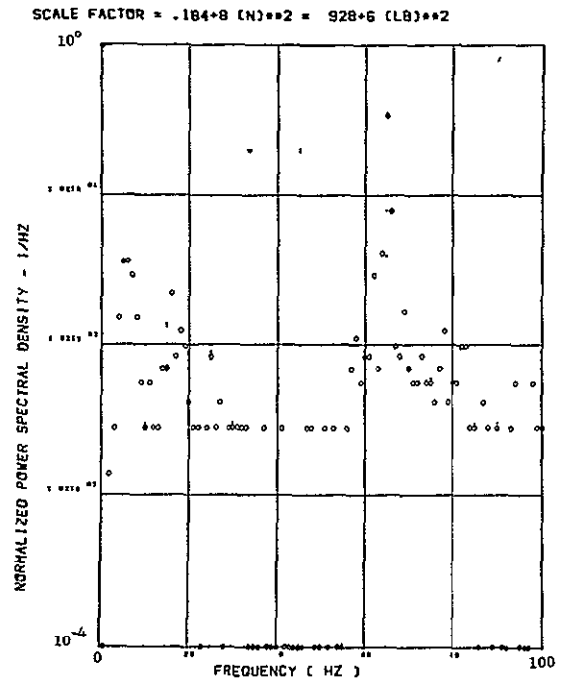

(h) - SW123 SHEAR AT WING STATION 1

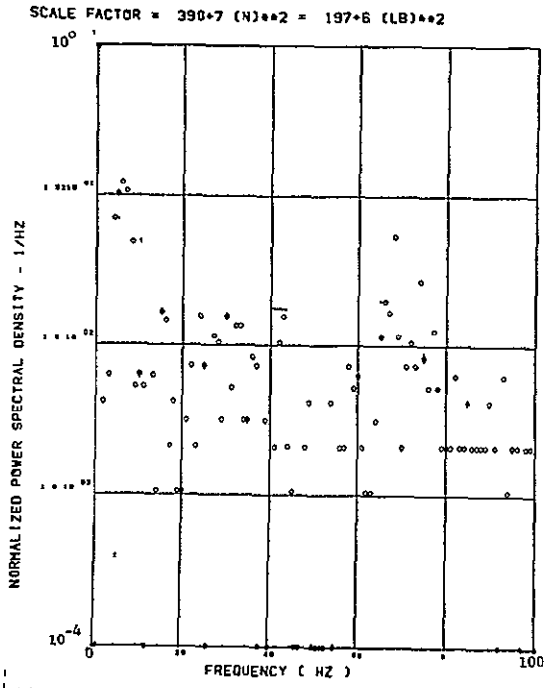

(i) - SW126 SHEAR AT WING STATION 2

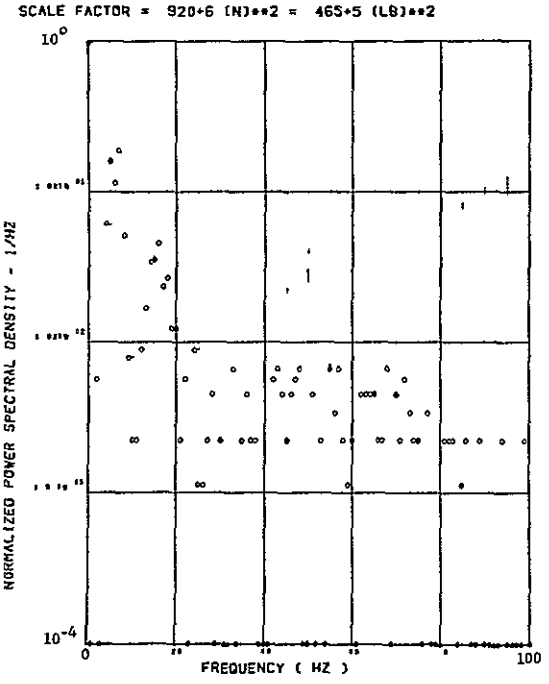

(j) - SW129 SHEAR AT WING STATION 3

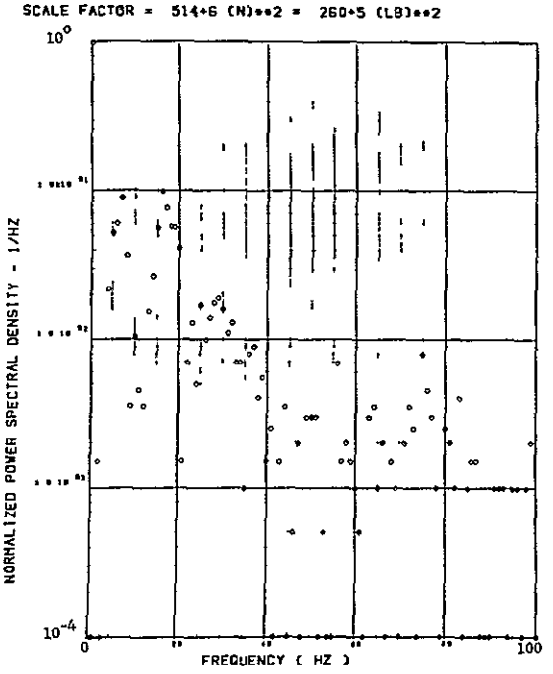

(k) - SW132 SHEAR AT WING STATION 4

Figure 24. Continued

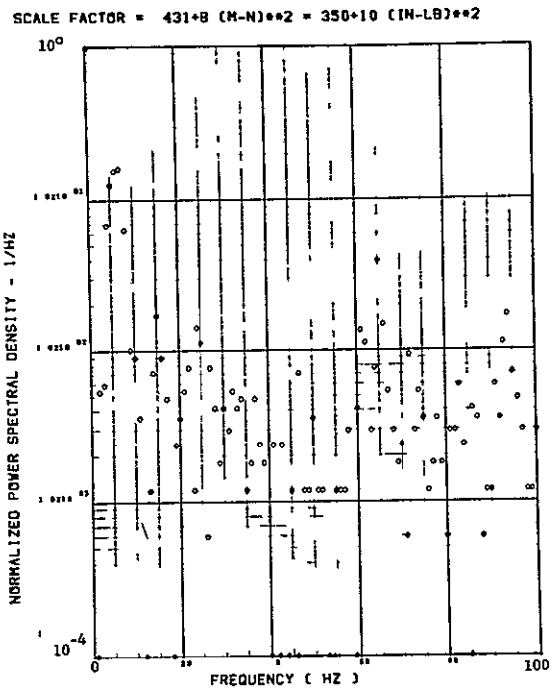

(l) - SW124 BENDING MOMENT AT WING STATION 1

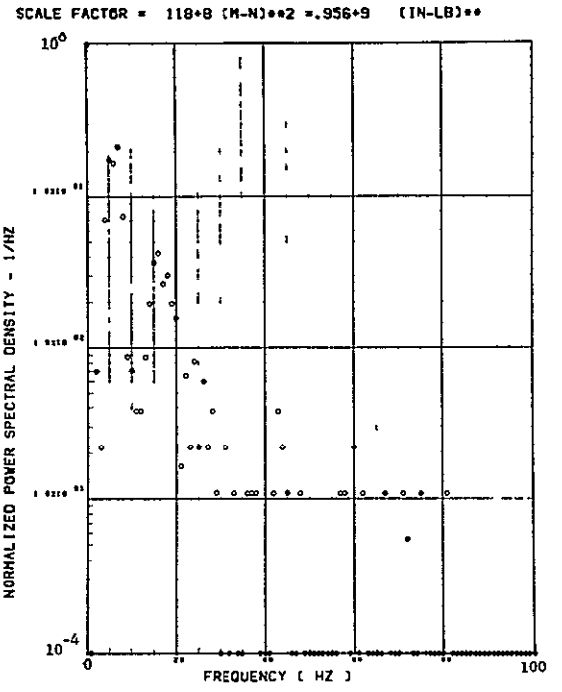

(m) - SW127 BENDING MOMENT AT WING STATION 2

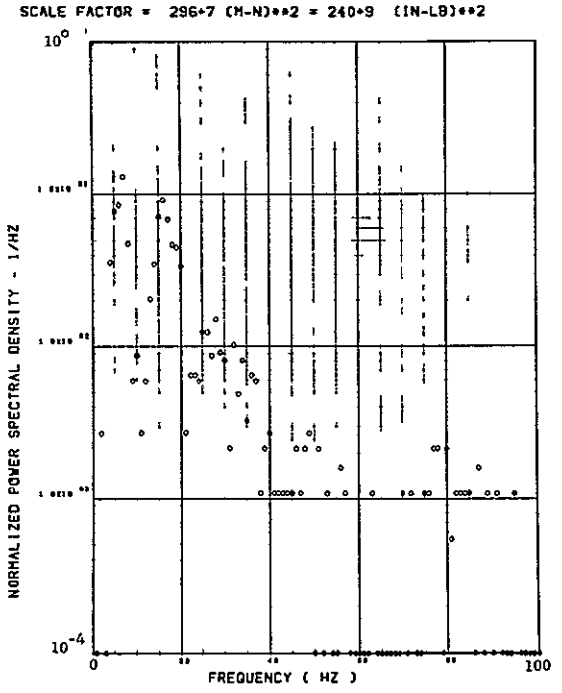

(n) - SW130 BENDING MOMENT AT WING STATION 3

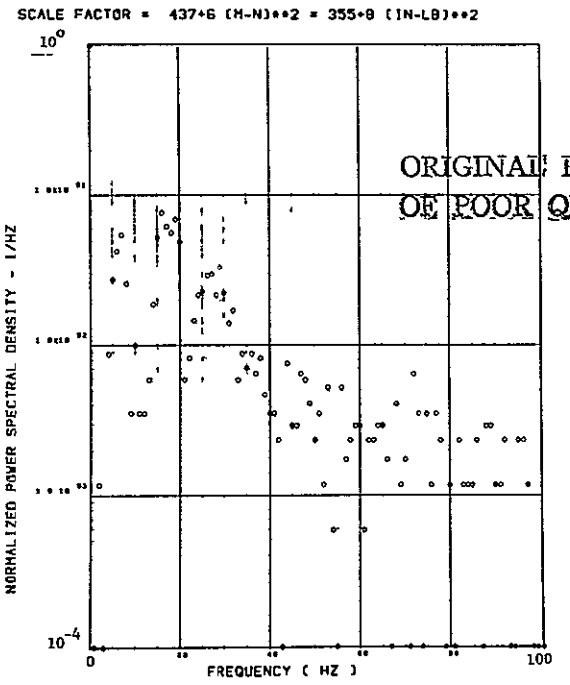

(o) - SW133 BENDING MOMENT AT WING STATION 4

Figure 24. Continued

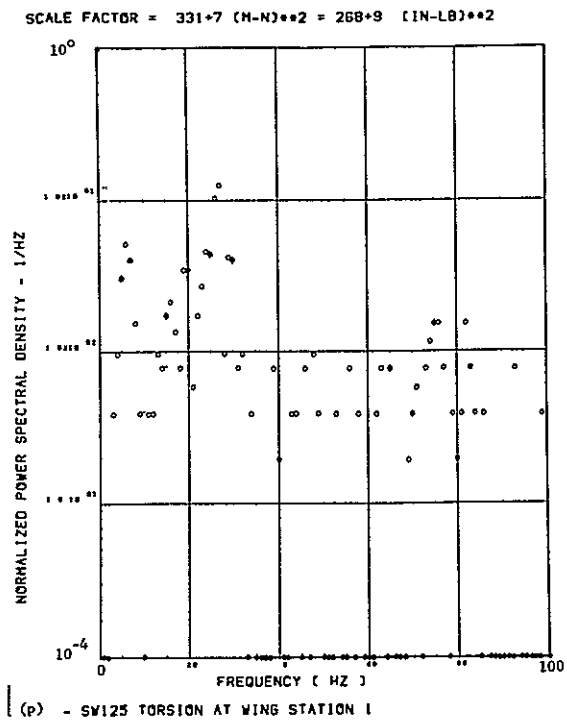

(p) - SW125 TORSION AT WING STATION 1

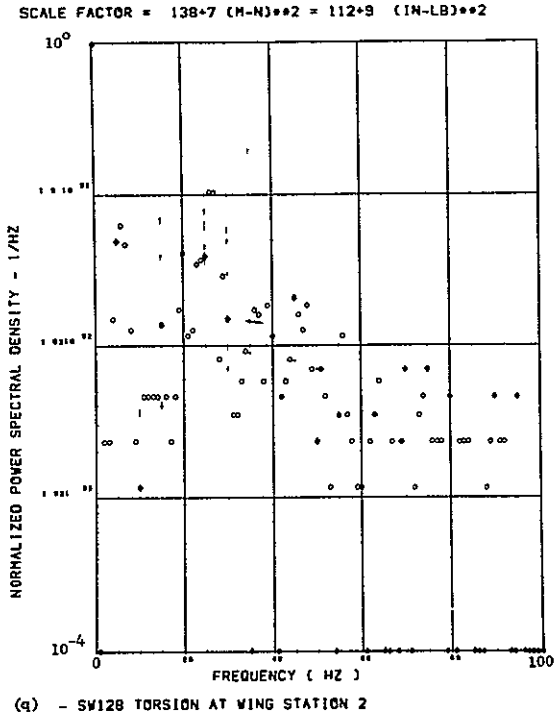

(q) - SW128 TORSION AT WING STATION 2

Data Not Available

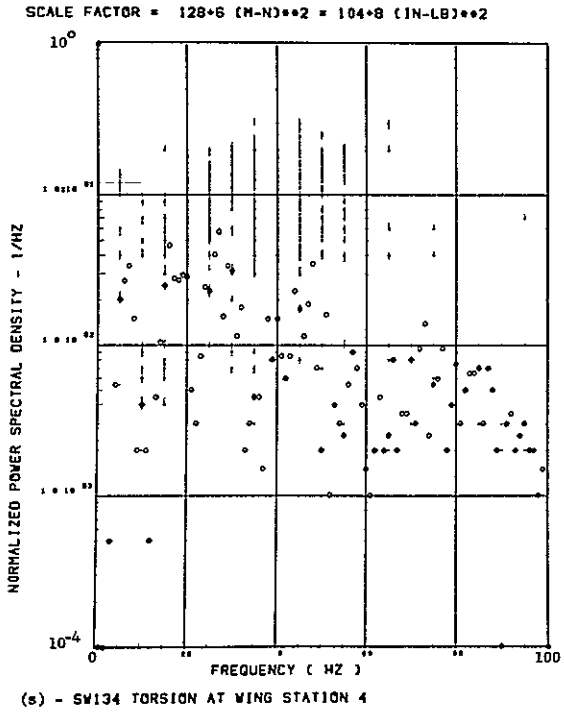

(s) - SW134 TORSION AT WING STATION 4

Figure 24. Concluded

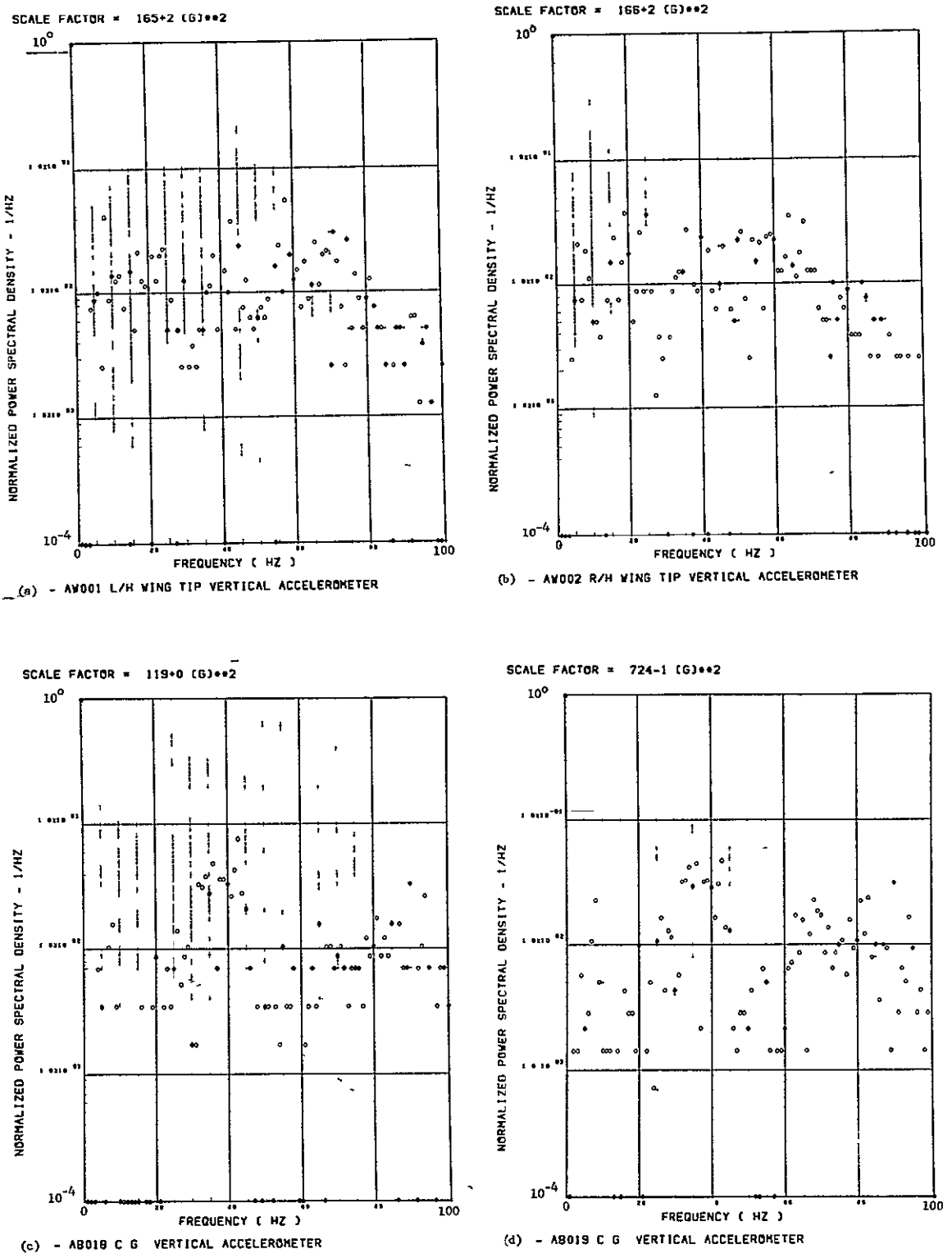

Figure 25. Power Spectra-Flight 77, Run S&C-R, Point 9, T_1=153318.5, ΔT=2 Sec, α_{Nom}=9.2 deg, $\Delta\alpha$=1.24 deg.

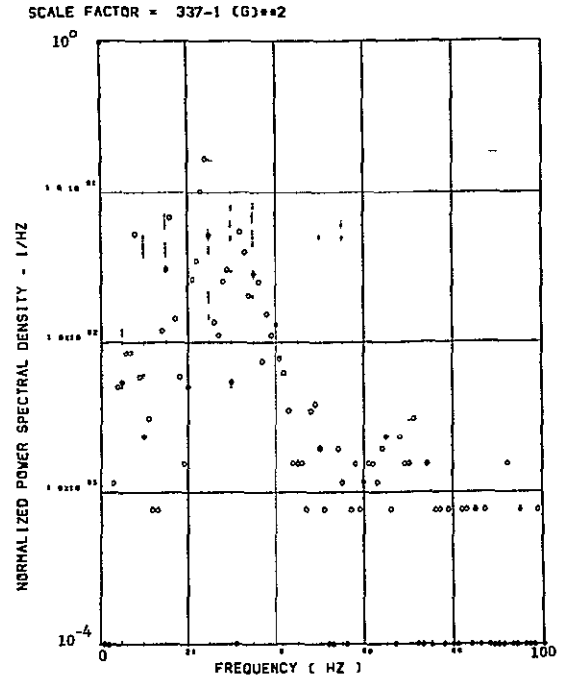

(e) - AF009 PILOT S SEAT VERTICAL ACCELEROMETER

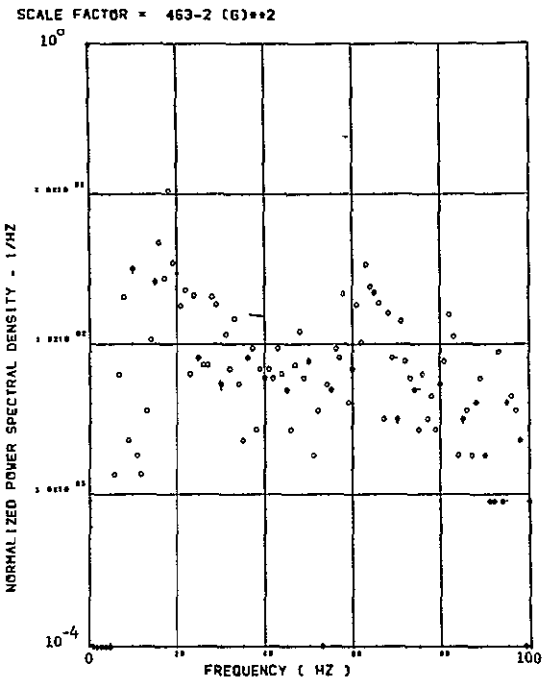

(f) - AF010 PILOT S SEAT LATERAL ACCELEROMETER

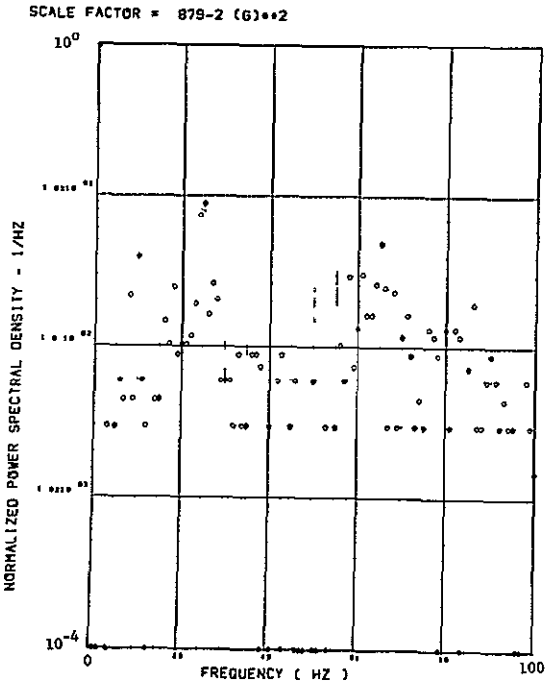

(g) - AB020 C G LATERAL ACCELEROMETER

Figure 25. Continued

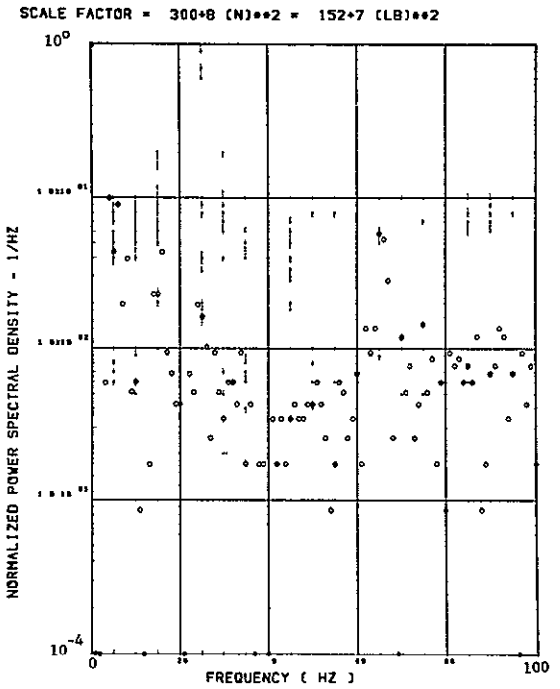

(h) I - SW123 SHEAR AT WING STATION 1

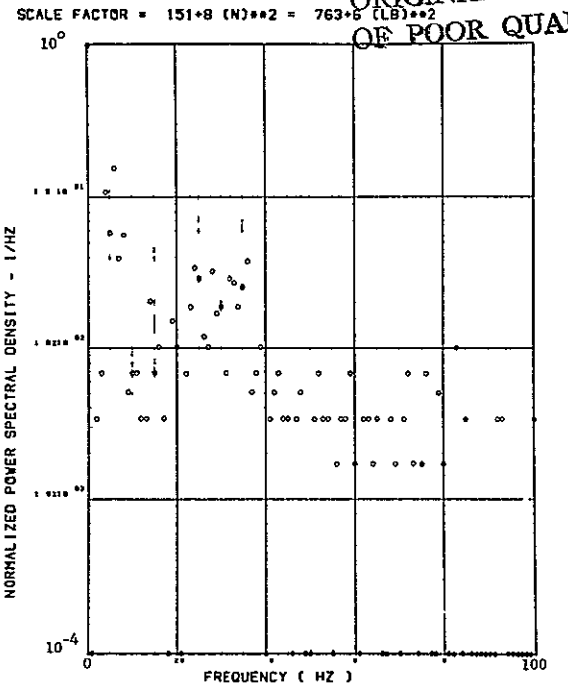

(i) - SW126 SHEAR AT WING STATION 2

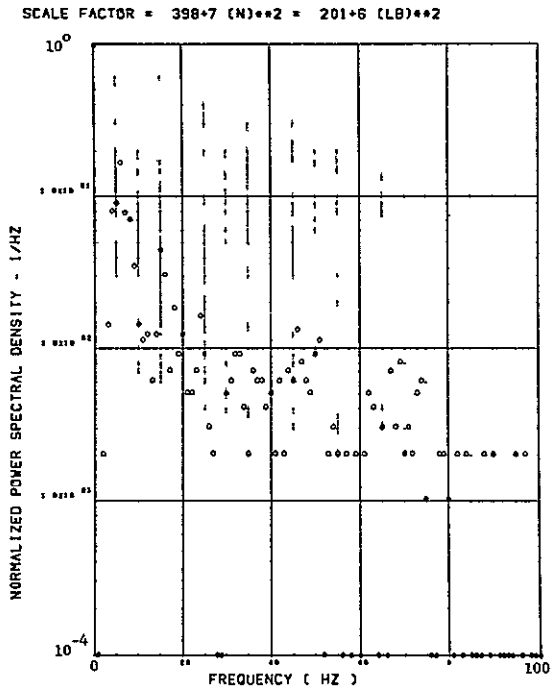

(j) - SW129 SHEAR AT WING STATION 3

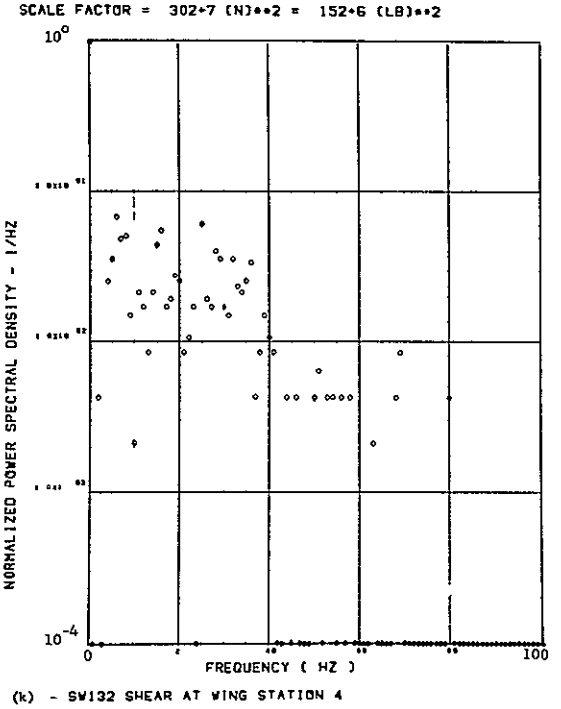

(k) - SW132 SHEAR AT WING STATION 4

Figure 25. Continued

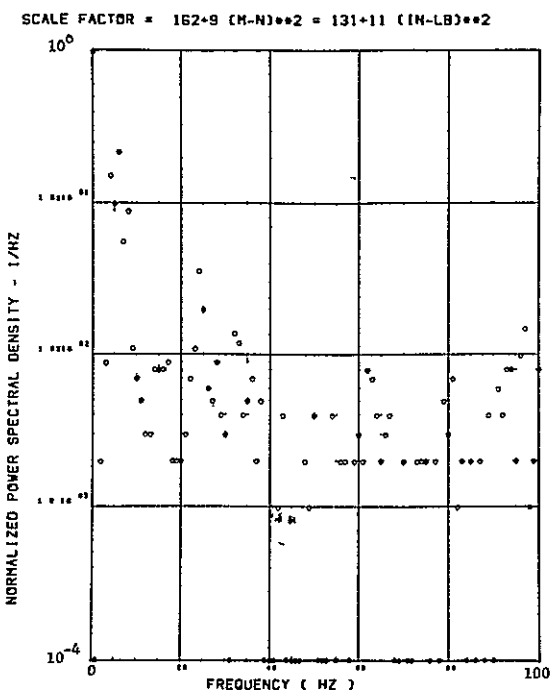

(l) - SW124 BENDING MOMENT AT WING STATION 1

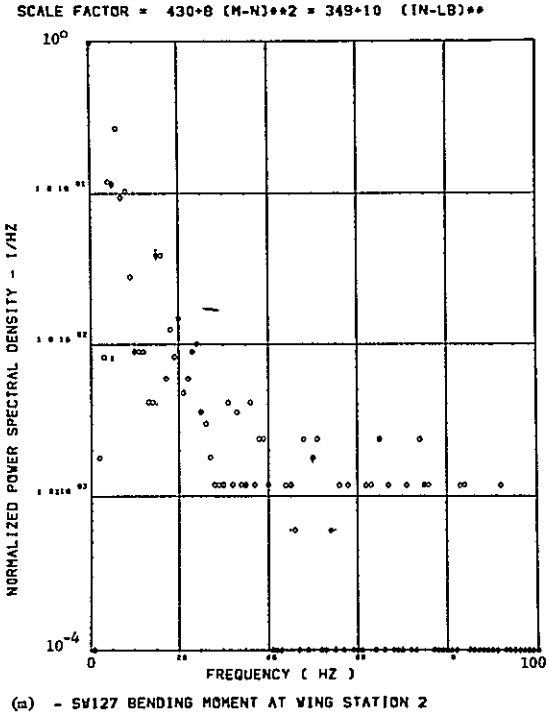

(m) - SW127 BENDING MOMENT AT WING STATION 2

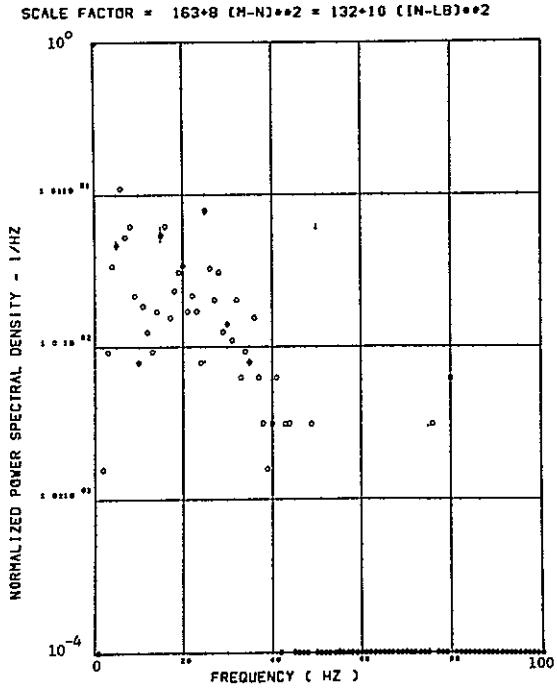

(n) - SW130 BENDING MOMENT AT WING STATION 3

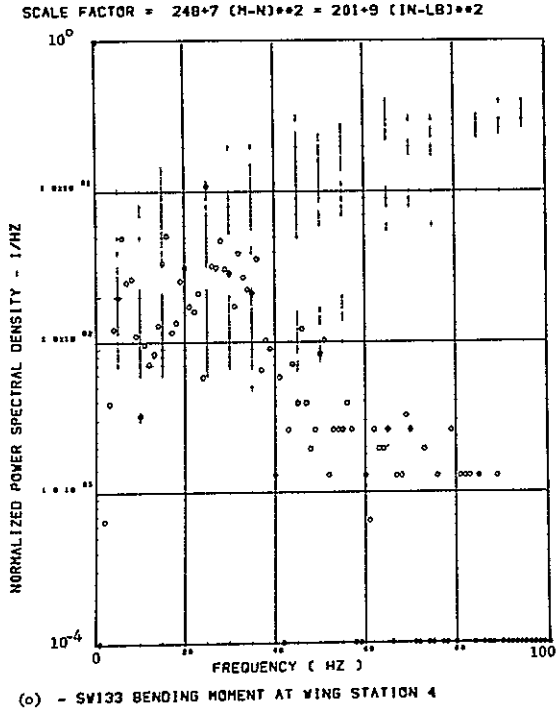

(o) - SW133 BENDING MOMENT AT WING STATION 4

Figure 25. Continued

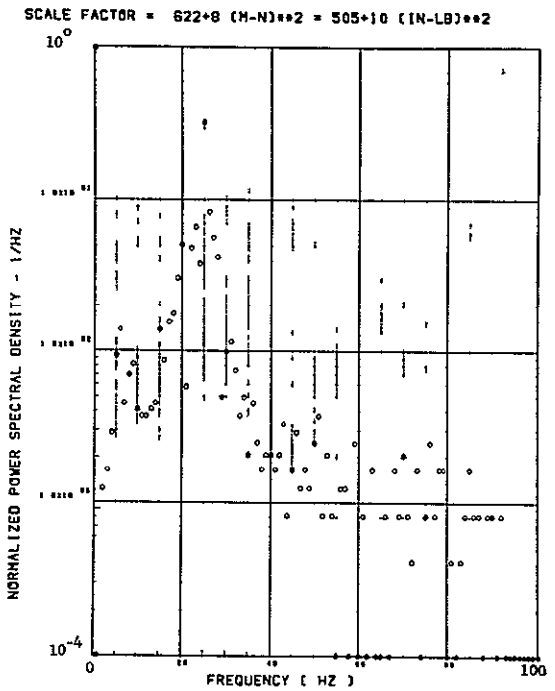

(p) - SW125 TORSION AT WING STATION 1

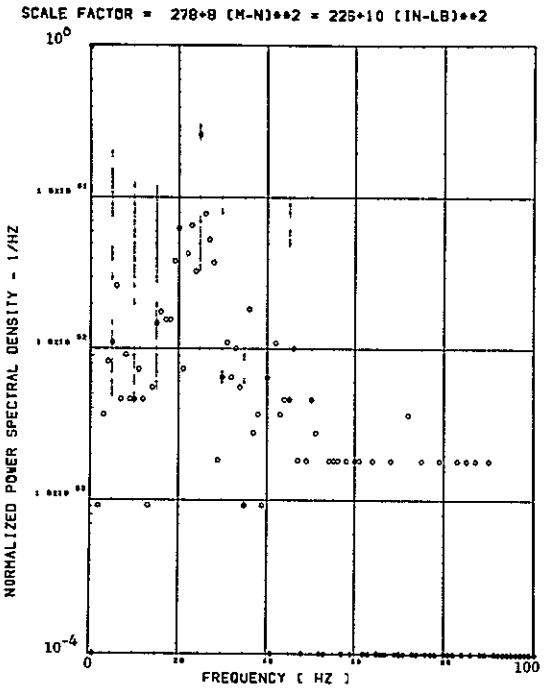

(q) - SW128 TORSION AT WING STATION 2

Data Not Available

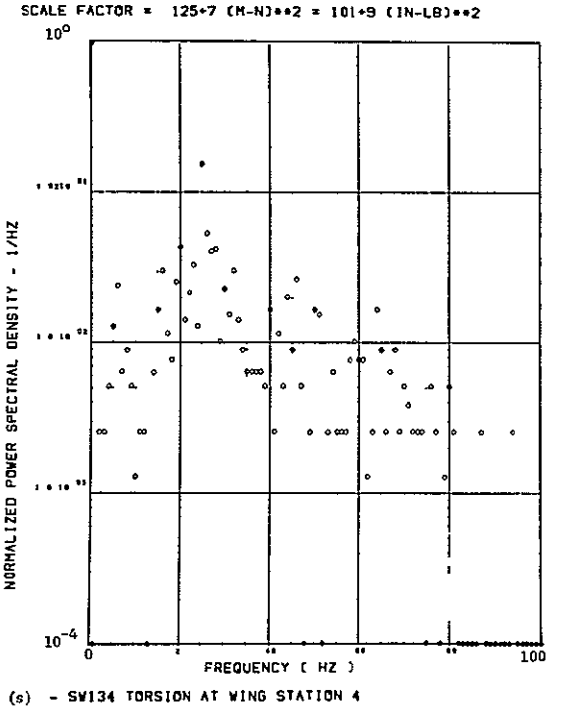

(s) - SW134 TORSION AT WING STATION 4

Figure 25. Concluded

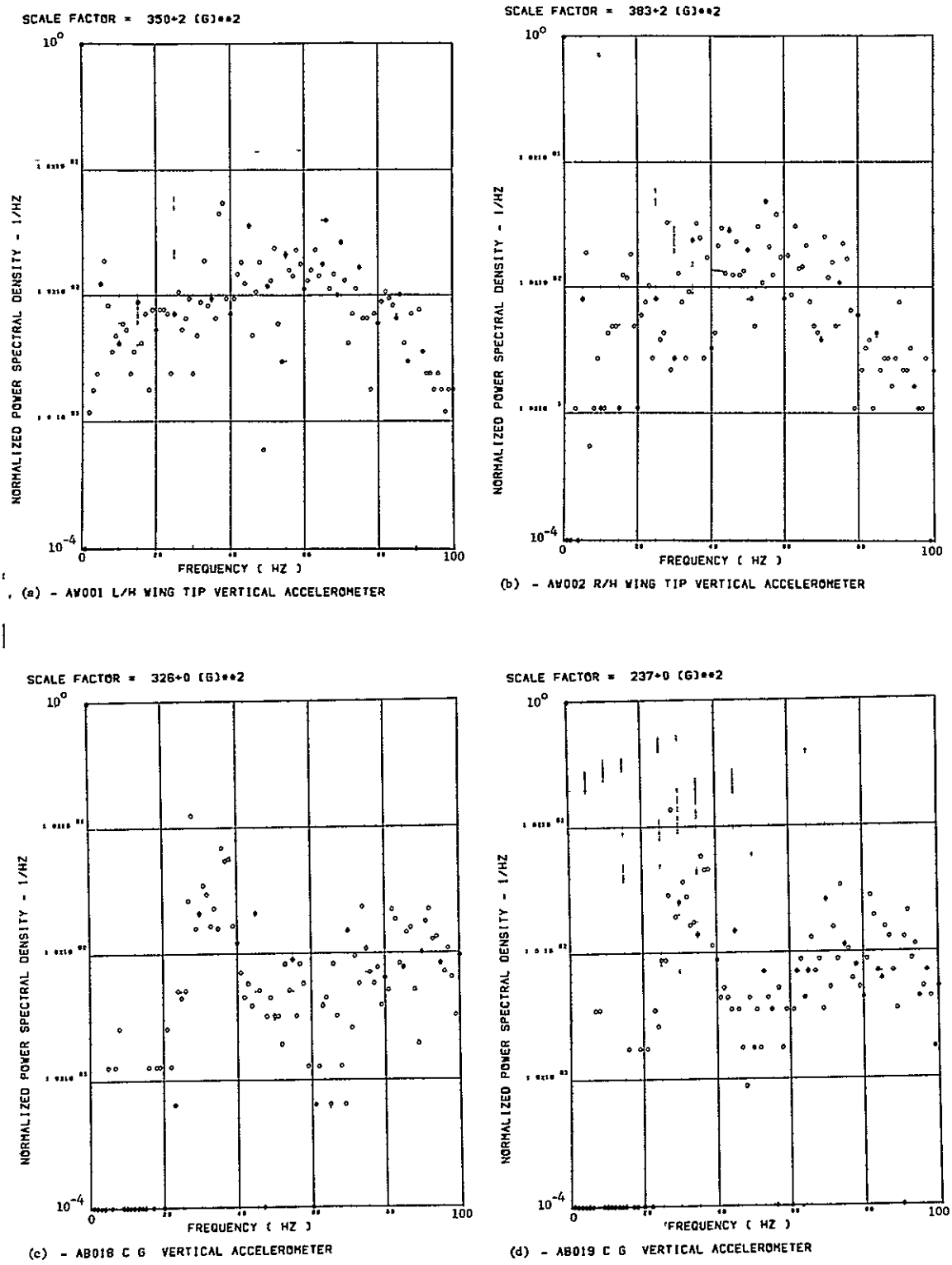

Figure 26. Power Spectra-Flight 77, Run S&C-R, Point10, T_1=153322.35, ΔT=2 Sec, α_{Nom}=12.2 deg, $\Delta\alpha$=2.55 deg.

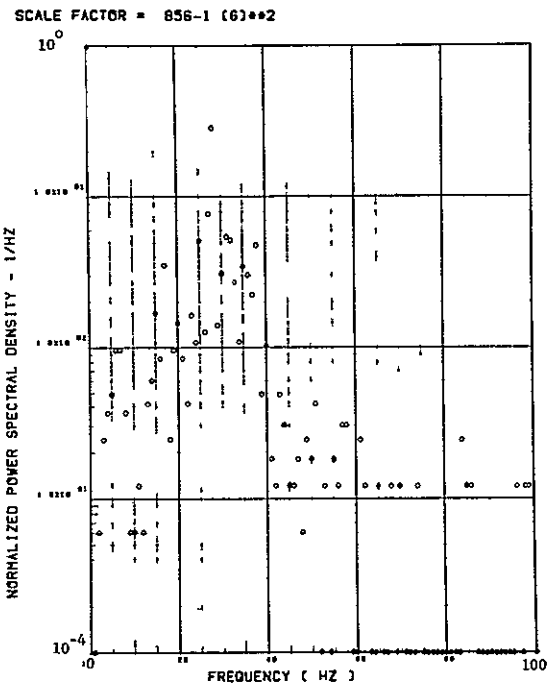

(e) - AF009 PILOT S SEAT VERTICAL ACCELEROMETER

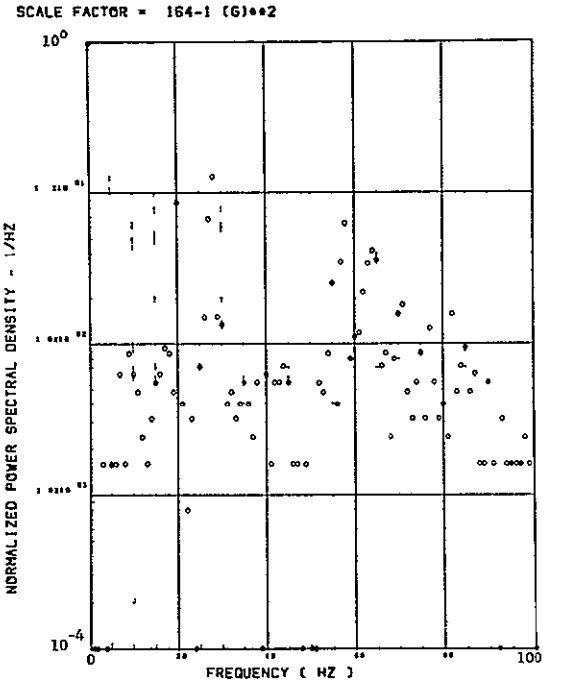

(f) - AF010 PILOT S SEAT LATERAL ACCELEROMETER

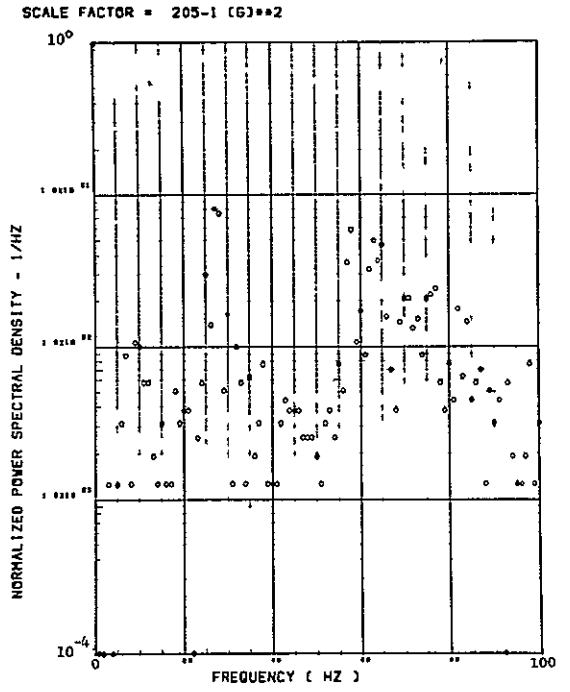

(g) - AB020 C G LATERAL ACCELEROMETER

Figure 26. Continued

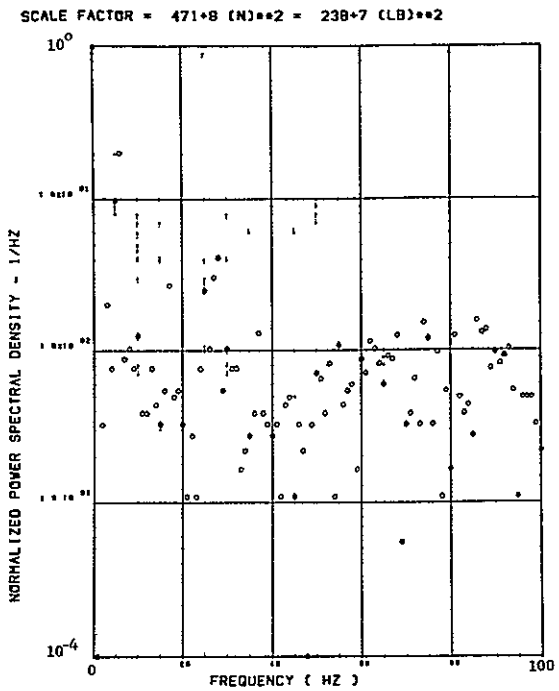

(h) - SW123 SHEAR AT WING STATION 1

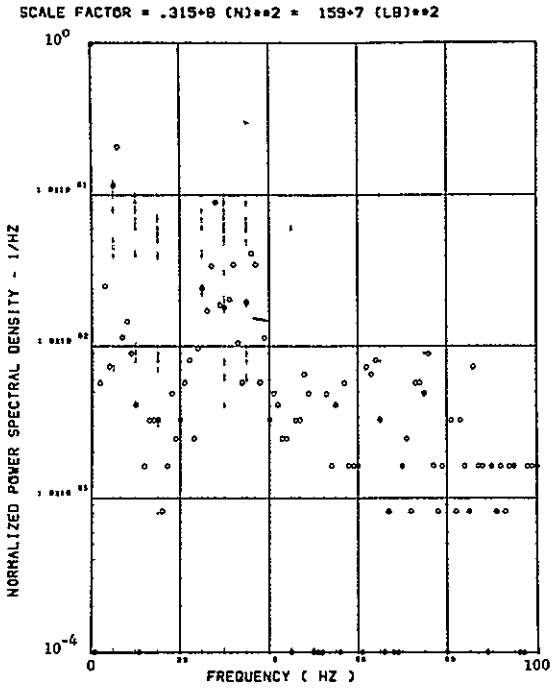

(i) - SW126 SHEAR AT WING STATION 2

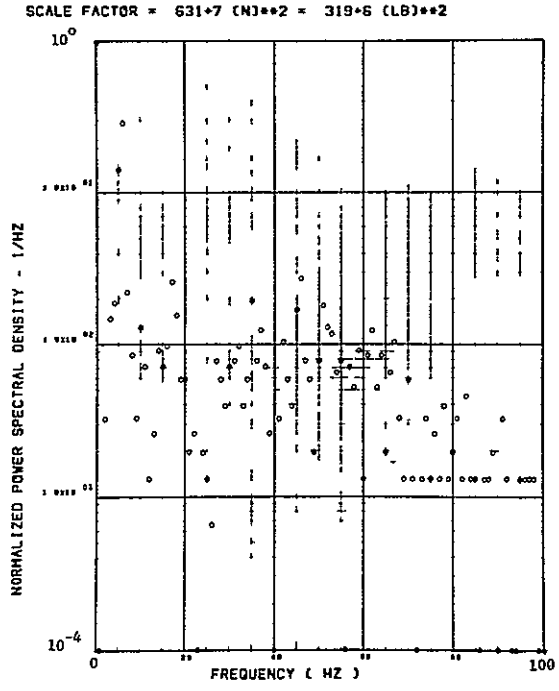

(j) - SW129 SHEAR AT WING STATION 3

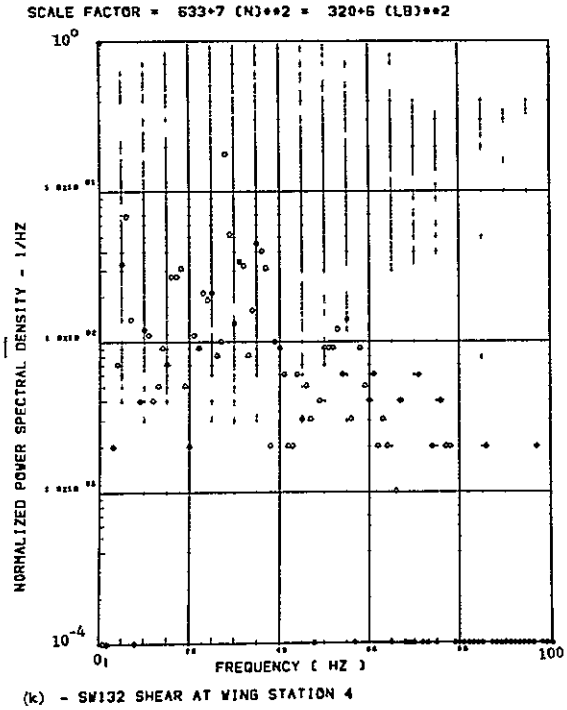

(k) - SW132 SHEAR AT WING STATION 4

Figure 26. Continued

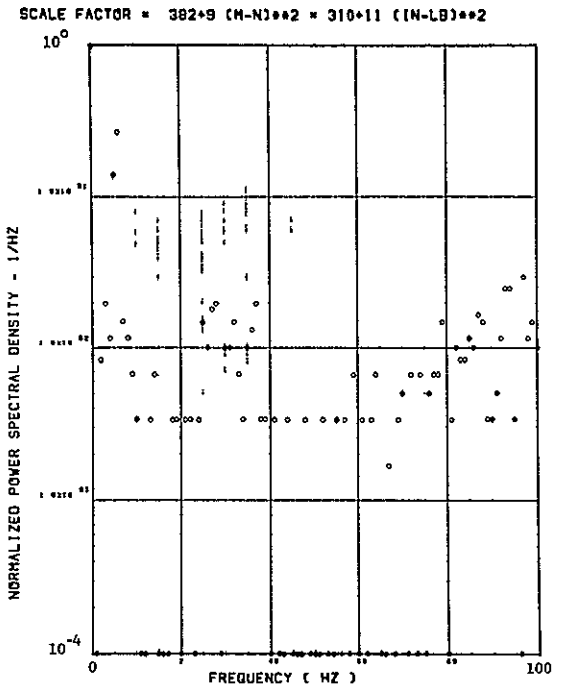

(l) - SW124 BENDING MOMENT AT WING STATION 1

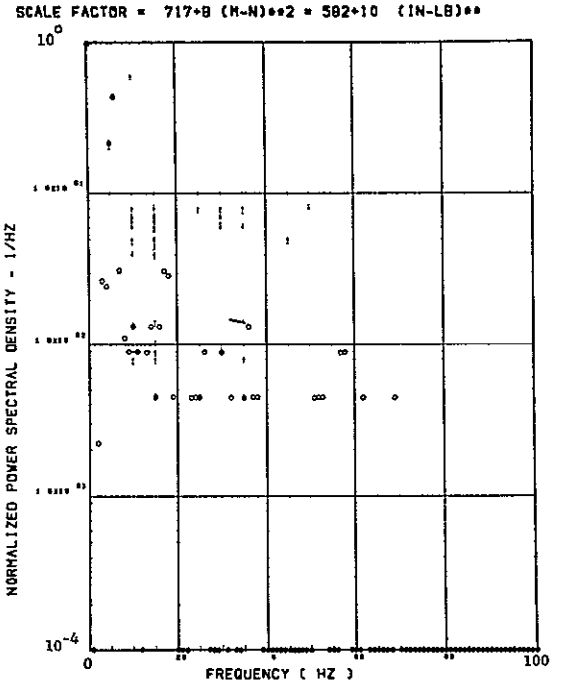

(m) - SW127 BENDING MOMENT AT WING STATION 2

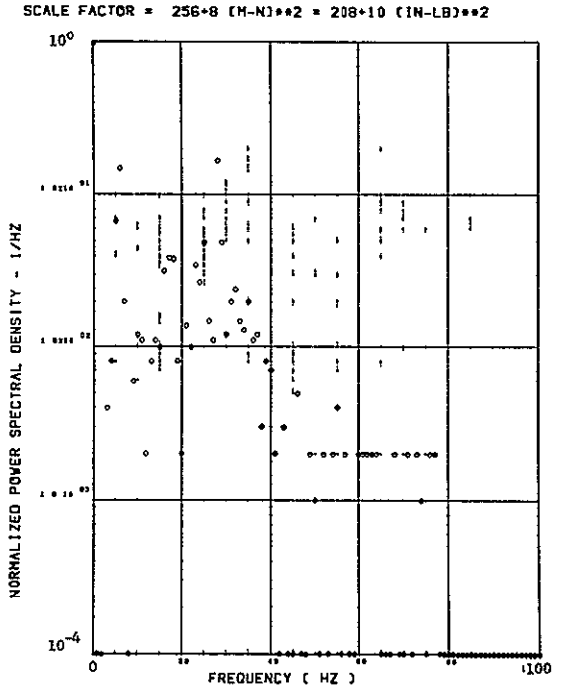

(n) - SW130 BENDING MOMENT AT WING STATION 3

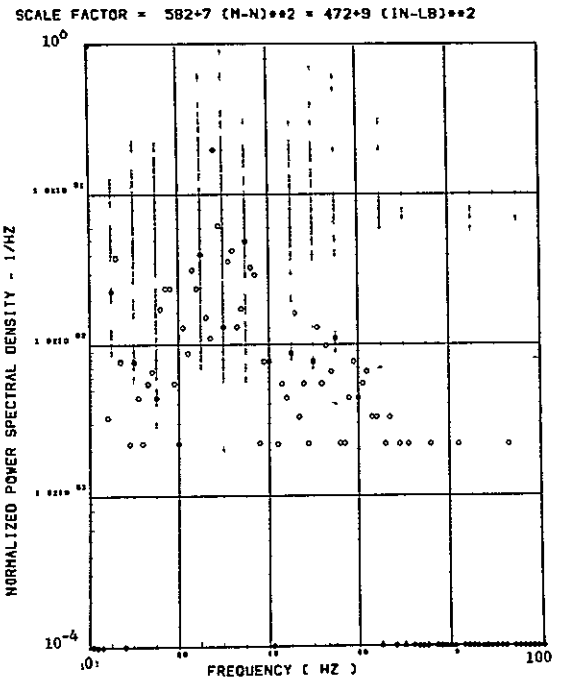

(o) - SW133 BENDING MOMENT AT WING STATION 4

Figure 26. Continued

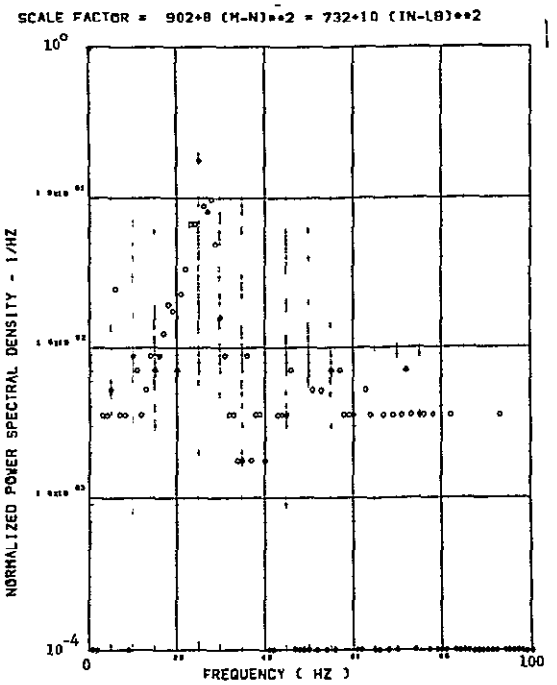

(p) - SW125 TORSION AT WING STATION 1

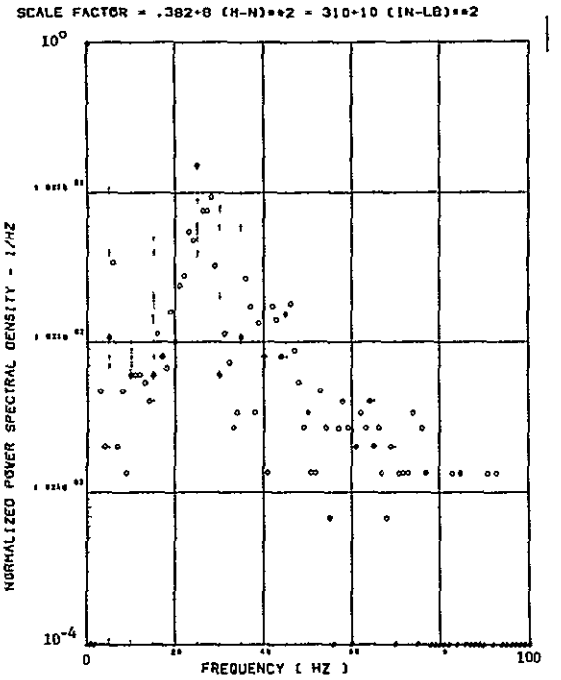

(q) - SW128 TORSION AT WING STATION 2

Data Not Available

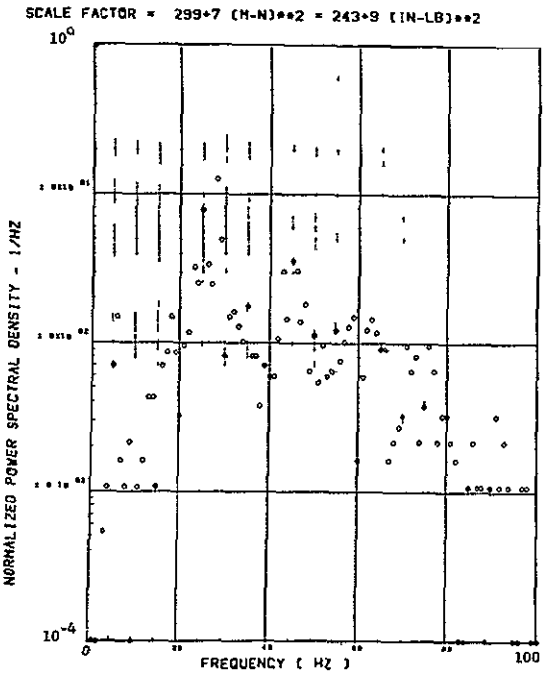

(s) - SW134 TORSION AT WING STATION 4

Figure 26. Concluded

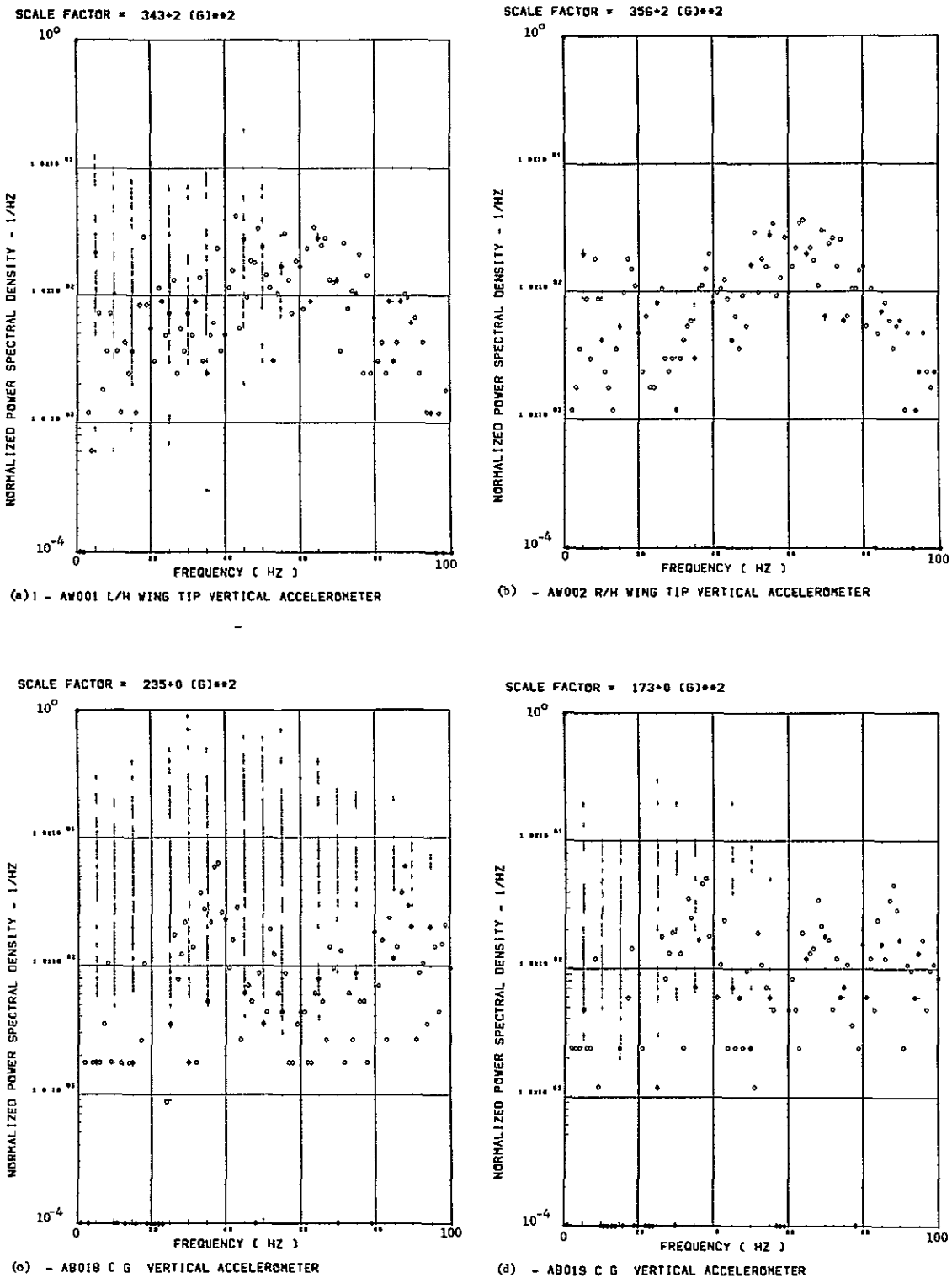

Figure 27. Power Spectra-Flight 77, Run S&C-R, Point 11 T_1=153324.35, ΔT=2 Sec, α_{Nom}=14.8 deg, $\Delta\alpha$=2.15 deg.

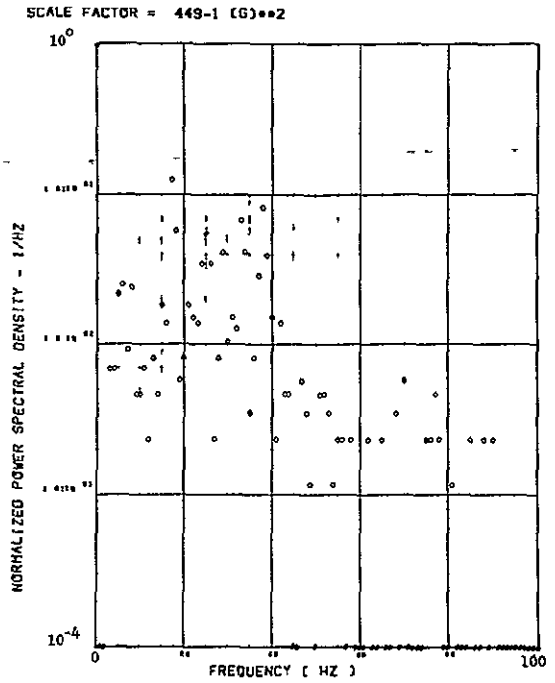

(e) - AF009 PILOT S SEAT VERTICAL ACCELEROMETER

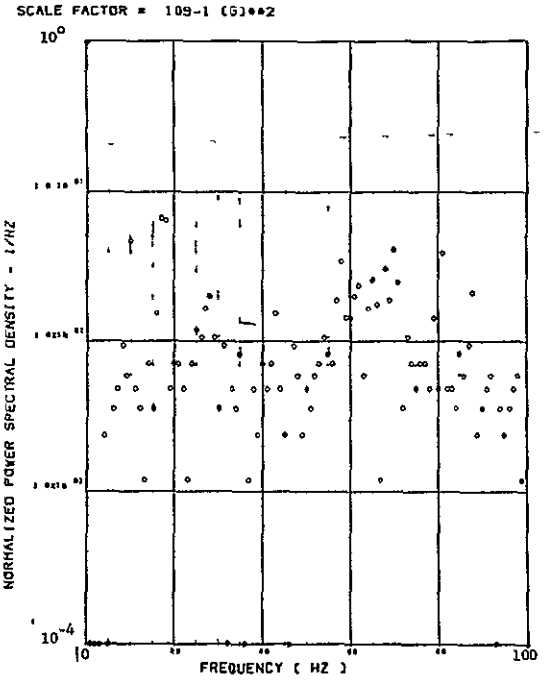

(f) - AF010 PILOT S SEAT LATERAL ACCELEROMETER

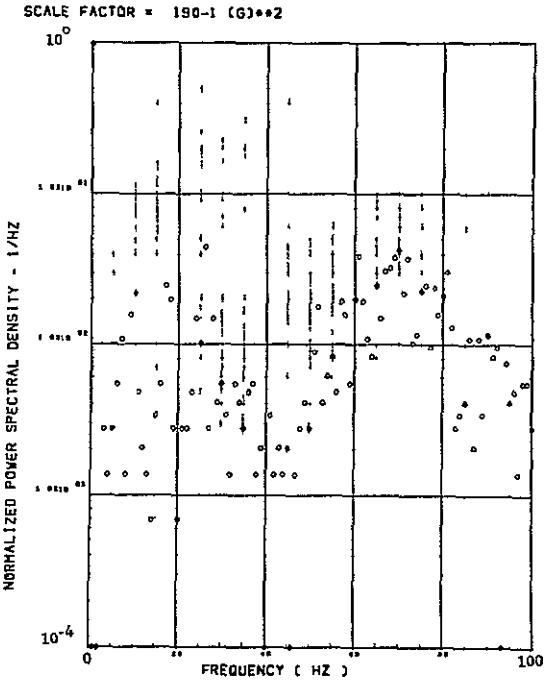

(g) - AB020 C G LATERAL ACCELEROMETER

Figure 27. Continued

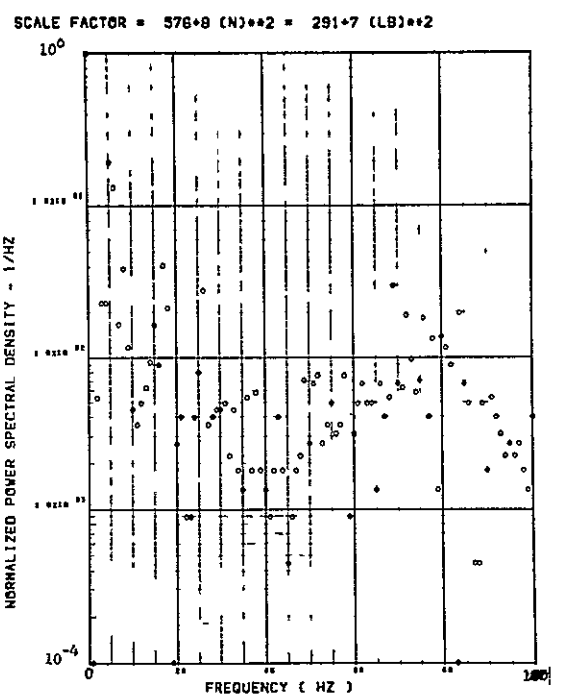

(h) | - SW123 SHEAR AT WING STATION 1

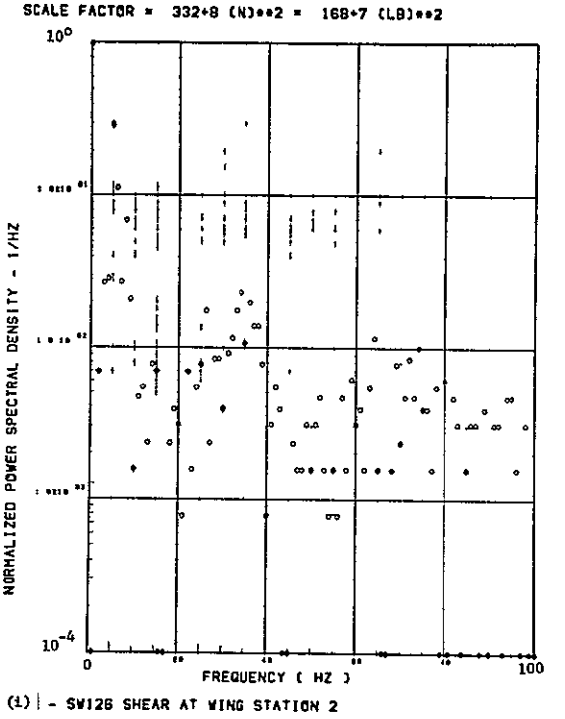

(i) | - SW126 SHEAR AT WING STATION 2

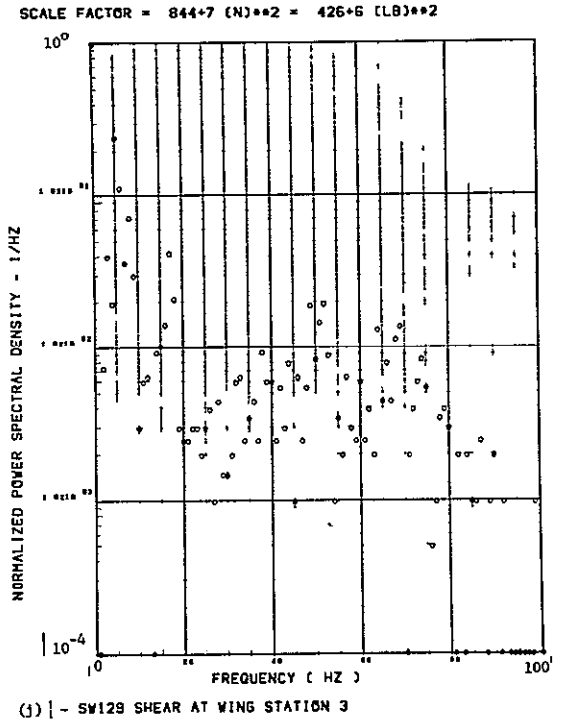

(j) | - SW129 SHEAR AT WING STATION 3

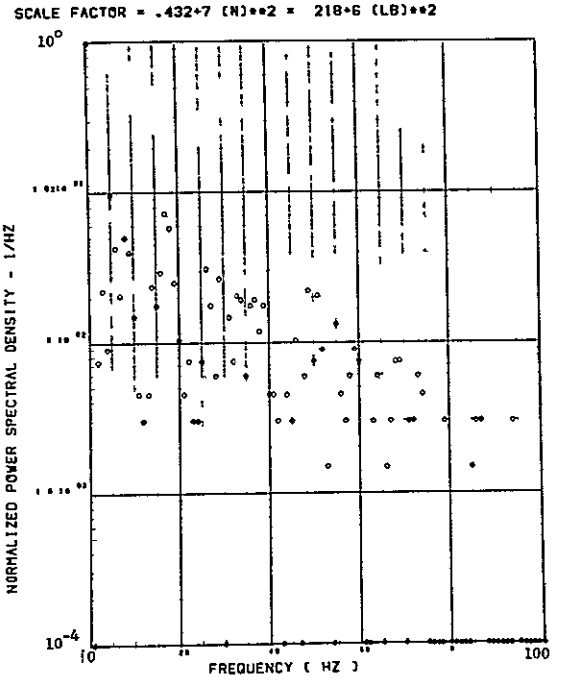

(k) | - SW132 SHEAR AT WING STATION 4

Figure 27. Continued

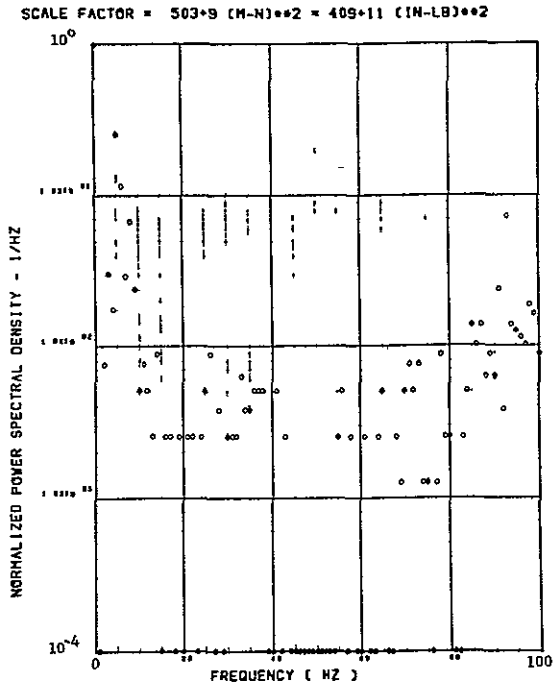

(l) - SW124 BENDING MOMENT AT WING STATION 1

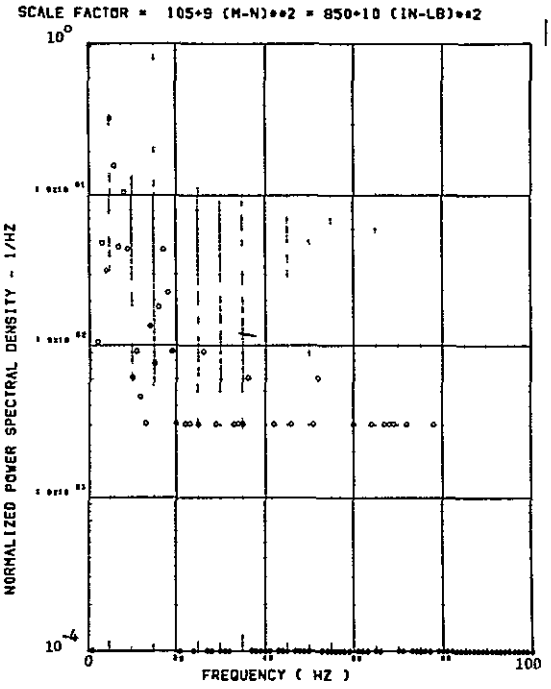

(m) - SW127 BENDING MOMENT AT WING STATION 2

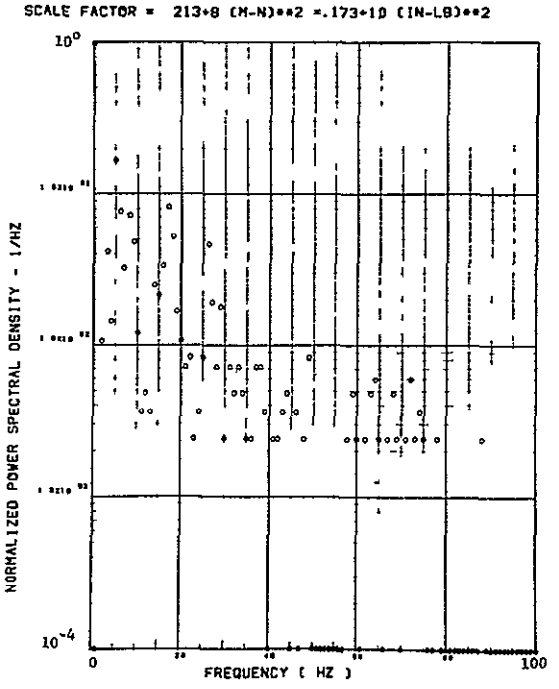

(n) - SW130 BENDING MOMENT AT WING STATION 3

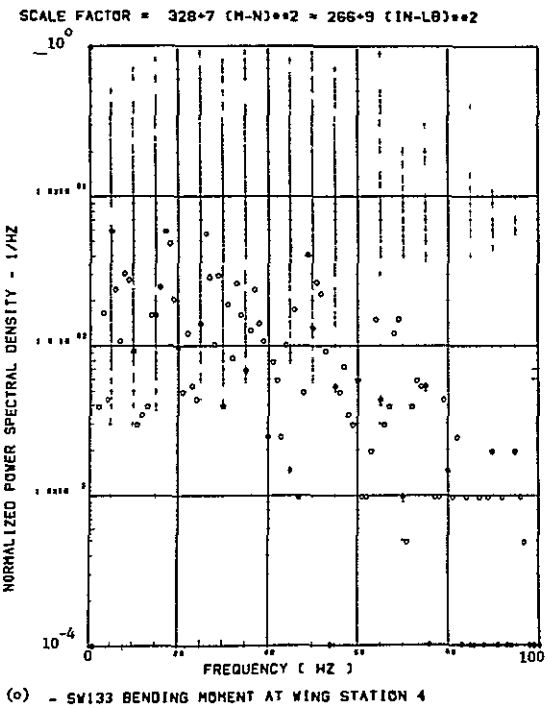

(o) - SW133 BENDING MOMENT AT WING STATION 4

Figure 27. Continued

ORIGINAL PAGE IS
OF POOR QUALITY

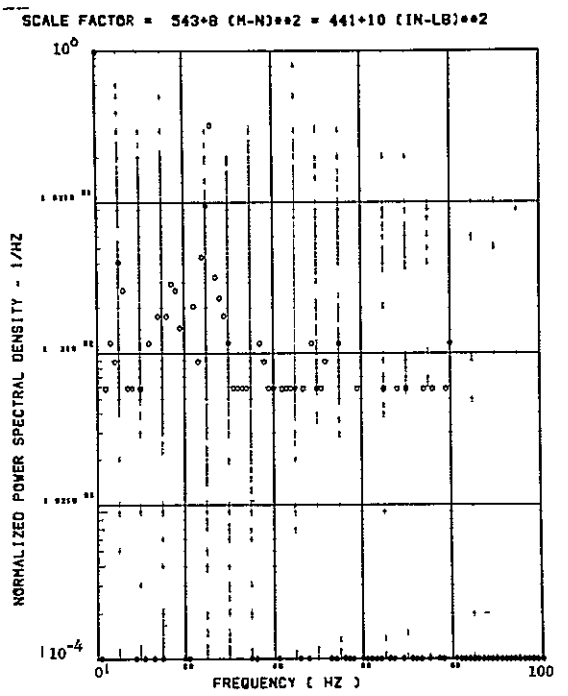

(p) - SW125 TORSION AT WING STATION 1

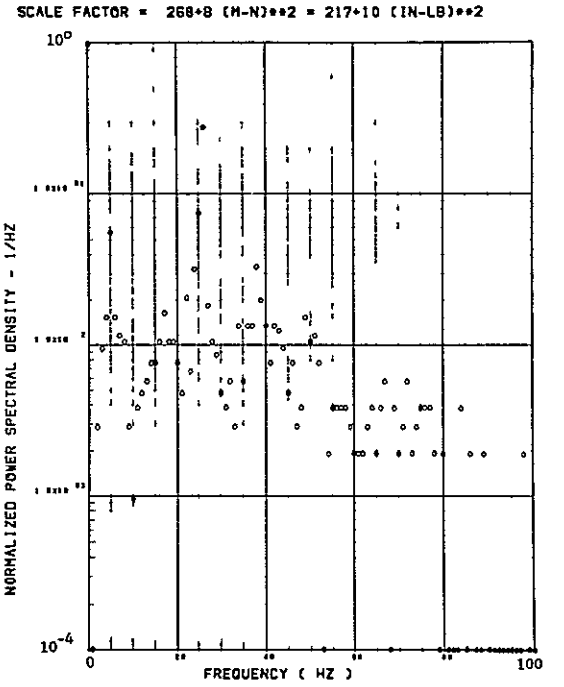

(q) - SW128 TORSION AT WING STATION 2

Data Not Available

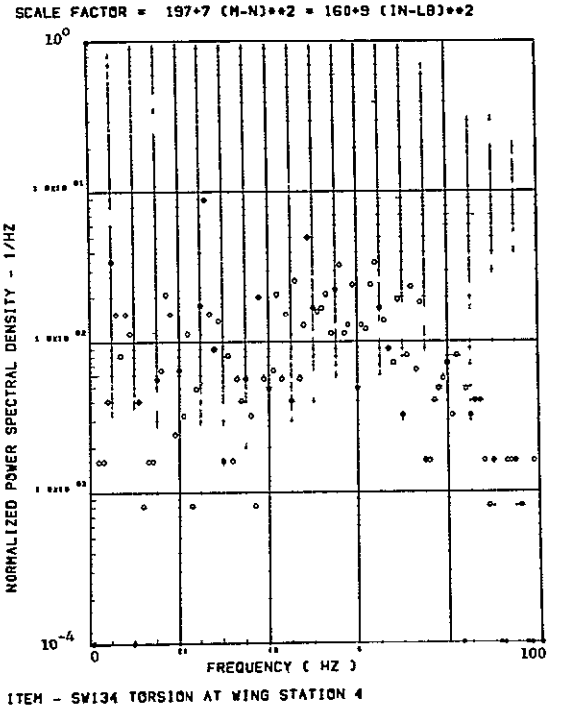

ITEM - SW134 TORSION AT WING STATION 4

Figure 27. Concluded

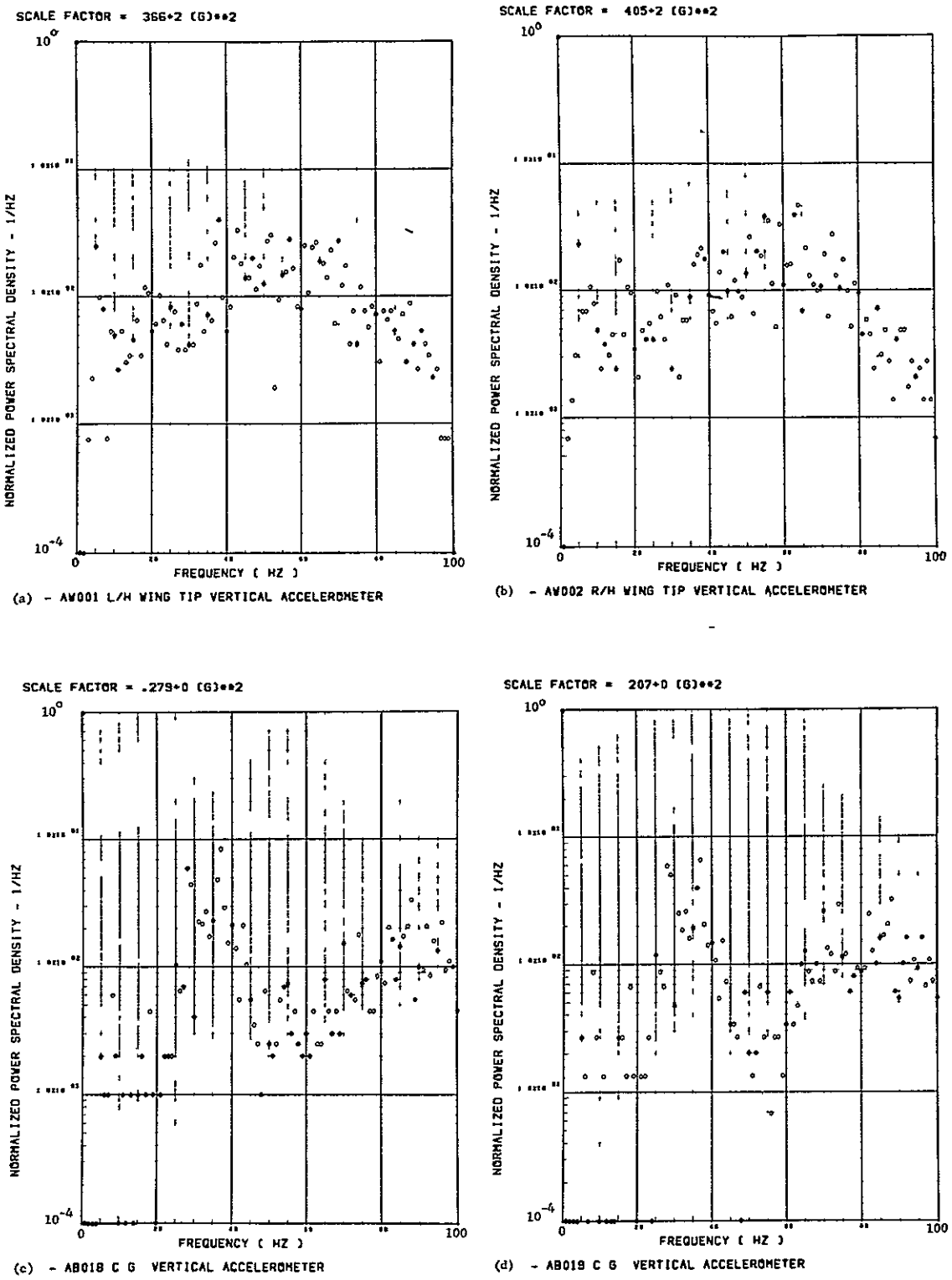

Figure 28. Power Spectra-Flight 77, Run S&C-R, Point 12, T_1=153323.0, ΔT=3 Sec, α_{Nom}=13.6 deg, $\Delta\alpha$=3.88 deg.

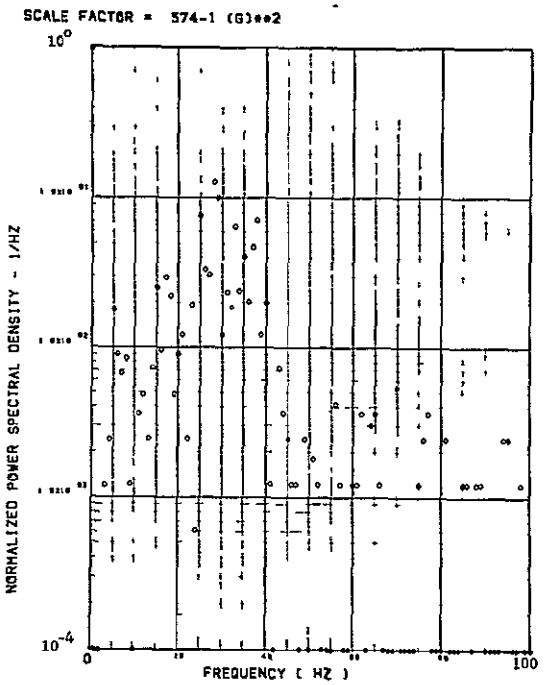

(e) - AF009 PILOT S SEAT VERTICAL ACCELEROMETER

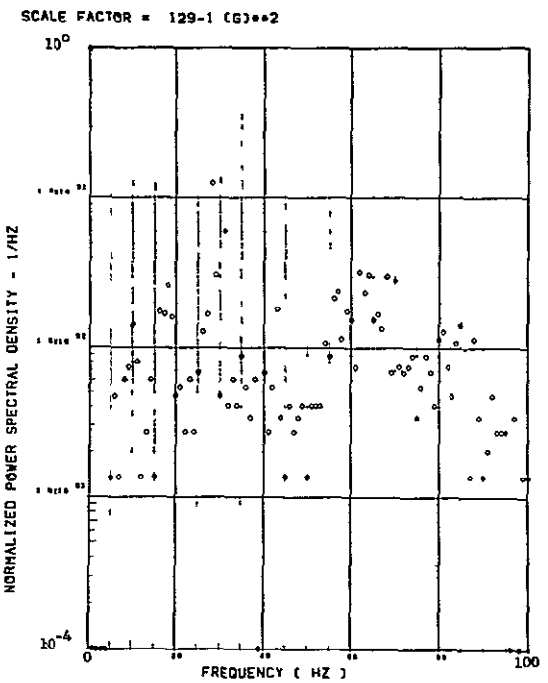

(f) - AF010 PILOT S SEAT LATERAL ACCELEROMETER

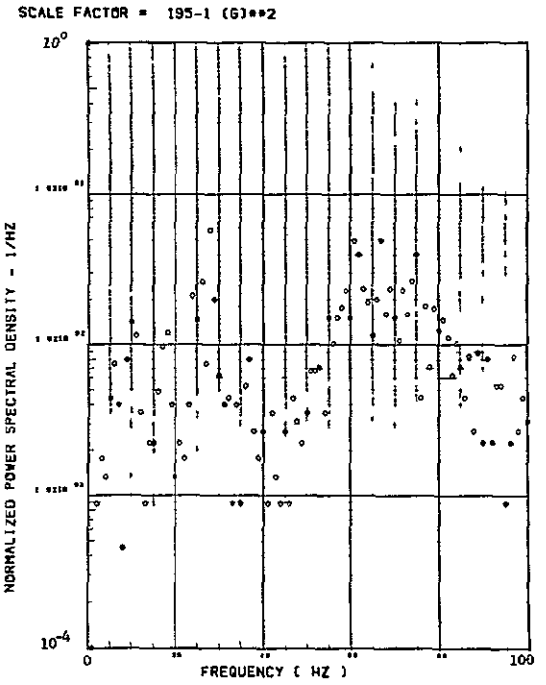

(g) - AB020 C G LATERAL ACCELEROMETER

Figure 28. Continued

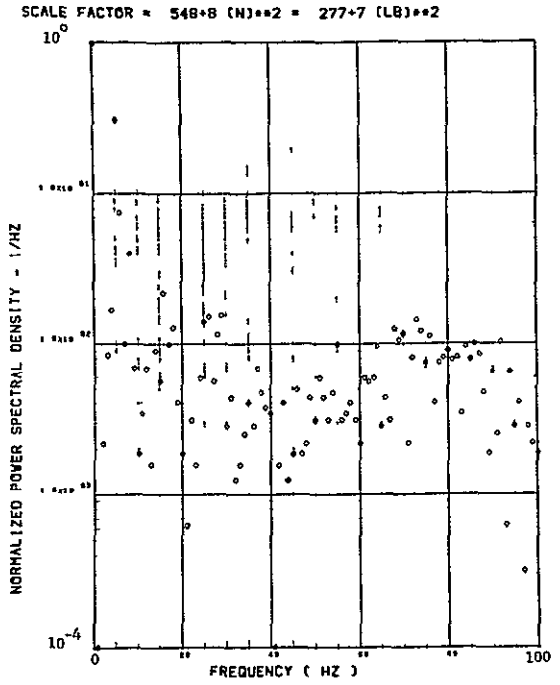

(h) - SW123 SHEAR AT WING STATION 1

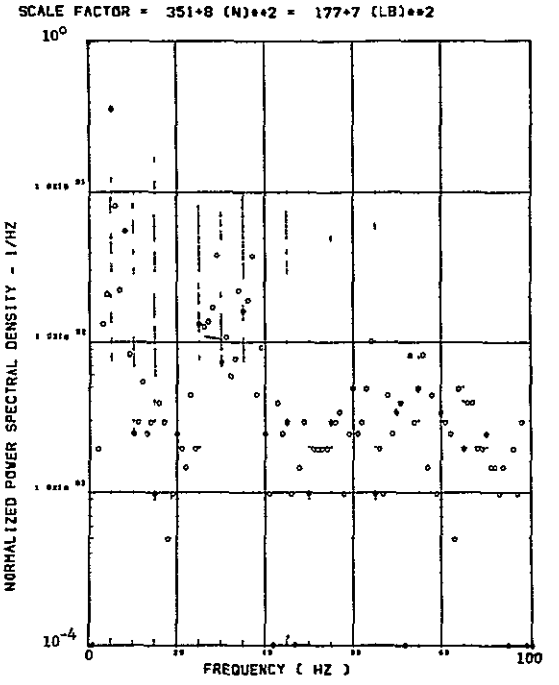

(i) - SW126 SHEAR AT WING STATION 2

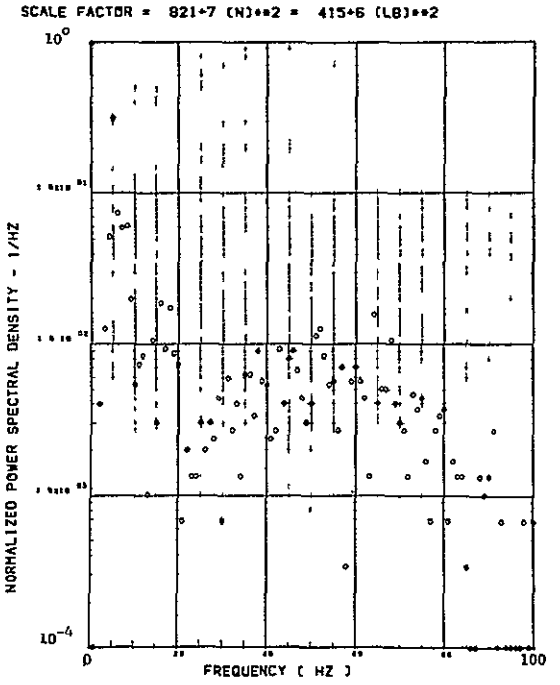

(j) - SW129 SHEAR AT WING STATION 3

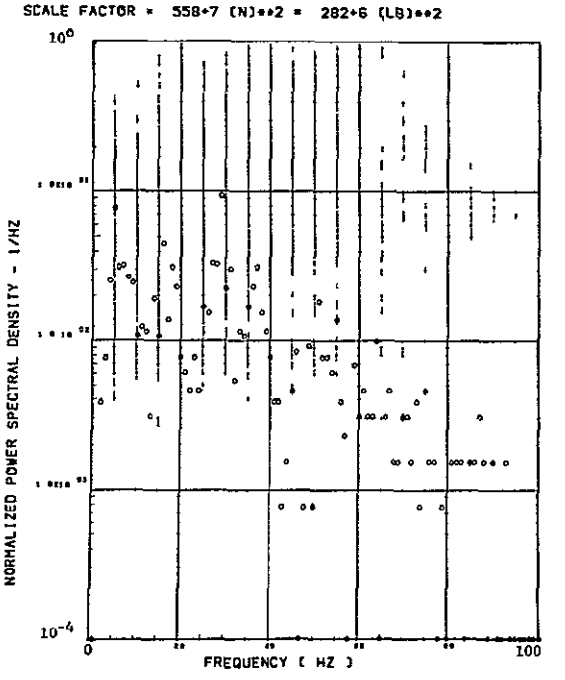

(k) - SW132 SHEAR AT WING STATION 4

Figure 28. Continued

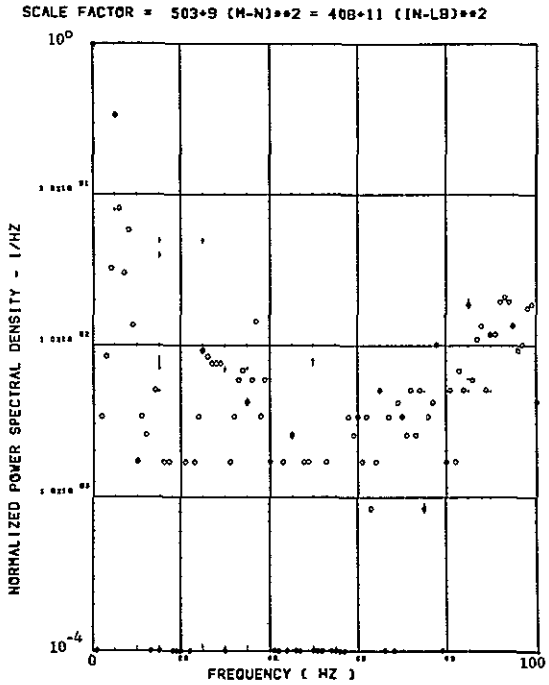

(l) - SW124 BENDING MOMENT AT WING STATION 1

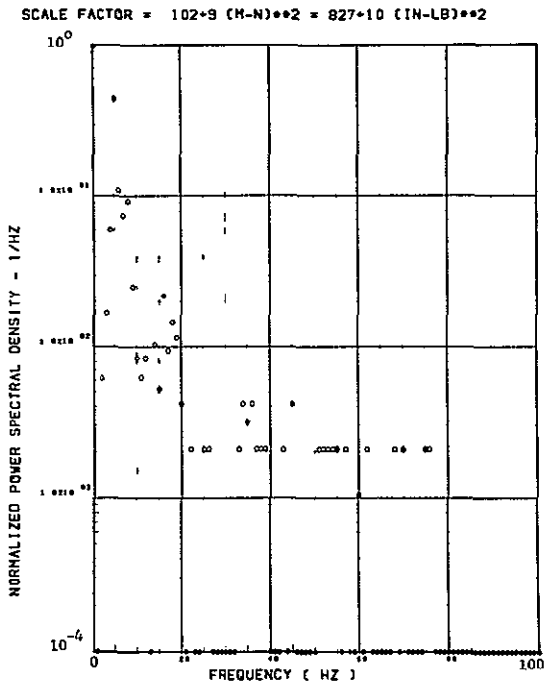

(m) - SW127 BENDING MOMENT AT WING STATION 2

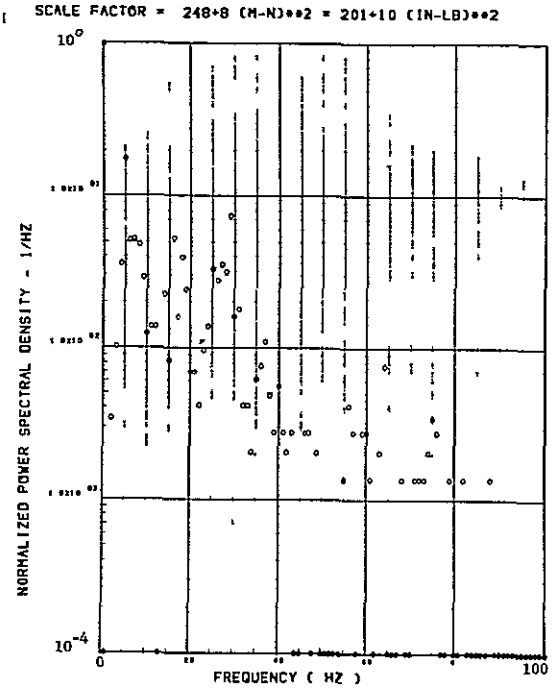

(n) - SW130 BENDING MOMENT AT WING STATION 3

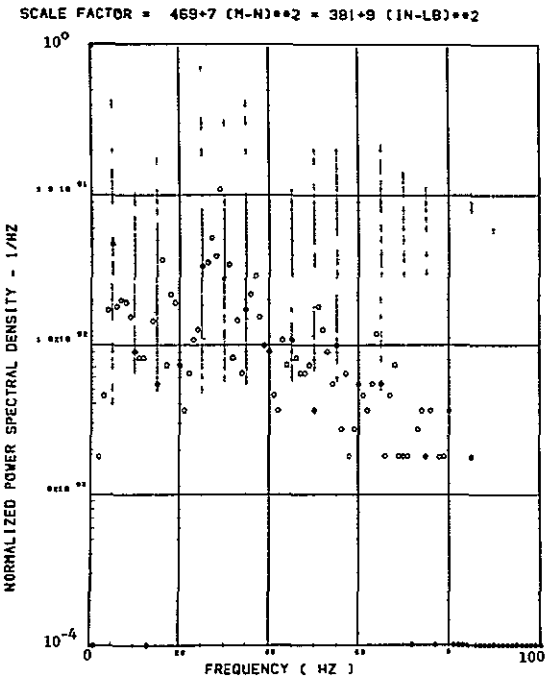

(o) - SW133 BENDING MOMENT AT WING STATION 4

Figure 28. Continued

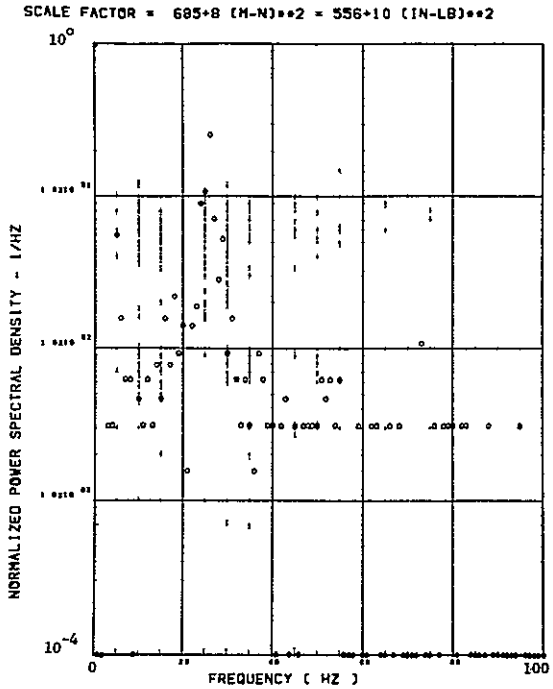

(p) - SW125 TORSION AT WING STATION 1

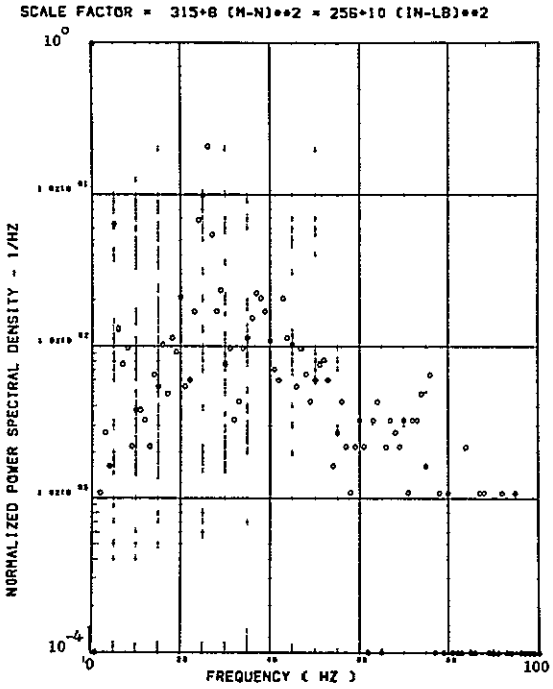

(q) - SW128 TORSION AT WING STATION 2

Data Not Available

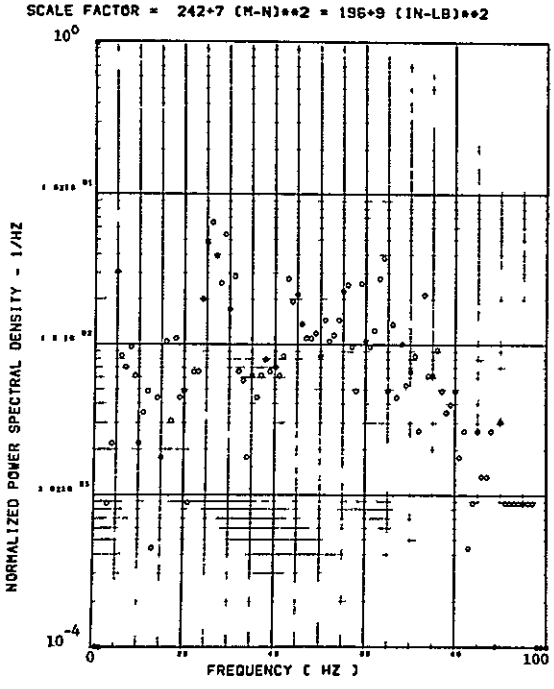

(s) - SW134 TORSION AT WING STATION 4

Figure 28. Concluded

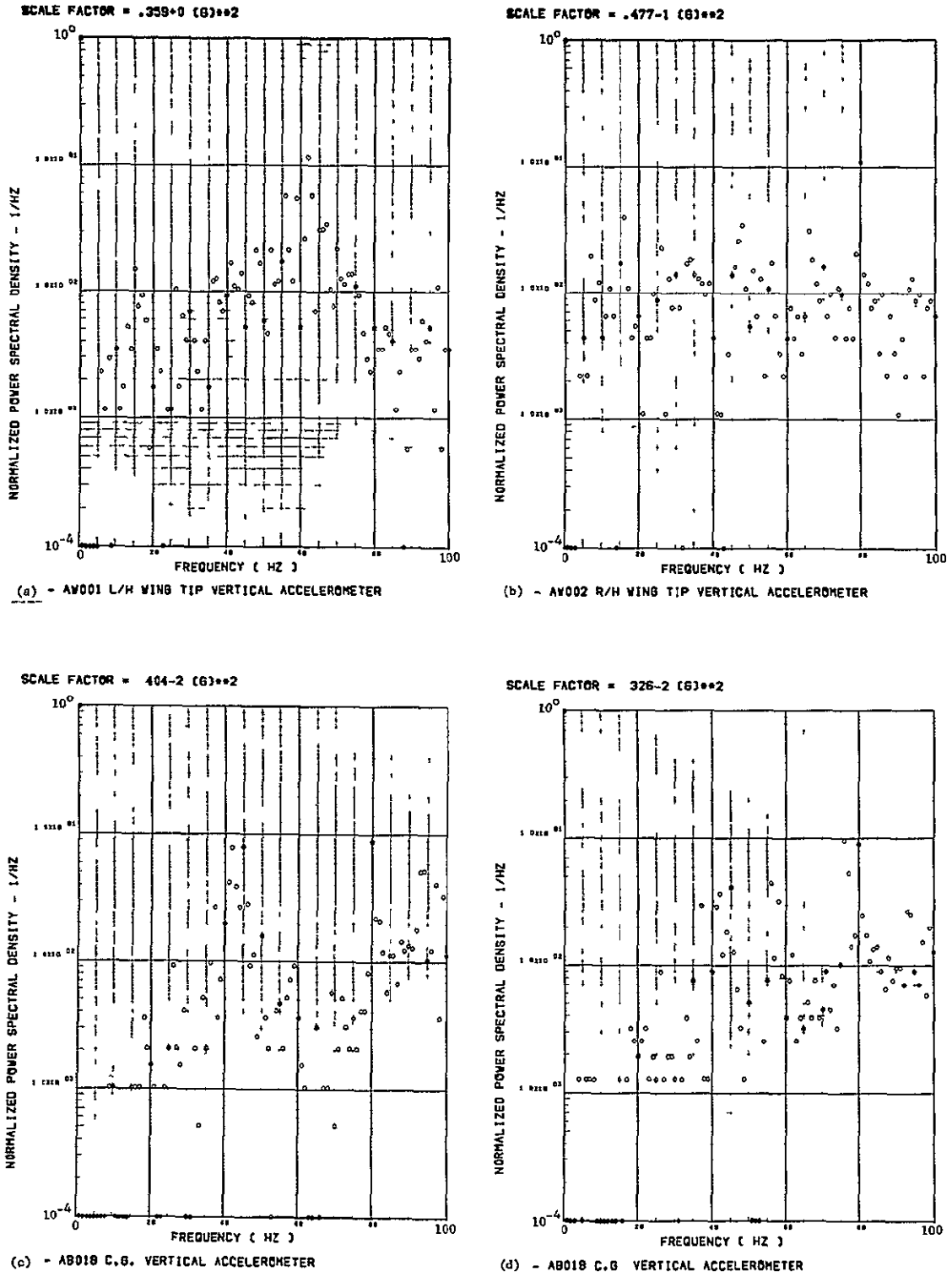

Figure 29. Power Spectra-Flight 78, Run 5, Point 1, T_1=114732.0, ΔT=1 Sec, α_{Nom}=2.60 deg, $\Delta\alpha = \pm .05$ deg.

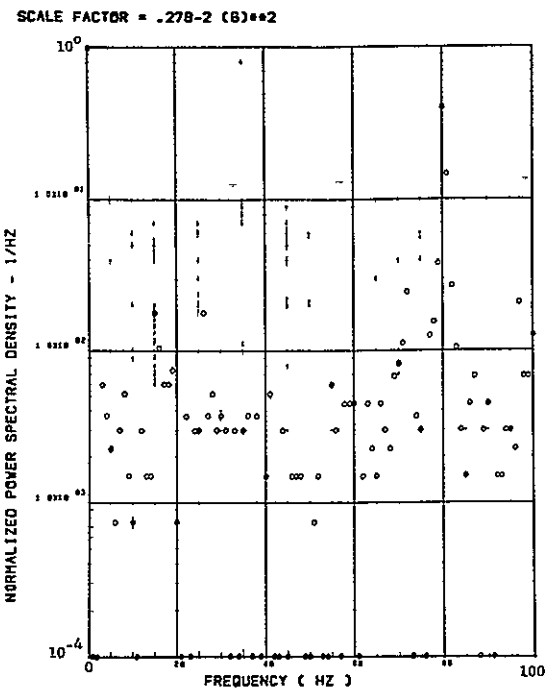

(e) - AF008 PILOT S SEAT VERTICAL ACCELEROMETER

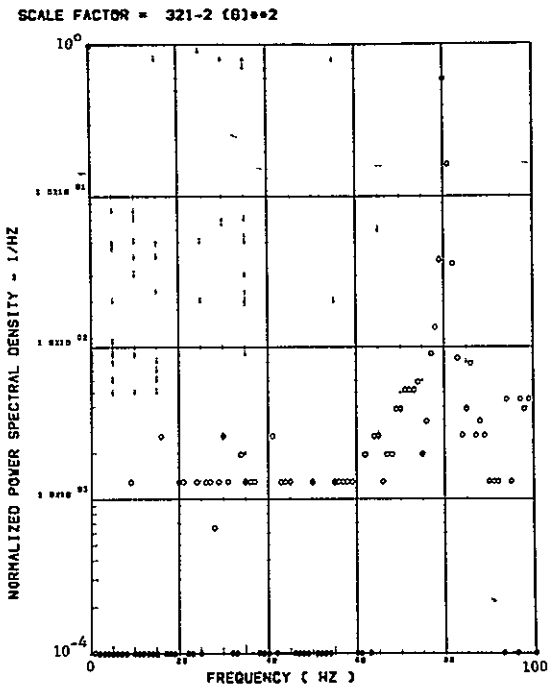

(f) - AF010 PILOT S SEAT LATERAL ACCELEROMETER

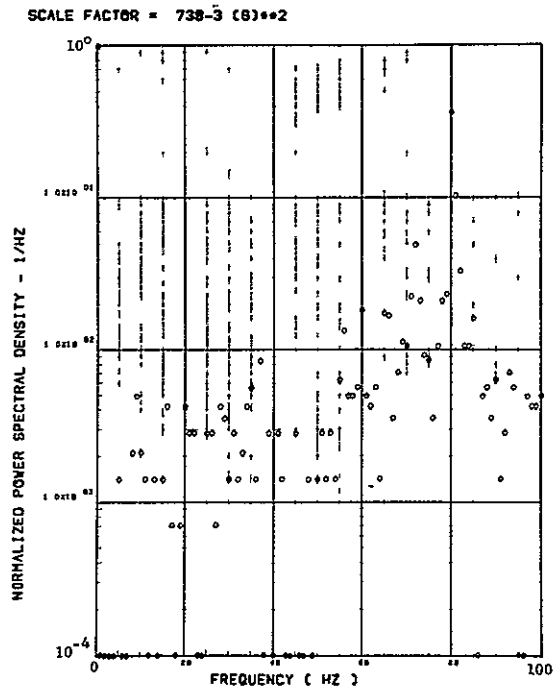

(g) - AB020 C.G. LATERAL ACCELEROMETER

Figure 29. Continued

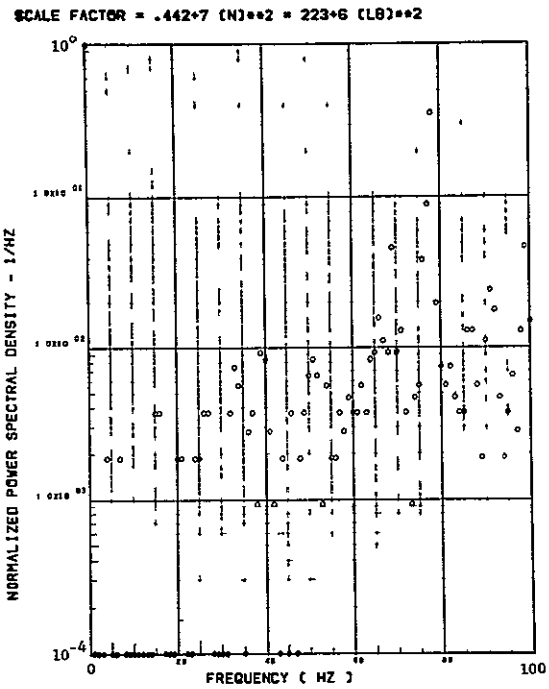

(h) - SW123 SHEAR AT WING STATION 1

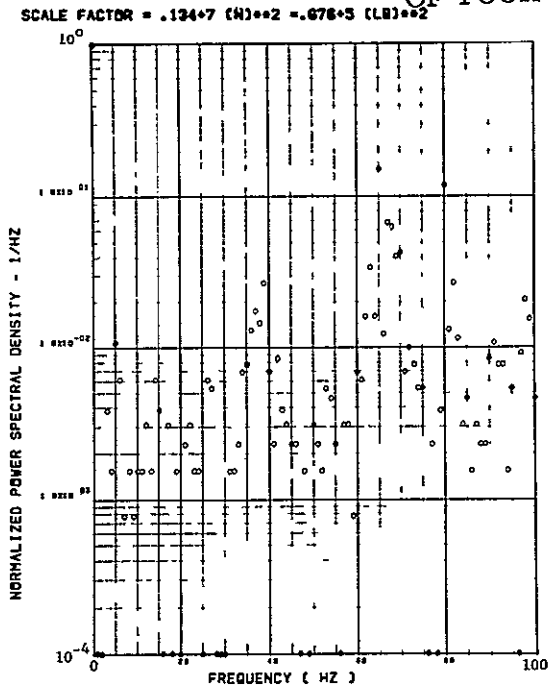

(i) - SW126 SHEAR AT WING STATION 2

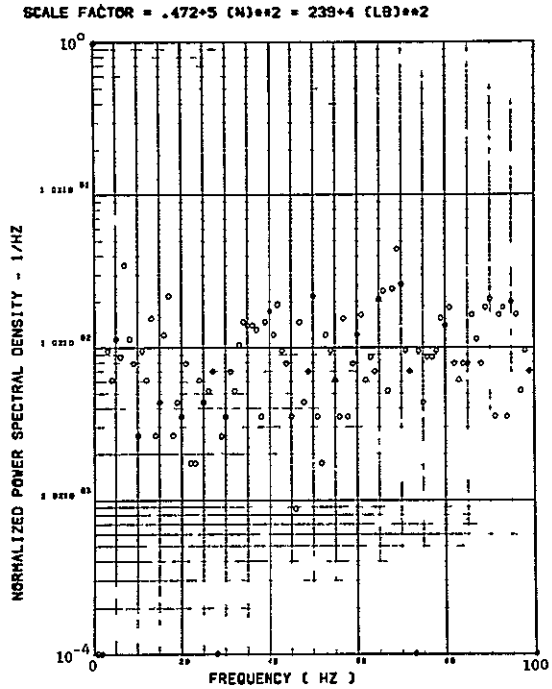

(j) - SW129 SHEAR AT WING STATION 3

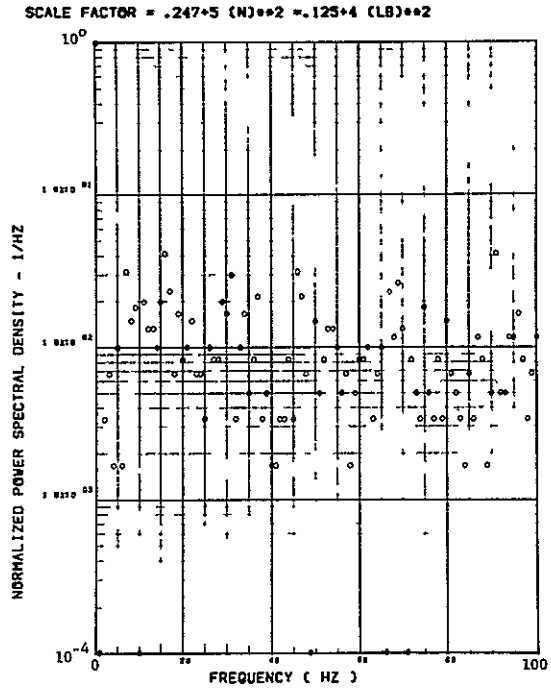

(k) - SW132 SHEAR AT WING STATION 4

Figure 29. Continued

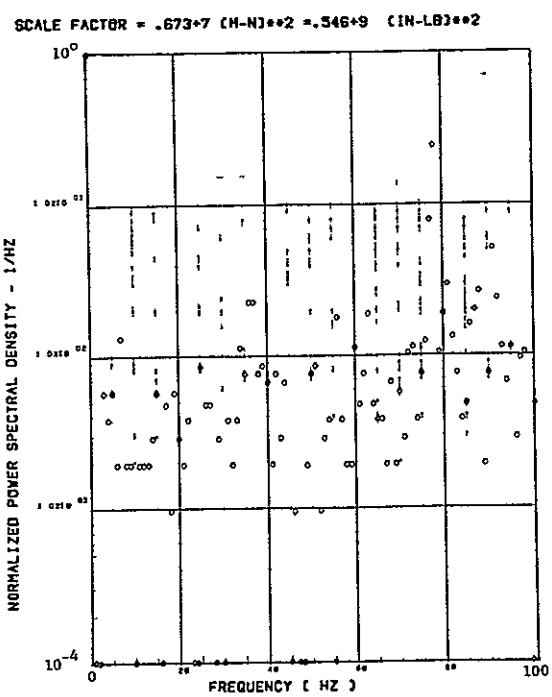

(l) - SW124 BENDING MOMENT AT WING STATION 1

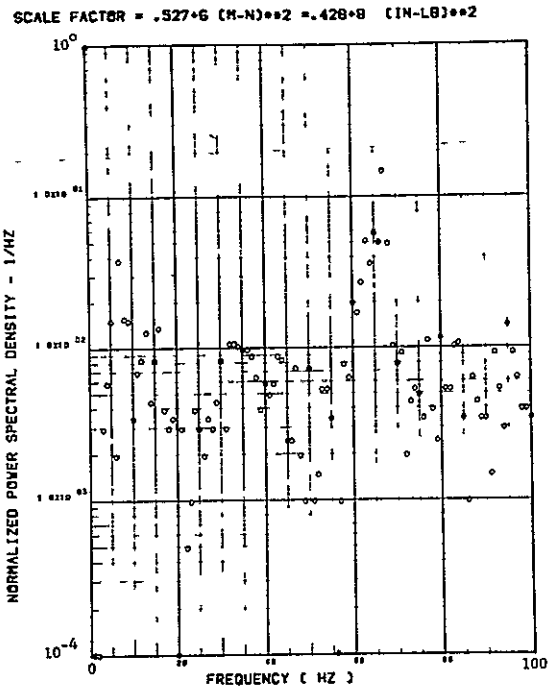

(m) - SW127 BENDING MOMENT AT WING STATION 2

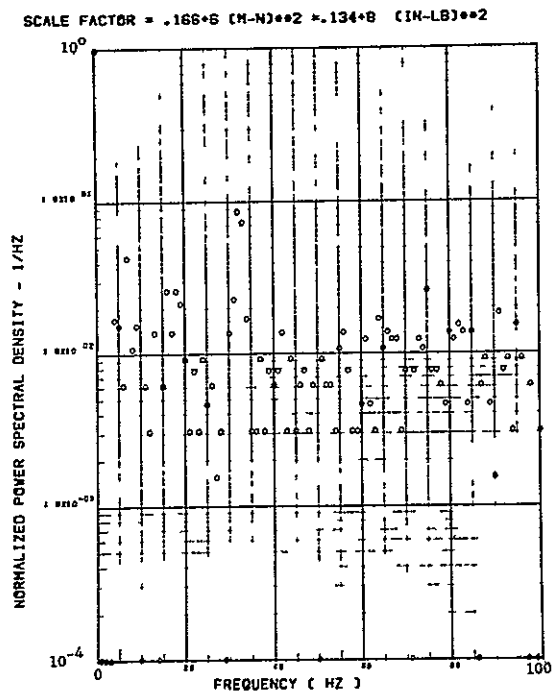

(n) - SW130 BENDING MOMENT AT WING STATION 3

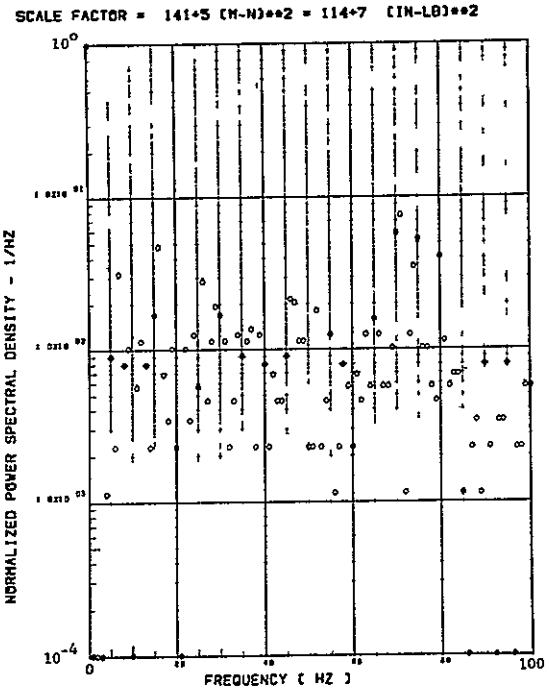

(o) - SW133 BENDING MOMENT AT WING STATION 4

Figure 29. Continued

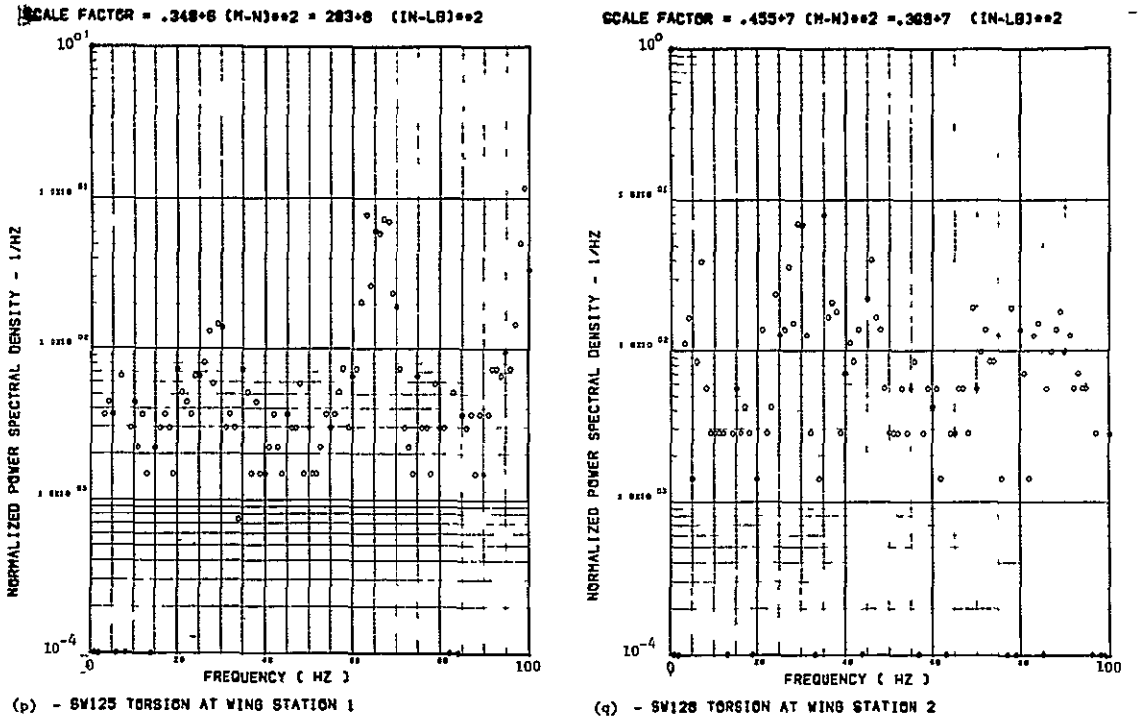

Data Not Available

Figure 29. Concluded

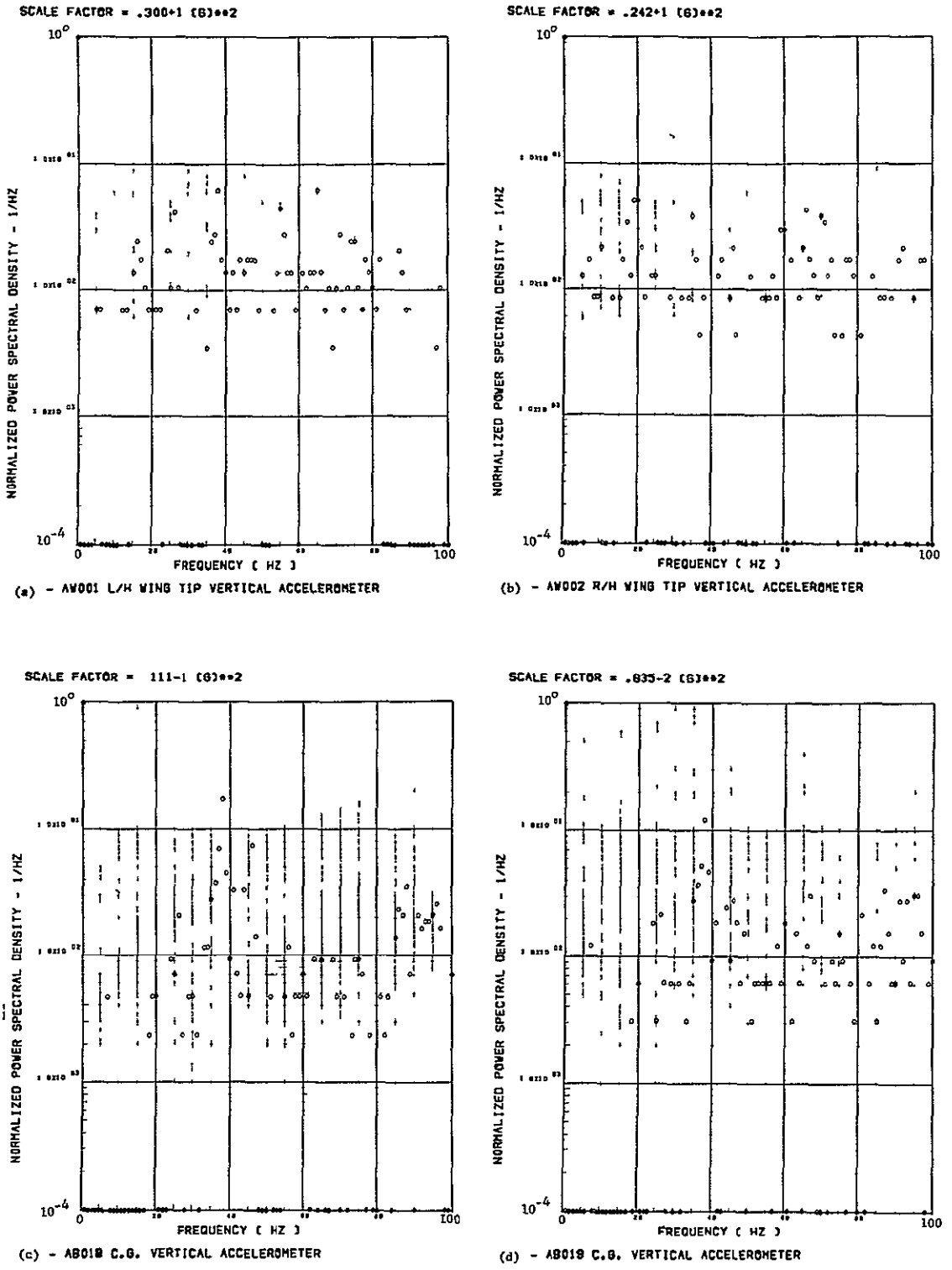

Figure 30. Power Spectra-Flight 78, Run 5, Point 2, T_1=114734.8, ΔT=1 Sec, α_{Nom}=5.1 deg, $\Delta\alpha$=3.8 deg.

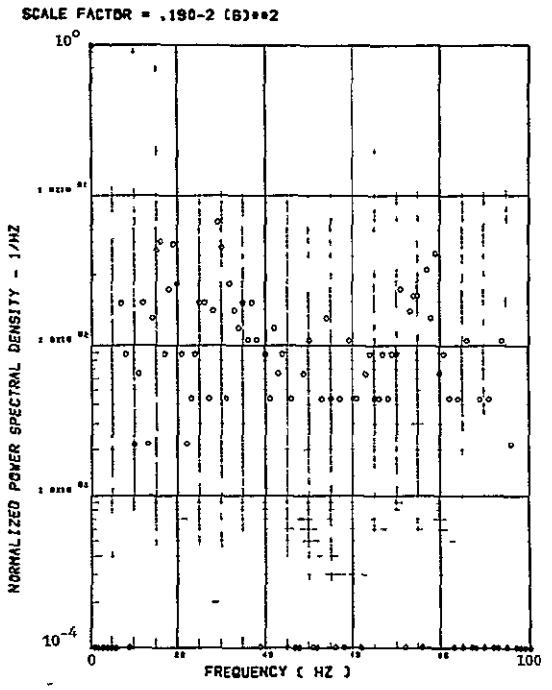

(e) - AF009 PILOT S SEAT VERTICAL ACCELEROMETER

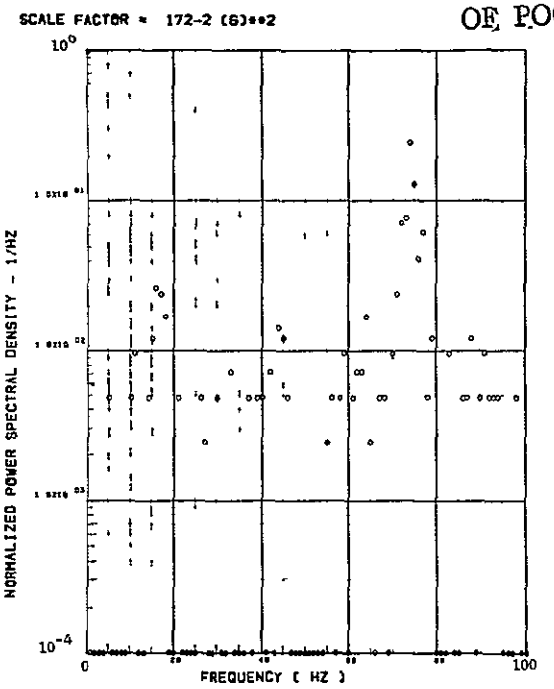

(f) - AF010 PILOT S SEAT LATERAL ACCELEROMETER

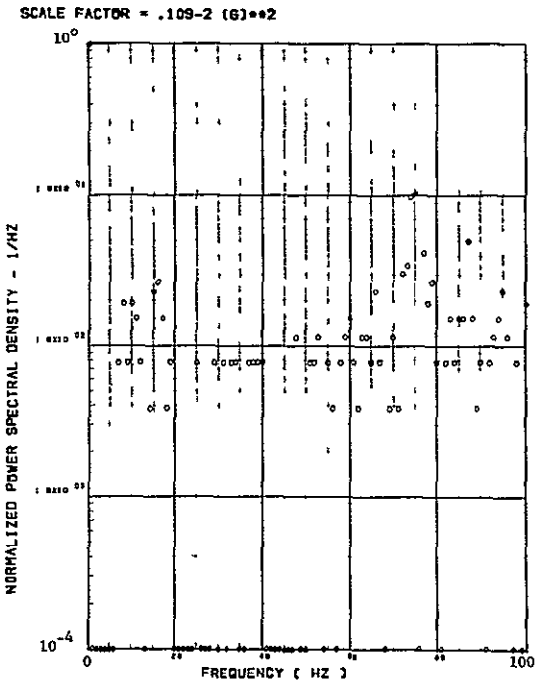

(g) - AB020 C G LATERAL ACCELEROMETER

Figure 30. Continued

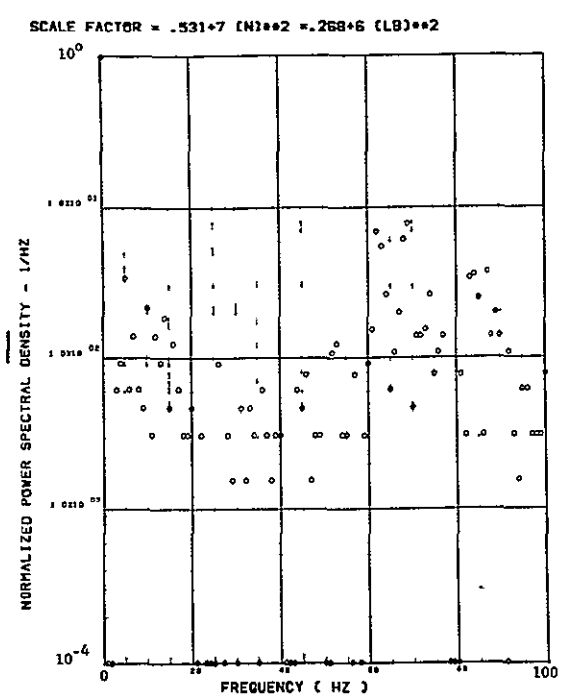

(h) - SW123 SHEAR AT WING STATION 1

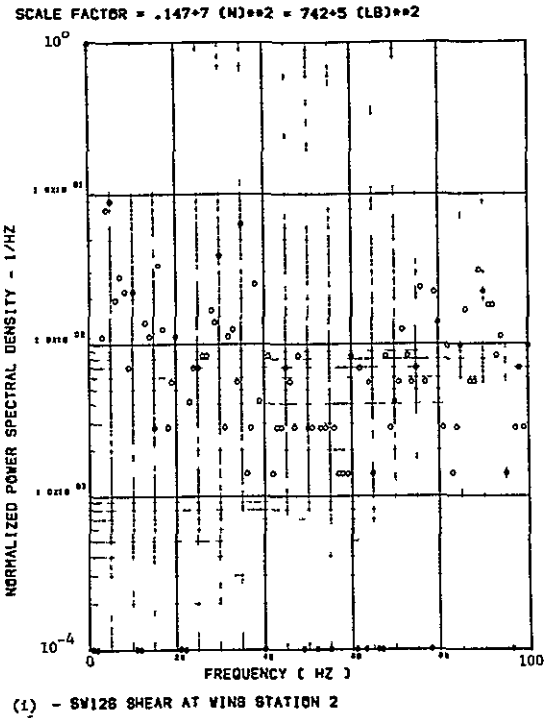

(i) - SW126 SHEAR AT WING STATION 2

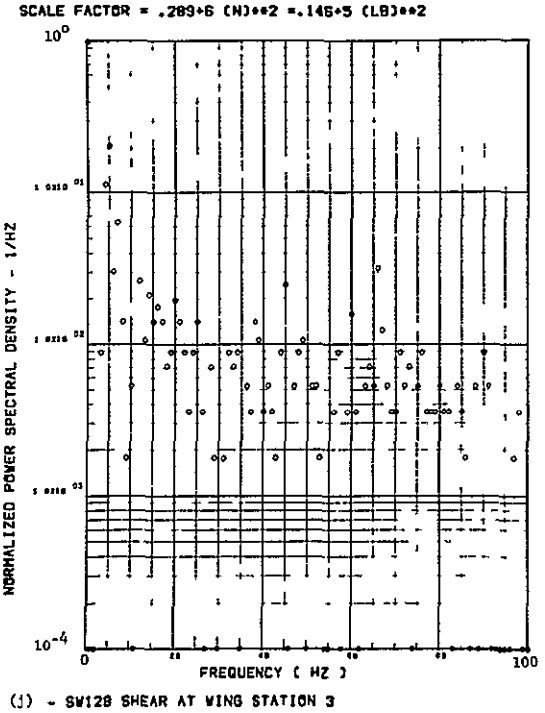

(j) - SW129 SHEAR AT WING STATION 3

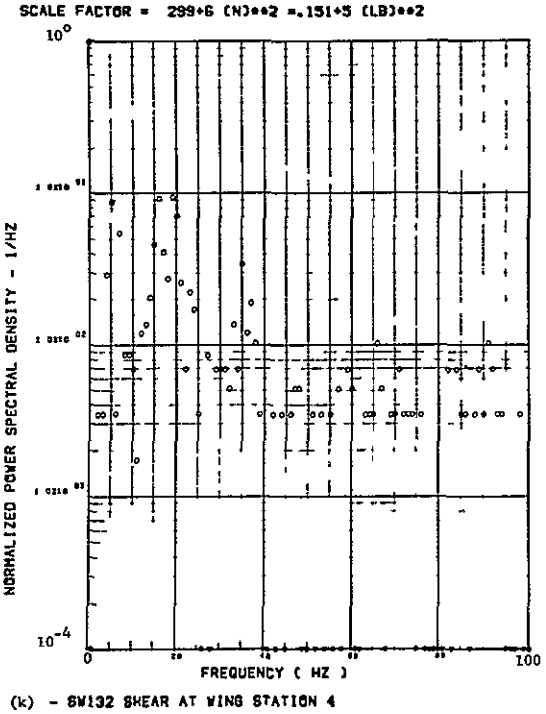

(k) - SW132 SHEAR AT WING STATION 4

Figure 30. Continued

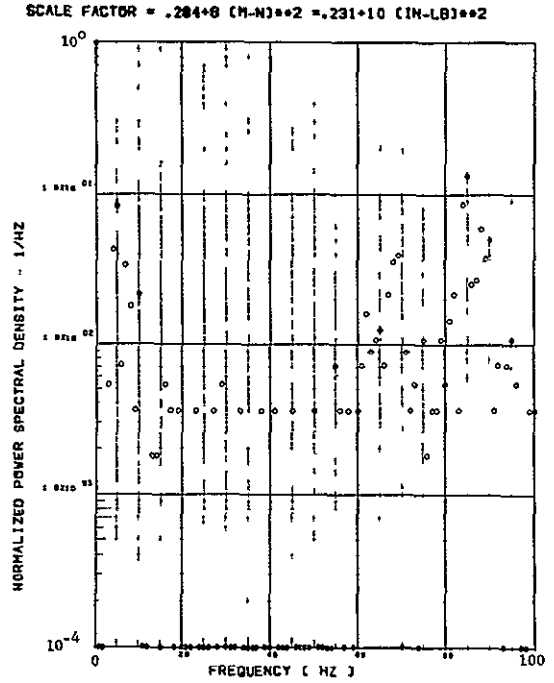

(l) - SW124 BENDING MOMENT AT WING STATION 1

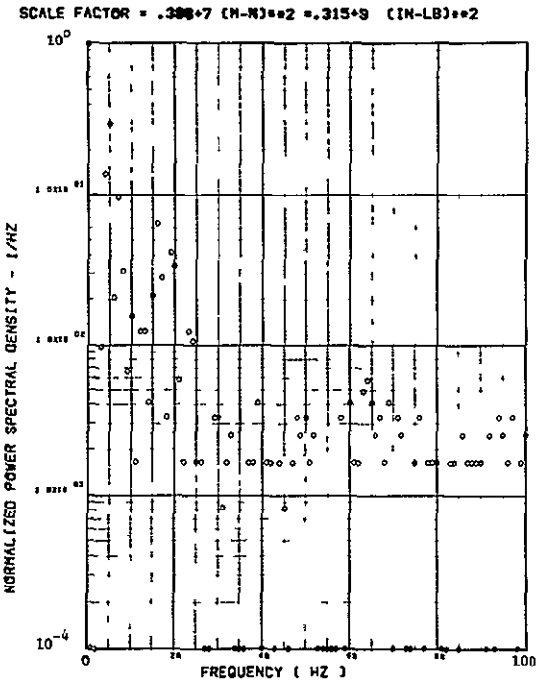

(m) - SW127 BENDING MOMENT AT WING STATION 2

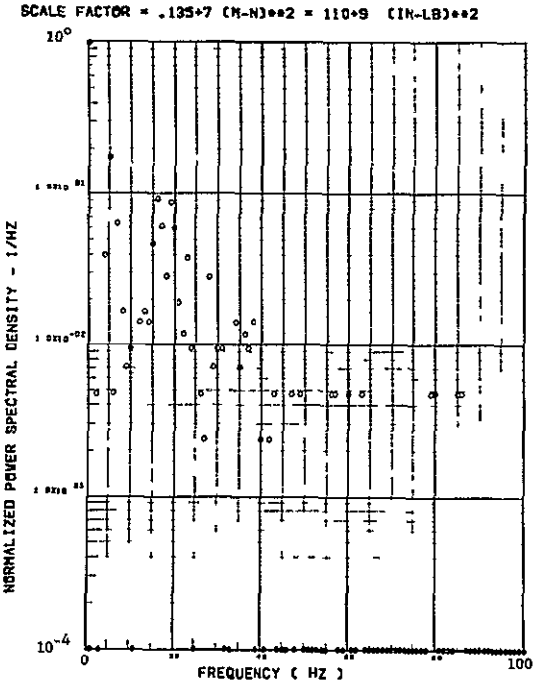

(n) - SW130 BENDING MOMENT AT WING STATION 3

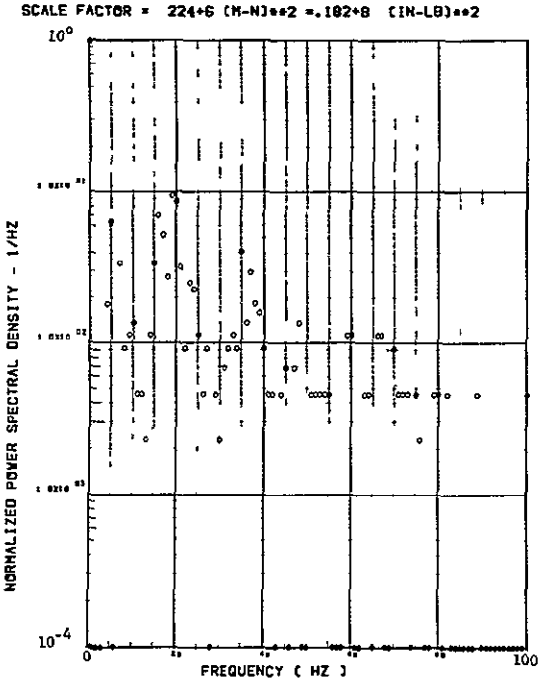

(o) - SW133 BENDING MOMENT AT WING STATION 4

Figure 30. Continued

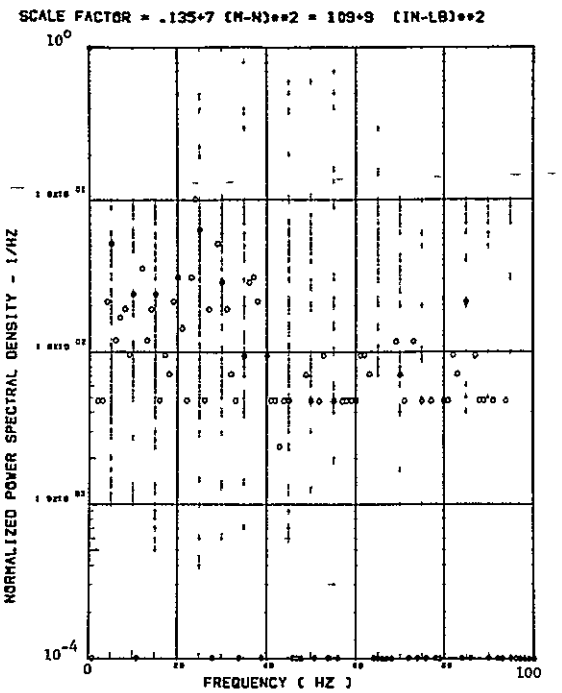

(p) - SW125 TORSION AT WING STATION 1

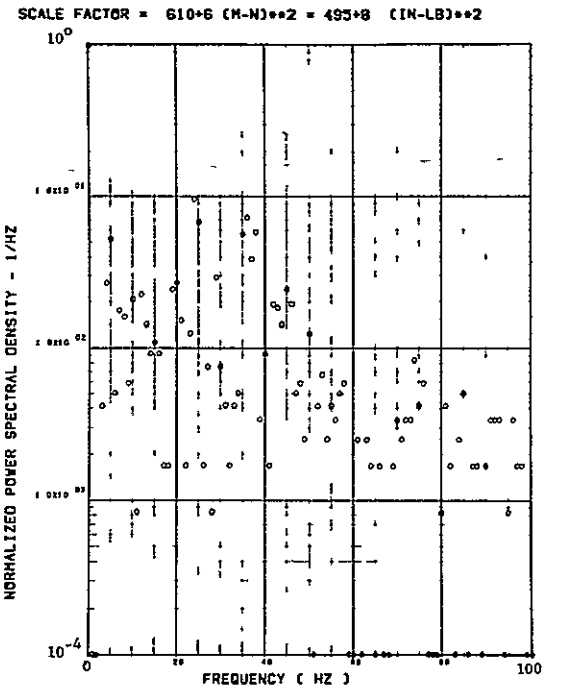

(q) - SW128 TORSION AT WING STATION 2

Data Not Available

Figure 30. Concluded

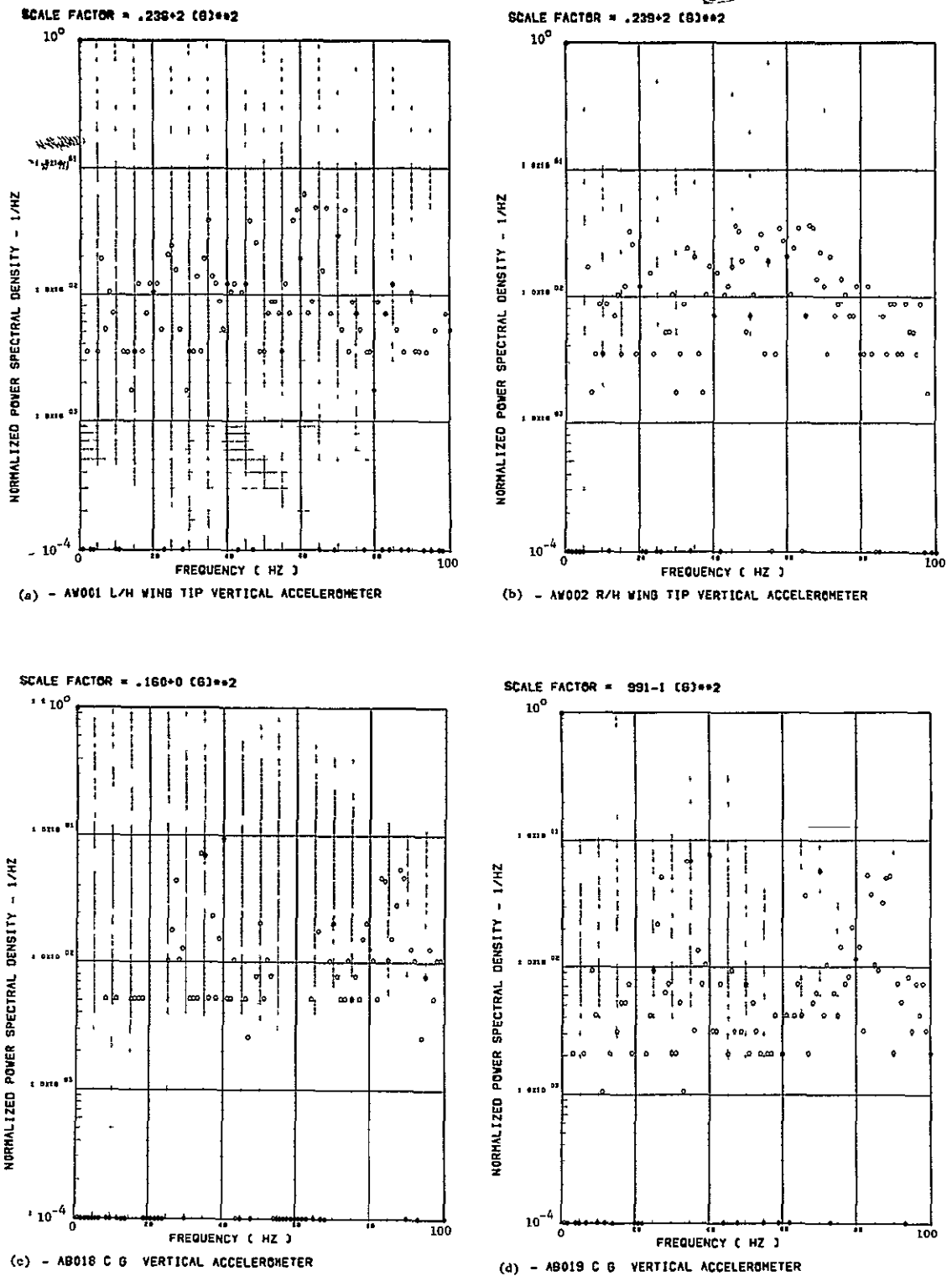

Figure 31. Power Spectra-Flight 78, Run 5, Point 3, T_1=114735.7, ΔT=1 Sec, α_{Nom}=9.2 deg, $\Delta\alpha$=4.20 deg.

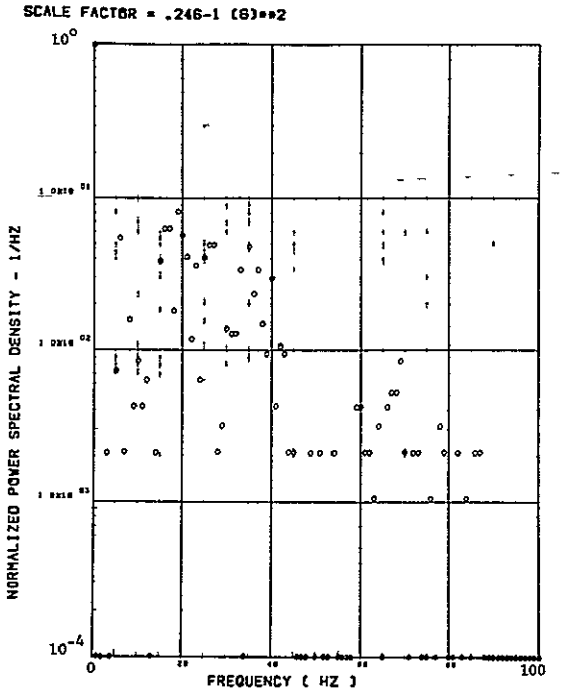

(e) - AF008 PILOT S SEAT VERTICAL ACCELEROMETER

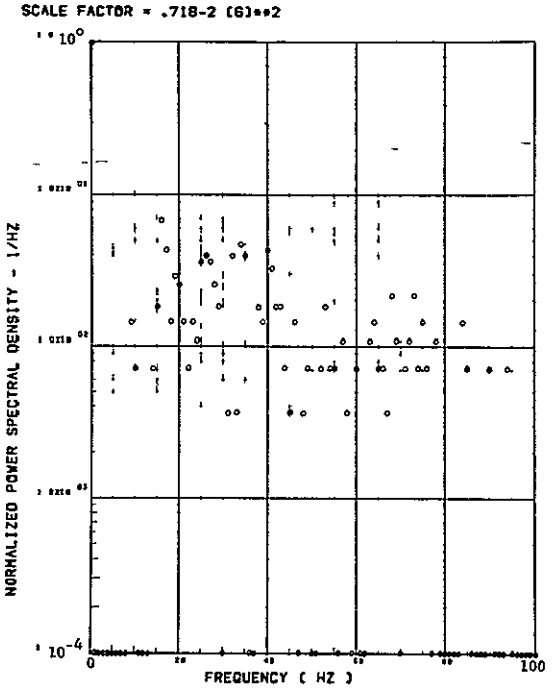

(f) - AF010 PILOT S SEAT LATERAL ACCELEROMETER

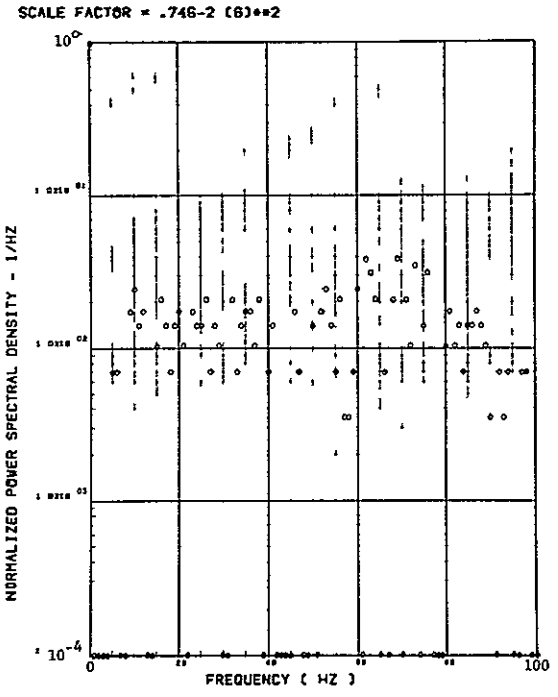

(g) - AB020 C G LATERAL ACCELEROMETER

Figure 31. Continued

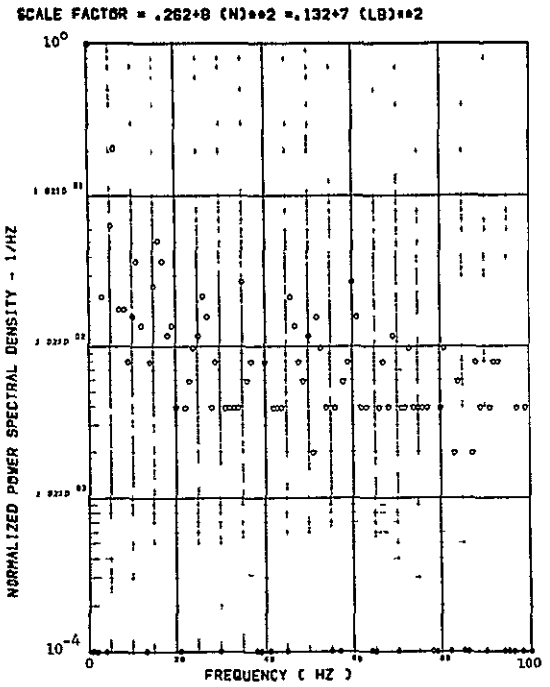

(h) - SW123 SHEAR AT WING STATION 1

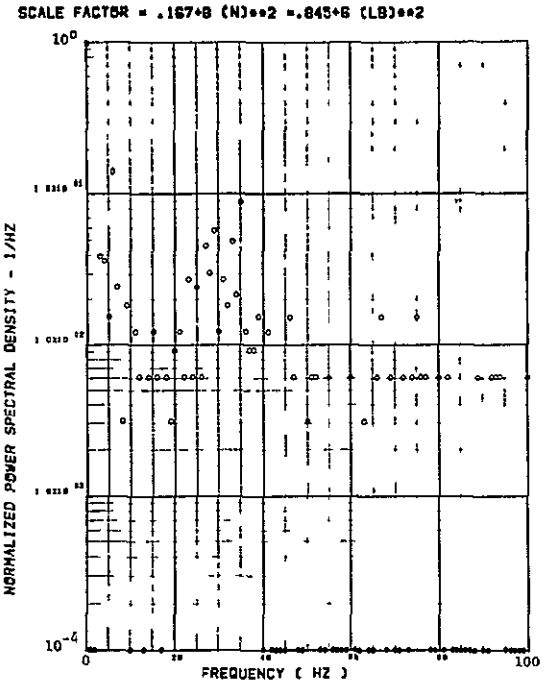

(i) - SW126 SHEAR AT WING STATION 2

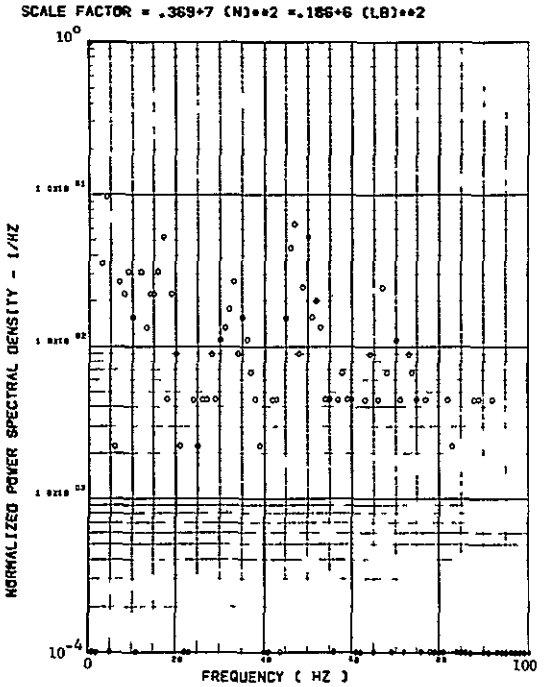

(j) - SW129 SHEAR AT WING STATION 3

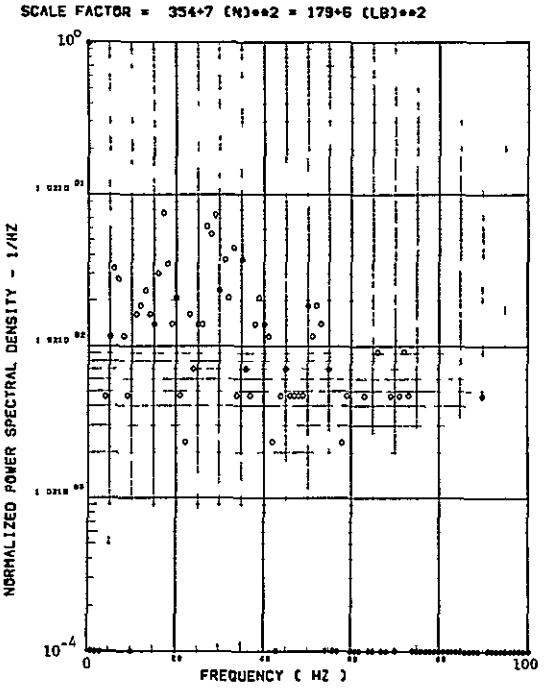

(k) - SW132 SHEAR AT WING STATION 4

Figure 31. Continued

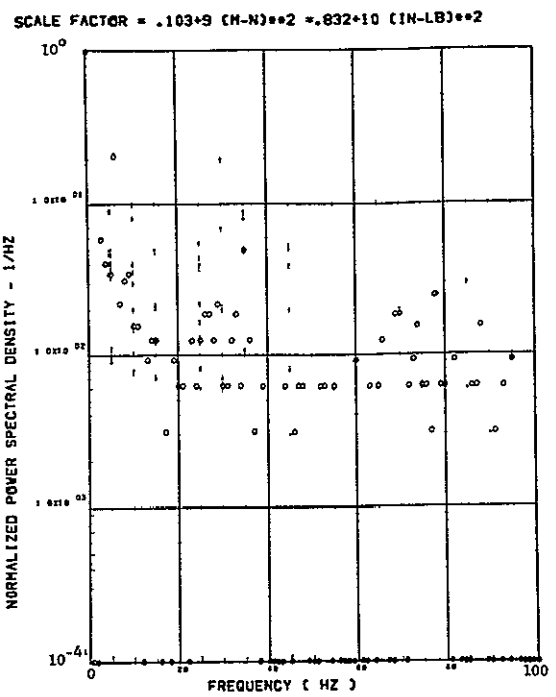

(l) - SW124 BENDING MOMENT AT WING STATION 1

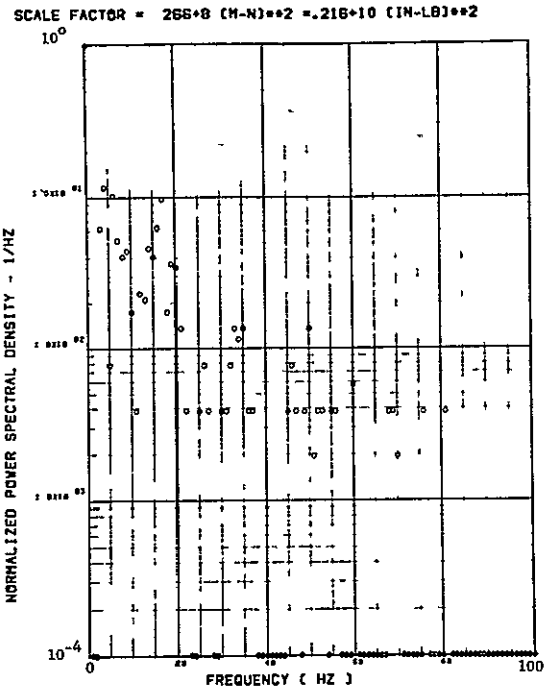

(m) - SW127 BENDING MOMENT AT WING STATION 2

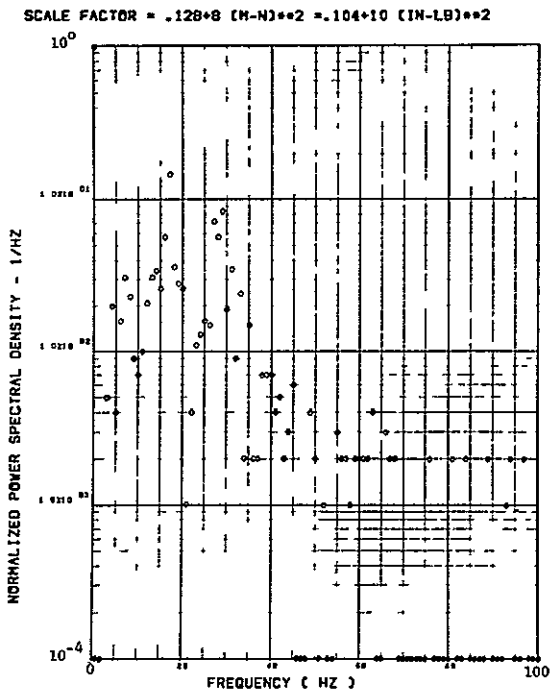

(n) - SW130 BENDING MOMENT AT WING STATION 3

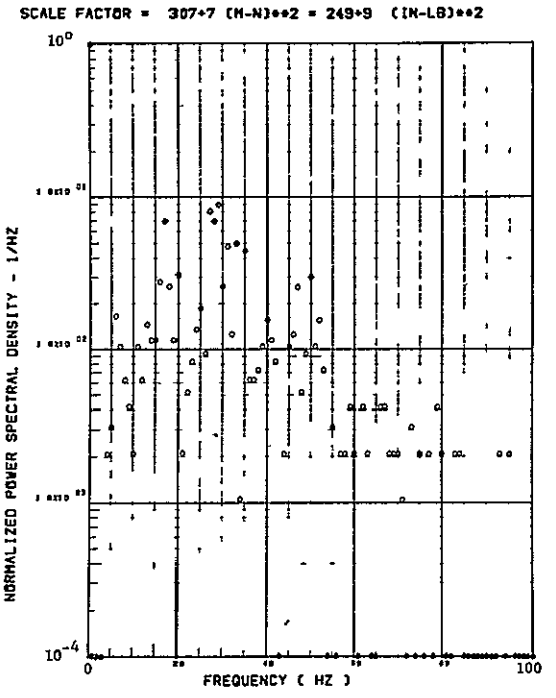

(o) - SW133 BENDING MOMENT AT WING STATION 4

Figure 31. Continued

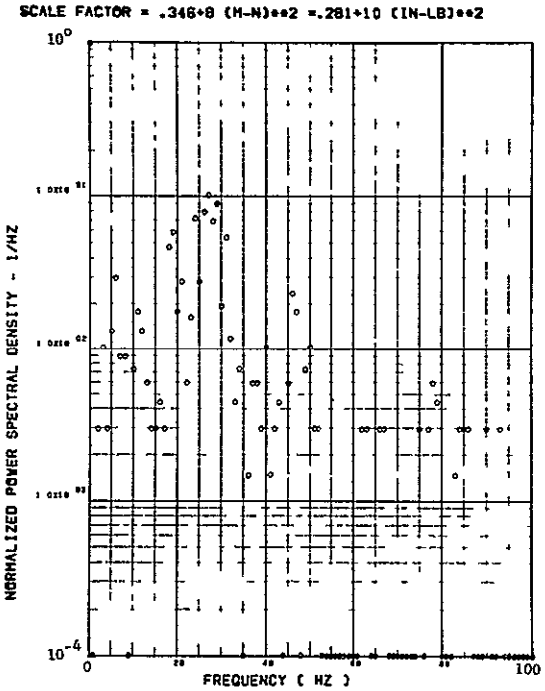

(p) - SW125 TORSION AT WING STATION 1

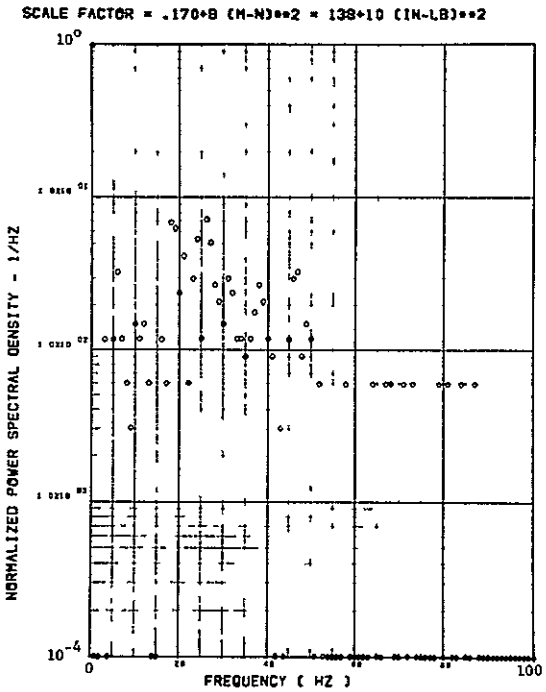

(q) - SW128 TORSION AT WING STATION 2

Data Not Available

Figure 31. Concluded

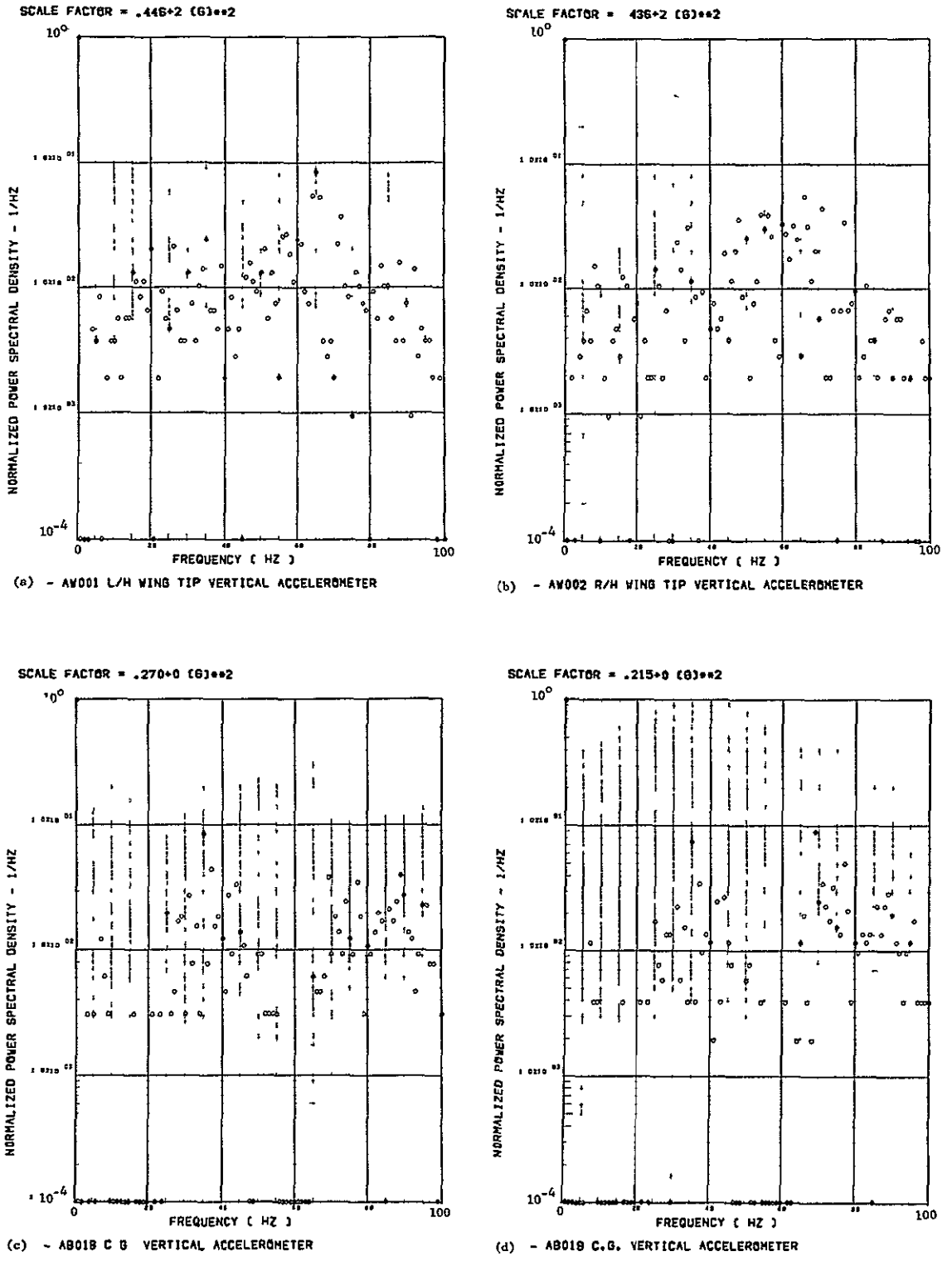

Figure 32. Power Spectra-Flight 78, Run 5, Point 4, T_1=114736.4, ΔT=1 Sec, α_{Nom}=12.2 deg, $\Delta\alpha$=4.30 deg.

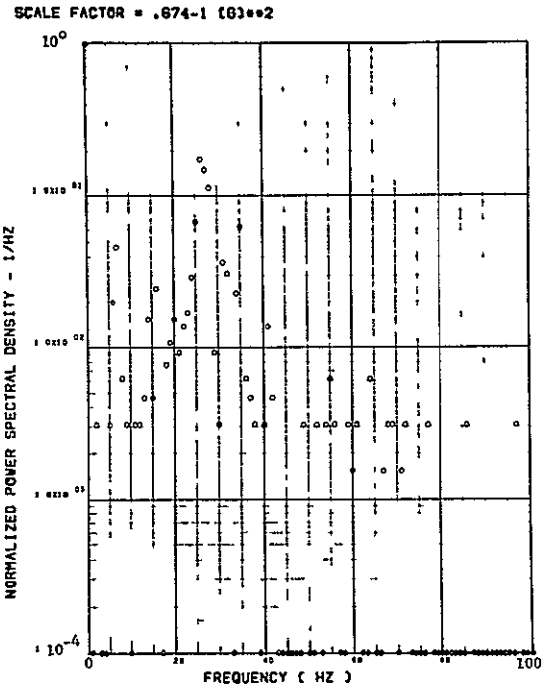

(e) - AF009 PILOT S SEAT VERTICAL ACCELEROMETER

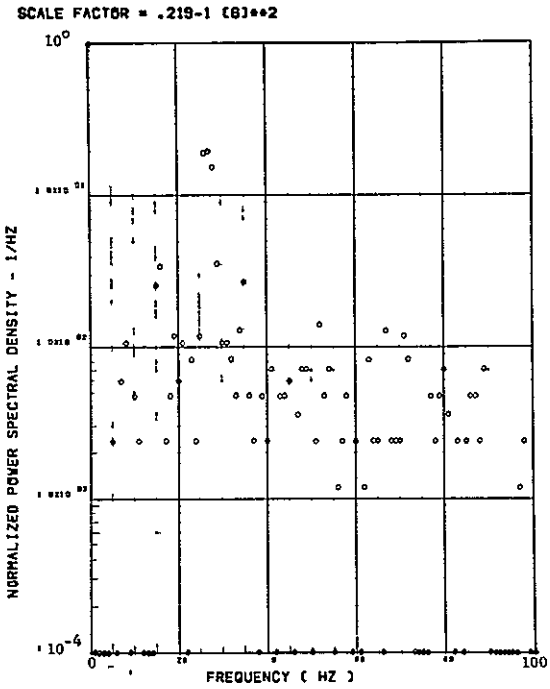

(f) - AF010 PILOT S SEAT LATERAL ACCELEROMETER

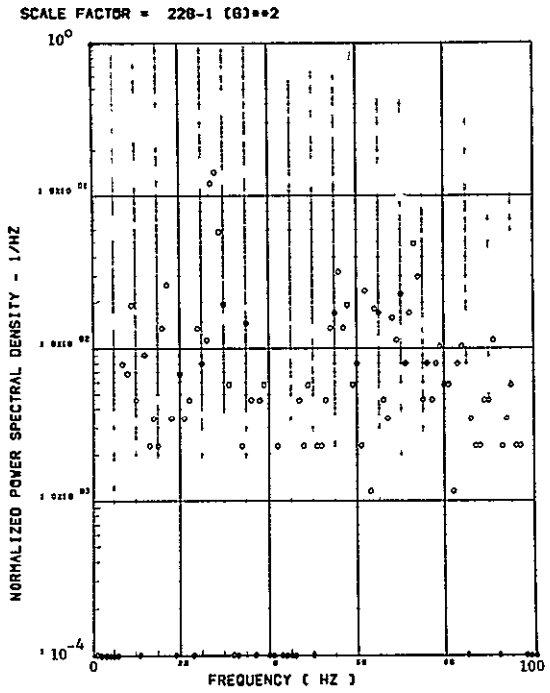

(g) - AB020 C G LATERAL ACCELEROMETER

Figure 32. Continued

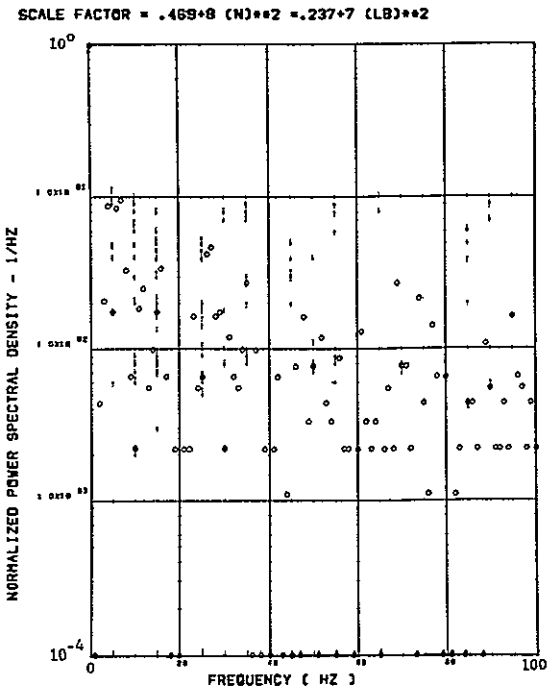

(h) - SW123 SHEAR AT WING STATION 1

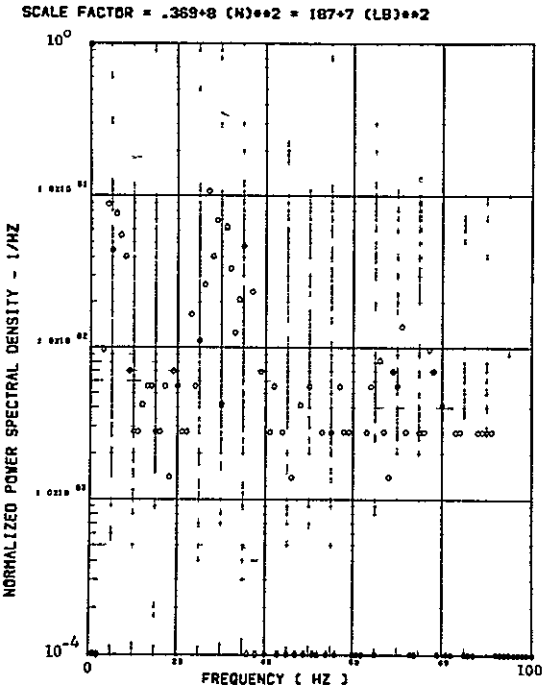

(i) - SW126 SHEAR AT WING STATION 2

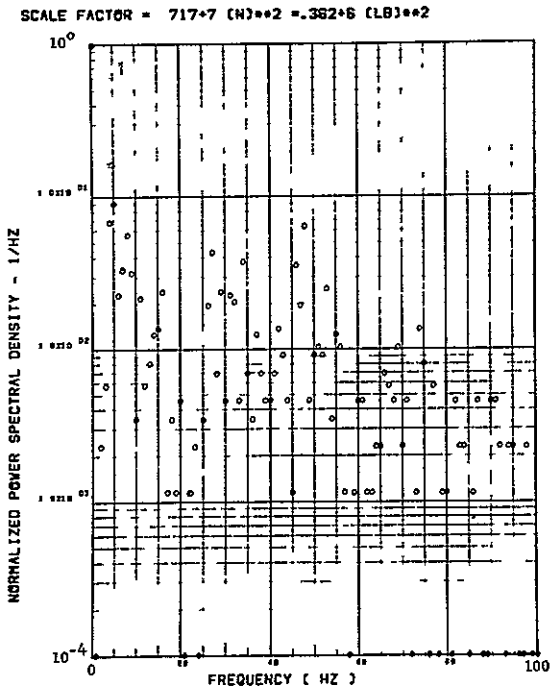

(j) - SW129 SHEAR AT WING STATION 3

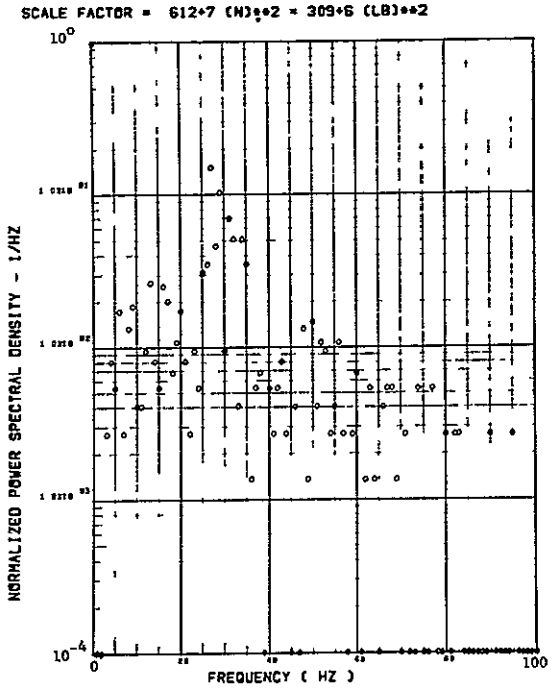

(k) - SW132 SHEAR AT WING STATION 4

Figure 32. Continued

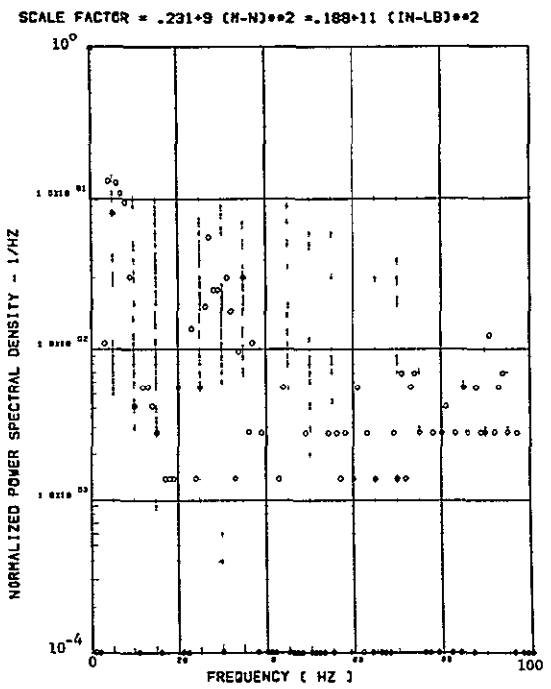

(l) - SW124 BENDING MOMENT AT WING STATION 1

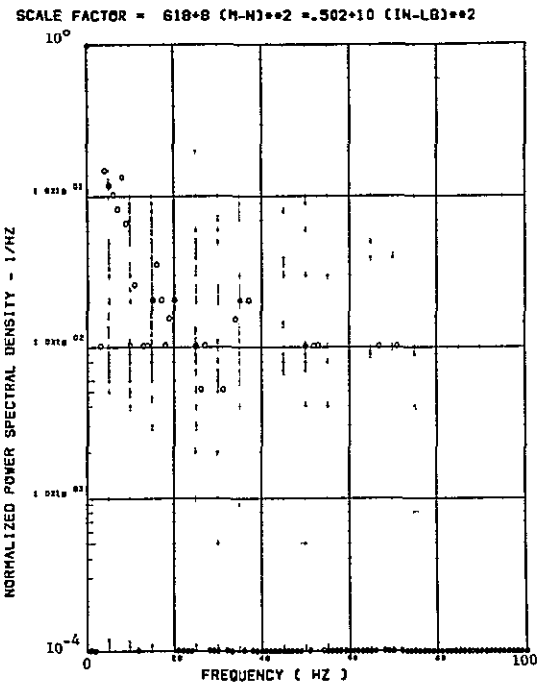

(m) - SW127 BENDING MOMENT AT WING STATION 2

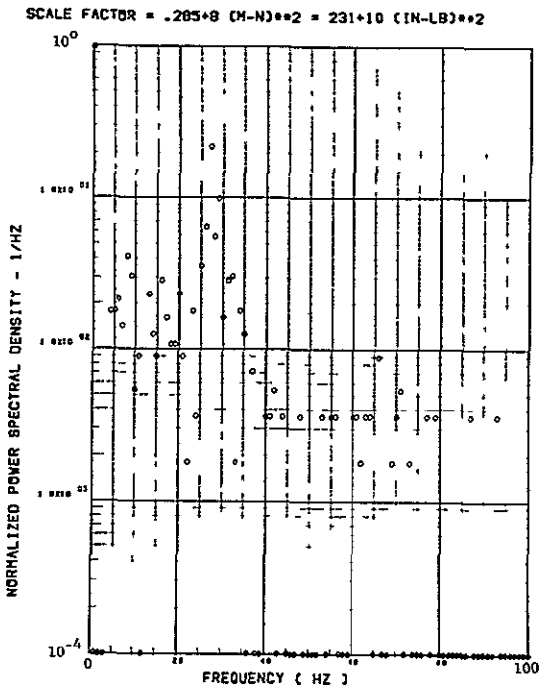

(n) - SW130 BENDING MOMENT AT WING STATION 3

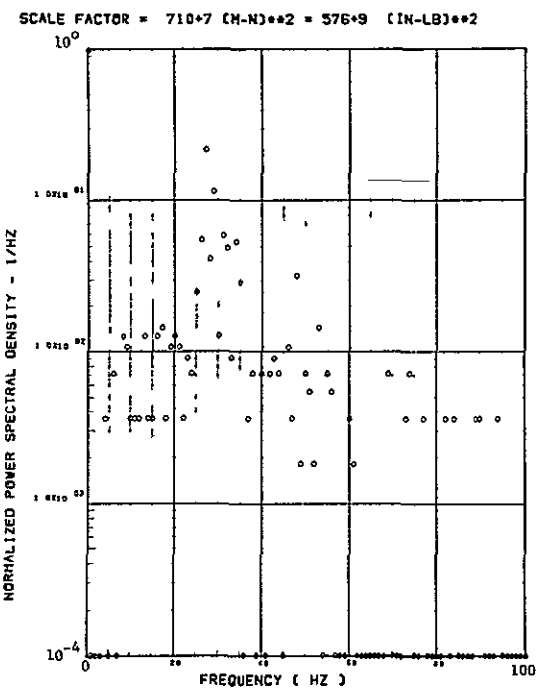

(o) - SW133 BENDING MOMENT AT WING STATION 4

Figure 32. Continued

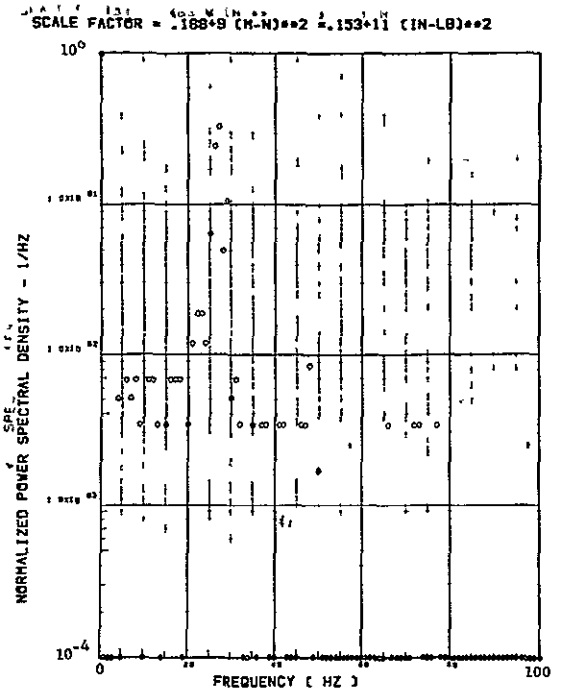

(p) - SW125 TORSION AT WING STATION 1

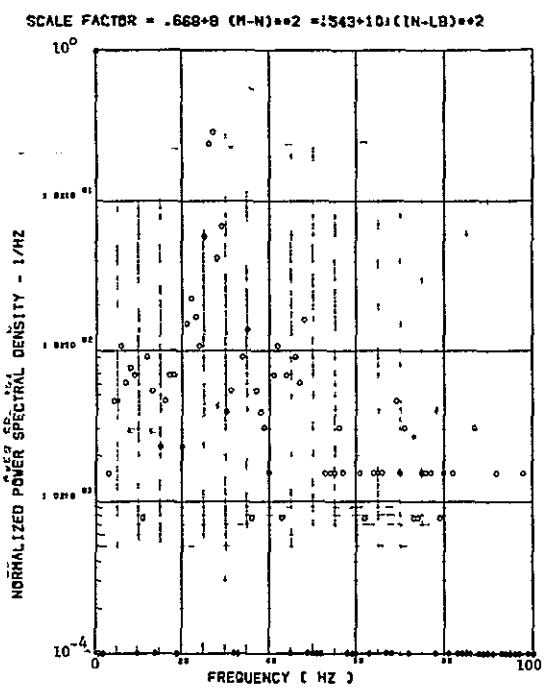

(q) - SW128 TORSION AT WING STATION 2

Data Not Available

Figure 32. Concluded

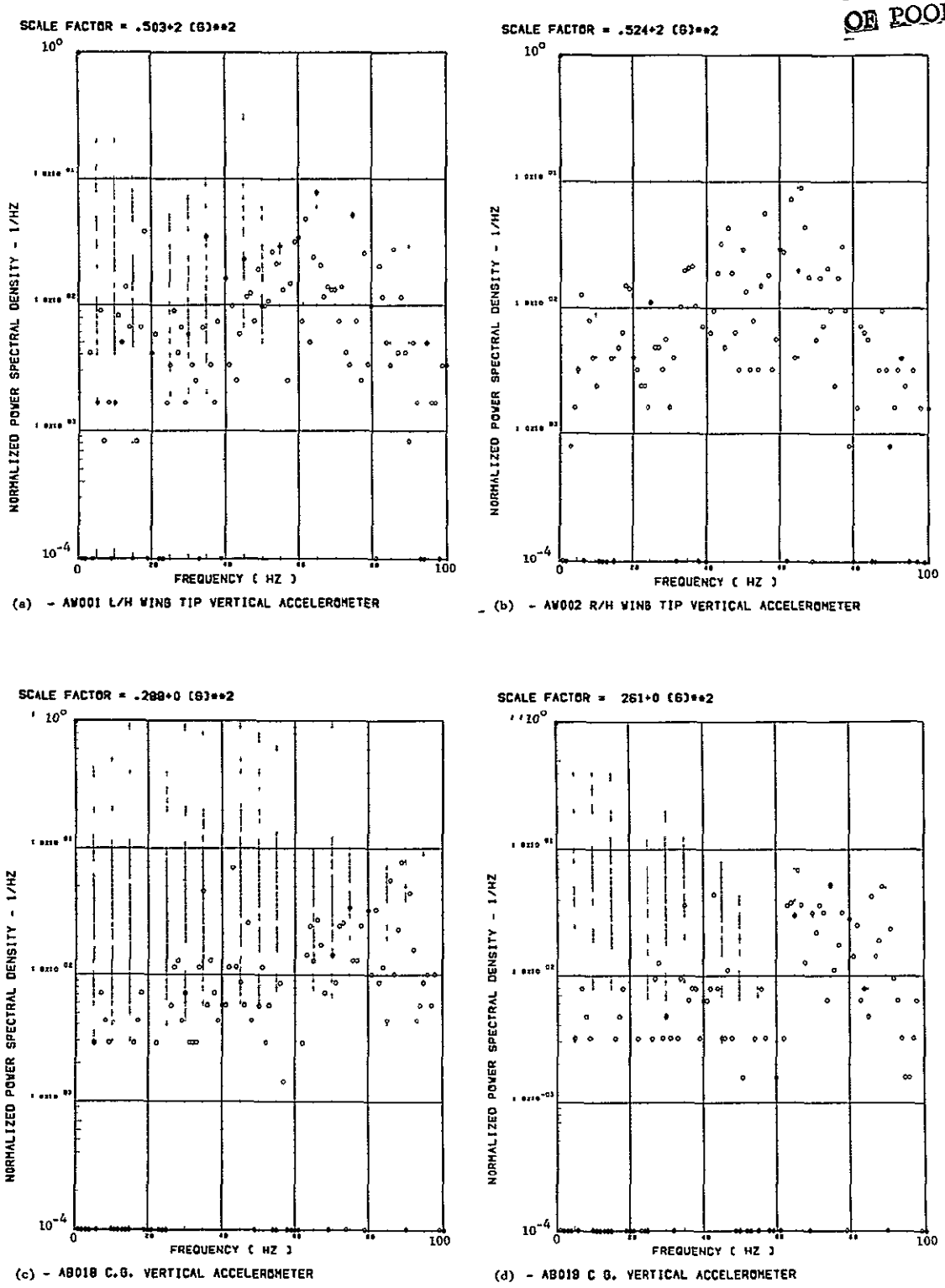

Figure 33. Power Spectra-Flight 78, Run 5, Point 5 T_1=114737.2, ΔT=1 Sec, α_{Nom}=14.6 deg, $\Delta\alpha$=2.05 deg.

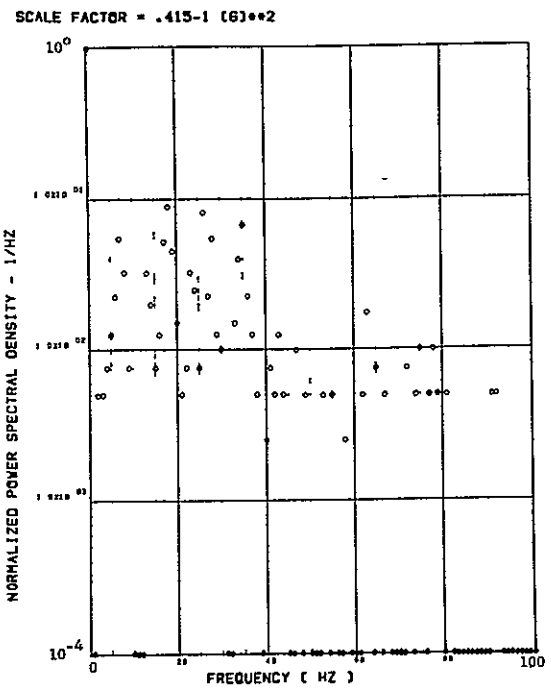

(e) - AF009 PILOT S SEAT VERTICAL ACCELEROMETER

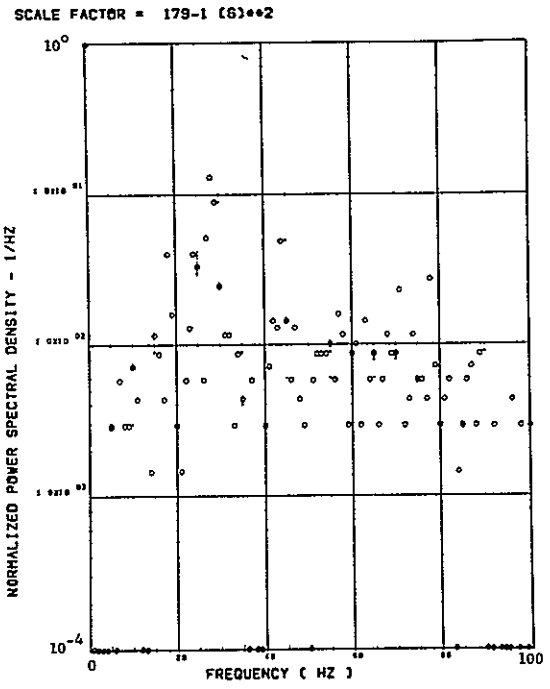

(f) - AF010 PILOT S SEAT LATERAL ACCELEROMETER

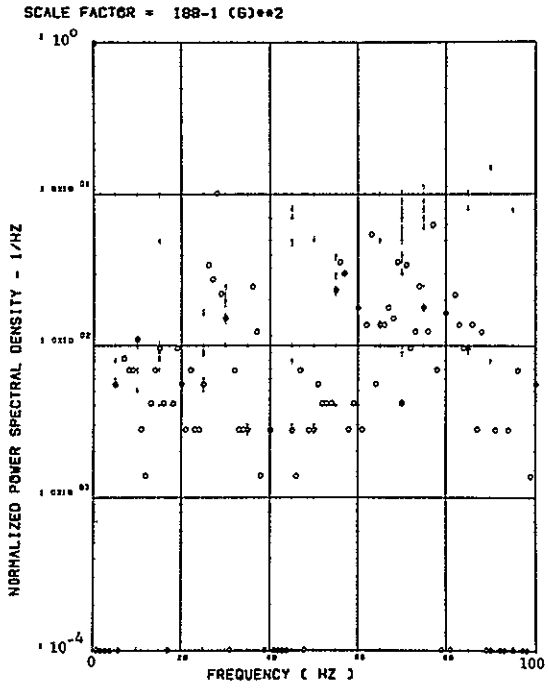

(g) - AB020 C.G. LATERAL ACCELEROMETER

Figure 33. Continued

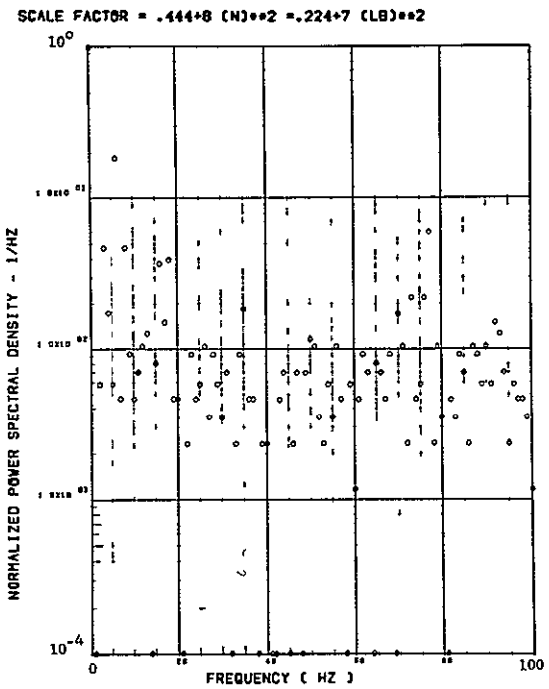

(h) - SW123 SHEAR AT WING STATION 1

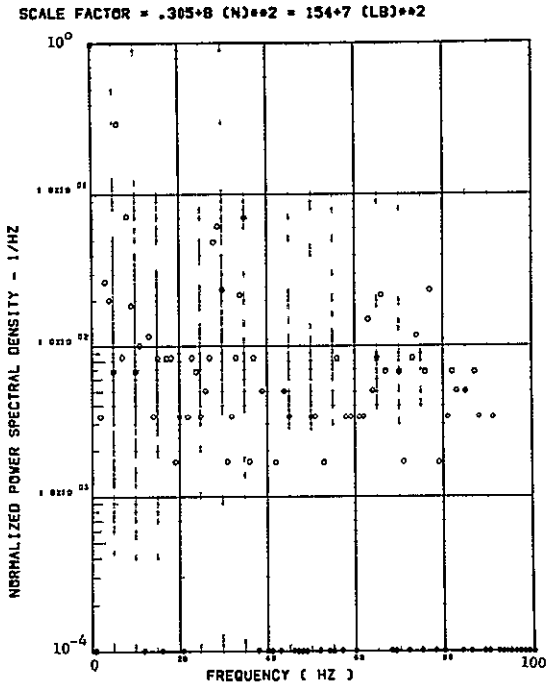

(i) - SW128 SHEAR AT WING STATION 2

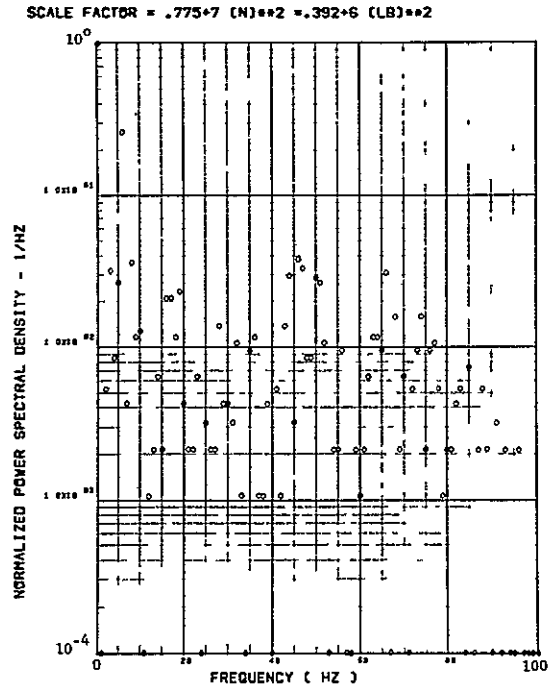

(j) - SW129 SHEAR AT WING STATION 3

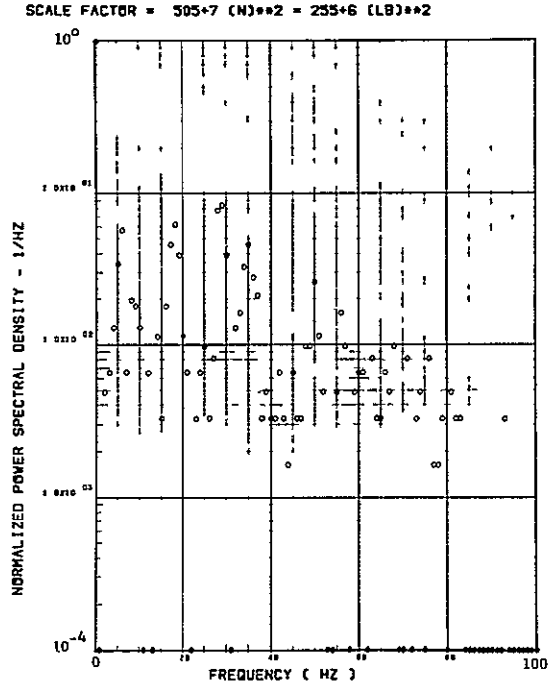

(k) - SW132 SHEAR AT WING STATION 4

Figure 33. Continued

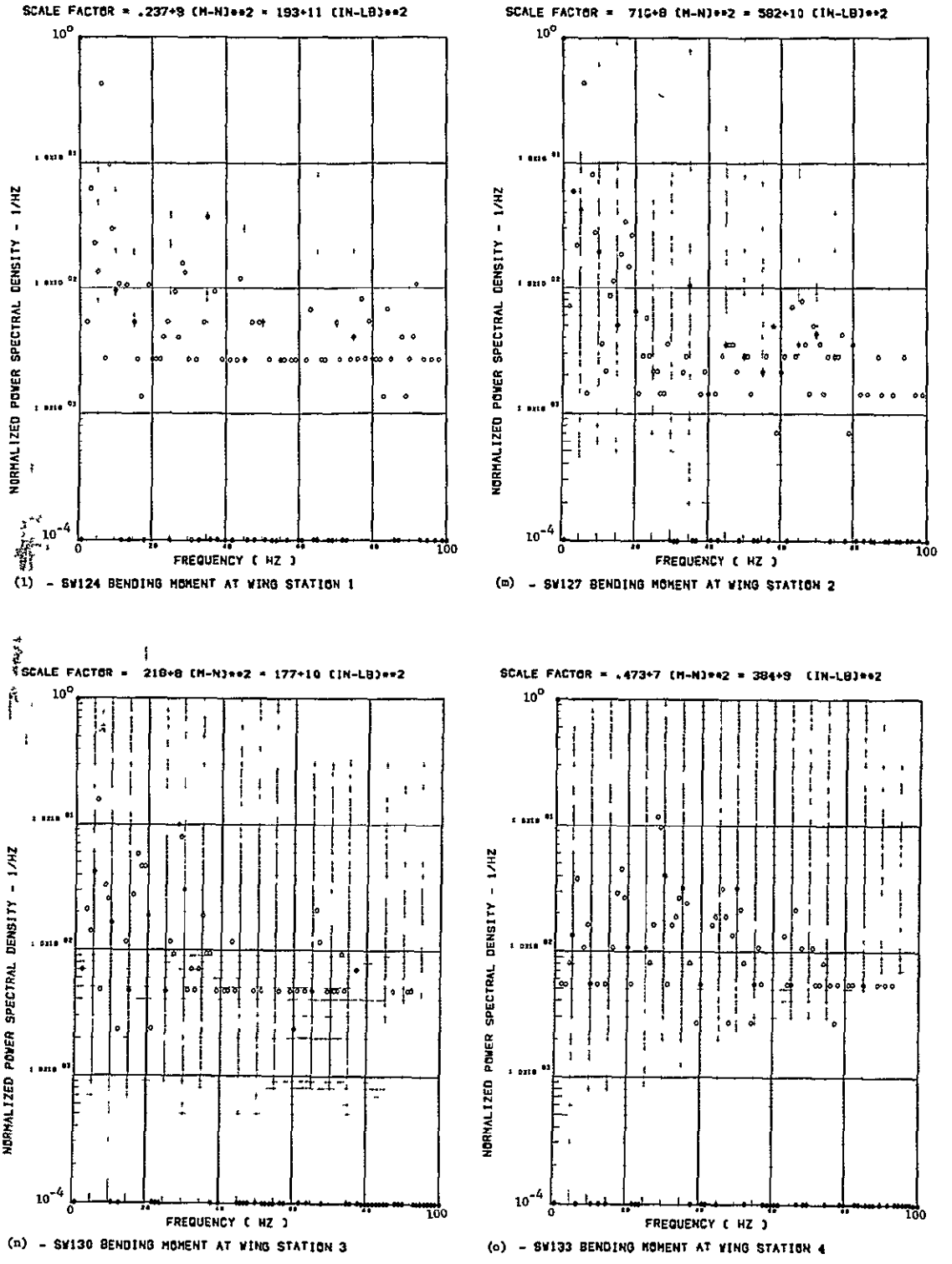

Figure 33. Continued

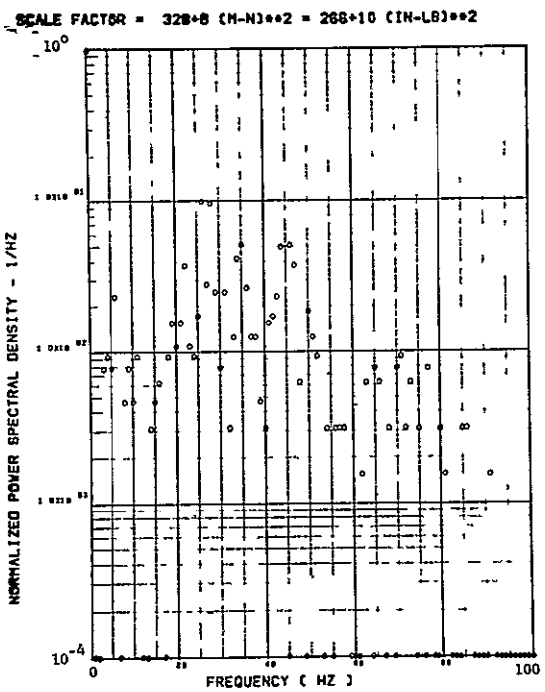

(p) - SW128 TORSION AT WING STATION 2

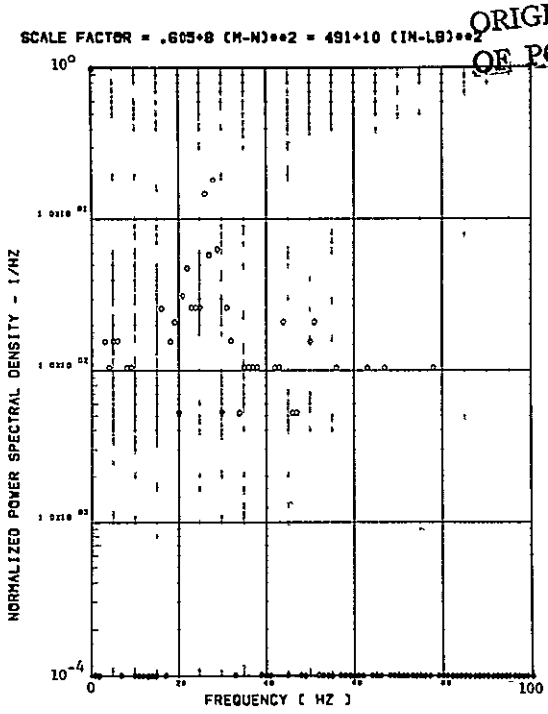

(q) - SW125 TORSION AT WING STATION 1

Data Not Available

Figure 33. Concluded

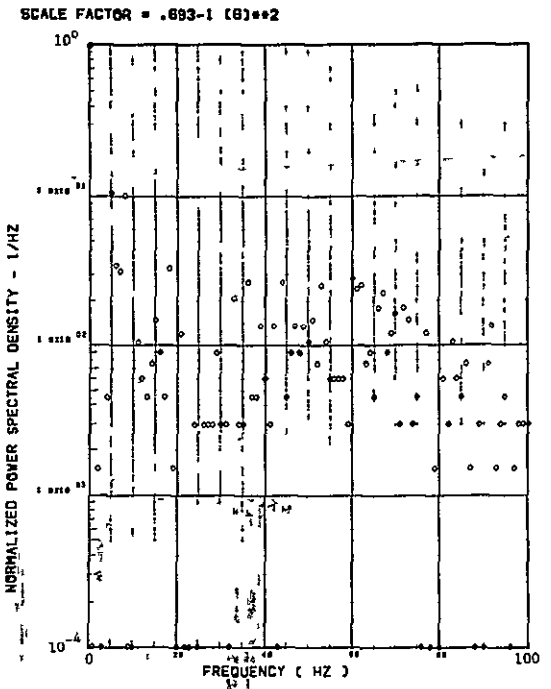

Data Not Available

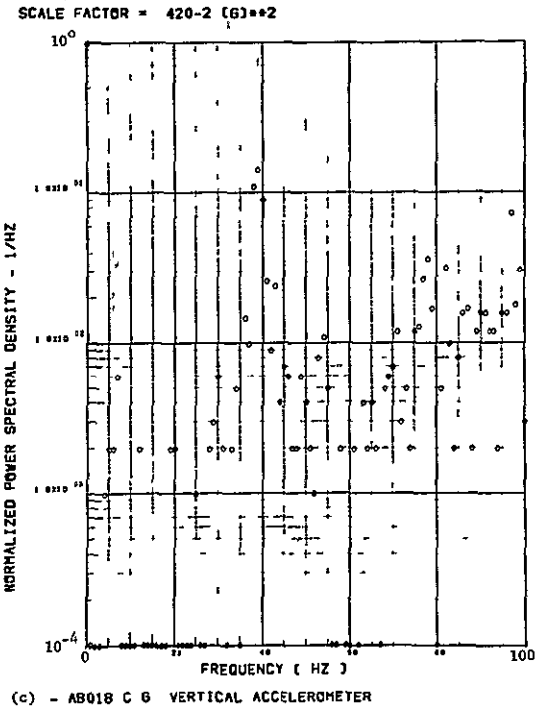

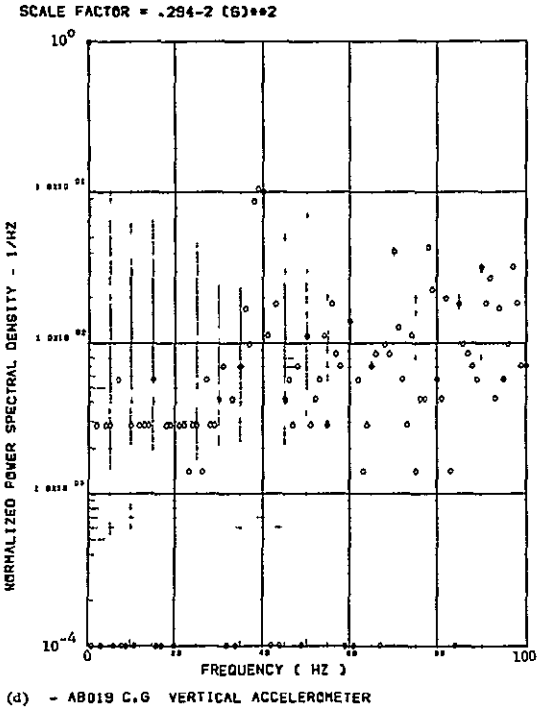

Figure 34. Power Spectra-Flight 79, Run 9R, Point 1 T_1=100109.4, ΔT=1 Sec, α_{Nom}=4.1 deg. $\Delta\alpha$=2.55 deg.

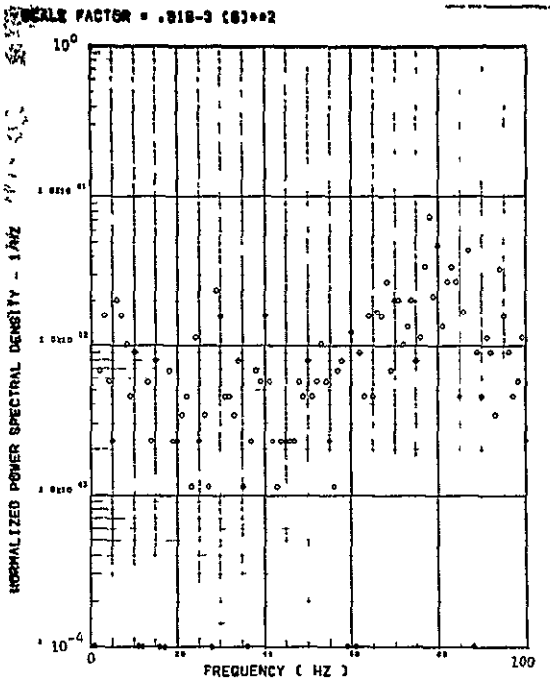

(e) - AF009 PILOT S SEAT VERTICAL ACCELEROMETER

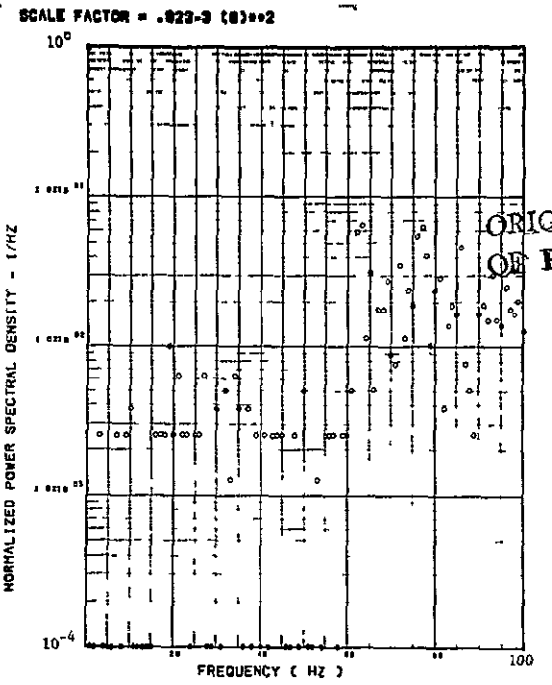

(f) - AF010 PILOT S SEAT LATERAL ACCELEROMETER

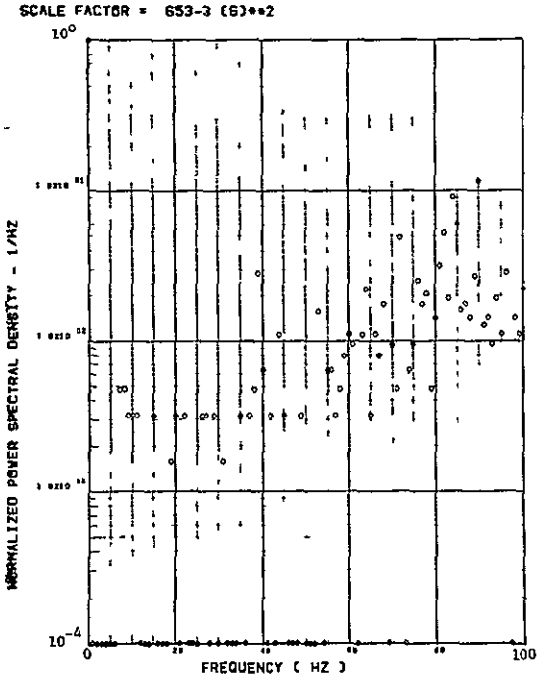

(g) - AB020 C G LATERAL ACCELEROMETER

Figure 34. Continued

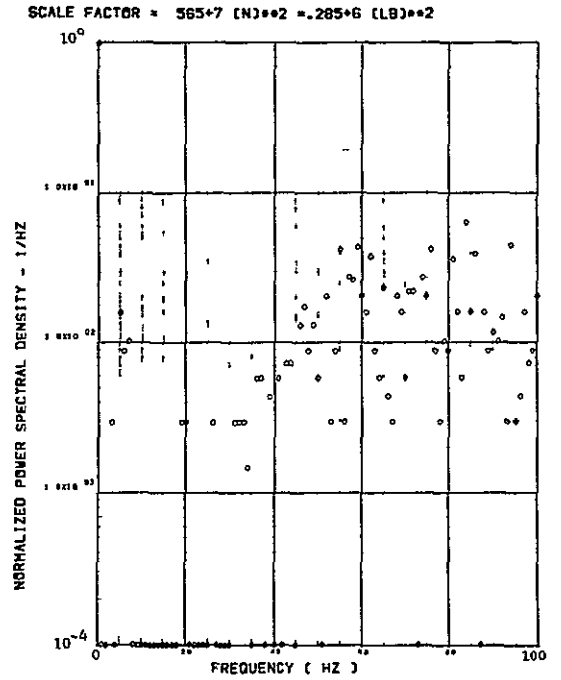

(h) - SW123 SHEAR AT WING STATION 1

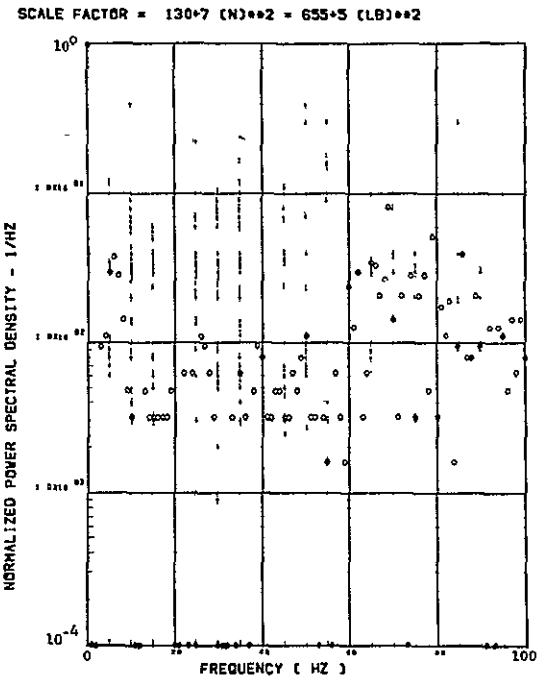

(i) - SW126 SHEAR AT WING STATION 2

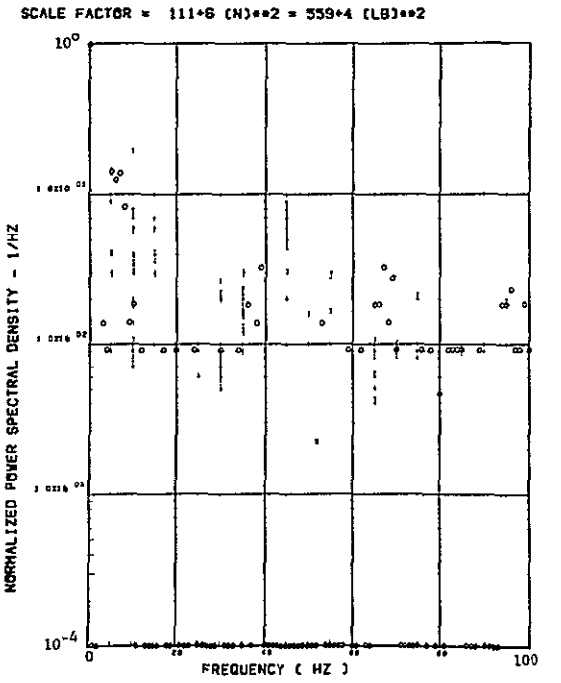

(j) - SW129 SHEAR AT WING STATION 3

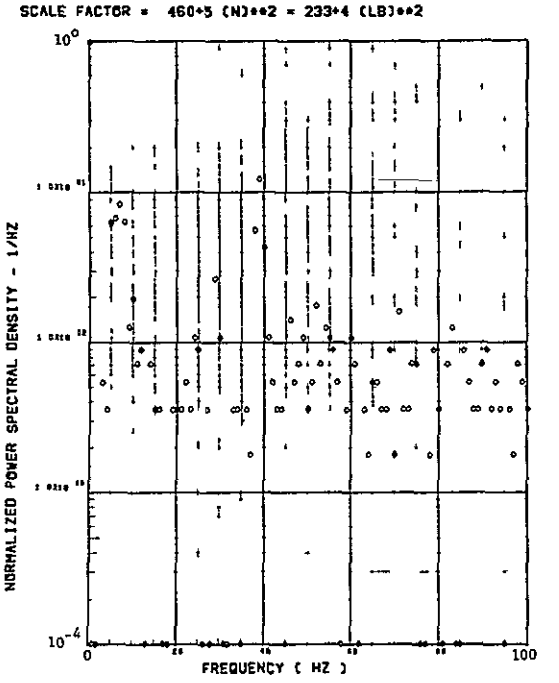

(k) - SW132 SHEAR AT WING STATION 4

Figure 34. Continued

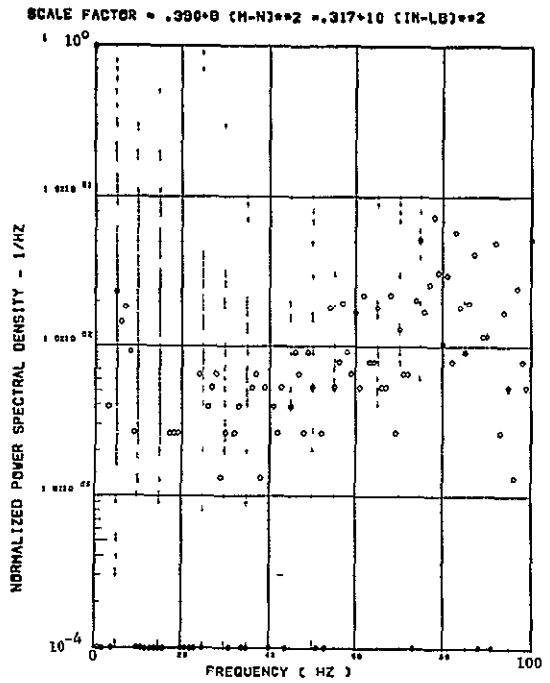

(l) - SW124 BENDING MOMENT AT WING STATION 1

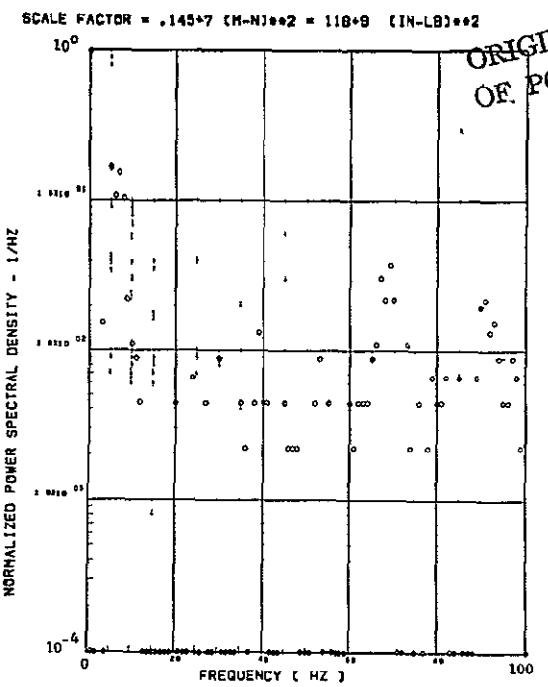

(m) - SW127 BENDING MOMENT AT WING STATION 2

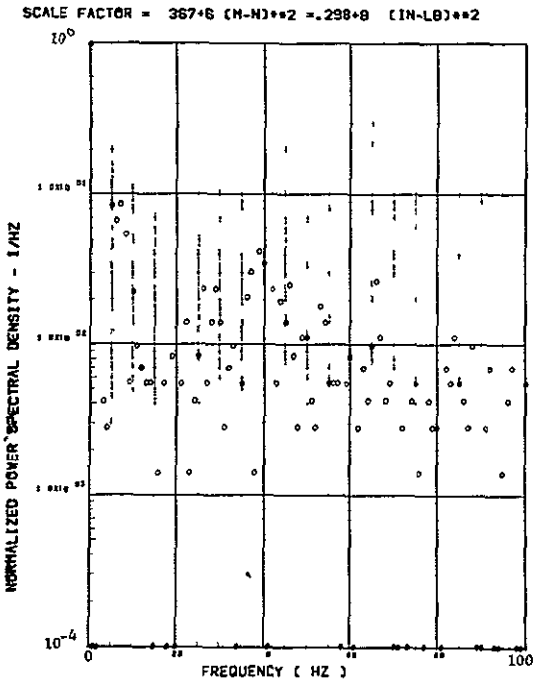

(n) - SW130 BENDING MOMENT AT WING STATION 3

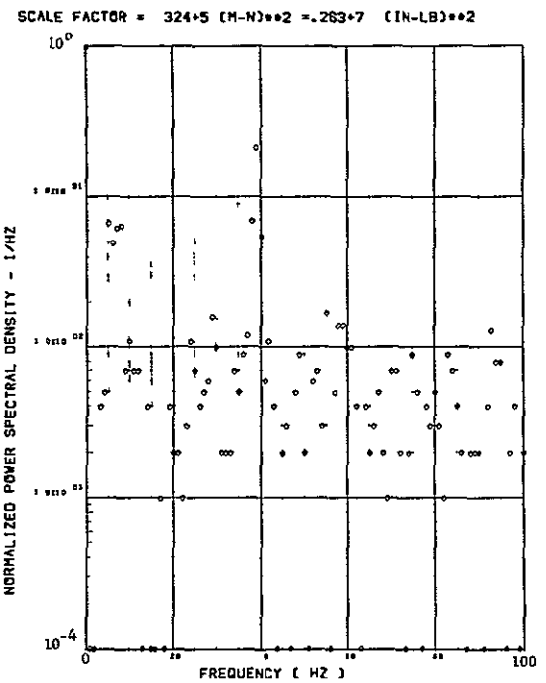

(o) - SW133 BENDING MOMENT AT WING STATION 4

Figure 34. Continued

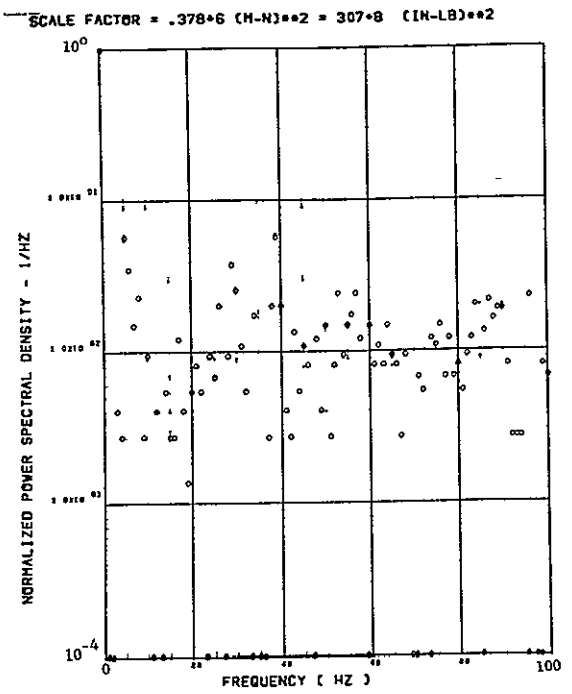

(p) - SW125 TORSION AT WING STATION 1

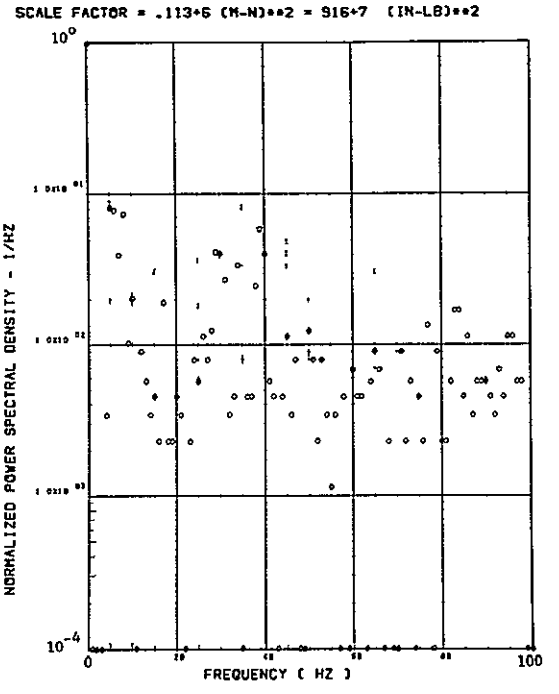

(q) - SW128 TORSION AT WING STATION 2

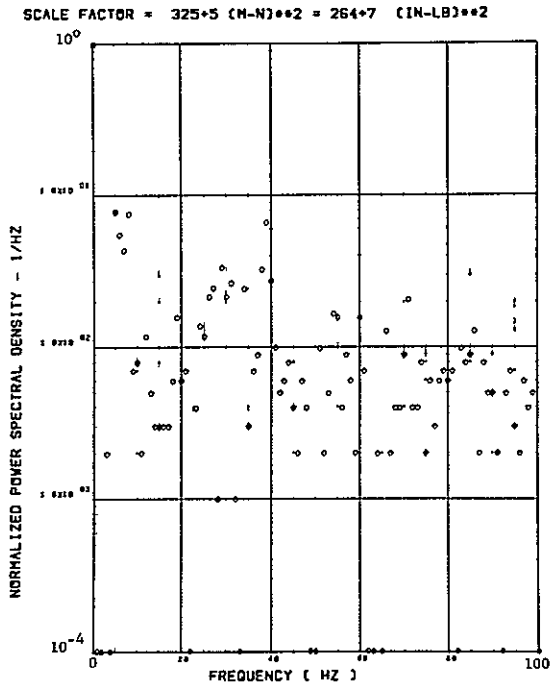

(r) - SW131 TORSION AT WING STATION 3

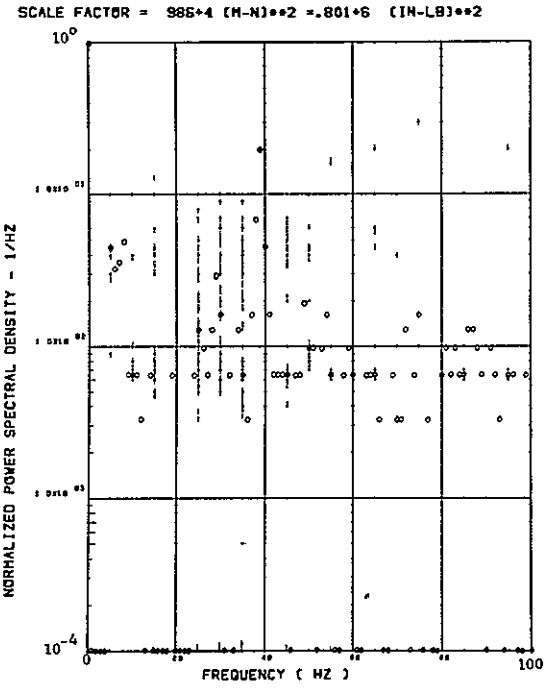

(s) - SW134 TORSION AT WING STATION 4

Figure 34. Concluded

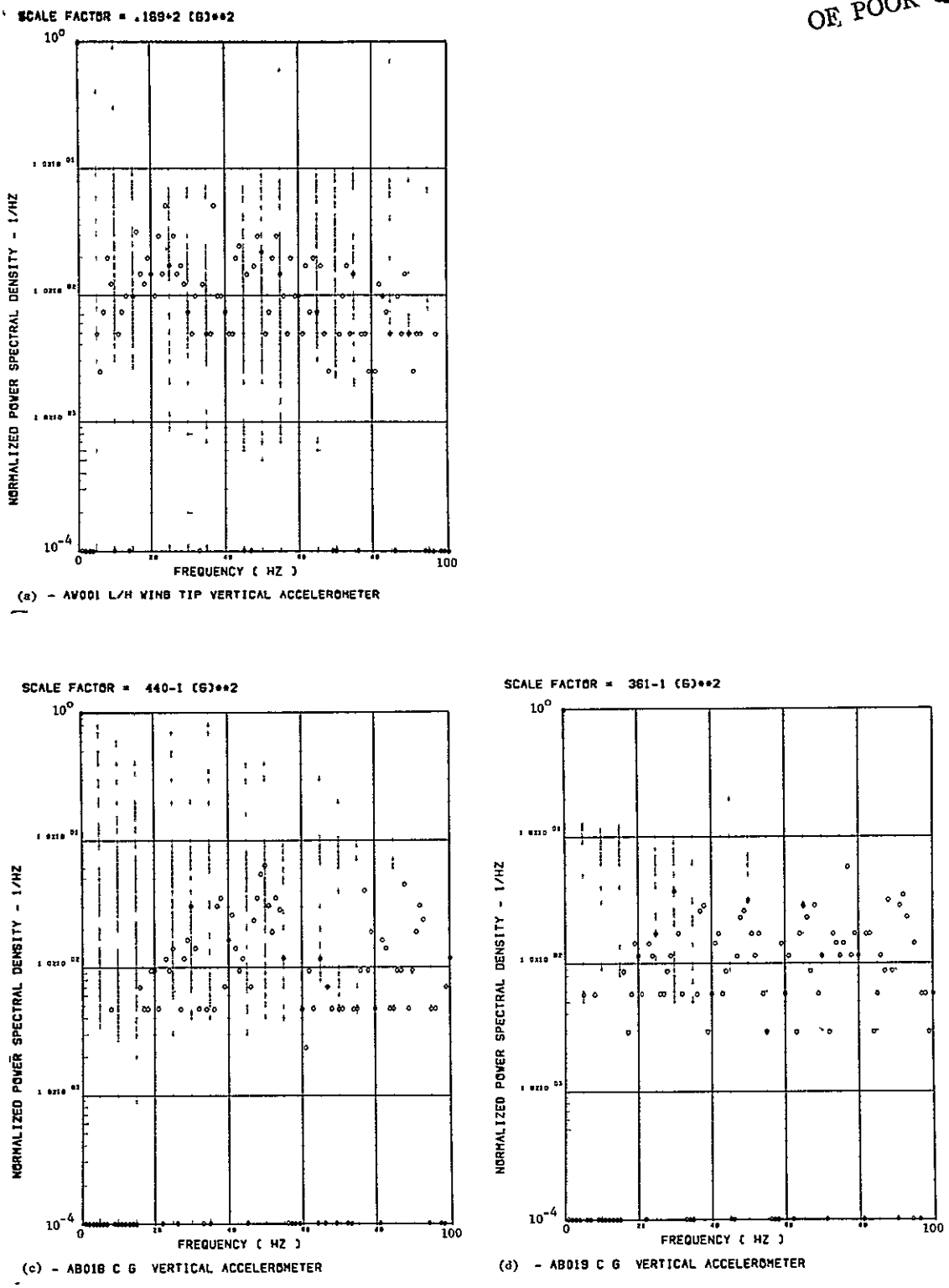

Figure 35. Power Spectra-Flight 79, Run 9R, Point 2, T_1=100110.3, ΔT=1 Sec, α_{Nom}=7.1 deg, $\Delta\alpha$=5.38 deg.

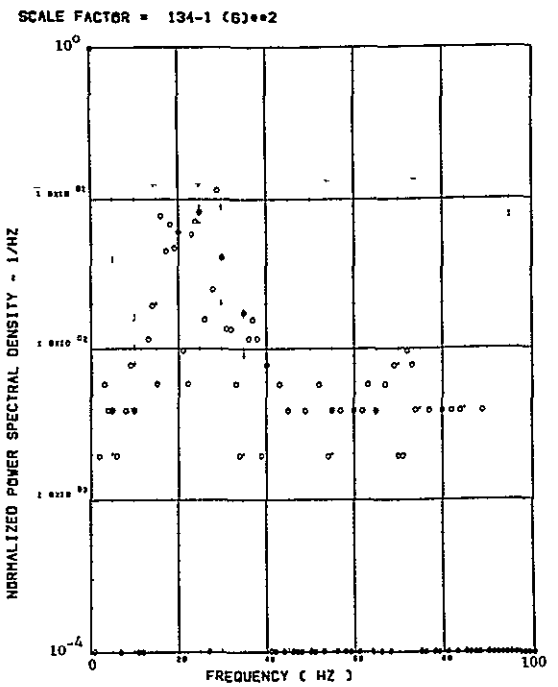

(e) - AF009 PILOT S SEAT VERTICAL ACCELEROMETER

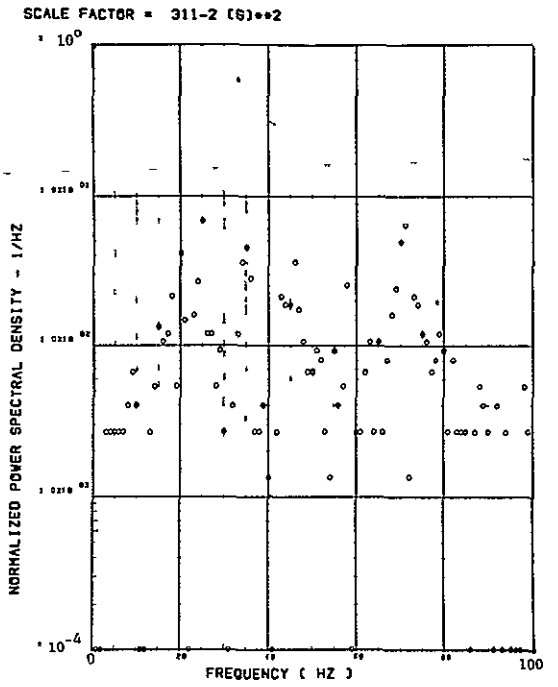

(f) - AF010 PILOT S SEAT LATERAL ACCELEROMETER

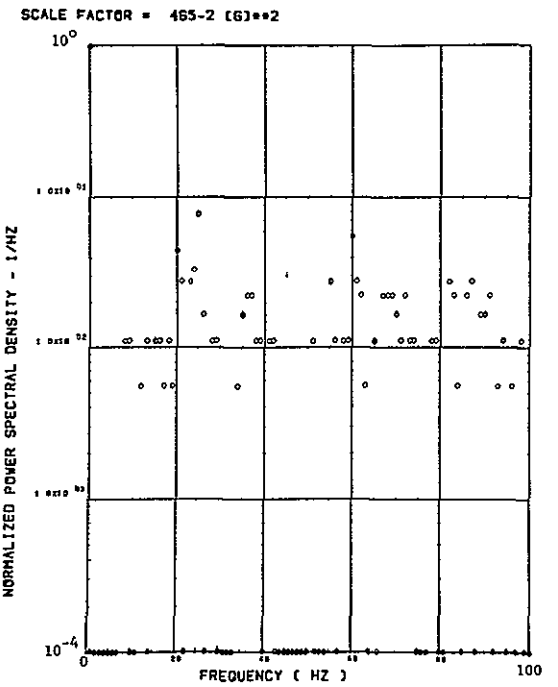

(g) - AB020 C G LATERAL ACCELEROMETER

Figure 35. Continued

C-3

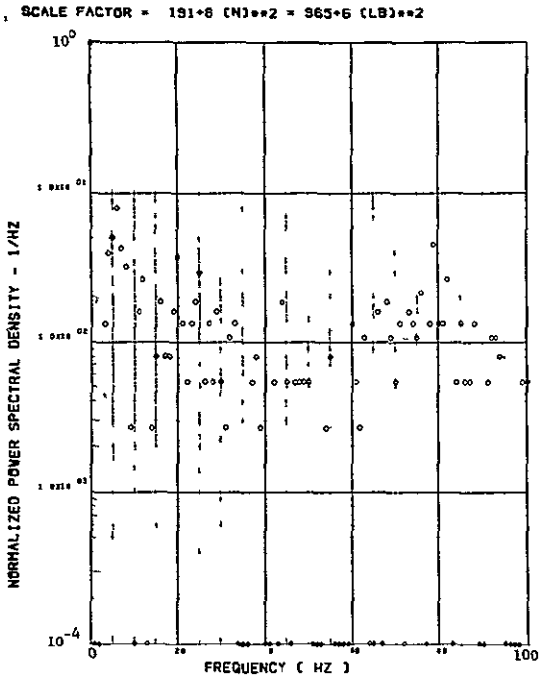

(h) - SW123 SHEAR AT WING STATION 1

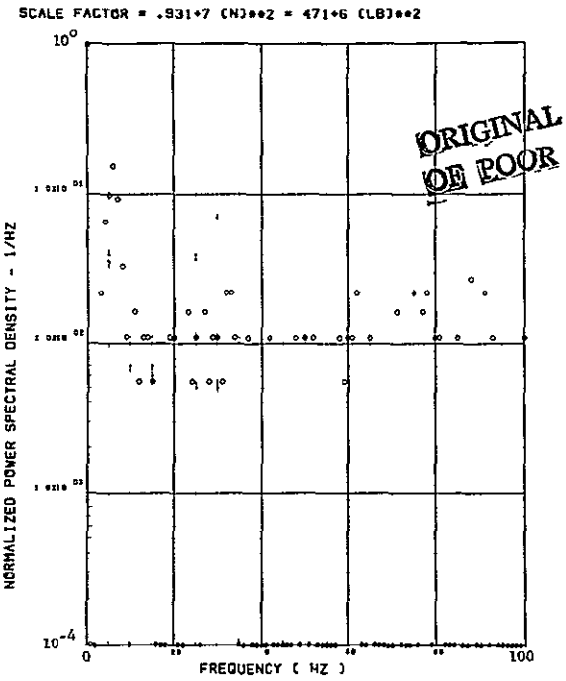

(i) - SW126 SHEAR AT WING STATION 2

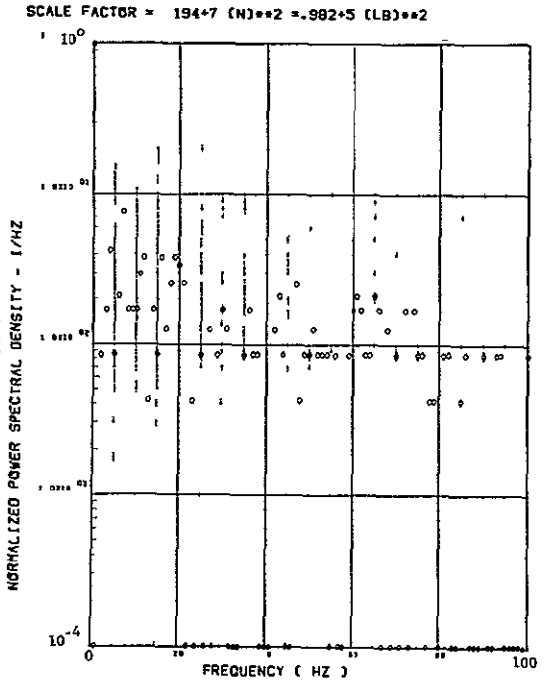

(j) - SW129 SHEAR AT WING STATION 3

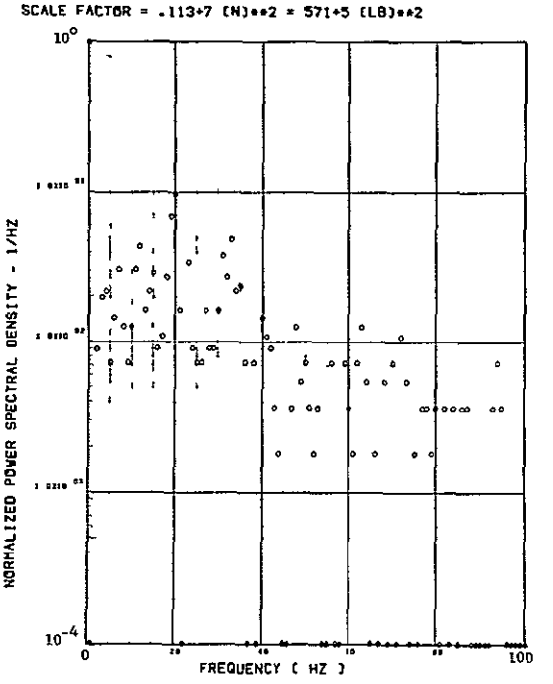

(k) - SW132 SHEAR AT WING STATION 4

Figure 35. Continued

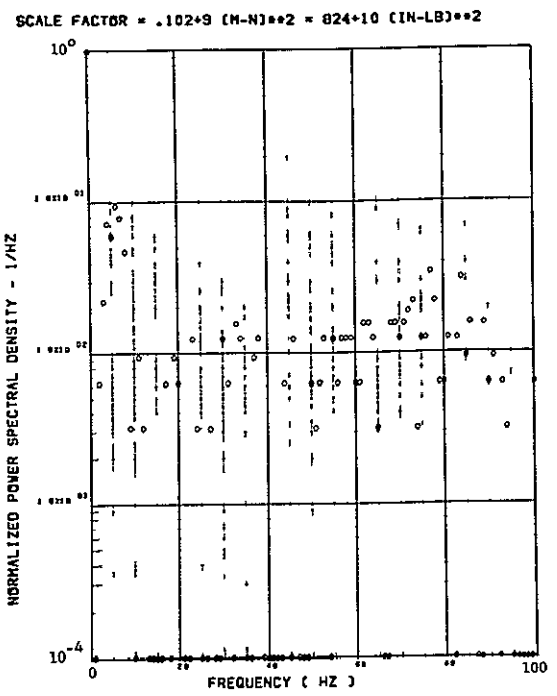

(l) - SW124 BENDING MOMENT AT WING STATION 1

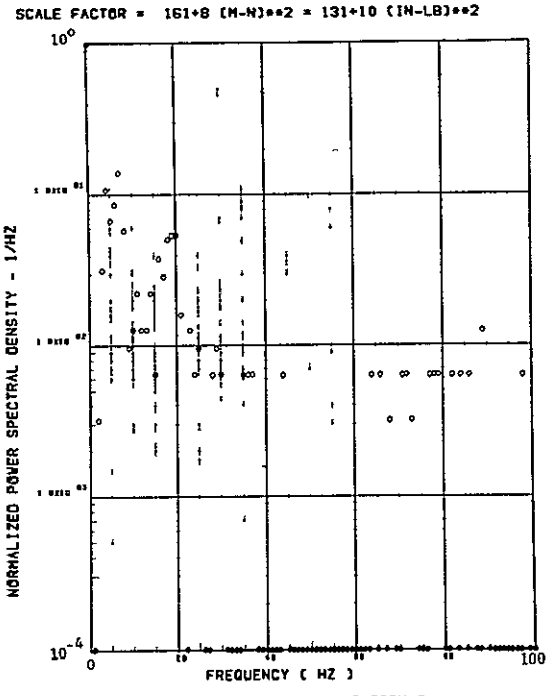

(m) - SW127 BENDING MOMENT AT WING STATION 2

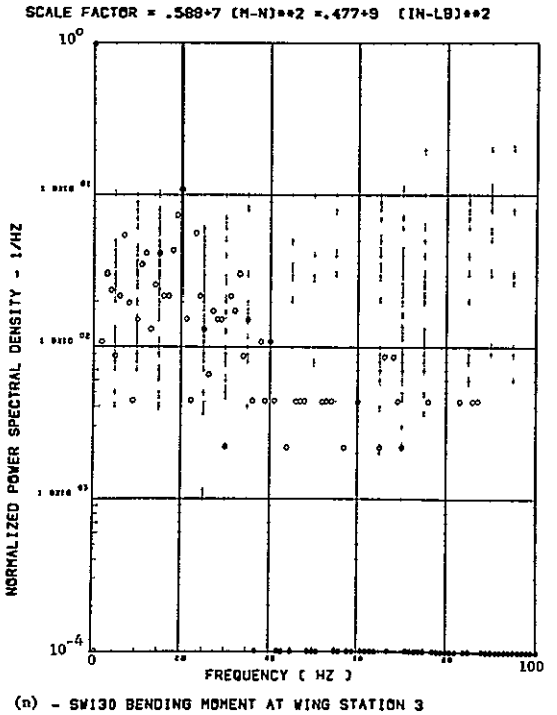

(n) - SW130 BENDING MOMENT AT WING STATION 3

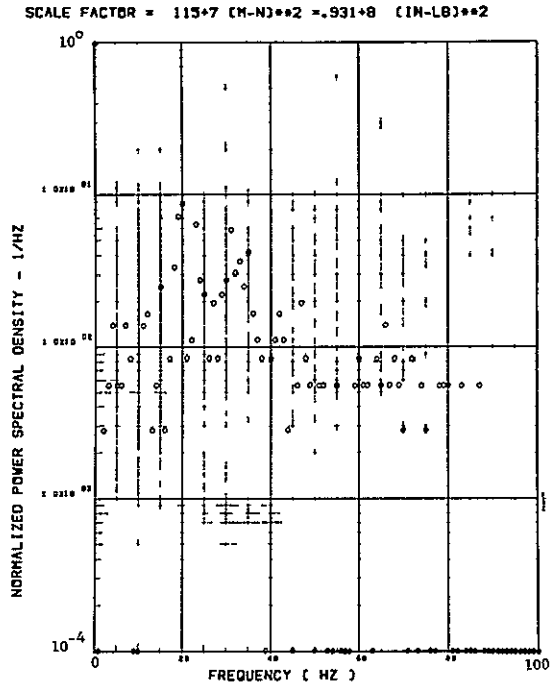

(o) - SW133 BENDING MOMENT AT WING STATION 4

Figure 35. Continued

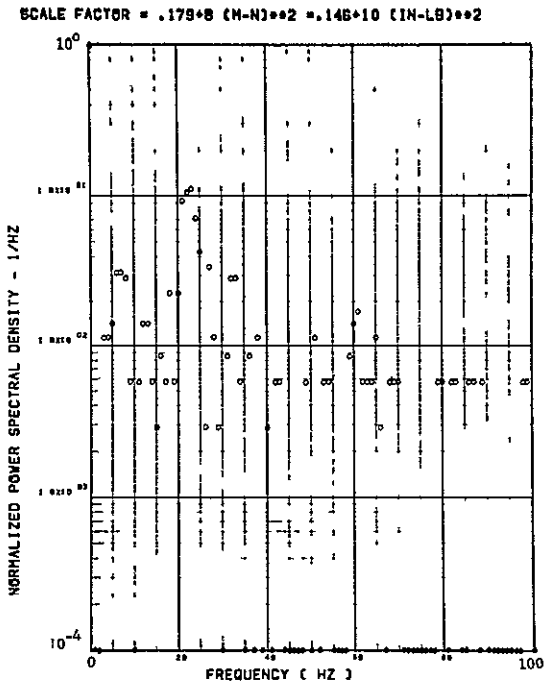

(p) - SW125 TORSION AT WING STATION 1

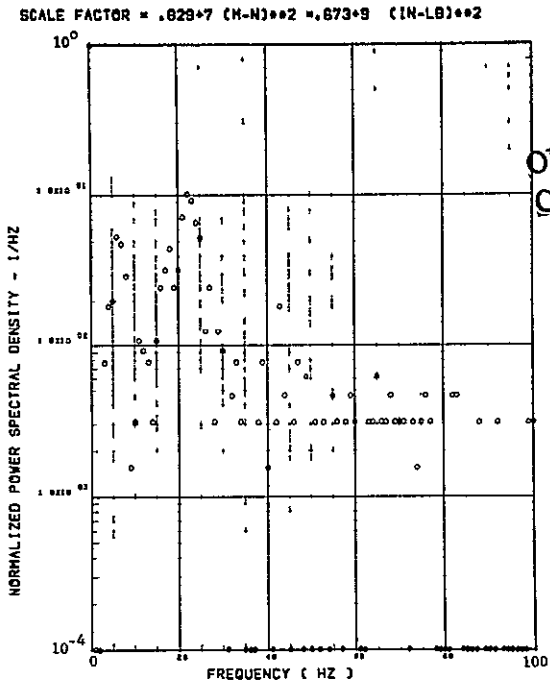

(q) - SW128 TORSION AT WING STATION 2

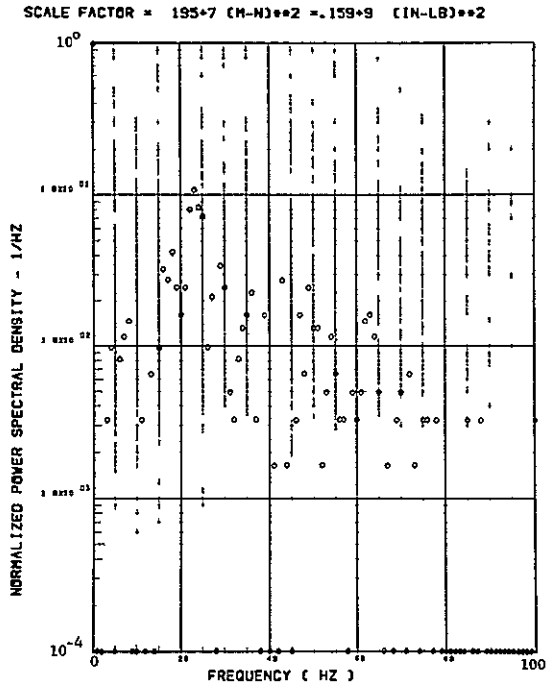

(r) - SW131 TORSION AT WING STATION 3

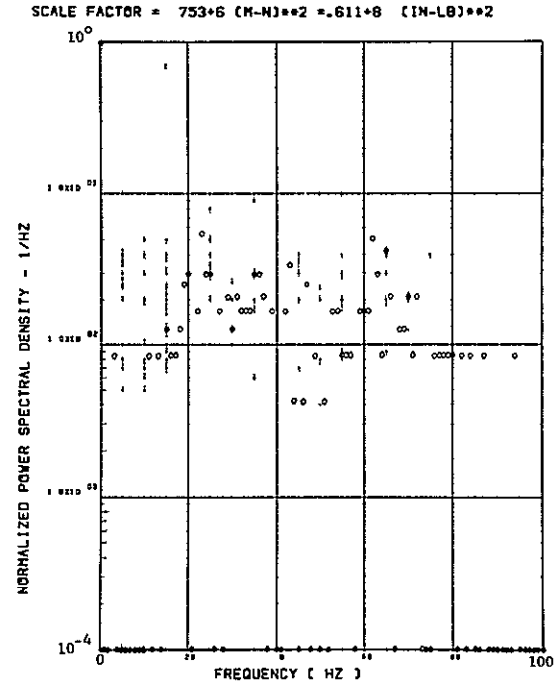

(s) - SW134 TORSION AT WING STATION 4

Figure 35. Concluded

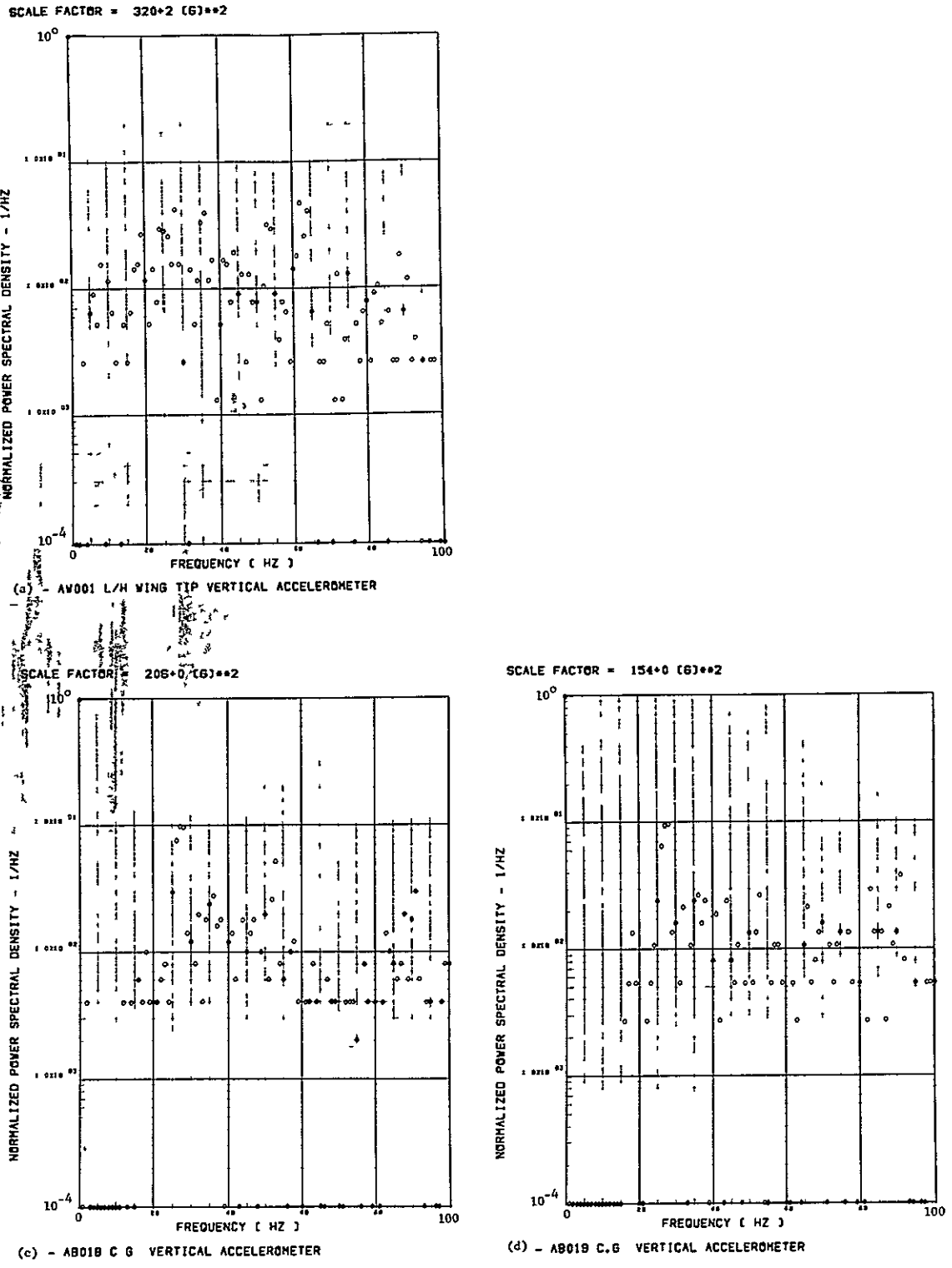

Figure 36. Power Spectra-Flight 79, Run 9R, Point 3, T_1=100110.6, ΔT=1 Sec, α_{Nom}=9.2 deg, $\Delta\alpha$=5.80 deg.

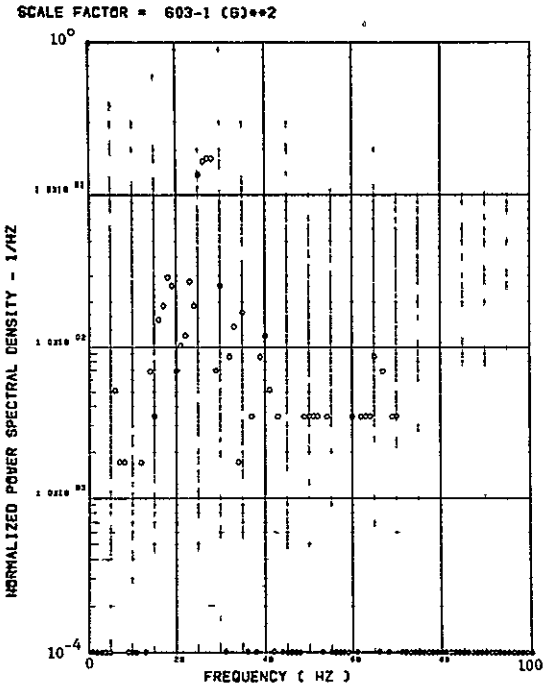

(e) - AF009 PILOT S SEAT VERTICAL ACCELEROMETER

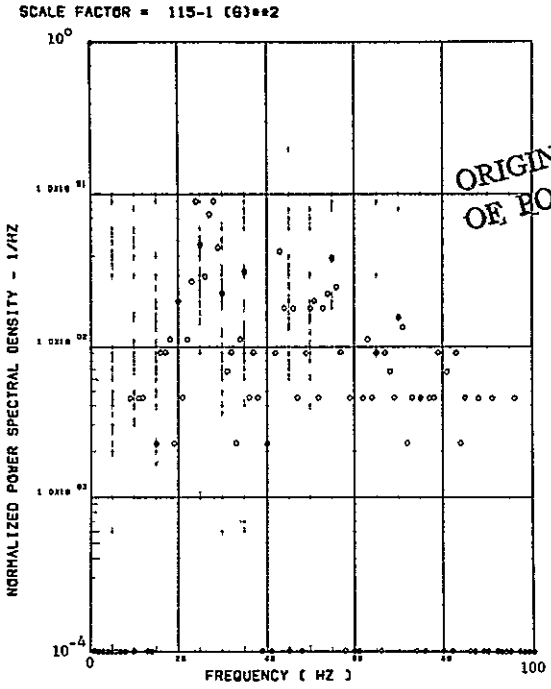

(f) - AF010 PILOT S SEAT LATERAL ACCELEROMETER

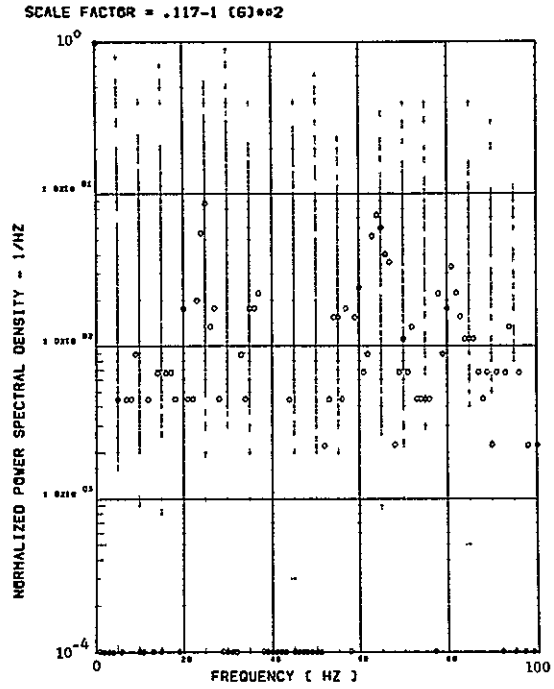

(g) - AB020 C G. LATERAL ACCELEROMETER

Figure 36. Continued

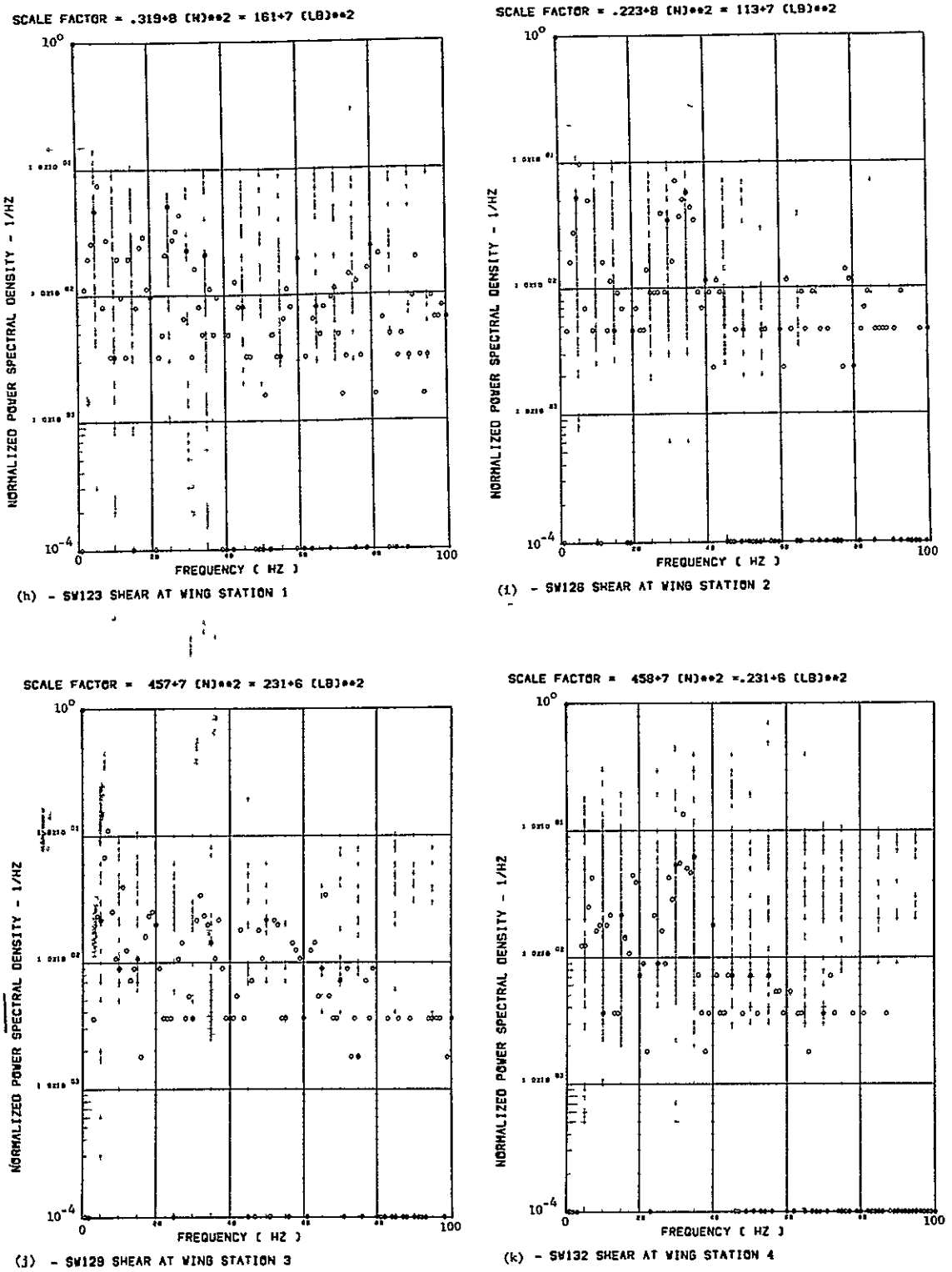

Figure 36. Continued

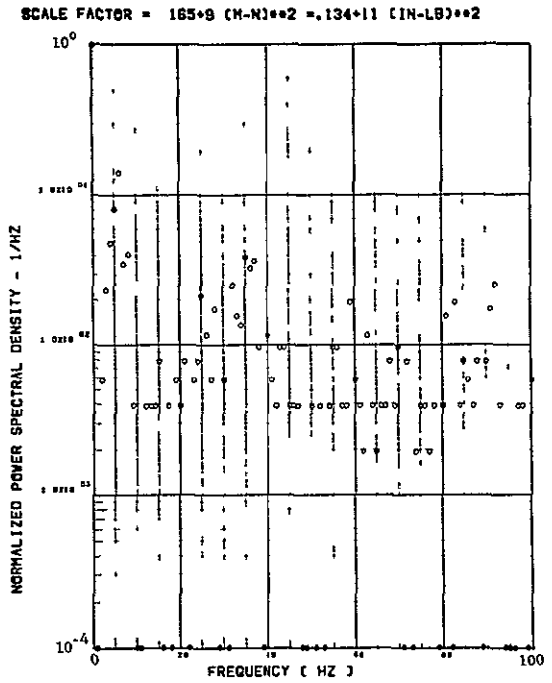

(l) - SW124 BENDING MOMENT AT WING STATION 1

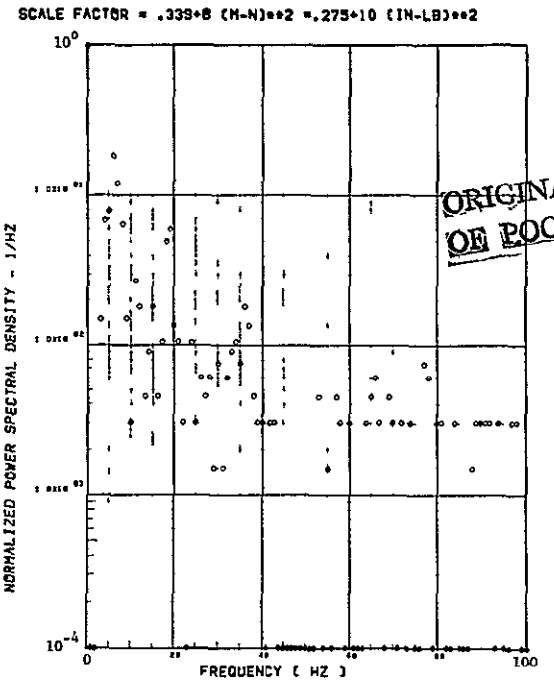

(m) - SW127 BENDING MOMENT AT WING STATION 2

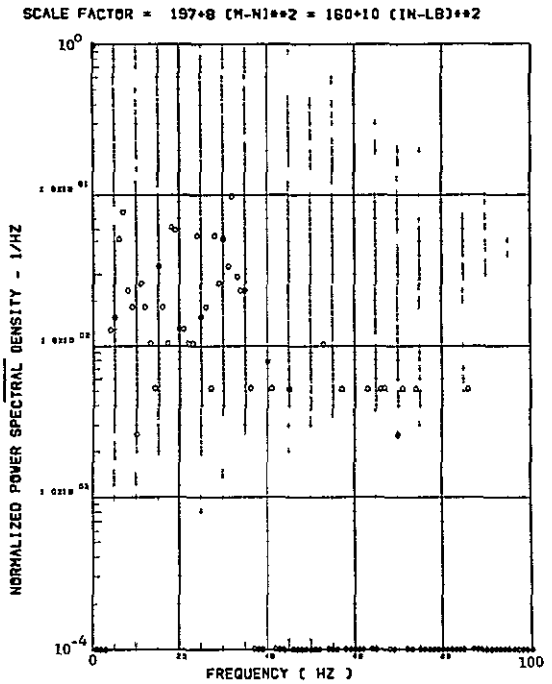

(n) - SW130 BENDING MOMENT AT WING STATION 3

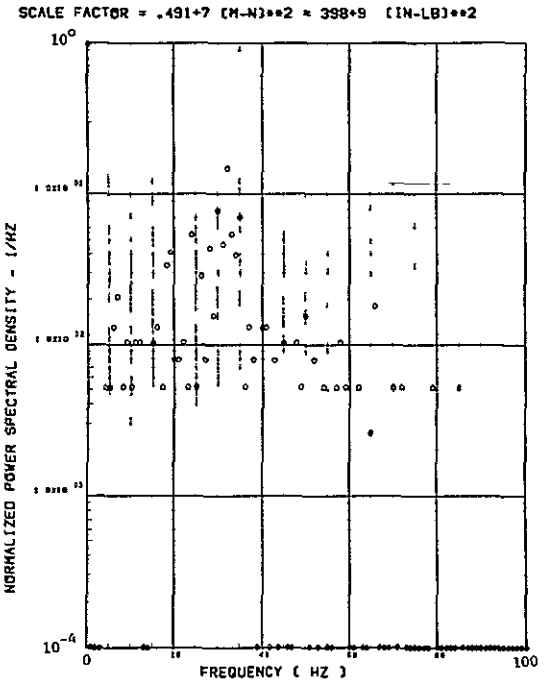

(o) - SW133 BENDING MOMENT AT WING STATION 4

Figure 36. Continued

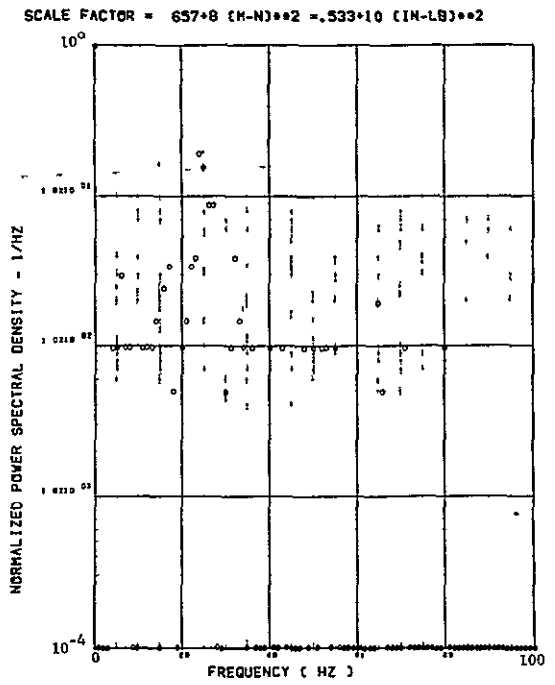

(p) - SW125 TORSION AT WING STATION 1

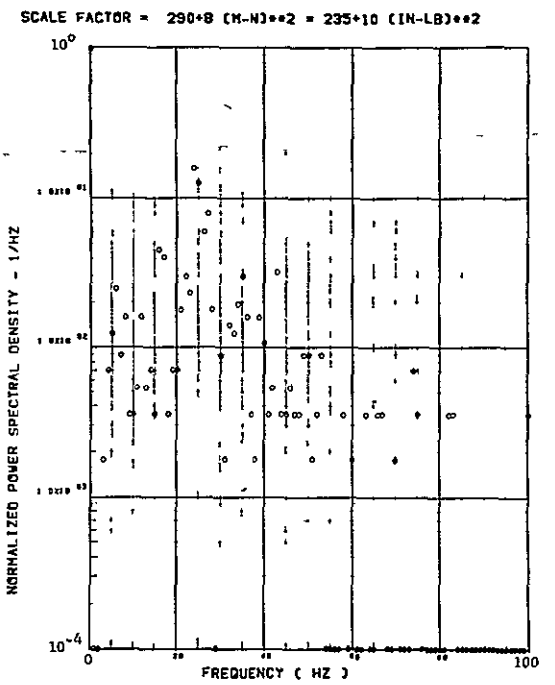

(q) - SW128 TORSION AT WING STATION 2

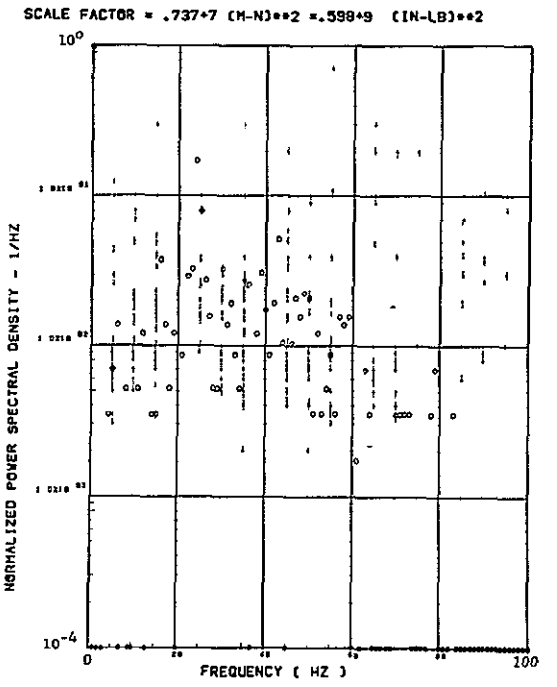

(r) - SW131 TORSION AT WING STATION 3

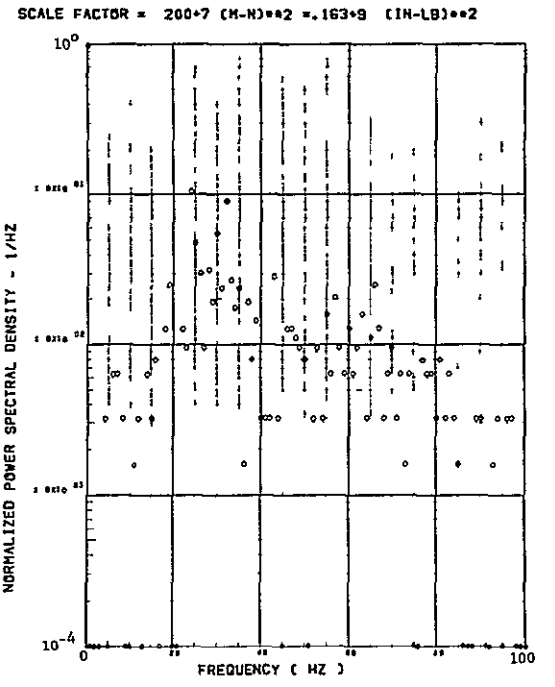

(s) - SW134 TORSION AT WING STATION 4

Figure 36. Concluded

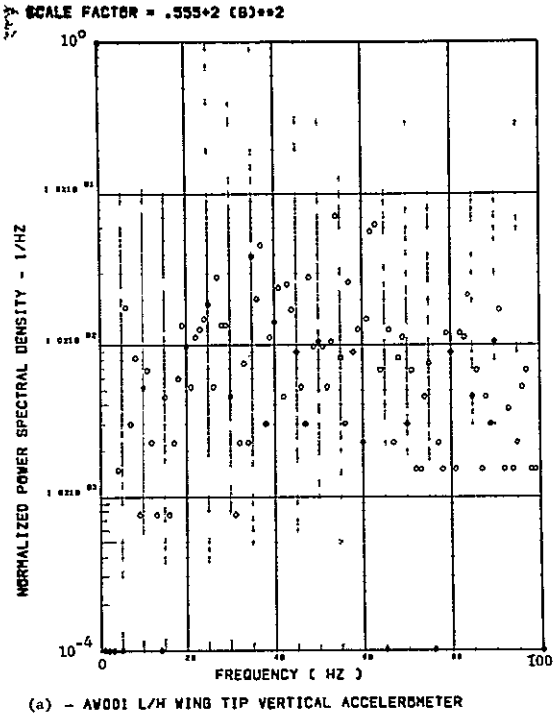

(a) - AW001 L/H WING TIP VERTICAL ACCELEROMETER

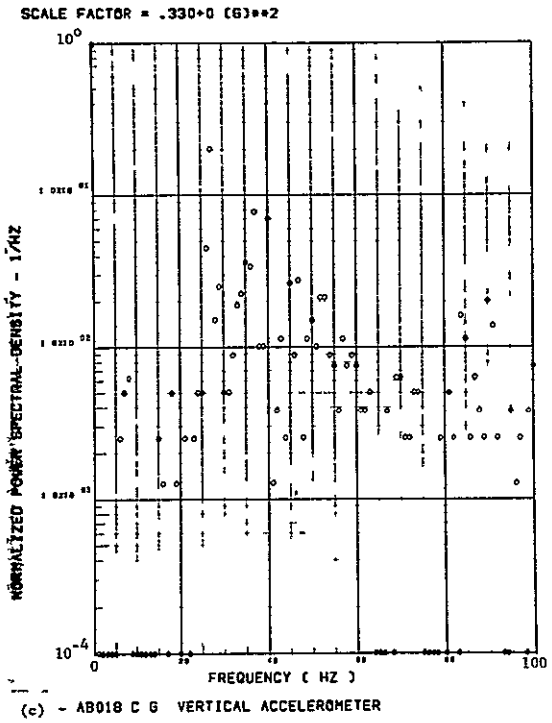

(c) - AB018 C G VERTICAL ACCELEROMETER

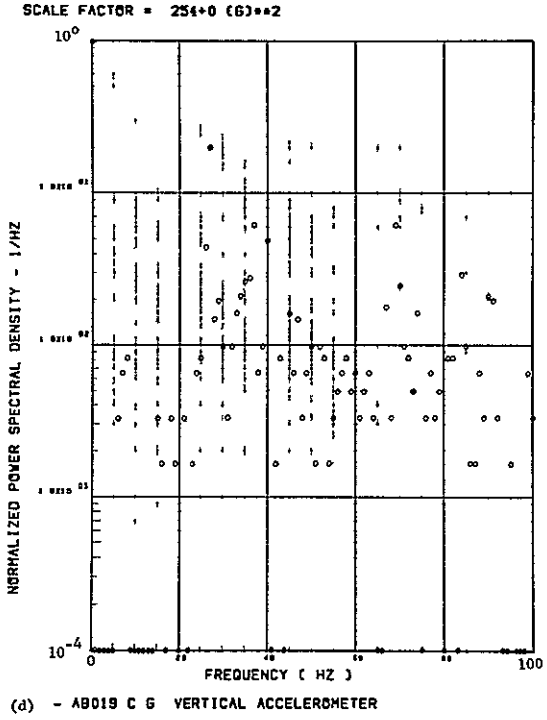

(d) - AB019 C G VERTICAL ACCELEROMETER

Figure 37. Power Spectra-Flight 79, Run 9R, Point 4 T_1=100111.15, ΔT=1 Sec, α_{Nom}=10.8 deg, $\Delta\alpha$=3.30 deg.

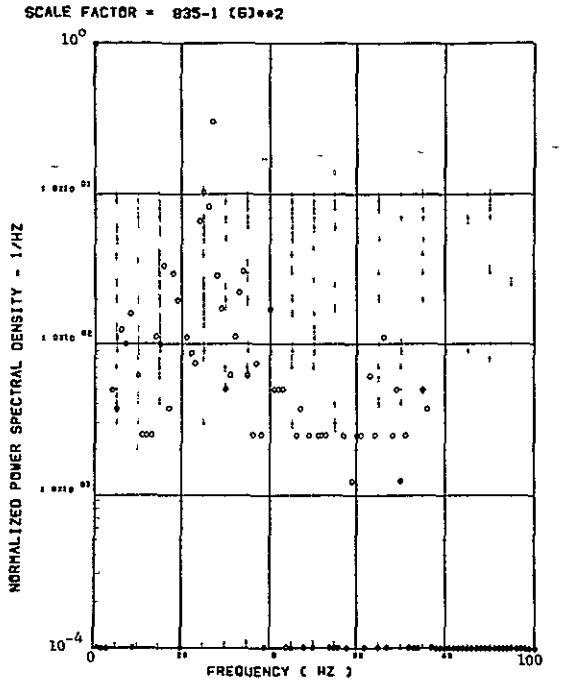

(e) - AF009 PILOT S SEAT VERTICAL ACCELEROMETER

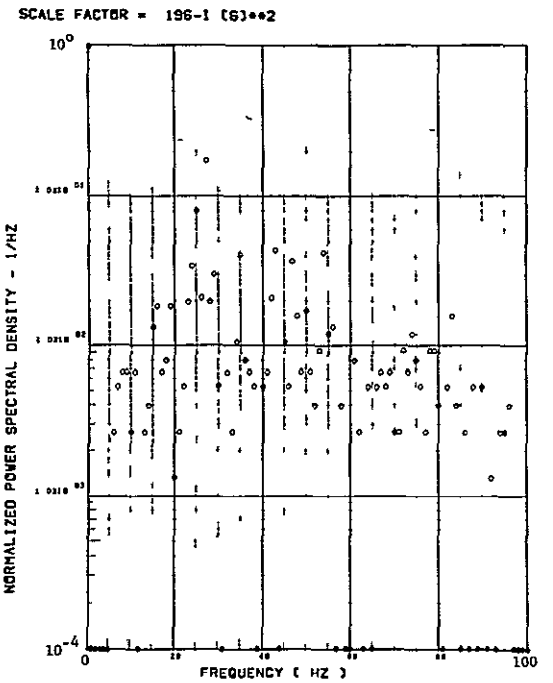

(f) - AF010 PILOT S SEAT LATERAL ACCELEROMETER

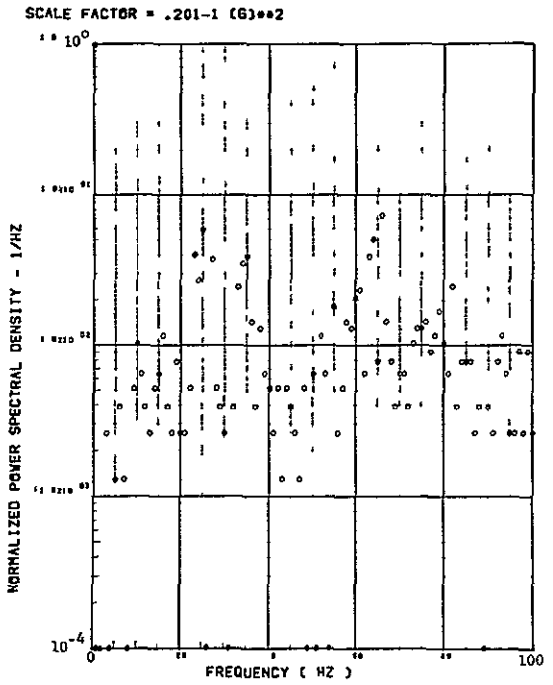

(g) - AB020 C G. LATERAL ACCELEROMETER

Figure 37. Continued

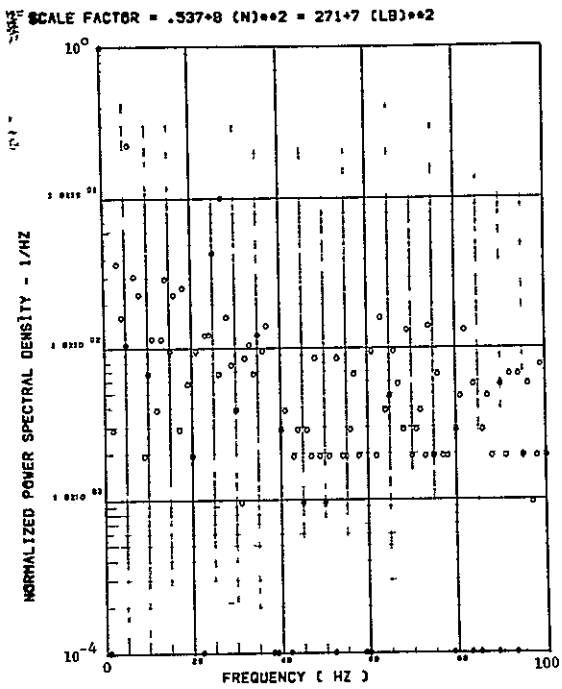

(h) - SW123 SHEAR AT WING STATION 1

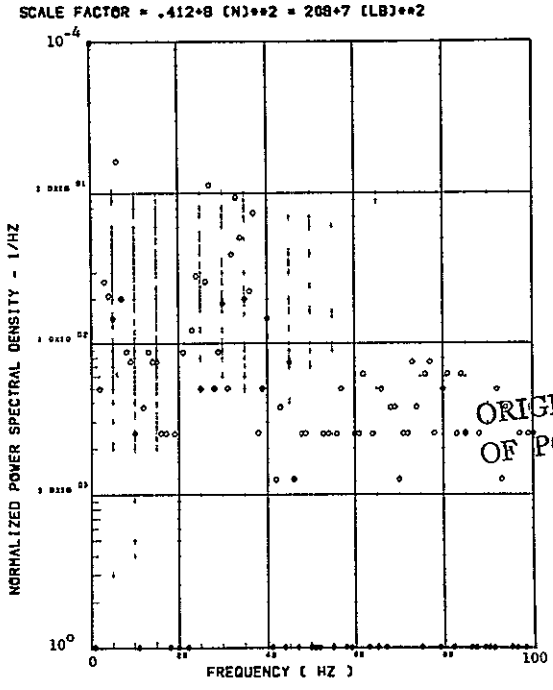

(i) - SW126 SHEAR AT WING STATION 2

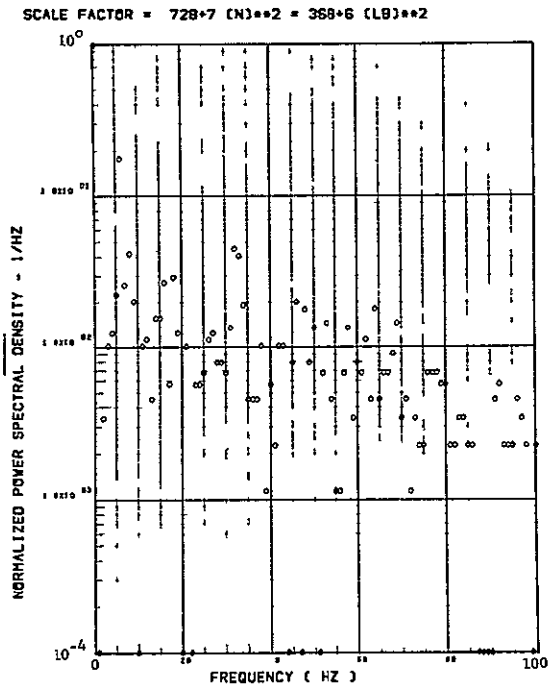

(j) - SW129 SHEAR AT WING STATION 3

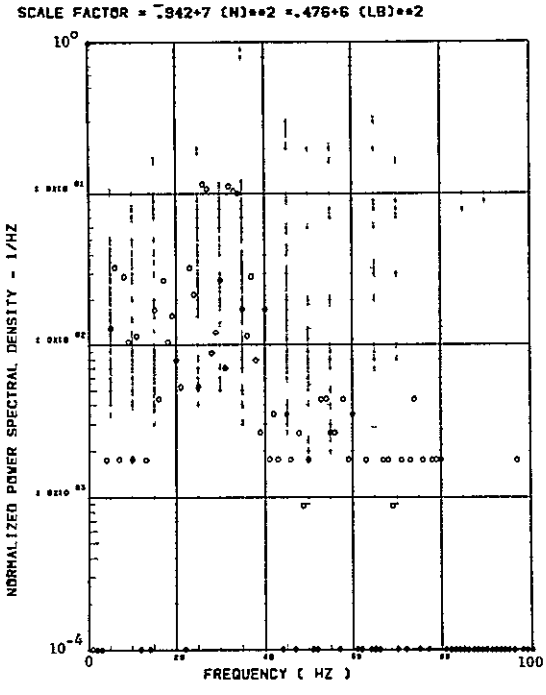

(k) - SW132 SHEAR AT WING STATION 4

Figure 37. Continued

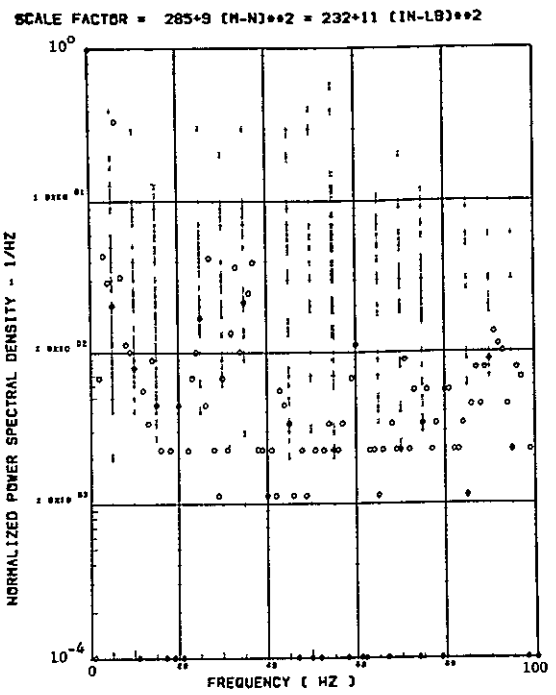

(l) - SW124 BENDING MOMENT AT WING STATION 1

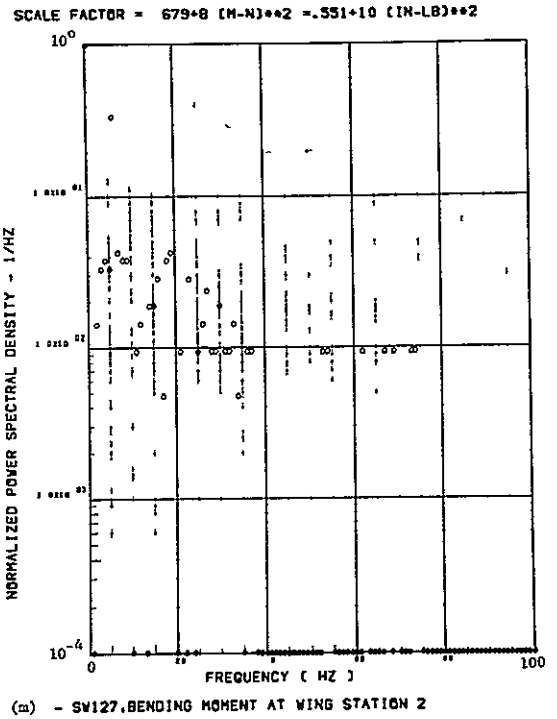

(m) - SW127,BENDING MOMENT AT WING STATION 2

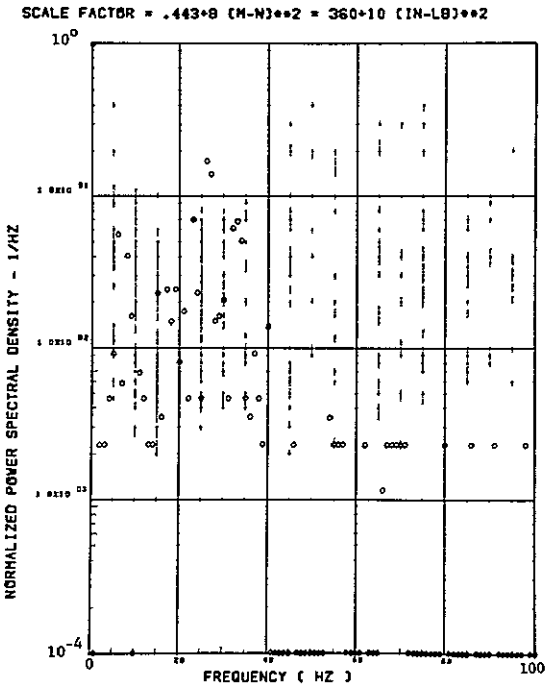

(n) - SW130 BENDING MOMENT AT WING STATION 3

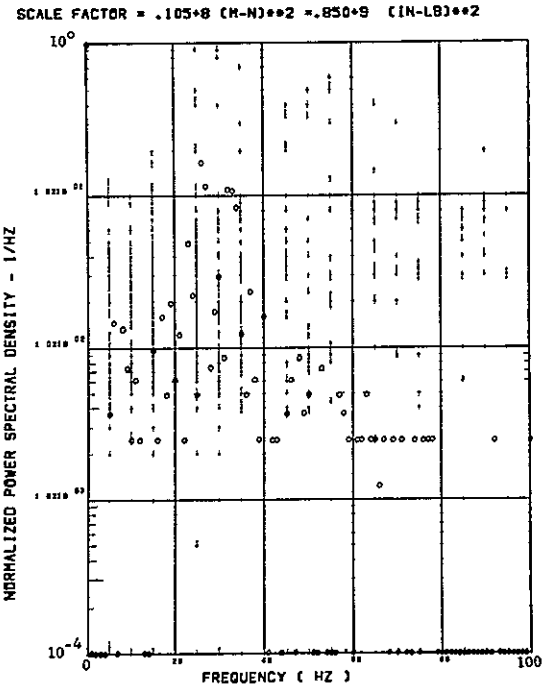

(o) - SW133 BENDING MOMENT AT WING STATION 4

Figure 37. Continued

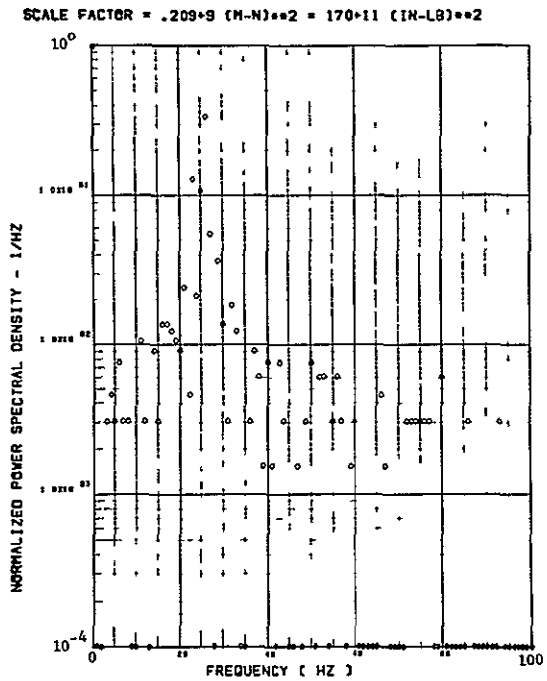

(p) - SW125 TORSION AT WING STATION 1

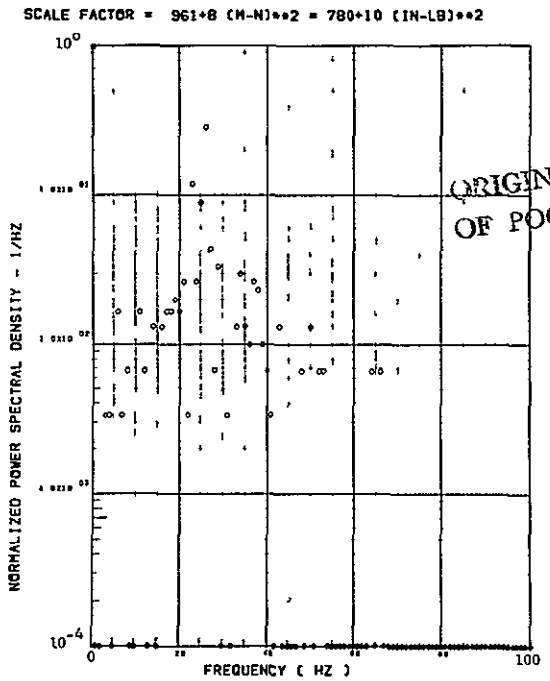

(q) - SW128 TORSION AT WING STATION 2

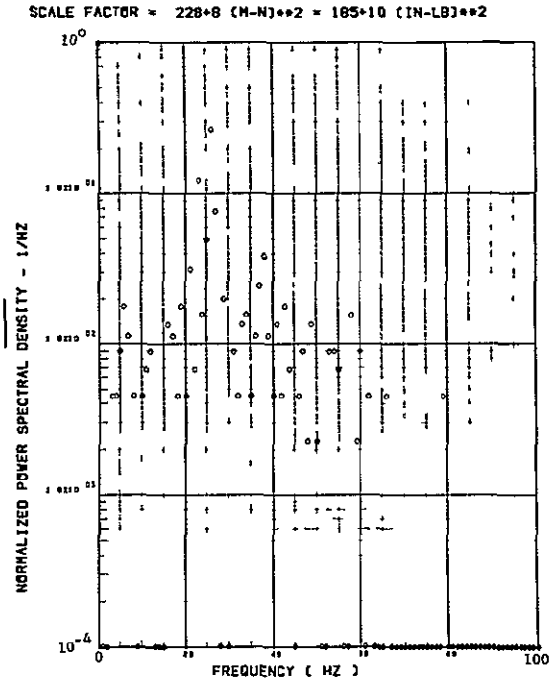

(r) - SW131 TORSION AT WING STATION 3

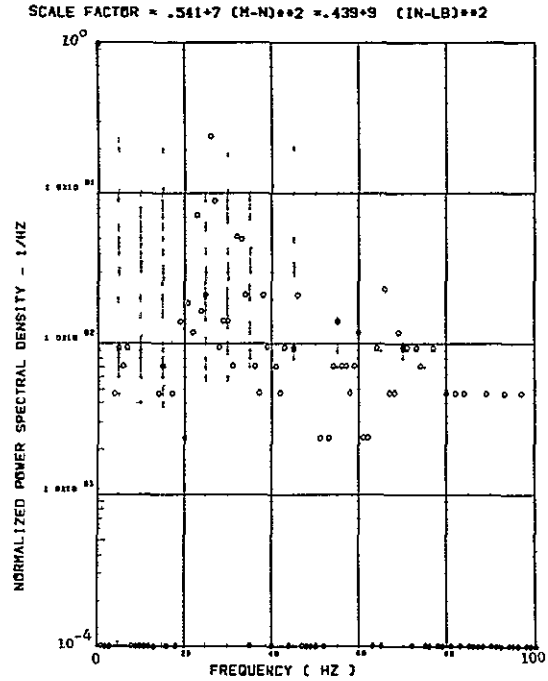

(s) - SW134 TORSION AT WING STATION 4

Figure 37. Concluded

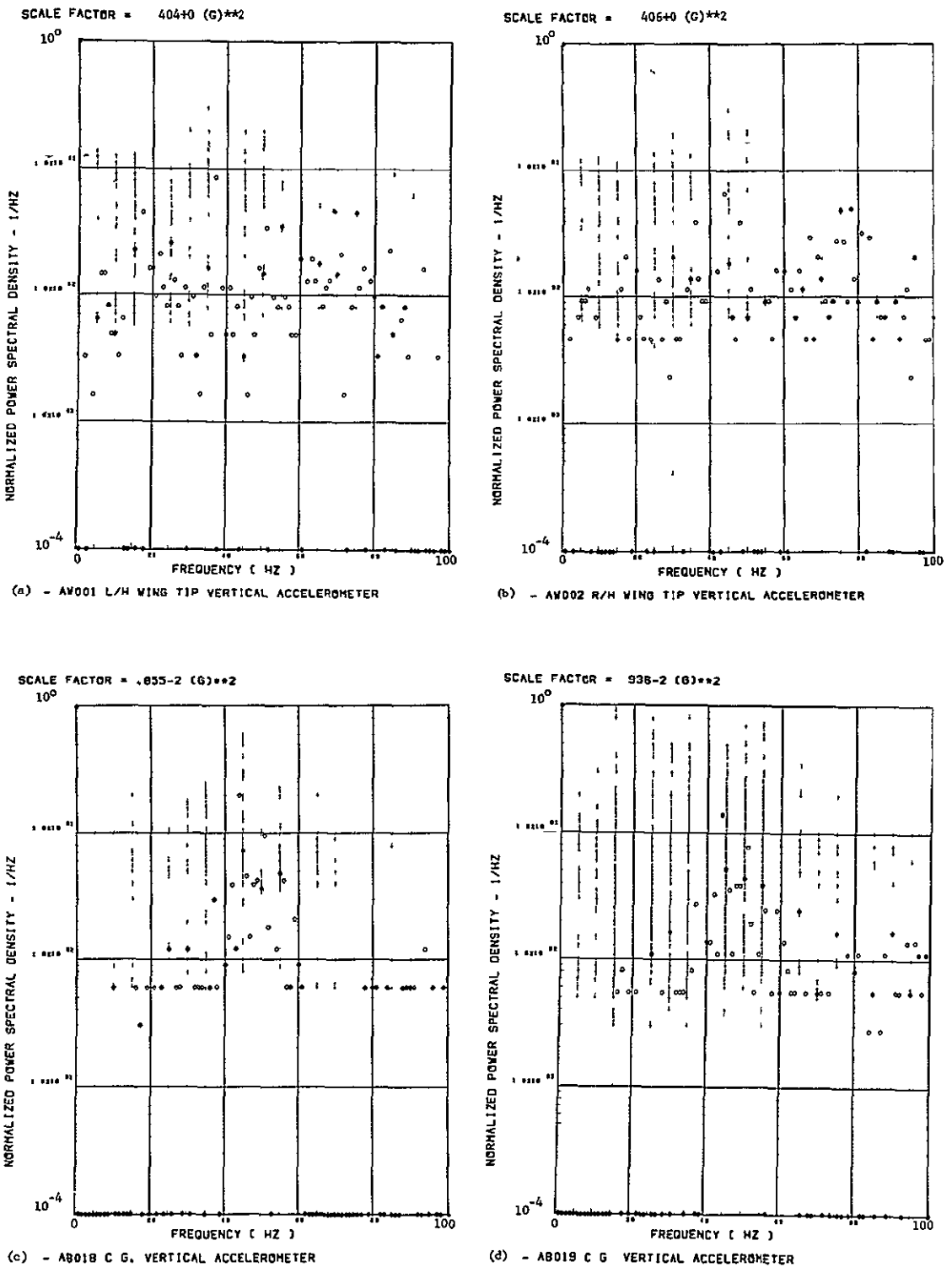

Figure 38. Power Spectra-Flight 60, Run 10, Point 1 T_1=100241.0, ΔT=1 Sec, α_{Nom}=3.5 deg, $\Delta\alpha = \pm .05$ deg.

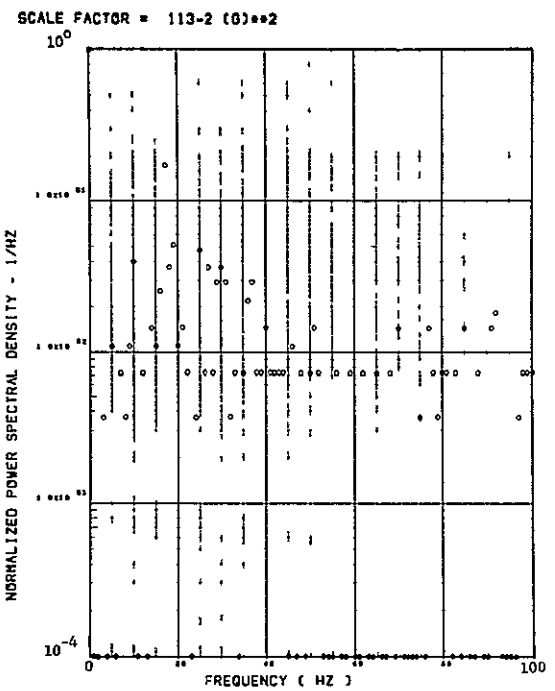

(a) - AF009 PILOT S SEAT VERTICAL ACCELEROMETER

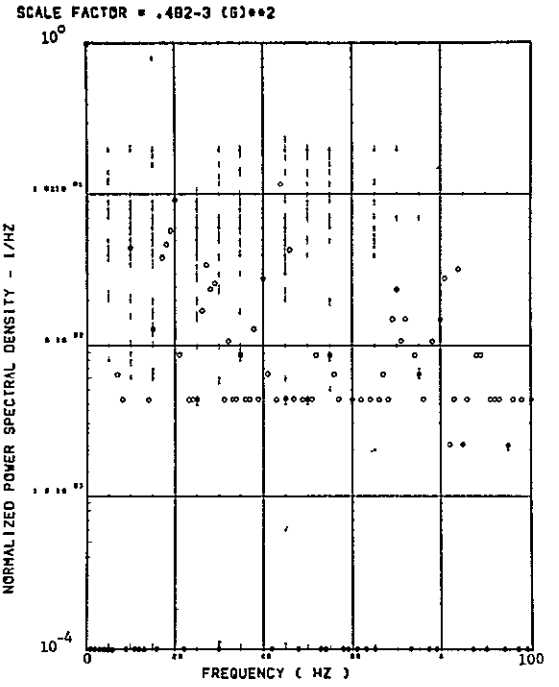

(f) - AF010 PILOT S SEAT LATERAL ACCELEROMETER

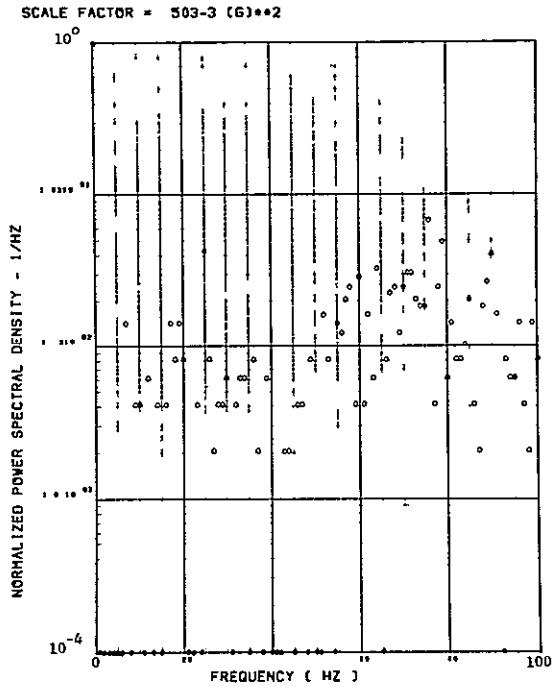

(g) - AB020 C G LATERAL ACCELEROMETER

Figure 38. Continued

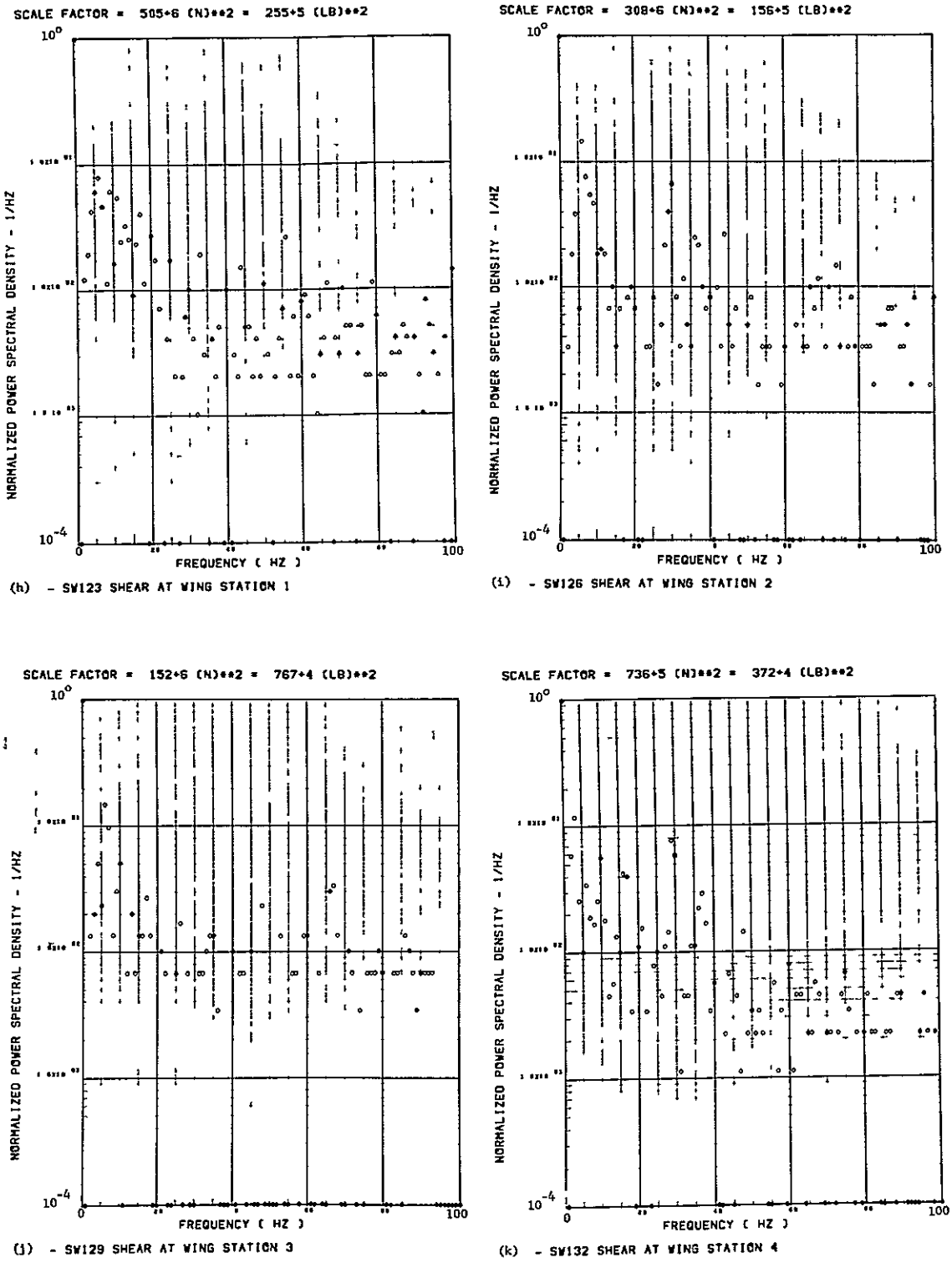

Figure 38. Continued

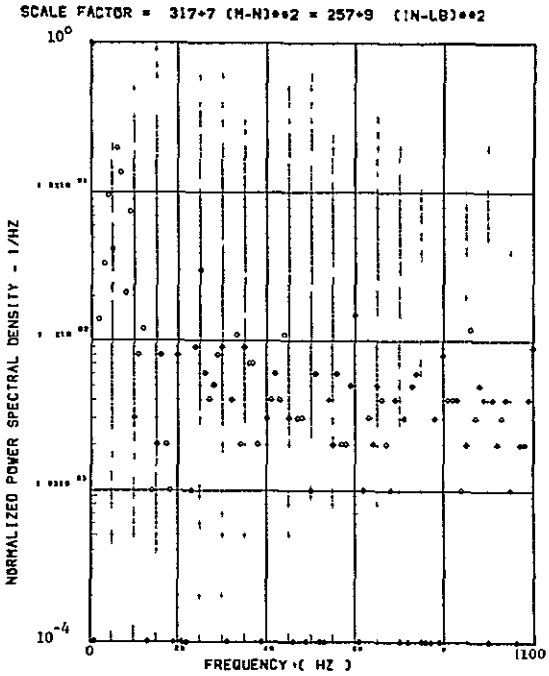

(l) - SW124 BENDING MOMENT AT WING STATION 1

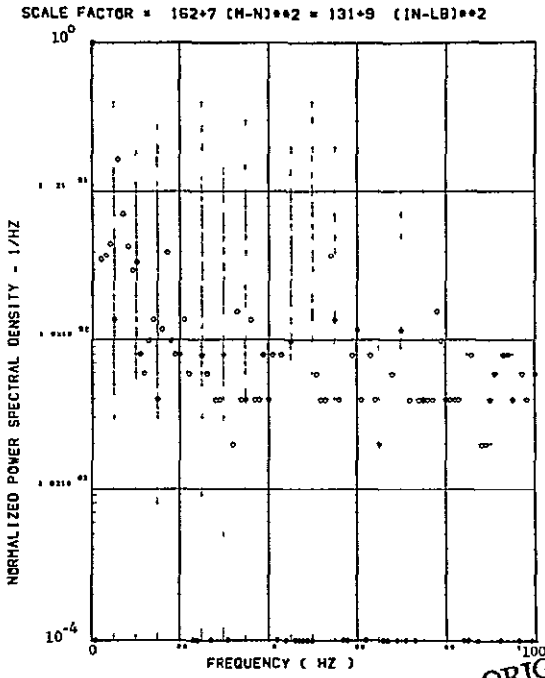

(m) - SW127 BENDING MOMENT AT WING STATION 2

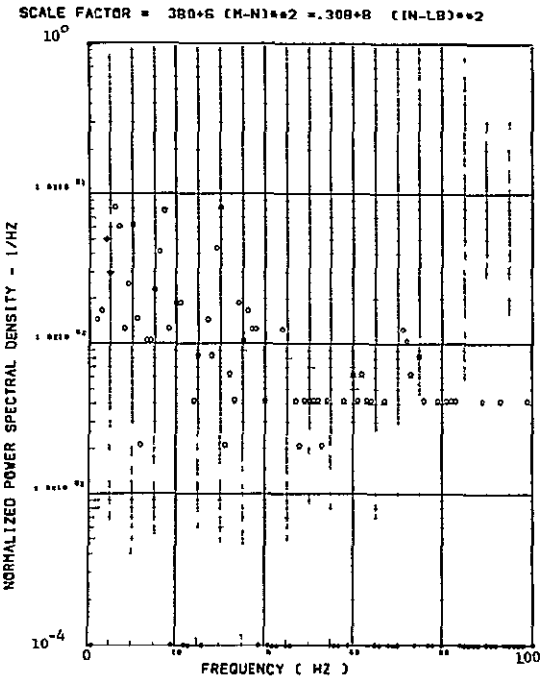

(n) - SW130 BENDING MOMENT AT WING STATION 3

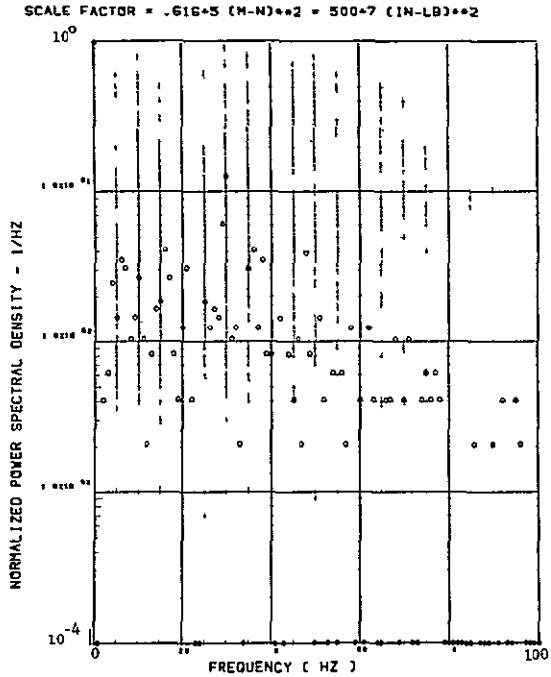

(o) - SW133 BENDING MOMENT AT WING STATION 4

Figure 38. Continued

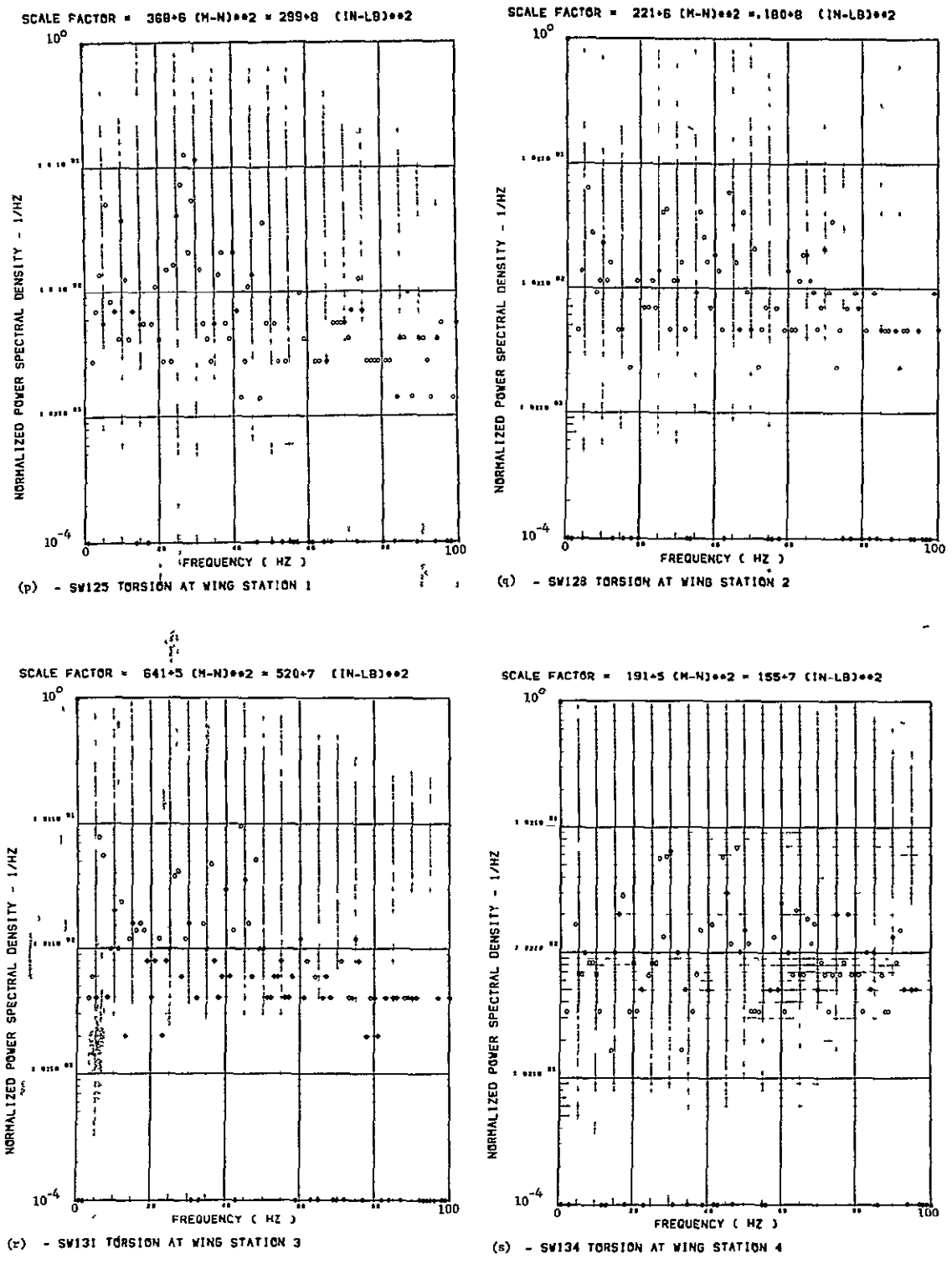

Figure 38. Concluded

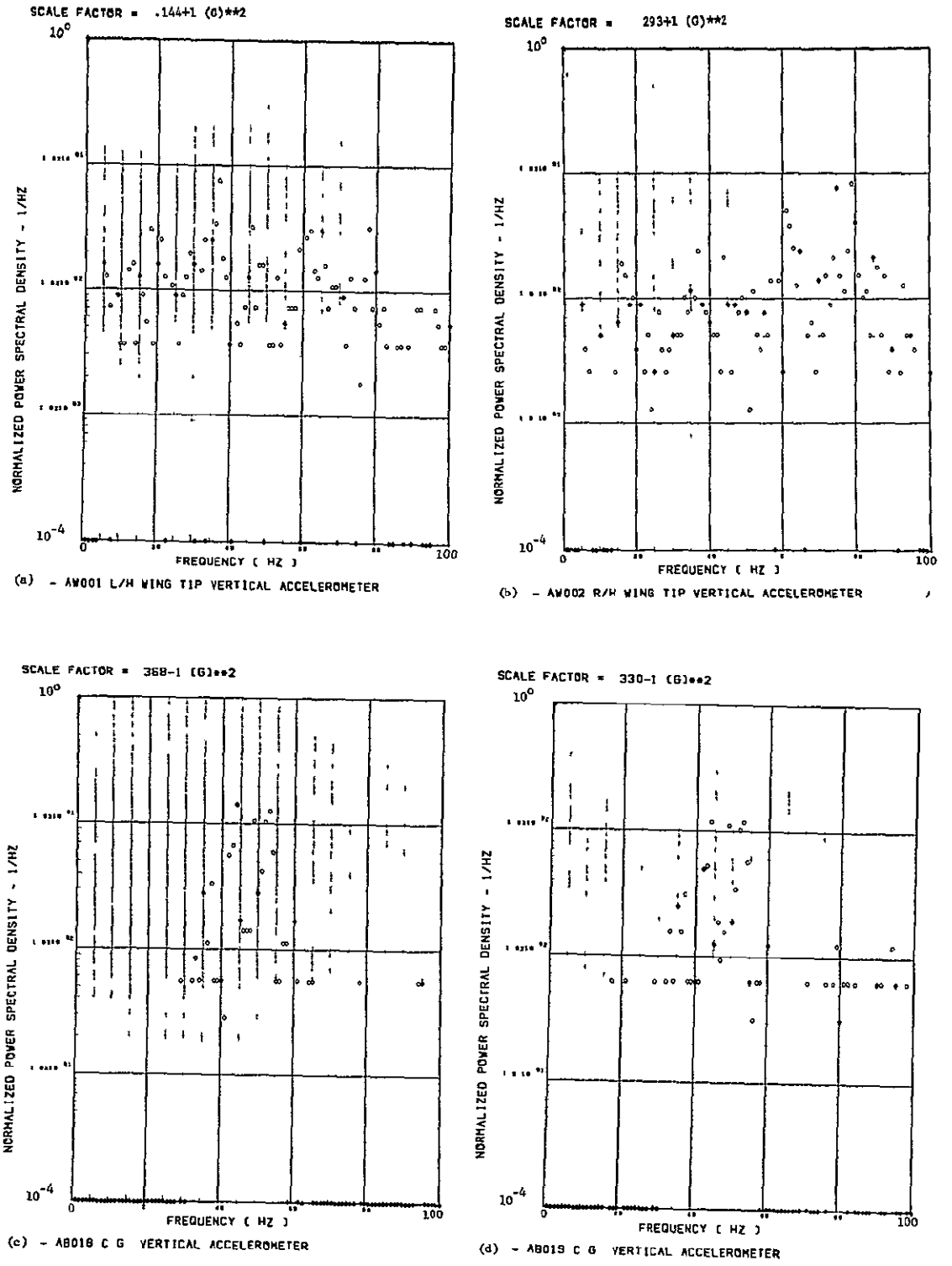

Figure 39. Power Spectra-Flight 60, Run 10, Point 2, T_1=100244.65, ΔT=1 Sec, α_{Nom}=5.15 deg, $\Delta\alpha$=6.60 deg.

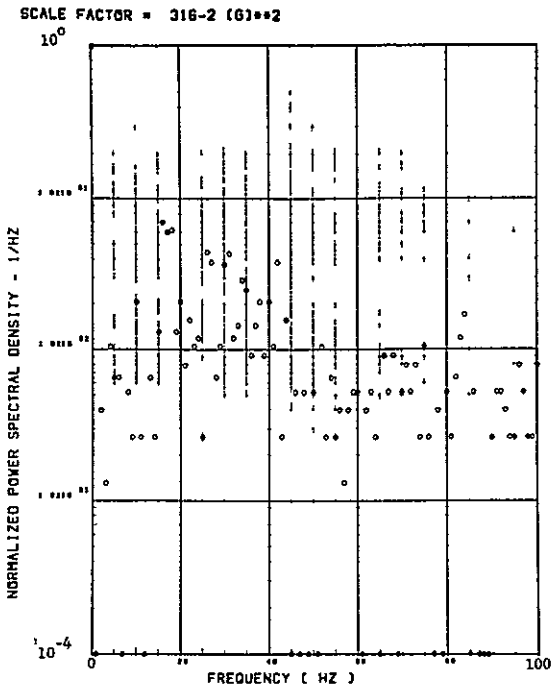

(e) - AF009 PILOT S SEAT VERTICAL ACCELEROMETER

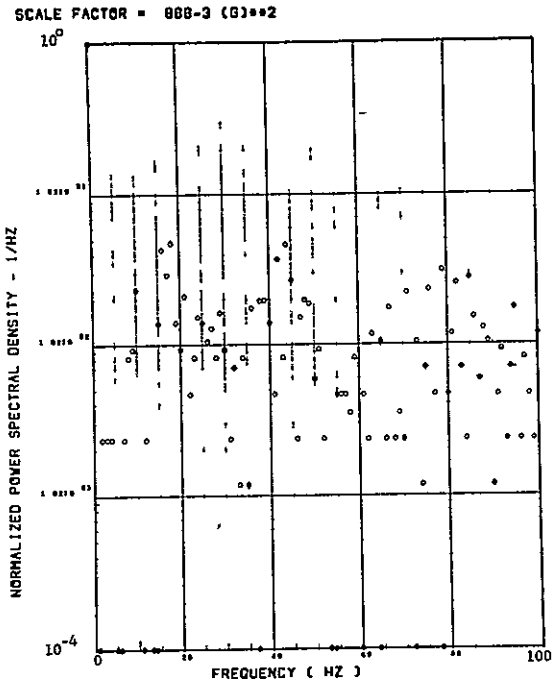

(f) - AF010 PILOT S SEAT LATERAL ACCELEROMETER

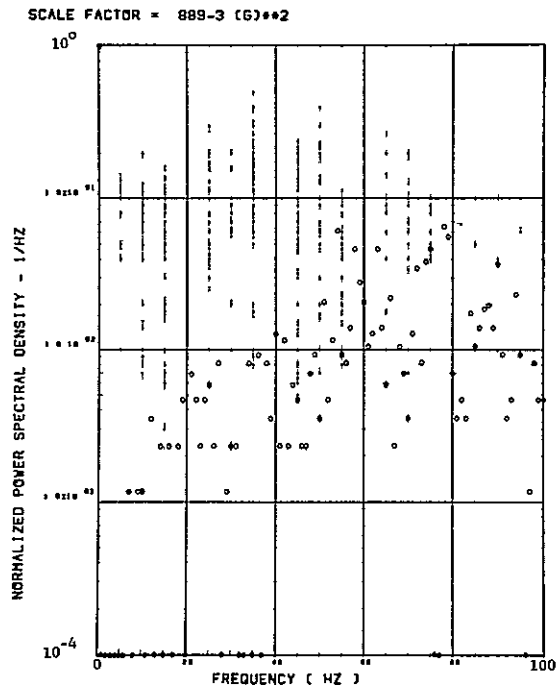

(g) - AB020 C G LATERAL ACCELEROMETER

Figure 39. Continued

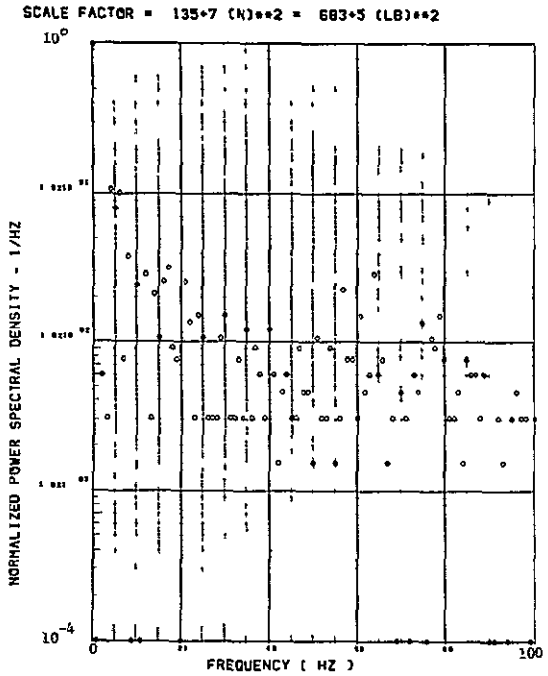

(h) - SW123 SHEAR AT WING STATION 1

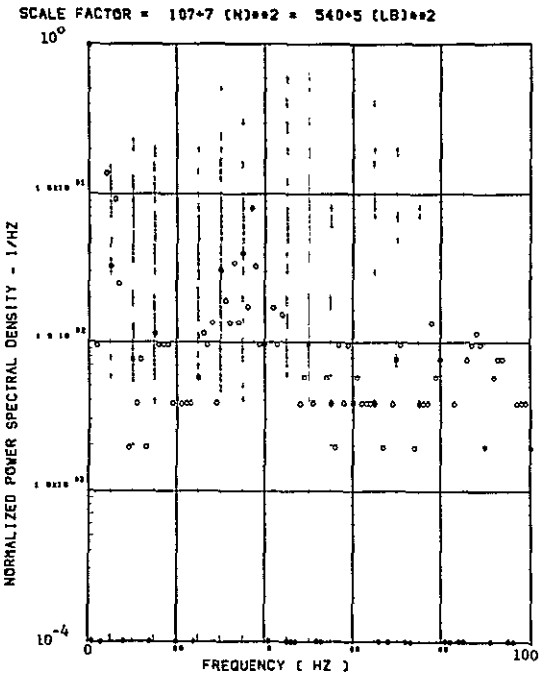

(i) - SW126 SHEAR AT WING STATION 2

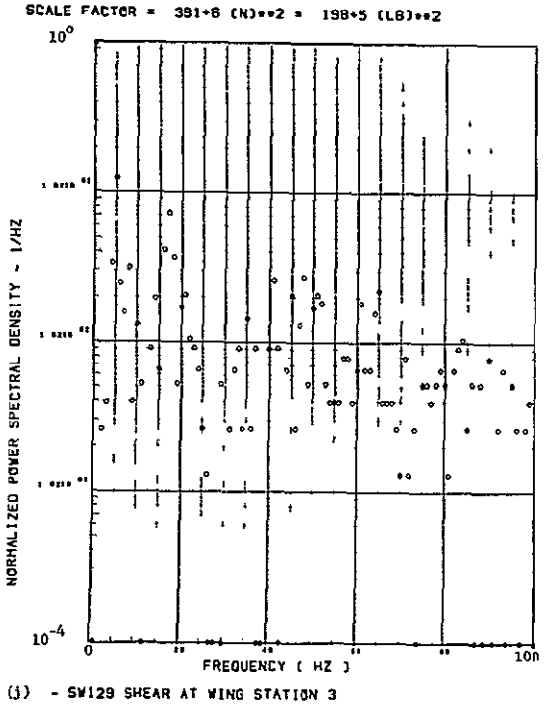

(j) - SW129 SHEAR AT WING STATION 3

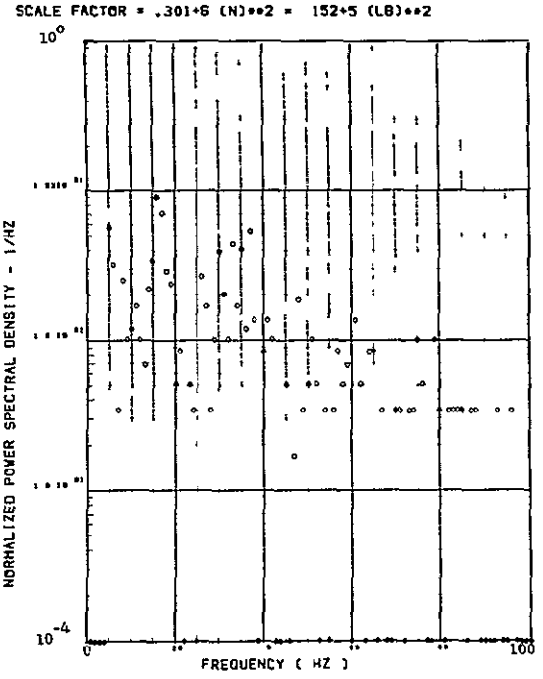

(k) - SW132 SHEAR AT WING STATION 4

Figure 39. Continued

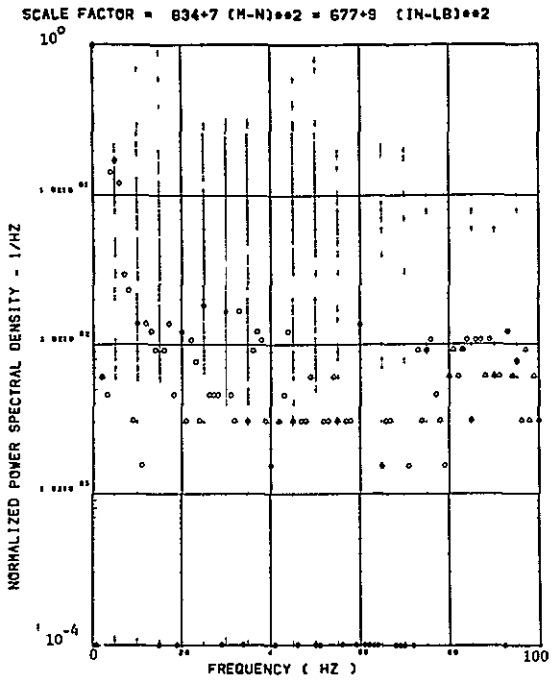

(l) SW124 BENDING MOMENT AT WING STATION 1

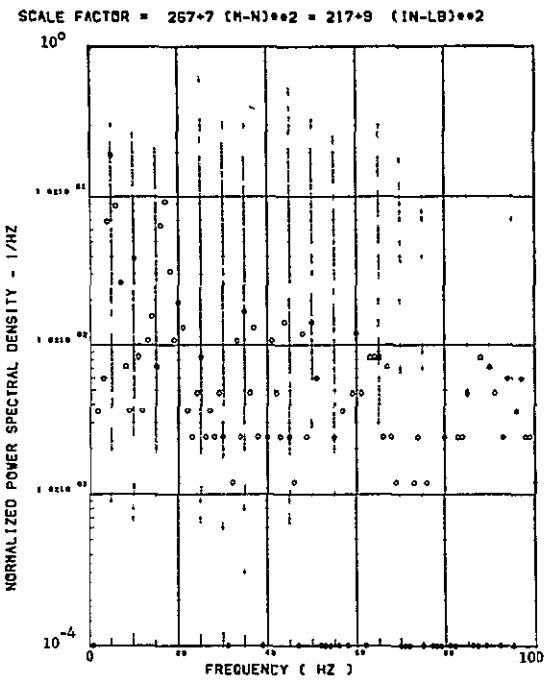

(m) - SW127 BENDING MOMENT AT WING STATION 2

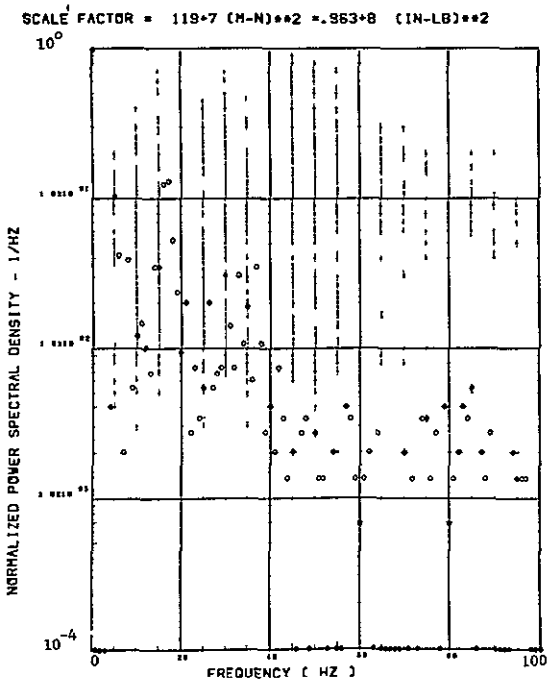

(n) - SW130 BENDING MOMENT AT WING STATION 3

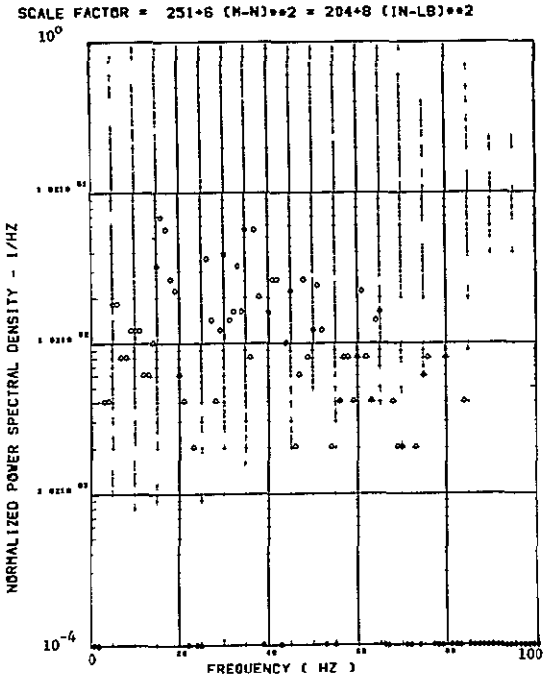

(o) - SW133 BENDING MOMENT AT WING STATION 4

Figure 39. Continued

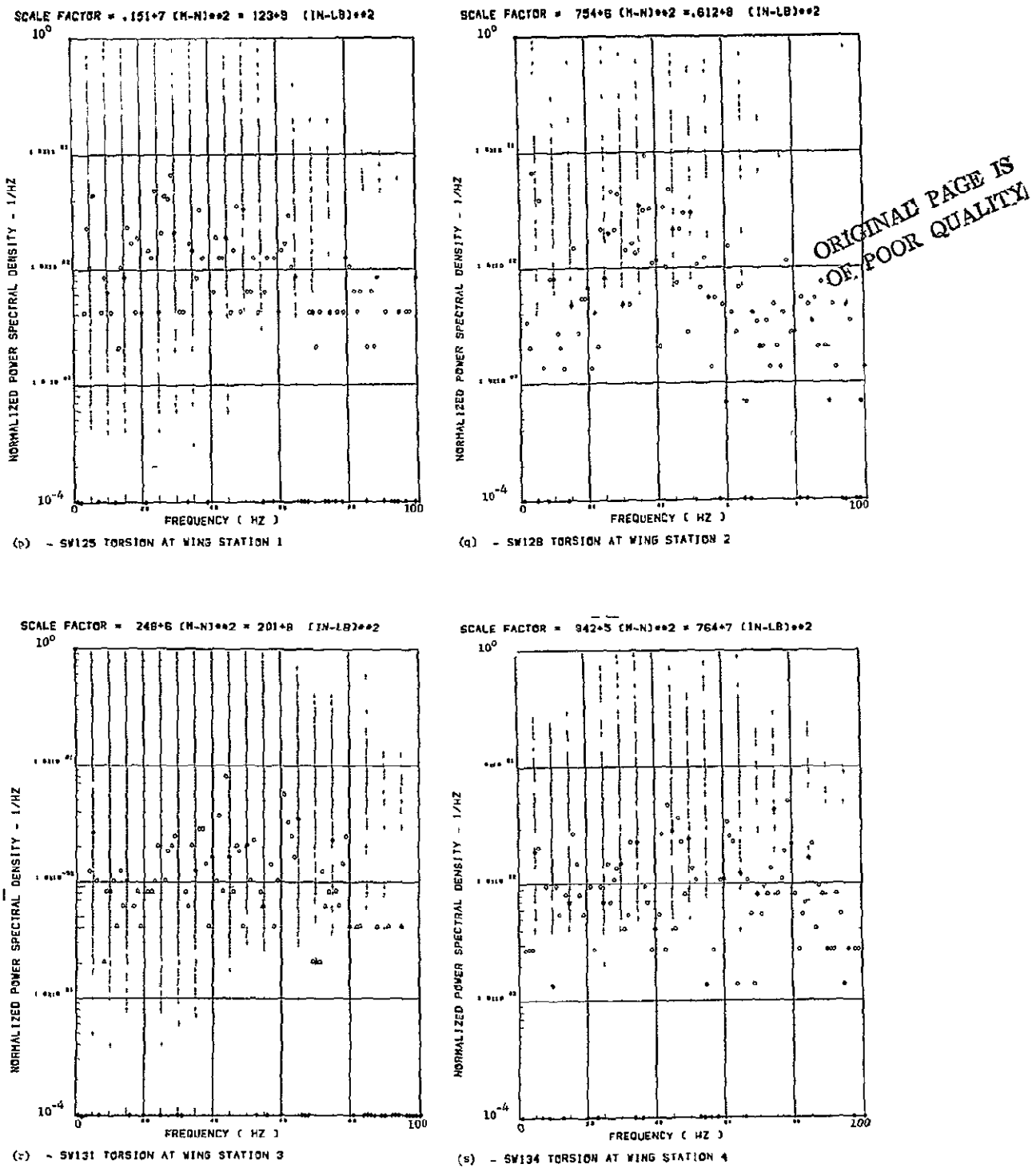

Figure 39. Concluded

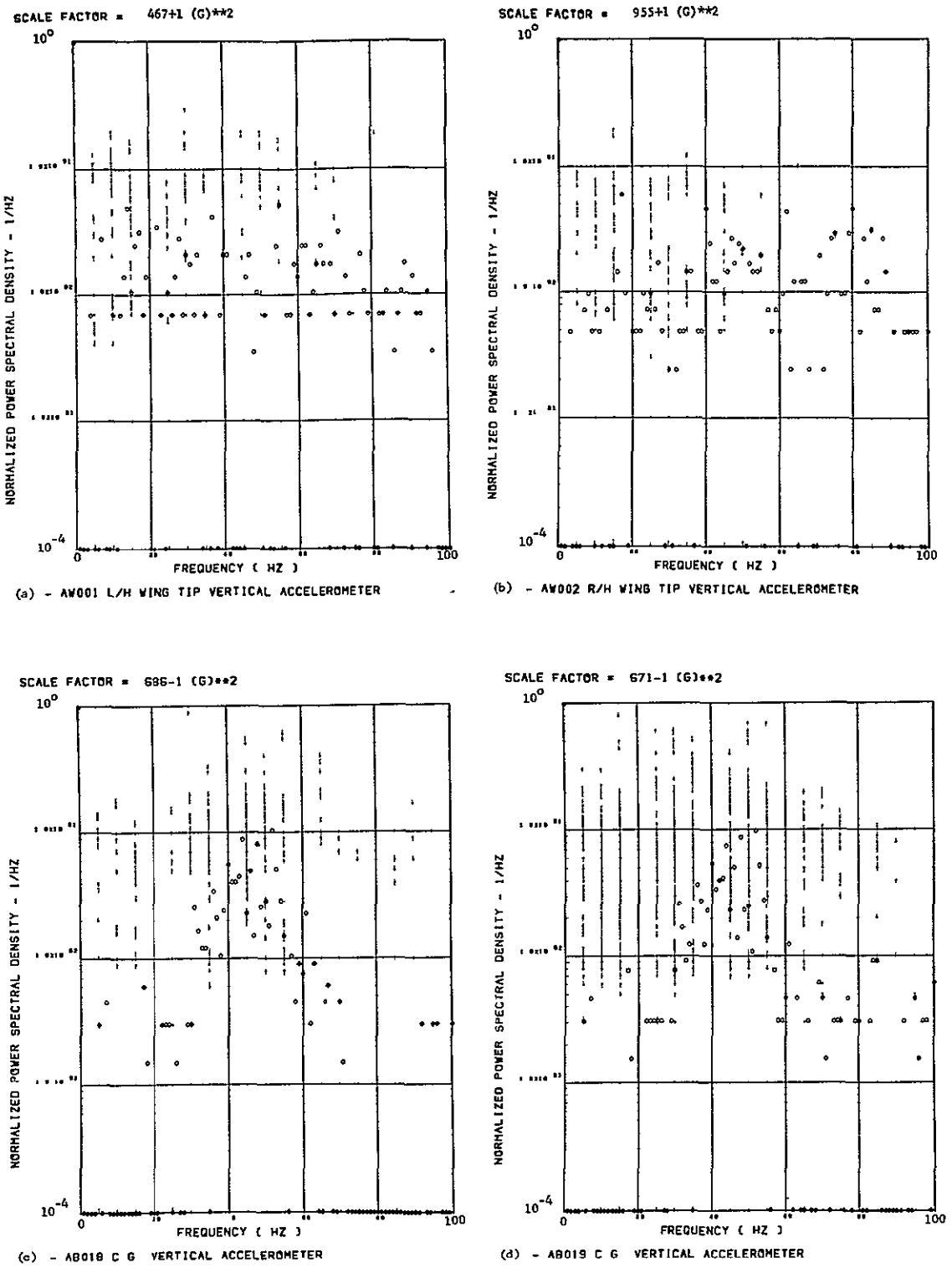

Figure 40. Power Spectra-Flight 60, Run 10, Point 3, T_1=100245.2, ΔT=1 Sec, α_{Nom}=9.3 deg, $\Delta\alpha$=5.95 deg.

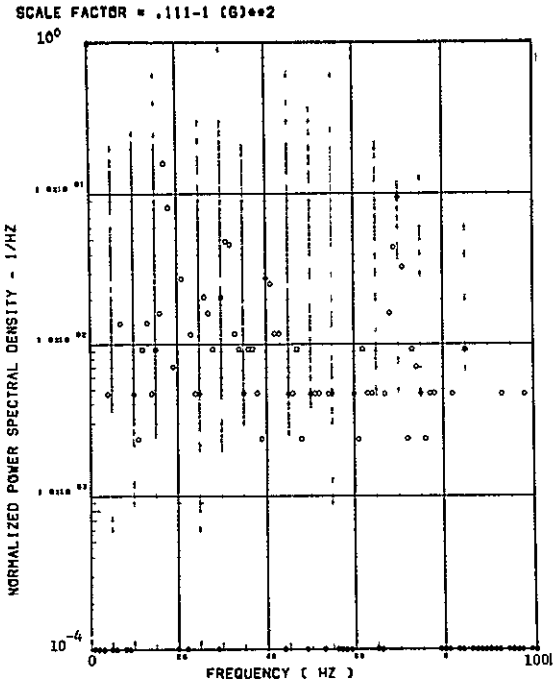

(e) - AF009 PILOT S SEAT VERTICAL ACCELEROMETER

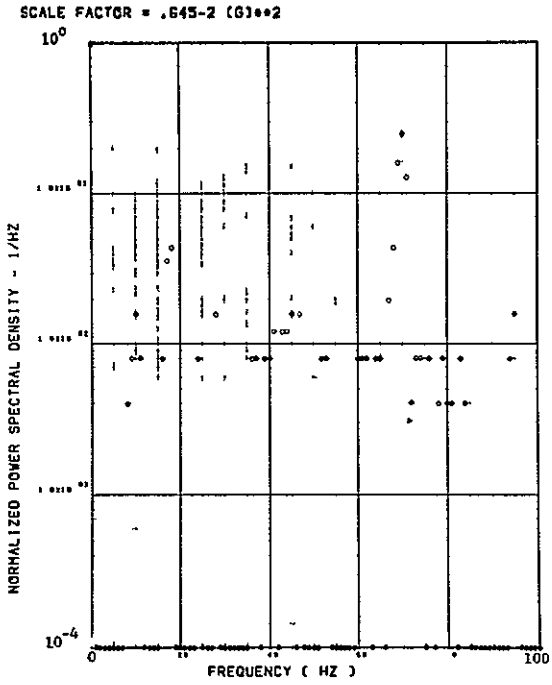

(f) - AF010 PILOT S SEAT LATERAL ACCELEROMETER

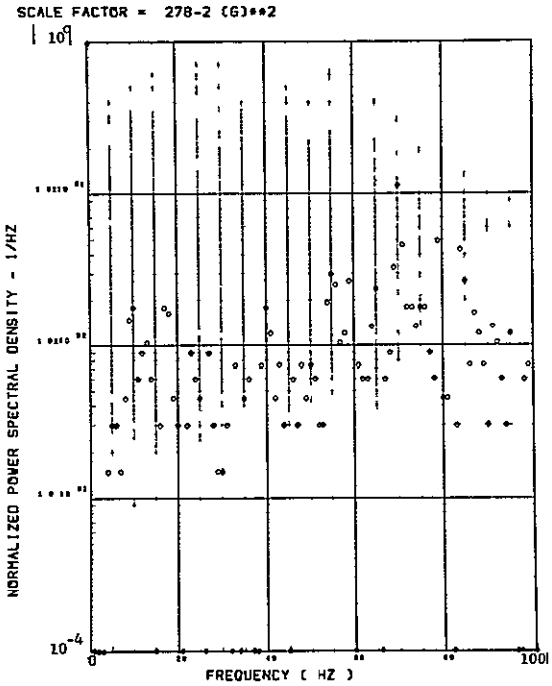

(g) - AB020 C G LATERAL ACCELEROMETER

Figure 40. Continued

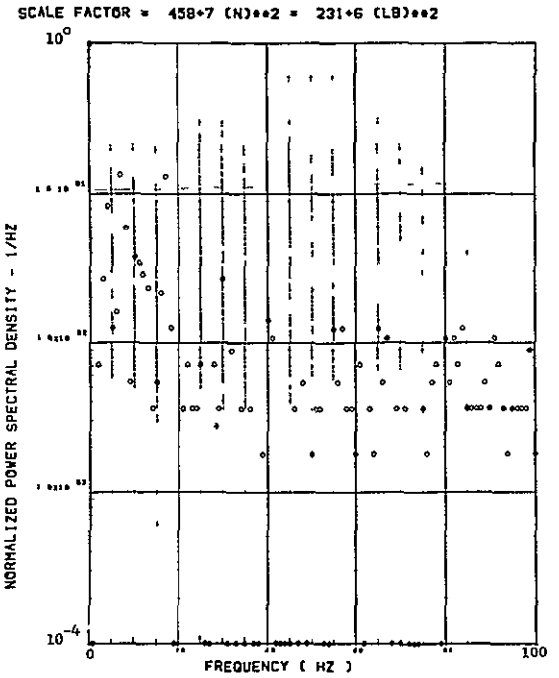

(h) - SW123 SHEAR AT WING STATION 1

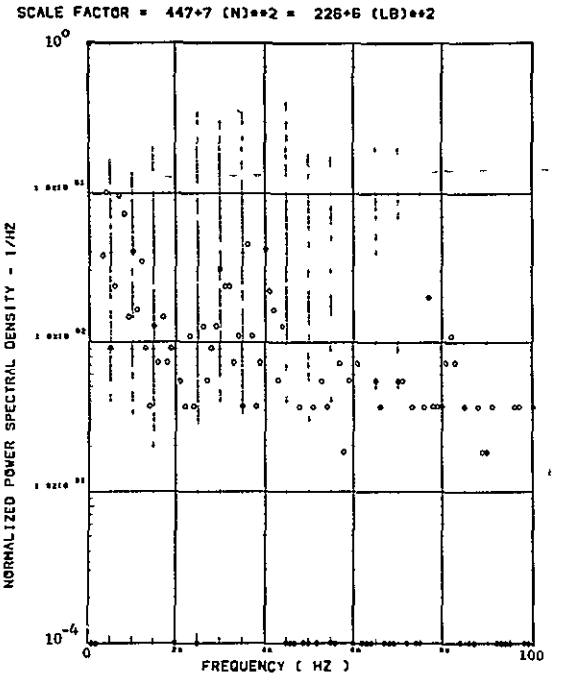

(i) - SW126 SHEAR AT WING STATION 2

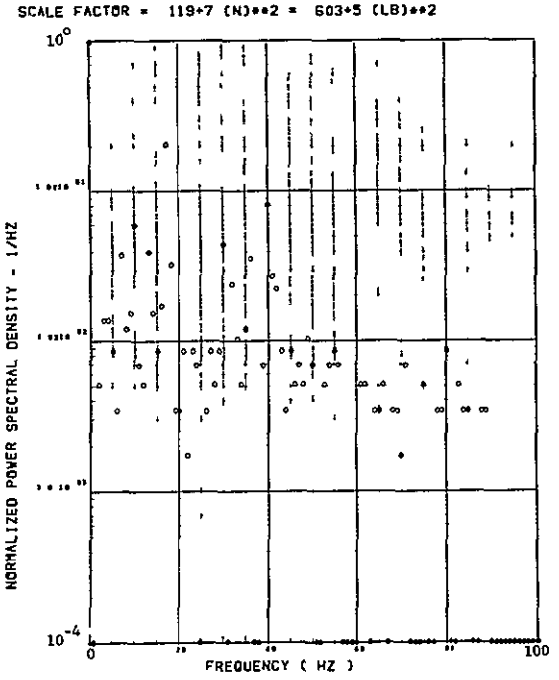

(j) - SW132 SHEAR AT WING STATION 4

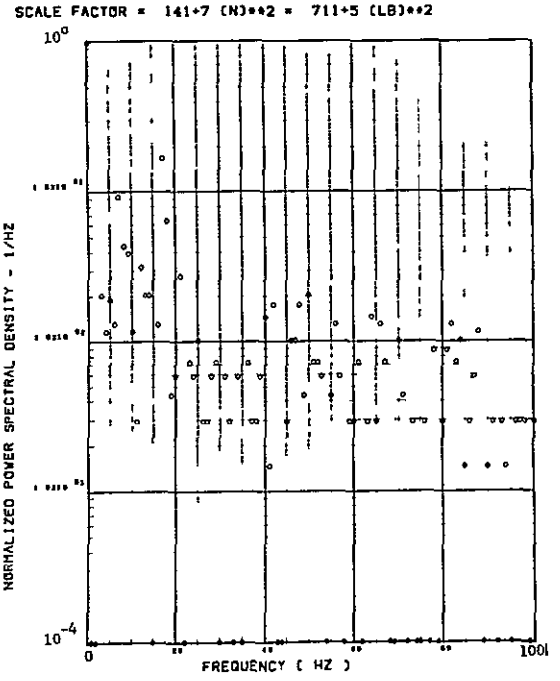

(k) - SW129 SHEAR AT WING STATION 3

Figure 40. Continued

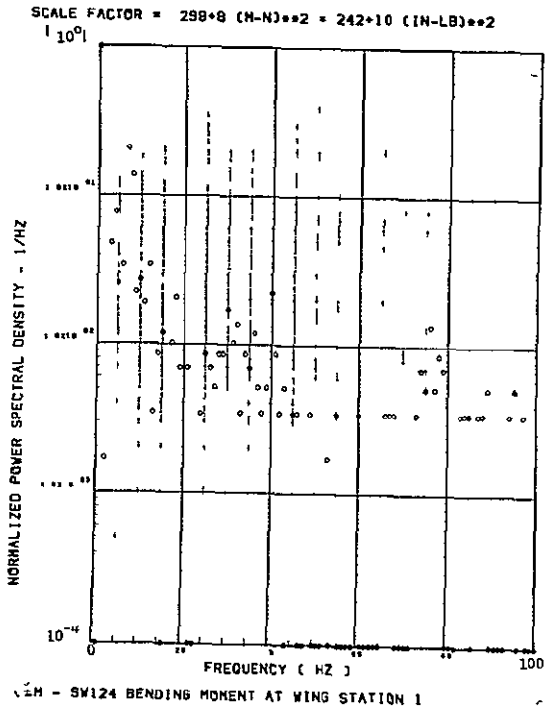

(m) - SW124 BENDING MOMENT AT WING STATION 1

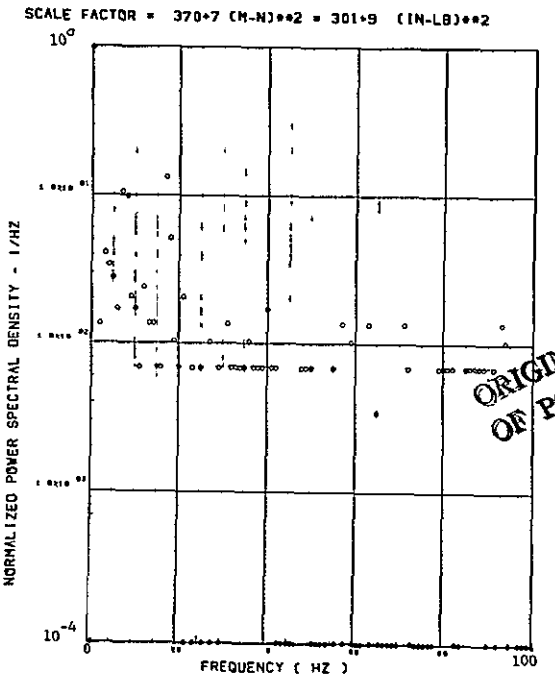

(n) - SW127 BENDING MOMENT AT WING STATION 2

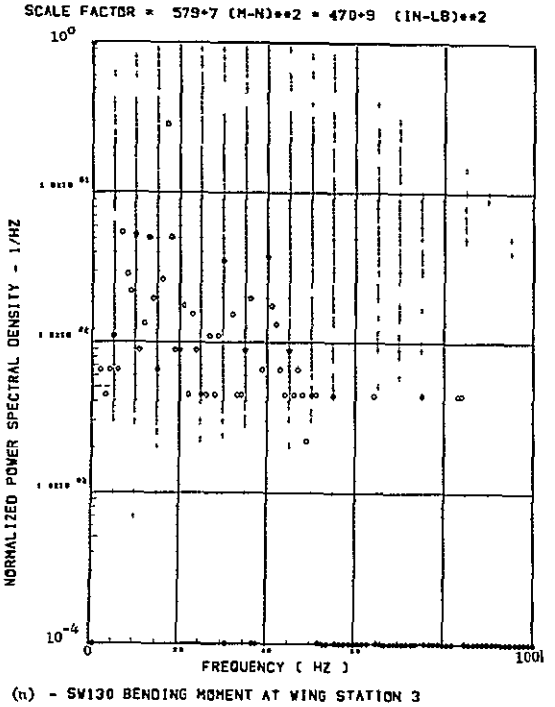

(n) - SW130 BENDING MOMENT AT WING STATION 3

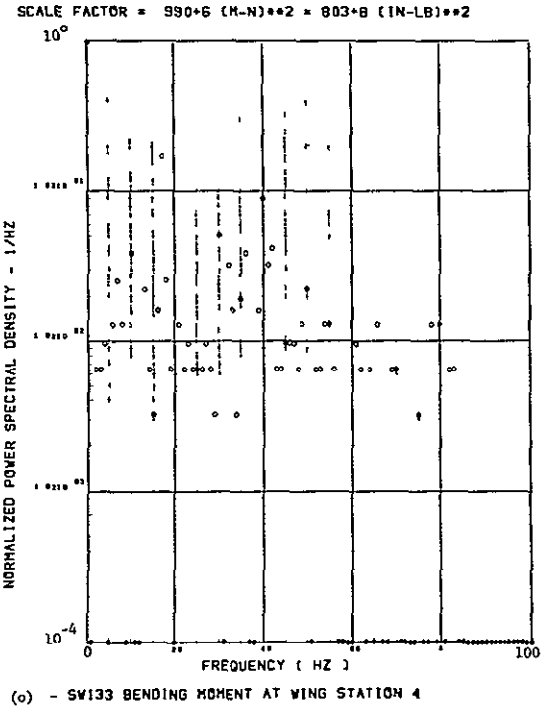

(o) - SW133 BENDING MOMENT AT WING STATION 4

Figure 40. Continued

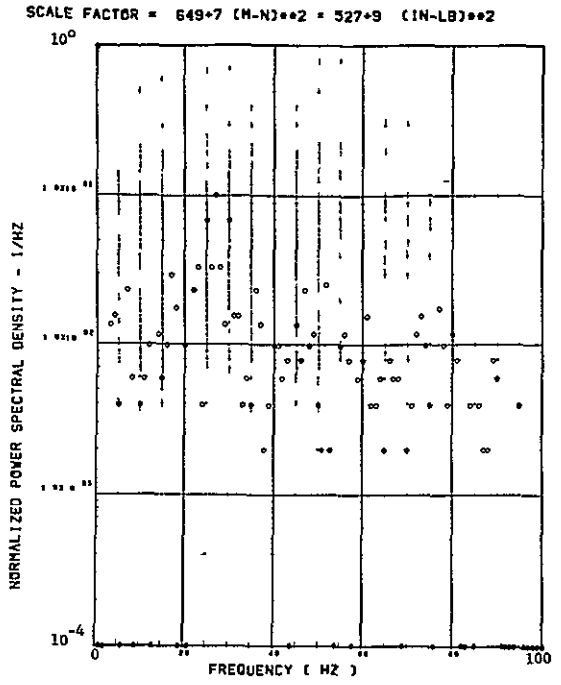

(p) - SW125 TORSION AT WING STATION 1

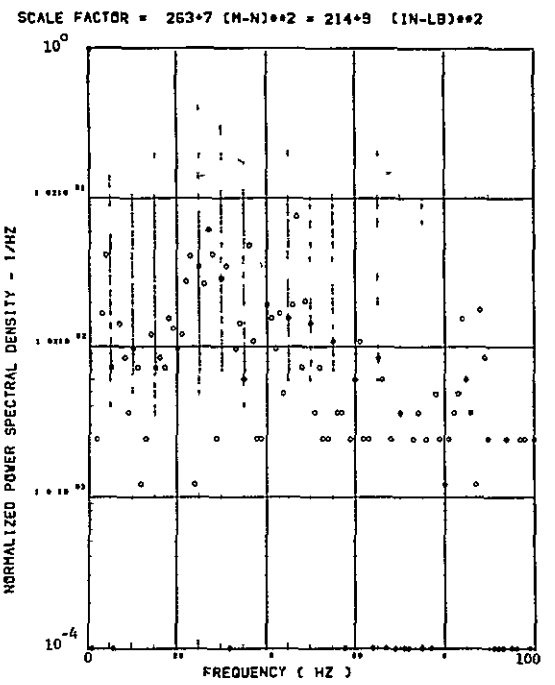

(q) - SW128 TORSION AT WING STATION 2

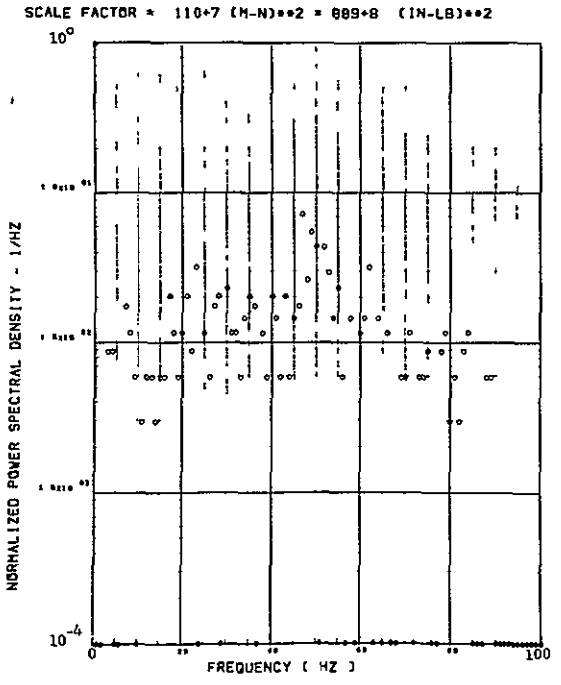

(r) - SW131 TORSION AT WING STATION 3

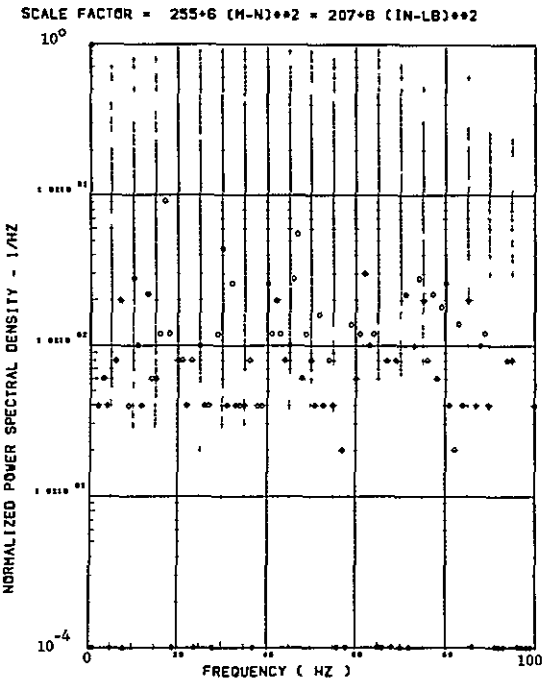

(s) - SW134 TORSION AT WING STATION 4

Figure 40. Concluded

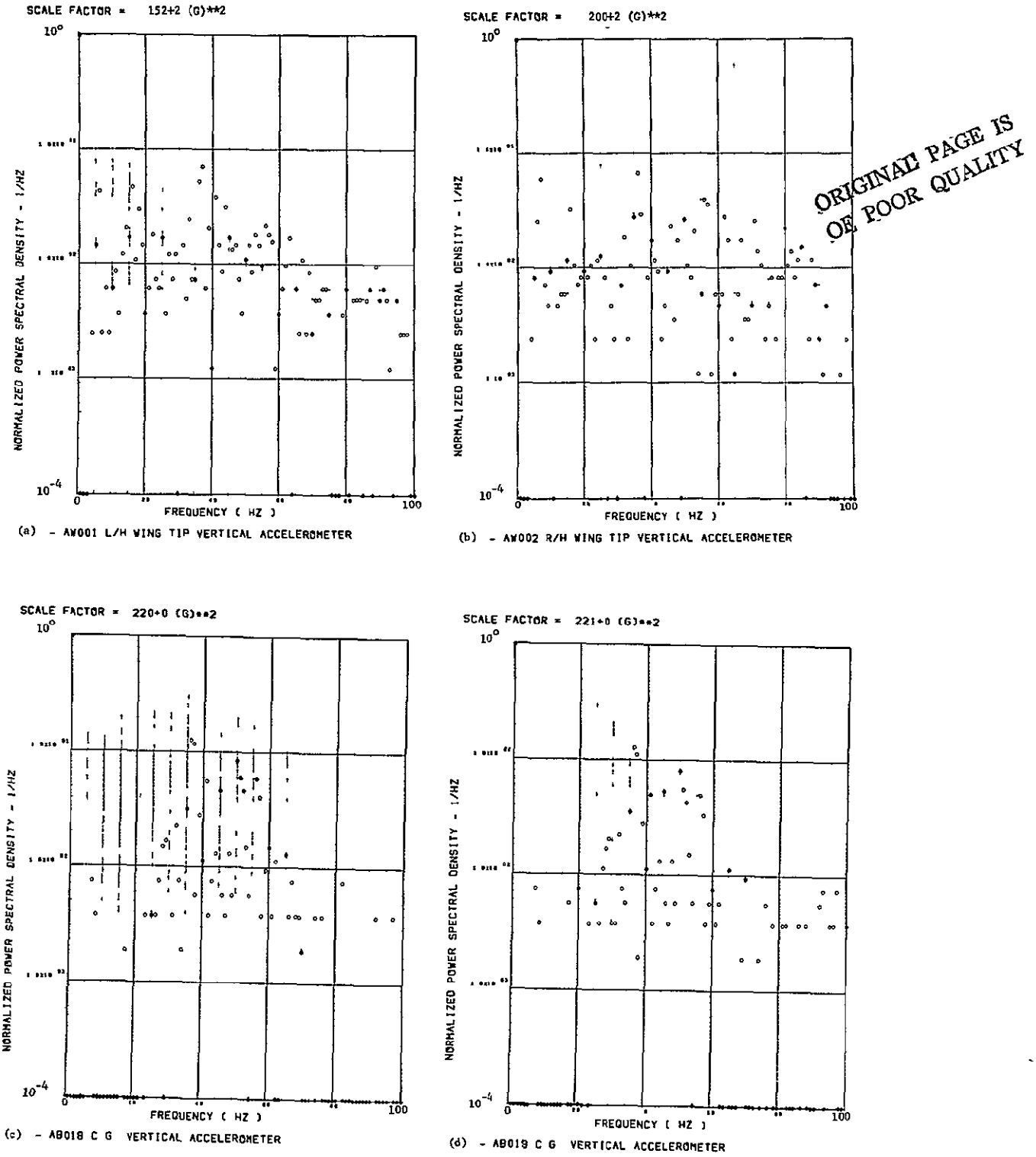

Figure 41. Power Spectra-Flight 60, Run 10, Point 4 T_1=100245.7, ΔT=1 Sec, α_{Nom}=12.3 deg, $\Delta\alpha$=6.53 deg.

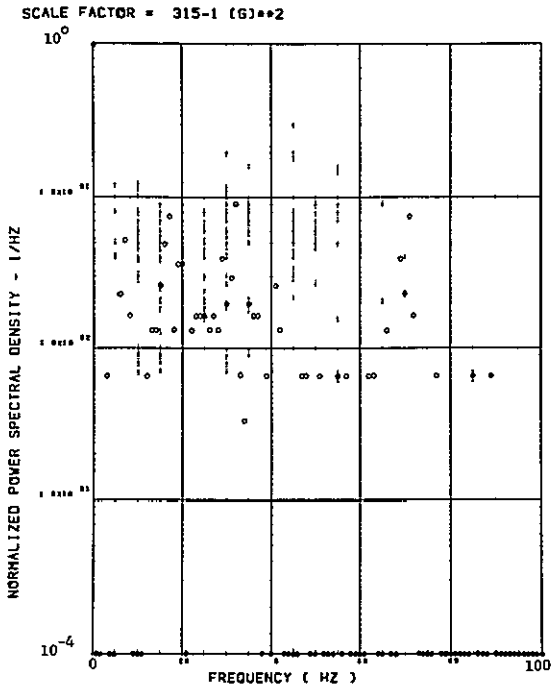

(e) - AF009 PILOT S SEAT VERTICAL ACCELEROMETER

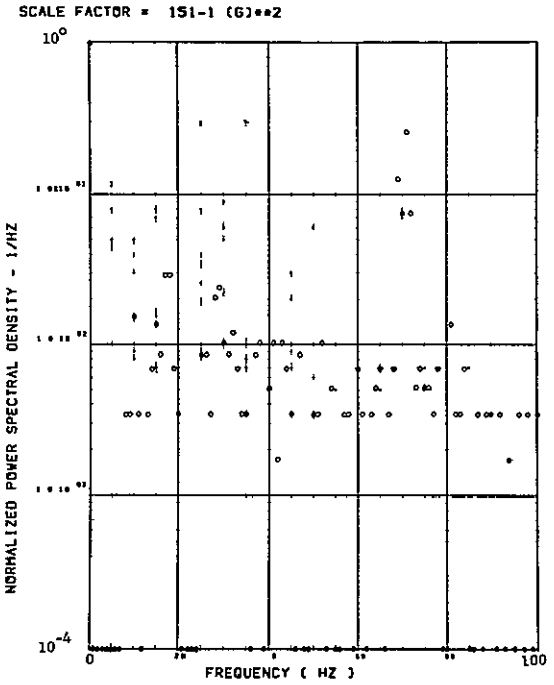

(f) - AF010 PILOT S SEAT LATERAL ACCELEROMETER

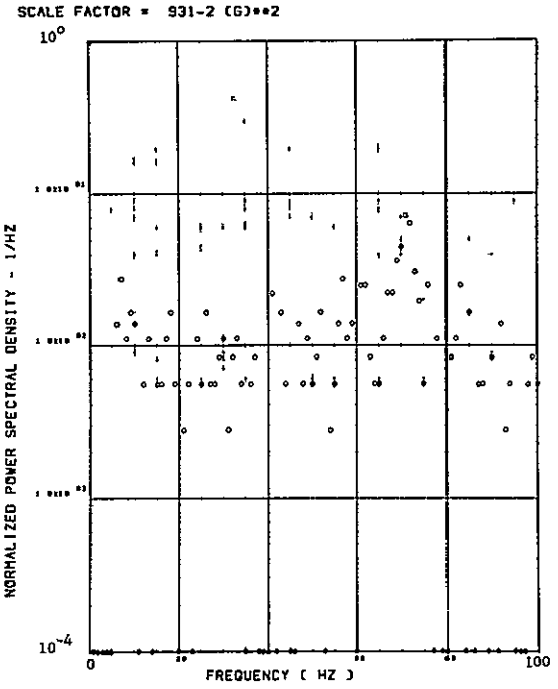

(g) - AB020 C G LATERAL ACCELEROMETER

Figure 41. Continued

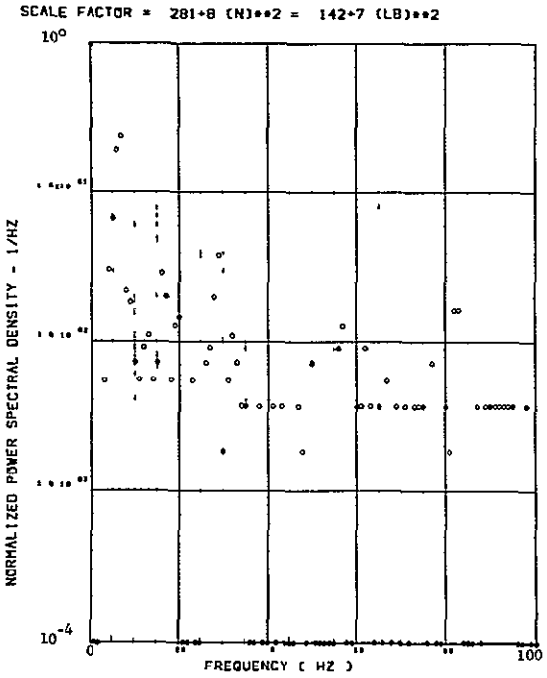

(h) - SW123 SHEAR AT WING STATION 1

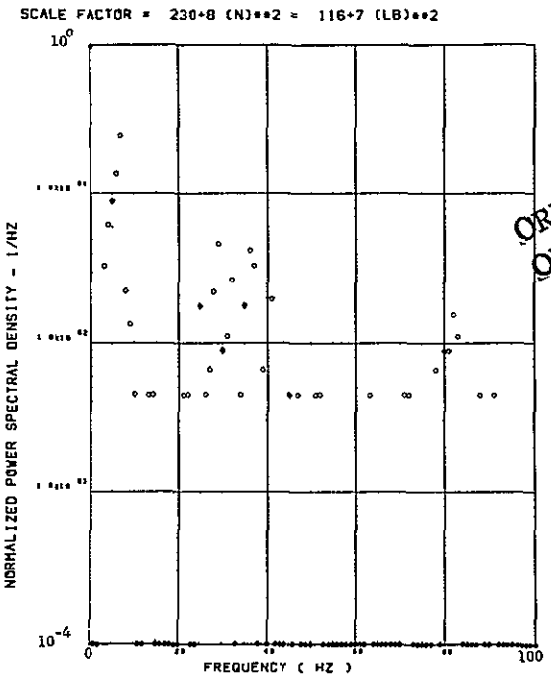

(i) - SW126 SHEAR AT WING STATION 2

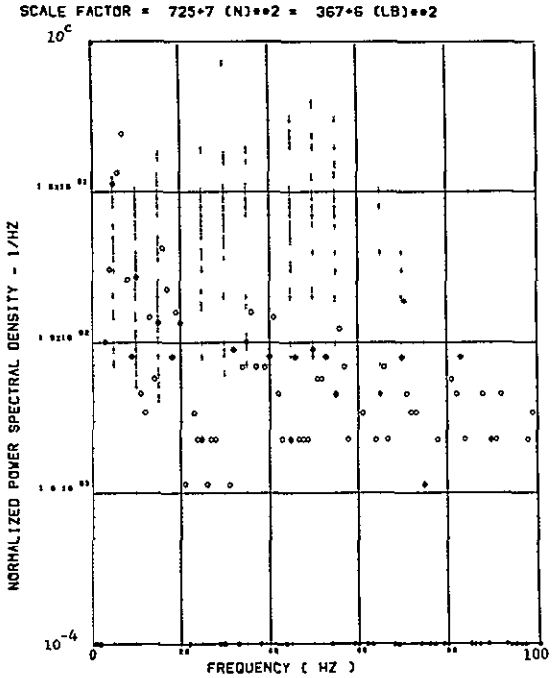

(j) - SW129 SHEAR AT WING STATION 3

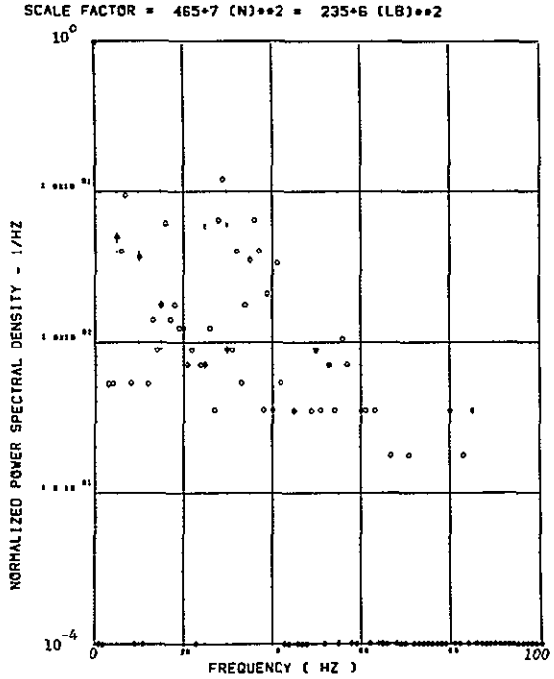

(k) - SW132 SHEAR AT WING STATION 4

Figure 41. Continued

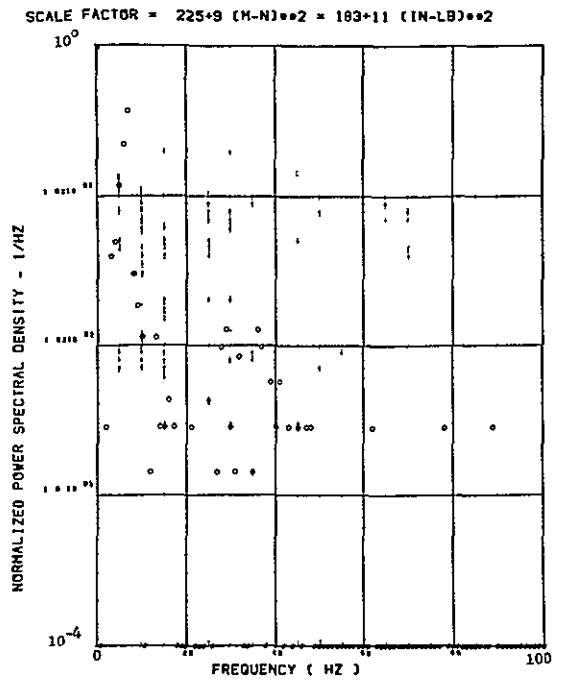

(l) - SW124 BENDING MOMENT AT WING STATION 1

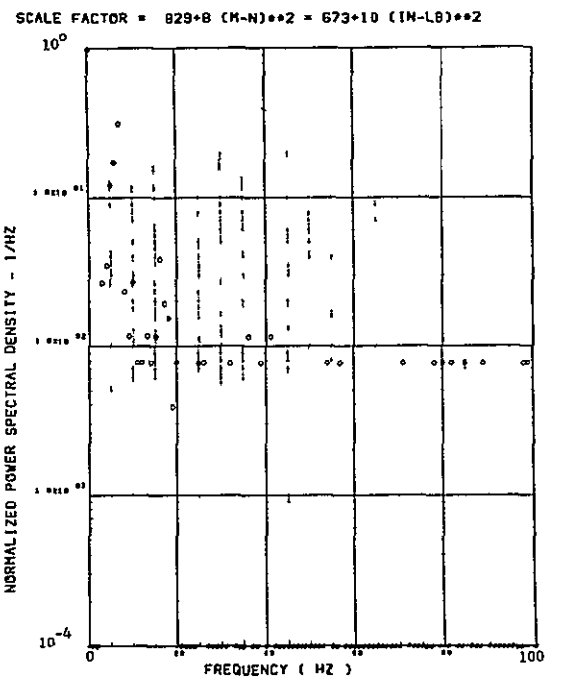

(m) - SW127 BENDING MOMENT AT WING STATION 2

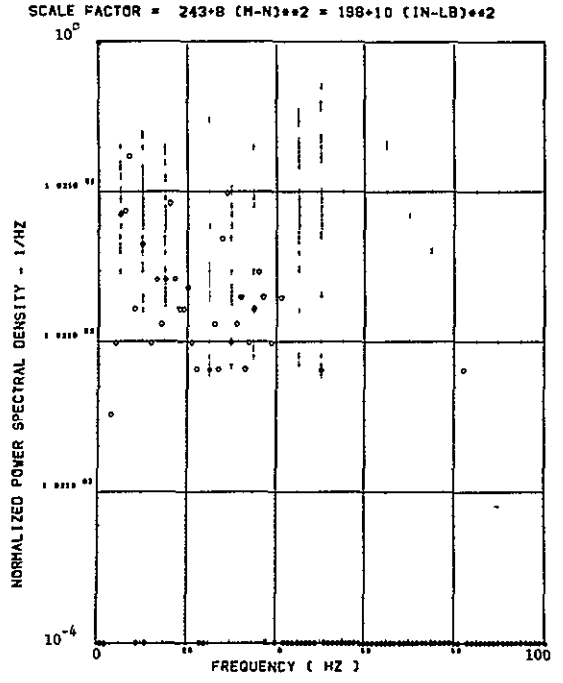

(n) - SW130 BENDING MOMENT AT WING STATION 3

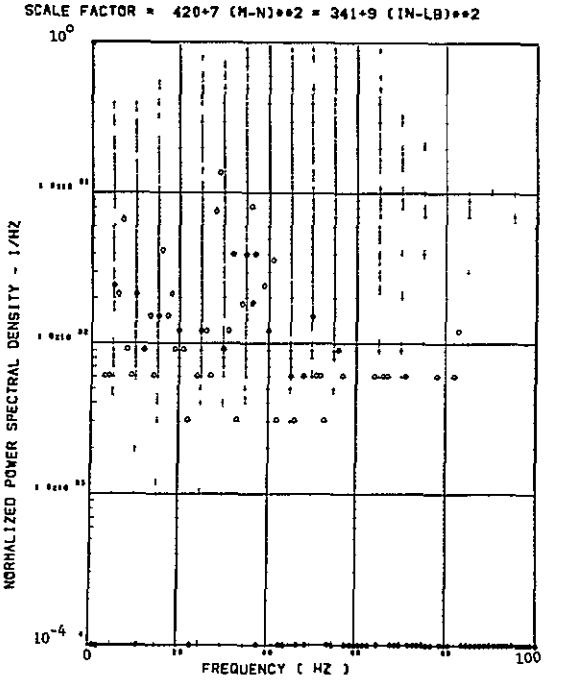

(o) - SW133 BENDING MOMENT AT WING STATION 4

Figure 41. Continued

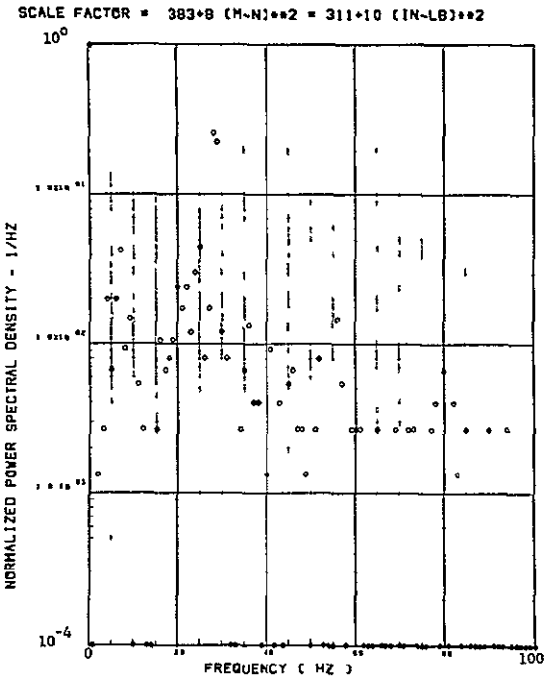

(p) - SW125 TORSION AT WING STATION 1

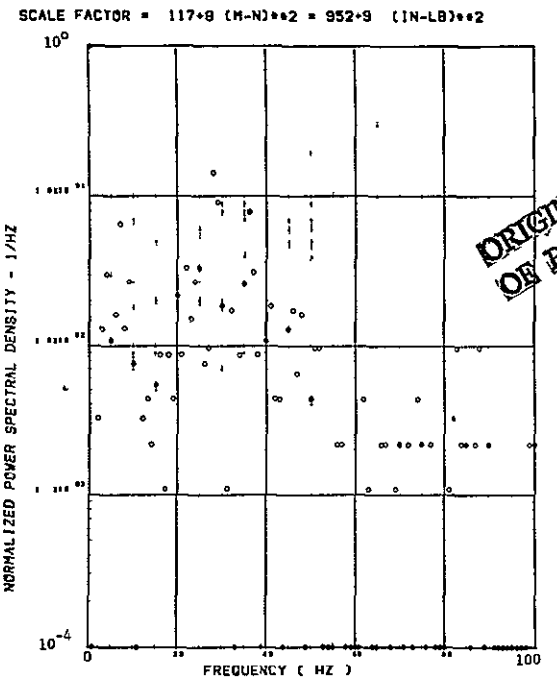

(q) - SW128 TORSION AT WING STATION 2

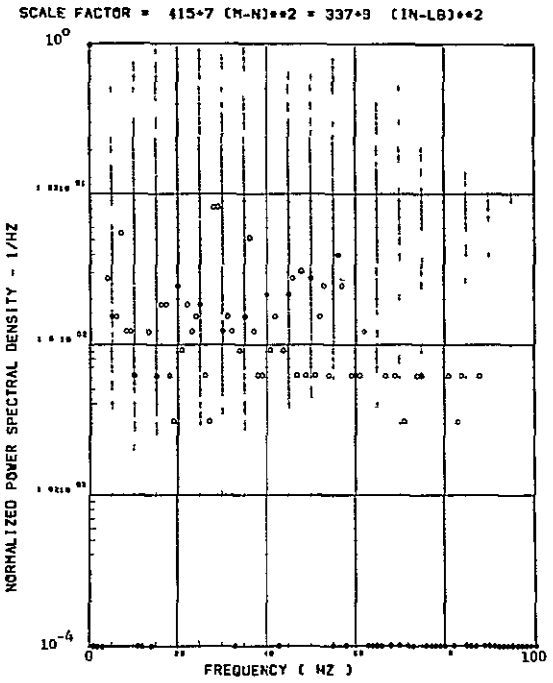

(r) - SW131 TORSION AT WING STATION 3

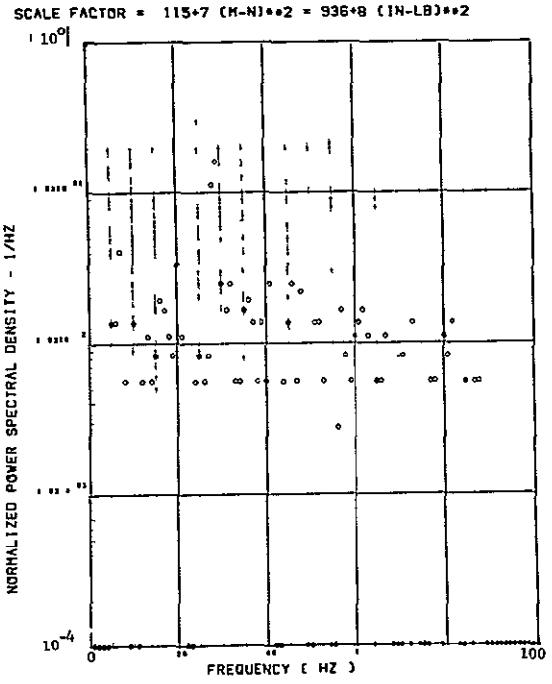

(s) - SW134 TORSION AT WING STATION 4

Figure 41. Concluded

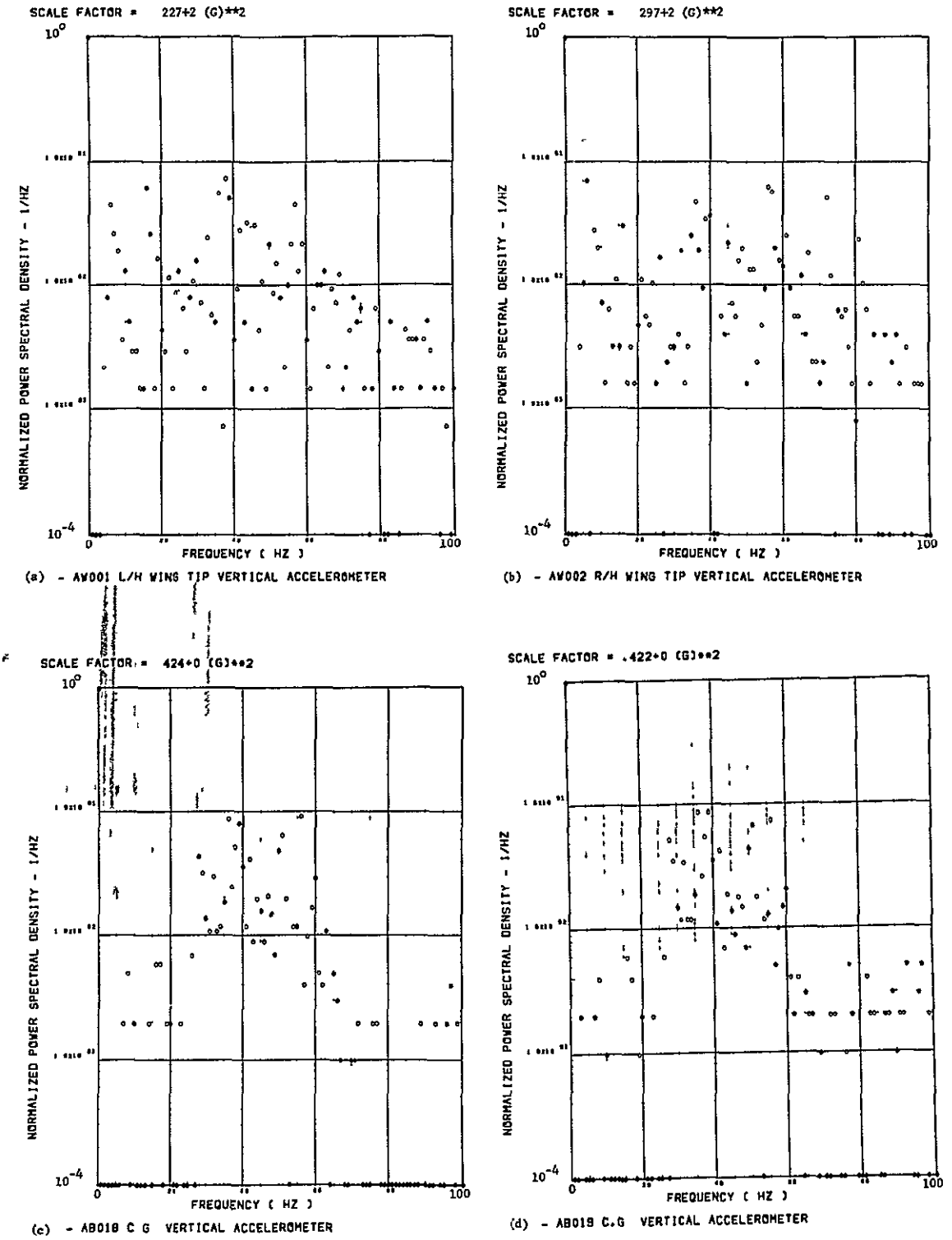

Figure 42. Power Spectra-Flight 60, Run 10, Point 5, T_1=100246.15, ΔT=1 Sec, α_{Nom}=14.8 deg, $\Delta\alpha$=4.30 deg.

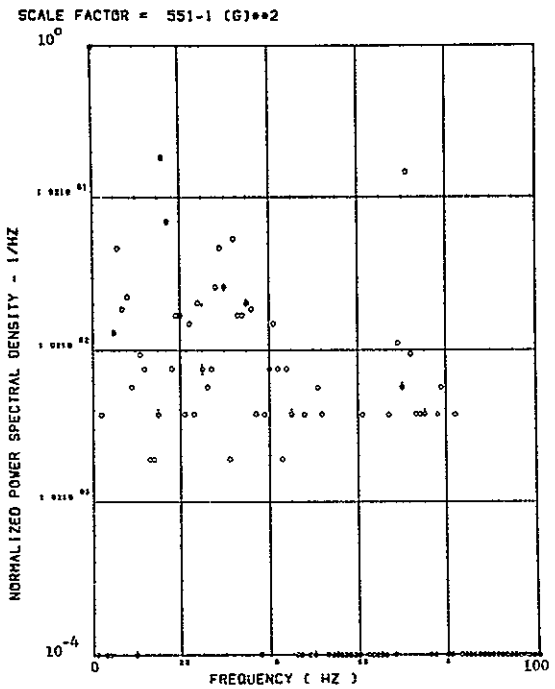

(e) - AF009 PILOT S SEAT VERTICAL ACCELEROMETER

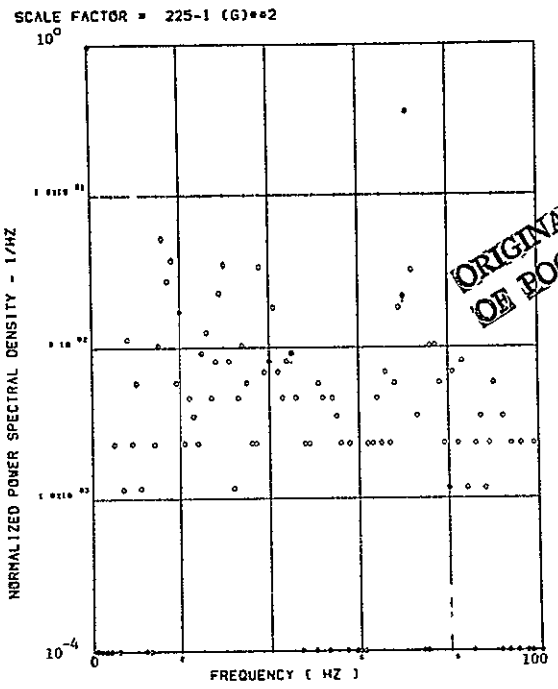

(f) - AF010 PILOT S SEAT LATERAL ACCELEROMETER

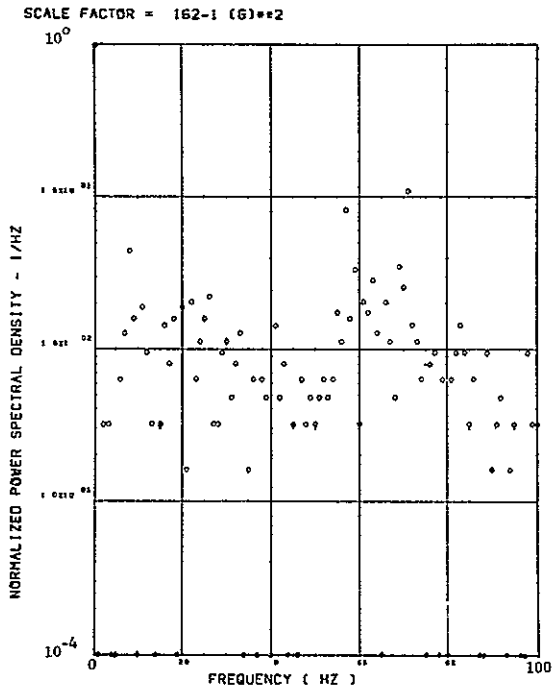

(g) - AB020 C G LATERAL ACCELEROMETER

Figure 42. Continued

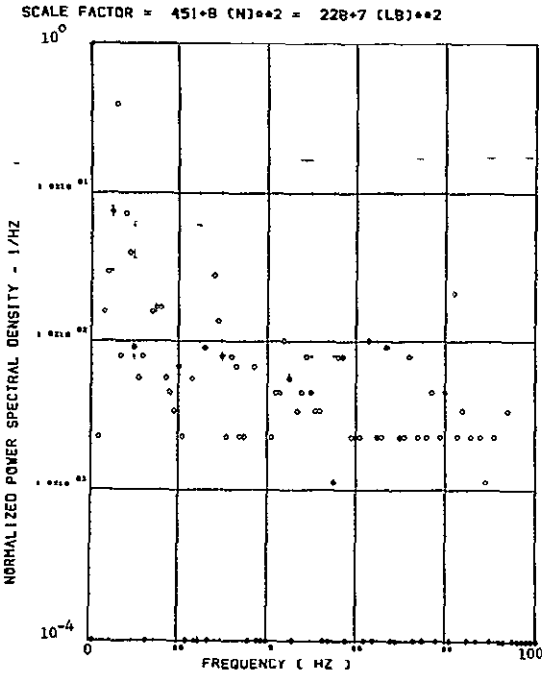

(h) - SW123 SHEAR AT WING STATION 1

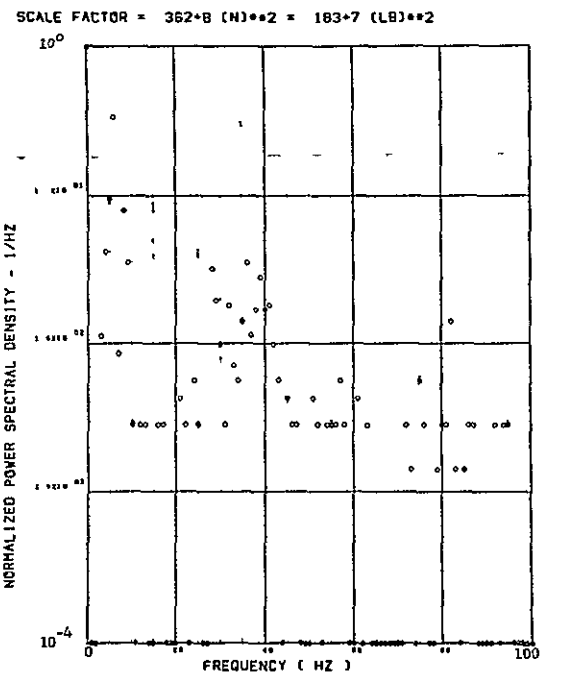

(i) - SW126 SHEAR AT WING STATION 2

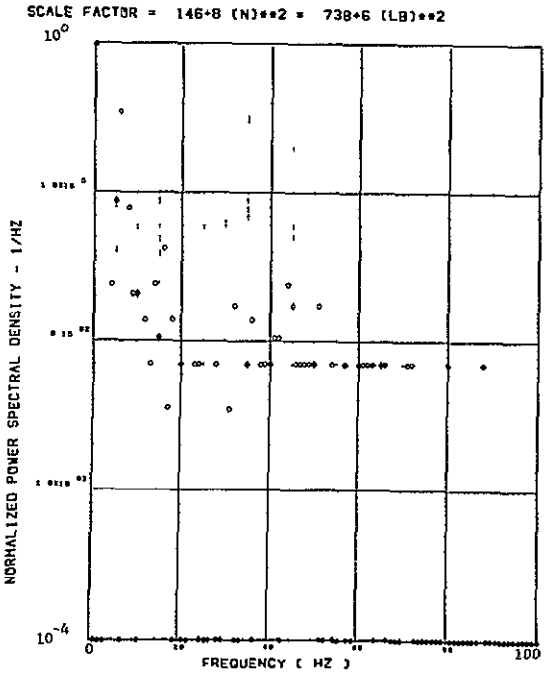

(k) - SW129 SHEAR AT WING STATION 3

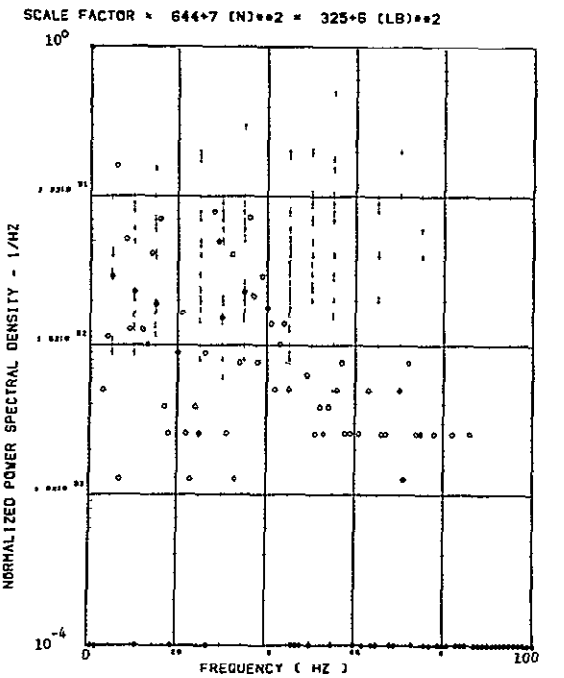

(j) - SW132 SHEAR AT WING STATION 4

Figure 42. Continued

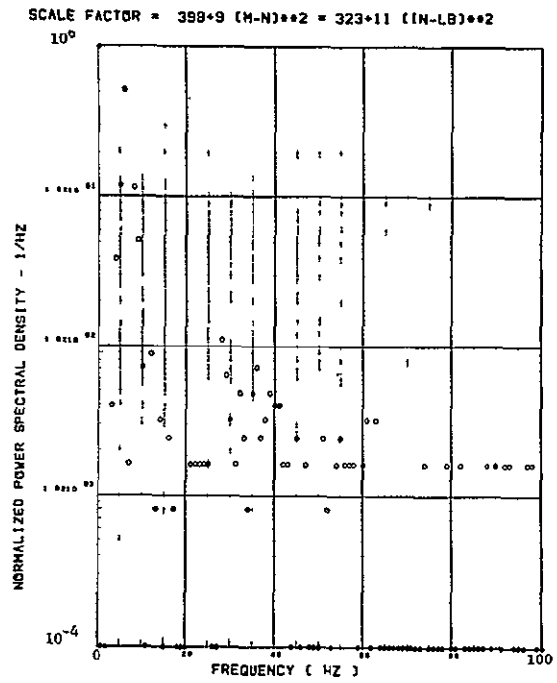

(l) - SW124 BENDING MOMENT AT WING STATION 1

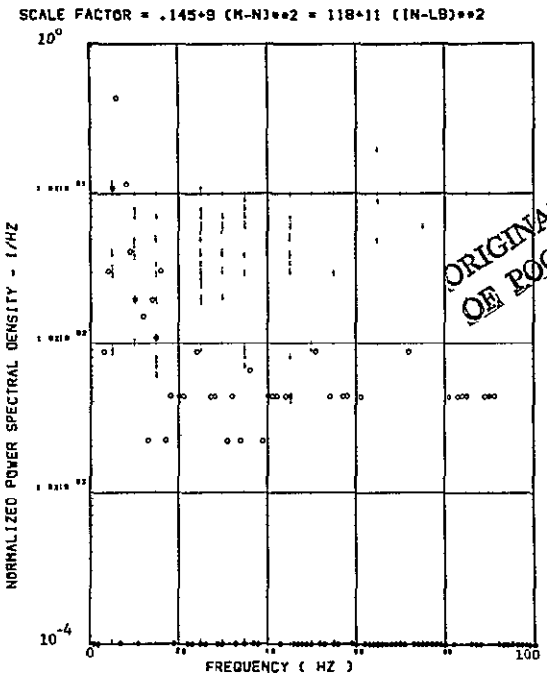

(m) - SW127 BENDING MOMENT AT WING STATION 2

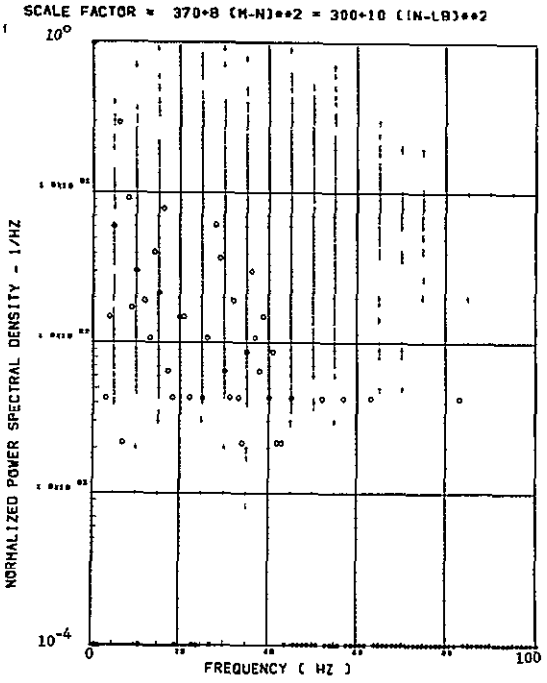

(n) - SW130 BENDING MOMENT AT WING STATION 3

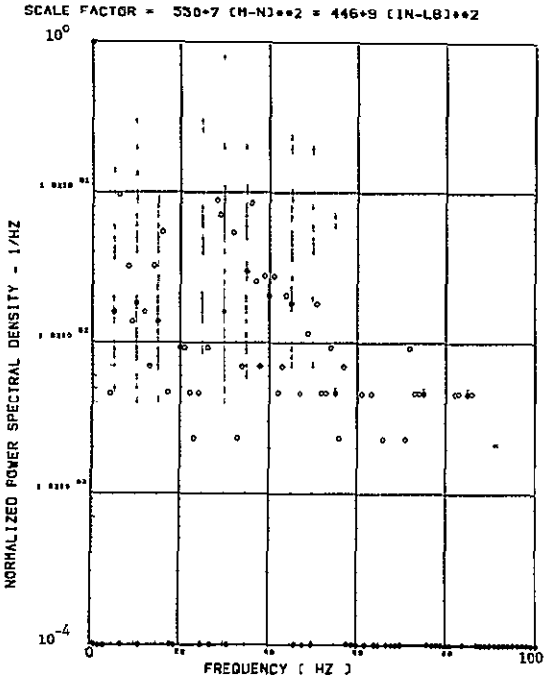

(o) - SW133 BENDING MOMENT AT WING STATION 4

Figure 42. Continued

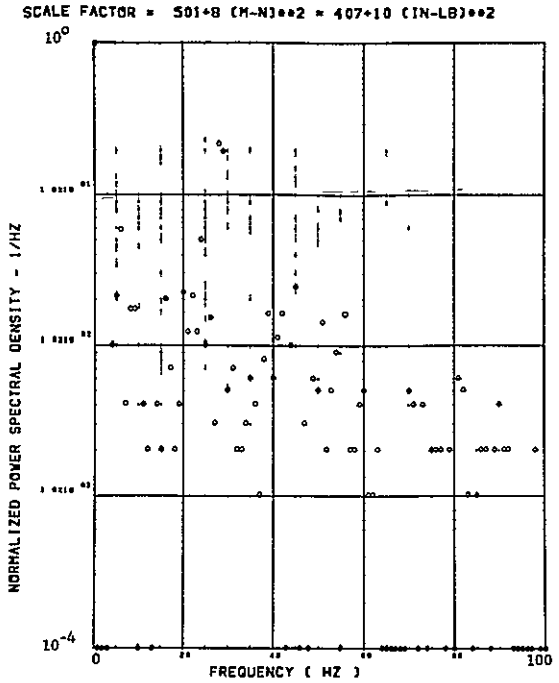

(p) - SW125 TORSION AT WING STATION 1

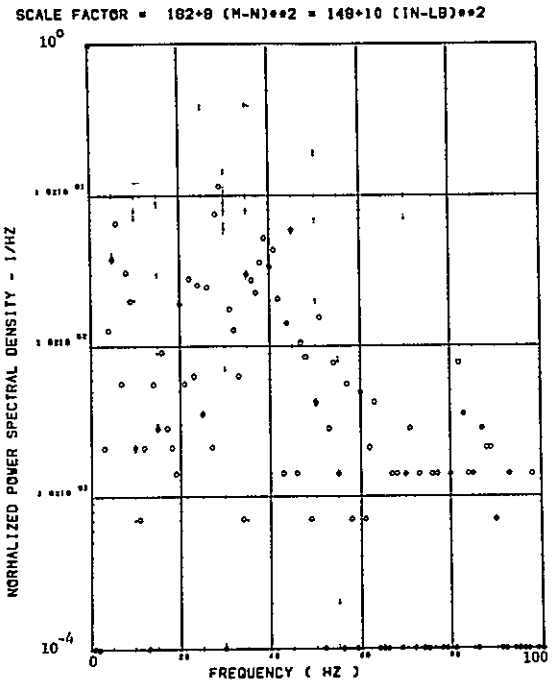

(q) - SW128 TORSION AT WING STATION 2

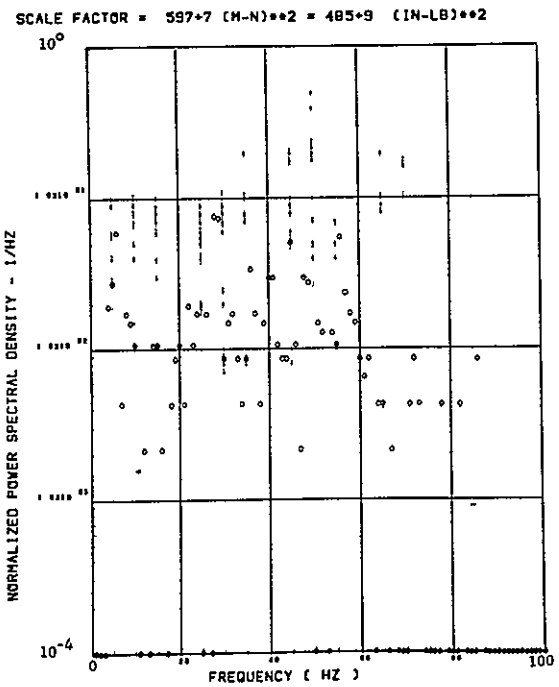

(r) - SW131 TORSION AT WING STATION 3

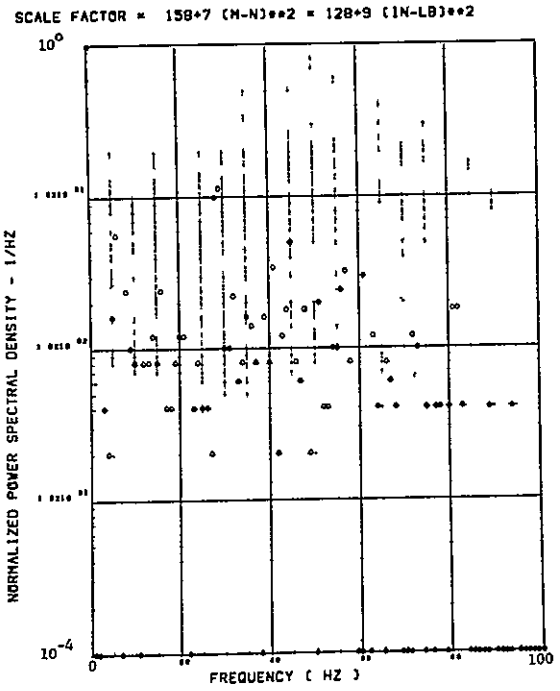

(s) - SW134 TORSION AT WING STATION 4

Figure 42. Concluded

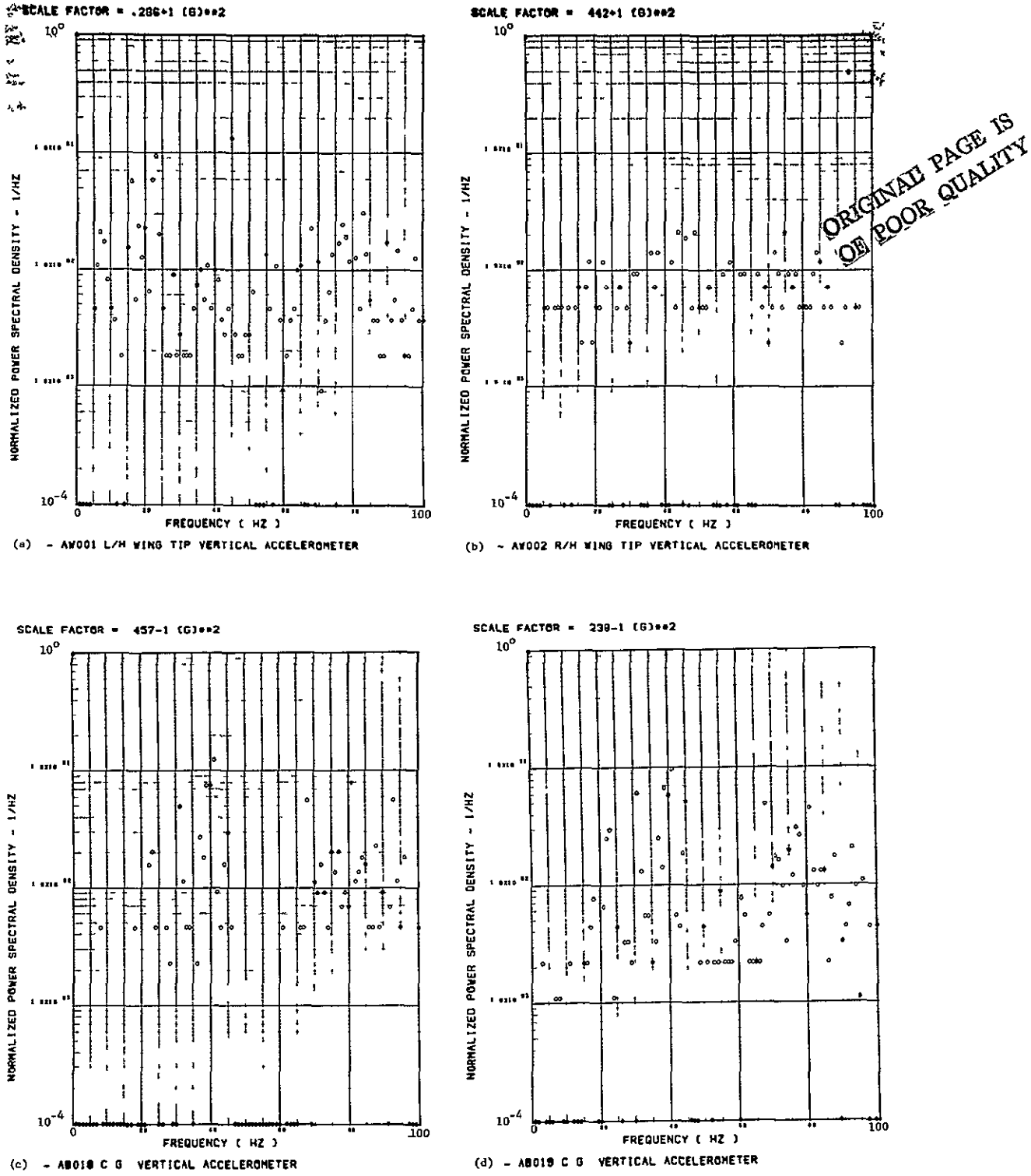

Figure 43. Power Spectra-Flight 78, Run 4, Point 1
T_1=114454.0, ΔT=1 Sec, α_{Nom}=3.3 deg.
$\Delta\alpha$=$\pm$.05 deg.

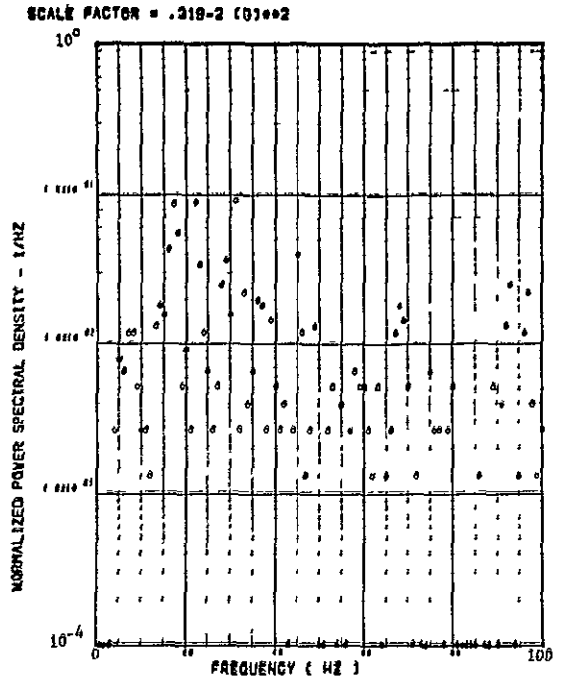

(e) = AF009 PILOT S SEAT VERTICAL ACCELEROMETER

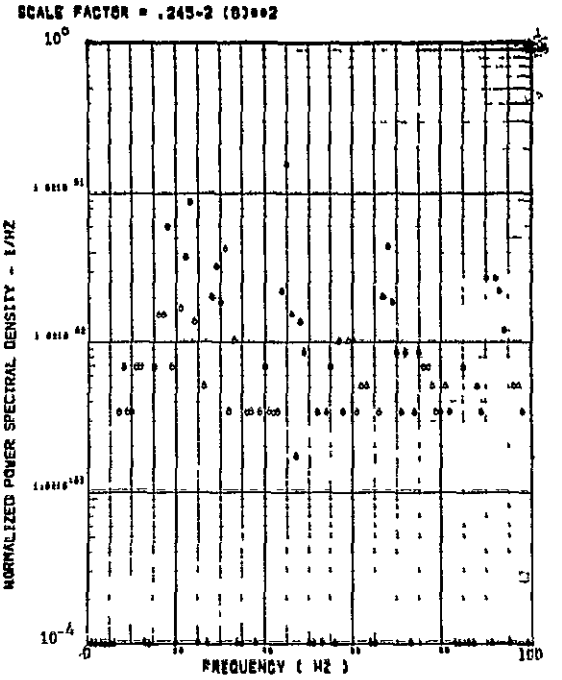

(f) = AF010 PILOT'S SEAT LATERAL ACCELEROMETER

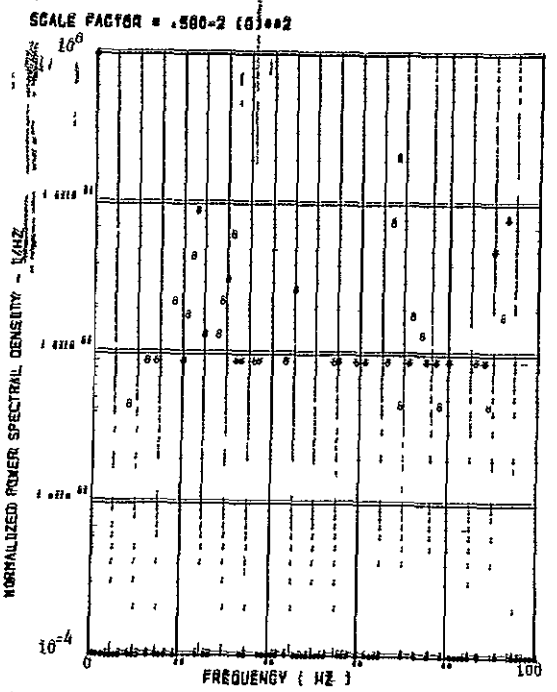

(g) = AB020 G.G. LATERAL ACCELEROMETER

Figure 43. Continued

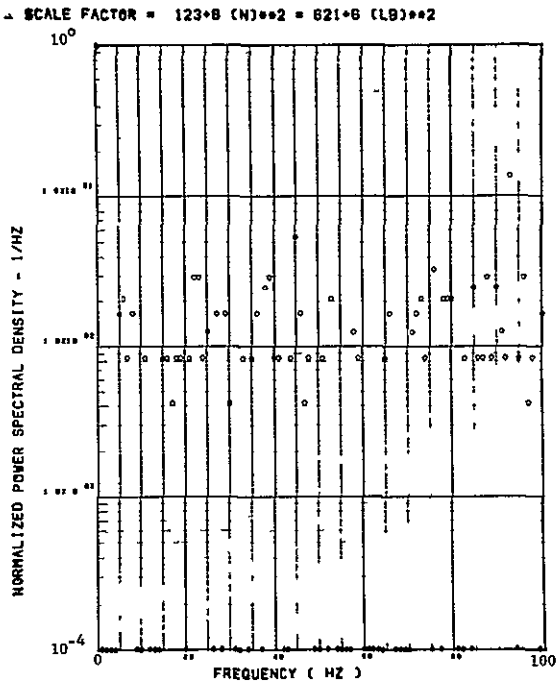

(h) - SW123 SHEAR AT WING STATION 1

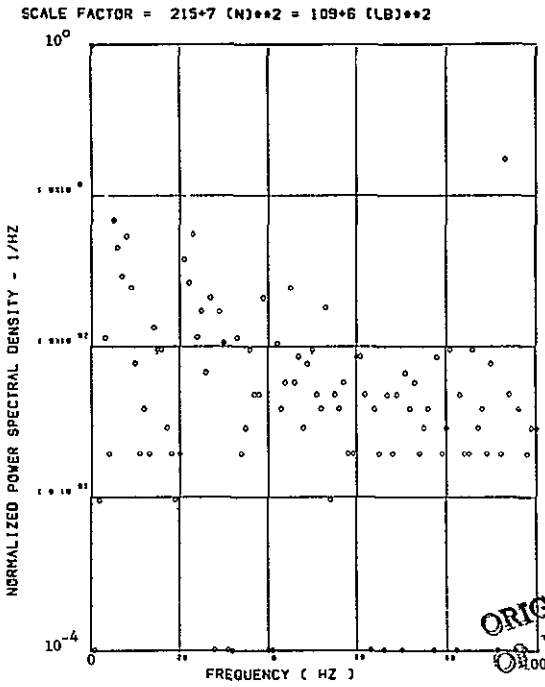

(i) - SW126 SHEAR AT WING STATION 2

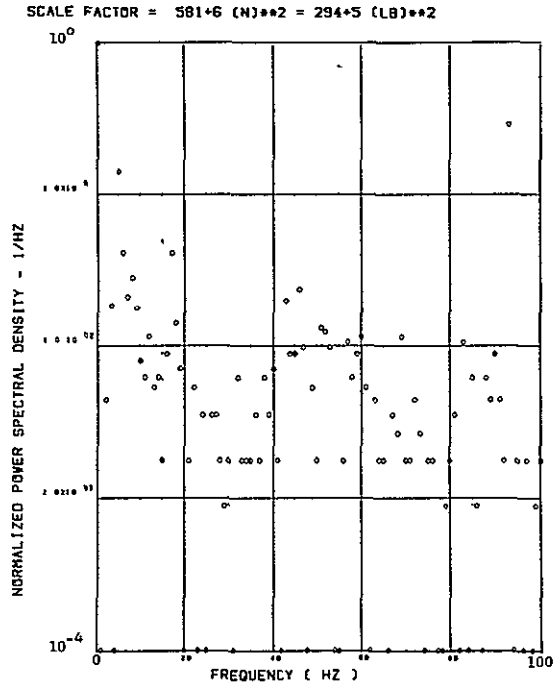

(j) - SW129 SHEAR AT WING STATION 3

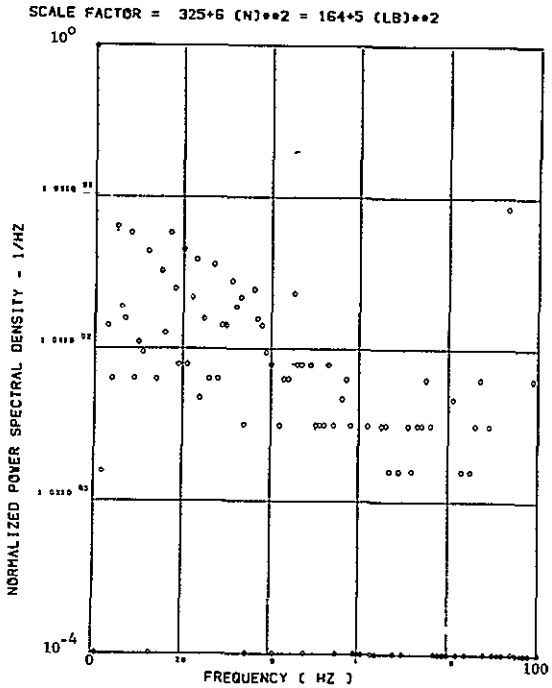

(k) - SW132 SHEAR AT WING STATION 4

Figure 43. Continued

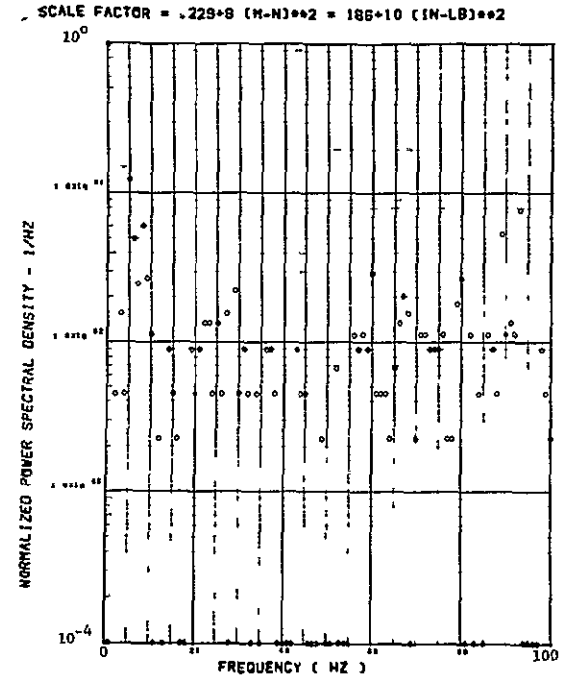

(l) - SW124 BENDING MOMENT AT WING STATION 1

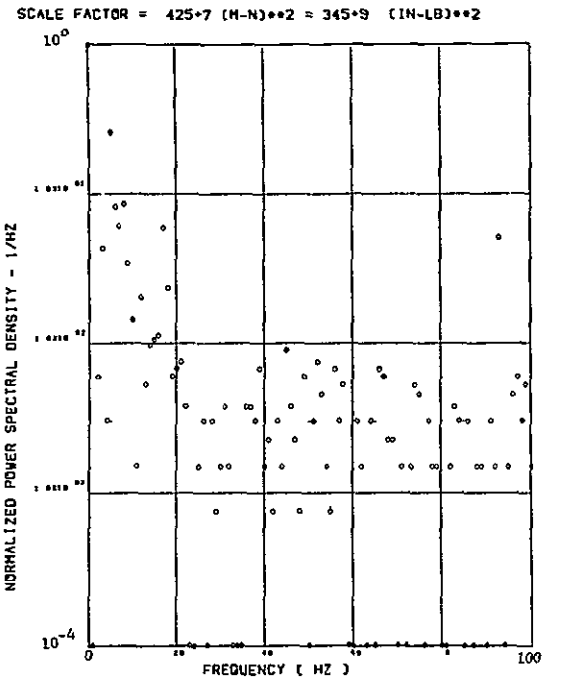

(n) - SW127 BENDING MOMENT AT WING STATION 2

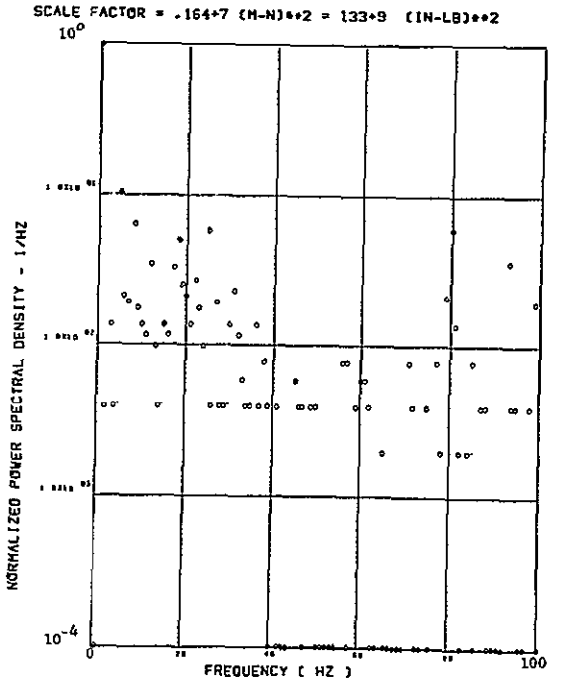

(n) - SW130 BENDING MOMENT AT WING STATION 3

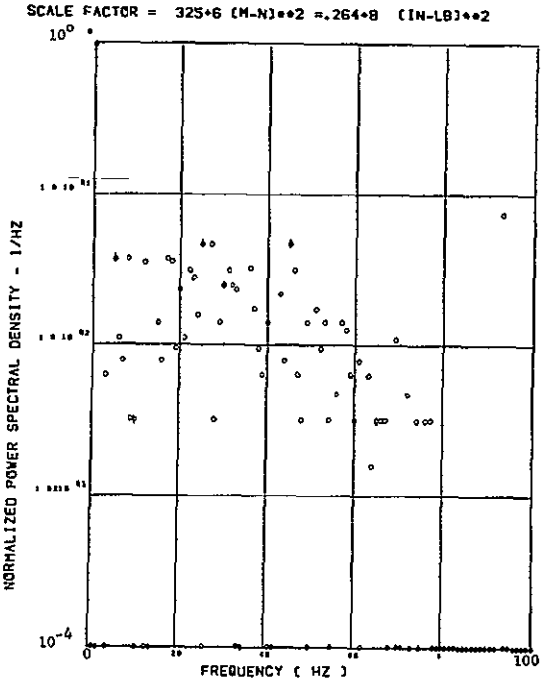

(o) - SW133 BENDING MOMENT AT WING STATION 4

Figure 43. Continued

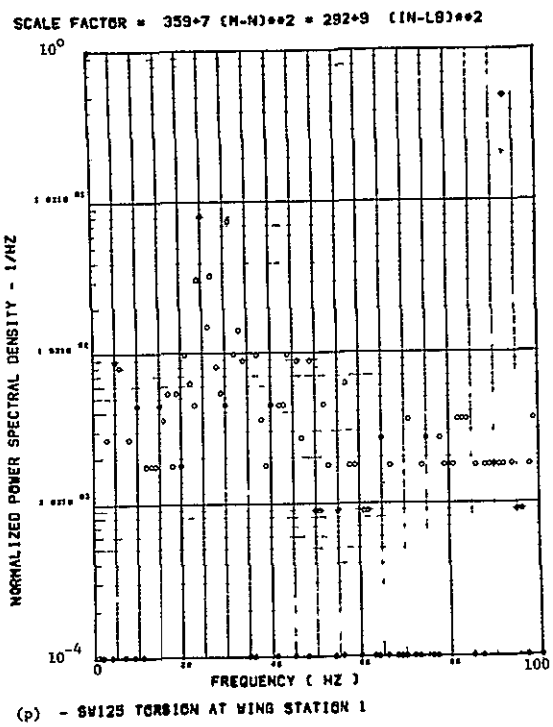

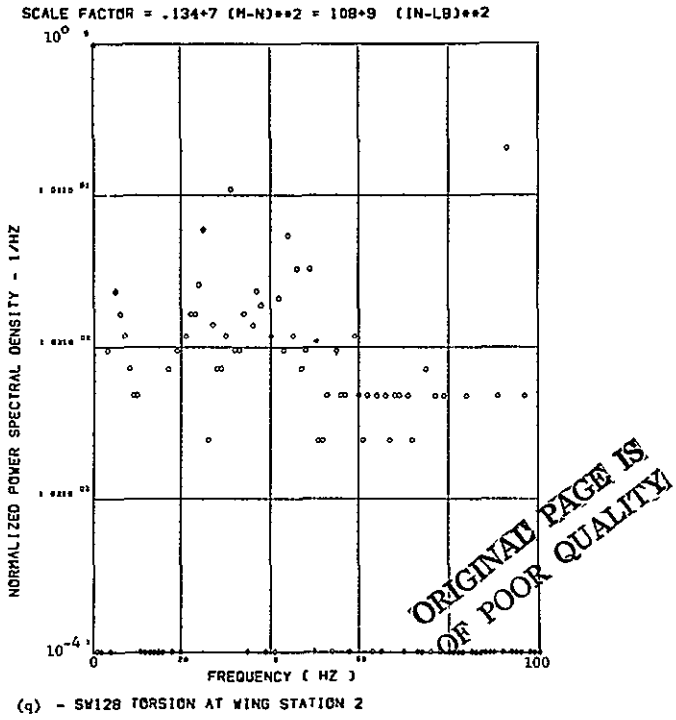

Data Not Available

Figure 43. Concluded

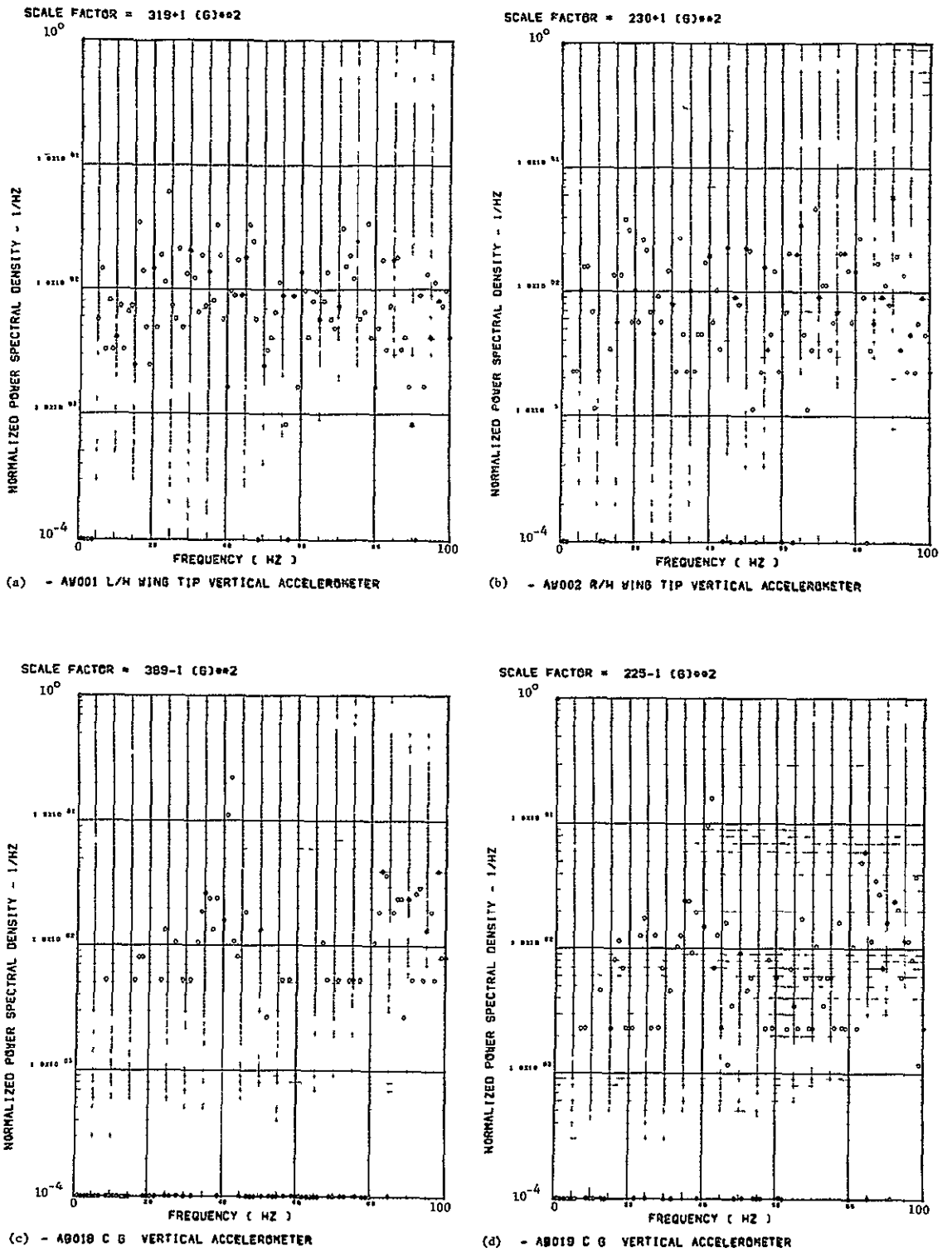

Figure 44. Power Spectra-Flight 78, Run 4, Point 2, T_1=114455.85, ΔT=1 Sec, α_{Nom}=6.35 deg, $\Delta\alpha$=4.00 deg.

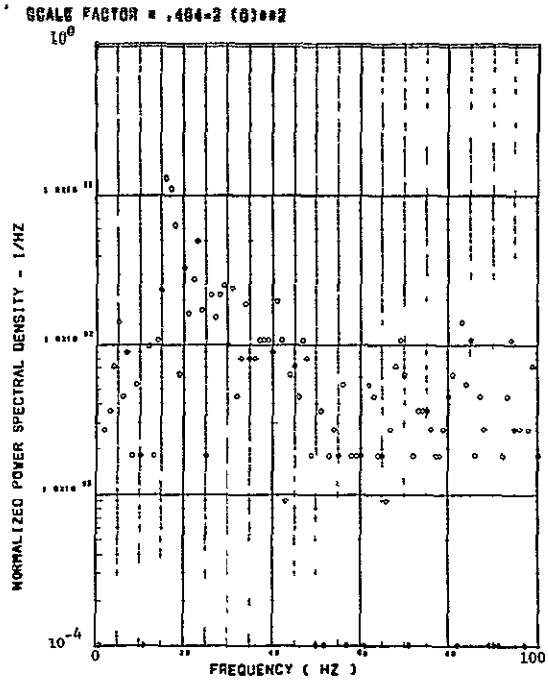

(e) - AF009 PILOT S SEAT VERTICAL ACCELEROMETER

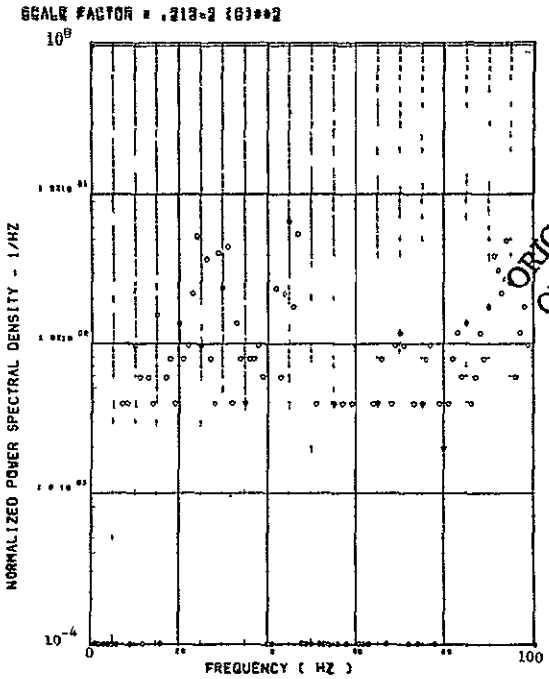

(f) - AF010 PILOT S SEAT LATERAL ACCELEROMETER

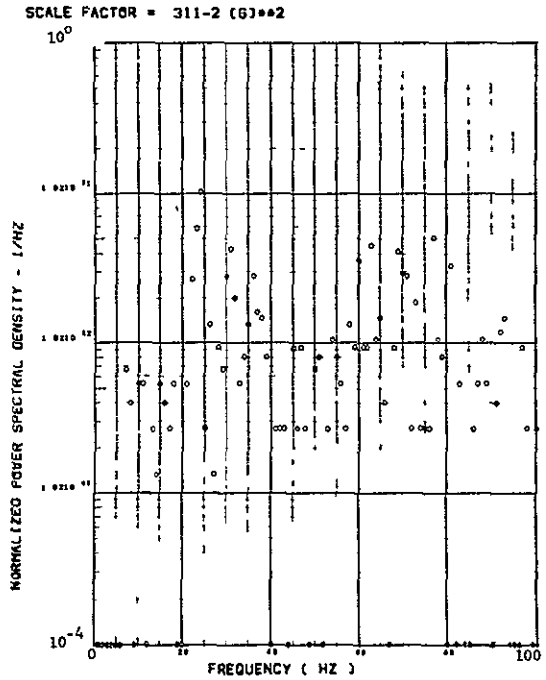

(g) - AB020 C G LATERAL ACCELEROMETER

Figure 44. Continued

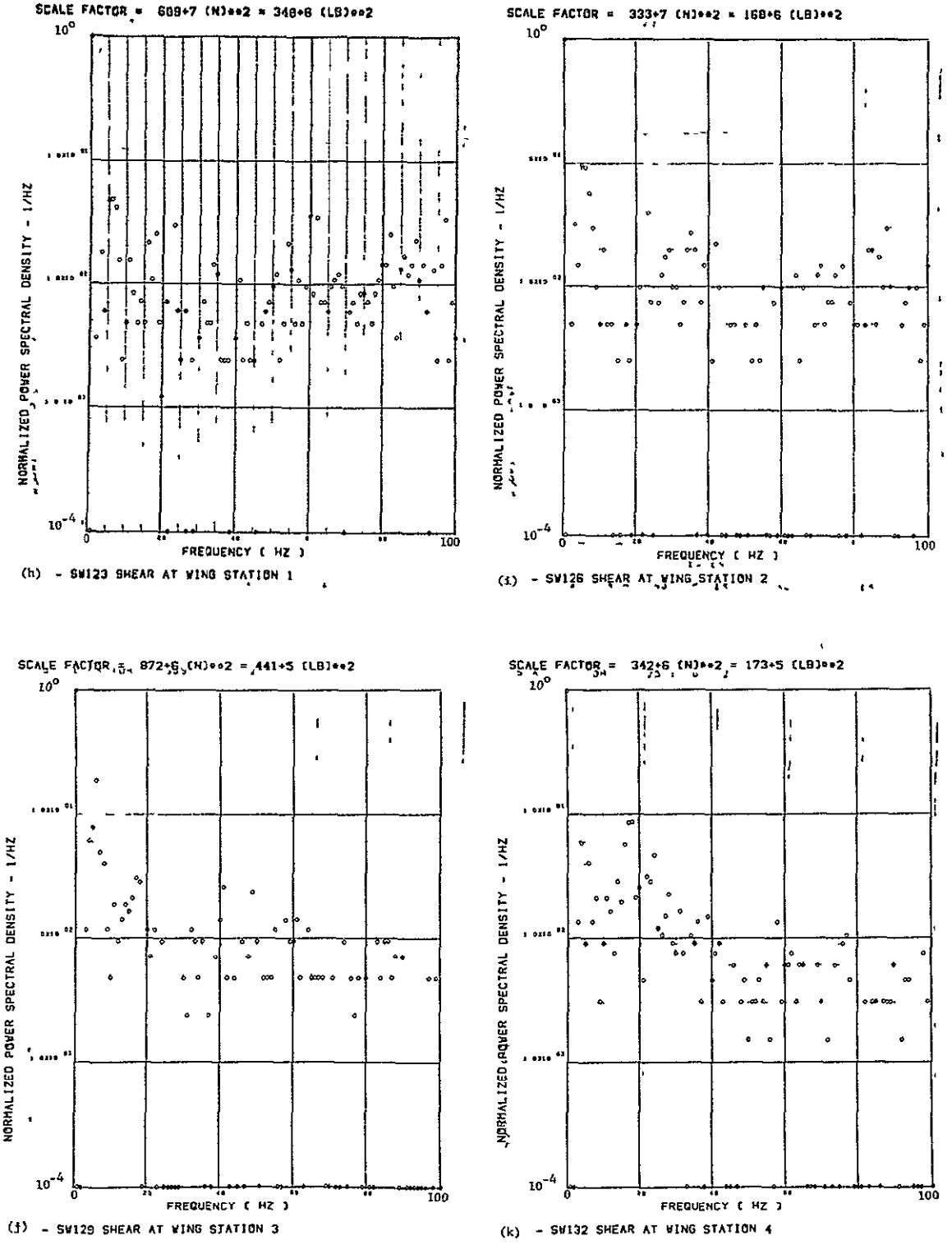

Figure 44. Continued

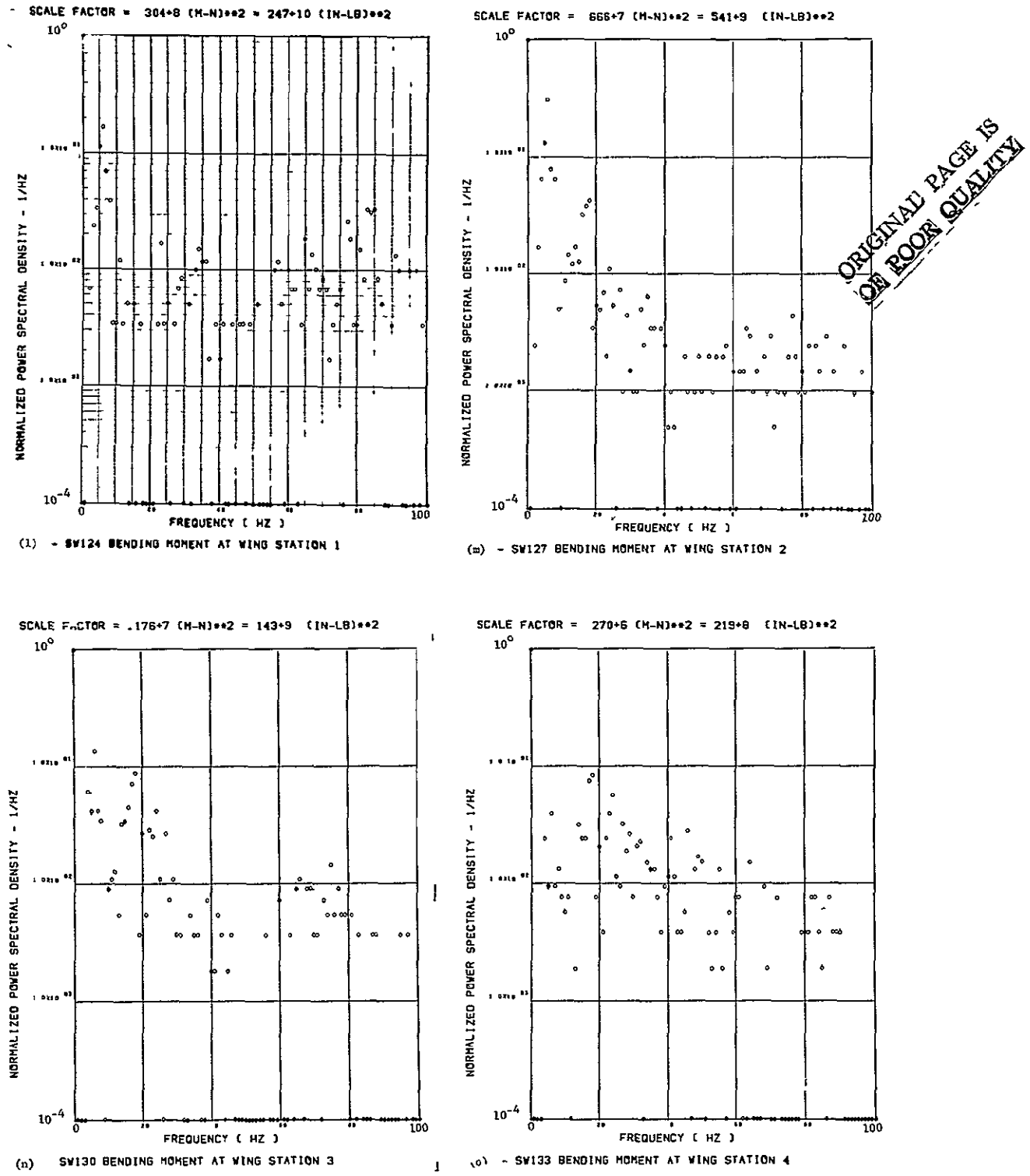

Figure 44. Continued

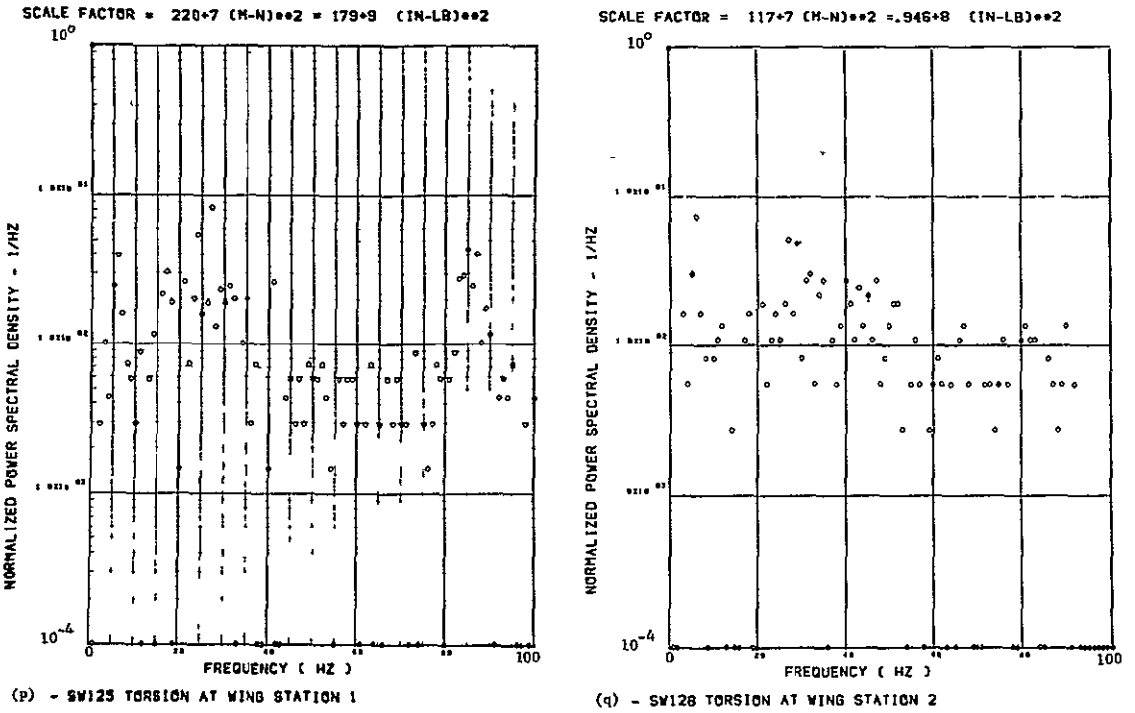

Data Not Available

Figure 44. Concluded

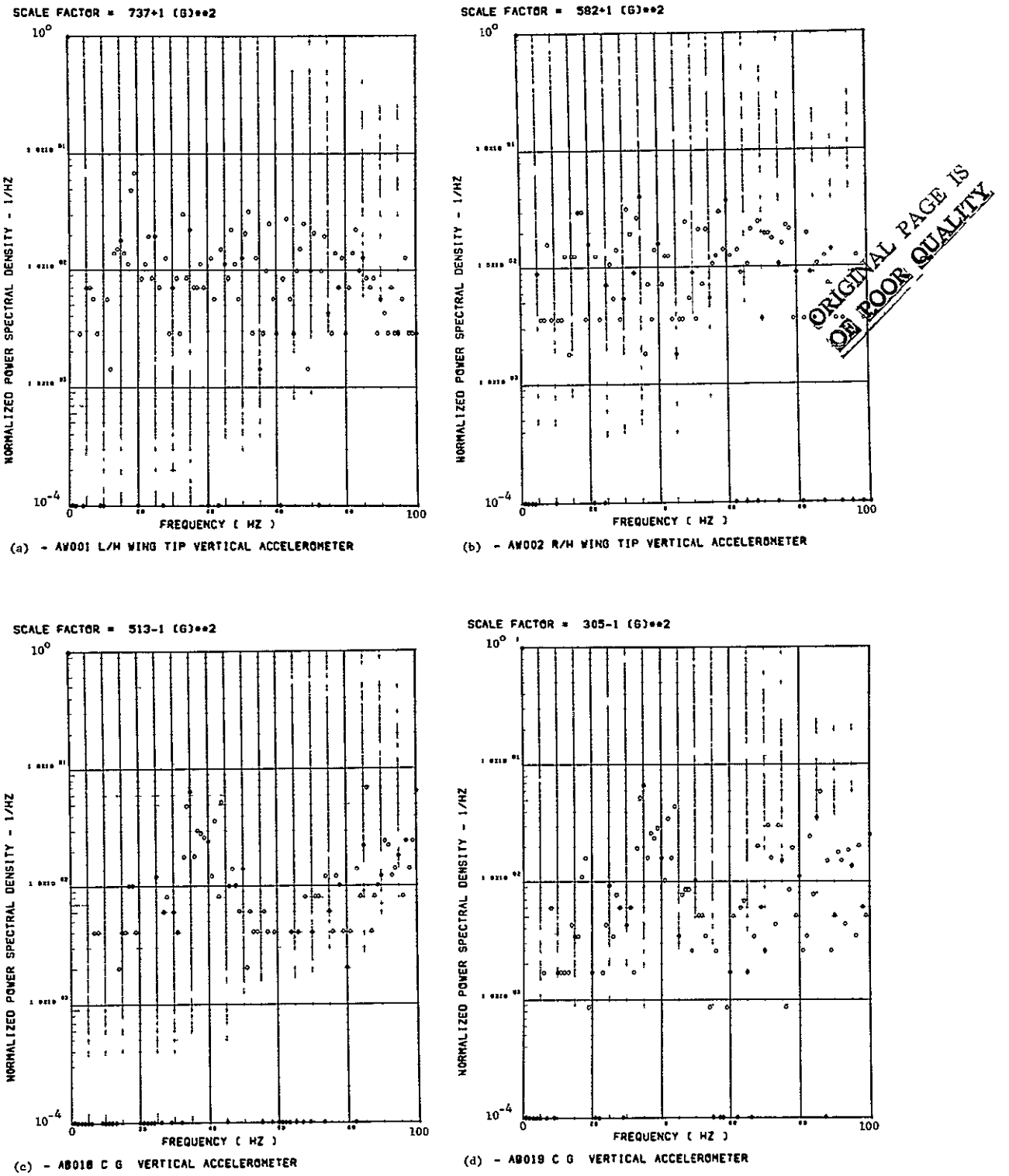

Figure 45. Power Spectra-Flight 78, Run 4, Point 3, T_1=114456.55, ΔT=1 Sec, α_{Nom}=9.40 deg, $\Delta\alpha$=4.95 deg.

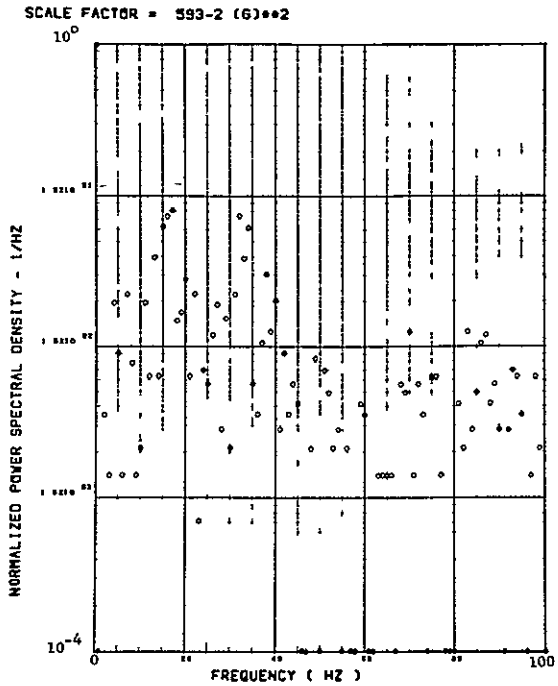

(e) - AF008 PILOT S SEAT VERTICAL ACCELEROMETER

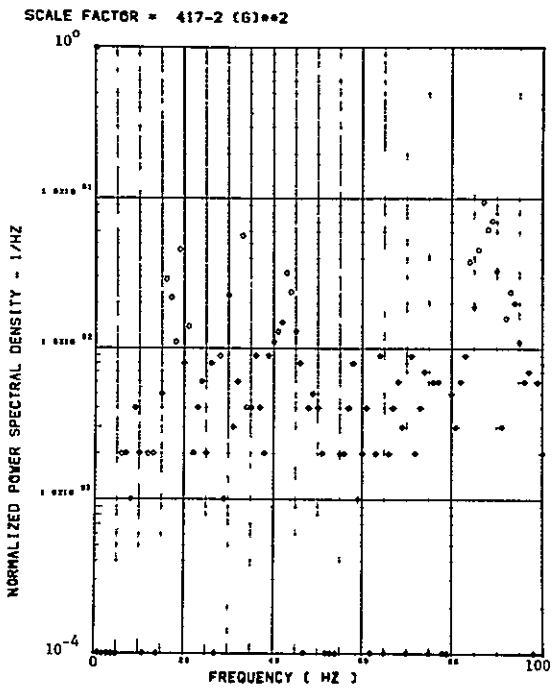

(f) - AF010 PILOT S SEAT LATERAL ACCELEROMETER

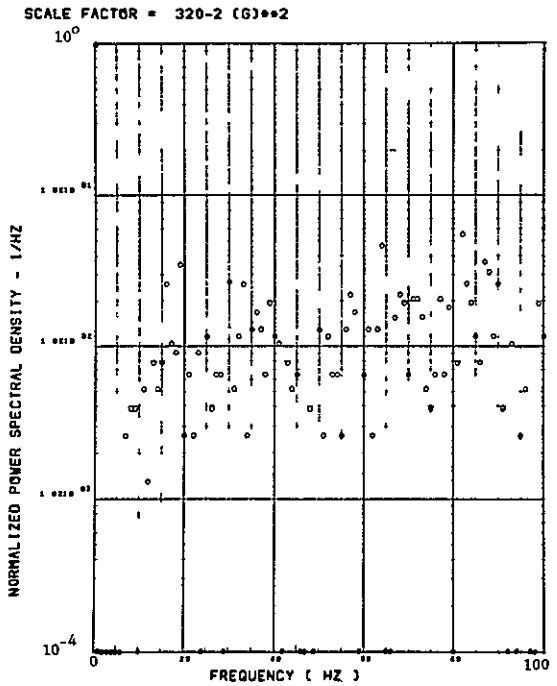

(g) - AB020 C G LATERAL ACCELEROMETER

Figure 45. Continued

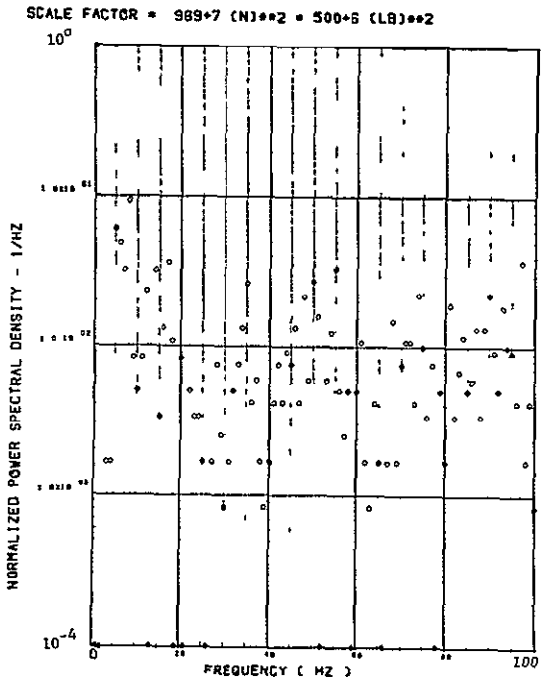

(h) - SW123 SHEAR AT WING STATION 1

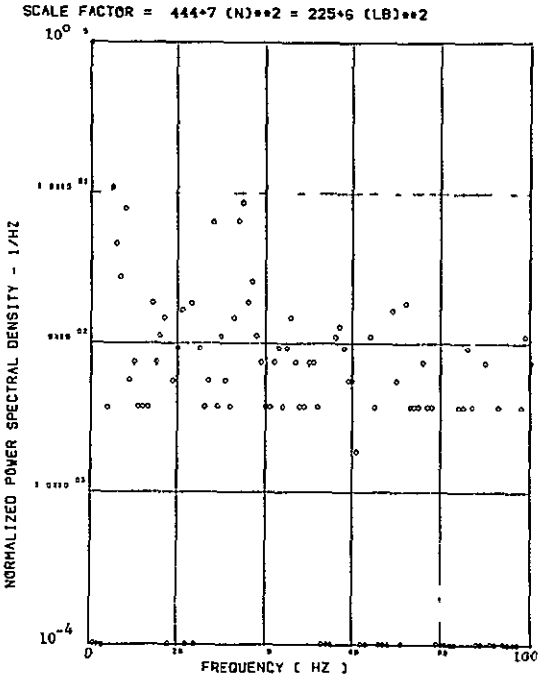

(i) SW126 SHEAR AT WING STATION 2

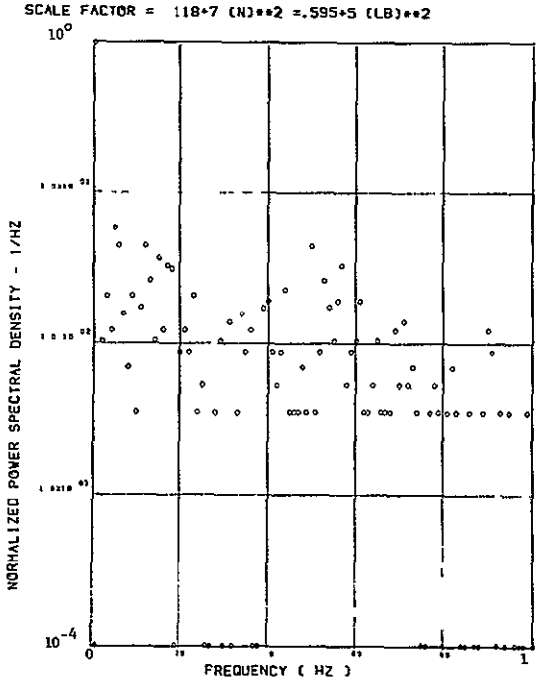

(j) - SW129 SHEAR AT WING STATION 3

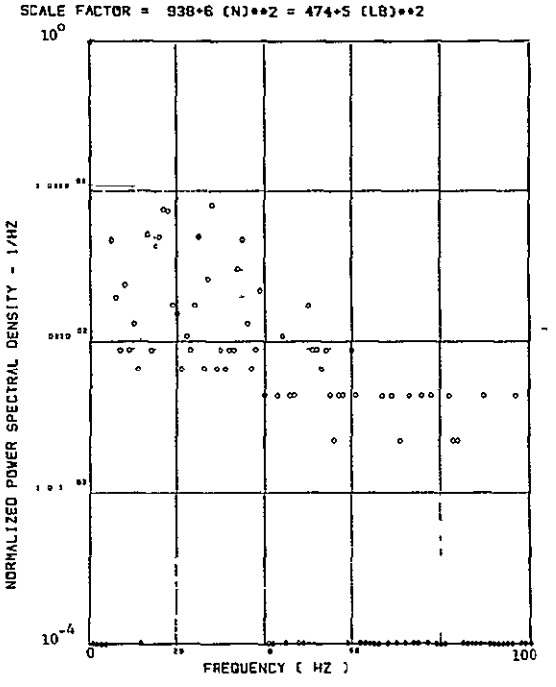

(k) SW132 SHEAR AT WING STATION 4

Figure 45. Continued

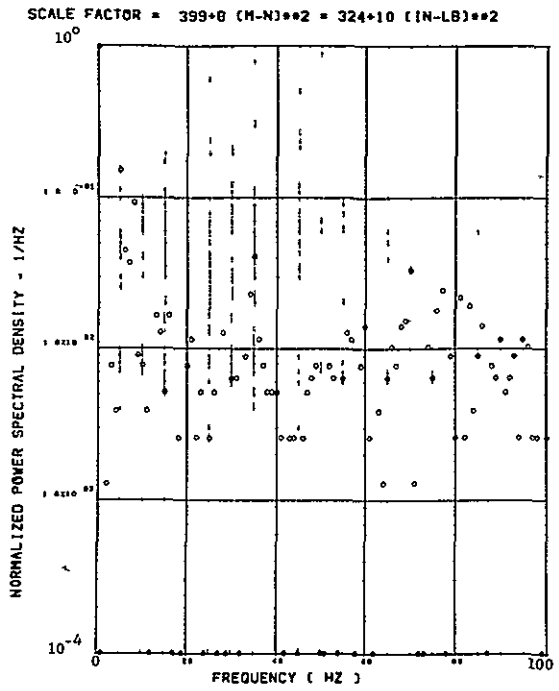

(l) - SW124 BENDING MOMENT AT WING STATION 1

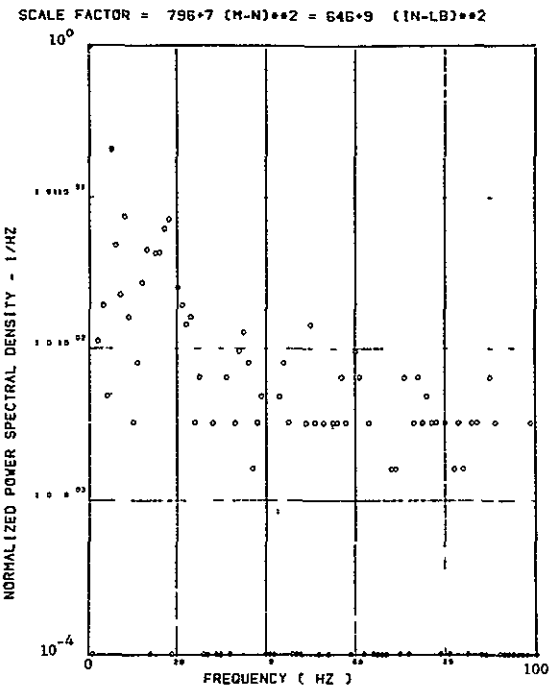

(m) - SW127 BENDING MOMENT AT WING STATION 2

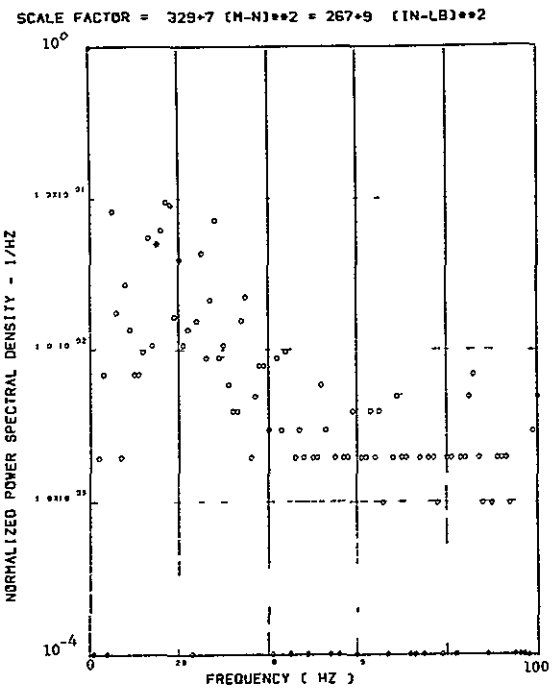

(n) - SW130 BENDING MOMENT AT WING STATION 3

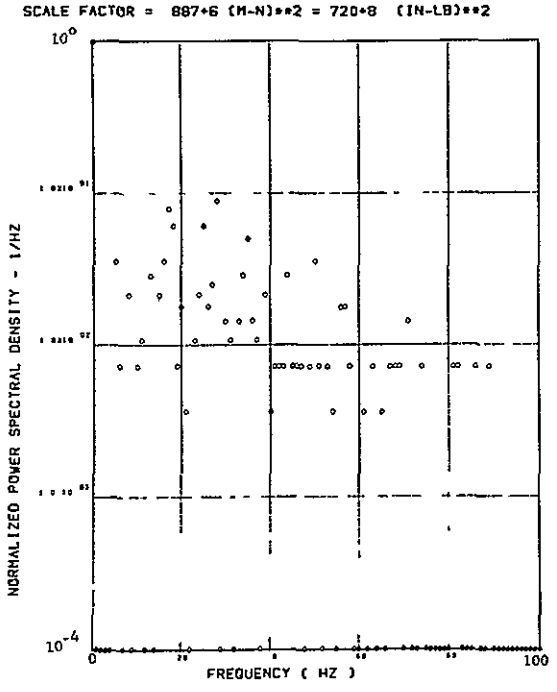

(o) - SW133 BENDING MOMENT AT WING STATION 4

Figure 45. Continued

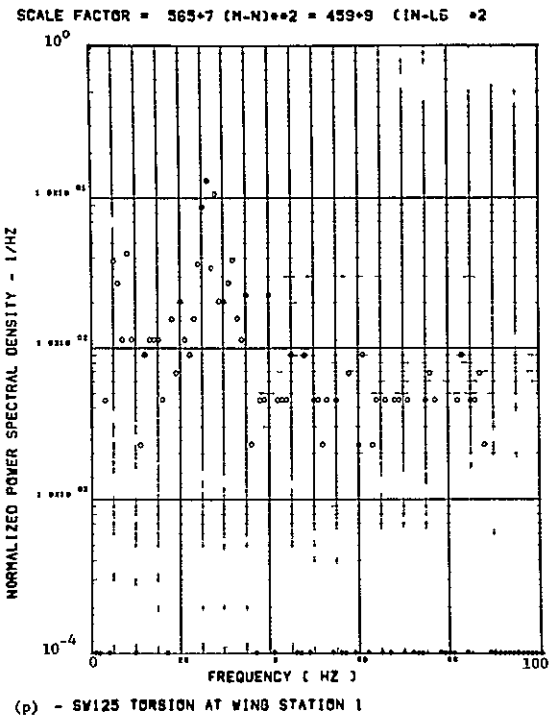

(p) - SW125 TORSION AT WING STATION 1

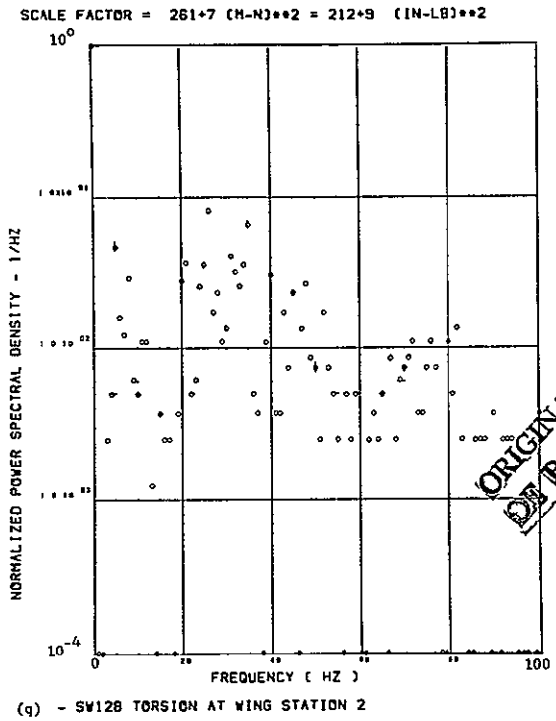

(q) - SW128 TORSION AT WING STATION 2

Data Not Available

Figure 45. Concluded

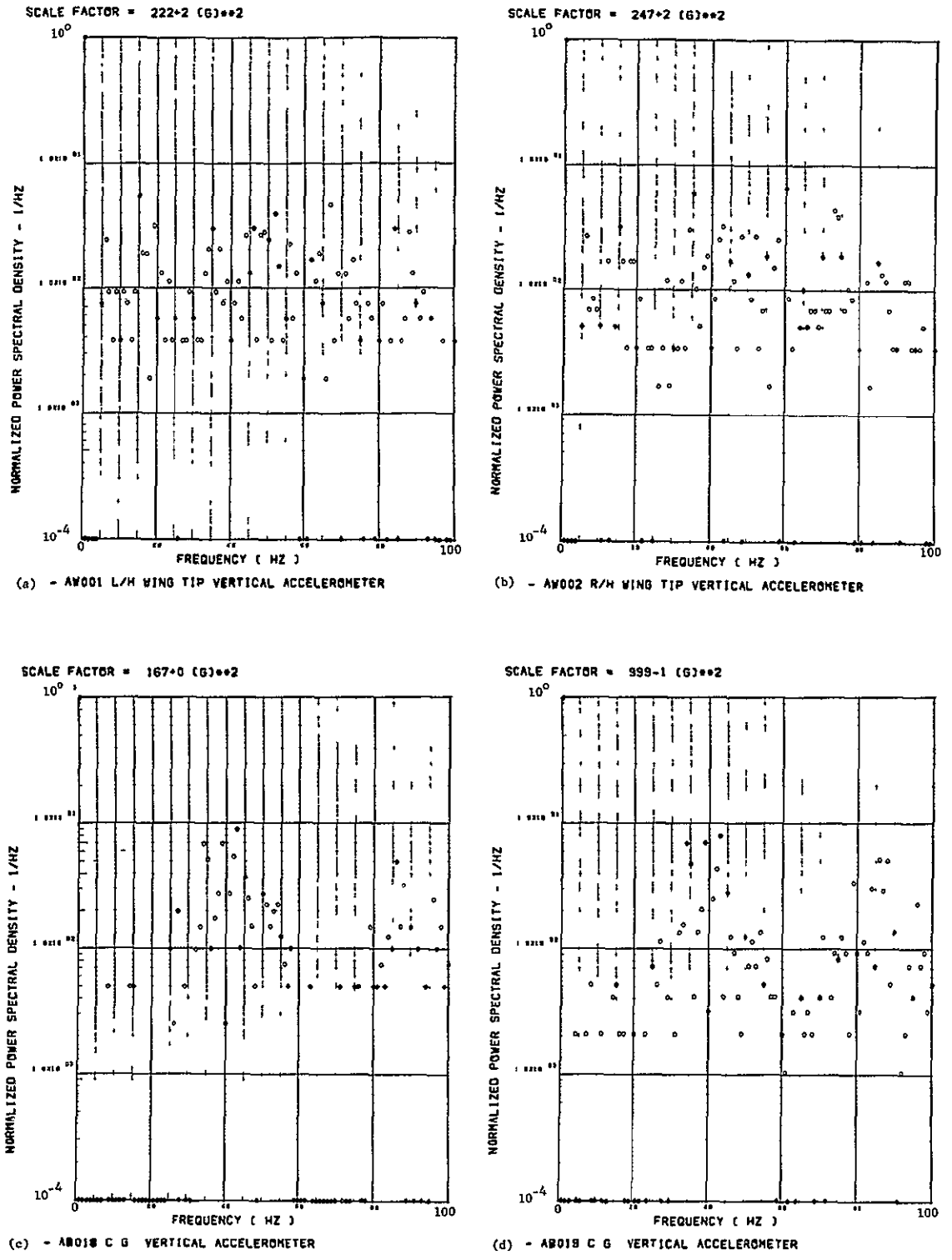

Figure 46. Power Spectra-Flight 78, Run 4, Point 4, T_1=114457.05, ΔT=1 Sec, α_{Nom}=12.0 deg, $\Delta\alpha$=5.45 deg.

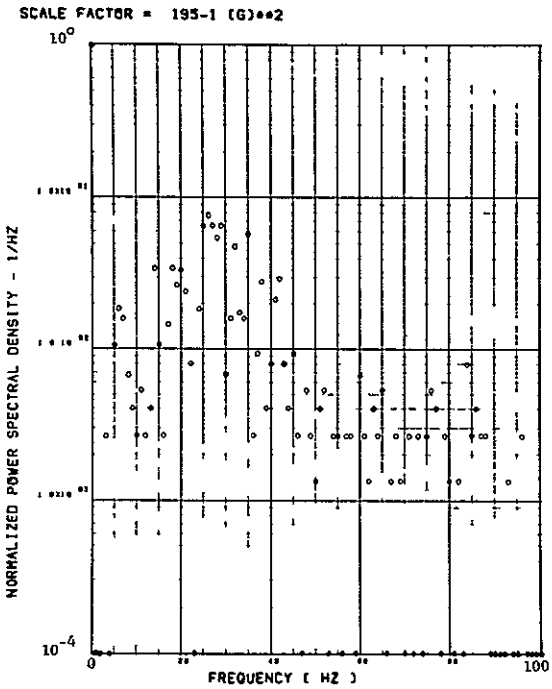

(e) - AF009 PILOT S SEAT VERTICAL ACCELEROMETER

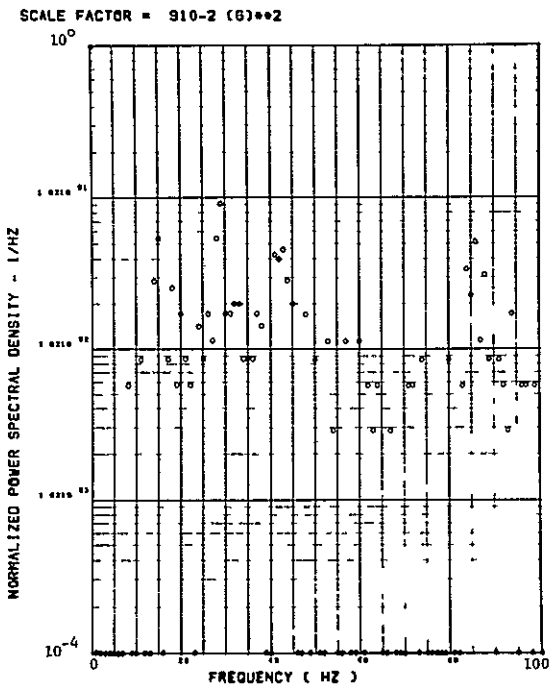

(f) - AF010 PILOT S SEAT LATERAL ACCELEROMETER

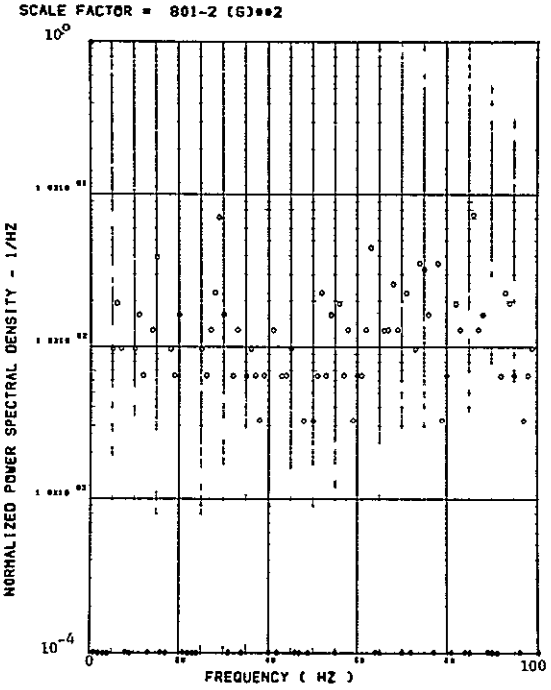

(g) - AB020 C G LATERAL ACCELEROMETER

Figure 46. Continued

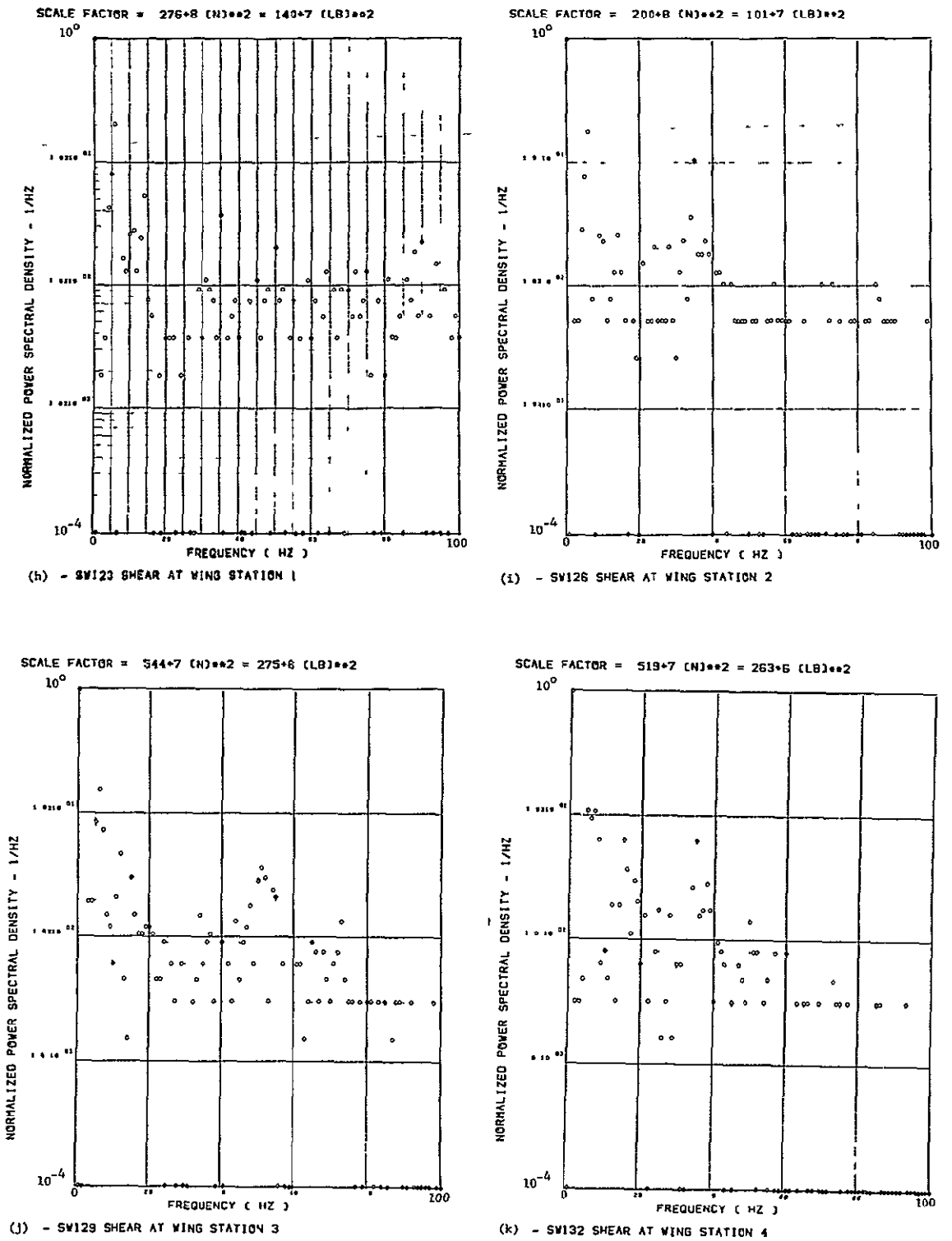

Figure 46. Continued

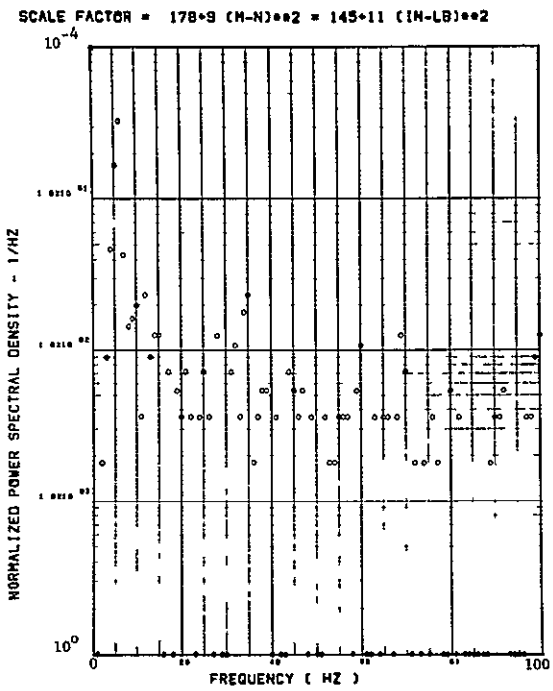

(l) - SW124 BENDING MOMENT AT WING STATION 1

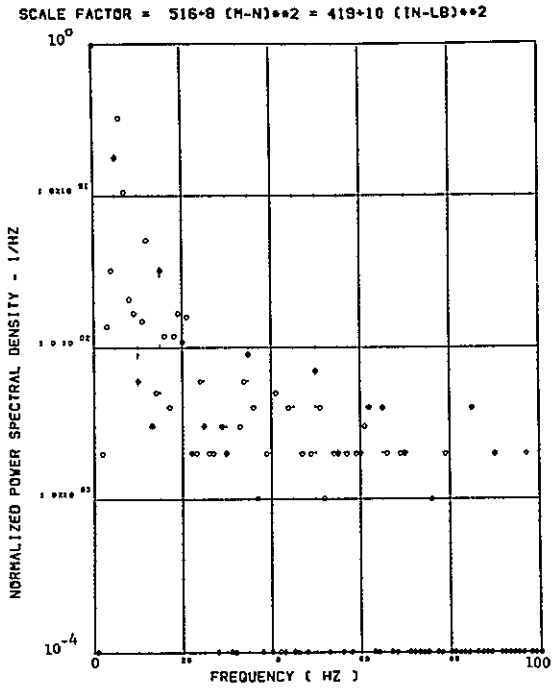

(m) - SW127 BENDING MOMENT AT WING STATION 2

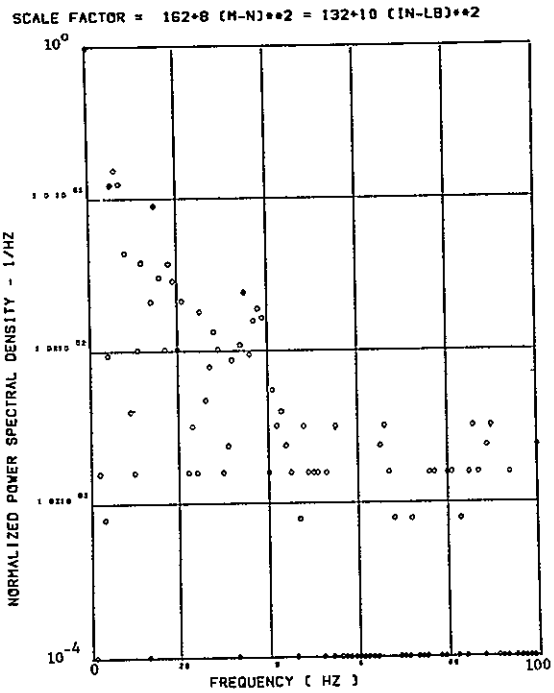

(n) - SW130 BENDING MOMENT AT WING STATION 3

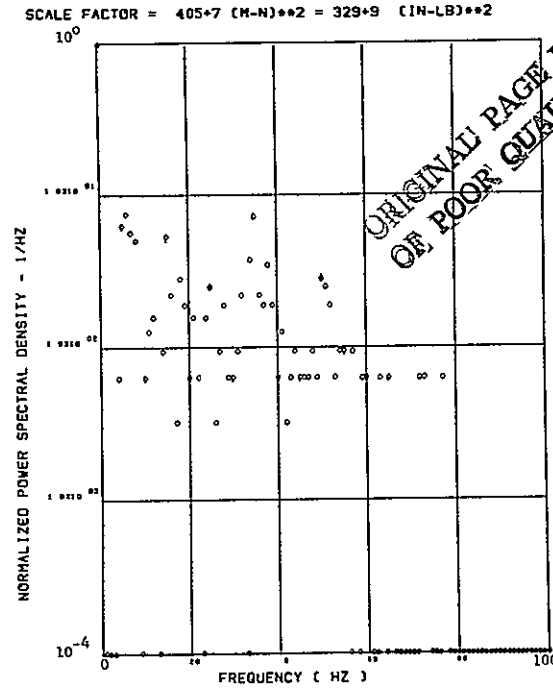

(o) - SW133 BENDING MOMENT AT WING STATION 4

Figure 46. Continued

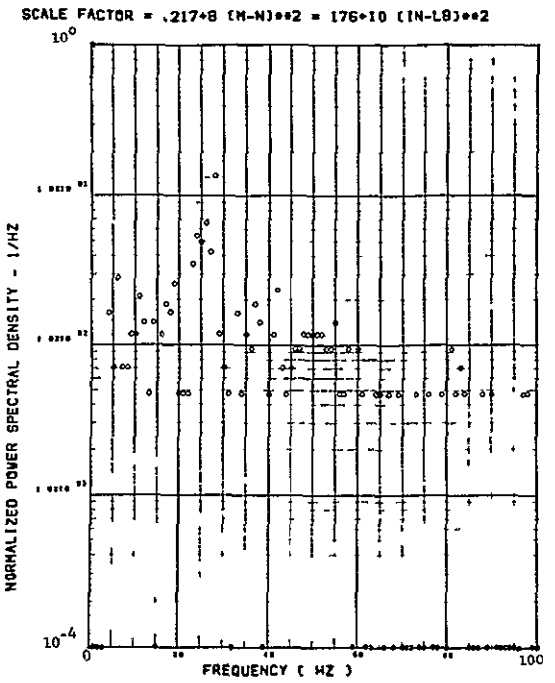

(p) - SW125 TORSION AT WING STATION 1

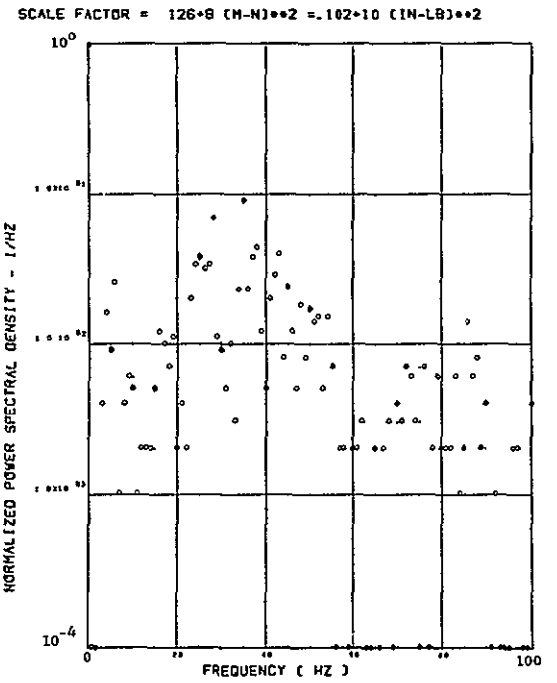

(q) - SW128 TORSION AT WING STATION 2

Data Not Available

Figure 46. Concluded

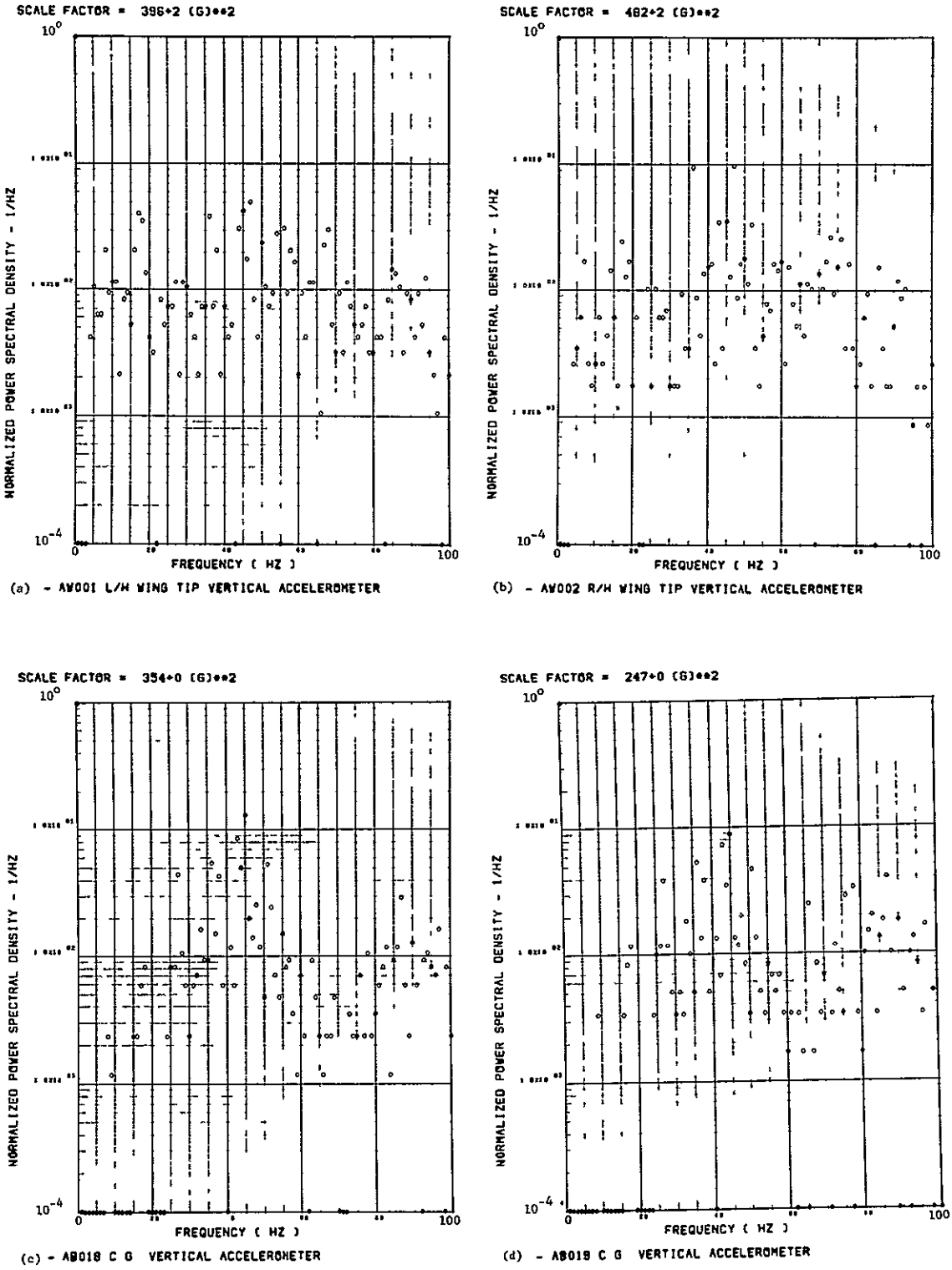

Figure 47. Power Spectra-Flight 78, Run 4, Point 5, T_1=11457.65, ΔT=1 Sec, α_{Nom}=14.6 deg, $\Delta\alpha$=4.20 deg.

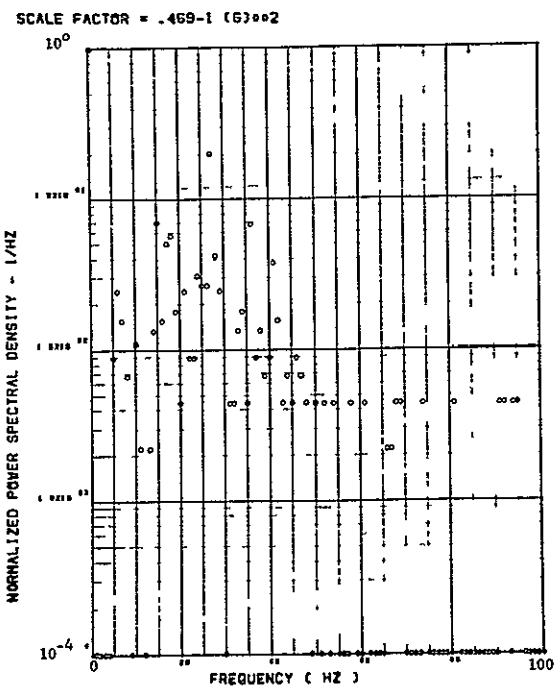

(e) - AF009 PILOT S SEAT VERTICAL ACCELEROMETER

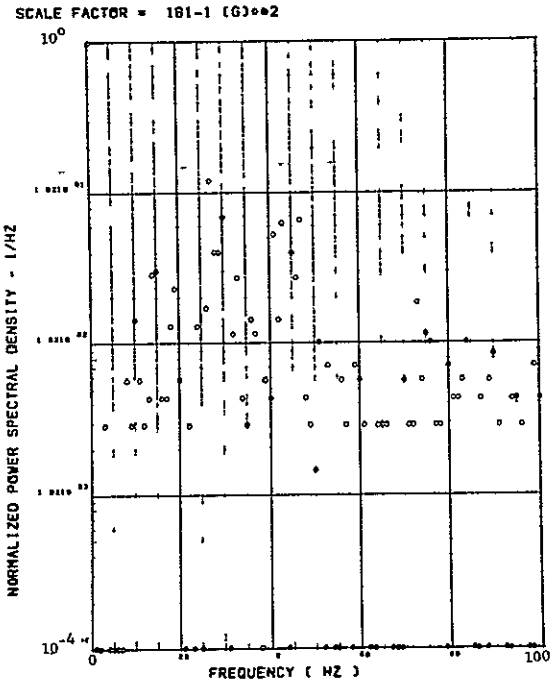

(f) - AF010 PILOT S SEAT LATERAL ACCELEROMETER

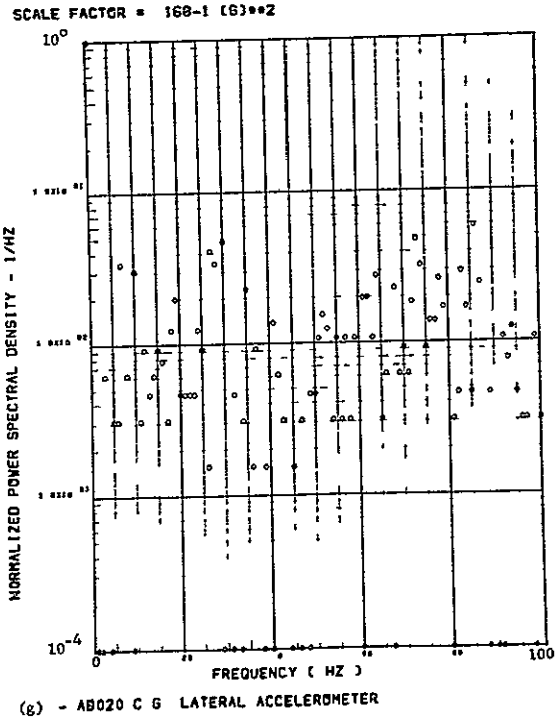

(g) - AB020 C G LATERAL ACCELEROMETER

Figure 47. Continued

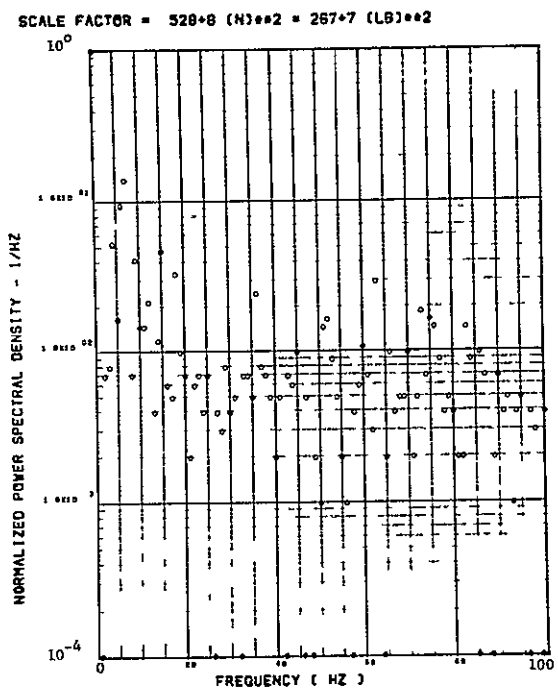

(h) - SW123 SHEAR AT WING STATION 1

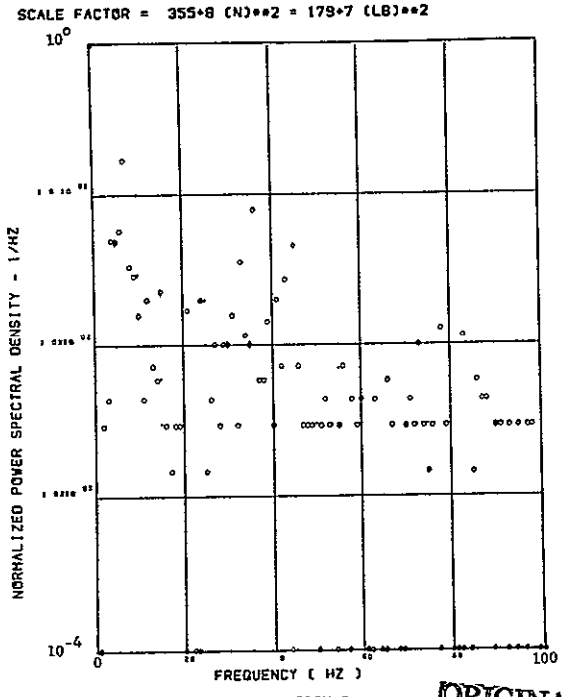

(i) - SW126 SHEAR AT WING STATION 2

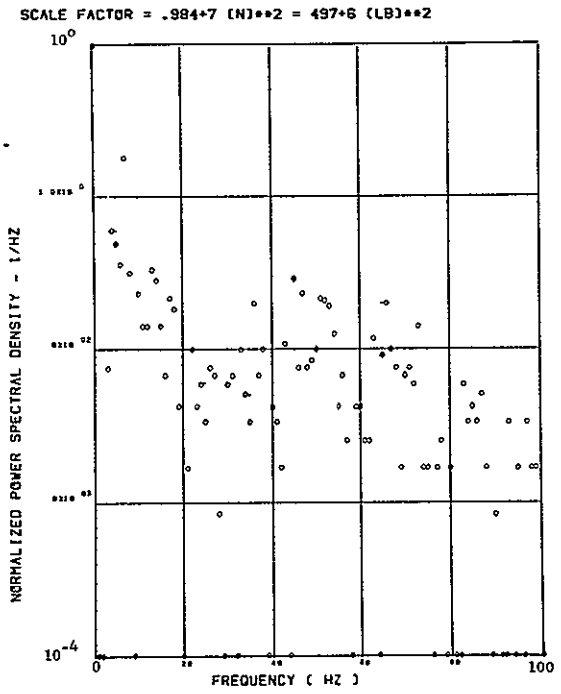

(j) - SW129 SHEAR AT WING STATION 3

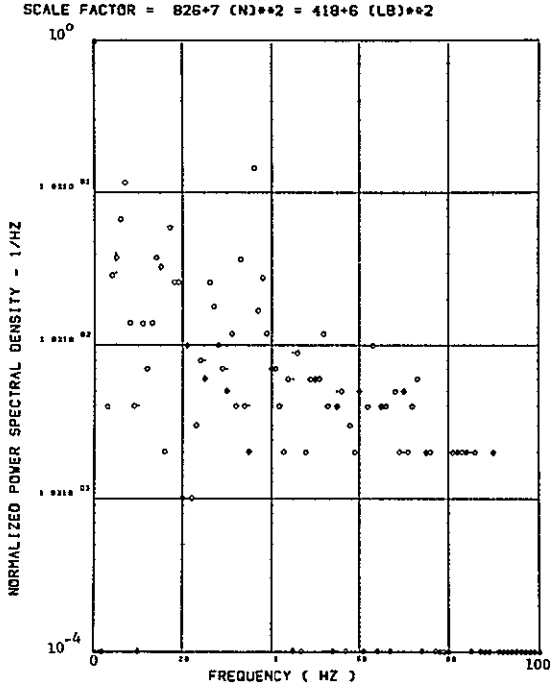

(k) - SW132 SHEAR AT WING STATION 4

Figure 47. Continued

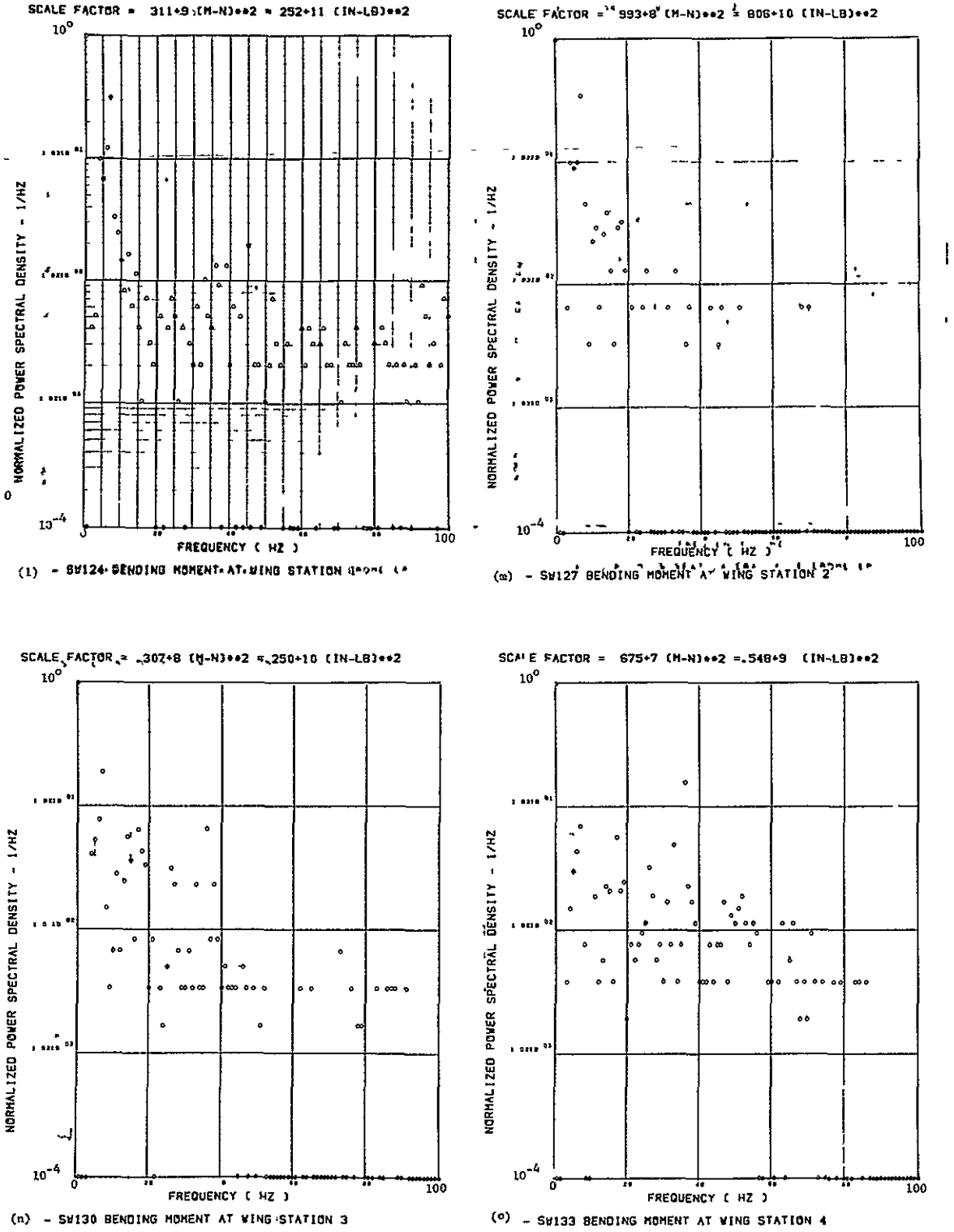

Figure 47. Continued

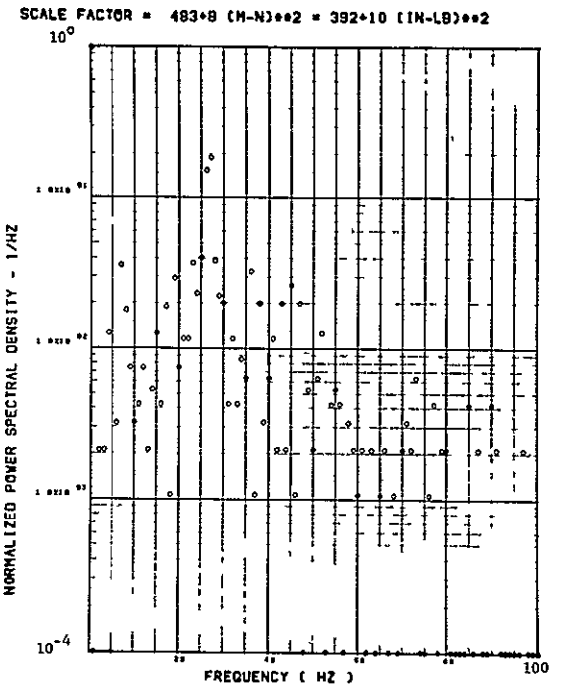

(p) - SW125 TORSION AT WING STATION 1

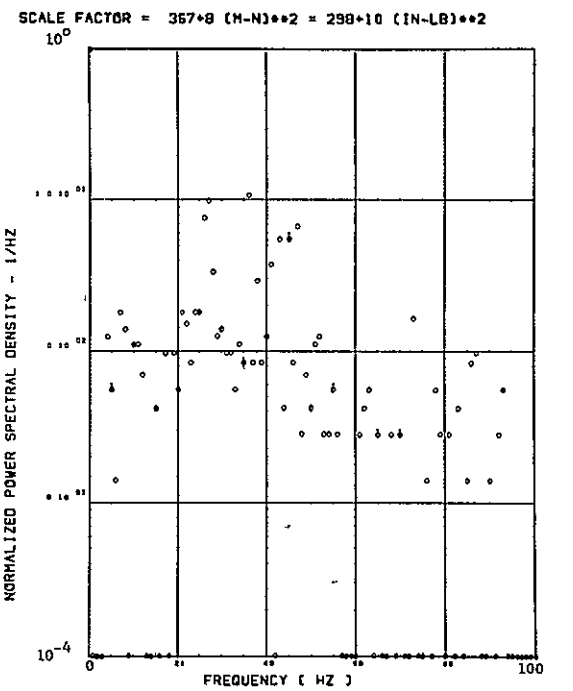

(q) - SW128 TORSION AT WING STATION 2

Data Not Available

Figure 47. Concluded

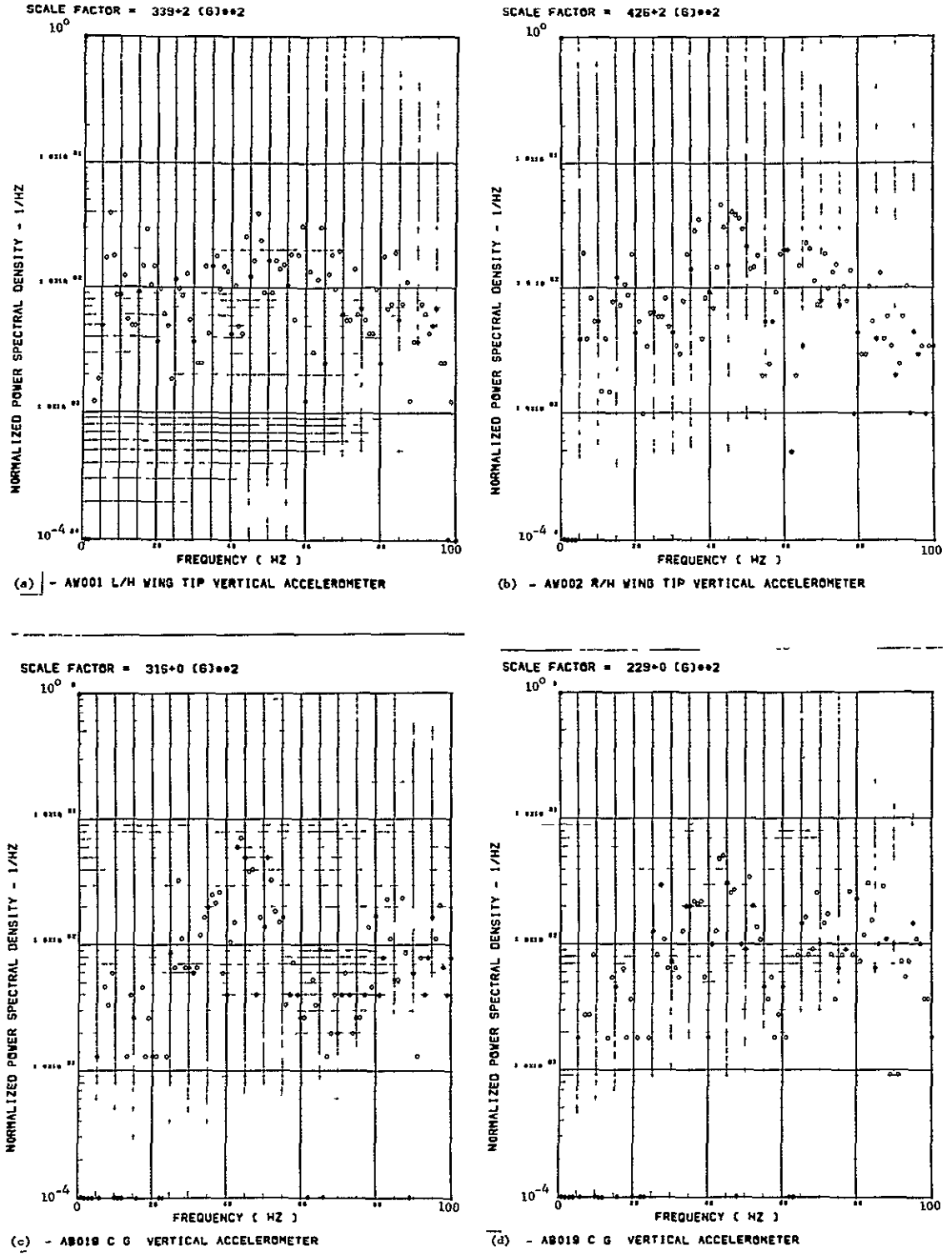

Figure 48. Power Spectra-Flight 78, Run 4, Point 6, T_1=114457.4, ΔT=1 Sec, α_{Nom}=13.6 deg, $\Delta\alpha$=5.55 deg.

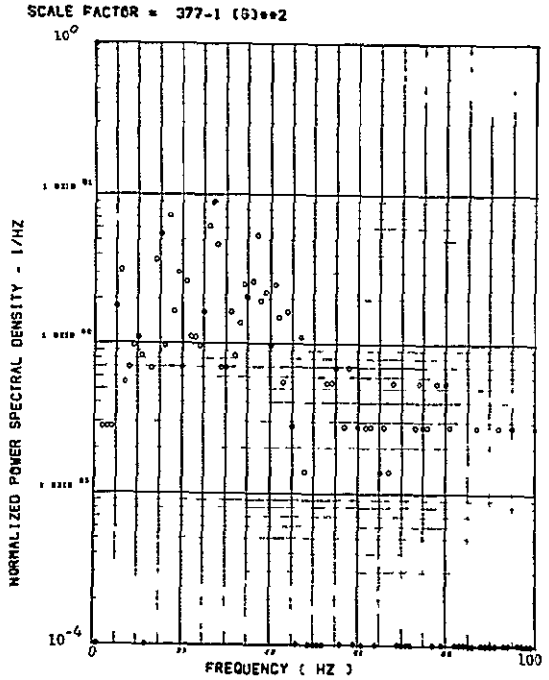

(e) - AF009 PILOT S SEAT VERTICAL ACCELEROMETER

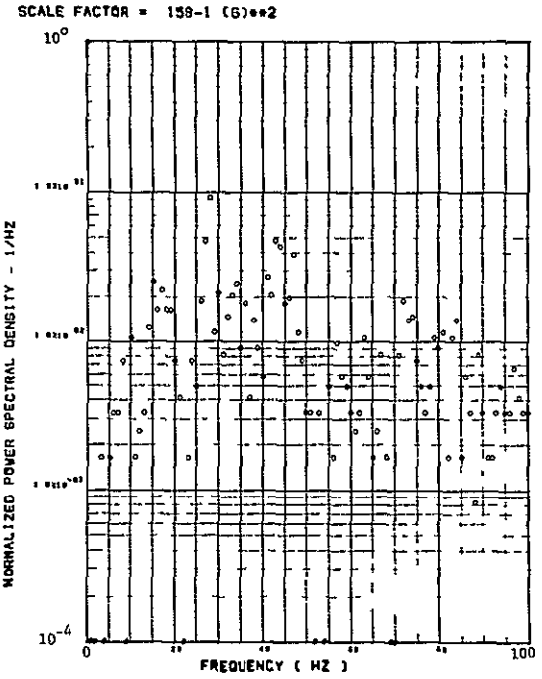

(f) - AF010 PILOT S SEAT LATERAL ACCELEROMETER

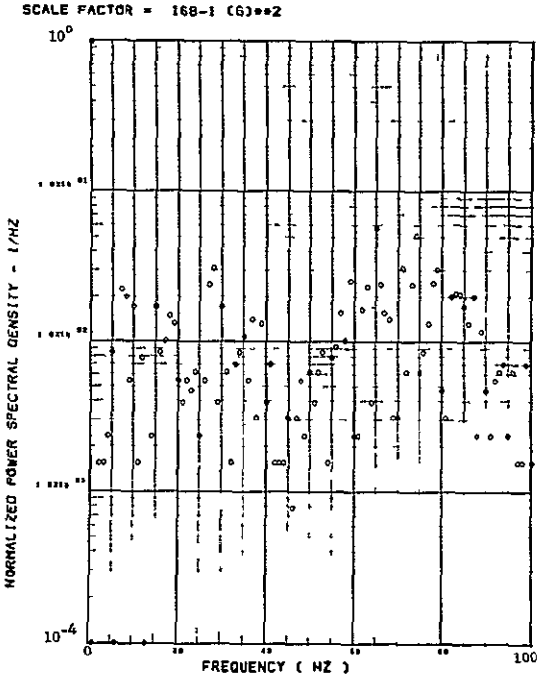

(g) - AB020 C G LATERAL ACCELEROMETER

Figure 48. Continued

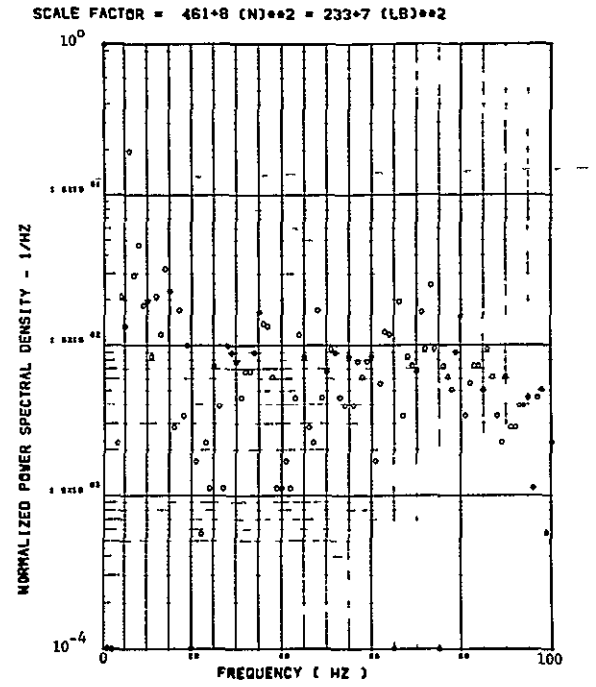

(h) - SW123 SHEAR AT WING STATION 1

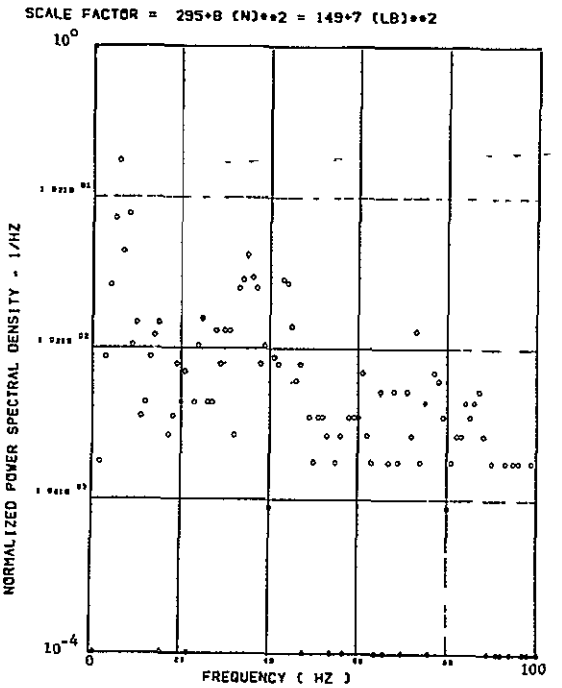

(i) - SW126 SHEAR AT WING STATION 2

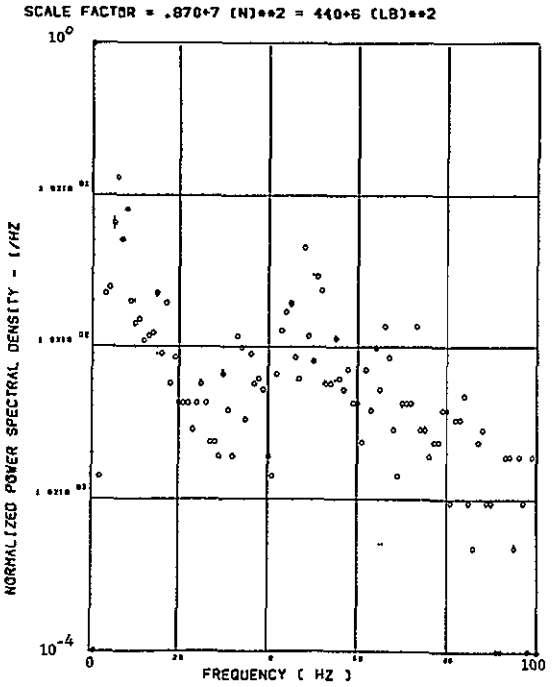

(j) - SW129 SHEAR AT WING STATION 3

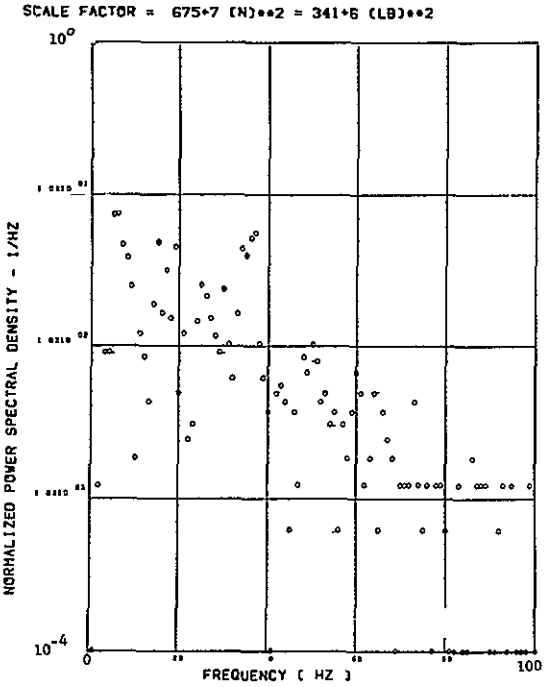

(k) - SW132 SHEAR AT WING STATION 4

Figure 48. Continued

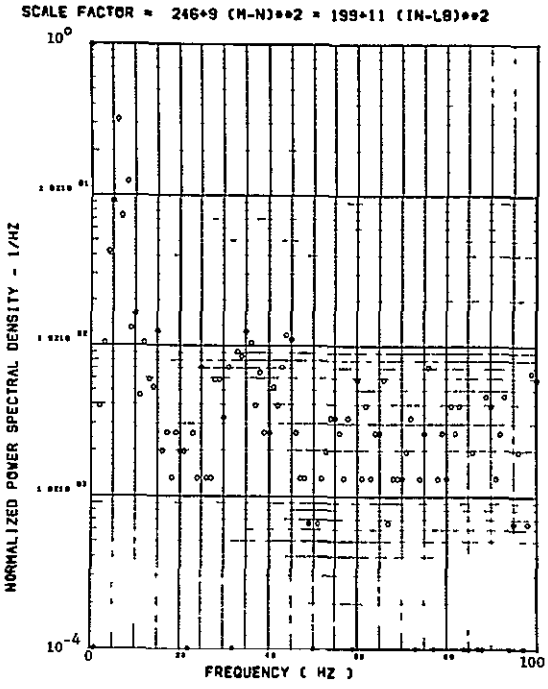

(l) - SW124 BENDING MOMENT AT WING STATION 1

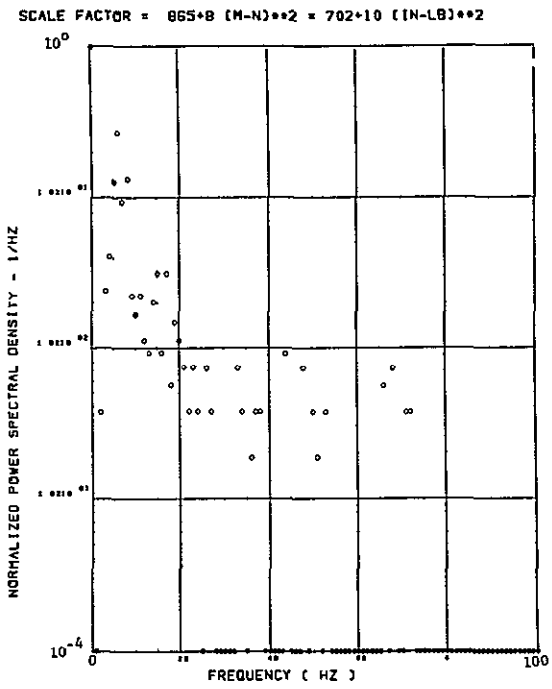

(m) - SW127 BENDING MOMENT AT WING STATION 2

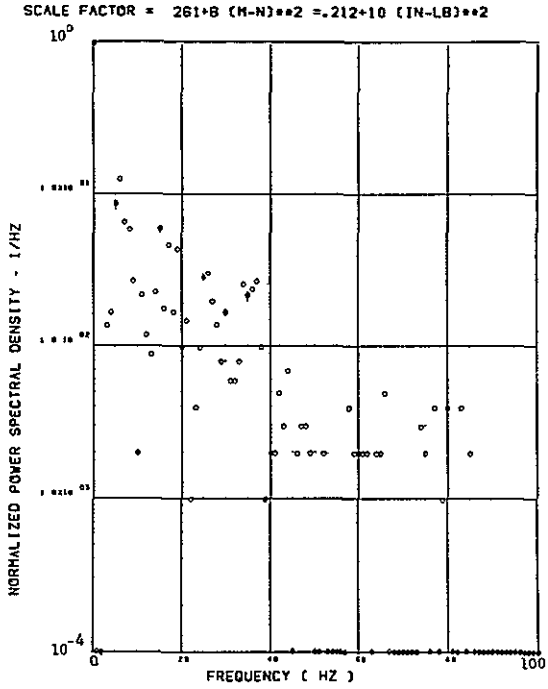

(n) - SW130 BENDING MOMENT AT WING STATION 3

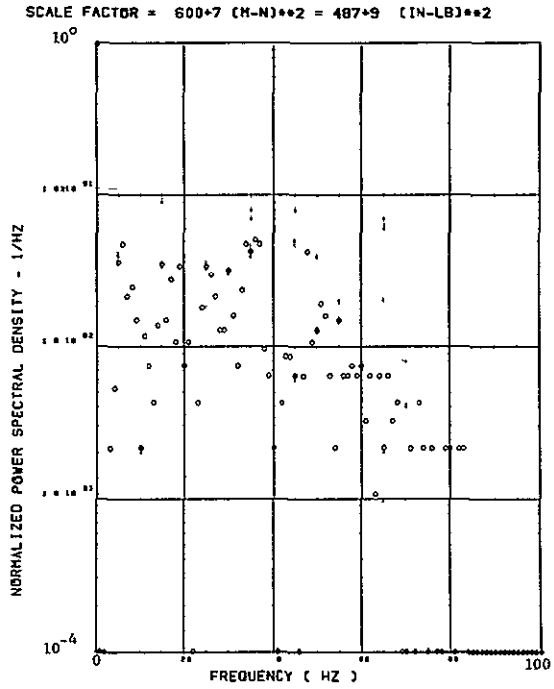

(o) - SW133 BENDING MOMENT AT WING STATION 4

Figure 48. Continued

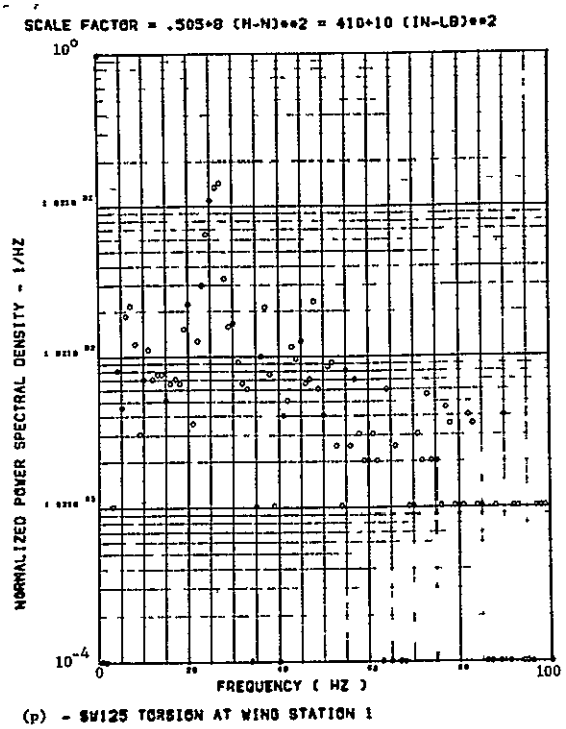

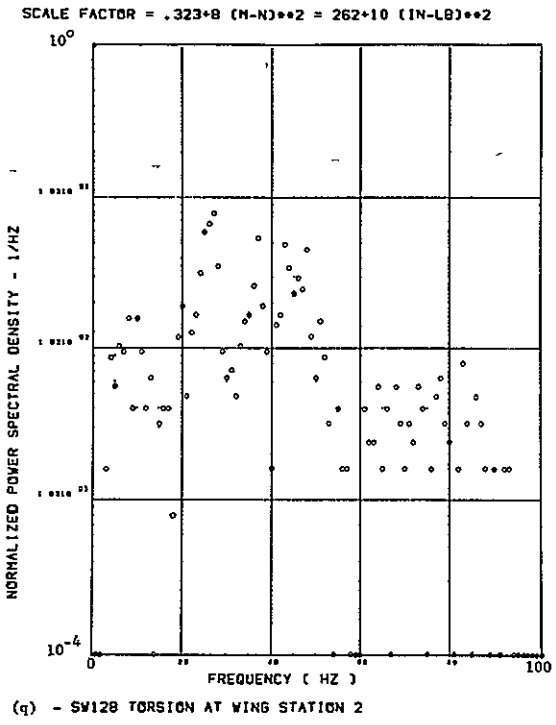

Data Not Available

Figure 48. Concluded

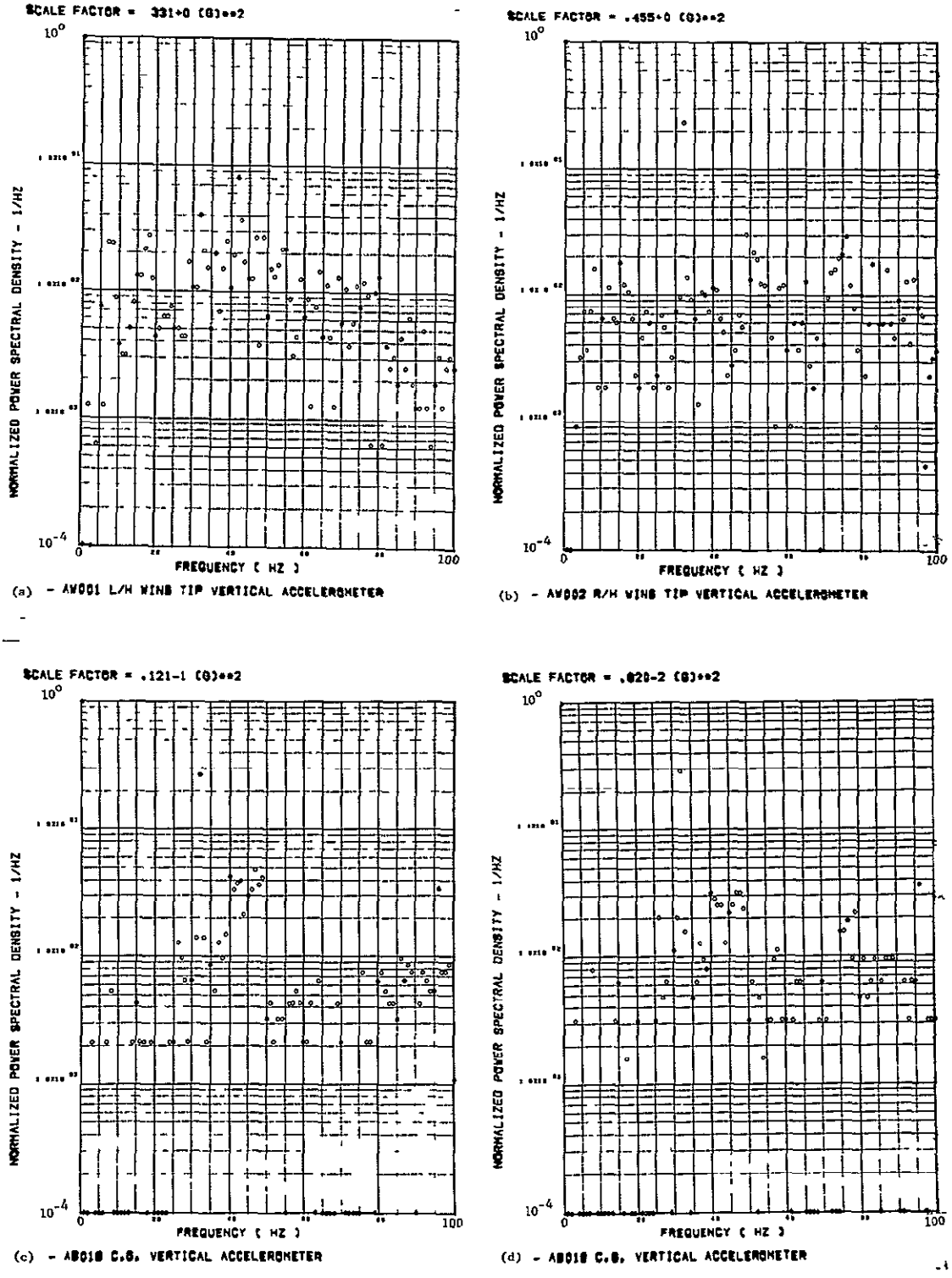

Figure 49. Power Spectra-Flight 70, Run 2, Point 1, T_1=124705.7, ΔT=2 Sec, α_{Nom}=2.10 deg, $\Delta\alpha = \pm .05$ deg.

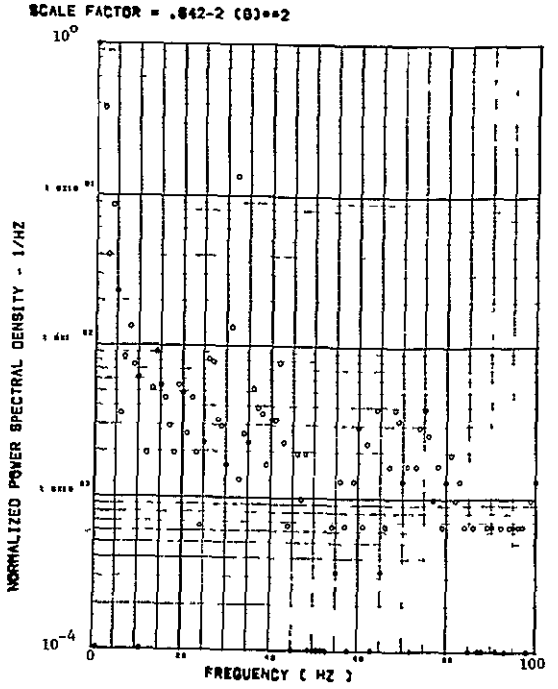

(e) - AF009 PILOT S SEAT VERTICAL ACCELEROMETER

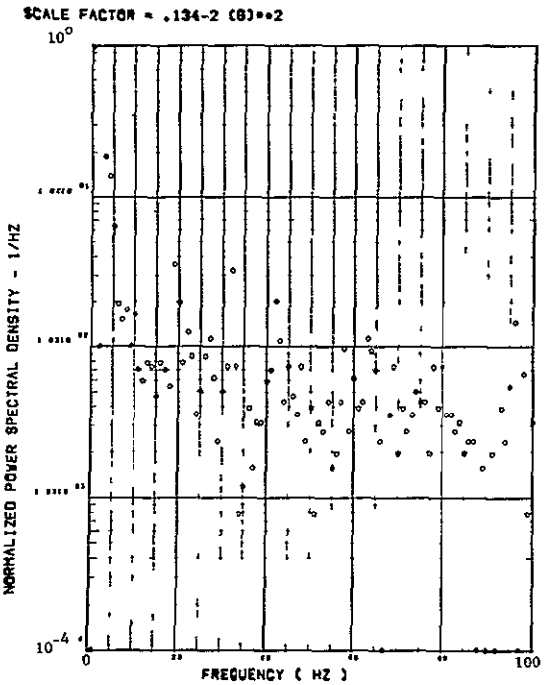

(f) - AF010 PILOT S SEAT LATERAL ACCELEROMETER

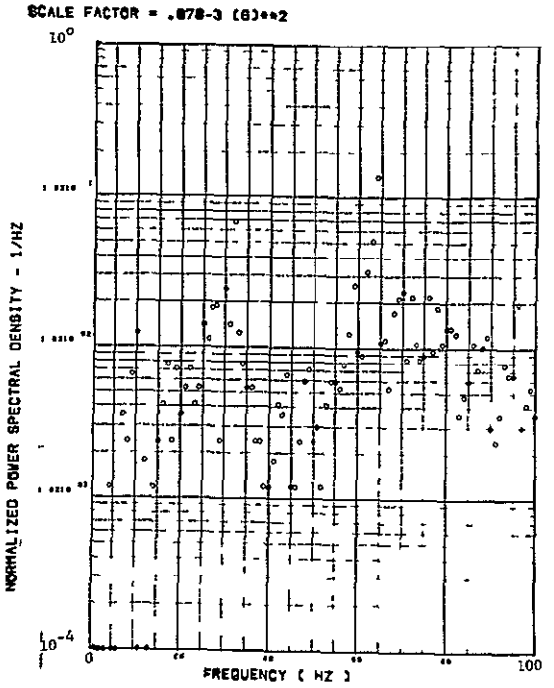

(g) - AB020 C.G. LATERAL ACCELEROMETER

Figure 49. Continued

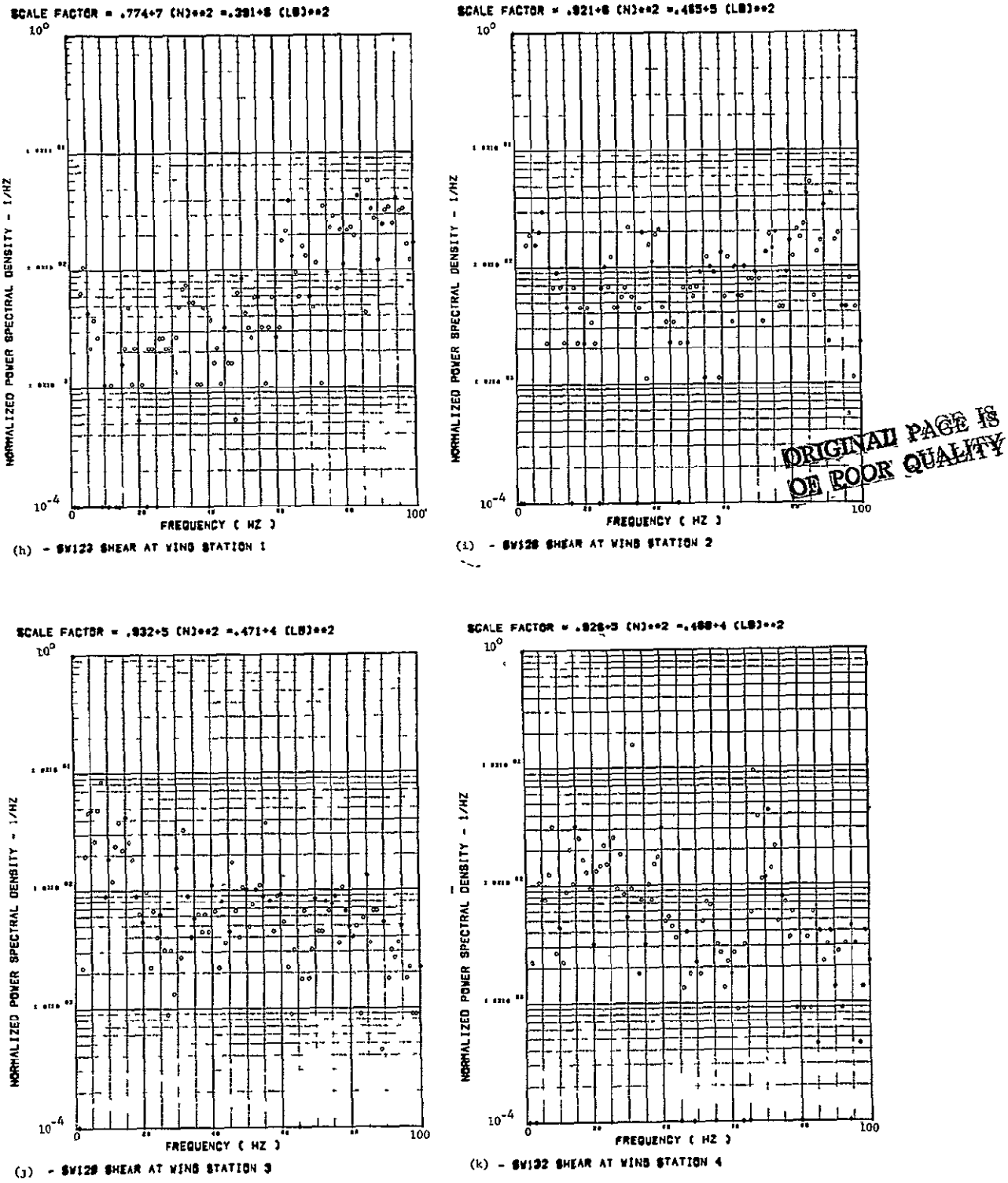

Figure 49. Continued

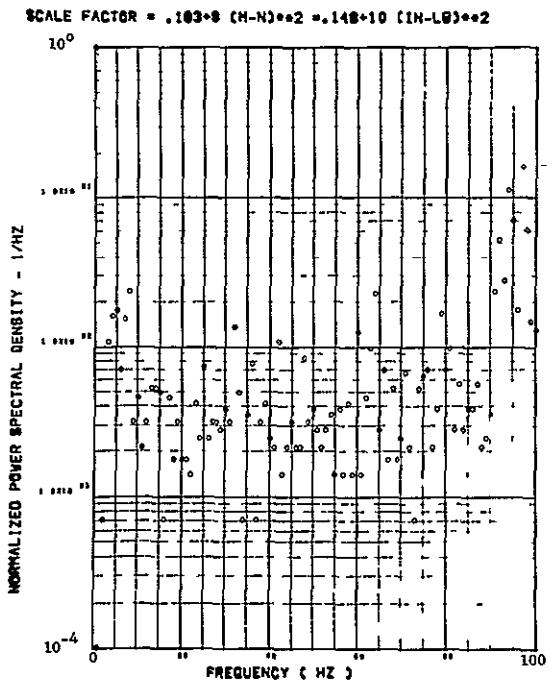

(l) - SW124 BENDING MOMENT AT WING STATION 1

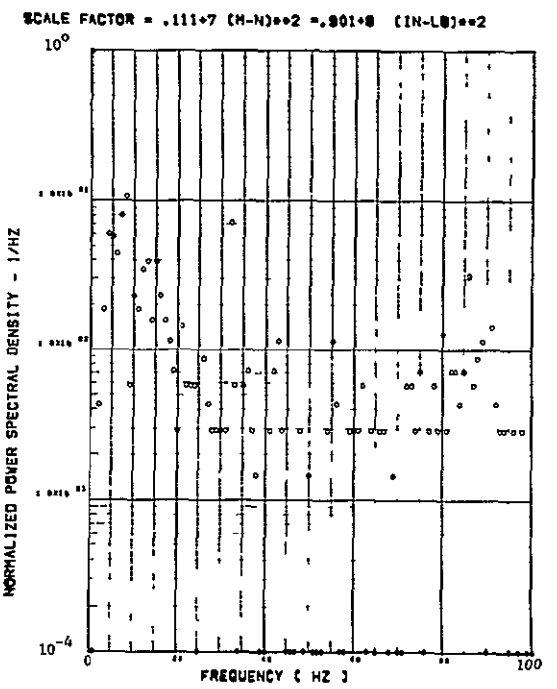

(m) - SW127 BENDING MOMENT AT WING STATION 2

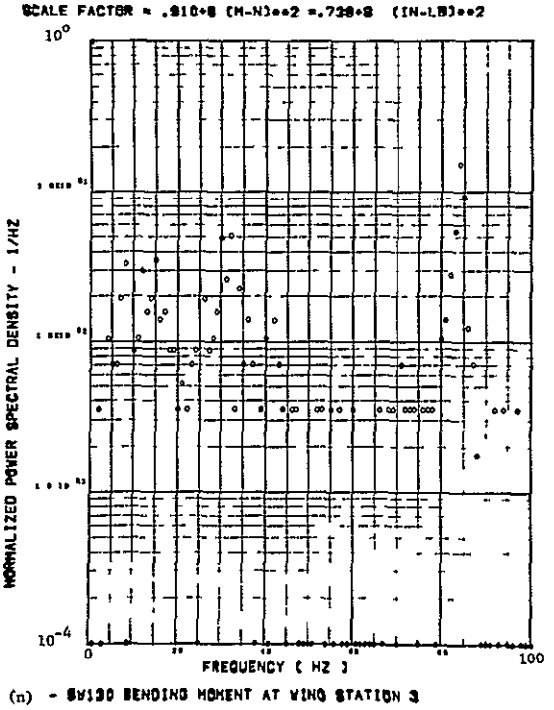

(n) - SW130 BENDING MOMENT AT WING STATION 3

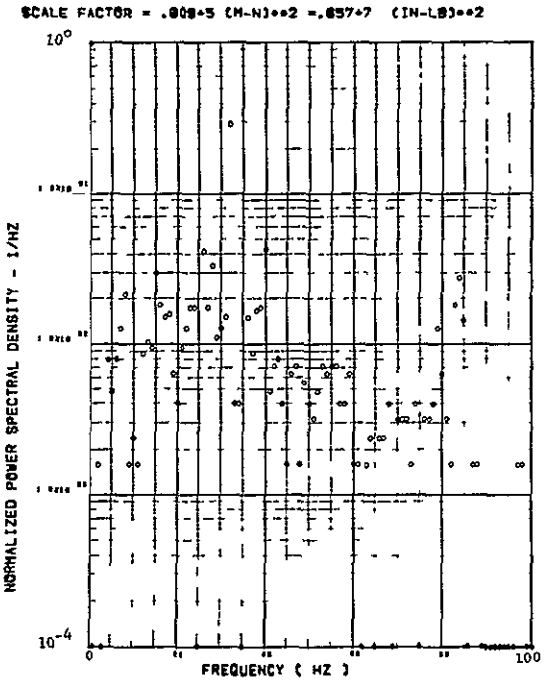

(o) - SW133 BENDING MOMENT AT WING STATION 4

Figure 49. Continued

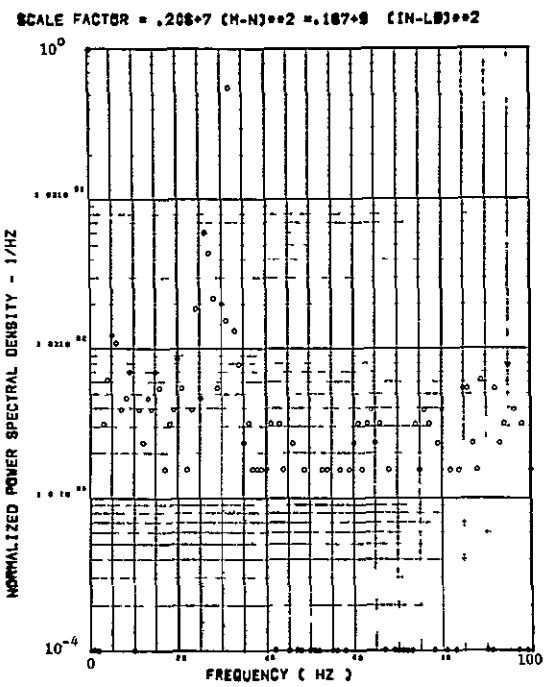

(p) SW125 TORSION AT WING STATION 1

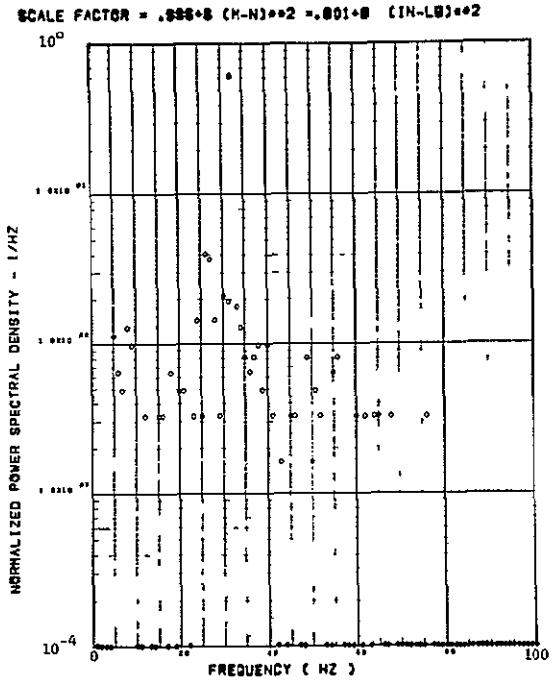

(q) - SW128 TORSION AT WING STATION 2

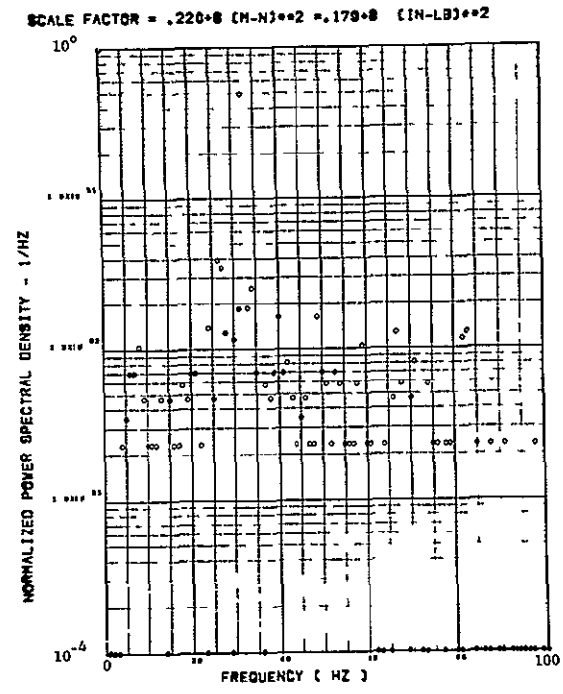

(r) - SW131 TORSION AT WING STATION 3

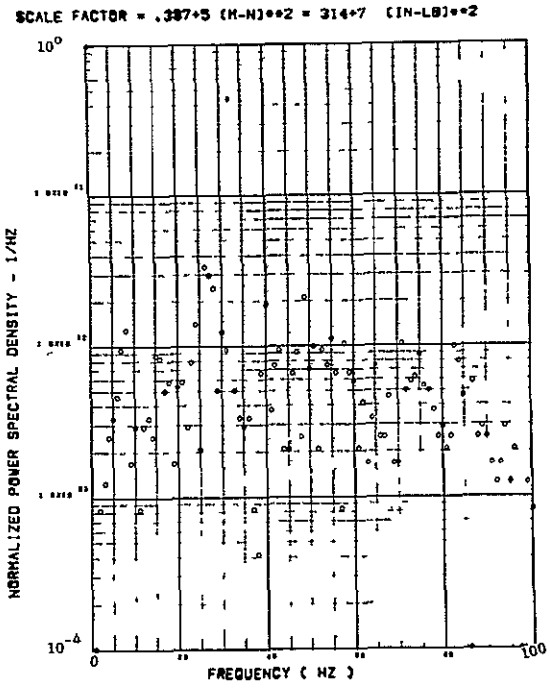

(s) - SW134 TORSION AT WING STATION 4

Figure 49. Concluded

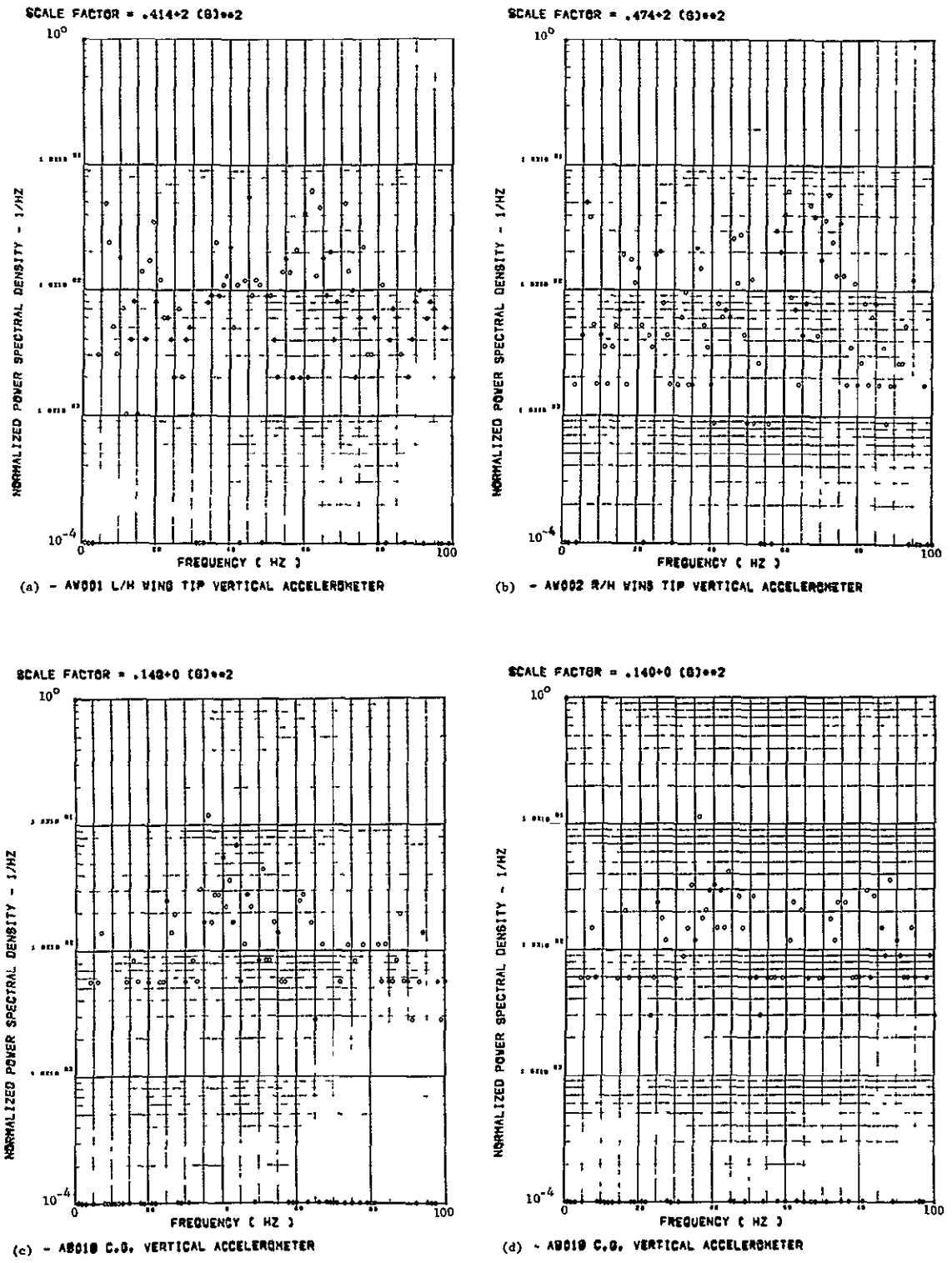

Figure 50. Power Spectra-Flight 70, Run 2, Point 2, T_1=124708.5, ΔT=1 Sec, α_{Nom}=12.3 deg, $\Delta\alpha$=4.20 deg.

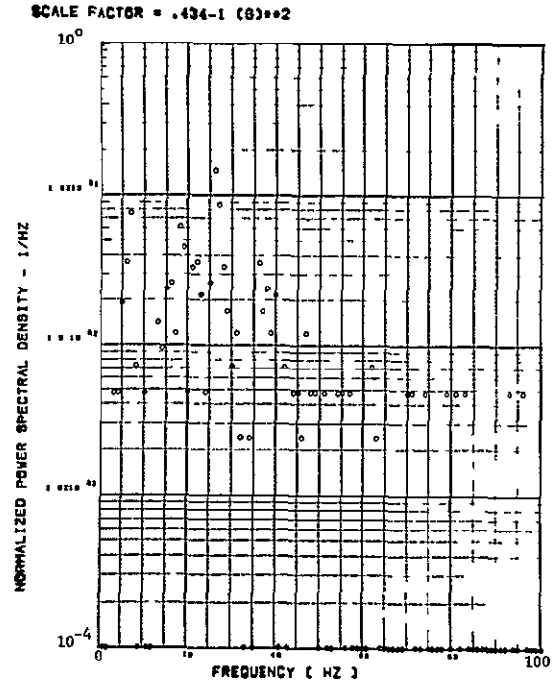

(e) - AF009 PILOT S SEAT VERTICAL ACCELEROMETER

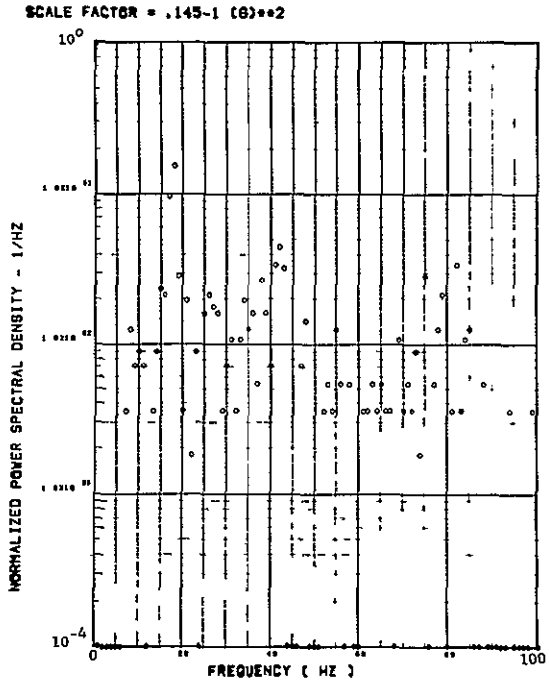

(f) - AF010 PILOT S SEAT LATERAL ACCELEROMETER

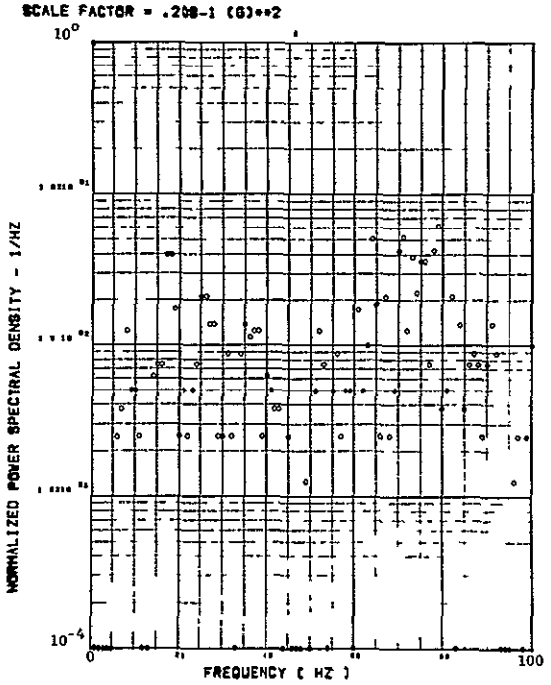

(g) - AB020 C.G. LATERAL ACCELEROMETER

Figure 50. Continued

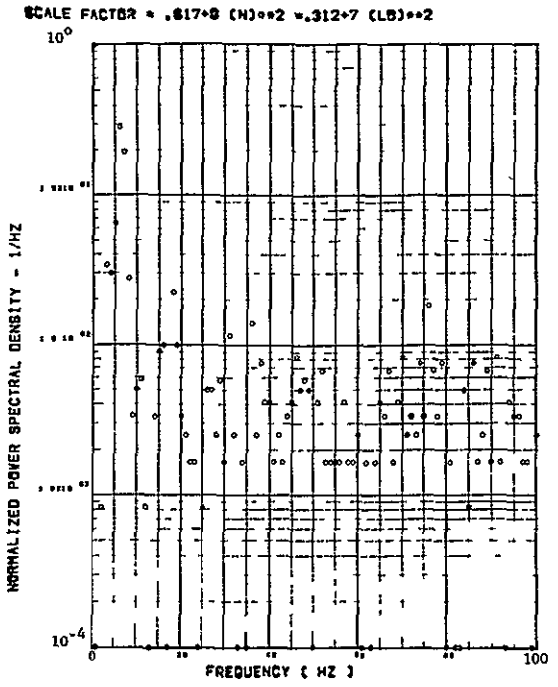

(h) - SW123 SHEAR AT WING STATION 1

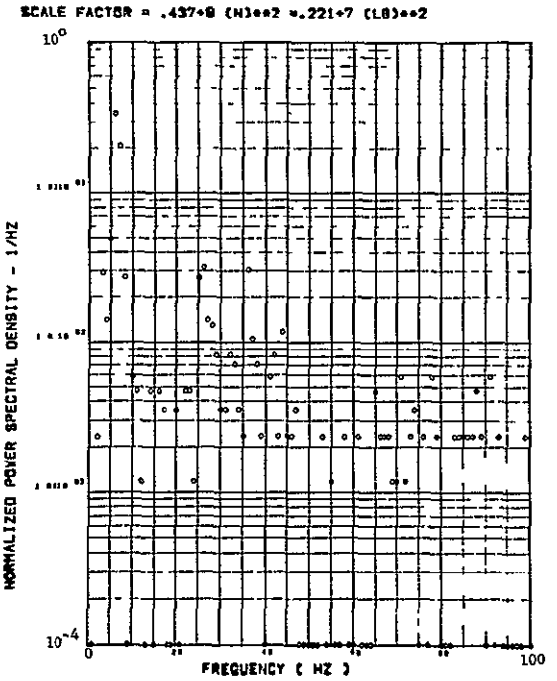

(i) - SW126 SHEAR AT WING STATION 2

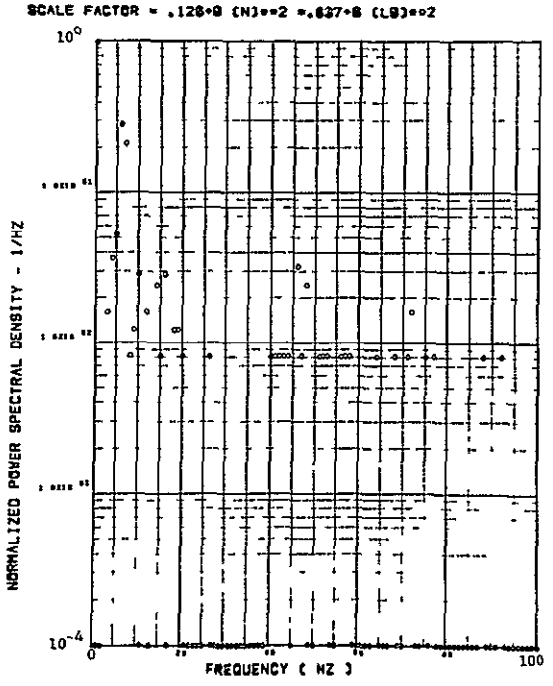

(j) - SW129 SHEAR AT WING STATION 3

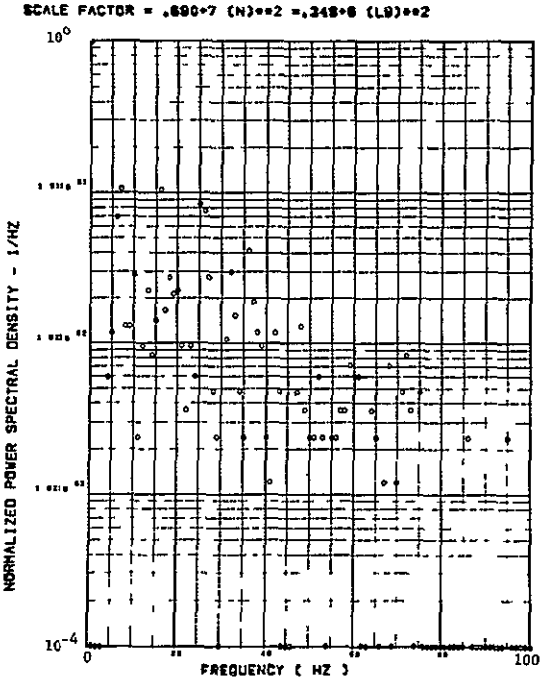

(k) - SW132 SHEAR AT WING STATION 4

Figure 50. Continued

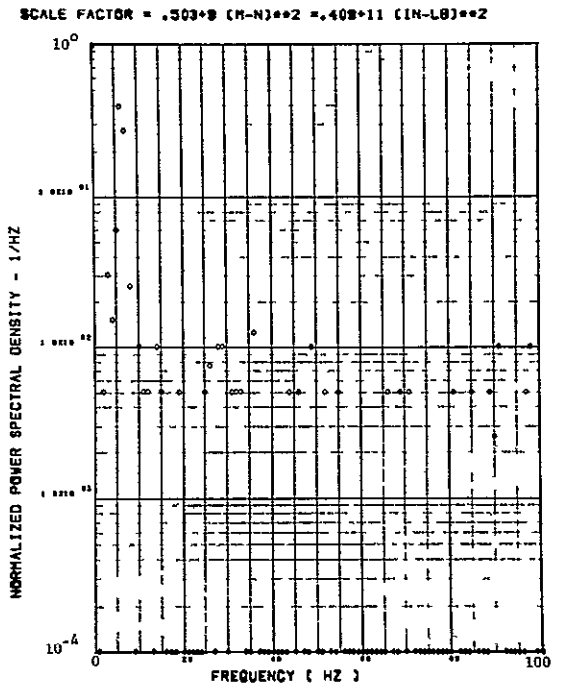

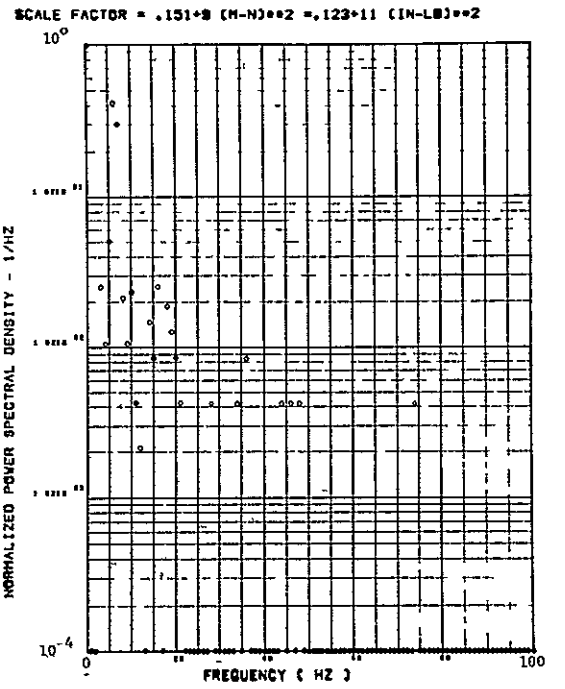

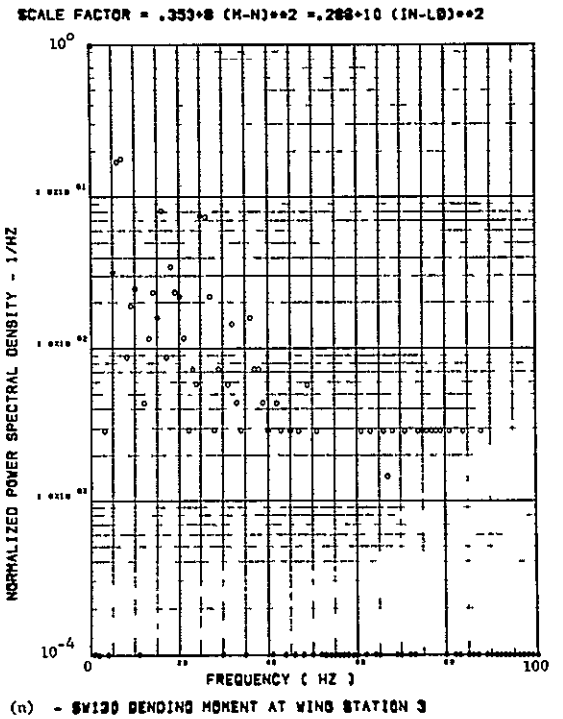

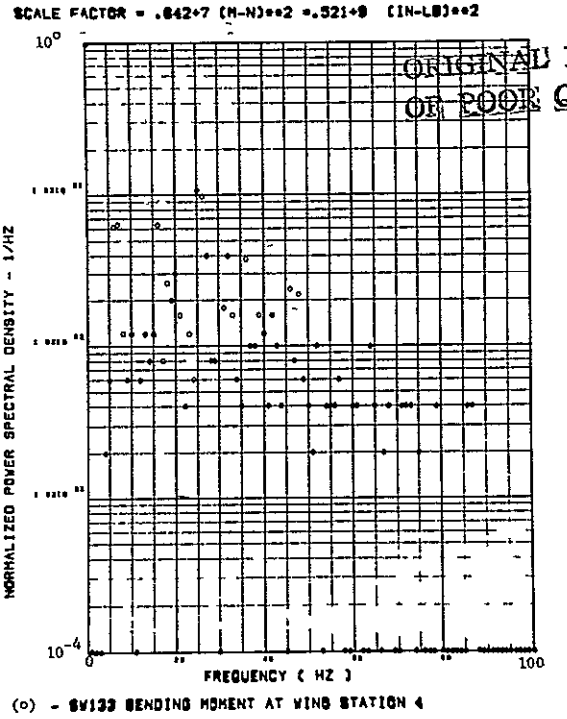

Figure 50. Continued

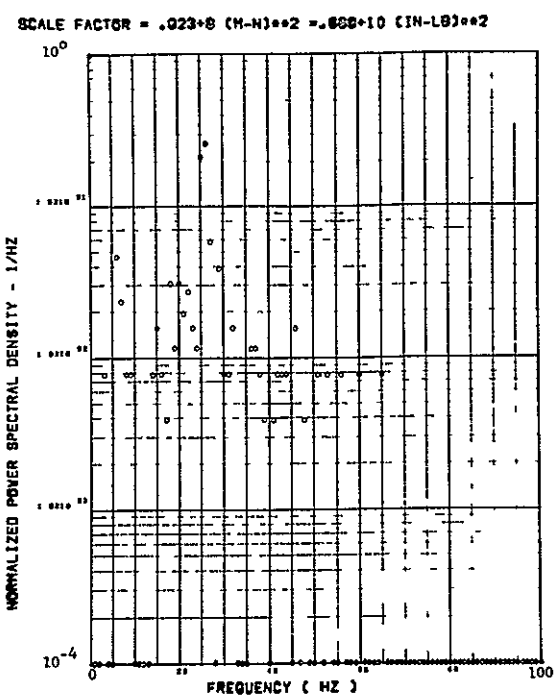

(p) - SW128 TORSION AT WING STATION 1

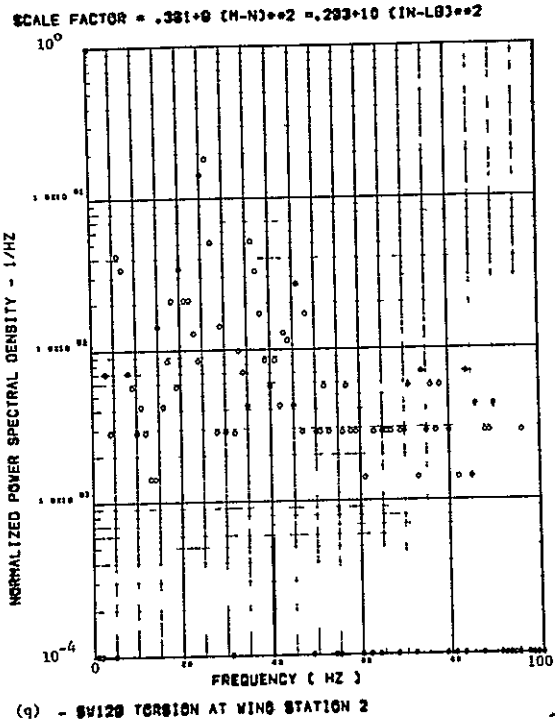

(q) - SW129 TORSION AT WING STATION 2

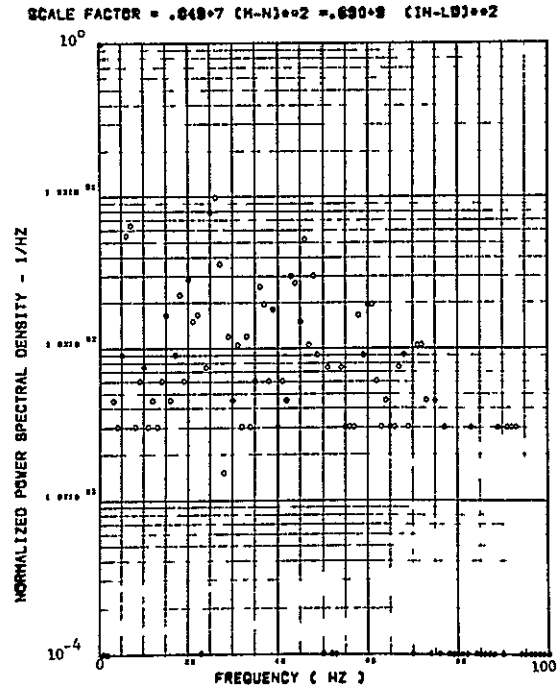

(r) - SW131 TORSION AT WING STATION 3

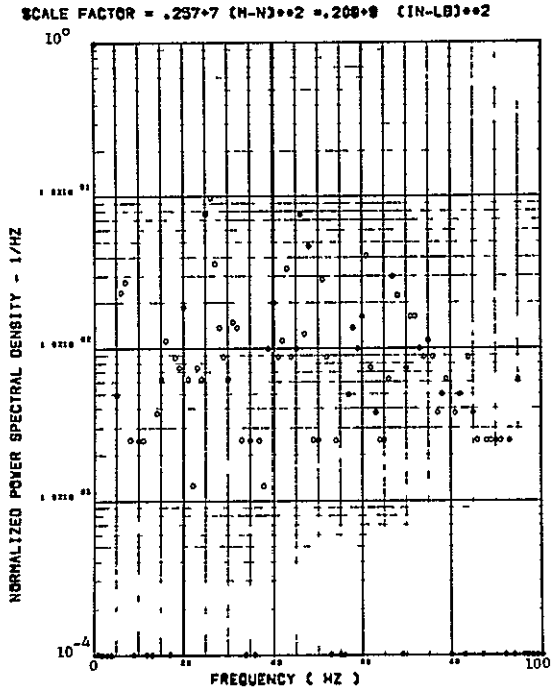

(s) - SW134 TORSION AT WING STATION 4

Figure 50. Concluded

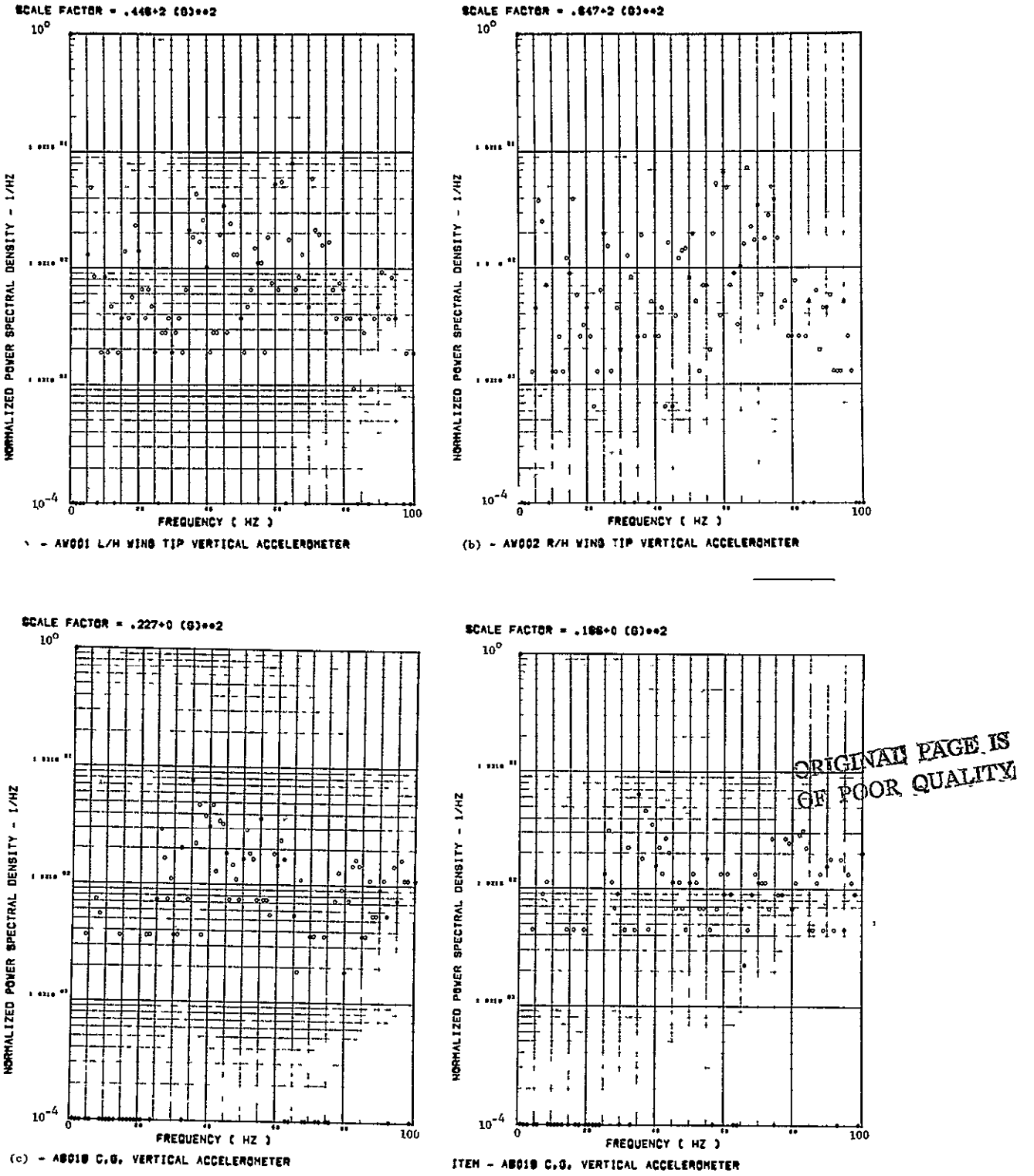

Figure 51. Power Spectra-Flight 70, Run 2, Point 3, T_1=124708.9, ΔT=1 Sec, α_{Nom}=12.5 deg, $\Delta\alpha$=1.30 deg.

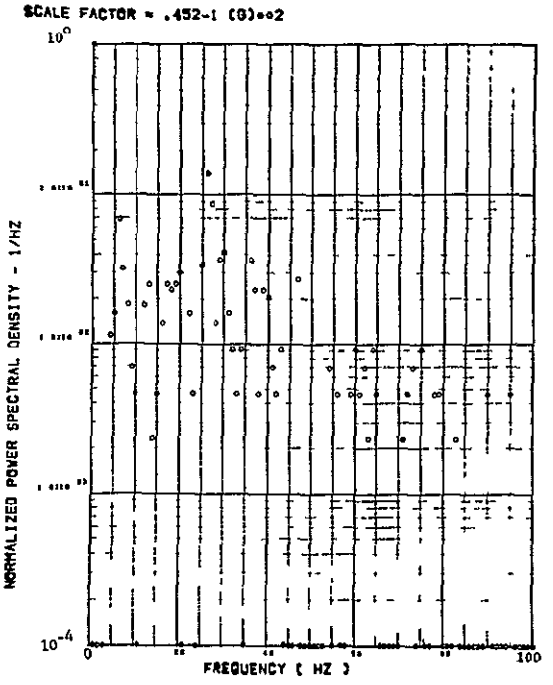

(e) - AF009 PILOT S SEAT VERTICAL ACCELEROMETER

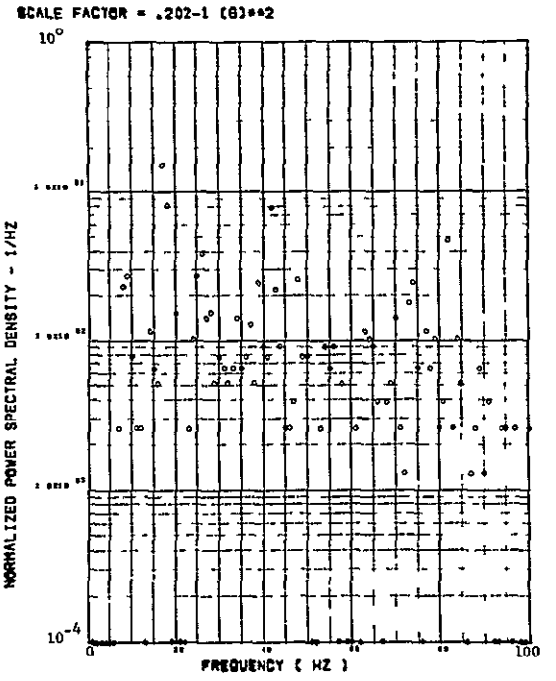

(f) - AF010 PILOT S SEAT LATERAL ACCELEROMETER

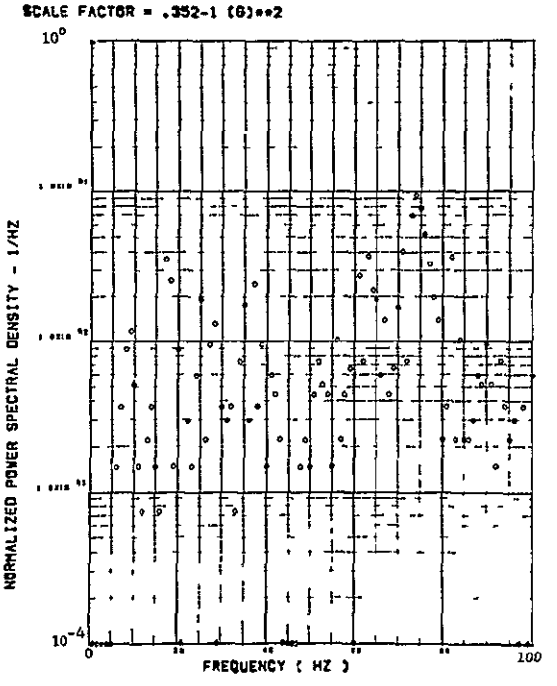

(g) - AB020 C.G. LATERAL ACCELEROMETER

Figure 51. Continued

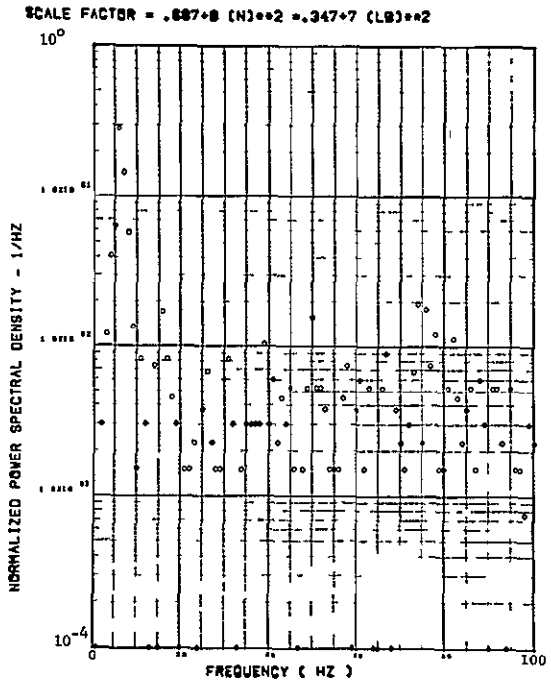

(h) - SW123 SHEAR AT WING STATION 1

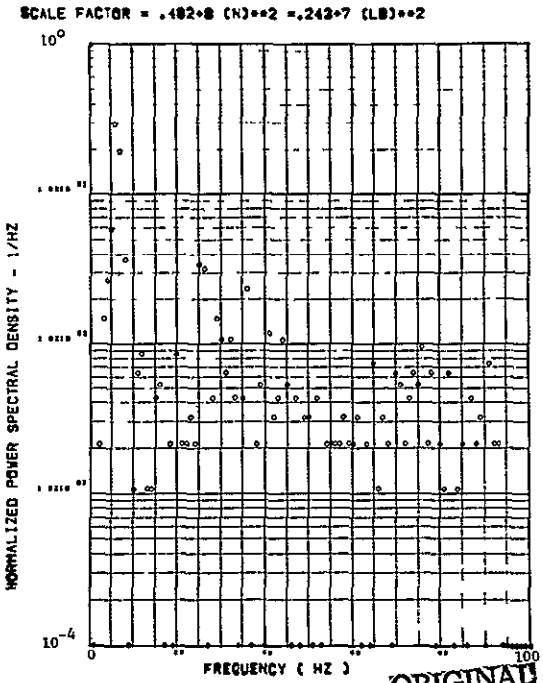

(i) - SW126 SHEAR AT WING STATION 2

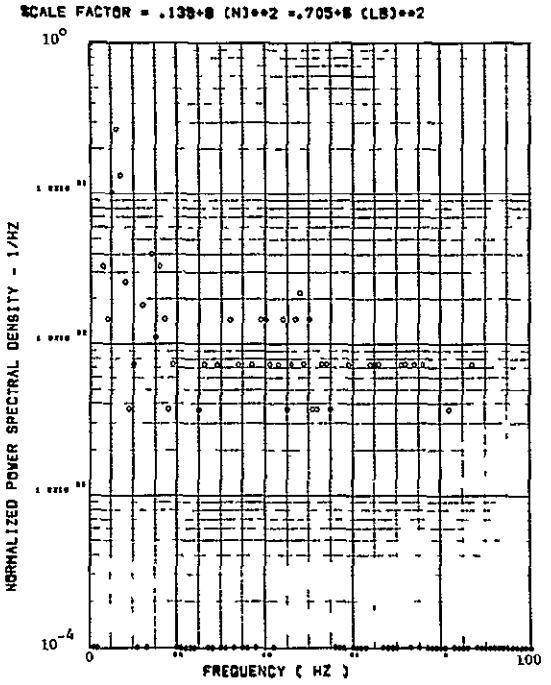

(j) - SW129 SHEAR AT WING STATION 3

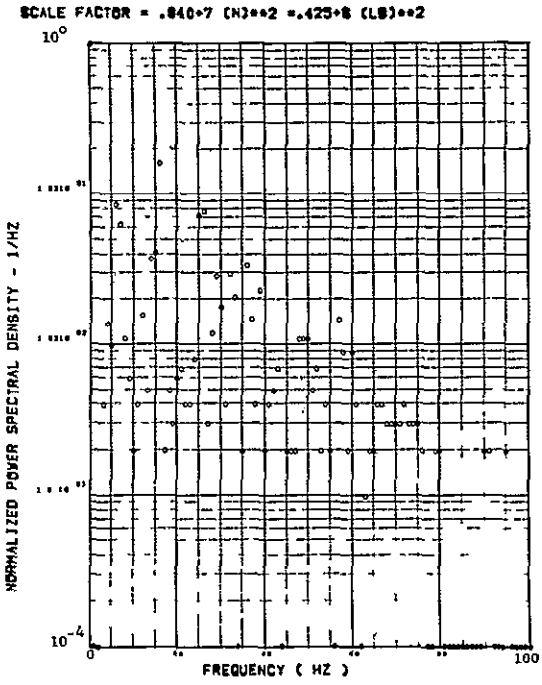

(k) - SW132 SHEAR AT WING STATION 4

Figure 51. Continued

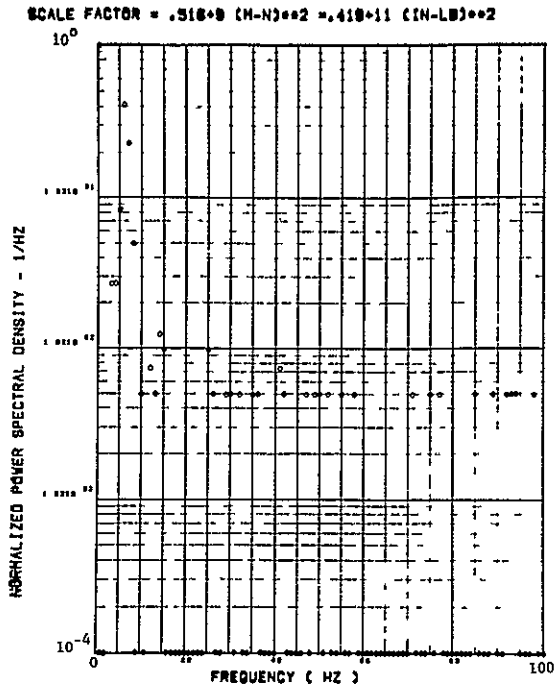

(l) - SW124 BENDING MOMENT AT WING STATION 1

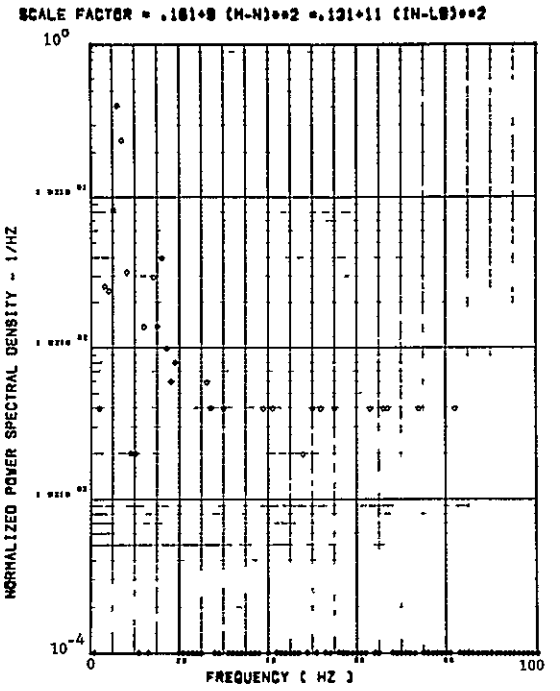

(m) - SW127 BENDING MOMENT AT WING STATION 2

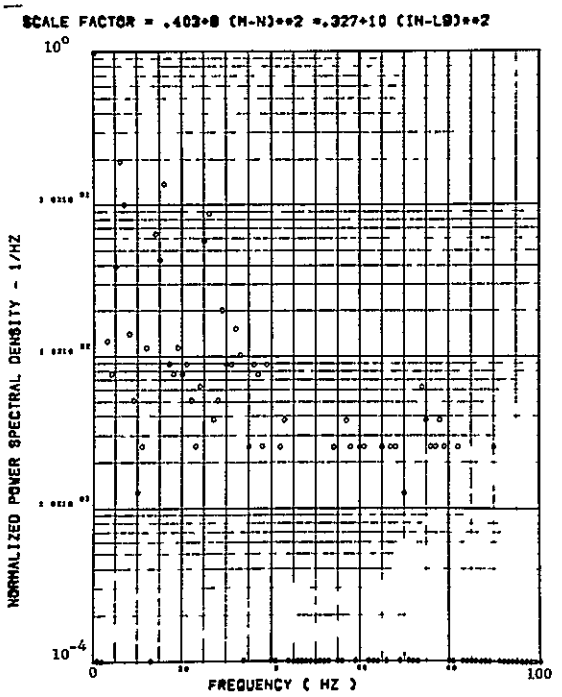

(n) - SW130 BENDING MOMENT AT WING STATION 3

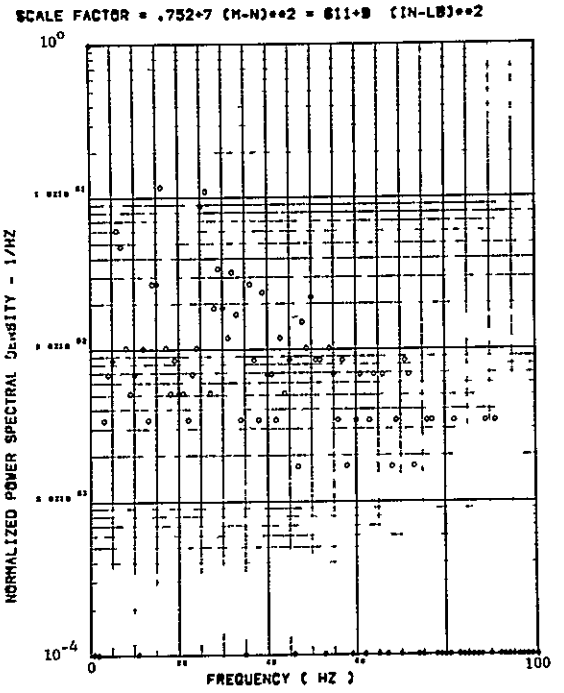

(o) - SW133 BENDING MOMENT AT WING STATION 4

Figure 51. Continued

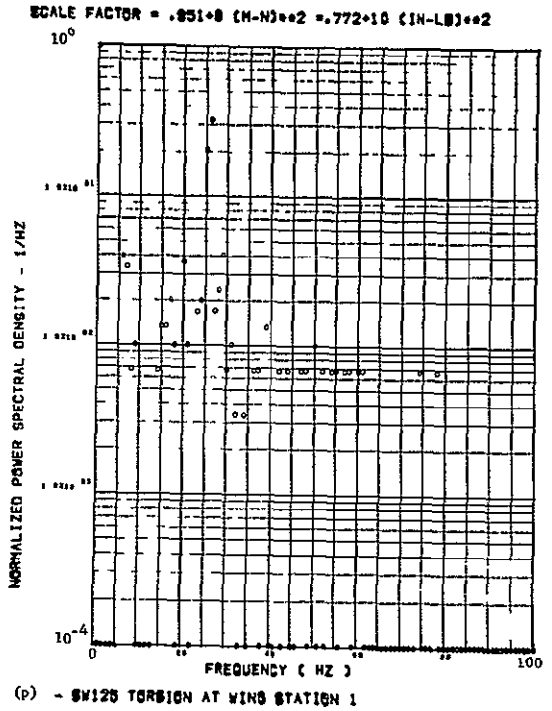

(p) - SW125 TORSION AT WING STATION 1

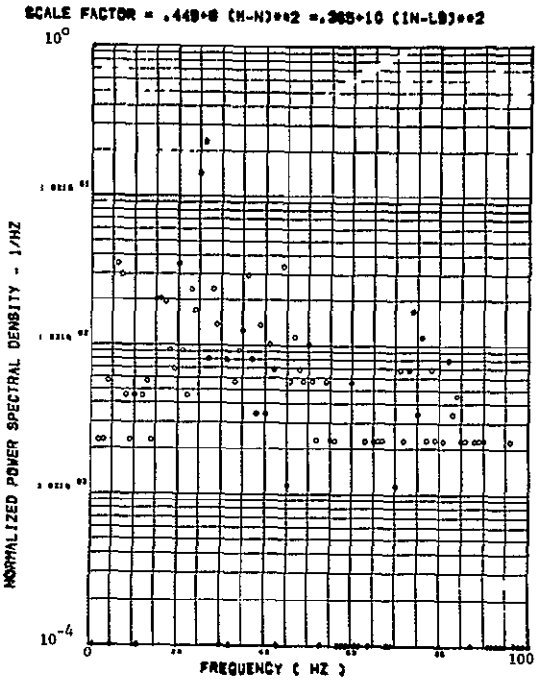

(q) - SW129 TORSION AT WING STATION 2

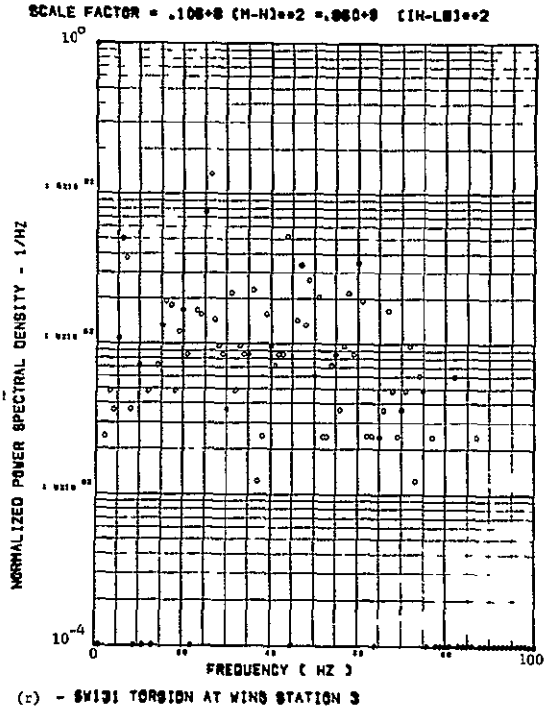

(r) - SW131 TORSION AT WING STATION 3

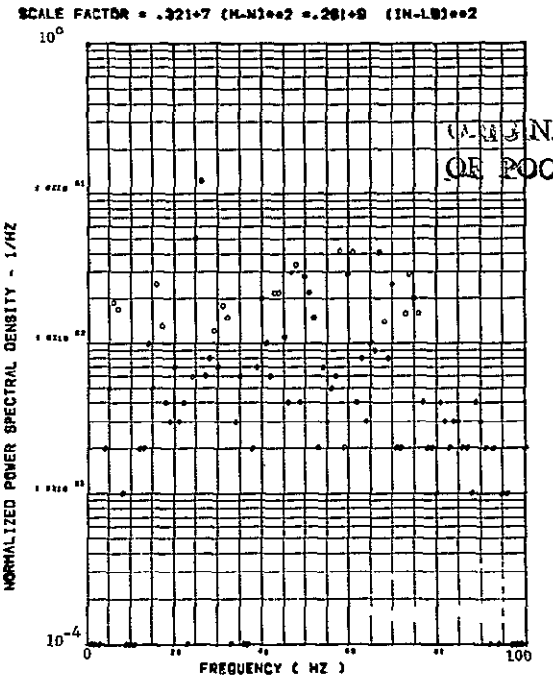

(s) - SW134 TORSION AT WING STATION 4

Figure 51. Concluded

REFERENCES

1. Coe, C.F., "The Effect of Model Scale on Rigid-Body Unsteady Pressures Associated with Buffeting," Proceedings of Symposium on Aeroelastic and Dynamic Modeling Technology, USAF (RTD TDR-63-4197, Part II), March 1964.

2. Ray, E.J., and Taylor, R.T., Buffet and Static Aerodynamic Characeristics of a Systematic Series of Wings Determined from a Subsonic Wind Tunnel Study, NASA TN D 5805, 1970.

3. Ray, E.J., Techniques for Determining Buffet Onset, NASA TM X-2103, November 1970.

4. Hanson, P.W., Evaluation of an Aeroelastic Model Technique for Predicting Airplane Buffet Loads, NASA TN D 7066, February 1973.

5. Friend, E.L., and Monaghan, R.C., Flight Measurements of Buffet Characteristics of the F-111A Variable Sweep Airplane, NASA TM X-1876, 1969.

6. Fischel, J., and Friend, E.L., Preliminary Assessment of Effects of Wing Flaps on High Subsonic Flight Buffet Characteristics of Three Airplanes, NASA TM X-2011, 1970.

7. Friend, E.L., and Sefic, W. J., Flight Measurements of Buffet Characteristics of the F-104 for Selected Wing-Flap Deflections, NASA TN D 6943, August 1972.

8. DeAngelis, M.V., and Banner, R.D., "Buffet Characteristics of the F-8 Supercritical Wing Airplane," Paper 7 in Supercritical Wing Technology. A Progress Report on Flight Evaluations, NASA SP-301, 1972.

9. Margolin, M., and Chung, J.G., "F-105F Transonic Buffet Study and Effect of Maneuvering Flaps, Air Force Flight Dynamics Lab, Technical Report AFFDL-TR-69-37, July 1969.

10. Titiriga, A., Jr., F-5A Transonic Buffet Flight Test, Air Force Flight Dynamics Lab, Technical Report AFFDL TR-69-110, December 1969.

11. Cohen, Marshall, Buffet Characteristics of the Model F-4 Airplane in the Transonic Flight Regime, Air Force Flight Dynamics Lab, Technical Report AFFDL-TR-70-56, April 1970.

REFERENCES, (Continued)

12. Emerson, E.G., F-106A Transonic Buffet Flight Test, Air Force Flight Dynamics Lab, Technical Report AFFDL-TR-70-87, June 1970.

13. Mullans, R.E., and Lemley, C.E., Buffet Dynamic Loads During Transonic Maneuvers, Air Force Flight Dynamics Lab, Technical Report AFFDL-TR-72-46, September 1972.

14. Anon., Turbulence Study of a Transonic Wind Tunnel and an Analysis and Tests of Aircraft Response to Turbulence, North American Aviation, Inc., Columbus Division, Report NA 63H-636, 1 October 1964.

15. Mayes, J.F., Lores, M.E., and Barnard, H.R., Transonic Buffet Characteristics of a 60 Degree Swept Wing with Design Variations, AIAA Paper No. 69-793.

16. Damstrom, E.K., and Mayes, J.F., Transonic Flight and Wind Tunnel Buffet Onset Investigation of the F-8D Aircraft - Analysis of Data and Test Techniques, AIAA Paper No. 70-341.

17. Post, J.P., Botman, M., and Bennett, R.V., An Analytical and Experimental Study of Aircraft Response to Buffeting, North American Aviation, Inc., Columbus Division, Report NA 60H-742, 6 September 1961.

18. Nevius, H.E., F-111A Ground Vibration Test No Wing Stores (Airplane 12), General Dynamics' Fort Worth Division Report FZS-12-167, 5 August 1966, and Supplement 1, 1 August 1967.

19. Nevius, H.E., F-111A Ground Vibration Tests No Wing Stores (Airplane 1-11), General Dynamics' Fort Worth Division Report FZS-12-060, 1 March 1965.